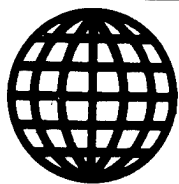


JPRS-JST-90-055

14 DECEMBER 1990



**FOREIGN
BROADCAST
INFORMATION
SERVICE**

JPRS Report

Science & Technology

Japan

ADVANCED COMPOSITE MATERIALS SYMPOSIUM

19980203 329

DTIC QUALITY INSPECTED 3

REPRODUCED BY
U.S. DEPARTMENT OF COMMERCE
NATIONAL TECHNICAL INFORMATION SERVICE
SPRINGFIELD, VA. 22161

DISTRIBUTION STATEMENT A

Approved for public release;
Distribution Unlimited

JPRS-JST-90-055
14 DECEMBER 1990

SCIENCE & TECHNOLOGY
JAPAN

ADVANCED COMPOSITE MATERIALS SYMPOSIUM

43070708 Tokyo ADVANCED COMPOSITE MATERIALS in English 2-3 Oct 90 pp 1-364

[10th Tsukuba General Symposium on Advanced Composite Materials Leading Part
for the 21st Century--Japan/France Joint Seminar held 2-3 Oct 90 in Tsukuba
City, sponsored by the Agency of Industrial Science and Technology, MITI]

CONTENTS

PROGRAM

◆◆◆ October 2, 1990 (Tuesday) ◆◆◆

10:00~12:00 GENERAL SESSION

(Room A)

10:00~10:10 [Opening Speech]

H. SUZUKI, Director-general for Technology Policy Coordination, Minister's
Secretariate, MITI

10:10~11:00 [Special Lecture]

"Social Impact of Advanced Technology in Japan" 1
Y. HAYASHI, President of Tokyo University of Information Sciences

11:00~12:00 [Key Note Speeches]

1. "Fracture and Fatigue of High Performance Composite Materials" 3
C. BATHIAS, Professor, Conservatoire National des Arts et Metiers
2. "Problems of Testing Methods for Advanced Composite Materials" 43
M. UEMURA, Professor, Nippon University

12:00~13:30 Lunch

13:30~16:50 SESSION I Life Prediction

(Room A)

Chairmen: S. MOMOSHIMA, Composites System Research Institute, Co.,Ltd.
G. VERCHERY, Ecole Nationale Supérieure des Mines de Saint-Etienne

- I-1 "Delamination Fatigue Crack Propagation in CF/PEEK Laminates" 57
M. HOJO, K. KEMMOCHI, and R. HAYASHI, Industrial Products Research
Institute, AIST, and K. TANAKA, Kyoto University
- I-2 "Microcomputer Aided Design and Control for Composite Structures" 64
G. VERCHERY, Ecole Nationale Supérieure des Mines de Saint-Etienne
- I-3 "Notch Sensitivity of Aramid Unidirectional Composites" 70
S. BANDO and M. OHNO, Kawasaki Heavy Industry Co.,Ltd.

(Coffee Break 15:00~15:20)

- I-4 "A Damage Statistical Micromechanic Modelization to a Discontinuous
Reinforcement Composite Aluminum-Carbon" 75
P. BREBAN, D. BAPTISTE, and D. FRANCOIS, Ecole Centrale de Paris
- I-5 "Reliability Evaluation of Static and Fatigue Strength of Carbon/Polyimide
Laminates" 91
T. SHIMOKAWA and Y. HAMAGUCHI, National Aerospace Laboratory, and
H. MITSUMA, National Space Development Agency of Japan
- I-6 "Damage Mechanics for 3D-Composite" 97
O. ALLIX and P. LADEVEZE, Ecole Normale Supérieure de l'Enseignement
Technique

16:50~17:50 SESSION II A Advanced Materials

(Room A)

Chairmen: M. MORITA, Toyama Prefecture University
R. NASLAIN, University of Bordeaux

- II-1 "Processing and Properties of Ceramic Matrix Composites for Applications in
Severe Aerospace Environments" 101
R. NASLAIN, University of Bordeaux, and J. C. CAVALIER, Societe Europeenne
de Propulsion
- II-2 "Fabrication and Properties of FGM" 107
I. SHIOTA, National Research Institute for Metals, and R. WATANABE,
University of Tokyo

9:30~12:00 SESSION IIB Advanced Materials

(Room A)

Chairmen: M. MORITA, Toyama Prefecture University
R. NASLAIN, University of Bordeaux

- II-3 "Silicon Carbide Fibres Reinforced Silicon Carbide and Glass Ceramic Composites" 116
M. PARLIER, T. GRENIER and J. F. STOHR, Office National d'Etudes et de Recherches Aeronautiques
- II-4 "New Design of Structural Ceramics -Nanocomposites-" 128
K. Niihara, Osaka University
- II-5 "Ceramic-Metal Nanocomposites" 134
A. ROUSSET, X. DEVAUX, M. BRIEU, Universite P. Sabatier, and A. MARCHAND, Laboratoire Louis Neel CNRS
- II-6 "Fabrication of Three-Dimensional Fabric Composites and Their Mechanical Properties" 144
E. AOKI, T. KITANO, Y. NAGATSUKA, and M. FUNABASHI, Research Institute for Polymers and Textiles, and K. FUKUTA, 3-D Composites Research Corporation
- II-7 "Growth, Structure and Properties of Fe/Ru Hexagonal Superlattices" 150
M. F. RAVET, M. MAURER, J. C. OUSSET and M. PIECUCH, Saint-Gobain

12:00~13:00 Lunch

13:00~15:00 POSTER SESSION Application and CAD/CAM

(Room A & C)

Chairmen: F. LESBRE, Service Technique des Constructions et Arms Navales
K. KEMMOCHI, Industrial Products Research Institute

- P-1 "The Use of Infrared Thermography to the Quality Assessment of Composite Materials Used in Military Ship Building" 159
F. LESBRE, Service Technique des Constructions et Arms Navales
- P-2 "Materials for Cryogenic Behavior" 165
M. SABRIE, Alstom
- P-3 "Computer Aided Design" 167
D. E. ROUVRAY, Engineering Systems Internationals and P. DESTUYNDER, Conservatoire National des Arts et Metiers
- P-4 "Development of High Performance Carbon/Carbon Composites for Space Applications" 169
T. MATSUSITA, H. MITSUMA, T. KOBAYASHI, Tsukuba Space Center, H. NAKAYAMA, A. SAKAI, Kawasaki Heavy Industry Co., Ltd., N. TSUCHIYA and T. KINJO, Kawasaki Steel Corp.

P-5	"Advanced Joint of 3-D Composite Materials for Space Structure"	175
	T. YAMAMOTO, Mitsubishi Heavy Industry Co.,Ltd. and T. HIROKAWA, Shikishima Canvas Co.,Ltd.	
P-6	"Superplastic Forging of SiCw Reinforced Aluminum Alloy"	181
	T. TSUZUKU, A. TAKAHASHI, C. FUJIWARA and A. SAKAMOTO, Mitsubishi Heavy Industry Co.,Ltd.	
P-7	"Approach to Control of Fibre Orientation on FRTP Injection Moulding"	187
	T. HIRAI, T. KATAYAMA, Dohshisha University and M. HIRAI, Osaka Prefectural College of Technology	
P-8	"Structural Analysis of Laminated Cylinder"	193
	A. NAKAZONO and K. NAKANO, Sumitomo Chemical Co.,Ltd.	
P-9	"New Thermoplastic Polyimide Composite for Aircraft Structure"	199
	T. NAGUMO, Fuji Heavy Industry Co.,Ltd. and H. SAKAI, Mitsui Toatsu Chemicals, Inc.	
P-10	"Safety Evaluation and Design of Filament Wound Structures -Cases of Pressure Vessels and Pipes-"	206
	M. KAWAHARA, T. MORI, Y. HIRASE, A. KATOH and T. ISHIHARA, Nippon Steel Co.,Ltd.	
P-11	"PRODACOM: Property Database for Advanced Composite Materials for Future Industries"	212
	M. MIKI, University of Osaka Prefecture, and Y. MINODA, Research and Development Institute of Metals and Composites for Future Industries	
P-12	"Japan-France Friendship Communication Monument, Colossal Structure Composed of Innovative Materials"	218
	H. SAITO, Secretariat of the Japanese Committee for the Japan-France Friendship Monument	
P-13	"Computer Aided Micro-damaging and Fracture Characterization of Composite Materials for Non-linear Structural Analyses and Crash Simulation"	223
	L. T. KISIELEWICZ, ESI Japan and K. ANDOH, Penta-Ocean Construction Co.,Ltd.	
P-14	"Grafting of Glass Surface"	229
	P. CHARTIER, Saint-Gobain Recherche	
P-15	"Influence of the Reaction Zone on the Interfacial Shear Stress in SiC/Titanium Alloy Composite"	235
	G. LAMANTHE, Y. KAGAWA, University of Tokyo, and A. OKURA, Inst. of Space and Astronautical Science	

(Coffee Break 14:40~15:00)

15:00~17:30 SESSION III Interface and Coatings

(Room A)

Chairmen: P. FAUCHAIS, University of Limoges France
R. HAYASHI, Industrial Products Research Institute

- III-1 "Plasma Sprayed Ceramic Coatings" 243
P. FAUCHAIS, A. VARDELLE, M. VARDELLE, J. F. COUDERT and A. GRIMAUD,
University of Limoges France
- III-2 "Recent Advancement in Thermal Barrier Coatings" 253
H. TAKEDA, T. SUZUKI, M. ITO and M. NAKAHASHI, Toshiba Co., Ltd.
- III-3 "Carbon Fiber Coating and its Influence on the Mechanical Behavior of
Composites" 259
J. BOUIX, R. FAVRE, C. VINCENT, H. VINCENT, S. CARDINAL, P. FLEISCHMANN,
P. F. GOBIN and P. MERLE, University of Lyon
- III-4 "Laser and Plasma Hybrid Spray Coatings on Carbon Fiber Reinforced Composite
Materials" 273
H. SHIMURA, S. SASAKI, Mechanical Engineering Laboratory, K. HASEGAWA
Kawasaki Steel Co., and K. HIRANO, Nippon Steel Co.
- III-5 "Interface Influence on Mechanical Properties of Composites" 279
J. P. FAIVRE, Saint-Gobain Group

11:00~12:00 SESSION IVA Database

(Room B)

Chairmen: S. NISHIJIMA, National Research Institute for Metals
D. R. VINARD, Saint-Gobain Aubervilliers

- IV-1 "Databases and Computer Assisted Manufacturing" 289
H. VIELLARD, CODATA-France
- IV-2 "IDAM: A Design Assist System for Composite Materials" 291
M. YOSHIOKA, M. HOJO, K. KEMMOCHI, Industrial Products Research Institute,
K. BAN, Rehabilitation Engineering Center for Employment Injuries, and
S. IYAMA, Toyo Engineering Co.
- IV-3 "Data Format, Structure and Transfer for Material Databases" 299
E. JULLIARD, Association Francaise de Normalisation
- IV-4 "Development of Fatigue Strength Design Support System" 321
T. SHUTO and T. OCHIAI, Mitsubishi Research Institute Co., Ltd.
- IV-5 "JICST/NRIM Materials Databases for Engineering Steels and Alloys" 327
Y. MONMA, K. KANAZAWA, M. SAKAMOTO, S. NISHIJIMA, National Research
Institute for Metals, K. SUZUKI and K. SHIMURA, JICST

Chairmen: Y. FUJIWARA, University of Tsukuba
M. CALISTE, Laboratoire National d'Essais

IV-6 "Certified Reference Materials"	333
M. CALISTE, Laboratoire National d'Essais	
IV-7 "The Materials Design Support Systems with Case-Based Reasoning"	338
Y. Fujiwara, University of Tsukuba	
IV-8 "Product Data Banks Requirements from Industrial Users"	347
D. R. VINARD, Saint-Gobain Aubervilliers	
IV-9 "Development and Application of Databases for Evaluation of Reliability in Structures of Heavy Electric Products"	353
T. INUKAI and N. OKABE, Toshiba Heavy Electric Co.,Ltd.	
IV-10 "The "Cetim-Materiaux" Database"	359
H. P. LIEURADE and C. LEBRETON, Centre Technique des Industries Mecaniques	

GENERAL SESSION

SPECIAL LECTURE
KEY NOTE SPEECHES

SOCIAL IMPACT OF ADVANCED TECHNOLOGY IN JAPAN

Yujiro HAYASHI

Tokyo University of Information Sciences
1200-2, Yato-machi, Chiba 280-01, Japan

ABSTRACT

Technology in the social context can be divided into two categories: exogenous technology and endogenous technology and this division is derived from the history of technology in society.

In the latter half of the nineteenth century Japan became a modern nation with a centralized government and its ultimate goal was the industrialization. Japan succeeded in accomplishing innovation three times so far and at present it is in the middle of the forth innovation, which centers around advanced technology.

Japan up to the Second World War experienced typical exogenous innovation. After the war it switched rapidly to endogenous innovation. In this paper I have clarified the cause and effect relationship of this period and described the social characteristics of present advanced technology and future prospects. Especially I have clarified what results were brought about by the science and technology promotion policy implemented in Japan after the war.

**FRACTURE AND FATIGUE OF HIGH
PERFORMANCE COMPOSITE MATERIALS**

Claude BATHIAS

Professor CNAM-Paris

Adjunct-Professor Georgia Tech-Atlanta

SUMMARY

INTRODUCTION

I - Application of fracture mechanics to composite materials

- 1.1 - Recapitulation of isotropic fracture criteria
- 1.2 - Relation between G and K
- 1.3 - Criteria for delamination

II - The mechanisms of damage

- 2.1 - General remarks
- 2.2 - Mechanisms of damage by delamination
- 2.3 - Remarks on the progression of damage mechanisms

III - Premature fracture in tension caused by a notch

- 3.1 - Notch effects
- 3.2 - Toughness of composite materials
- 3.3 - Application of Whitney and Nuismer criteria
- 3.4 - Effect of a notch on the fatigue strength
- 3.5 - Notch effect in compression

IV - Damage at the Notch tip

- 4.1 - Damage in simple tension
- 4.2 - The effects of fatigue on the damaged zone
- 4.3 - The influence of stacking orientation
- 4.4 - Damage zone in compression

CONCLUSION

FRACTURE AND FATIGUE OF HIGH PERFORMANCE COMPOSITE MATERIALS

CLAUDE BATHIAS

Professor at C.N.A.M./Paris and Adjunct-Professor at Georgia Tech/Atlanta

INTRODUCTION

The fracture in high performance composite material structures is of a quite different nature from these of metallic components. Failure, due to fatigue, is to be feared much less in the first case than in the second. On the other hand, the most worrying causes of damage are the stress concentrations round about notched and holes, as well as the splitting (into two) of the composites due to delamination.

The delamination, which in first approximation, implies flaw in the plane, can be treated by fracture mechanics, the latter allowing one to compare very easily the toughness of laminated composites as opposed to that of metallic alloys. Such an approach is of particular interest when one intends substituting metal by a composite.

Fracture mechanics lead, as it were, to measuring the properties of composites with respect to fracturing, and this at several scales. From the microscopic point of view, fracture originates from the cracking of the matrix, the reinforcements and the interfaces ; all these mechanisms which can be studied by fracture mechanics. From the macroscopic point of view, the total breakdown of the material can be investigated in the same manner, and it is only this approach, in actual fact the most useful to the engineer, which will be discussed hereafter.

More difficult is to apply fracture mechanics to notched laminated plate. In some cases where a quasi-isotropic lay-up exists it is always possible to use fracture mechanics to predict the failure of notched plates. However, where a strong orthotropic effect appears fracture mechanics criteria are not working very well. Other criteria such as Nuisner and Whitney approach is recommended.

In this paper we summarize some solutions for fracture in tension, in shear, in compression either in monotonic or in cyclic loading.

I - APPLICATION OF FRACTURE MECHANICS TO COMPOSITE MATERIALS

1.1 - Recapitulation of isotropic fracture criteria

When one considers the fracturing of notched composite material plates or the splitting (into two) of composites due to delamination, one is tempted to apply the fracture criteria of linear mechanics. In comparison with metallic materials, the situation will be simplified for the high performance composite materials, thanks to their quasi elastic behaviour, but it will be complicated by anisotropy. Other criteria, for example that of damage characteristics of fracturing based on a density of flaws, have been proposed in literature relative to the subject [1], but it calls upon a local approach. The determination of local stresses, ply per ply, being at the present time very expensive using a three dimensional method, the criteria of fracture mechanics remain very interesting, wherever they are applicable.

A priori, in order to escape from the difficulties present by anisotropy in composites, one will preferably use the dissipated energy G from which one will possibly be able to extract a stress intensity factor. In both cases, it will be convenient

to use the fracture criterium defined by the critical value G_c or K_c .

1.2 - Relation between G and K

For isotropic solids, there exists a simple relation between G , K and Young's modulus E , namely :

$$K = \sqrt{GE}$$

Thus, one will always be able to calculate K from a measurement of G by compliance, as long as the behaviour of the material remains essentially linear. Nevertheless, the "macroscopic" anisotropy of the material must be such that fracturing takes place in plane of symmetry identical, macroscopically speaking, to the plane of the notch from where the fracturing has originated. Any and all branching off and/or change in mode results in the probleme becoming even more complex, whether it be a question of metals or composites. In reality, anisotropy does not present an obstacle to the application of fracture mechanics to composites, with the exception of some special cases, for example unidirectional composites subjected to stress under tension along to the direction of the fibers [1 to 9].

On the reflexion, it is clear, at the microscopic scale, that metals are highly anisotropic because of the disorientation of the grains, the distribution of the symmetrical elements being naturally more random than in composites. Finally, it is anisotropy at the macroscopic scale which counts in the fracture analysis for the energy criterion G .

The "plasticity" effect for high performance composites is small and more easily disregarded than in the case of metals. The anisotropic effect is not problematic for many quasi-isotropic composites and for the treatment of delamination. On the other hand, the branching off of fracturing in composites represents a big problem.

1.3 - Criteria for delamination

Damage due to intralaminar delamination is expressed by an even interfacial debonding which produces a splitting (into two) of the composite thicknesswise. This type of even damage which spreads parallel to a face, under tensile and shear stress, can be treated successfully by fracture mechanics. Several authors [10 to 25] have illustrated the advantages and the limitations of applying the concept of the rate of dissipated energy G to delamination. In particular, one must know the orientation of the notch and of the flaw propagation plane in relation to the principal axes of symetry of the composite, as well as the stress mode. Once these conditions are fulfilled the estimation of the delamination is carried out, either in terms of G , or in terms of the stress intensity factor K .

From the experimental point of view, delamination propagation is especially studied using bars or beams (DCB tests samples), to which we will also limit ourselves. In very rare cases, see, for example O'BRIEN works [10, 11], delamination is studied on the edge of thin plates, the results obtained being in conformity with those of the beams, but more difficult to express.

For fiberglass or carbon fiber composites, the experiment shows that the unstable critical value G_c or K_c can be properly determined from delamination contained within the beams, in mode II [22]. In mode I, it is found that before instability there is useally a stable propagation of the delamination. Thus during stable

propagation G_{IC} is constante but where the crack is short G_{IC} depends of the length of the delamination (figure 1). In conclusion, it is appropriated to use R curve concept to characterize the delamination resistance, including G_{IC} at initiation and G_{IC} for stable propagation.

In addition to the delamination fracture conditions, it is also quite interesting to know how the latter spreads under cycle stress. Amongst the solutions to be considered at the present time, fracture mechanics offer an efficient means for estimating the growth of delamination under fatigue by expressing the growth rate da/dN in terms of ΔK , G_{max} . In glassfiber/epoxy composites a power relation is verified, both in mode I and in mode II and for several types of fabric or ply symmetry (figures 2 and 3). The existence of a delamination threshold (ΔK threshold) which defines a stress below which the growth stops is also verified. Compared with the other mechanical properties, this delamination threshold is particularly high ; it is, furthermore, higher in mode II than in mode I. The experiment shows, all in all, that the delamination in glassfiber composites is faster under tension (mode I) than under shear, and that, contrary to what one might think, the stress frequency between one and several tens of hertz has no influence on the delamination growth rate.

Similar results are obtained in high modulus composite materials, reinforced with carbon fibers, in mode I and II. In any case, an increase in the load ratio R produces a difference in the delamination process.

If the curve da/dN is plotted versus ΔK , the delamination rate increases with R ratio but if G_{max} is used the delamination rate decreases.

II - THE MECHANISMS OF DAMAGE

2.1 - General remarks

Considering only polymer-matrix composites reinforced by long fibers, it is acknowledged that the first damages that appear under loading are matrix cracks, before the fracture of the fibers. These are microcracks with an initial size of the thickness of one layer, and their presence constitutes the initiation of damage. Propagation will develop next, by a multiplication of cracks building to a critical density and resulting in the development of delamination, until the eventual fracture of the fibers, should that arise.

The initiation and propagation of damage depend on the stacking of the composite layers. In cross-worked layers the first microcracks are produced in the layers for which the fibers are the most disoriented with respect to the tensile axis (a layer at 90° , for example) and then in the least disoriented layers (layers at 45° and 0° , for example).

According to the stacking sequence of the layers, the interlaminar tensile stresses σ_{33} and the interlaminar shear stress τ eventually result in the formation of cracks between the layers ; this leads to delamination, a serious type of damage because it will spread, separate the layers of the composite and allow, in time, the fracture of the fibers.

The series of elementary damage-matrix cracking-delamination-fracture of fibers take place with all sorts of variations, depending on the orientation of the layers, the geometry, and the introduction of forces. Before entering into detail, it should be noted that there is no basic difference between the phenomenon of delamination and the fissuring of the matrix. To see this, let us consider some specific cases in which

delamination is initiated and propagates in mode I or mode II, both simple modes of deformation. Such an approach cannot be applied to a plate subjected to tension because the local forces are mixed (tension and shear). It is thus reasonable to turn to the delamination of a bar or a DCB (Double Cantilever Beam) specimen.

2.2 - Mechanisms of damage by delamination

Locally, on the microscopic scale, the mechanisms of delamination are basically the same in tension and in shear. Still, the principal plane of decohesion is strongly influenced by the maximum shear stress. In general, decohesion is produced at the interface between fiber and matrix, except in mode II where the delamination has a tendency to leave the interface and cut through the resin in order to stay within the conditions of maximum shear (for example, the plane of the neutral axis in a bending bar).

In carbon or glass fiber fabrics delamination progresses, in mode I, along the longitudinal fibers while bypassing the arrays of transversal fibers (figure 4). In stacked woven composites delamination in mode I always follows the interface of a layer at zero degree, then deviates from that path under the influence of decohesions propagating on the interface of layers oriented differently. That is how "splintered" reliefs form (figure 5), which are consequently caused by the interaction of interlaminar and intralaminar cracks.

On a smaller scale, delamination brings mechanisms of resin cracking into play, among which is the fracture of the resin bridges between fibers that leaves, on the delamination surface, tongues of material that do not seem to depend on the type of stress (tension, shear, fatigue). Smooth surfaces are observed in the imprint of the fibers, under simple loading and even in fatigue, with the exception of the imprints left by glass fibers and sometimes in the resin clusters, where fatigue striations are visible.

Thus delamination progresses essentially by interlaminar fissuring, which is responsible for the separation of the composite material in its thickness, but it is also associated with a very significant network of intralaminar cracks that depend on the fiber orientation given to each of the composite layers. Some of the intralaminar cracks are induced by the interlaminar cracks. In laminated carbon fiber composites, long intralaminar cracks are observed perpendicular to the plane of delamination in the layers at zero degrees (figure 6). These cracks appear a little ahead of the delamination front under the action of triaxial stresses [22] before any decohesion at the interfaces between layers. It seems then that the actual phenomenon of delamination is caused by previous damaging of the resin ahead of the front resulting first in the formation of intralaminar cracks.

Ultimately, the mechanisms of delamination occur locally in a damaged zone encompassing the delamination front, a zone that can be readily detected with radioscopy or tomodensitometry (figure 7). The network of microcracks leads to a local decrease in the Hounsfield density in the first layers around the mean plane of delamination. It is evident from these investigations that the head of the delamination front is probably closed because of stress relaxation from the formation of microcracks and in spite of the fact that residual compressive stresses due to plastic deformation cannot exist in composites.

In conclusion, it appears that the first microcracks forming in front of a delamination, in mode I or in mode II, are intralaminar in nature for a DCB specimen. The intralaminar cracks only appear later, in the form of segments that interfere with the intralaminar cracks. This conclusion holds true for composites made up of unidirectional layers or of weaves, which present a quasi-isotropic stacking.

The microscopic mechanisms involve numerous changes of planes and the formation of "splinters" during delamination, so that delamination cannot be considered, in any case, as a simple decohesion between two adjacent layers.

These mechanisms show, in addition, that the role of the fracture strength of the resin is thereby just as important as that of the fiber/matrix interface in these problems of delamination. Hence the present interest in thermoplastic resins which have more toughness than thermosetting resins.

2.3 - Remarks on the progression of damage mechanisms

Considering once again a laminated plate, the series of damages will be slightly different from the one described in section 2.2, especially because the delamination is initiated and propagates in a mixed mode of deformation (I + II). In the case of a quasi-isotropic stacking delamination will be facilitated by the presence of layers oriented at 45°, adjacent to the outer layer at 0°. On the other hand, a 0/90 sequence retards the beginning of delamination. As delamination is delayed, the first microcracks in the layers at 90° develop into significant deformations. And as in the DCB specimens, delamination is initiated after the fissuring of the layers at 90°.

The ductility of the matrix obviously plays an important role. For carbon fiber composites, the epoxy resin 914 does not crack before attaining a 70% elongation to fracture while the resin 5208 cracks before 50%. Thermoplastic resins further improve on this behaviour. On the other hand, it does not seem that carbon fibers with an increased elongation to fracture (1.8 %) play as important a role as the resin [8]. It is reasonable, however, to distinguish between the behaviour of the matrix in fixed load and fixed displacement conditions ; in the latter case it is less important to have a ductile matrix.

The role of the environment, humidity and temperature, will not be discussed here. Nevertheless, it is useful to specify that aging at elevated temperature or in humidity leads to a softening of the matrix and a reduction of internal stresses, which reduces the tendency for crack initiation [26].

III - PREMATURE FRACTURE IN TENSION CAUSED BY A NOTCH

3.1 - Notch effects

In the absence of brittleness, it is observed that the presence of a notch or a hole appreciably increases the apparent yield strength and even the ultimate tensile strength of metals. This phenomenon is due to the effect of triaxial stresses at the notch tip that results in a confinement of plastic deformation and slows the spread of plasticity. For example, the yield strength of a 2024T351 aluminium alloy, which is about 300 MPa, increases to 550 MPa in the presence of a notch with a theoretical stress concentration factor $K_t = 3.3$.

In carbon fiber composites the effect of a notch is totally different [27 to 29]. For quasi-isotropic stacking orientations a hole or a notch cuts the ultimate tensile strength in half.

In the case of an isotropic stacking with an arrangement (0/+45/90/-45)_S, the residual strength falls to 260 MPa for an original tensile strength of 535 MPa. An increase in the number of layers at 0° significantly reduces this effect.

In a general way the notch effect depends on the geometry. Figure 8 gives the fracture results for quasi-isotropic carbon fiber composites (0,90,0±45,0)_S, results

which show that the residual strength tumbles from 80% to 20% of the nominal strength when the size of the notch increases [29]. A notch having the same diameter as a hole is even more serious.

Technologically, the substitution of a metallic alloy by a composite must be carried out considering that the admissible stress around a hole is about two to three times lower in the composite.

It is worth mentioning that the behaviour of the composite is distinctly different under cyclic loading.

The fatigue behaviour of notched composites is slightly unaffected by the notch with respect to the static residual strength.

These observations show, therefore, that the substitution of a metal by a composite reverses the problems, the design of a metallic part requiring a careful fatigue study while the same part made of carbon fiber composites will have to be studied instead for resistance to static forces.

3.2 - Toughness of composite materials

For carbon fiber composites having quasi-isotropic macroscopic properties, linear mechanics is quite applicable, especially in relation to the size and geometrical effects [27, 28]. Nevertheless, in the general case an orthotropic approach is necessary.

In carbon fiber composites with an isotropic stacking orientation, the critical stress intensity factor K_{IC} (which is an indication of a material's fracture toughness) is between 40 and 50 MPa \sqrt{m} for stacked woven plates 2 mm thick, with layers oriented at 45° intervals.

This factor falls to 30 and 20 MPa \sqrt{m} if the number of layers at 30° and 0° is increased (figure 9).

It should be noted that a high-strength aluminium alloy with the same 2 mm thickness attains a K_{IC} of 80 MPa \sqrt{m} . A priori, the composite's toughness in the limit of small thicknesses is much less than that of rival aluminium alloys ; the situation is different, however, for large thicknesses.

In effect, up to a thickness of 10 mm the value of K_{IC} for the composite remains constant while that of the alloy tumbles by about 50 %. It follows that the toughness of composites with respect to metals is small, and all the more so when the thickness of the plate is small. From the parts design point of view, a new difference appears between metal and composite : while fracture mechanics recommends small thicknesses to guarantee better toughness for metals, the same criteria applied to composites tend to recommend the opposite.

The materials that will best resist tearing for a given load are thick, stacked woven composites.

3.3 - Application of Whitney and Nuismer criteria

An other approach to predict the fracture of a notched plate has been proposed by Whitney and Nuismer using the stress at the tip of the notch.

Since the point stress criterion and the average stress criterion were established by Whitney and Nuismer, a number of articles have been published [30 to 37] for the strength prediction of notched composite laminates under uniaxial load. All the criteria associate with a characteristic dimension that expresses the characteristic damage zone size. The characteristic dimension was considered as a universal

constant ; then it was treated as a function of the hole diameters. Although these criteria containing the characteristic dimension can provide a good agreement with experimental data for the strength prediction, they leave much to be done for the explication and study of the damage mechanism in notched laminates.

3.3.1 - Point stress criterion (WN-A) and average stress criterion (WN-B) from Whitney and Nuismer

The two criterion are no more than based on the stress distribution along the ligament of notched laminates. According to the first criterion :

$$\frac{\sigma_N}{\sigma_0} = \frac{2}{2 + \xi_1^2 + 3\xi_1^4 - (K_T - 3)(5\xi_1^6 - 7\xi_1^8)} \quad (1)$$

$$\xi_1 = \frac{R}{R + d_0} \quad (1.a)$$

$$K_T = 1 + \sqrt{\frac{2}{A_{22}} \left(\sqrt{A_{11}A_{22}} - A_{12} + \frac{A_{11}A_{22} - A_{12}^2}{2A_{66}} \right)} \quad (1.b)$$

According to the second criterion :

$$\frac{\sigma_N}{\sigma_0} = \frac{2(1 - \xi_2)}{2 - \xi_2^2 - \xi_2^4 + (K_T - 3)(\xi_2^6 - \xi_2^8)} \quad (2)$$

$$\xi_2 = \frac{R}{R + a_0} \quad (2.a)$$

where, all symbols are explicated in [30-37].

3.3.2 - Point strength model (Tan-A) and minimum strength model (Tan-B) from S.C Tan

The two models are based on the stress distribution around the hole. In the first model, the ratio of two first ply failure (FPF) strengths is proposed to be the same as the ultimate strength reduction factor (SRF), i.e.

$$SRF = \frac{\sigma_N}{\sigma_0} = \frac{\text{FPF notched strength at } (b_1, 0)}{\text{FPF unnotched strength}} \quad (3)$$

In the second model, the strength distribution along a curve which is parallel to the hole contour with a characteristic distance b_0 apart is considered. The curve is called as the characteristic curve. Along it, the FPF strength is calculated point by point, the ratio of the minimum FPF notched strength to the unnotched strength is proposed to be the same as the strength reduction factor i.e.

$$SRF = \frac{\sigma_N}{\sigma_0} = \frac{\text{Minimum FPF notched strength at } c}{\text{FPF unnotched strength}} \quad (4)$$

where σ_N and σ_0 are the notched ultimate strength and the unnotched ultimate strength respectively ; b_1 is the characteristic dimension ; c is the characteristic curve of which the equation is as follows :

$$\frac{x^2}{(a+b_0)^2} + \frac{y^2}{(a+b_0)^2} = 1 \quad (4.a)$$

b_0 is also the characteristic dimension. FPF strength can be determined with the Tsai-Wu quadratic failure criterion [36] containing the stress interaction term $F_{12}^* = -0.5$. The stress distribution of infinite symmetric laminate with a hole was derived by using a complex variable technique following Lekhnitskii's approach [36] a superposition principle. The expressions of the stress distribution can be found [34].

3.3.3 - Modification for Tan's models

The characteristic dimensions in Tan models are only determined in laminate. But, since a first ply failure strength is considered, it is more reasonable to calculate them in this ply. After the first ply failure, one can recalculate the laminate rigidity and determine a new characteristic dimension in the second failure ply. This implicates that Tan models are useful for a progressively degraded laminate. This modification for Tan models makes it possible to study the notched laminate damage mechanism, including the failure sequences (by calculating the security coefficients of each ply), the failure locations (by calculating the failure angles around the hole in each ply), and the failure moments (by calculating the ratio of the first damage charge to final fracture charge). The calculation is carried out with a VAX 780.

3.3.4 - Experimental validation

Laminate T300/Epoxy is used, of which the stacking sequences are as follows :

$$X : (0/0/45/45/-45/-45/90/90)_S$$

$$J : (0/90/45/-45/-45/45/90/0)_S$$

All specimens are cut from a 300x600 plate. They have a fixed ratio of width to diameter, equal to 5. They are respectively 15, 25, 40, 50 mm wide by 250 mm long including 75 mm of each end tap. Each ply has the same thickness of 0.125 mm. The machining of specimens is carried out with diamond tools. The elastic properties of each ply in the notched laminates are given in reference [38].

The comparisons between the ultimate strength predictions and the experimental data are illustrated in figures 10 and 11. All the predictions agree reasonably well with the experimental data. In particular, the prediction of the minimum

strength model is more accurate than that of the others due to the consideration of the stress distribution around the hole other than along the ligament. It can be seen from these figures that the characteristic dimension is a function of stacking sequences.

After the first laminate degradation (90° ply fails), the following +45° and -45° plies can be retrained as the so-called first failure plies, and a new SRF-Radius relation that can also give a good prediction result can be calculated by using the Tan models and the classical lamination theory. Based on the same treatment for 0° ply, after the second laminate degradation (+45° and -45° plies fail), an other new SRF-radius relation can also give a good prediction.

1) Failure locations

The failure initiation location, θ , the angles between the 1-axis and the normal vector of the tangent at the hole contour are calculated and shown in figure 12.

From figure 12, it can be seen that the predicted final failure locations in the 0° ply (Fra.) are almost identical with those in the 90° ply. This result is similar to that given by Tan (6). From photo A4, it can be seen that the path followed by final fracture in 0° plies is influenced both by cracks in 45° plies and by those in 90° plies.

In 90° ply, the results measured experimentally for specimen X agree well with those calculated at larger radius but are not very good at smaller radius because of very deep pre-damage around the hole. The agreements are better in +45° and -45° plies than in 90° ply. It is difficult to measure precisely these angles. The failure locations are significantly influenced by the pre-damage around the hole, especially in 90° ply.

In general, the hole size and form can be changed by the pre-damage. The contributions of pre-damaged regions to laminate properties must be considered, then an equivalent radius between the original radius and pre-damaged hole radius can be introduced so as to predict precisely the failure locations.

2) Initiation and growth of damage

The stresses at the first damage P_1 (cracks in 90° plies) and at the final fracture P_U are calculated and respectively shown in figure 13. It can be seen from the two figures that the two curves calculated are almost "parallel". In fact, the ratio calculated of P_1 to P_U can be treated as a material constant. The ratio is independant of the hole radius, of the models, and of the characteristic dimensions. It can be also seen that all experimental points are smaller than those from calculations because of the pre-damage.

The stresses at the second damage (cracks in +45° and -45° plies) P_2 are also calculated and shown in figure 13. It can be seen that P_1 and P_2 change with the hole radius at an identical tendency. This means that the influences of pre-damages on P_1 and on P_2 are the same.

In conclusion :

1) These criteria and models used in the present study can give good results for the strength prediction of notched laminates, but the minimum strength model is the most accurate.

2) The characteristic dimensions are not only a function of the stacking

sequences but are different in different plies of a laminate.

3) The so-called combining method proposed in the present study can make Tan's models useful for a laminate of which the rigidity has been progressively degraded and can be used for studying the notched laminate damage mechanism, including the failure sequences, the failure locations, and the failure growth.

4) The failure sequences of notched and unnotched laminates for the same configurations are identical, and several main damage stages predicted agree well with the experimental results ; the failure angles around the hole in each ply change with the hole size. The ratio calculated of the stress at the first damage P_1 to that at the final fracture P_U is independent of the hole radius, of the models, and of the characteristic dimensions. It can be treated as a material constant. The experimental value of the ratio is smaller than that from calculations because of the pre-damage around the hole. The value calculated of P_2/P_U changes slightly with hole radius and is larger than the values from experiments.

3.4 - Effect of a notch on the fatigue strength

It is well known today that all metals are very notch sensitive and that their endurance limit then falls in significant proportions. In composite materials this phenomenon is practically unknown, which endows them with a definite advantage with respect to metals.

The most spectacular illustration is undoubtedly the Williams experiment [39] in which he shows that a composite plate with carbon fibers, quasi-isotropic, notched, presents an endurance limit greater than the residual strength of the material, even greater than the endurance limit of the unnotched material, on the condition that the load is applied in increasing stages.

Endurance curves determined [40] for the quasi-isotropic composites T300/5208 and 914 show that the fatigue limit in repeated tension of the notched material does not differ by more than 10 % from that of the unnotched material. As we will see later on, these results are explained by the stress relaxation caused by damaging.

Other studies [41 and 42] lead to the same conclusion : composite materials, although very sensitive to the effect of a notch under simple loading, are no longer sensitive to this under cyclic loading. Comparing the notch effect in samples of aluminium alloy 7075T6 and of quasi-isotropic carbon fiber composite with a K_t of 3.1, it is found [43] that the stress concentration factor K_f in fatigue is less than 1 in the composite and equal to 2.5 in the alloy, for a lifetime N_f of 10^7 cycles. It now remains to be seen whether this result can be generalized no matter what the fatigue loading and in particular in the case where one part of the cycle includes compression.

3.5 - Notch effect in compression

Monotonic loading

To study compression loading, we suggest to use a CT specimen with a notch to avoid macrobuckling [44].

For a quasi isotropic T300/N5208 composite, the cracking of the specimen

under the monotonic compression loading can be considered as macroscopically elastic. The figure 14 shows that, during the test the slope of compression curve load-opening displacement stays unvarying, although the first damages occur early, at about 60~70 % of ultimate load (P_u). This signifies that the stiffness of the specimen or the response of the opening displacement transducer is not sensible to the first damage.

The results of mechanical tests carried out on different specimens for several notch lengths shows clearly that the failure stress is not a simple function of notch length. The curvature radius of notch tip ρ has an important influence. This conclusion is logical because, in the case that $\rho \neq 0$, the stress field at the vicinity of the notch tip is not only governed by the notch length but also by ρ .

Fatigue Loading

In a general manner, the damage evolution of compression cyclic specimen does not end by a brutal propagation. As for monotonic compression specimen, the compliance transducer is not sensible to the first damages. The figure 15 gives typical curves of compression fatigue. We can see that the significant stiffness degradation of the specimen occurs as about, in the case of C-T loading, 3/4 of the life time and, in the case of C-C loading, 4/5 of the life time. The growth of the compliance due to damage is later but more pronounced for the second case than for the first one. This remark leads us to think that the damage mode depends the fatigue ratio R , in such fashion that when R tends to 1, the damage mode becomes this of monotonic compression [7].

For compact specimens $W = 75$, $a^* = 34$ mm, $\rho = 4$ mm, some observations have to be noted out : under C-C fatigue loading, the "no damage", threshold is found at 60~70% of P_u . In the case of C-T loading, the life time tends to the infinity when the maximum applied load is inferior to 42 % of P_u . The endurance limit is smaller in the second situation than in the first one. So we can conclude that the C-T fatigue is the most dangerous loading mode for the material.

In the case where the loading is in alternating compression-tension, the S_d/UTS ratio is in the neighborhood of only 33 % with respect to ultimate tensile strength but close to 50 % with respect to compression strength. It emerges from these observations that there exists radically different behaviors in carbon-epoxy composite materials according to whether or not a notch is present and whether the load is in tension or compression. The situation can be schematically as shown in figure 16. (the crossbatched rectangles represent the behavior of the notched plates).

IV - DAMAGE AT THE NOTCH TIP

4.1 - Damage in simple tension

Considering the significant notch effects observed in composite materials, numerous studies have been begun on damage at the notch tip in order to determine and predict fracture from the stress concentration.

In the presence of a notch or a hole, damage starts near the edge of the notch and propagates in the course of loading ; these two phases of initiation and propagation can be separated, and both depend on the composite's stacking orientation. The case of quasi-isotropic materials will be examined first, then materials with other types of stacking orientation.

One of the most powerful methods for studying the damaged zone at a notch tip consists in making use of radiography in conjunction with an impregnation of the composite with an opacifying agent (zinc tetrabromoethane or iodide) (figure 17).

With the aid of this technique, let us examine the damage at the notch tip in rectangular plates and compact specimens presenting 16, 32, 64 carbon fiber layers in a quasi-isotropic stacking $(0/+45/90/-45)_S$.

In the course of tensile loading the first damages appear at one-third of the fracture load, at first in the layers at 0° . The size of the damaged zone increases with the applied force according to a function of K^2 or K^3 . It is to be emphasized that this zone is about twenty times larger than the plastic zone in metals would be, calculated by the Irwin relation [6].

The fracture of the plates is produced when the size of the damaged zone reaches a dimension of the order of 10-20 mm, depending on the stacking considered and with a noticeable effect of the notch configuration [6, 7]. For greater loads the damaged zone is smaller in CT (Compact Tension) specimens than in CCT (Center Crack Tension) specimens.

The shape of the damaged zone depends on the stacking orientation and the stress state at the notch tip. In a compact specimen the damaged zone has a tendency to round off, while in flat specimens with a centered notch the zone tends to grow symmetrically in the planes of maximum shear. The number of layers, for a given stacking, does not seem to influence the size of the damaged zone [6].

Comparing the mechanical behavior of notched composites to that of metals, it has been emphasized that the size of the damaged zone is significantly greater than that of the plastic zone. But other differences are worth bringing up. In the case of metals, a release of energy takes place in the plastic zone that opposes the development of the process of brittle fracture. For composites, the damaged zone is already the result of the propagation of fracture (delamination, fracture of fibers, etc...) which remains in the elastic range.

The difference between these mechanisms at the notch tip is evidenced by a study of the fracture surfaces.

The fracture of a metal is limited by the plastic zone ; that of the composite is sustained inside the damaged zone.

4.2 - The effects to fatigue on the damaged zone

In the same specimens as before, damage is found in the same way at the notch tip ; under cyclic stresses it grows as the number of cycles increases [7, 27].

For repeated loads limited to between $2/3$ and $3/4$ of the ultimate tensile strength, cracks advance in the layers oriented at 45° with respect to the notch, up to a lifetime of 5×10^6 cycles.

The cracks in the layers at 0° , parallel to the notch, advance relatively little in the course of loading except in the proximity of the cracks oriented at 45° . A damaged zone is thus formed in the shape of butterfly wings oriented in the directions of maximum shear and, in general, asymmetrical after 10^6 to 10^7 cycles and equal to the size it would have been under simple tension, to a first approximation. But its shape seems to be clearly influenced by the macroscopic shear, which often introduces an asymmetry in the damaged zone, already observed by several authors (and which does not exist in simple loading), because delamination progresses faster between the first layers near the surface, oriented 0° - 45° .

4.3 - The influence of stacking orientation

We have just seen that, under both simple and cyclic stresses, a localized damage exists at the notch tip and that the microscopic development of this damage depends on the loading. But it also depends on the stacking orientation of the composite, which makes any attempt at generalization difficult.

On the other hand, a tendency clearly emerges for the blunting of the notch effect, a tendency which strongly depends on the cracking of the layers at 0° ("splitting"), when these layers exist. It is evident that adding more fibers in the direction of loading will increase the toughness while spreading the splitting effect, ending in fracture from the hole but parallel to the direction of loading. In this case fracture mechanics is not applicable.

4.4 - Damage zone in compression

4.4.1 - Evolution of damage around the hole

As discussed early, the compliance transducer is not sensible to the first damages, in the both cases of monotonic compression loading and cyclic compression loading. By contrast, the lateral transducer and the strain gage show an excellent sensibility to these. In the figure 15, we can distinguish three steps on the curve of the lateral transducer. From beginning, the curve increases with an important slope, and reveals the initiation and the progression of damages. The X-rays photo (above the curves) taken in this step gives the confirmation. The increase of this curve continues until a plateau which corresponds to the seconds step. In this step, damages propagate stably, and only the strain gage can reveal this, because it is placed more far from the notch tip than the lateral transducer. In the last step, the damages progress quickly, until the final failure. All the three curves recorded by the compliance transducer, the lateral transducer and the strain gage have a very strong slope. It has to point out that the slope of the strain gage curve changes the sign, and the curve can decrease until below 0. This signifies that the concerned region is in a tension state. The final form of damage zone has a quasi elliptical form (figure 18).

4.4.2 - Microscopic aspect of damage zone in compression

The X-ray technique is very efficient to visualize the damage from and its progression, but this technique gives only projected images through the whole specimen thickness. For observe closely the damage progression and to help understand the mechanisms acting, the micrographic sections were taken before and after the final failure.

From different microscopical observations, a general conclusion can be given : the damage mechanisms change from a loading mode to an another, but in all cases, the delamination is the principal mode of damage propagation in the compression laminate specimens [44].

Monotonic loading

The damage, or more exactly the delamination is initiated, at first time in the most external interfaces. But this initiation is very limited before the final failure. The micrographic section effected at 95 % of Pu shows that the delaminations are confined

at the notch tip and in the external interfaces.

When the applied load reaches P_u , the closing of the notch becomes so hard and the energy accumulated at the notch tip attains the critical value, the breakdown of the specimen occurs brutally. The figure 19 shows a photo of the micrographic section A-A of a failed specimen. We can differentiate three zones. The first, near the notch tip, corresponds to a generalized crushing damage zone. In the second zone, the crushing damages tend to be transformed to delaminations and then to propagate in the external plies, because in these locations the necessary propagation energy is less. The change of propagation planes happens by breaking adjacent laminas, and indeed the 90° plies which are very difficult to break, as they have the same orientation than the delamination propagation. This change is possible because the energy liberation due to the crushing damage of the first zone is very brutal and important. The delaminations, limited now in the external interfaces, progress in the third zone which is in tension.

On the section B-B, we can observe an irregular damage distribution. Some delaminations at the specimen center can be more important than those external. This is the consequence of the brutality of the final failure.

From these observations, it will be reasonable to think that the final failure of the monotonic compression specimen occurs brutally at the last moment, under the crushing form at the notch tip and this crushing damage begins at same time in the all specimen thickness. This consideration is very important for the application of the fracture mechanics to characterize the monotonic compression failure, which is discussed later.

Cyclic loading

Since the applied load is inferior to the critical value for the monotonic generalized damage, the first damages of cyclic loading, confined at the notch tip and limited in the external interfaces, can not progress quickly. But as the resin is sensible to the cyclic loading, these delaminations can propagate slowly. The exterior plies grow weak progressively due to the degradation of the resin between the fibers and begin to bend with an increase amplitude as function of number of cycles. This induces the delamination of the second adjacent plies, and then the third, the forth..., until the final failure. For this reason, the brutal breaking is not observed in the compression fatigue specimen.

In the A-A section of a C-C fatigue specimen, we can observe that in the second zone of damage progression, there is no fracture of the 90° plies. That is, the accumulated energy at the damage tip is not sufficient to break these plies for changing the propagation direction.

In the A-A section of a C-T fatigue specimen, there is a very good regularity of the damage distribution. The first damage state is practically absent, and the delamination tips can be included inside a quasi parabolic curve.

In the micrographic sections B-B (figure 19), we can compare easily the regularity of the damage distribution of C-C and C-T specimens which is quasi parabolic, with the monotonic compression specimen. It has also to point out that with these sections, we can distinguish more clearly the difference between C-C failure and C-T failure : in the first case, the microcracks don't exist, and the damages are essentially delamination and plie fractures due to bending and buckling in these plies. In the second case, by influence of the positive loading, microcracks are formed in the 90° and $\pm 45^\circ$ plies. The microcracks are aided by the delamination of the adjacent plies and aid mutually the progression of these delamianaions. This is why the C-T

fatigue is the most dangerous loading mode for the laminate materials.

4.4.3 - Characterization of the compression damage

The damage mechanisms discussed early lead us to think that, it is reasonable to try to use the linear fracture mechanics to characterize the compression failure of this material. For this purpose it is convenient to take the generalized plane stress consideration in the determination of stress field.

Calculation of stress and displacement fields

Since the considered medium is a macroscopically orthotropic plate containing a notch, to calculate the stress field in the specimen, especially near the notch tip, a theoretical analyses was necessary. To simplify the calculation, we have replaced the notch by an elliptical hole of which the curvature radius of the top is same than this of the hole. The validity of this approximation is discussed in [8]. The used method was based on the so called "modified mapping-collocation" technique developed early by O. Bowie with the following mapping formulation [45].

$$z_j = \omega(\zeta_j) = \frac{L_j}{2} \left(\zeta_j + \frac{m_j}{\zeta_j} \right) \quad (1)$$

where $z_j = x + \mu_j y$ the complex planes representing the physical region of the specimen, $L_j = a + i\mu_j b$, $m_j = (a + i\mu_j b)/(a - i\mu_j b)$, and $\mu_j = a + ib$, the roots of the characteristic equation determined by the specimen anisotropy :

$$a_{11}\mu^4 - 2a_{16}\mu^3 + (a_{66} + 2a_{12})\mu^2 - a_{26}\mu + a_{22} = 0 \quad (2)$$

This mapping carries the unit circle $\zeta = \sigma$ and its exterior into an ellipse along the modified notch and its exterior respectively.

The representation of the stress function can be given as follow :

$$2\text{Re} \left\{ \eta_{1i} \left[S \Phi_2(\zeta_1) + T \overline{\Phi_2\left(\frac{1}{\zeta_1}\right)} \right] + \eta_{2i} \Phi_2(\zeta_2) \right\} = \overline{X}_i \quad (3)$$

$$\text{or} \quad 2\text{Re} \left\{ \eta_{1i} \left[S \sum_{n=-\infty}^{\infty} a_{n2} \zeta_1^n + T \sum_{n=-\infty}^{\infty} \overline{a_{n2}} \zeta_1^{-n} \right] + \eta_{2i} \sum_{n=-\infty}^{\infty} a_{n2} \zeta_2^n \right\} = \overline{X}_i \quad (4)$$

where $S = (\mu_1 - \mu_2)/(\mu_1 - \mu_1)$, $T = (\mu_1 - \mu_2)/(\mu_1 - \mu_1)$, X_i represents the boundary conditions in the direction i ($i = 1, 2$), η_{1i} , η_{2i} are constants depending the nature of boundary conditions X_i :

- for force resultant conditions

$$\eta_{11} = \mu_1, \eta_{21} = \mu_2, \eta_{12} = \eta_{22} = 1$$

- for displacement conditions

and $a^*_{n2} = c^*_{n2} + id^*_{n2}$, complex coefficients to determinate for verifying the equation (4).

The following procedure was tried and found good to resolve the equation (4) :

1. Truncation of the infinite expansion in equation (4) to a suitable number of positive and negative powers n_1, n_2 respectively.
2. Selection of points around the external boundary in a fairly uniform manner and writing force boundary conditions at each of the direct locations. The number of points was so arranged that the number of boundary equations thus obtained was about twice or triple the number of unknowns a^*_{n2} .
3. Selection of the unknowns in such a manner that the equations in step 2 are satisfied in a least-square sense.

A computer code was developed in order to determine the coefficients of the stress function a^*_{n2} and to calculate the stress fields by the following relation :

$$\sigma_{ij} = 2 \sum_{n=-n_1}^{n_2} n c^*_{n2} \text{Re} \left\{ \eta_{1i} \frac{S \zeta_1^{n-1} - T \zeta_1^{n+1}}{\omega_1(\zeta_1)} + \eta_{2i} \frac{\zeta_2^{n-1}}{\omega_2(\zeta_2)} \right\} - 2 \sum_{n=-n_1}^{n_2} n d^*_{n2} \text{Im} \left\{ \eta_{1i} \frac{S \zeta_1^{n-1} + T \zeta_1^{n+1}}{\omega_1(\zeta_1)} + \eta_{2i} \frac{\zeta_2^{n-1}}{\omega_2(\zeta_2)} \right\} \quad (5)$$

where $\eta_{ji} = \mu_j^2$ when $\sigma_{ij} = \sigma_{xx}$, $\eta_{ji} = \mu_j$ when $\sigma_{ij} = \sigma_{xy}$ and $\eta_{ji} = 1$ when $\sigma_{ij} = \sigma_{yy}$.

Calculation of the rate of dissipated energy for monotonic failure initiation

Since the monotonic compression failure occurs immediately after its initiation, the characterization or the establishment of the criterion for this damage state is essentially. With the knowledge of the stress and displacement fields, the rate of dissipated energy can be determined by integrating the expression $\sigma_2 du_1$ from B to A [10] :

$$G_1 = \frac{\partial U}{\partial a^*} = \int_B^A \sigma_2 du_1$$

The signification of a^* , B and A are indicated in the figure 20-a.

In practice, the damage does not begin on the all width of the notch, the integration must be effected from B to A^* . The point A^* or the width of damage zone is determined by the point criterion of NUISMER-WHITNEY lied in the vertical direction and in the revers manner. That is, knowing the compression resistance of the material σ_{yc} and applied stress state σ_{ij} , we determine the interval d_1 between which the stress $\sigma_{yy} \geq \sigma_{yc}$ (figure 20-b).

Since the damage width d_1 is not null when damage occurs, the energy of failure initiation must be carried on an energy by unit damage volume. To avoid

confusion, we denote this energy by L_1 :

$$L_1 = \frac{1}{d_1} \int_B^{A^*} \sigma_{2i} du_i \quad (6)$$

The index 1 signifies that, macroscopically the loading is in mode I. The compression failure occurs when $L_1 \geq L_{1c}$. In the calculation of L_1 , if the applied stress is very less, the width of damage zone d_1 can be not initiated.

Application and discussions

(1) Monotonic damage

The results of calculation are shown in the figure 21 for both the compact specimens and the rectangular specimens. The failure initiation energy can be considered as constant for all specimens, except there is a small difference between compact specimens and rectangular specimens. We think that this difference comes from the use of the anti-buckling devices for the rectangular specimens, since some authors have found early that the anti-buckling devices can cause some small change of the material behavior. So it is convenient to take $1.138.10^7 \text{ J/m}^3$ as the energy of the monotonic failure initiation. Of course, this energy can also be used for establish the catastrophic failure criterion because of the brutality of the monotonic damage progression.

(2) Fatigue damage

With the definition of the rate of dissipated energy by unite volume [45], we can summarize all results of endurance tests in the same curve $L_{1\max} - N_f$, where $L_{1\max}$ corresponds to the maximum load in the cyclic loading. It has to underline that the rate of dissipated energy used here has only an indicative signification, by the reason that the damage mode in the monotonic specimen and in the cyclic specimen is quite different. We have chosen this parameter for the fatigue damage characterization because it should exist a relation between the monotonic failure energy and cyclic failure energy. Thus, with this parameter $L_{1\max}$ we can give an indicative idea on the compression fatigue resistance of this notched laminate material.

To describe the fatigue damage propagation, we have interpolated the specimen compliance $Comp$ and the damage length A as function of number of cycles of a specimen.

The final results of the calculation for the damage progression are illustrated in the figure 22.

We can discern three different stages on this curve. The first which has a very high slope, corresponds to the beginning of damage. The second, less vertical, represents the state of the stable propagation, and this leads into the last state of damage until the final failure. The second stage is the most interesting for the characterization of the fatigue damage. Since this part is a straight line, we can choose the Paris law to describe this stable progression of damage, that is :

$$dV/dN = 7.34 \cdot 10^{-18} (L_{1\max})^{0.862}$$

The unit of V , N and $L_{1\max}$ are respectively m^3 , cycle and J/m^3 .

CONCLUSION

The essential of the approach presented herewith concerns the study of fracture criteria and the damage mechanisms up to the microscopic scale. On both cases, the application of the concepts of fracture mechanics leads to global or local analysis which allow one to suitable characterize the behaviour of materials.

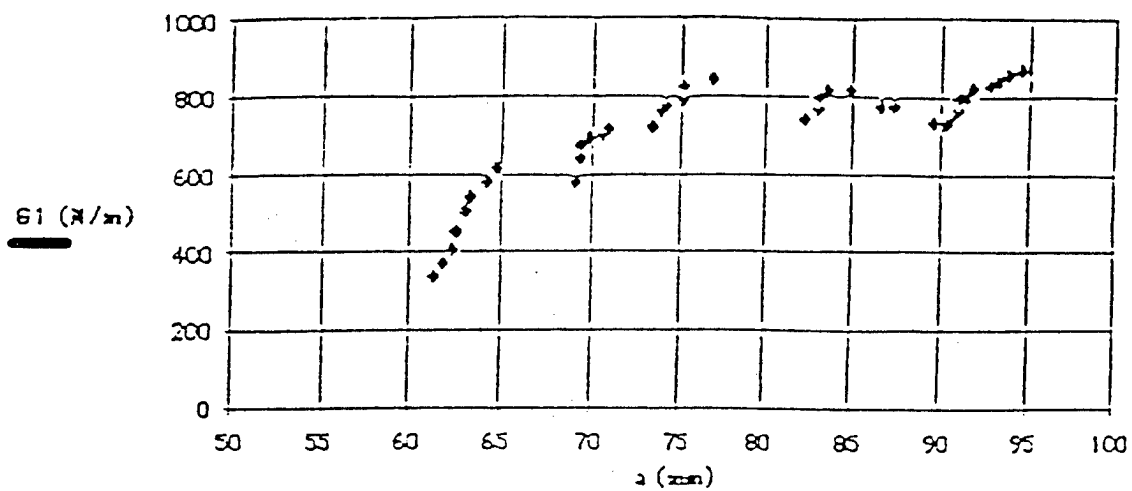
The problem in question can only be solved by calculating the stress intensity factor or the rate of dissipated energy for a given structure. The calculation of K or G in quasi isotropic composite materials subjected to stress in simple modes does not present any particular difficulty. However, anisotropy and mutiaxial loading seriously complicate the calculation, the results of which to date remain unreliable.

All things considered, the application of fracture mechanics to composite materials results in one being able to solve numerous problems, in particular those posed by delamination, and one can conclude herewith in favour of its success, here as elsewhere, it being understood that much more remains to be done.

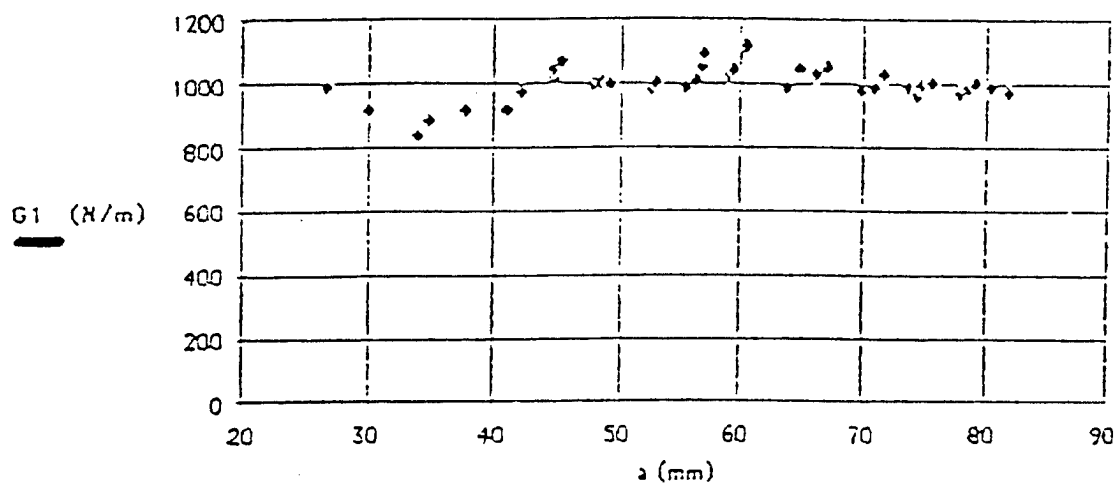
REFERENCES

- 1 - K. REIFSNIDER, Life Prediction Analysis, ICCMVI, pp 41-43, 1987.
- 2 - E. WU, Fract. Mech. of anisotropic plates, Composites Materials, Vol. 1, pp 20-43, 1968.
- 3 - J.F. MANDELL, S.S. WANG, Journal of Composite Materials, pp 266-287, 1975.
- 4 - J.C. HALPIN, L. NICOLAS, G. CAPRINO, Composites, pp 223-227, 1979.
- 5 - A.W. HOLDSWORTH, M.J. OWEN, S. MORRIS, Journal of Composite Materials, pp 117-119, 1977.
- 6 - C. BATHIAS, R. ESNAULT, J. PELLAS, Composites, pp 195-200, 1981.
- 7 - C. BATHIAS, The Damaging of Composite Materials : Mechanisms and Detection, Kluwer Academic Publishers, pp 627-657, 1989.
- 8 - P.T. CURTIS, Investigation of the tensile fatigue behaviour of improved carbon fibre composite materials, ICCM 6, pp 54-64, 1987.
- 9 - S. PARHIZGAR, L. ZACHARY, C.T. SUN, Application of principles of linear fracture mechanics of the composites materials, International Journal of Fracture, 2, pp 3-15, 1982.
- 10 - T.K. O'BRIEN, N.J. JOHNSTON and al, ASTM STP 937, pp 199-221, 1987.
- 11 - S.A. SALPEKAR and T.K. O'BRIEN, NASA TM 102591, March 1990.
- 12 - M. HOJO, Near Threshold Propagation of Delamination Fatigue cracks in CFRP Laminates, Report n° 87-14, The Royal Institute of Technology, Stockholm.
- 13 - D.J. WILKINS, J.R. EISENMANN, R.A. CAMIN, W.S. MARGOLIS and R.A. BENSON, Characterizing delamination growth in graphite epoxy, ASTM STP 723, 1981.
- 14 - C. BATHIAS, Evaluation de la qualité des joints collés par la mécanique de la rupture, Rapport SNIAS, P.V. n°34618, 1977.
- 15 - MOSTOVOY, BERSCH, RIPLING, Fracture toughness of adhesive joints, Aerospace adhesives and elastomers, Dallas, SAMPE, vol. 2, 1970.
- 16 - H.T. CORTEN, Journal of Adhesion, 3, 103, 1971.
- 17 - E.J. RIPLING, S. MOSTOVOY, H.T. CORTEN, Journal of Adhesion, 3, 107, 1971.
- 18 - S. MOSTOVOY, E.J. RIPLING, R.L. PATRICK, ASTM. Spec. Tech., Pub. 360, 5, 1963.
- 19 - G.G. TRANTINA, Combined mode crack extension in adhesive joints, TAMP Report 352, Univ. of Ill., 1971.
- 20 - K.L. DEVRIES, M.L. WILLIAM, M.D. CHANG, Exp. Mech., 14, 89, 1974.
- 21 - S. MOSTOVOY, E.J. RIPLING, Flaw tolerance of a number of commercial and experimental adhesives, Adhesion Science and Technology, Ed. Lieng-Huang Lee, 1975.
- 22 - D. LEFEBVRE, C. BATHIAS, ICCM 5, pp 331-345, The Metallurgical Society, 1985.
- 23 - W.W. STINCHCOMB, K.L. REIFSNIDER, P. YEUNG and J. MASTERS, Effects of ply constraint on fatigue damage development in composite material laminates, ASTM STP 723, pp 64-84, 1981.
- 24 - J.C. LENAIN and A.R. BUNSELL, The resistance to crack growth of asbestos cement, J. Mat. Sci., 14, pp 321-332, 1979.
- 25 - F.H. CHANG, D.E. GORDON and A.H. GARDNER, A study of fatigue damage in composite by nondestructive testing techniques, ASTM STP 636, pp 57-72, 1977.
- 26 - S.M. BISHOP, The effect of environment on the fatigue damage development in notched carbon fibre-composite, ICCM 6, pp 4139-4149, 1987.
- 27 - R. ESNAULT, D. ALLIAGA, C. BATHIAS, Endommagement et rupture par traction

- et fatigue de deux matériaux composites entaillés à fibres de verre et de carbone, JNC, Paris, Septembre 1982.
- 28 - A.S. WANG, Fracture mechanics of sublaminate cracks in composite materials, Comp. Tech. Review, Vol. 6, n°2, pp 45-62, 1984.
 - 29 - G. DOREY, Impact damage in composites, ICCM 6, pp 3,1-3,26, 1987.
 - 30 - J.M. WHITNEY and R.J. NUISMER, Stress fracture criteria for laminated composite containing stress concentration, J. Composite Materials, Vol. 8, pp 253-265, July 1974.
 - 31 - R.J. NUISMER and J.M. WHITNEY, Uniaxial fracture of composite laminates containing stress concentrations, Fracture Mechanics of Composites, ASTM STP 593, pp 117-142, 1975.
 - 32 - H.J. KONIH and J.M. WHITNEY, Approximate stress in an orthotropic plate containing a circular hole, J. Composite Materials, Vol. 9, pp 157-166, April 1975.
 - 33 - R. BYRON PIPES et al, Notched strength of composite materials, J. Composite Materials, vol. 13, pp 148-160, 1979.
 - 34 - SENG CHUAN TAN, Fracture strength of composite laminates with an elliptical opening, Composite Science and Technology, 29, pp 133-152, 1987.
 - 35 - S.C. TAN, Laminated composites containing an elliptical II : Experment and model modification, J. Composite Materials, vol.21, pp. 949-968, octobre 1987.
 - 36 - S.W. TSAI and H.T. HAHN, Introduction to composite materials, Technomic, 1980.
 - 37 - C. CAMPELLO, C. BATHIAS et al, Etude de d'endommagement de plaque stratifiée contenant un trou circulaire sous chargement quasi-statistique, Paris, pp 149-161, Pluralis, 9-11 Septembre 1986.
 - 38 - J. XIAO, D. LAI, C. BATHIAS, Euromech Colloquium 269, to be published, décembre 1990.
 - 39 - S.V. RAMANI and D.P. WILLIAMS, Notched and Unnotched Fatigue Behavior of Angle-Ply Graphite/Epoxy Composites, STP 638, pp 27-46, 1977.
 - 40 - M. ROUCHON and M. LIBERGE, Endommagement des matériaux composites carbone-epoxy, report CEAT n°5213, 1986.
 - 41 - C.E. BAKIS and W.W. STINCHCOMB, Response of Thick, Notched Laminates Subjected to Tension-Compression Cyclic Loads, STP 906, pp 314-334, 1986.
 - 42 - P.A. LAGACE and S.C. NOLET, Effect of Ply Thickness on Longitudinal Splitting and Delamination in Graphite-Epoxy Under Compressive Cyclic Loading, STP 906, pp 335-360, 1986.
 - 43 - D. SCHUTZ and J.J. GERHARZ, Fatigue Strength at a Fibre Reinforced Materials Composites, pp 245-250, Octobre 1987.
 - 44 - D. LAI and C. BATHIAS, The Compression Fatigue Resistance of a Carbon -Epoxy Composite Plate Containing a Hole, ICM 5, pp 1231-1238, 1987.
 - 45 - D. LAI and C. BATHIAS, ASTM STP 1005, to be published, 1990.



a) VETROTEX Glass fiber/Epoxy Resin E60, th=3mm , a = 60.5mm - V = 2mm/min



b) VETROTEX Glass fiber/Epoxy Resin B89, th=20mm , a = 19mm - V = 0.2mm/min

Fig.1 Woven glass fibers epoxy composite delamination, Test DC3 - mode I

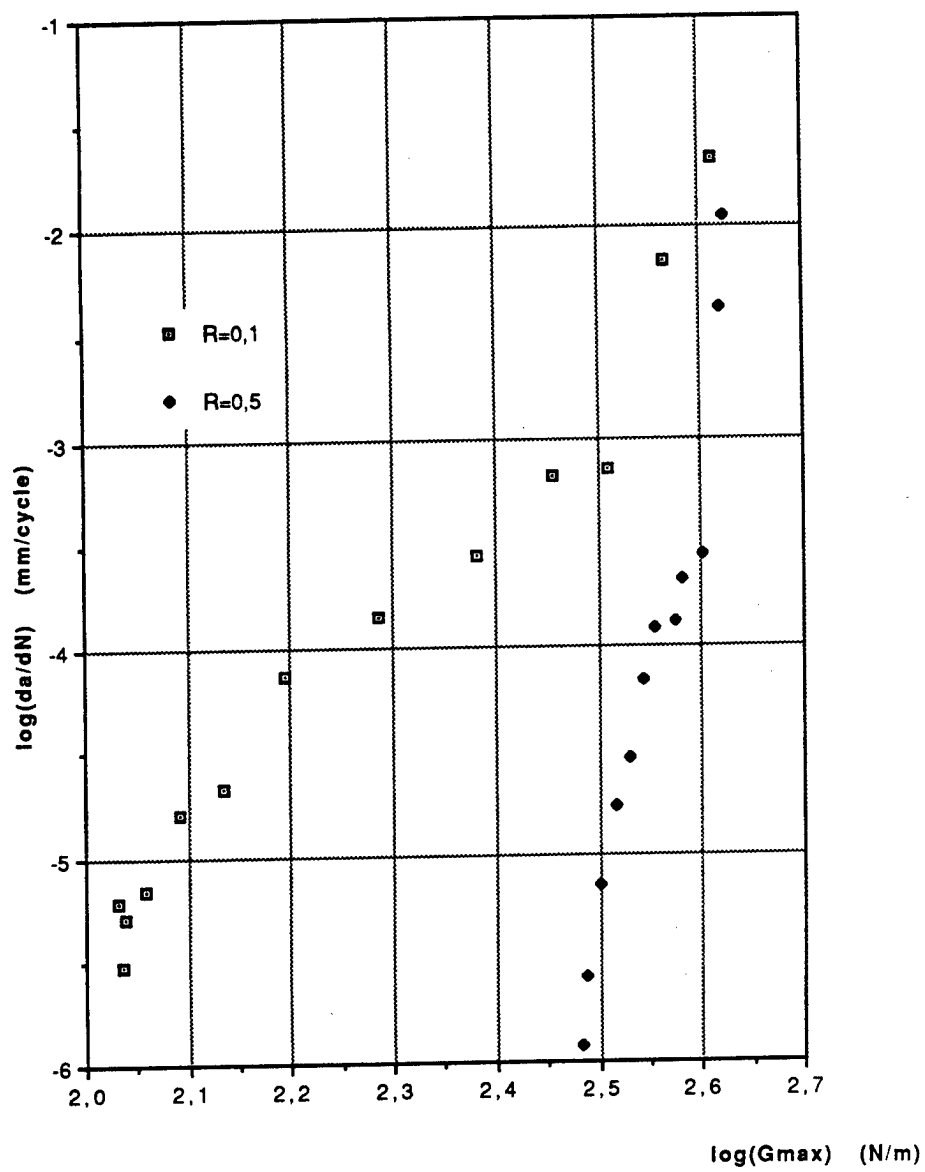


Fig.2 Influence of R ratio on the growth rate vs strain energy release rate
(Fatigue, delamination mode I GFRP U.D. th = 3mm, f = 10Hz)

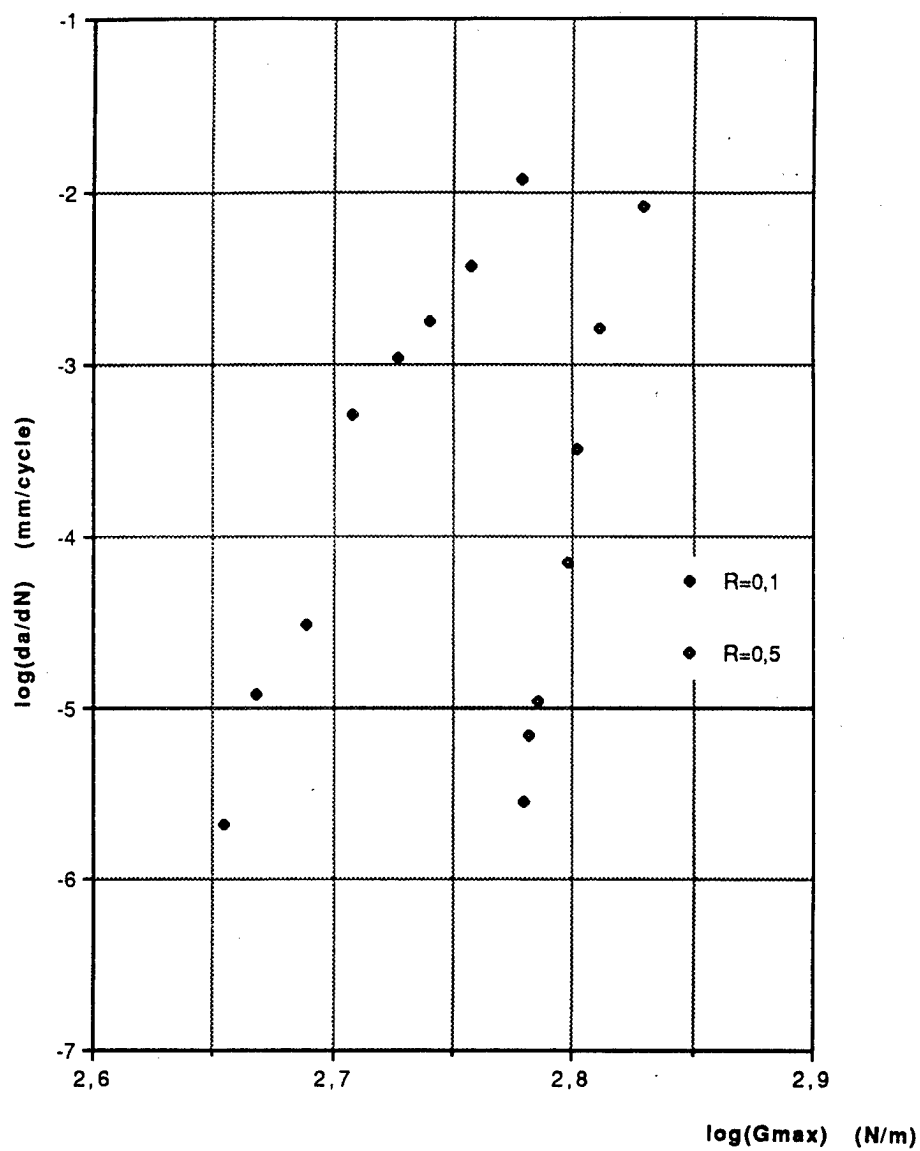
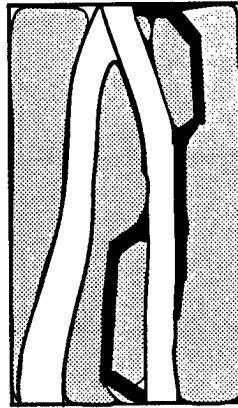
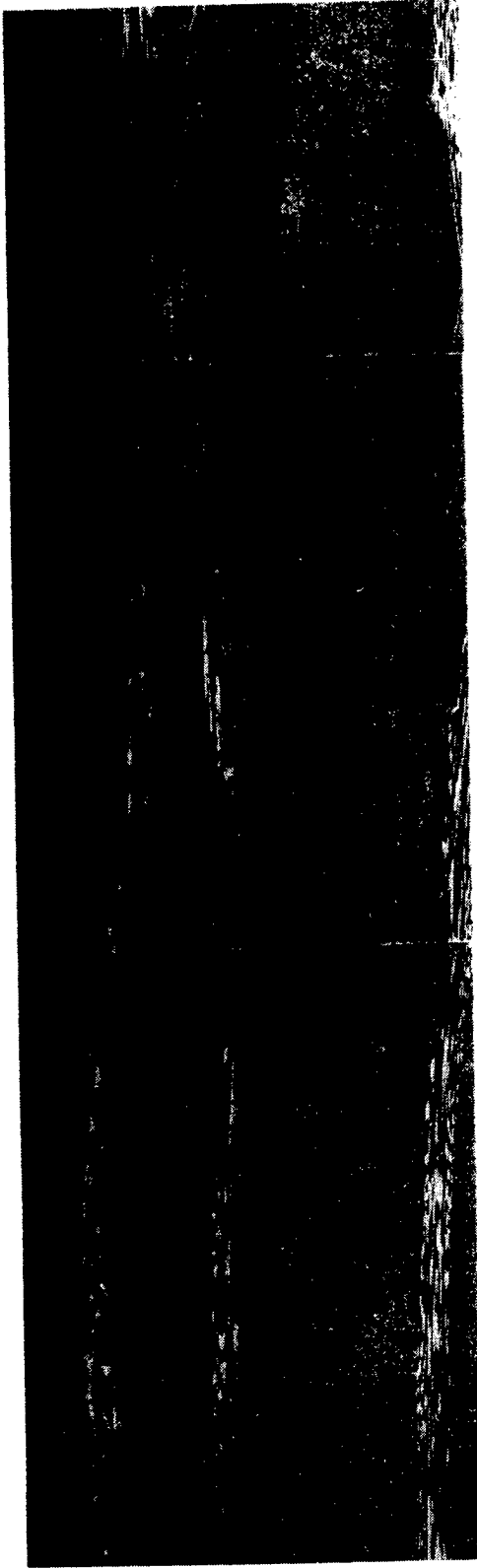


Fig.3 Influence of R ratio on the growth rate vs strain energy release rate
(Fatigue, delamination mode II GFRP U.D. th = 3mm, f = 5Hz)



warp fibers
 woof fibers
 path of delamination

Fig.4 Microscopic path of delamination in composites
(carbon woven).

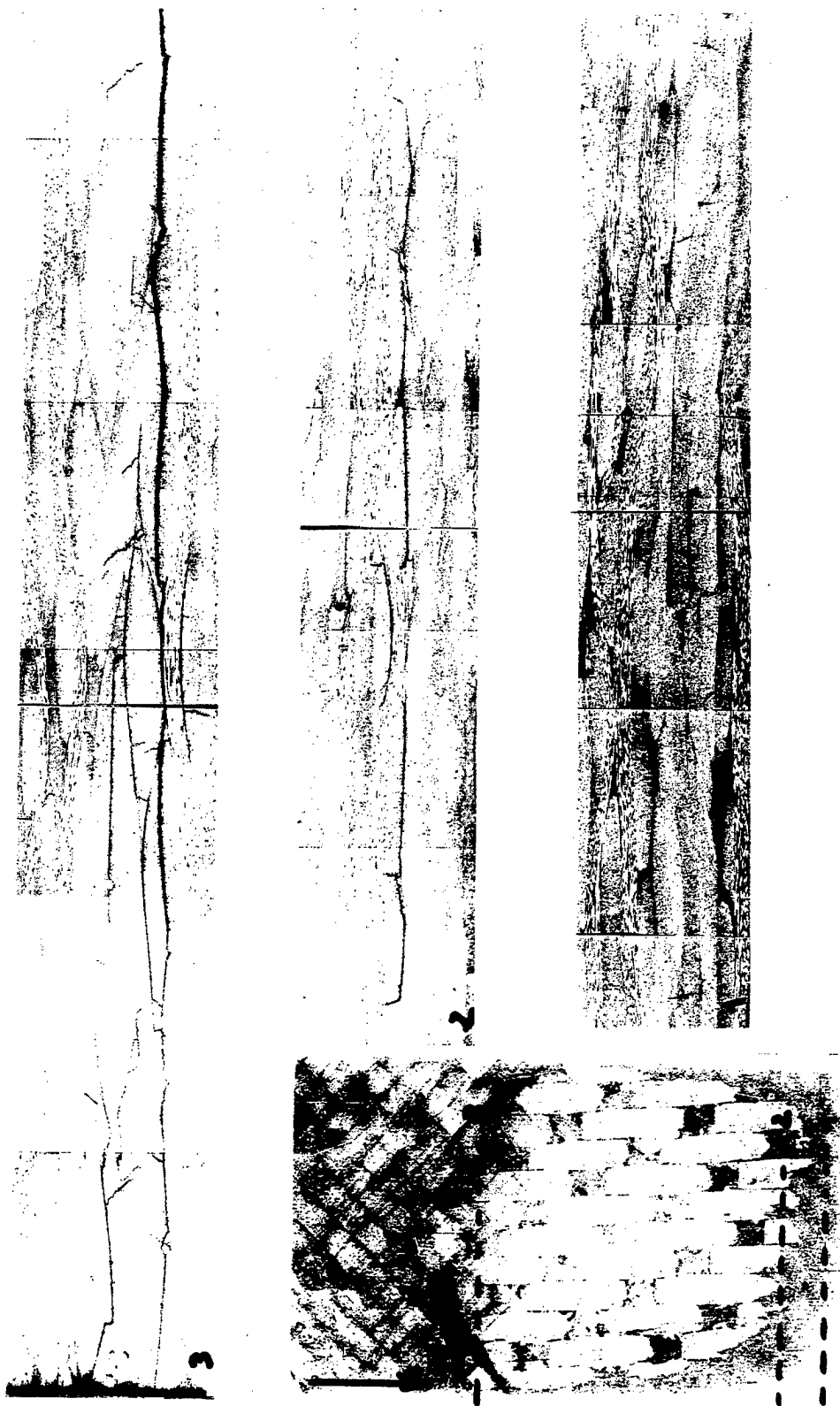


Fig.5 Interlaminar matrix microcracks in front of a delamination in T300/5208 woven composite material after fatigue — Three cross sections (X50).



X Ray Radiography



X Ray Tomography

Fig.6 Delamination front in DCB specimens - quasi isotropic T300/5208 laminate -
Notice the microcracks in front of the tip of the delamination after fatigue

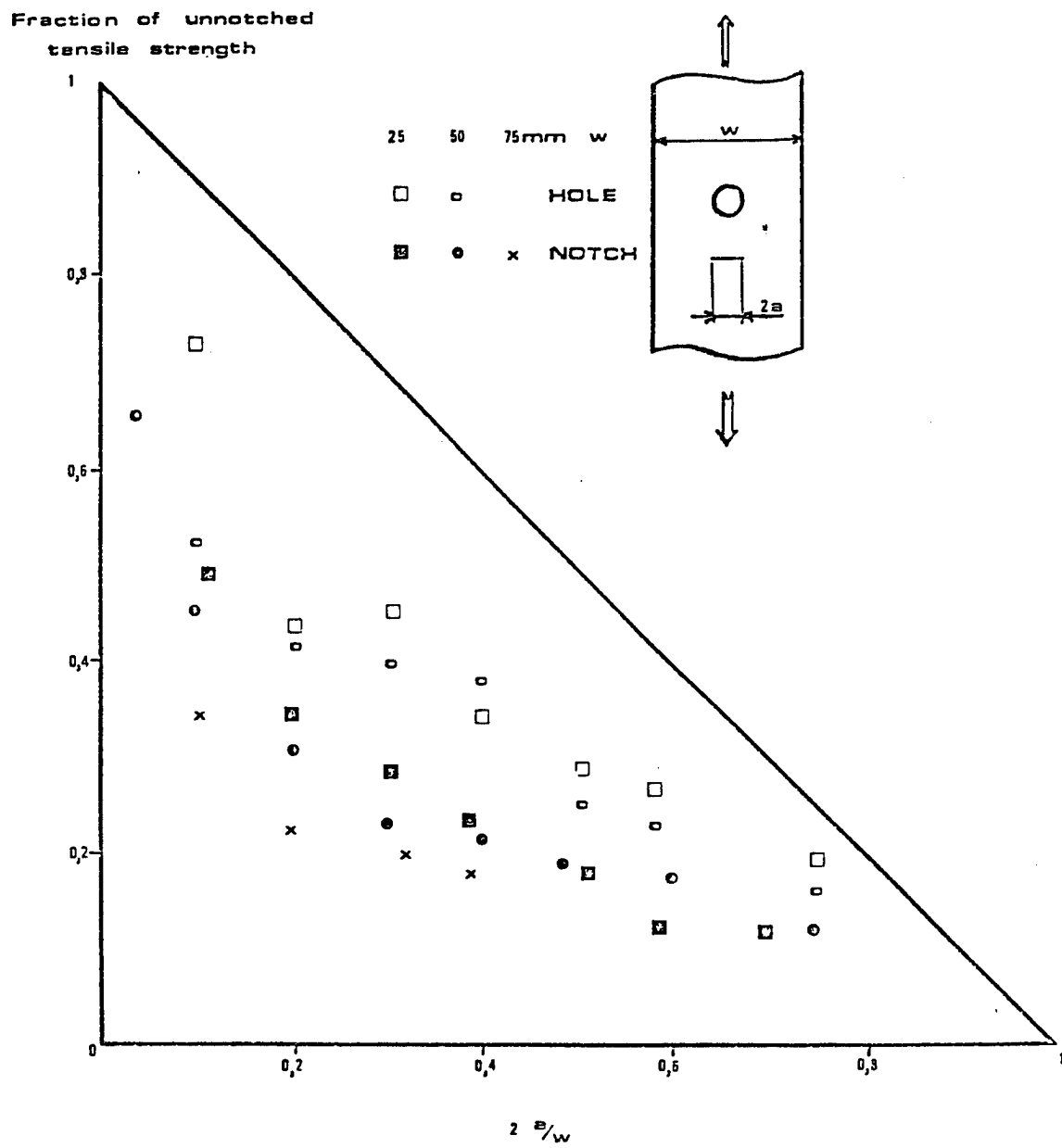
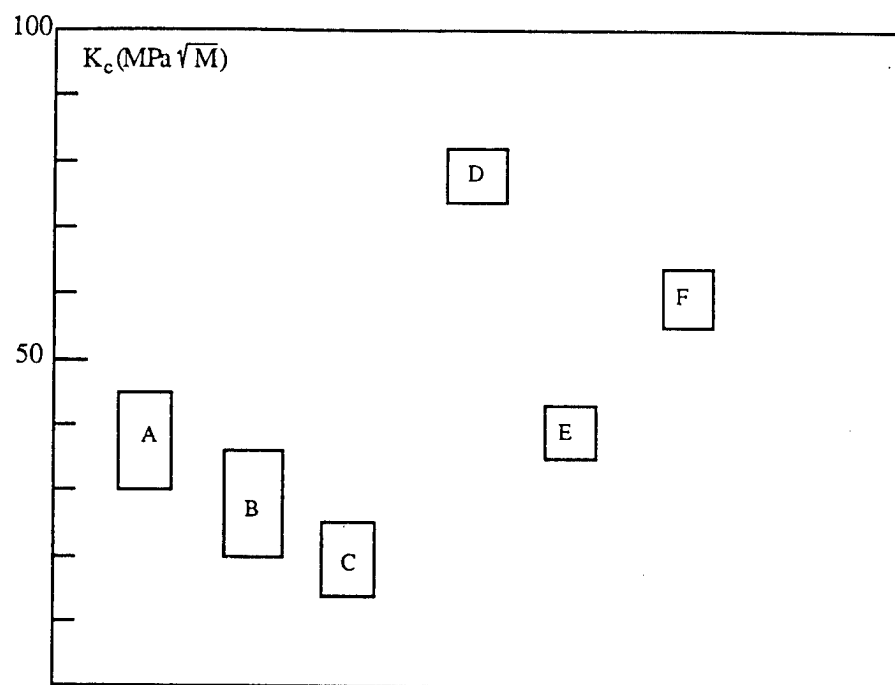


Fig.8 Notch effect in a CFRP (0/90/0/±45/0)_s in tension (by DOREY)



T300/914—Thickness (2 to 20 mm)

A—(0/45/90/-45)s

B—(0/30/60/90)s

C—(0/45/-45/0)s

D—7075 T7351 (1.6mm)

E—7075 T7351 (12mm)

F—2024 T351 (1.6mm)

Fig.9 Schematic comparison between the toughness of composite materials and aluminium alloys.

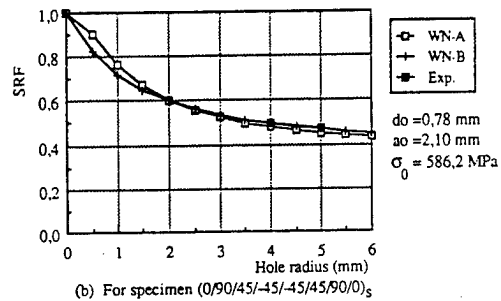
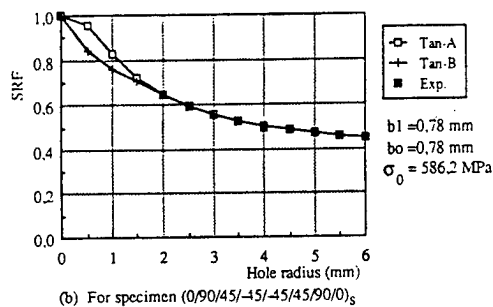
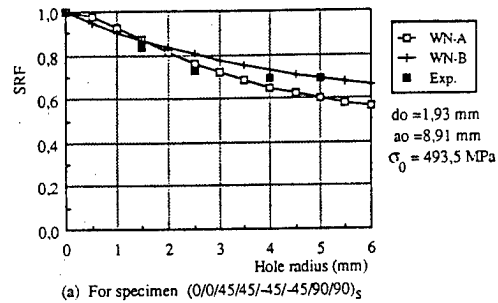
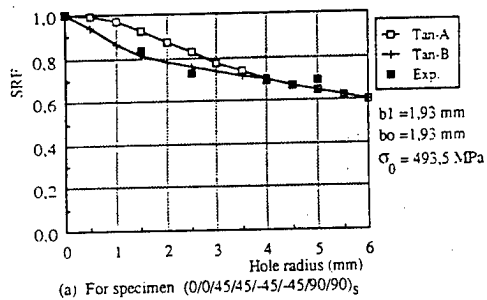


Fig.10 Comparison between the experimental results and the Tan models.

Fig.11 Comparison between the experimental results and the criteria WN.

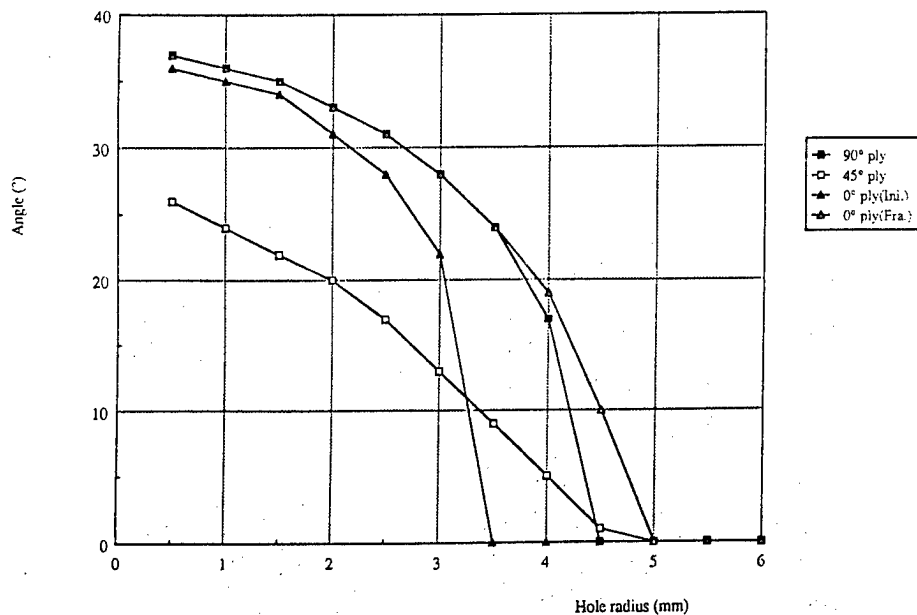


Fig.12 Failure initiation locations around the hole in 90°, 45° and 0° plies and final location in 0° ply for specimen (0/0/45/45/-45/-45/90/90)_S.

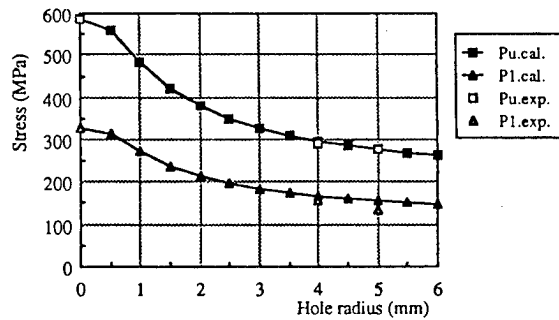
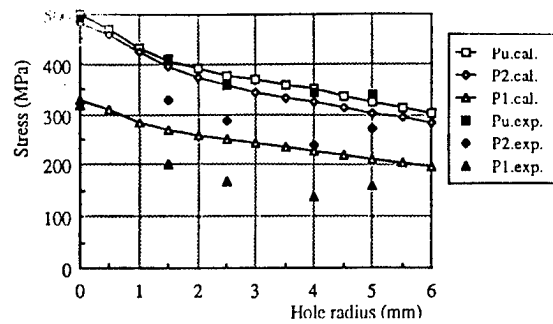


Fig.13b Comparisons of P1 and Pu between the results from experiments and from calculations with the model Tan-B for specimen (0/90/45/-45/-45/45/90/0)_S

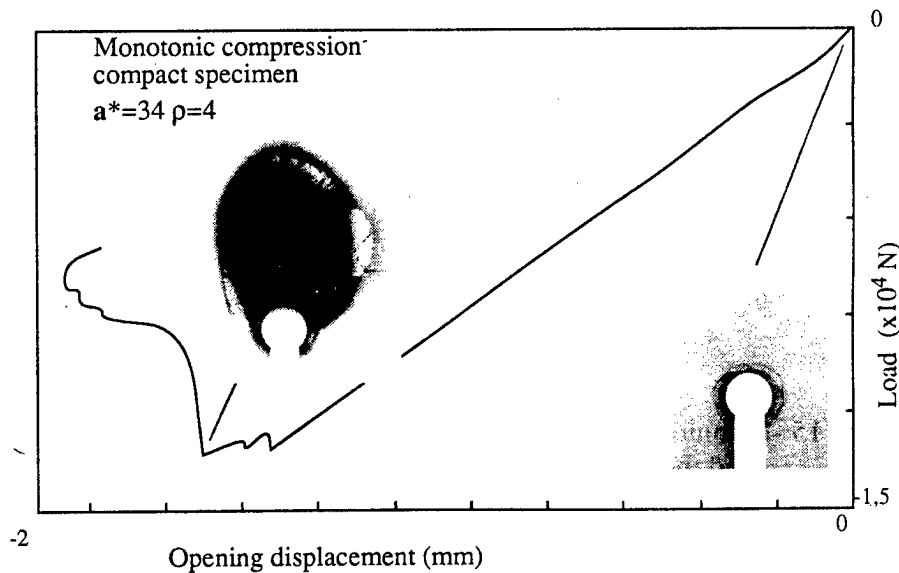


Figure 14 - Mechanical behaviour of CT specimen in compression (by D. LAI)

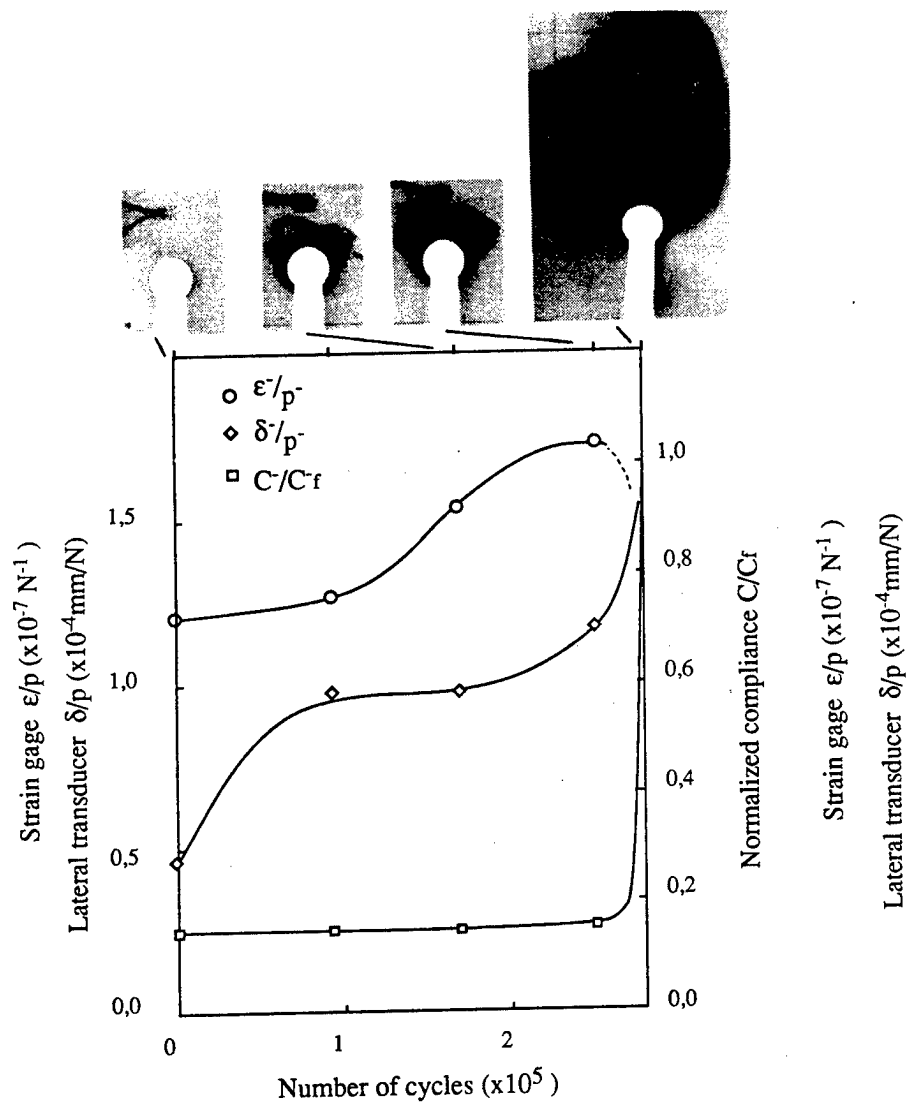


Figure 15 - Evolution of the compliance, the longitudinal strain and the transverse strain in C-C fatigue

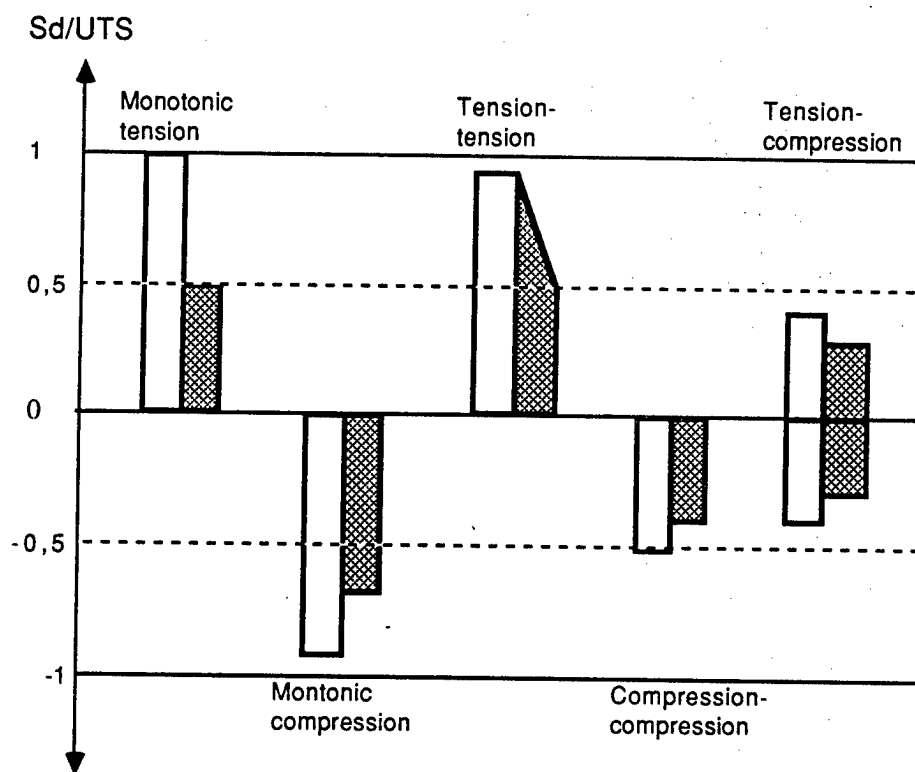


Fig.16 Schematic review of the fatigue limits versus UTS of notched and unnotched composite materials.

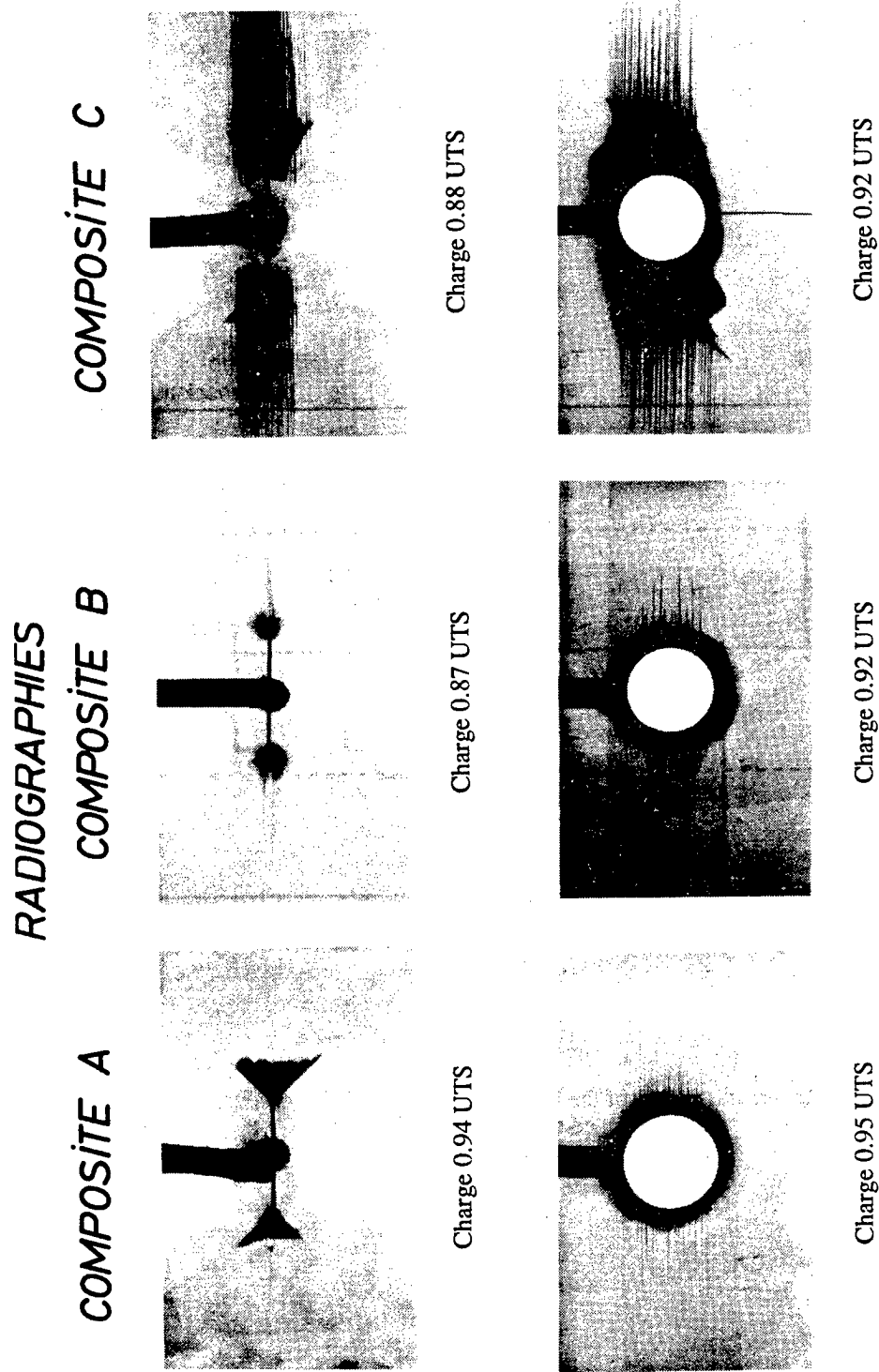


Fig.17 Damage zones around a notch or a hole under monotonic loading

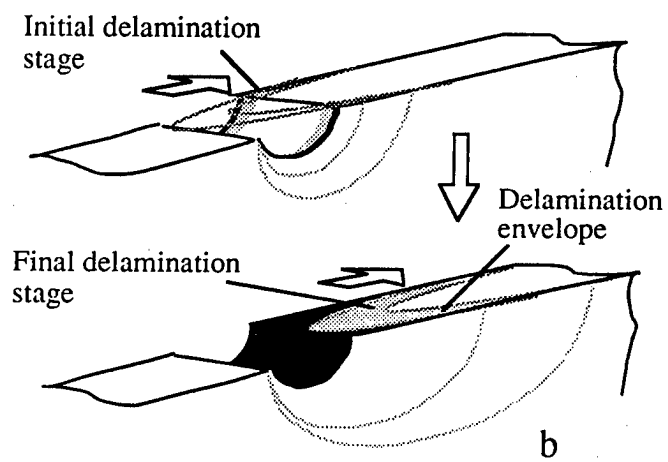
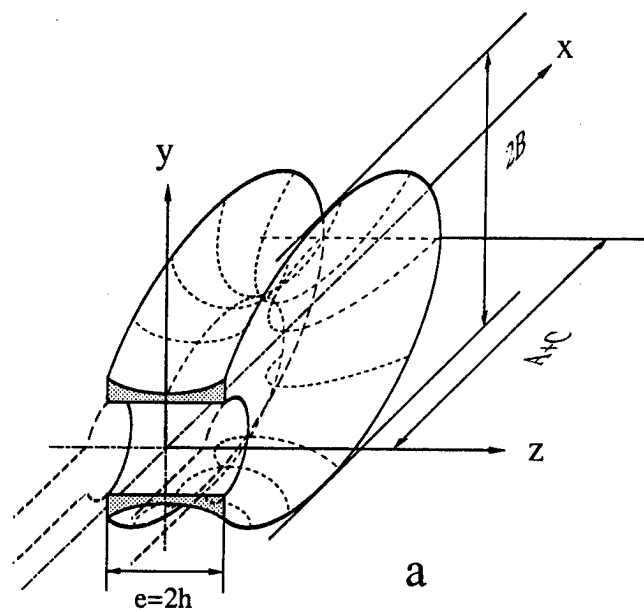


Figure. 18 - Modelisation of the damage zone at the tip of a notch in compression cyclic loading

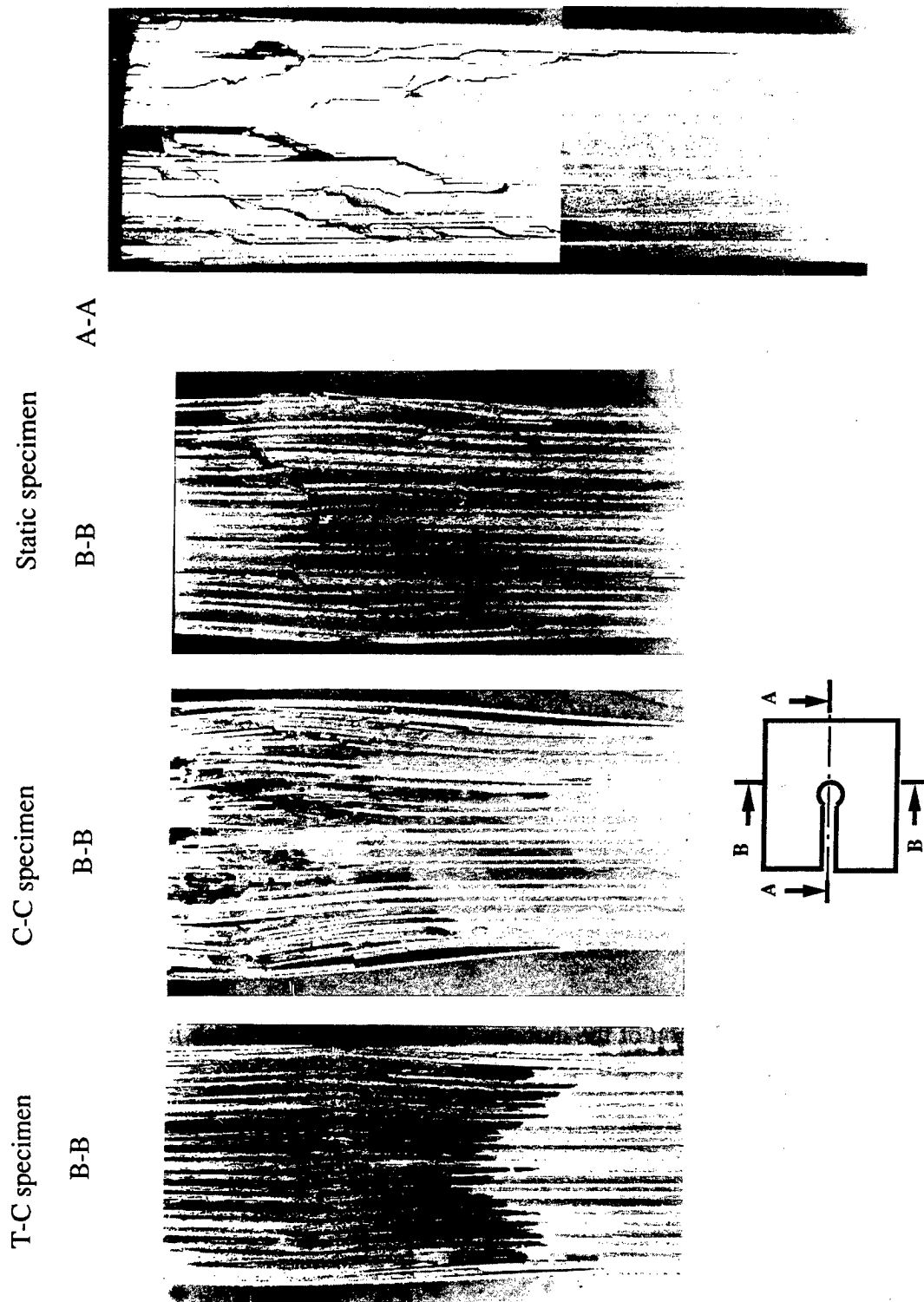


Figure 19 - Micrographic sections of static and cyclic specimens

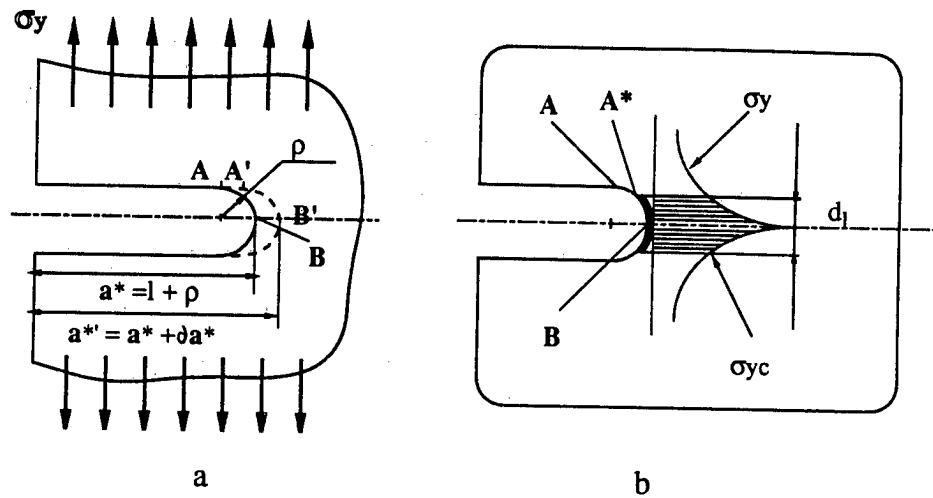


Figure 20 - Modelisation of a notch in compression loading

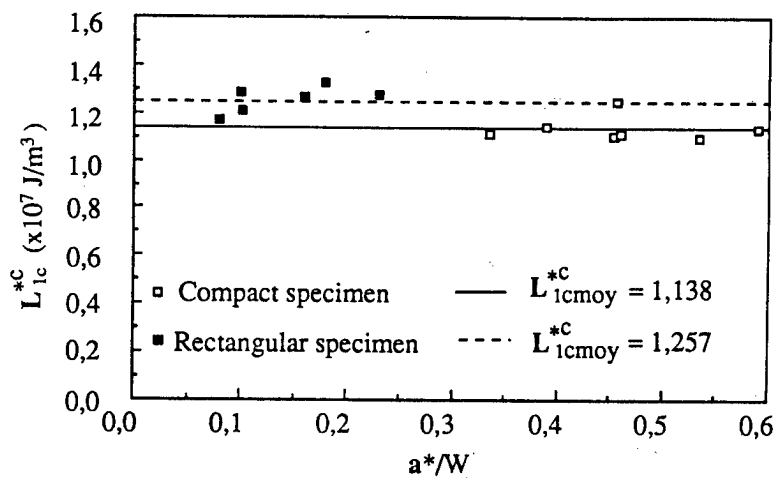


Figure 21 - The critical strain energy release rate versus the geometry of a notch in monotonic compression

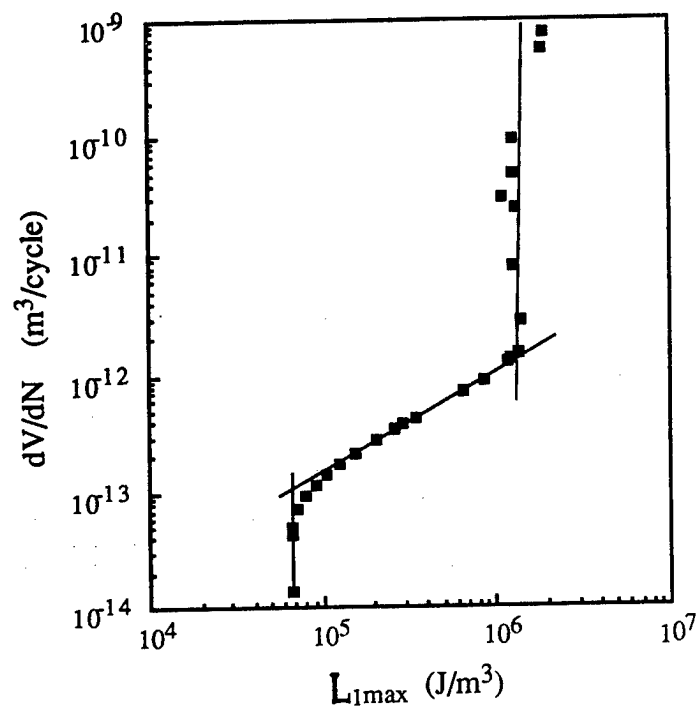


Figure 22 - Growth of the damage zone at the tip of a notch in tension-compression fatigue

PROBLEMS IN MECHANICAL TESTING METHODS OF ADVANCED COMPOSITE MATERIALS

Masuji Uemura

Department of Mechanical Engineering
College of Industrial Technology, Nihon University,
1-2-1, Izumicho, Narashino, Chiba 275, Japan

ABSTRACT

This paper summarizes a series of research works performed in my laboratory in Tokyo University and Nihon University. They include the analytical and experimental studies on the mechanical testing methods in order to obtain the fundamental and reliable mechanical properties used for structural design, such as tensile, flexural and in-plane shear properties of advanced composites. As an extreme case, the unidirectional carbon-fiber reinforced plastics is used as a specimen material. The stress and deformation distributions are analysed by the finite element method numerically and by basing on the finite deformation theory. Based on the good agreements between the experimental and analytical results, the present testing methods are discussed or criticised and the recommendations for improving them are proposed.

1. INTRODUCTION

The mechanical testing methods for advanced composites developed recently, have not yet been fully established internationally^{1,2)} and many problems remain to be solved. The reason for it results from extreme anisotropy, low shear rigidity, coupling effects and various fracture mechanisms etc.. And it is difficult to specify the testing methods for evaluating reasonably the mechanical properties used for structural design, because of existence of lots of influence factors³⁾. Under such present circumstances, the seven developed nations are now cooperating to contribute to the establishment of reliable international specifications for testing methods as VAMAS project (Versailles Project of Advanced Materials and Standards). Some part of this research has been performed to meet this project.

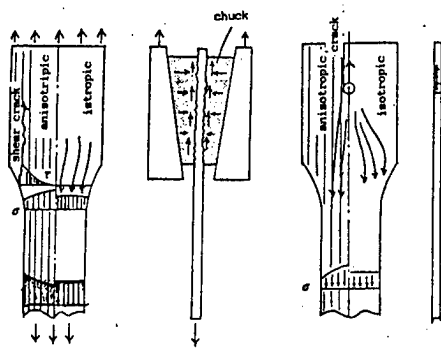
2. SIGNIFICANCE OF STANDARD TESTING METHODS

- The significance to establish the standard testing methods should be
- (1) To avoid the large scatters of mechanical properties determined by various testing methods and to put them in order in design manual.
 - (2) To discuss the merits or the demerits of the properties of various composites through the relative comparison by the unified testing method.
 - (3) To present the useful design data obtained under the similar stress states in practical service

3. PROBLEMS ENCOUNTERED IN TESTING METHODS FOR ADVANCED COMPOSITE MATERIALS

- (1) The stress can not be dispersed from the highly stressed regions under concentrated loads due to extreme anisotropy and low shear modulus. Accordingly, the Saint-Venant principle used in elasticity can not be applied.

As an example, consider the stress flows and the tensile stress distributions in both isotropic and anisotropic dumbbell-type specimens as shown in Fig.1. In isotropic specimen, the tensile stress in parallel part becomes almost uniform because of high shear modulus; On the other hand, in the anisotropic specimen, the tensile stress is not uniform due to low shear modulus along fibers, and the shear cracks are apt to occur in the region with curvature because of low shear strength along fibers. Further, the shear deformation can not be neglected in some case, e.g., in the bending of thick beam.



(a) tension through chuck (b) tension through pin

Fig. 1. Stress flow in tensile specimen.

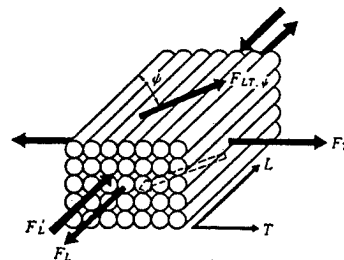


Fig. 2. Four fundamental fracture strengths of unidirectional fiber-reinforced composite.

(2) Because of existence of various fracture mechanisms, it is difficult to realize the specified fracture mode in testings.

The four fundamental strengths corresponding to four kinds of fracture modes in a unidirectional layer in laminated structures as shown in Fig. 2 are as follows.

- ① Tensile strength, F_L , in the fiber direction due to tensile fracture of fibers
- ② Compressive strength, F'_L , in the fiber direction accompanying fiber buckling and shear deformation of matrix
- ③ Tensile strength, F_T , transverse to fibers due to interfacial separation
- ④ Shear strength, F_{LT} , which varies with the angle ϕ between shearing and fiber directions, along fiber-matrix interface

These failure strengths vary with properties of fibers and resins, curing conditions and fiber content, etc.. The variations of experimental values of unidirectional CFRP(T300) with fiber volume fraction, V_f , are shown in Fig. 3. F_T and $F_{LT,0} = F_{LT}$ are much lower than F_L and F'_L resulting in probable fractures at the interface.

Accordingly, the desired fracture properties can not be obtained frequently because of preceding F_T or F_{LT} fractures, such as F_{LT} fracture in tensile test as shown in Fig. 1.

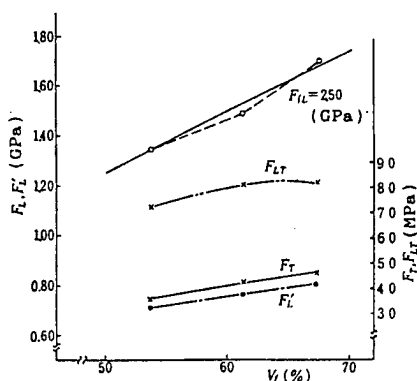
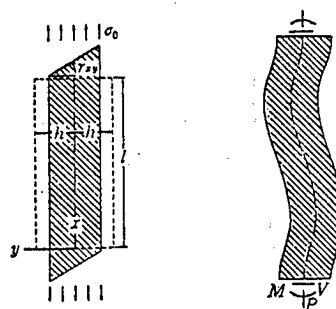


Fig. 3. Effect of fiber volume fraction of failure strength of unidirectional CFRP composite.



(a) Uniform tension (b) Effect of end constraint
Fig. 4. Deformation of specimen where tension is applied oblique to fiber direction.

(3) The coupling and cross-elasticity effects in anisotropic composites generate complicated stress and deformation states. When the tension is applied obliquely to the fiber direction, the rectangular specimen deforms obliquely or is crooked without or with end constraint, respectively, as shown in Fig. 4.

When a laminate having different fiber directions in each layer, e.g., a symmetric angle-ply laminate is subject to tension, as shown in Fig.5, the complicated three-dimensional stresses including interlaminar shear stress take place near free edges, and the in-plane fracture is preceded by unexpected delamination.

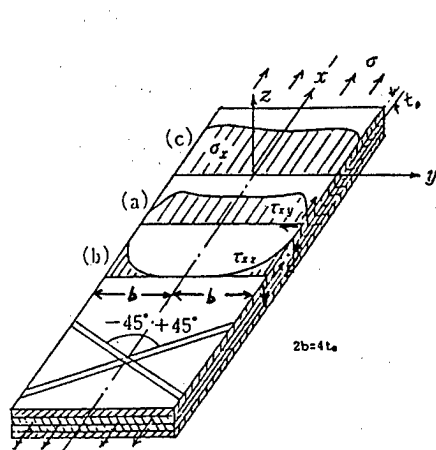


Fig.5. Widthwise stress distribution in angly ply laminate under uniaxial tension

4. PROBLEMS IN FLEXURAL TESTING METHOD

3-point and 4-point flexural tests have been widely recommended as standard methods by ASTM, ISO and JIS²⁾. However, in the unidirectional advanced composites with extreme anisotropy, there exist lots of problems as discussed below.

4.1 Comparison of Stress Distributions in the Vicinity of Loading Point with Those Derived from Elementary Beam Theory (E.B.T.)

The local stress distributions through the thickness in the vicinity of loading point in 3-point bending are analysed by using the two-dimensional anisotropic elasticity theory. The load by loading nose with radius, R_n , is assumed to distribute as a function of $[1 + \cos(\pi x/\epsilon)]$ (2ϵ : breadth of loading) as shown in Fig.6.^{4,5)}. The distributions of following normalized stresses derived from E.B.T. are shown in Fig.6.

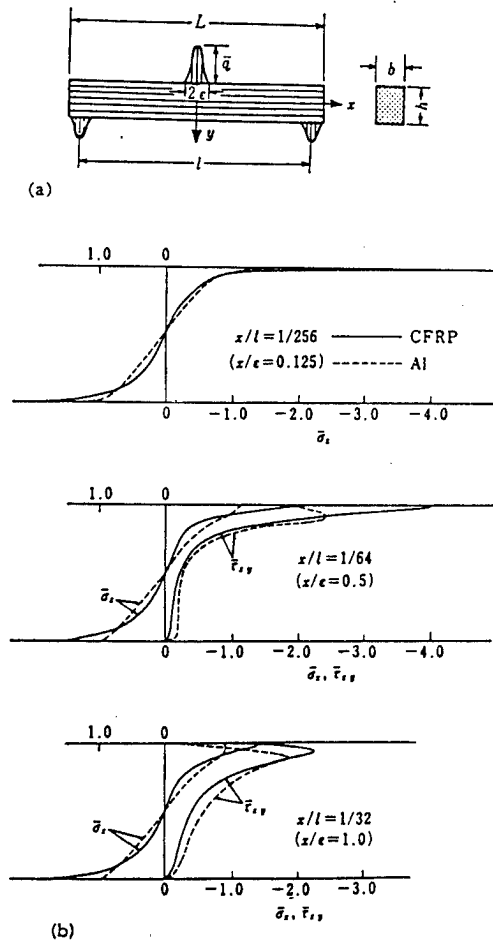


Fig. 6. Stress distributions in the vicinity of loading point in 3-point bending ($l/h=4$, $\epsilon/h=1/8$).

$$\bar{\sigma}_x = \frac{\sigma_x}{(3Pl/2bh^2)}, \quad \bar{\sigma}_y = \frac{\sigma_y}{(P/\epsilon b)}, \quad \bar{\tau}_{xy} = \frac{\tau_{xy}}{(3P/4bh)} \quad (1)$$

The elastic constants used for numerical calculation of unidirectional CFRP ($V_f=60\%$) are:

$$\begin{array}{llll} \text{T800; } E_L = 139.4 \text{ GPa, } E_T = 8.33 \text{ GPa, } \nu_L = 0.32, & G_{LT} = 4.84 \text{ GPa} \\ \text{T300; } E_L = 120.0 \text{ GPa, } E_T = 6.00 \text{ GPa, } \nu_L = 0.40, & G_{LT} = 3.00 \text{ GPa} \end{array} \quad (2)$$

The maximum axial stress of σ_x and maximum shearing stress of τ_{xy} in the vicinity of the central loading point are much higher than those derived by E.B.T.. The maximum values $(\sigma_x)_{max}$ and $(\tau_{xy})_{max}$ increase with decreases in l/h , ϵ/h and radius of loading nose, R , in highly anisotropic composites, such as CFRP. And so, flexural strengths defined by E.B.T. are very questionable. In addition, the interlaminar shear strength has been usually determined by the 3-point short beam bending test. Accordingly, the ILSS value defined by E.B.T. is open to discussion.

4.2 Effect of Large Deflection on Load-Central Deflection Curve and Maximum Flexural Edge Stress

(1) Analytical formulas

The nonlinearity results from the changes of contact points and directions of reaction forces, and the horizontal thrust in addition to the large deflection. The analytical formulas derived by the author and based on the finite deformation theory are as follows⁶⁾.

(1) Load (P)—Central Deflection (δ) Relation

$$\left. \begin{aligned} \text{3-point bending: } \frac{Pl^2}{48 E_L I} &\approx \frac{\delta}{l} \frac{1 - \frac{9}{2} \frac{R}{l} \frac{\delta}{l}}{\left(1 - 6 \frac{R}{l} \frac{\delta}{l}\right)^3} \left[1 - 12.34 \left(\frac{\delta}{l}\right)^2 + 161.6 \left(\frac{\delta}{l}\right)^4 - \dots \right] \\ \text{4-point bending (N=3, one-third points loading):} \\ \frac{23 Pl^2}{1,296 E_L I} &\approx \frac{\delta}{l} \frac{1 - \frac{144}{23} \frac{R}{l} \frac{\delta}{l}}{\left(1 - \frac{36 \times 72}{23^2} \frac{R}{l} \frac{\delta}{l}\right)^3} \left[1 - 14.38 \left(\frac{\delta}{l}\right)^2 + 129.6 \left(\frac{\delta}{l}\right)^4 - \dots \right] \end{aligned} \right\} \quad (3)$$

where $I = bh^3/12$.

(2) Maximum Flexural Edge Stress

$$\left. \begin{aligned} \text{3-point bending:} \\ \frac{\sigma_b}{\left(\frac{3}{2} \frac{P_{max} l}{bh^2}\right)} &= \begin{cases} 1 + 6 \left(\frac{\delta}{l}\right)^2 - 4 \frac{h}{l} \cdot \frac{\delta}{l} - 6 \frac{R}{l} \cdot \frac{\delta}{l} - \mu \left(2 \frac{\delta}{l} - \frac{4}{3} \frac{h}{l}\right) & \text{(tension side)} \\ 1 + 6 \left(\frac{\delta}{l}\right)^2 - 2 \frac{h}{l} \cdot \frac{\delta}{l} - 6 \frac{R}{l} \cdot \frac{\delta}{l} - \mu \left(2 \frac{\delta}{l} - \frac{2}{3} \frac{h}{l}\right) & \text{(compression side)} \end{cases} \\ \text{4-point bending:} \\ \frac{\sigma_b}{\left(\frac{P_{max} l}{bh^2}\right)} &= \begin{cases} 1 + \frac{4,644}{529} \left(\frac{\delta}{l}\right)^2 - \frac{180}{23} \frac{h}{l} \cdot \frac{\delta}{l} - \frac{324}{23} \frac{R}{l} \cdot \frac{\delta}{l} - \mu \left(\frac{78}{23} \frac{\delta}{l} - \frac{h}{l}\right) & \text{(tension side)} \\ 1 + \frac{4,644}{529} \left(\frac{\delta}{l}\right)^2 - \frac{144}{23} \frac{h}{l} \cdot \frac{\delta}{l} - \frac{324}{33} \frac{R}{l} \cdot \frac{\delta}{l} - \mu \left(\frac{78}{23} \frac{\delta}{l} - \frac{h}{l}\right) & \text{(compression side)} \end{cases} \end{aligned} \right\} \quad (4)$$

where μ is the friction coefficient at the supporting nose, and R is the radius of nose

In such modified formulas proposed by ASTM, ISO and JIS²⁾, the effects of radius of curvature of noses, R , and friction at noses are not taken into consideration.

(2) Comparison of experimental and analytical P versus δ/l diagrams

The experimental diagrams in unidirectional CFRP specimens are shown under various values of R in Fig.7(a) and (b) for the cases of 3-point and 4-point bendings, respectively. The slopes of P - δ diagrams become steep with an increase of R . The good agreement can be seen in these nonlinear relations.

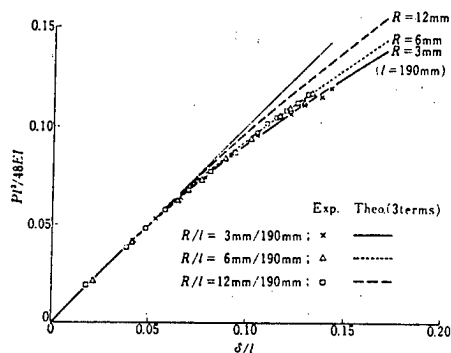


Fig. 7(a) Load versus central deflection relation in 3-point bending.

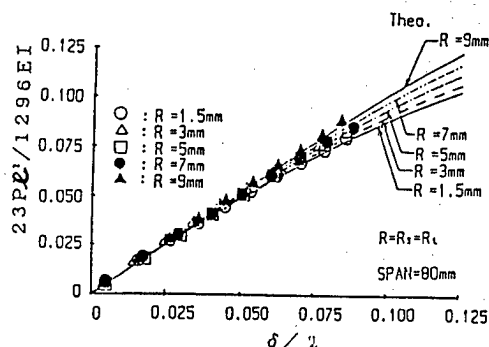
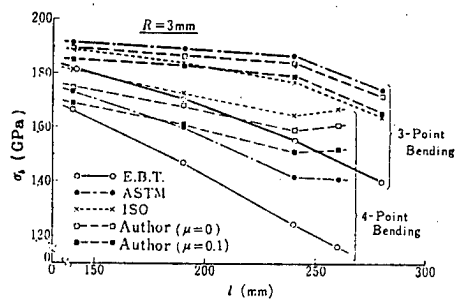


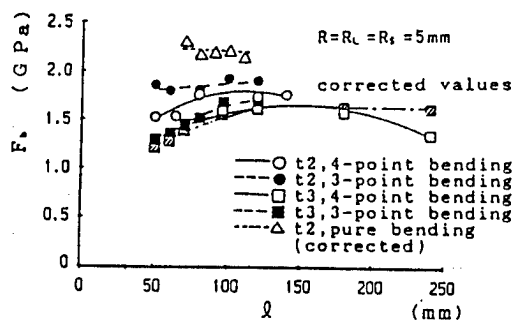
Fig. 7(b) Effect of radius of nose, R , on load versus deflection diagrams in 4-point bending

4.3 Effects of Various Factors on Flexural Strength

Denoting the radius of loading and supporting noses as R_L and R_S , respectively, R is used when $R_L = R_S = R$. In the flexural tests, span l , thickness t and R were varied to discuss their effects. Experimental values of flexural strengths, F_b , defined by E.B.T. are shown in Fig. 8.



(a) T300 CFRP
(long span l)



(b) T800 CFRP
(short and long spans l)

Fig. 8 Variations of flexural strengths with span in various loading methods

(1) Effects of loading modes

Variations of F_b in CFRP (T 300) and (T 300) specimens with span under three kinds of loading methods, that is, 3- and 4-point bendings and pure bending are shown in Fig. 8(a) and (b), respectively. The F_b values obtained by 3-point bending are much higher than those obtained by 4-point bending.

The fracture crack originates just beneath the loading point under stress concentration and then propagates accompanying the interlaminar shear delamination in both 3- and 4-point bendings as shown in Photo. 1.

The F_b values in 3-point bending are defined by using the maximum bending moment at the one central point; however, in 4-point bending, the maximum bending moment extends over between the two loading points. It is considered that the fracture is not governed only by the local maximum stress at a point, but influenced by the over-all stress around the fracture point. Accordingly, 4-point bending will give the lower strength from the viewpoint of probability of

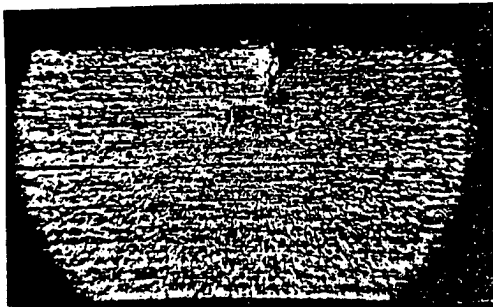
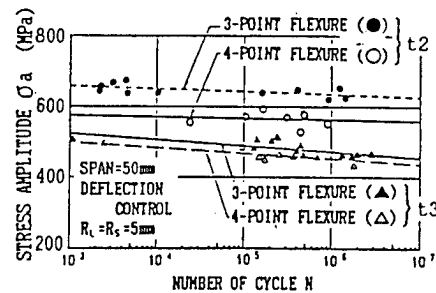


Photo.1. Local fracture behaviors beneath loading point in 4-point bending ($R=2\text{mm}$)



Case of deflection control

Fig. 9. Fatigue S-N diagrams under two kinds of loading modes and specimen thicknesses

fracture, but the conservative and useful values for practical structural design. Such an effect of loading mode can be seen also in the fatigue tests. The S-N curves are shown in Fig. 9. The fatigue strengths under 3-point bending are higher than those under 4-point bending for both thicknesses $t=2$ and 3mm .

In order to avoid the fractures just beneath the loading noses due to the stress concentration observed in 3- and 4-point bending methods, a test fixture was developed in my laboratory to apply the pure bending moment without any loading point over the span. The fracture occurred between both tabs without stress concentration. The almost constant F_b values of $2.2\sim 2.3\text{GPa}$ obtained under pure bending are much higher than those under 3- and 4-point bendings and seem to give the real flexural strength.

(2) Effects of span length and thickness

- ① The F_b values obtained under long span $l>120\text{mm}$ seem to be lower as seen in Figs. 9(a) and (b), but the corrected F_b values by use of Eq. (4) become nearly constant independently of span. The F_b values become lower under high loads in the short range of span as seen in Fig. 8(a). It results from the high local stress concentration at loading point.
- ② The F_b values for $t=2\text{mm}$ are higher than those for $t=3\text{mm}$ in the case of statical test as shown in Fig. 8(b). This fact can be seen also in fatigue test as shown in Fig. 9. The reasons for it are considered as follows.
 - (a) Since the fracture load becomes higher approximately in proportion to t^2 , the stress levels just beneath the loading point for thicker specimens are higher than those for thinner ones.
 - (b) The thicknesswise stress gradient in the thinner specimen is steeper than in the thicker one under the condition of constant flexural stress. Accordingly, the highly-stressed region close to both surfaces is narrow and is sustained by the lowly-stressed region, resulting in low probability of fracture.
- ③ The optimal ratio of span to thickness seems to be about 40 in the case of $t=2\sim 3\text{mm}$, where the F_b values defined by E.B.T. are almost constant.

(3) Effect of radius of loading nose

The experiments were carried out under 3- and 4-point bendings with $l=80\text{mm}$ and $t=2\text{mm}$, that is, under the optimal ratio of $l/t=40$.

The variations of F_b values with radius of loading nose, R_l , are shown in Fig. 10. F_b values decrease with radius of R_l less than 5mm in both cases of 3- and 4-point bendings. It results from the fracture just beneath the loading nose owing to the stress concentration. If the F_b values in the range of larger R_l are corrected by use of the Eq. (4), they become almost constant.

Similarly, in the S-N curves in the fatigue tests, the stress amplitude σ_a values under $R=5\text{mm}$ are higher than those under $R=2\text{mm}$ as shown in Fig. 11.

(4) Effect of insertion of film beneath loading point

As expected from the experimental evidences above described, the experiments for the effect of film inserted between nose and specimen were carried out under 4-point bending.

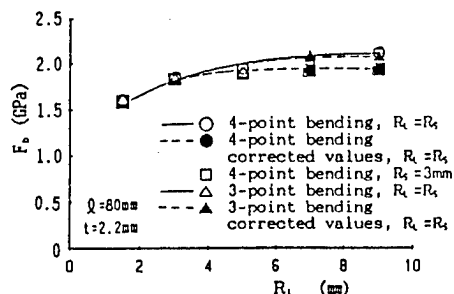


Fig. 10 Variation of flexural strength, F_b , with radius of loading nose, R_n

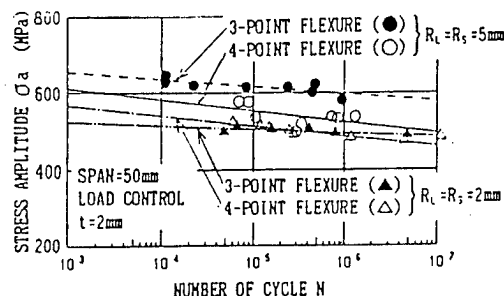


Fig. 11 Effects of nose radius and flexural loading methods on S-N curves

The flexural strengths, F_b , increase with total thickness, t , as shown in Fig.12. However, the F_b values are almost constant independently of t , in the range below $t_r = 0.05\text{mm}$ where no effect of cushion is observed. As the total thickness, t , is increased, the fractures do not occur at the loading point due to stress concentration, but occur in the central region under constant bending moment between the two loading points. The alleviation of stress concentration due to film insertion can be numerically verified by FEM.

4.4 Recommendations for Flexural Tests

- (1) The failures in 3- and 4-point bending methods took place just beneath the loading points without showing the so-called flexural fractures. On the other hand, the fractures under pure bending moment occur between both ends without stress concentration, giving the higher real bending strengths compared with 3- and 4-point bending tests. Accordingly the pure bending test is recommended for advanced composites.
- (2) As for the optimal ratio of span to thickness (l/t), it seems to be around 40 in 3- and 4-point bending methods.
- (3) Comparing only 3- and 4-point bending methods, the latter has several advantages over the former, that is, exhibits a region of uniform bending moment without shear under lower stress concentration, even though the F_b values become lower from the view of probability of fracture.
- (4) As for the radius of curvature of noses, the optimal R_n value is recommended to be about 5mm in 3-point bending and 3 to 4mm in 4-point bending in order to avoid the stress concentration. The optimal R_s value is recommended to be about 3mm in order to avoid the effect of movement of contact point.

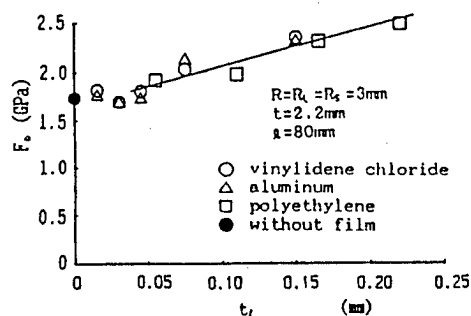


Fig.12 Variations of flexural strength, F_b , with total thickness, t , of various films

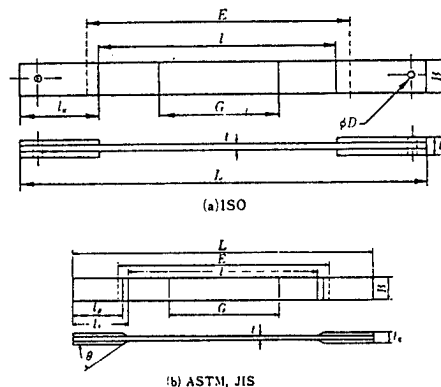


Fig. 13 Tensile specimens proposed for oriented composites.

5. PROBLEMS IN TENSILE TESTING METHODS

Even though there are few cases where the F_L fracture governs the structural design, there are much problems in tensile testing methods to obtain the F_L values.

5.1 Difficulties Involved in Tensile Tests

(1) The problems in the case when the tension is applied obliquely to the fiber direction are discussed in §3(3).

(2) The Dumbbell-type specimens used for quasi-isotropic plate are undesirable since most fractures occur near the transient portion between the curved and the parallel regions in oriented composites, as explained by Fig.1 in §3(1).

The coupon-type specimens were proposed for oriented composites as shown in Fig.13, but the fractures occur frequently near the tab ends or in the grips due to stress concentration. Occasionally, the tabs tear off especially in thick specimens by debonding.

5.2 Problems in Tensile Tests by Use of Ring Specimens

(1) Problems in NOL ring.

In order to overcome the difficulties described above, NOL ring specimen as shown in Fig.14 has been widely used to determine the tensile strength of unidirectional filament-wound composites⁷⁾. However, the considerable bending moment is superposed at the fracture points near the split in the dee-fixture as seen from the numerical results in Fig.15(a)⁷⁾. Hence, the experimental fracture strength decreased appreciably with an increase of ring thickness. Accordingly the race-track(RT) type ring specimen as shown in Fig.14(b) is considered to be effective in reducing this disadvantage, as seen from Fig.15(b). The advantage of RT ring is that the hoop stress is nearly uniform; however, it is a trouble to have a fabrication device so as to have constant thickness around RT ring.

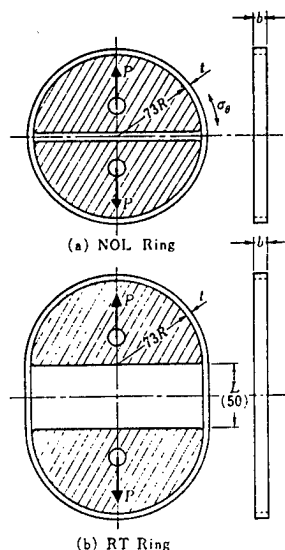


Fig. 14 Configurations of tensile ring specimens.

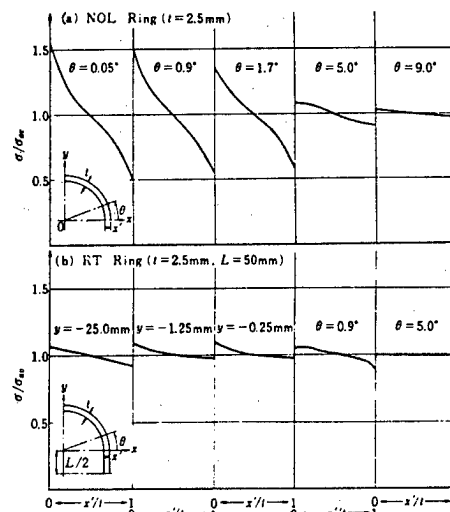


Fig. 15 Distributions of hoop strains through the thickness along ring.

5.3 Thicknesswise-cut Tensile Specimen

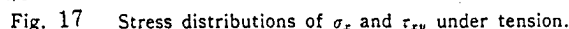
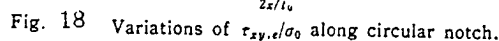
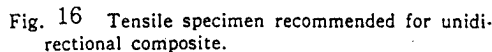
In order to overcome the above-mentioned disadvantages, a thicknesswise-cut tensile specimen is recommended to obtain the reliable tensile strength, F_L .

(1) Circular notch

The specimen should be cut with a large radius of curvature, R_1 , thicknesswise rather than widthwise as shown in Fig.16, to reduce the shear stress.

(2) Stress distributions around circular notch

The distributions of axial stress, σ , and shearing stress, τ , obtained numerically are shown in Fig.17 for $R_1/t=50/3$ and CFRP(T300). The distributions



(3) Tensile experimental results

6. PROBLEMS IN IN-PLANE SHEAR TESTING METHODS

6.1 Disadvantages in Picture-Frame Loading Method and Their Revisions¹⁰⁾

(1) Location of corner pin

(2) Split of pin

(3) Insertion of plate

The inside corners of frames do not contact with specimen surfaces as shown in Fig.21(a). Accordingly, thin plate inserted between frame and specimen, is connected with specimen through by small pins around corners as shown in Fig.21(b). As a result, the more uniform shear stress distribution can be obtained as seen in Fig.22.

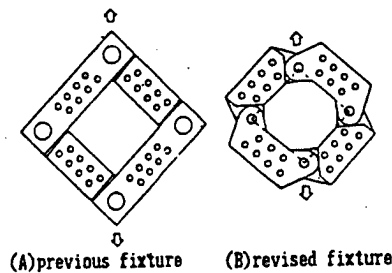


Fig.19 Picture-frame fixtures

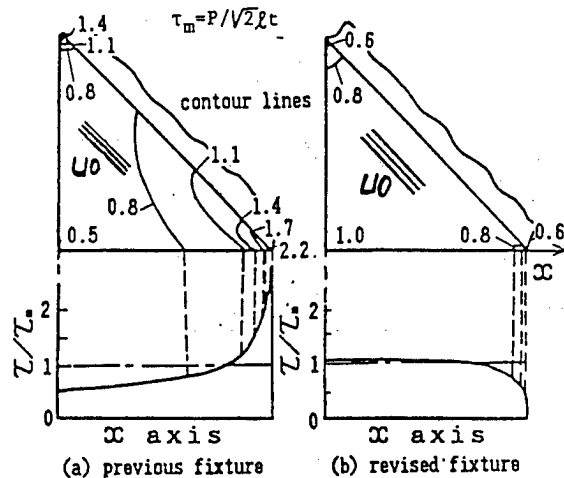


Fig.20 Comparison of shear stress distributions obtained by FEM in U0 specimen

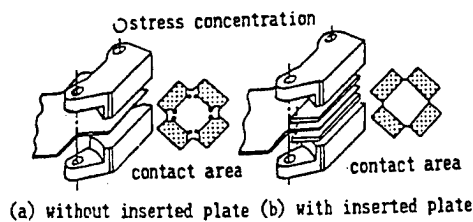


Fig.21 Compositions of revised fixtures

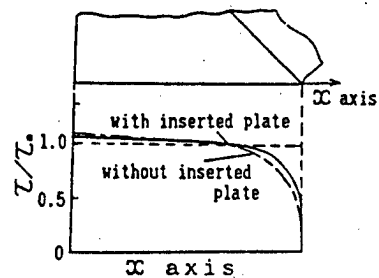


Fig.22 Comparison of principal shear stress distributions obtained by FEM in U0 specimen

(4) Effect of radius of curvature, R, at specimen corners

It seems that the stress concentration will originate at corner under small R; however, the corner sharpness has no effect on stress concentration, because the location of pin coincides with the corner. That is, the corners are allowed to be rectangular and it makes the cutting of specimen easier.

Table 2. Comparison of moduli and shear strengths obtained by various kinds of test methods and specimens (MPa)

test method	specimen	shear modulus G_{LT}		shear strength F_s	
		(U0)	(U90)	(U0)	(U90)
picture-frame	previous	6210	←	34.3	←
	revised	5020	←	82.1	←
rail shear	two-rail	3920	4210	48.8	61.0
	three-rail	3820	3920	43.6	77.1
45° off-axis tension		3920	←	48.3	←
theoretical		5290	←	—	—

(5) Comparison of experimental results obtained by both types of picture-frame

The shear strengths obtained in the three kinds of specimens are compared in Table 2. In the case of previous type of frame (A), the fracture strengths were lower because of the premature fracture originating from corners. On the other hand, in the case of revised type of frame (B), the higher shear strengths were obtained with accompanying lots of failure cracks along fibers extending over the whole specimen under uniform shear. These experimental evidences shows the effectiveness of the revision.

6.2 Disadvantages of Rail-Shear Method and Their Revision³

(1) Stress distributions in U0 specimens and experimental results

Fig. 23 shows the rail-shear fixtures with specimens whose merits are considered to be simple and economical. However, as seen from Fig. 24(a) for U0 specimens where fibers are arranged in the tensile direction, the tensile stress σ_T normal to fibers concentrates at both edges. Since σ_T is about one and a half times τ_{LT} , and F_T is smaller than F_{LT} , it is clear that the F_T fracture is preceded by the F_{LT} fracture at corners.

The experimental shear strengths of U0 specimens obtained by 2-rail shear method are compared with those by other methods in Table 2. The F_s values are much lower than those obtained by the revised picture-frame fixture. Also in the 3-rail shear method, almost the same F_s values were obtained.

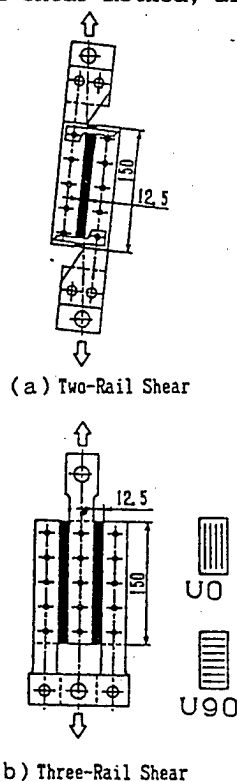


Fig. 23. Rail shear fixtures with specimens

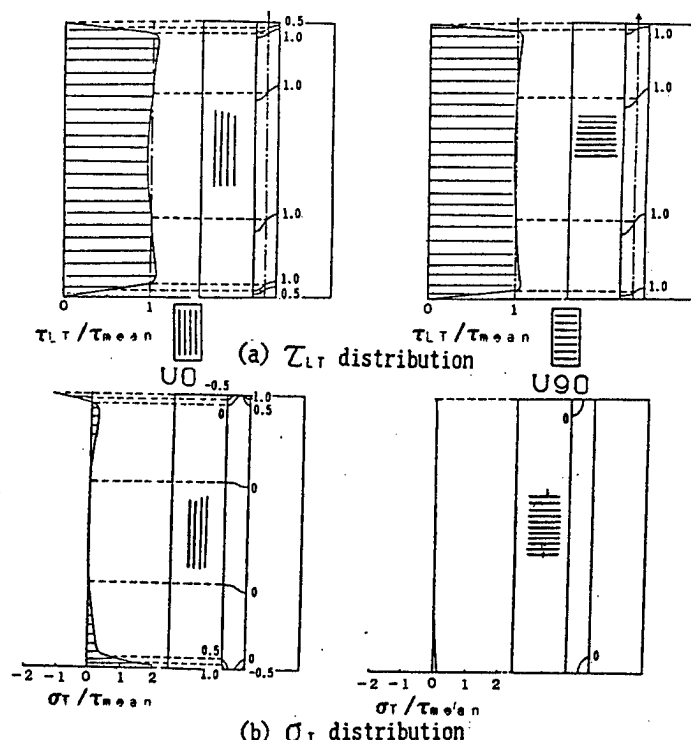


Fig. 24. shear stress distributions and contour lines in both U0 and U90 specimens obtained by FEM

(2) Revision by changing the fiber direction to normal to tensile direction

In order to overcome the F_T fractures at corners described above, The U90 specimen where the fibers are arranged normal to tensile loading direction, is recommended as shown in Fig. 24. The tensile stress, σ_T at corners in U90 specimens are about one sixth compared with in U0 specimens. Accordingly, the F_T fracture will occur instead of the σ_T fracture. As seen from Table 2, the shear strengths in U90 specimens are much higher than in U0 specimens. The shear stress versus shear strain curves are shown in Fig. 25. In contrast with U0 specimens, the fracture strains in U90 specimens increase very much without showing the brittle behaviors due to the F_T fracture.

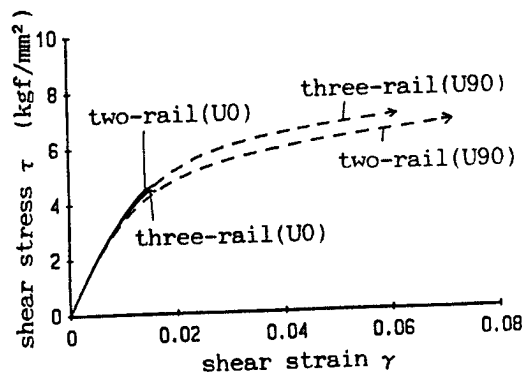


Fig. 25. Mean shear stress versus shear strain diagrams at center in rail-shear methods

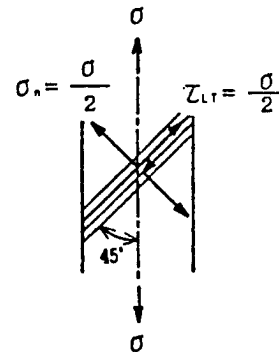


Fig. 26. Stress components under tensile stress in unidirectional specimen

6.3 Disadvantage of 45-deg off-Axis Tensile Test

According to JIS specification⁹⁾, the tensile test of coupon specimen with fibers oriented in the 45° direction to the loading axis as shown in Fig. 26 may be substituted for a shear test. However, in this method, the tensile stress component $\sigma/2$ normal to fibers acts on the shearing plane along fibers in addition to the shear stress component $\sigma/2$, which presents a combined stress state. Since the fundamental strength, F_t , is about one half of fundamental shear strength, F_{11} , the premature tensile fracture is preceded by the shear fracture. The experimental results are compared with the other methods in Table 2. The shear strengths F_s defined for U0-specimens are only about one half of those obtained by the revised frame fixture, suggesting the inadequacy of the off-axis tensile testing methods to obtain the fundamental shear properties, especially of the unidirectional composites.

7. Conclusion

In view of the present situation that the mechanical testing methods for advanced fiber-reinforced composites have not yet been established, the developmental research work on fundamental tensile, flexural and in-plane shear testing methods have been performed, basing on the experiments and the numerical analyses.

In the highly anisotropic composite materials such as unidirectional CFRP having various fracture mechanisms, the careful attention should be paid to obtain the reasonable desired properties because of various influence factors on mechanical properties. It should be avoided to apply correspondingly the testing methods for isotropic materials.

The author would like to express my sincere thanks to the many collaborators in my laboratory for their assistants in experiments and numerical analyses.

References

- 1) Tensile testing methods ; ASTM D3039-74(76), ISO-3268(1978), JIS K-7113(1981)
- 2) Flexural testing methods ; ISO TC61-WG2-TG11
- 3) M.Uemura ; Trans. Japan Soc. Comp. Mat., 10, 1 (1984), 7-16 (in English)
- 4) H.Yoshida and M.Uemura ; Bull. Ind. Prod. Res. Inst., No.88 (1979) 9/14 (in Japanese)
- 5) H.Yoshida, M.Uemura & Y.Yamaguchi ; Jour. Japan Soc. Comp. Mat., 5, 2 (1979) 62/67 (in Japanese)
- 6) M.Uemura, H.Iyama & Y.Yamaguchi ; Reinforced Plastics, Japan Reinforced Plastic Association, 24, 1 (1973) 13/20 (in Japanese)
- 7) M.Uemura and M.Murata ; Jour. Japan Soc. Mat. Sci., 27, 301 (1978) 1001/1007
- 8) M.Uemura, H.Iyama & Y.Yamaguchi ; Jour. Japan Soc. Comp. Mat., 2, 1 (1976) 20/26 (in Japanese)
- 9) JIS K 7059, Testing Method for In-Plane Shear Properties of Glass Fiber Reinforced Plastics, (1987/3/01)
- 10) M.Uemura & H.Iwai ; Proc. of ICCM VII, vol.3 (Gunzhou, China) (1989) 489/494

SESSION I

LIFE PREDICTION

This page intentionally left blank

PROPAGATION OF DELAMINATION FATIGUE CRACKS IN CF/PEEK LAMINATES

Masaki Hojo*, Keisuke Tanaka**, Kiyoshi Kemmochi*,
and Ryuichi Hayashi*

* Structure Technology Dept. Industrial Products Research
Institute, AIST, MITI, Higashi, Tsukuba 305, Japan

**Dept. of Engineering Science, Kyoto University, Sakyo-ku,
Kyoto 606, Japan

ABSTRACT

The effect of the stress ratio on the near-threshold growth of delamination fatigue cracks was investigated with unidirectional laminates made from ICI APC-2 thermoplastic prepregs (AS4/PEEK). Tests were carried out under mode I opening loading by using double cantilever beam specimens with a special loading device. The crack growth rate under different stress ratios was a unique function of the equivalent stress intensity range proposed by the authors. The fatigue crack growth rate near the threshold was mainly controlled by the stress range rather than by the maximum stress. The fatigue crack growth resistance of APC-2 laminates was much higher than that of conventional CF/epoxy laminates even near the threshold region. This increase of resistance, however, was smaller than that of fracture toughness. The difference of the growth behavior between CF/PEEK and CF/epoxy laminates was discussed on the basis of the fractographic observation and mechanism consideration.

INTRODUCTION

The use of composite materials in primary structures offers significant weight saving due to their high specific strength. Today, structures made of carbon fiber reinforced plastics (CFRP) have been applied to the vertical and horizontal stabilizers of commercial aircraft such as Airbus A320. Composite structures used as primary structures require performance reliability based on damage tolerance. Conventional CFRP laminates made of brittle epoxy matrix have very low interlaminar strength, manifested as a low threshold of delamination fatigue crack growth and a low static fracture toughness(1-3). Hence, the improvement of delamination strength of CFRP laminates is of current interest in their structural applications.

Polyetheretherketone(PEEK) is a new semicrystalline thermoplastic matrix resin which is expected to improve significantly the interlaminar strength. The interlaminar fracture toughness of CF/PEEK laminates was reported to be 3 to 4 times higher than that of conventional CF/epoxy laminates (where the toughness is expressed in terms of the stress intensity factor)(4). On the other hand, very little is known about the effect of cyclic loading on the delamination growth behavior in CF/PEEK laminates. Although Prel et al.(5) carried out mode I and mode II delamination fatigue crack growth tests by using DCB and CBEN specimens, they dealt only with crack growth at very high rates. Recently,

TABLE 1. Material and mechanical properties.

Prepreg Carbon fiber Matrix	ICI APC-2 Hercules AS4 ICI PEEK
Volume fraction of fiber	62%
Constitution of laminate	(0) ₄₈
Crystallinity	34%
Elastic constants (GPa)	$E_1=134$, $E_2=8.9$, $G_{13}=5.1$ $\nu_{13}=0.37$
Fracture toughness	K_{IC} (MPa $m^{1/2}$) G_{IC} (N/m)
	4.7 1700

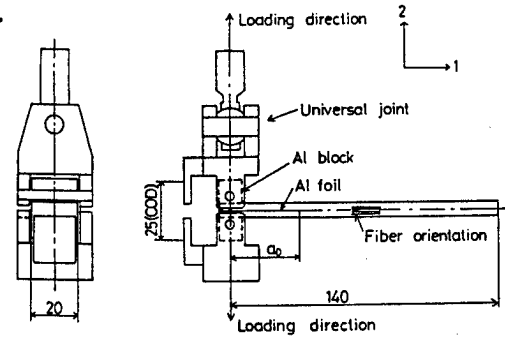


Fig. 1. DCB specimen with pins and Al blocks (dimensions are in mm).

O'Brien(6) reported on the basis of the results of edge delamination tests that the delamination onset in CF/PEEK laminates under fatigue loading was observed at significantly lower strain levels than its delamination onset under static loading was.

In the present study, the load-shedding condition to obtain the fatigue crack growth data near the threshold region was first established. Then, the effects of the stress ratio (the mean stress) on the near-threshold growth of delamination fatigue cracks were investigated. The results were compared with our previous results for CF/epoxy laminates(3,7).

EXPERIMENTAL PROCEDURE

Material and specimen

The laminates were made from prepregs of ICI APC-2 (AS4/PEEK). The unidirectional laminates (thickness=6mm) were fabricated by ICI Wilton. The constitution of laminates, their elastic moduli, and their fracture toughness for mode I delamination are summarized in TABLE 1. The fracture toughness tests were carried out by loading the specimen which had a fatigue crack made at the threshold condition. The fracture toughness value shown in TABLE 1 is expressed by the propagation value in the stable growth region.

Tests of delamination fatigue crack growth were carried out under mode I opening loading by using double cantilever beam specimens with a special loading device. Figure 1 shows the loading apparatus. Crack opening displacement on the load line was measured by an extensometer attached to the loading apparatus as shown in Fig. 1.

Fatigue tests

Tests were carried out with a computer-controlled fatigue testing system established by the authors(3,7). The energy release rate, G and the stress intensity factor, K were also calculated by the same procedure as before. In each test, the stress ratio, R , of the minimum to the maximum load was kept constant to be 0.2 or 0.5. A

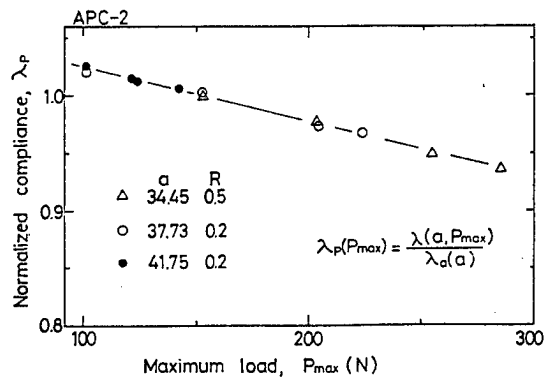


Fig. 2. Relation between normalized compliance and maximum load in G-decreasing test.

normalized gradient of energy release rate, $(1/G)dG/da$, was also controlled during load shedding. The frequency of stress cycling was 10 Hz. The testing environment was air of 50%RH at 23°C. The length of a crack was computed from the measurement of the compliance of the specimen(7). Slight dependency of load on the compliance was observed. The compliance, λ , was expressed by functions of maximum load, P_{max} and crack length, a , as follows:

$$\lambda = \lambda_a(a) \lambda_p(P_{max}) \quad (1)$$

Experimental results showed that λ_p is a simple linear function of P_{max} as shown in Fig. 2. Thus, this equation was used in order to get accurate crack length measurement near the threshold region.

EXPERIMENTAL RESULTS AND DISCUSSION

Effect of load shedding condition

Experiments were first conducted under several G-gradients to establish the testing condition. Here, G-gradient, $(1/G)dG/da$, is twice as much as K-gradient, $(1/K)dK/da$. The relation between the crack propagation rate, da/dN , and the energy release rate range, ΔG , is shown in Fig. 3, where $\Delta G = G_{max} - G_{min}$ (G_{max} and G_{min} are the maximum and minimum values of the energy release rate corresponding to the maximum and minimum loads). The result obtained under the steepest G-gradient (-2.8 mm^{-1}) did not coincide with the results under the other two conditions. Thus the allowable limit of the G-gradient for the load decreasing test of CF/PEEK laminate is -0.87 mm^{-1} . Since this allowable limit is lower than that for CF/epoxy laminate, the influence of plastic deformation near the crack tip on crack growth might be large for the case of CF/PEEK laminate (7). Subsequent tests were conducted at a G-gradient below this limit.

Effect of stress ratio

Figure 4 shows the relation between the crack propagation rate, da/dN , and the stress intensity range, ΔK , under $R=0.2$ and 0.5 , where $\Delta K = K_{max} - K_{min}$ (K_{max} and K_{min} are the maximum and minimum values of the stress intensity factor corresponding to the maximum and minimum loads). For each case of the stress ratio, da/dN is expressed as a power function of ΔK in the region where da/dN is larger than about 10^{-10} m/cycle . Below this region, da/dN deviates to the lower rate, and there exists a growth threshold for fatigue cracks. When compared with our previous study on CF/epoxy(3), the downward deviation in the da/dN vs. ΔK relation is not so clear near the threshold region. However, the slope is steep enough to suggest the existence of the growth threshold in practical applications. The exponent of the power function and the R -dependence on da/dN are smaller than those for CF/epoxy. Crack closure was not detected for the present tests.

For the case of CF/epoxy laminates, the growth rate under different stress ratios was fairly well correlated to ΔG . Thus, da/dN is plotted against ΔG in Fig. 5. The R -dependence is larger than that on the da/dN vs. ΔK relation.

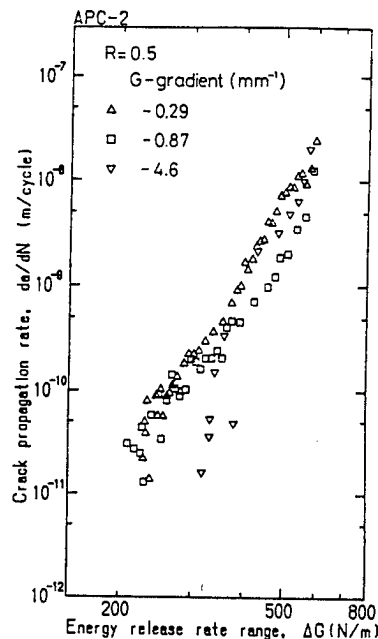


Fig. 3. Effect of normalized gradient of energy release rate.

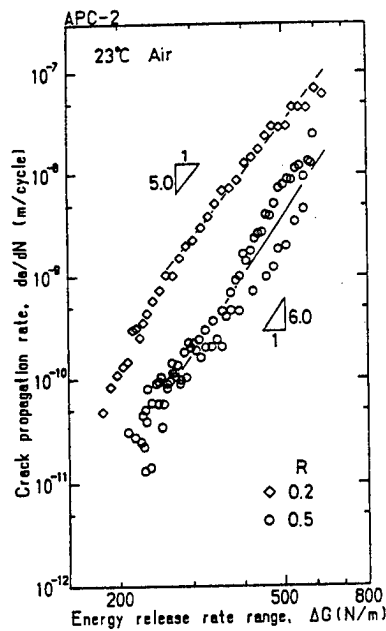


Fig. 4. Relation between crack propagation rate and stress intensity range.

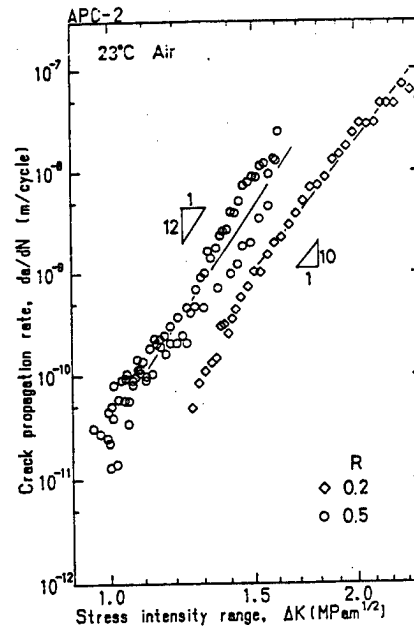


Fig. 5. Relation between crack propagation rate and energy release rate range.

Controlling fracture mechanics parameter

In our previous analysis of the near-threshold crack growth(3), we proposed the following equivalent stress intensity range, ΔK_{eq} as a controlling parameter for fatigue crack growth under various R values:

$$\Delta K_{eq} = \Delta K(1-R)^{-\gamma} = \Delta K^{(1-\gamma)} K_{max}^{\gamma} \quad (2)$$

where γ indicates a relative contribution of the maximum stress to the cyclic stress in determining the crack growth rate. ΔK_{eq} can be regarded as an equivalent parameter of ΔK at R=0 to which the R dependency of ΔK is converted.

In Fig. 6, ΔK at $da/dN=10^{-10}$ m/cycle is plotted against a stress ratio parameter, $(1-R)$, in order to obtain γ values. The results of the CF/epoxy laminate (T300/914) are also shown with the triangle marks in this figure(3). The exponent of a straight line fit of data gives the γ values. For the case of CF/PEEK laminate, the γ values is 0.36. This low value of γ suggests that the mechanism of fatigue crack propagation is mainly controlled by the stress intensity range (ΔK) like in metallic materials. On the other hand, the results of CF/epoxy laminate fit to the line at the slope of 0.85. This slope means that the contribution of the maximum stress intensity factor (K_{max}) is larger than that of stress intensity range (ΔK)(3). The influence of the stress ratio on the growth resistance is com-

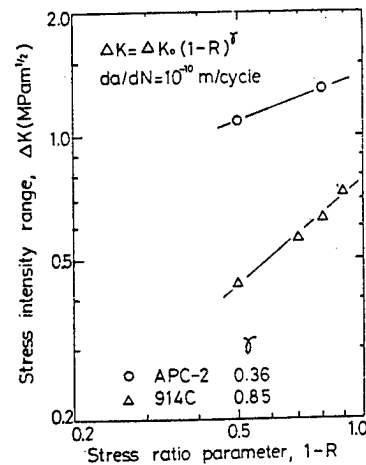


Fig. 6. Relation between stress intensity range and stress ratio parameter at $da/dN=10^{-10}$ m/cycle.

pletely different between CF/PEEK and CF/epoxy.

Open marks in Fig. 7 shows the relation between da/dN and ΔK_{eq} . The influence of the stress ratio is minimal for the whole region. This means that ΔK_{eq} is the controlling fracture mechanics parameter for APC-2 laminate.

Comparison with CF/epoxy

As mentioned above, the γ values in Eq. (2) are different between CF/PEEK and CF/epoxy laminates. While ΔK of CF/PEEK laminate is only 1.8 times that of CF/epoxy laminate under $R=0$, the difference in ΔK is much larger at higher R values as shown in Fig. 6. Figure 7 compares the relations between da/dN and ΔK_{eq} for APC-2 (CF/PEEK) and 914C (CF/epoxy) laminates. The resistance of the former material against fatigue crack growth is much higher than that of the latter material. When compared at the same growth rate, ΔK_{eq} value for APC-2 laminate is about twice as much as that for 914C laminate. When compared at the same ΔK_{eq} , da/dN for APC-2 laminates is about 4 orders of magnitude lower than that for 914C laminates. The exponent of the power function for APC-2 laminates reduced to three fourths.

TABLE 2 shows the values of $\Delta K_{eqth}/K_{IC}$ for CF/epoxy (914C, P305) and CF/PEEK (APC-2) where ΔK_{eqth} is the ΔK_{eq} value at the crack growth threshold. The value of $\Delta K_{eqth}/K_{IC}$ for APC-2 laminate is 0.25 and is much smaller than those for CF epoxy laminates. Thus, the remarkable increase of fracture toughness, K_{IC} , for APC-2 laminates contributes only 50% to the increase of fatigue crack growth resistance near the threshold region. This fact indicates that the contribution of fatigue is very important in damage-tolerance design. Similar tendency with toughened matrix systems in the high growth rate region was reported by Mall et al(8).

Fractographic Observation

Figure 8 presents scanning electron micrographs of the fracture surfaces under static and fatigue loading. The arrow indicates the growth direction. Each pair of micrographs shows the fracture surface of almost the same place at different magnifications. The fracture surface of static fracture shows remarkable ductility. Drawing of matrix resin is dominant. On the other hand, significantly

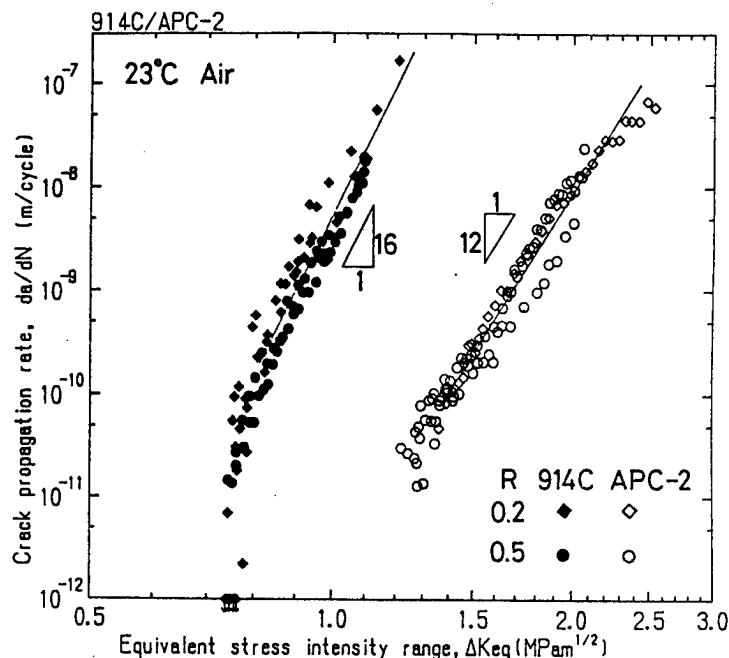


Fig. 7. Relation between crack propagation rate and equivalent stress intensity range for CF/PEEK (APC-2) and CF/epoxy(914C) laminates.

TABLE 2. Threshold conditions compared with fracture toughness.

Material	K_{IC} (MPam ^{1/2})	ΔK_{eqth} (MPam ^{1/2})	$\Delta K_{eqth}/K_{IC}$
914C	1.4	0.75	0.54
APC-2	4.7	1.2	0.25

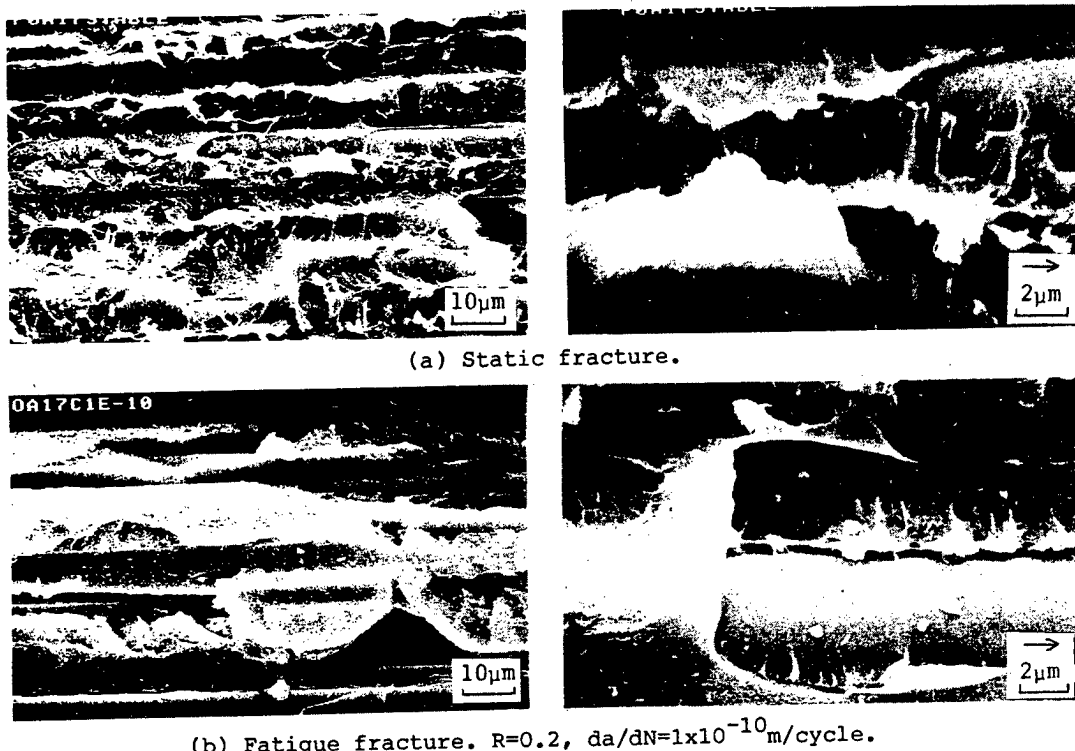


Fig. 8. Scanning electron micrographs of fracture surfaces.
Arrow shows growth direction.

rough surface without drawing of matrix was observed under fatigue loading. This roughness means that the process zone at the crack tip is much larger than that for CF/epoxy laminates(3). Small ductility in the SEM of higher magnification and the large process zone suggest that contribution of cyclic plastic deformation is large(9). The difference of the fracture surface between static and fatigue fracture indicates a difference in mechanism of fracture. These facts agree with the higher contribution of cyclic stress on the fatigue crack growth. For the case of CF/epoxy laminates, contribution of maximum load was high, and no significant difference was observed between fracture surfaces of fatigue fracture and of static fracture(3).

CONCLUSIONS

The crack propagation rate under different stress ratios was expressed as a unique power function of the equivalent stress intensity range at the growth rates above about 10^{-10} m/cycle. Below this region, there was a growth threshold. The degree of contribution of the stress range was high. Fractographic observation also showed the difference in the mechanism of fracture between fatigue and static loading.

CF/PEEK laminates are more resistant to fatigue crack growth, showing a higher growth threshold, lower crack growth rates and a lower exponent in the power relation. On the other hand, the ratio of the the fatigue threshold to the fracture toughness in the CF/PEEK laminates decreased in comparison with the CF/epoxy laminates. This fact indicates the significance of fatigue consideration in damage-tolerance design.

ACKNOWLEDGMENT

We would like to thank Prof. Claes-Göran Gustafson of the Norwegian Institute of Technology for his valuable discussion. This work is supported by the MITI program of R&D Project on Basic Technologies for Future Industries.

REFERENCES

1. Wilkins, D. J., Eisenmann, J. R., Camin, R. A., Margolis, W. S., and Benson, R. A., "Characterizing Delamination Growth in Graphite-Epoxy", ASTM STP 775 (1981) 168-83.
2. Bathias, C., and Laksimi, A., "Delamination Threshold and Loading Effect in Fiber Glass Epoxy Composite", ASTM STP 876 (1985) 217-237.
3. Hojo, M., Tanaka, K., Gustafson, C.-G., and Hayashi, R., "Effect of Stress Ratio on Near-threshold Propagation of Delamination Fatigue Cracks in Unidirectional CFRP", Composite Sci. Tech., 29 (1987) 273-230.
4. Leach, D. C., and Moore, D. R., "Toughness of Aromatic Polymer Composites Reinforced with Carbon Fibres", Composite Sci. Eng., 23 (1985) 131-161.
5. Prel, Y. J., Davies, P., Benzeggagh, M. L., and de Charentenay, F.-X., "Mode I and Mode II Delamination of Thermosetting and Thermoplastic Composites", ASTM STP 1012 (1989) 251-269.
6. O'Brien, T. K., "Fatigue Delamination Behavior of PEEK Thermoplastic Composite Laminates", J. Reinforced Plast. Compos., 7 (1988) 341-359.
7. Hojo, M., Gustafson, C.-G., Tanaka, K., and Hayashi, R., "Mode I Propagation of Delamination Fatigue Cracks in CFRP", Advanced Materials for Severe Service Applications, Elsevier, (1987) 353-372.
8. Mall, S., Yun, K.-T., and Kochhar, N. K., "Characterization of Matrix Toughness Effect on Cyclic Delamination Growth in Graphite Fiber Composites", ASTM STP 1012 (1989) 296-310.
9. Crick, R. A., Leach, D. C., Meakin, P. J., and Moore, D. R., "Interlaminar Fracture Morphology of Carbon Fibre/PEEK Composites", J. Mat. Sci., 22 (1987) 2094-2104.

Microcomputer Aided Design for Composite Structures

G.Verchery

Mechanical & Materials Engineering Department
Ecole Nationale Supérieure des Mines de Saint-Etienne
42023 ST ETIENNE CEDEX 2, France

ABSTRACT

First the paper discusses the conditions to meet in order to develop an efficient and user-friendly program for the design of composite structures with micro-computers. The two-level design concept is explained : first, the structural level, then the material one. The approximating material concept is presented as a tool to solve the material-level design. Finally, the finite element aided structural design using fast re-analysis is examined and exemplified with a description of the main features and facilities of the FEAD-LASP program. Appendix 1 presents a new method of solution without boundary conditions for the singular equilibrium equations, which extends widely the re-analysis applicability and speed. Appendix 2 introduces the basic formulas defining distance and relative deviation concepts for plane anisotropic systems.

GENERAL PRESENTATION

Introduction

Finite element structural programs are presently available for main-frame, mini- and micro- computers. Many of them offer facilities for composite structures. They are primarily analysis tools, which means they have to operate with fixed data. Although very efficient in analysis, these classical finite element programs are not well suited for design, as design incorporates more or less massively modifications of the data in its process. While finite element analyses of structures might be currently used in the design process for isotropic homogeneous structures, for composite structures, the available performances of programs are generally not sufficient for design, due to the huge amount of data to deal with. General purpose finite element programs can be used directly to check the influence of only a limited number of data parameters. Coupling of such programs with optimization methods needs very large computing facilities, inducing costs and times unacceptable for most of the users. Finally, artificial intelligence methods are not yet effective, due to their present status as well as the small amount of available expertise to introduce in them.

Tentative definition of aided-design programs

In our opinion, a sensible approach should rely on fast simple programs devoted to typical applications. They could be used as an aid for preliminary design for structures or parts of structures (afterwards general purpose finite element programs could be used to assess and verify the global solution). At present, it seems not possible to include in these simple programs some automatic processes of design, so the control of the iterative design process should be let in the hand of the designer. With these limited aims, microcomputers appear of course as the convenient tool. Recent developments in microcomputer programming also permit to build programs which are user-friendly (interactive and self-explanatory) and portable. Finally, there is a special interest in significant decrease of computational time, in order to reduce the waiting times for the user : only seconds or a few minutes are acceptable in an interactive package. Special techniques of computation and simplifications of the studied parts must be used to obtain the required speed of treatment. The FEAD-LASP program described hereafter was developed according to these views.

The two-level design

The complete design problem for laminated composite structures is to determine the material itself : natures, thicknesses, orientations, stacking sequences of the plies. From a mathematical point of view, the optimal design can be obtained only by solving this problem, using optimization methods. However, due to the large number of variables, it is generally a very difficult task. On the other hand, good designs can be obtained in a much simpler way. The principle consists in splitting the design problem in first a structural problem with stiffnesses as variables to determine, then a material problem with laminate parameters as variables. Practically, the first level is the search of optimal or, more simply, improved structural properties. Then, the second step should be apparently the search of a material possessing the above structural properties, but such a problem may have no solution, or the solution may be too hard or too long to find. So the problem definition to retain is an extended one, which is the search of a material providing **exactly or approximately** the required stiffnesses. This definition is made possible by the concept of approximating material, explained hereafter.

Designing materials

The prediction of the effect of stacking sequences on stiffness properties of laminates generally is correctly solved by the classical laminated plate theory and its more sophisticated extensions or improvements. However, from the design point of view, very few general methods or results are available. Derived from a description of anisotropic properties of two-dimensional systems using a method of complex polar representation, some new methods for design of laminates with given stiffness properties have been introduced by the author, in various papers summarized in [1]. Further, with this method, a way was introduced to quantify the difference between two anisotropic materials, which allows to define the concept of anisotropic materials nearly equal. From this concept, available rules and methods can be extended to the design of laminates with nearly required properties, and new types of

materials, such as nearly quasi-homogeneous, nearly orthotropic, nearly isotropic materials, can be defined and extend widely the possible solutions for design problems.

THE FEAD-LASP PROGRAM

General Description of FEAD-LASP

The program FEAD-LASP (Finite Element Aided Design for Laminated and Sandwich Plates) was developed to give very fast analyses in order to make possible the design process of a structure through re-analyses under slightly modified conditions (loads, boundary conditions, materials properties). Speed in the analysis has been obtained by simplification of the analysed structure and limitations in its generality, improvements in the numerical methods used, selection of easy-to-use and efficient computers or micro-computers, use of user-friendly techniques. It is presently limited to the analysis and design of laminated and sandwich rectangular plates in linear elasticity. FEAD-LASP is structured with three main levels : i) a fully interactive data input module, ii) a fast finite element analysis module, and iii) an interactive re-analysis module. A more detailed presentation can be found in [2].

Interactive Data Input

The data input part was developed to be very easy to use and self explanatory, based on Macintosh-like interface techniques (using mouse, windows, pull-down menus for data input, verification and modification). The materials properties can take into account the characteristics of general laminated and sandwich plates (extended laminated plate theory, including in-plane, bending, bending-membrane coupling and transverse shear stiffnesses). However the geometry is limited to rectangular panels, which nevertheless covers a wide domain of practical needs. Finally, boundary conditions are given by specifying zero or prescribed displacements at nodes. Loads are not input at this level but in the re-analysis module.

Fast Finite Element Analysis

This module was developed from parts of a classical finite element program for plates in bending and in-plane deformation, with a 16-node thick plate element with transverse shear, in which the materials properties of the laminate or sandwich are input using an equivalent material. However, pre-defined regular meshes are used and a faster method for the formation and assembly of the stiffness matrices of the elements was derived and tested, using precomputation and storage of dimensionless parts of the stiffness matrix. This reduces the corresponding time very significantly,

Re-analysis Process

At present, the program incorporate efficient re-analysis facilities only for loading. The process is the following : first, 25 loading cases are solved simultaneously from the beginning (these cases correspond to concentrated normal unit force at each corner node of the elements). Any practical loading can be described as a linear combination of these 25 basic cases. For each loading, the data input process provides the 25 load coefficients and the solution is obtained by the same linear combination of the 25 basic

cases. This combination is almost instantaneous and the process can be re-applied by the designer as many times as required. Also, some current load cases, such as uniform pressure, gravity load, linear load, are pre-defined.

Computer Implementation

The program is written in Fortran 77 and operates on Apple Macintosh II microcomputers. Versions for IBM-PC/AT or compatible microcomputers and low cost work-stations (Apollo DN-3000 & DN-4000) are in development. To run the program satisfactorily, it is necessary to have a graphic display and an arithmetic coprocessor. The minimal required configuration for storage capacity is 10 Mbytes hard disc drive and 640 Kbytes of RAM memory. However a 20 Mbytes hard disc drive is recommended.

Developments in Progress

The implementation of automatic re-analysis for both loadings and displacement boundary conditions is currently developed. Though increasing somewhat the first analysis phase, it will improve the power and the speed of re-analysis. This method of re-analysis for displacement boundary conditions is based on the principle presented in the following Appendix for solving the singular linear equations of equilibrium for structures without prescribed displacements.

REFERENCES

- [1] Verchery G., "Designing with anisotropy", Textile Composites in Building Construction, Part 3, edited by P.Hamelin & G.Verchery, Pluralis, Paris, 1990, pp.29-42.
- [2] Aivazzadeh S., Ghazal A., Verchery G., Zidani F., Chu D., "Finite element aided design of laminated and sandwich plates", Proceedings of the Seventh International Conference on Composite Materials (ICCM 7, Guangzhou, China, 22-24 Nov. 1989), edited by Wu Yunshu, Gu Zhenlong & Wu Renjie, International Academic Publishers, Beijing, 1989, pp.346-351.
- [3] Verchery G., "Régularisation du système de l'équilibre des structures élastiques discrètes - How to solve the singular equilibrium system of discrete elastic structures", Comptes Rendus de l'Académie des Sciences, Paris, Vol.311, Series II, No 6, 13 Sept.1990, pp.585-589.

Please refer to these basic papers for complete analysis of the literature and detailed lists of references.

APPENDIX 1 - SOLVING STRUCTURAL EQUILIBRIUM WITHOUT BOUNDARY CONDITIONS

Taking advantage of the fact that the rigid body motions are the singularities of the equilibrium system of discrete elastic structures, this system can be solved prior to assigning the displacement boundary conditions. With this method, the re-analyses under various boundary conditions are made easier. This can be applied to aided design, which requires fast re-analysis processes for full efficiency. The theoretical principle is outlined hereafter.

The equilibrium system for discrete elastic structures

$$(A-1) \quad K u = f$$

is singular and the eigenvectors for the zero eigenvalue of the symmetrical positive stiffness matrix are the r rigid body motions. In the classical solving process, this system is modified using the prescribed displacement boundary conditions, which results in a regular system. Whereas it is then possible to solve for several right-hand-side loads, this process does not permit to change the displacement boundary conditions without coming back to the original system. The present method introduces a universal regularization, not dependent on particular boundary conditions.

Let R be the $n \times r$ matrix, the columns of which are the orthonormal eigenvectors for the zero eigenvalue :

$$(A-2) \quad K R = 0.$$

The condition for the system (A-1) to have solutions is :

$$(A-3) \quad R^T f = 0$$

which assesses the static equilibrium of the forces f . The regularized matrix K_a is defined as :

$$(A-4) \quad K_a = K + a R R^T.$$

which has the same eigenvectors as K and $R R^T$, with a as eigenvalue for the R eigenvectors. Consequently, this matrix is regular for any non-zero a , and the system

$$(A-5) \quad K_a v = f$$

can be solved. It can be shown that its solution is a particular solution to system (A-1), from which it is possible to express the general solution as :

$$(A-6) \quad u = K_a^{-1} f + R w$$

in which w is a r -parameter vector defining the actual rigid body motion.

This completes the solution for statically determinate structures. Further analysis is required for statically indeterminate structures, as the determinations of the load vector f and the rigid body motion vector w are required, prior to apply Eq. (A-6). The process is described in [3], together with details on the method.

APPENDIX 2 - DISTANCE CONCEPT IN ANISOTROPY

Polar notations

The polar notation for an elasticity type 2-D fourth order tensor T is introduced by the following relations between the

cartesian components and the polar components T_0 , T_1 , R_0 , R_1 , q_0 and q_1 :

$$\begin{aligned} T_{xxxx} &= T_0 + 2T_1 + R_0 \cos 4q_0 + 4R_1 \cos 2q_1 \\ T_{xxxy} &= R_0 \sin 4q_0 + 2R_1 \cos 2q_1 \\ T_{xxyy} &= -T_0 + 2T_1 - R_0 \cos 4q_0 \\ T_{xyxy} &= T_0 - R_0 \cos 4q_0 \\ T_{xyyy} &= -R_0 \sin 4q_0 + 2R_1 \sin 2q_1 \\ T_{yyyy} &= T_0 + 2T_1 + R_0 \cos 4q_0 - 4R_1 \cos 2q_1 \end{aligned}$$

Norms

The polar notation naturally induces a norm concept for tensors. As example, from the four polar components of an elasticity type 2-D fourth order tensor \mathbf{T} , we define a norm $N(\mathbf{T})$, invariant under changes of the frame of reference, equal to the square root of the weighted sum of the squares of the norms of these four polar components (the weights are related to the representation of general fourth rank tensors) :

$$\{N(\mathbf{T})\}^2 = (T_0)^2 + 2(T_1)^2 + |R_0 e^{4iq_0}|^2 + 4|R_1 e^{2iq_1}|^2$$

Distances

These mathematical concepts of norms help to quantify the difference between two anisotropic materials. This is done through the definition of distances between tensorial properties of two materials.

For elasticity type 2-D fourth order tensors \mathbf{T}' and \mathbf{T}'' , the distance between two materials is defined as the norm $N(\mathbf{T}' - \mathbf{T}'')$ of the difference tensor $\mathbf{T}' - \mathbf{T}''$.

Obviously, when $N(\mathbf{T}'' - \mathbf{T}') is equal to zero, then the two tensors \mathbf{T}' and \mathbf{T}'' are identical, which means that the two materials are identical from the point of view of the property described by these tensors.$

Relative deviation

As the distances are obviously dependant on the system of units in use, it is usefull to further introduce the relative deviation between two materials, as the ratio of the distance to the norm of one of the tensors :

$$D(\mathbf{T}', \mathbf{T}'') = N(\mathbf{T}'' - \mathbf{T}') / N(\mathbf{T}')$$

These non-dimensional quantities are well suited to quantify the difference between the two materials. Specially, if these deviations are less than a small quantity (.01 or .001 for instance), the difference between the tensors is small and we designate such materials as nearly equal materials for the corresponding physical property.

Notch Sensitivity of Aramid Unidirectional Composites

S. Bando^{*}, M. Ohno^{**}

^{*}Helicopter Engineering Dep., Aerospace Engineering Division,
Kawasaki Heavy Industries, Gifu 504, Japan

^{**} Materials & Process Engineering Section, Engineering Department,
Kawajū Gifu Engineering, Gifu 504, Japan

ABSTRACT

In the case of the fatigue strength of the aramid unidirectional composite, high notch sensitivity was found out.

On the contrary, the static and fatigue strength of the glass composites and the static strength of the aramid composites has no or less notch sensitivity. By 3 dimensional FEM analysis combined with the tensile and interlaminar shear fatigue test results, this phenomenon can be well explained.

INTRODUCTION

In general, unidirectional composites are believed to have a low notch sensitivity and used for helicopter rotor system.

In order to design a light weight rotor by using aramid fiber, we conducted the tensile fatigue test of notched and unnotched coupon test specimens, which consist of 20 ply laminates and ply orientation was $[(\pm 45^\circ)/0^\circ]_s/(\pm 45^\circ)_s$.

We found out the very high notch sensitivity (Fig.1) and fiber failure mode along the transverse direction at high cycle region (Fig.2) in aramid composites.

But, in the case of glass composites, we found out the low notch sensitivity (Fig.3) and shear failure mode along 0° direction (Fig.4).

To understand these phenomenon, we have conducted the tensile fatigue test and the short beam shear fatigue test by unidirectional coupon specimen, and also analyzed the stress distribution by 3D-FEM around the hole of the notched specimen.

As the results of these analysis, in the case of glass composites, we found out that the shear failure is likely to occur near the hole and the stress concentration will disappear (Fig.5).

But on the contrary, tensile failure is likely to occur in aramid composites (Fig.6).

As shown in Fig.8, actual notch effects of aramid composites were complicated. From the static strength to 10^4 cycle region fatigue strength, the strength was nearly equal to the estimated value of the Point Stress Criteria (Fig.7). But in high cycle region, fatigue strength reached to the estimated strength based on Peak Stress Criteria.

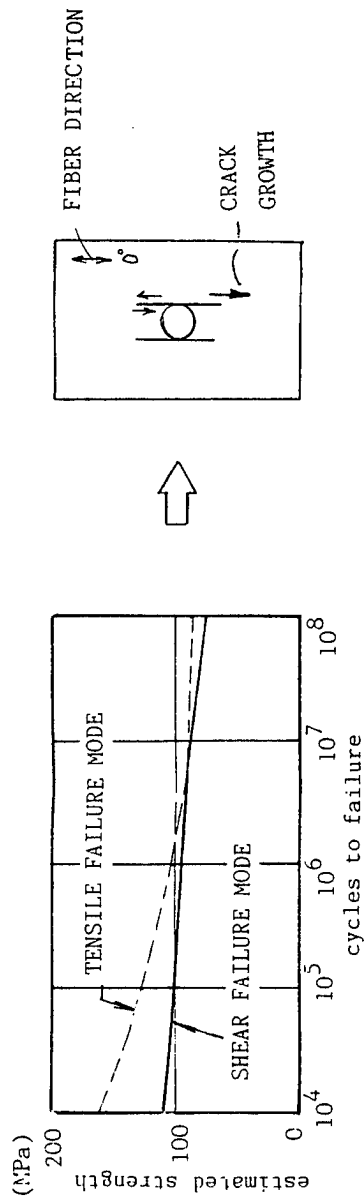


Fig. 5 Estimated failure mode of notched glass unidirectional composite specimen

GLASS COMPOSITE FAILURE MODE ; TENSILE STRENGTH IS STRONGER THAN THE SHEAR STRENGTH, THEN THE SHEAR FAILURE LIKELY TO OCCUR.

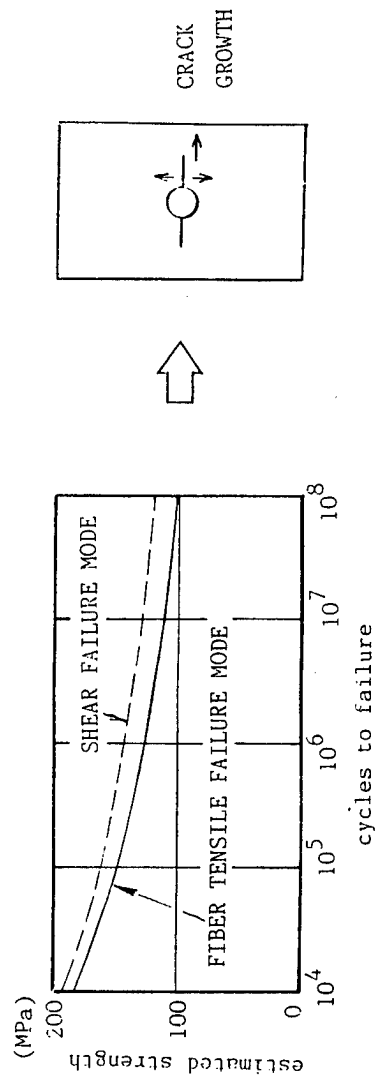


Fig. 6 Estimated failure mode of notched aramid unidirectional composite specimen

ARAMID COMPOSITE FAILURE MODE ; SHEAR STRENGTH IS STRONGER THAN THE FIBER STRENGTH, THEN THE FIBER FAILURE LIKELY TO OCCUR.

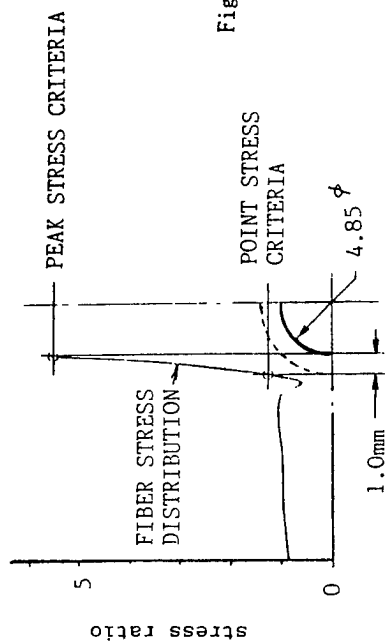


Fig. 7 Point stress criteria and peak stress criteria

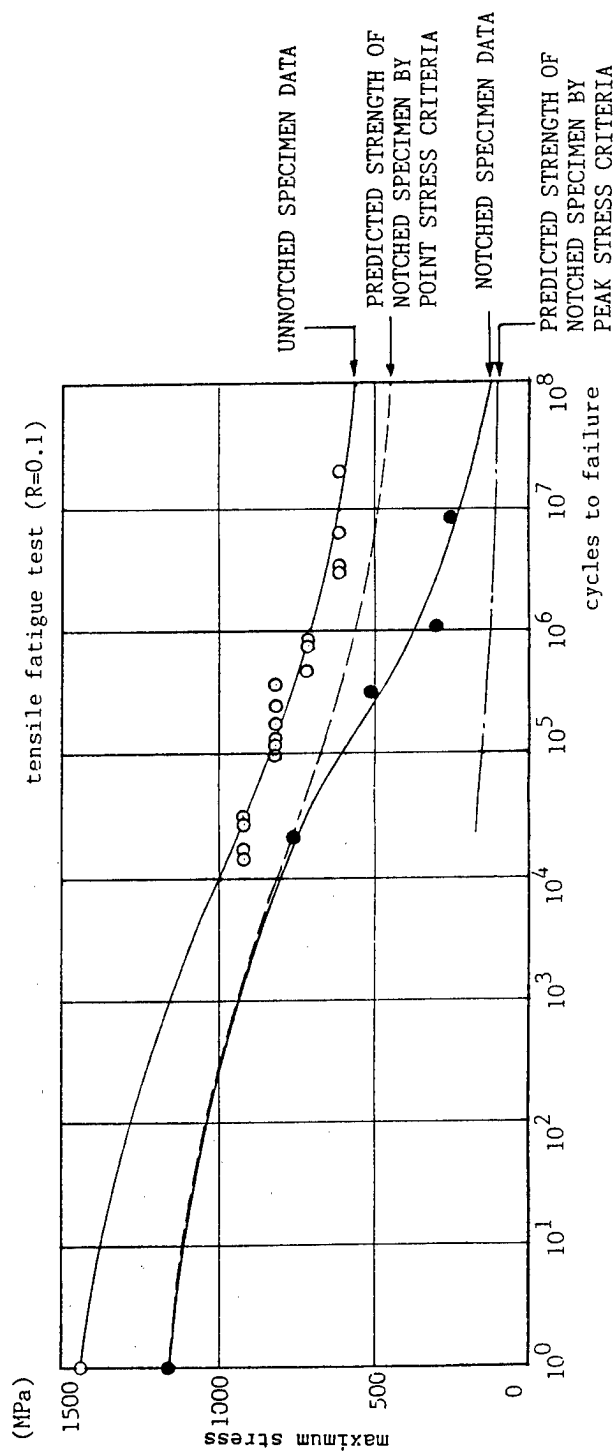


Fig. 8 Comparison between the estimated strength and the test data of notched aramid composite

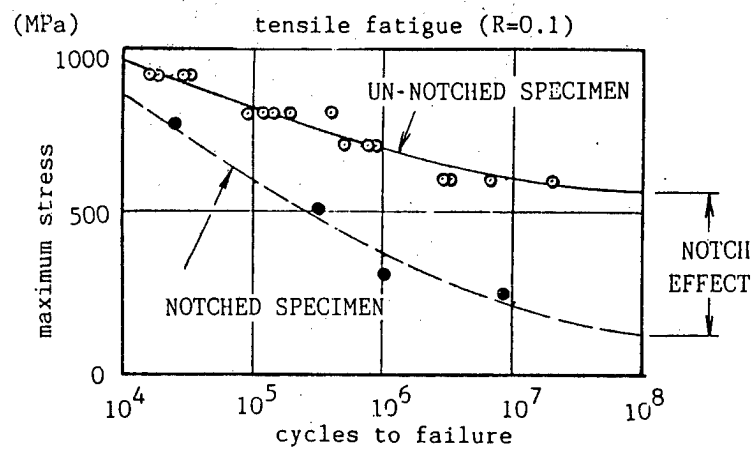


Fig.1 Tensile fatigue test results
of aramid fiber composite
exhibits high notch sensitivity

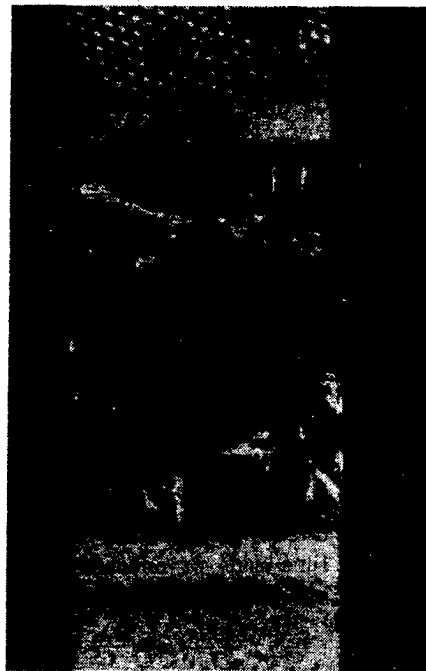


Fig.2 Failure mode of notched aramid
specimen (fiber failure)

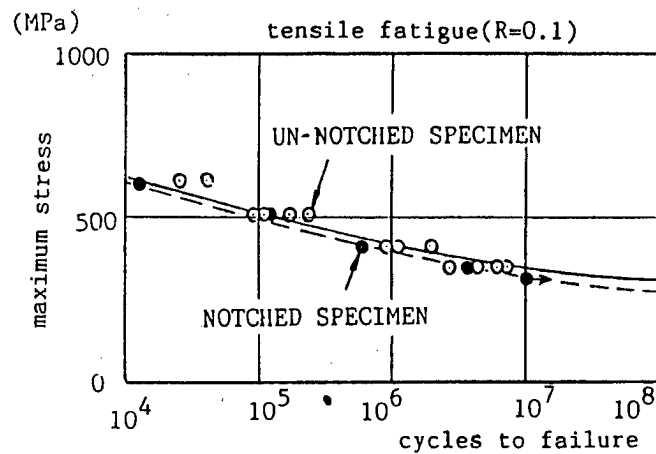


Fig.3 Tensile fatigue test result of glass fiber composite shows low notch sensitivity

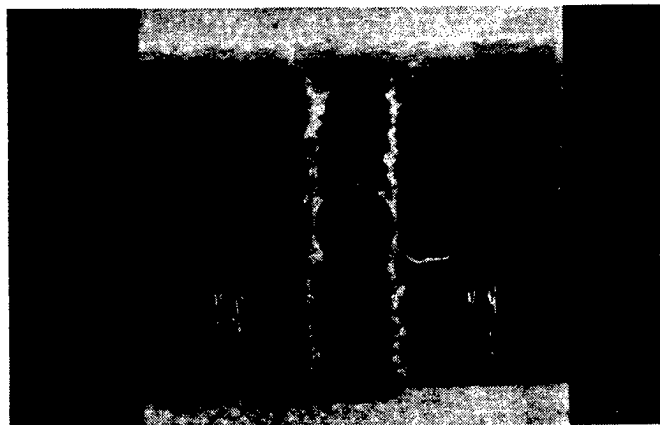


Fig.4 Failure mode of notched glass specimen (shear failure)

A DAMAGE STATISTICAL MICROMECHANICS MODELIZATION TO A DISCONTINUOUS REINFORCEMENT COMPOSITE ALUMINUM-CARBON.

PH. BREBAN, D. BAPTISTE, D. FRANCOIS

Laboratoire de Mécanique des Sols Structures et Matériaux,
CNRS - URA 850
Ecole Centrale Paris, Gde Voie des Vignes,
92295 Châtenay Malabry CEDEX, FRANCE

Abstract - A new solid phase coextrusion process to manufacture metal matrix composites has been developed. As part of this study, the influence of following parameters on the behavior and damage mechanisms of the composite was investigated : aspect ratio of the fibers, orientation of reinforcement and local concentration distribution. This has been achieved through an equivalent inclusion analytical approach based on a micro-macro modelization. The prediction of the elastic constants, the coefficients of thermal expansion and the yield criterion can be determined from the microstructure. Finite element calculations complete this model by computing a three phase basic cell. The influence of the distribution of fibers on the development of local plasticity has been demonstrated. It appears that the configuration of fibers side by side has a dramatic effect on the propagation of damage which occurs at the fiber tip. An analytical criterion for damage initiation has also been suggested. These results are compared with in situ tensile tests performed inside a scanning electron microscope, where every stages of the failure mechanism can be observed.

NOMENCLATURE

Σ	=	macro-stress field applied to the elementary representative volume (ERV)
E	=	macro-strain field in the composite corresponding to Σ
σ	=	disturbed stress field
D	=	total volume of the ERV
$\langle \cdot \rangle_V$	=	average quantity over the volume V
C_m	=	elastic characteristics of the matrix
C_f	=	elastic characteristics of the fiber
E_0	=	strain field related to Σ
\bar{E}	=	strain field related to the average value of σ over the matrix volume
e^*	=	eigenstrain in Eshelby's theory
l/d	=	length to diameter ratio of the fibers

INTRODUCTION

Most of discontinuous metal matrix composites (DMMC) studied at the moment are manufactured by three main technologies [1]:

- Squeeze- casting
- Compo-casting
- Powder metallurgy

But the relatively high cost of these processes restricts the field of their application. To prevent this limitation, we have improved a solid phase coextrusion process in order to obtain in a single operation a discontinuous fibers composite. This technology has been developed with an aluminum matrix reinforced by T300 graphite fibers (diameter, 7 μ m). When increasing the rate of reinforcement (15 to 30% in

volume), some difficulties were noticed to impregnate the tows of fibers. One solution is proposed which consists in the infiltration of 5 to 10 mm long fibers with a technology near to the one of powder metallurgy. The final product presents bundles of fibers well infiltrated by the matrix, but not evenly distributed in the aluminum. The mechanical properties are subsequently improved compared to the matrix. The longitudinal Young's modulus is 25% higher, and the strength to failure is two times more important.

In order to better improve the mechanical properties by controlling the manufacturing parameters, the influence of the microstructure has been evaluated through an analytical modelization. The major drawback of this approach is that it does not take into account the thermoelastoplastic behavior of the matrix. Finite element calculations were developed on different three phases basic cells to complete the model and better understand the appearance and evolution of damage related to the local geometrical distribution of fibers. The poor effect of fibers side by side has been displayed. A damage initiation criterion based on physical observations has been suggested through the comparison of residual stresses and the local stress field around the fiber when loading the composite.

The achieved results were compared with in situ tensile tests performed in the SEM. A good agreement between calculations and experiments is noticed.

MICROSTRUCTURE OF THE COMPOSITE

The material selected for the experiments is a 1050Al (A5) - 20vol.% T300 carbon fibers reinforced metal-matrix composite. It was extruded at low speed and high temperature according to the developed process. The final product is a plate of rectangular section ($40 \times 7 \text{ mm}^2$). The material presents a good impregnation of fibers even in the middle of bundles (figure 1). The aspect ratio of fibers (length divided by diameter) is relatively small, about 5 in average. This parameter can be related to the geometry of the flow in the die, and it appears here not to have been optimized. An important heterogeneity of local volume fraction can also be noticed with some areas almost free of reinforcement and others with more than 50vol.%. The last important point to be remarked is the large distribution of orientation of the fibers compared with the extrusion axis (vertical on fig. 1). This disorientation occurred principally in the plane of the plate. Thus tensile properties of the composite are not optimal in the extrusion direction, but are improved perpendicularly.

ANALYTICAL MODELIZATION OF THE COMPOSITE BEHAVIOR

The important anisotropy of carbon fibers requires a three dimensional approach taking into account all the coefficients of the stiffness matrix. An equivalent inclusion method based on Eshelby's theory [2] has been chosen. Among different models inspired by the self consistent scheme, TANAKA and MORI's model, presented by TAYA [3] in the case of metal matrix composites, appears to give an explicit and relatively simple solution to the modelization of discontinuous metal matrix composites. It had been tested previously on a 2124Al-25vol.% SiCw composite with a good agreement with experiments. An attempt is made to clarify and generalize this approach in term of a micro-macro relationship.

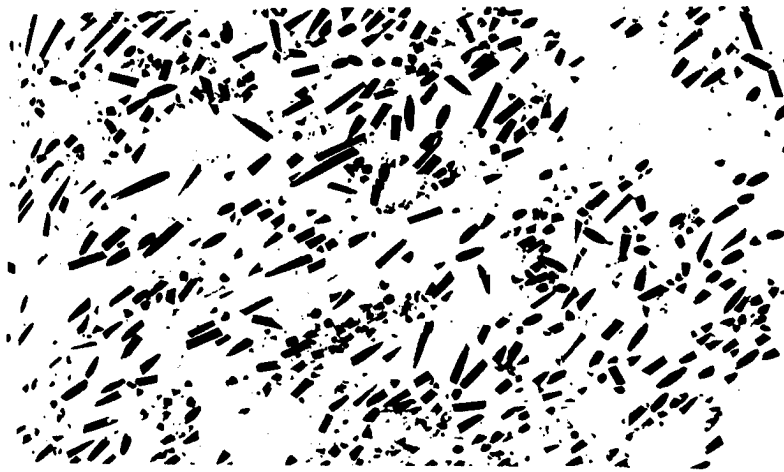


Fig. 1. Distribution of fibers in the studied composite.

The macro scale corresponds to the elementary volume representative of the structure. This volume includes all microstructural parameters such as distribution of fiber length, disorientation of the reinforcement and local heterogeneity of volume fraction. The cell is submitted to a uniform macro-stress Σ . The presence of numerous fibers disturbs locally the uniform stress field. Thus the total stress field at any point of the space can be decomposed into the uniform and disturbed stress fields (σ). These two stresses can be associated to strain fields through the stiffness tensor of the matrix (we assume that the properties of the aluminum in the matrix are the same as the control metal) :

$$\Sigma = C_m E_0$$

$$\langle \sigma \rangle_{D-\Omega} = \frac{1}{D-\Omega} \int_{D-\Omega} \sigma dV = C_m \bar{E}$$

where $\langle \rangle_{D-\Omega}$ denotes the average quantity over the matrix volume (D total volume, Ω fiber volume). The evaluation of σ requires to write the behavior of a single fiber surrounded with the others. Let us introduce at the micro scale a short fiber characterized by its stiffness, aspect ratio and orientation in a small volume of matrix. The constitutive equation completed with the equivalent inclusion theory provides a relation of localization where e^* represents the eigenstrain.

$$e^* = Q(1/d, \theta, \varphi, C_m, C_f)(E_0 + \bar{E})$$

Q is the localization tensor which only depends on the characteristic parameters of this fiber and of the matrix.

The homogenization consists in writing that the disturbed stress field vanishes in average over the entire volume of the composite.

$$\int_{D-\Omega} \sigma dV + \int_{\Omega} \sigma dV = 0$$

The problem can then be solved. The total strain field E associated to the uniform stress field Σ is determined

$$E = E_0 + \frac{1}{D} \int_{\Omega} e^* dV$$

The linear relation between Σ and E gives the stiffness matrix of the composite.

RESULTS

Effect of fiber aspect ratio

In the particular case where all fibers are well oriented and identical, the previous equations become very simple. This formulation is first used to predict the effect of variable aspect ratio on longitudinal and transverse Young's modulus for different composites. Figure 2 presents the curves obtained for a 2124Al-20vol.% SiCw composite (2-a), a 2024Al-20vol.% C composite (2-b) and the studied material (2-c). The difference of reinforcement between an isotropic fiber (SiC) and a greatly anisotropic one (Carbon - [4]) is shown on the first two diagrams. An important point to be noticed is the saturation of the curve for a lower threshold in the case of carbon fibers. Beyond an aspect ratio of 15 no significant increase of the elastic properties has to be expected. The very low transverse modulus of T300 carbon fibers has an important impact on the longitudinal modulus of the composite. The two last diagrams compare two different matrix with no important differences. The influence of the properties of fibers appears to be predominant on the elastic characteristics of the composite.

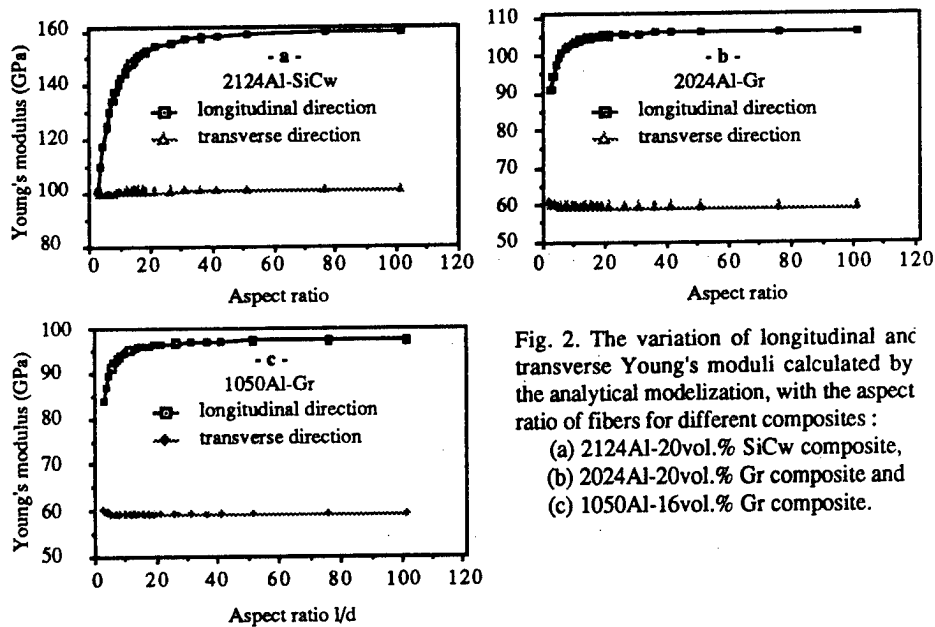


Fig. 2. The variation of longitudinal and transverse Young's moduli calculated by the analytical modelization, with the aspect ratio of fibers for different composites :
(a) 2124Al-20vol.% SiCw composite,
(b) 2024Al-20vol.% Gr composite and
(c) 1050Al-16vol.% Gr composite.

Effect of fibers disorientation

Other developments of the same formulation can be made, such as the effect of scattered fiber aspect ratio [5], but the most important microstructural parameter is the disorientation of fibers. TAYA and al.[6] have studied the effect of a distribution of orientation on the longitudinal Young's modulus. The developed formalism allows the same study on all the coefficients of the stiffness matrix. We represent on figure 3 the evolution of the longitudinal and transverse modulus with different distribution for the studied composite. In our case, the disorientation occurs symmetrically in the plane of the plate so that we only consider one angle of disorientation. The results show that this parameter cannot be neglected, excepted for narrow angle distributions (less than 20° of disorientation). The diagram of figure 4 presents the half of a theoretical distribution

which gives the same results as experimental measurements. The left side corresponds to the well oriented fibers owing to the extrusion process, when the uniform part represents the randomly oriented fibers prior to manufacturing. Thus, a criterion to measure the efficiency of the extrusion process has been pointed out, taking into account that an efficient extrusion has to rub the uniform part.

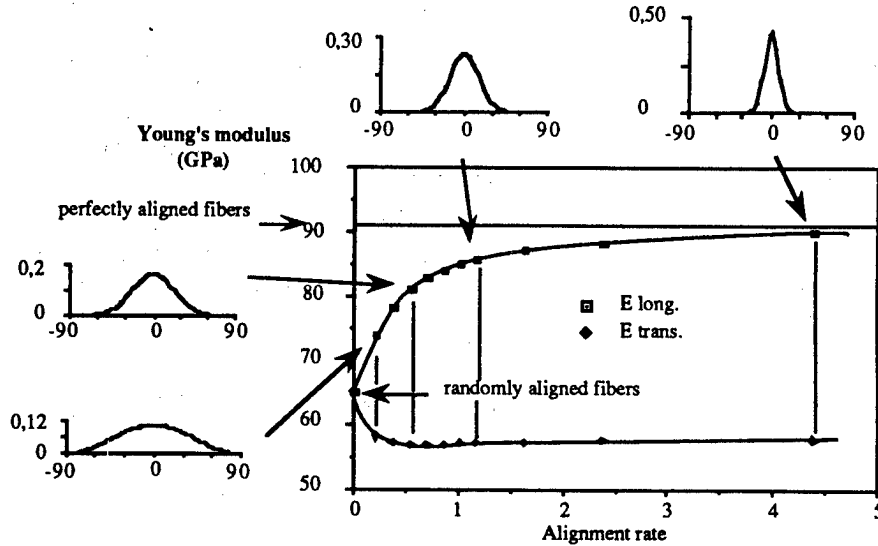


Fig. 3. The variation of longitudinal and transverse Young's moduli of the studied composite, calculated by the analytical modelization, with a characteristic parameter of the narrowness of the fiber angle distribution. Different distributions representing the fiber fraction with a given disorientation are presented.

Effect of local volume fraction

The last microstructural parameter to be modelize is the effect of a local volume fraction distribution. This has been achieved through the introduction at the micro-scale of a term of short range interaction between the fibers (δ^*). δ^* corresponds to the difference between the eigenstrains calculated with the local volume fraction and the average one.

$$\delta^* = e^*(f_i) - e^*(f)$$

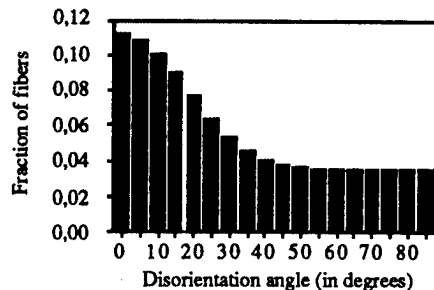


Fig. 4. The half of a theoretical fiber angle distribution which gives the same results as the experimental tests.

Figure 5 shows the evolution of longitudinal and transverse moduli with the main volume fraction, for a given distribution. All the points correspond to the same average fiber rate. The longitudinal modulus exhibits a small decrease when increasing

obtained for the 2124Al-20vol.% SiC_w are in good agreement with measurements made by CHAMBOLLE [9] with an average aspect ratio of the whiskers of 5. For longer fibers, this model seems to overestimate the axial flow stress, mainly because it neglects the initiation of local plasticity around the fibers due to residual stresses. The very small incidence of the aspect ratio on the transverse properties can be noticed. The two last diagrams display the influence of the matrix alloy which is much more important in this case. Figure 7 presents the influence of thermal residual stresses on the yield criterion. We can verify that the matrix is initially in tension at least in the fiber axis. The important coupling between longitudinal and transverse directions explains the behavior perpendicularly to the fibers.

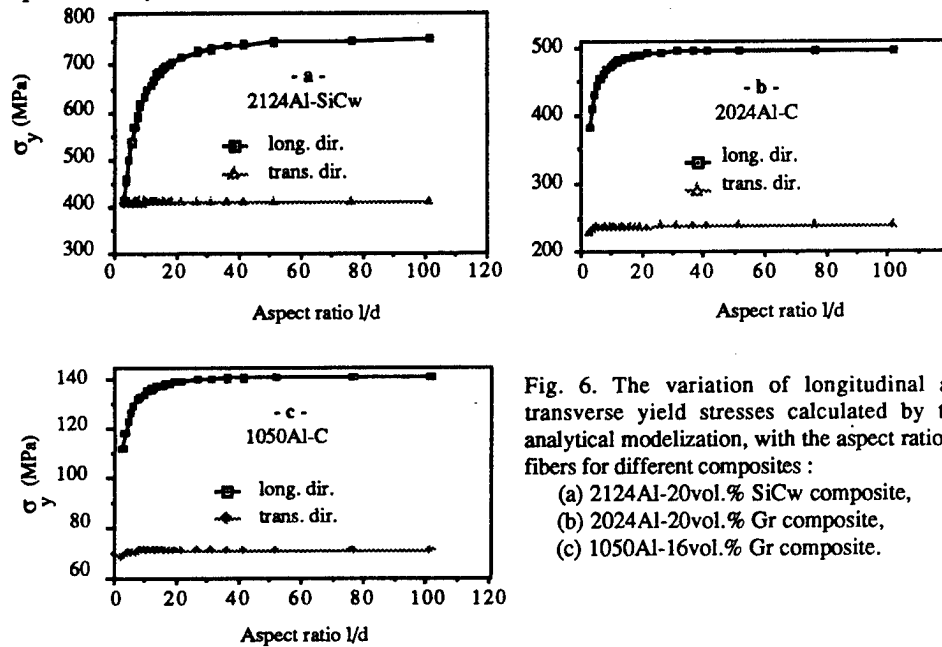


Fig. 6. The variation of longitudinal and transverse yield stresses calculated by the analytical modelization, with the aspect ratio of fibers for different composites :

- (a) 2124Al-20vol.% SiC_w composite,
- (b) 2024Al-20vol.% Gr composite,
- (c) 1050Al-16vol.% Gr composite.

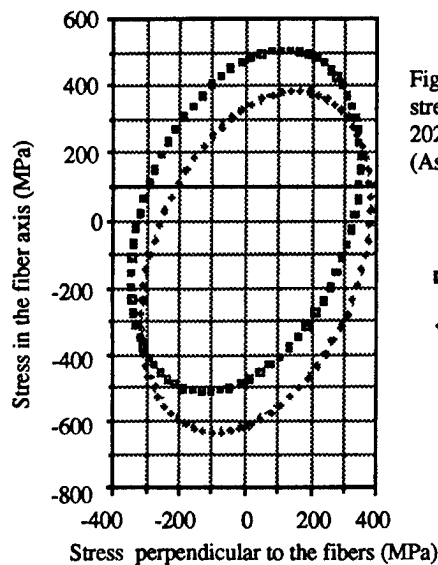


Fig. 7. Influence of the residual stresses on the yield surface of a 2024Al-20%vol. Gr composite. (Aspect ratio of fibers $l/d = 10$).

- without residual stresses
- ◆ with residual stresses

the fiber volume fraction in the bundles. The effect on the transverse one appears to be neglectable. Nevertheless this parameter is less important than the disorientation of fibers.

Extensions of the modelization

An extension of the modelization was carried out by TAYA and al. [7] to calculate the coefficients of thermal expansion (CTE). The previous generalized formulation is also extended to thermal loadings. The evolution of the CTE in the longitudinal and transverse directions with the volume fraction of fibers for two different aspect ratios has been calculated. In the particular case of carbon fibers, the increase of transverse thermal expansion for composites with 25vol.% of fibers is noticeable. The value exceeds the CTE of the matrix and can set a problem for an application requiring dimensional stability. The influence of the fiber aspect ratio is negligible. Thermal residual stresses have also been calculated. This model gives no influence of this stress field on the elastic constants but displays a translation of the threshold surfaces.

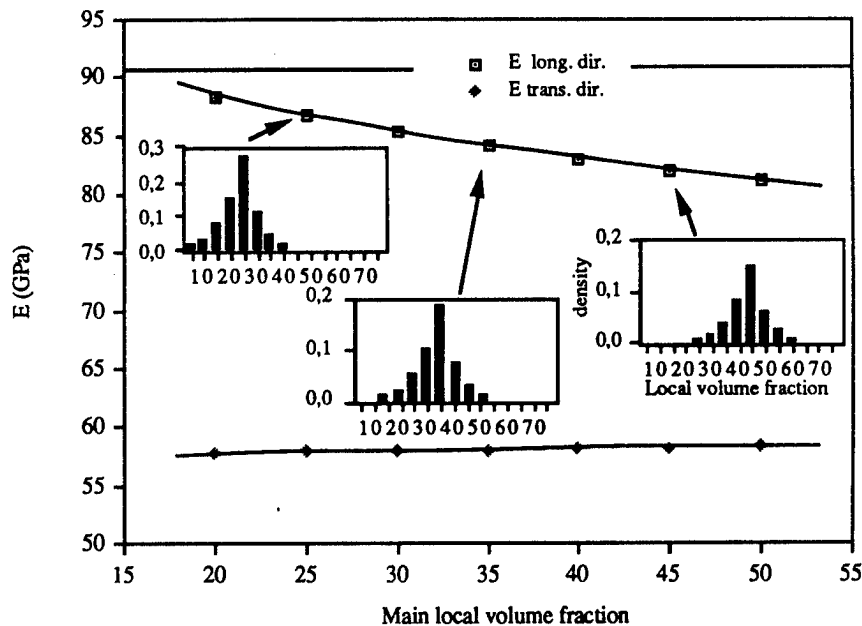


Fig. 5. The variation of the longitudinal and transverse Young's moduli with a distribution of local volume fraction. Each case corresponds to the same average volume fraction (20%).

The last extension to be presented here is the calculation of the Hill criterion for plasticity. The experiments on DMMC have shown that strain localization involving local plasticity appears at very small stresses near fiber tips without generating a macro plasticity. So a yield criterion has to take into account the average stress over the matrix volume. An attempt was made by W. J. CLEGG [8] to modelize the tensile behavior of particle reinforced MMC with a similar approach, using a Tresca criterion for the matrix and involving elastic residual stresses. The aluminum is supposed here to plastify according to a Mises criterion. When the stress $\Sigma + \langle \sigma \rangle_{p,q}$ reaches the flow limit, the Hill criterion is assumed to be verified by the composite. Yield stresses in longitudinal and transverse directions for the same three different composites as previously described, are presented figure 6. The shape of the curves is identical to the evolution of the Young's moduli, with the same saturation for a threshold value of the aspect ratio. Results

APPROACH TO DAMAGE MODELIZATION

Experimental observations

In situ tensile tests on micro-samples have been performed in a SEM, in order to identify the physical parameters of damage. The sample was chosen for its large distribution of local volume fraction, at least at the surface. The different steps of damage can be listed :

- + strain localization in the bundles of fibers,
- + cavity nucleation at the fiber tips,
- + cavity growth and coalescence,
- + crack propagation with a plastic area in front of the crack tip.

We measured the load during the test which allows us to correlate the observations to the macro-tensile behavior (figure 8). Cavity nucleation just begins when the stress reached the macro-yield stress of the composite.

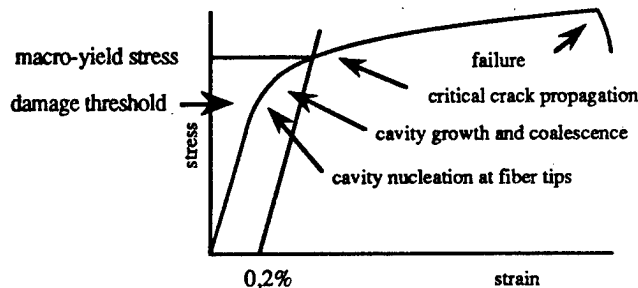


Fig. 8. The different steps of damage propagation correlated to the macro behavior of the studied composite.

Analytical approach

We are able to calculate the residual stresses at the fiber interface. Fracture surfaces show that no reaction occurred during the manufacturing process between carbon and matrix; so only residual stresses assure the binding of fibers. When an external load is applied to the composite, the stresses just outside the fiber can be obtained by a relation depending on the stress inside the fiber and the eigenstrain [15].

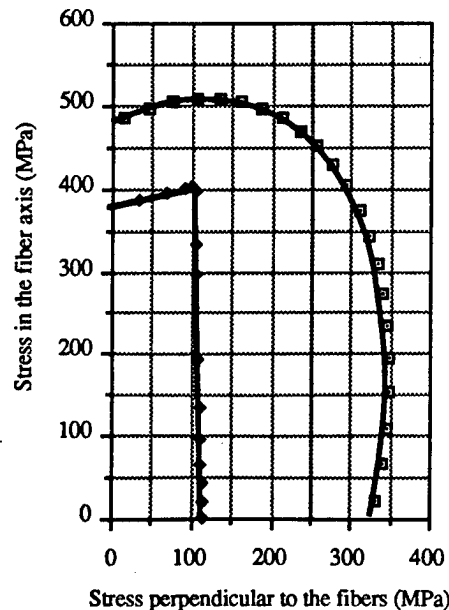


Fig. 9. Comparison between the yield criterion and the damage threshold calculated by the analytical approach for a 2024Al-20%vol. Gr composite

- ◆ Damage threshold
- Yield surface

The damage threshold is supposed to be reached when the normal stress to the considered point of the interface is equal to the residual stress. Thus, a single criterion allows the modelization of an anisotropic phenomenon as presented figure 9. We can see a critical angle corresponding to the transition between the interface at the fiber tip and the one along the fiber. The comparison between the yield and damage surfaces presents a good agreement with figure 8.

In the particular case of perfectly aligned and equi-distributed fibers, figure 10 shows an increase of the damage stress in the longitudinal direction with the fibers aspect ratio. This parameter has a small influence on the transverse direction. The critical angle also varies with the length to diameter ratio of the fibers. The approximate value of this angle corresponds to the acceptable disorientation angle of the fibers in the case of elasticity ($\sim 20^\circ$). Figure 11 presents the evolution of the damage threshold surface with the fiber volume fraction for a composite with a fiber aspect ratio of 10. The decrease of the damage stress in both longitudinal and transverse directions with the reinforcement rate is noticeable. This tends to confirm the fact that damage first appears in the areas with an important local volume fraction.

In order to clarify this point, we have introduced in the calculation of the damage threshold surface the effect of a distribution of local volume fraction. We have plotted figure 12 the damage stress, for a given distribution, in different tensile directions. The shape of the concentration distribution has a negligible influence. Thus, the influence of rich in fibers areas is clearly demonstrated.

This approach displays the important influence of the local volume fraction in the damage initiation of a metal matrix composite.

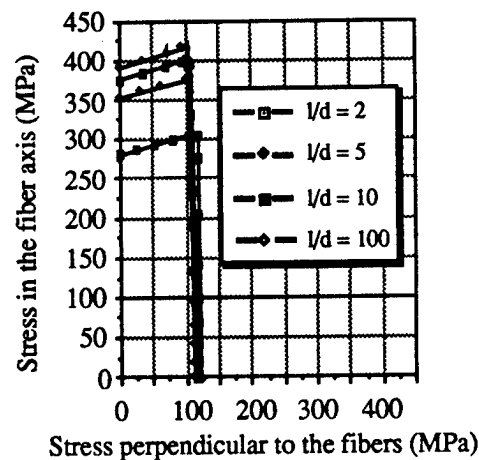


Fig.10 : Evolution of the damage threshold surface with the fiber aspect ratio for a 2024Al-Gr composite with a fiber volume fraction of 20%

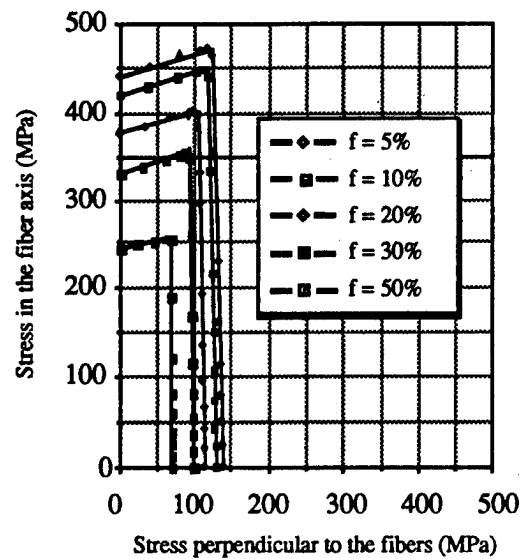


Fig.11 : Evolution of the damage threshold surface with the fiber volume fraction for a 2024Al-Gr composite with a fiber aspect ratio of 10

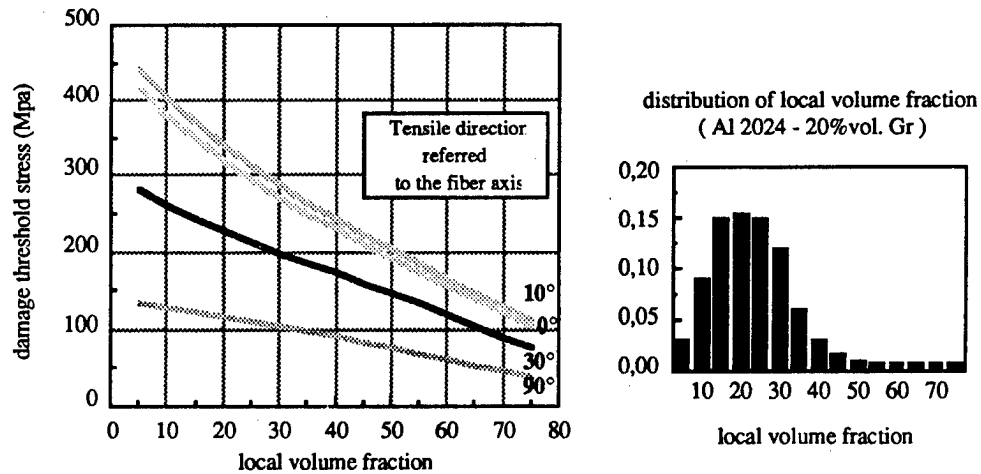


Fig.12 : Evolution of the damage threshold surface with the tensile stress orientation for a 2024Al-Gr composite with a given distribution of local volume fraction

Since we know the relation between the local volume fraction density and the damage stress, we determine the proportion of damaged material as a function of the applied stress. (figure 13)

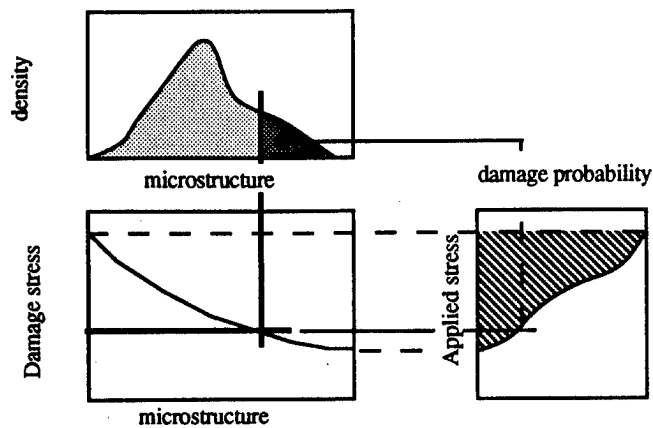
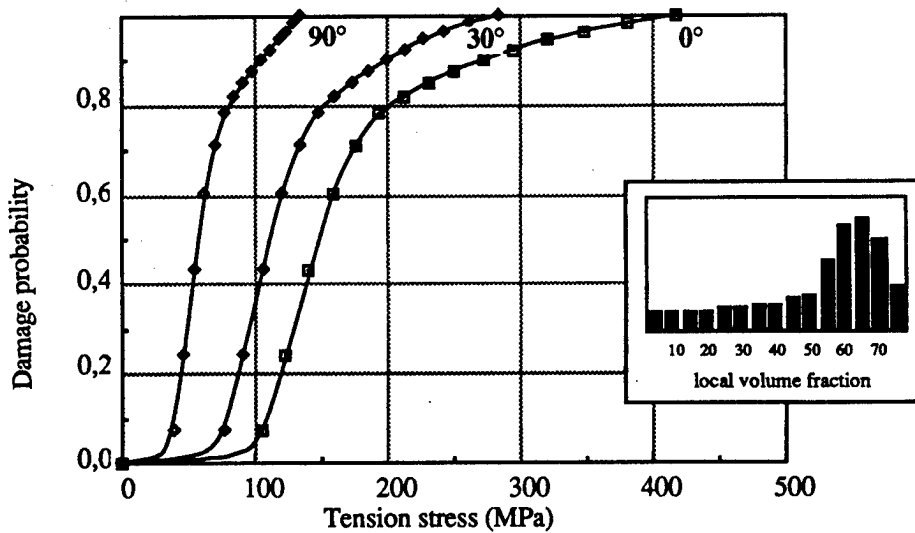


Fig 13: Method to calculate the damage probability.

We present, on figure 14, for different orientation of the tensile stress, the damage probability, considering two different distributions of the local volume fraction, but with the same macroscopic volume fraction. We point out the importance of the shape of the distribution on the mean value and the scatter of the damage stress. The anisotropy in the different directions is also well taken into account.



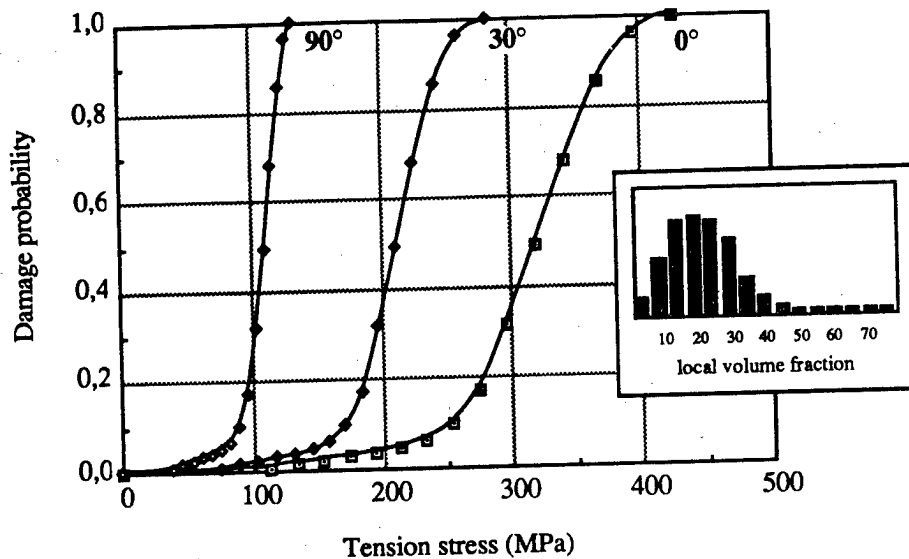


Fig.14: Damage probability as a function of the applied stress for different directions of loading and two local volume fraction distributions.

We point out the importance of the shape of the distribution on the mean value and the scatter of the damage stress. The anisotropy in the different directions is also well taken into account.

Numerical approach

A more accurate modelization of the behavior of these composites requires to take into account the thermoelastoplastic behavior of the matrix, and to predict the evolution of damage, which is different for particle and short fiber reinforcement [10]. An attempt is made to study the influence of the distribution of short fibers ($l/d=10$) on the last point.

A numerical approach has already been undertaken by CHRISTMAN and al. [11] on two phases basic cells. In a first computation, the circular cylindrical cell around the fiber was required to remain a circular cylinder throughout the deformation history. According to TVERGAARD [12], this approximation is close to a 3D periodic homogenization. The modeled behavior overestimates the experimental one. A second set of boundary conditions consists in maintaining the outside of the cylinder stressfree. This underestimates the experimental results. An in-between situation has been investigated by surrounding the matrix phase with a third phase constituted by the equivalent homogeneous material. We assumed an infinite strength for the fiber-matrix interface.

Six different axisymmetrical basic cells have been computed. Each one contains the same volume fraction of reinforcement even at the local scale. The first five ones contain a T300 carbon fiber ($l/d=10$), the last one is reinforced by an equivalent homogeneous composite with 50 vol.% of fibers which represents a bundle of fibers well infiltrated. The reinforcement phase is surrounded with a 2024 aluminum alloy. The proportion of matrix "seen" by the fiber tip decreases along the cells, excepted for the last one. The behavior of fibers is anisotropic elastic. The one of the matrix is isotropic thermoelastoplastic with non linear kinematic hardening. The behavior of the EHM is anisotropic thermoelastoplastic with linear kinematic hardening. The different coefficients of the EHM were calculated by the analytical model.

Each cylinder was cooled from manufacturing temperature to room temperature in order to take into account the residual stresses. Then the cells were loaded in tension. By measuring the mean stress and the displacement for different steps of loading at the top frontier between the matrix and the EHM, we can plot a micro behavior curve which includes the cooling and the tension loading. The evolution of the thermoplastic behavior must be noticed, but with a poor impact on the elastic part. We can remark a change in the sign of residual stresses when the fiber tip does not see a lot of matrix. This situation is near to a configuration of continuous fibers which can explain the observed compressive stresses.

The slope of the curve at the beginning of the mechanical loading gives a local Young's modulus. This has been plotted figure 13 as a function of the thickness of matrix between two neighboring fibers. The configuration of fibers which corresponds to the composite modelization is also mentioned :

- 1- a situation of fibers close to their neighbors,
- 2- a homogeneous distribution,
- 3- a close tip to tip fibers configuration.

The value obtained for a bundle of fibers is also indicated.

We study the development of plasticity in an average configuration. Plasticity first extends in the matrix along the fiber. Then the EHM starts yielding at the bottom of the cell. This rapidly stops to continue at the top of the fiber with an important localization near the fiber tip . The maximum value of the equivalent plastic strain near the fiber tip, for a same macro-stress corresponding to the macro yield strength of the composite, has been plotted on the same kind of diagram as on fig.15 (figure 16). The main directions for plasticity development have also been shown.

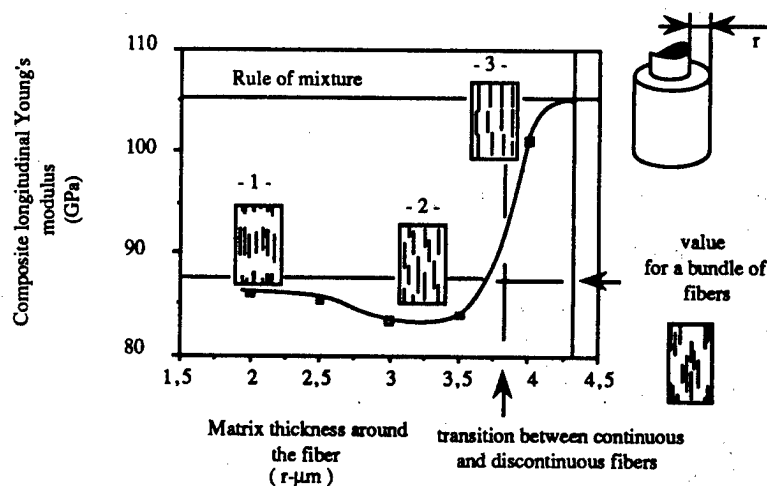


Fig. 15. The variation of the local longitudinal Young's modulus given by the numerical approach, with the matrix thickness around the fibers.

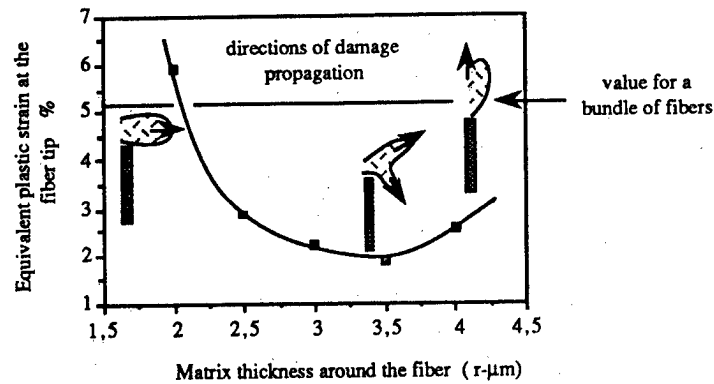


Fig. 16. The variation of the maximum equivalent plastic strain at the fiber tip given by the numerical approach, with the matrix thickness around the fibers. All these values are measured for the same stress level corresponding to the macro yield stress of the composite.

DISCUSSION

LEMAITRE [13] has shown that the damage parameter D was linearly dependent on the equivalent plastic strain. So we qualitatively explain fig.14 in terms of initiation and propagation of damage. The better situation is clearly the middle one. Fibers close to their neighbors are much more sensitive to plastic localization and damage occurs more rapidly. The evolution of damage as determined by the finite element model has also been sketched for each configuration. The left one shows a propagation perpendicularly to the fiber axis. The middle one presents two major directions correlated to the propagation of shear bands. For the third one, the evolution occurs along the fiber axis.

Both figures 15 and 16 show that a bundle of fibers can be represented by a configuration of fibers close to their neighbors.

According to LEMAITRE [14], the plastic strain threshold for initiation of damage in such aluminum alloys is 3%. This limit is only exceeded in the bundles of fibers. Such conclusions have to be moderated by the fact that the matrix is not exactly in the same metallurgical state as the control alloy but microhardness values obtained by CHRISTMANN and al. [11] have suggested that the same mechanical characteristics can be adopted which has been done here for both modelizations.

The fracture surfaces observation shows a difference between areas of bundled fibers and isolated ones. We can check (Figure17-a) that the damage has locally propagated perpendicularly to the fiber axis when an isolated fiber displays a propagation along the matrix interface fig. 17-b. This tends to confirm the calculated directions of damage propagation.

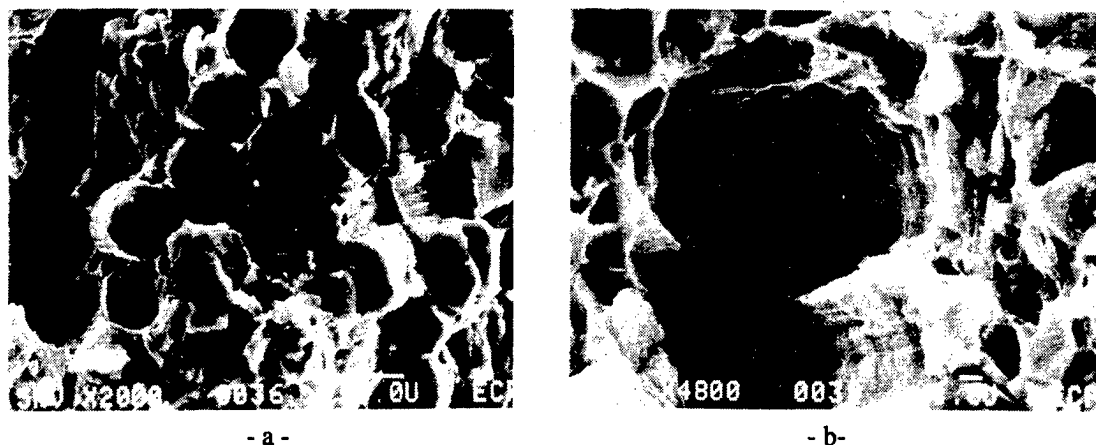


Fig. 17. Fracture surface morphology in different areas, (a) fibers near to their neighbors and (b) a fiber embedded in the matrix.

In fact, we observed that the first step of damage initiation corresponds to a debonding of carbon-matrix interface. The numerical computation assumes a perfect interface, so this method does not describe the real process. A better description is made with the previous analytical approach. This model also allows to take into account the effect of distribution of different microstructural parameters as seen before, which is fundamental for the prediction of a local damage criterion.

CONCLUSION

In this study, the influence of different microstructural parameters on the mechanical properties of a Gr-Al composite has been investigated. Two models have been presented : an analytical one, based on a micro-macro modelization. This provides the influence of fiber length, distribution of orientation and local volume fraction on the stiffness matrix, the coefficients of thermal expansion, the Hill criterion for plasticity, and a criterion of damage initiation. In order to confirm these results a finite element model has been developed which gives informations on the influence of local fibers distribution on the initiation and propagation of damage.

We have outlined the ill effect of carbon fibers anisotropy on the elastic characteristics of the composite. The choice of a strong matrix is more important for the increase of the flow stress. A fiber disorientation of less than 20° induces only a 2% drop of the stiffness, but transversely oriented fibers have a more considerable effect. A distribution of local volume fraction induces a small decrease of the elastic characteristics.

Taking into account the residual stresses generated by the cooling from the manufacturing temperature, a configuration of bundled fibers with little matrix inbetween has been shown to induce an earlier initiation of damage by cavity nucleation at the fiber tips. Damage tends to propagate in the direction of the crack that is to say perpendicularly to the fiber axis. The better configuration corresponds to homogeneously distributed fibers.

To go further in the modelization of the behavior of DMMC it appears indispensable to take into account the void formation in the matrix through a local damage criterion that we can build on the analytical modelization. This seems to be the best way to succeed in the good prediction of a fracture criterion.

The developed models are included in a more general scheme to predict a damage probability of a structure.

Acknowledgments - This work has been supported by the Ets R. CREUZET for the manufacturing of the composites and the AEROSPATIALE, through a CIFRE contract.

REFERENCES

- 1 M. G. McKIMPSON and T. E. SCOTT (1989) Processing and properties of Metal Matrix Composites Containing Discontinuous Reinforcement. *Mat. Sci. Eng.* A107, 93-106
- 2 ESHELBY J. D. (1957) The Determination of the Elastic Field of an Ellipsoidal Inclusion and Related Problems. *Proc. Roy. Soc. London Series A* 241, 376-396
- 3 TAYA M. and MURA T. (1981) On Stiffness and Strength of an Aligned Short Fiber Containing Fiber-End Cracks Under Uniaxial Applied Stress. *J. Appl. Mech.* 48, 361
- 4 KOWALSKI I. M. (1986) Determining the Transverse Modulus of Carbon Fibers *SAMPE J.*, 38
- 5 TAYA M. and TAKAO Y. (1987) The effect of Variable Fiber Aspect Ratio on the Stiffness and Thermal Expansion Coefficients of a Short Fiber Composite. *J. Comp. Mat.* 21, 140
- 6 TAKAO Y., CHOU T. W. and TAYA M. (1982) Effective Longitudinal Young's Modulus of Misoriented Short Fiber Composites. *J. Appl. Mech.* 49, 536-540
- 7 TAYA M. and TAKAO Y. (1985) Thermal Expansion Coefficients and Thermal Stresses in an Aligned Short Fiber Composite With Application to a Short Carbon Fiber/Aluminium. *J. Appl. Mech.* 52, 806
- 8 CLEGG W. J. (1988) A Stress Analysis of the Tensile Deformation of Metal-Matrix Composites. *Acta Met.* 36 2141-2149
- 9 CHAMBOLLE D., BAPTISTE D. and BOMPARD Ph. (1989) Damage Micromechanisms and Micromechanic Modelization of Al-SiCw Composites *Proc. Mecamat 89* (to be published).
- 10 VASUDEVAN A. K., RICHMOND O., ZOK F. and EMBURY J. D. (1989) The Influence of Hydrostatic Pressure on the Ductility of Al-SiC Composites. *Mat. Sci. Eng.* A107, 63-69
- 11 CHRISTMAN T., NEEDLEMAN A., NUTT S. and SURESH S. (1989) On Microstructural Evolution and Micromechanical Modelling of Deformation of a Whisker-reinforced Metal Matrix Composite. *Mat. Sci. Eng.* A107, 49-61
- 12 TVERGAARD V. (1982) *Int. J. Fract.* 18, 237
- 13 LEMAITRE J. (1984) *J. Eng. Mat. Tech.*
- 14 LEMAITRE J., CHABOCHE J. L. (1985) *Mécanique des Matériaux Solides*. DUNOD
- 15 MURA T. and TAYA M. (1985) Recent Advances in Composites in the United States and Japan (edited by J. R. Vinson and M. Taya). *ASTM STP864*, 209

RELIABILITY EVALUATION OF STATIC AND FATIGUE STRENGTHS
OF CARBON/POLYIMIDE LAMINATES

Toshiyuki Shimokawa, Yasumasa Hamaguchi

Airframe Division, National Aerospace Laboratory
6-13-1 Ohsawa, Mitaka, Tokyo 181, Japan

and

Hidehiko Mitsuma

System Engineering Department, Tsukuba Space Center,
National Space Development Agency of Japan
2-1-1 Sengen, Tsukuba, Ibaragi 305, Japan

ABSTRACT

The objective of this study is to evaluate the reliability of the static and fatigue strengths of T-800H/PMR-15 carbon polyimide laminates. Static tests at various temperatures and fatigue tests at room temperature were conducted for smooth specimens and circular hole notched specimens. Static tests provided the mean and averaged scatter of static strength as a function of temperature, and the distribution form of tensile strength. Fatigue tests yielded S-N relationships under three kinds of stress ratios. Moreover, the residual static strength of the unbroken specimens was investigated.

INTRODUCTION

Carbon/polyimide composites are high temperature materials having possibility of operating in 260°C-320°C range and promising candidates for primary structures of HOPE (H-II Orbiting PlanE), which is a small space shuttle planned at NASDA (National Space Development Agency of Japan). However, since these materials are not fully matured, in order to apply for practical structures many test data should be accumulated and used for advancing these materials more reliable.

Only a few papers[1,2] with respect to the data on static strength of Celion 3K and 6K/PMR-15 systems are published. NAL (National Aerospace Laboratory) and NASDA selected T-800H/PMR-15 system and have been evaluating the reliability of this material, as a part of the joint research programs to develop HOPE between both institutes. The elaborate reliability evaluation of this system has not been found so far. Obtained results will be returned to the laminate-manufacturing companies and used to modify the cure cycle and so on.

In the present study, static tests for smooth and notched specimens were carried out at various temperatures. The mean and averaged scatter of static strength and the distributional form of tensile strength are evaluated. Fatigue tests for notched specimens were conducted at room temperature and yielded the S-N relationships under three kinds of stress ratios. The reduction of fatigue strength is discussed. Moreover, the residual static strength of the unbroken specimens was investigated. The influence of fatigue damage on the residual static strength is discussed.

MATERIALS AND SPECIMENS

The materials tested are T-800H/PMR-15 laminates. Static test specimens were manufactured by two companies, A and B. The laminate ply lay-up is (+45/0/-45/90)_{4s}. Fatigue test specimens were manufactured by A company. The laminate ply lay-up is (+45/0/-45/90)_{3s}. The prepreg tapes for the static tests and fatigue tests were supplied from different companies. Figure 1 indicates the specimen configurations. Smooth and circular hole notched specimens were used for static tests. Circular hole notched specimens were used for fatigue tests. Specimen thickness is represented by nominal values calculated from nominal prepreg tape thickness. Net area stress is used for stress in notched specimens.

STATIC TESTS

Tension and compression tests were conducted at NAL, A, and B companies. Four data sets for each test case is normal, where each test case is defined by the combination of smooth or notched specimen, tension or compression test, and test temperature. Four data sets come from the combination of the test laboratory and laminate-manufacturing company, i.e., (NAL, A), (NAL, B), (A, A), (B, B). However, one to three data sets exist in some cases. The number of observations in one data set is two to four, except for 30 in only one data. Test temperatures were -100°C, -50°C, room temperature, and +300°C. At -100°C and -50°C there is one data set each and no difference in the amount of scatter is assumed at these temperatures. The estimates of scatter in static strength at these low temperatures were averaged. In this case the temperature was represented by -50°C in drawing graphs. The parameters to measure the mean and scatter of static strength were estimated assuming the normal distribution.

Numbers of Specimens and Data Sets

Table 1 presents numbers of specimens tested and data sets. The total degrees of freedom can be calculated by subtracting the number of data sets from the number of specimens tested.

Table 1 Number of specimens; also, number of data sets in parenthesis.

Specimen & load	-100°C	-50°C	RT	+300°C
Smooth, tension	3(1)	3(1)	39(4)	10(4)
Smooth, compression	3(1)	3(1)	14(4)	8(3)
Notched, tension	3(1)	3(1)	13(4)	10(4)
Notched, compression	3(1)	3(1)	13(4)	10(4)

Mean Static Strength

Strength considered is represented by x . Individual sample, i.e., data set, is indicated by j , and the number of data sets by m . The sample size in the sample j is denoted by n_j . An arbitrary strength observation is expressed by x_{ji} . The mean in the sample j , $\hat{\mu}_j$, is given by

$$\hat{\mu}_j = (\sum x_{ji})/n_j. \quad (1)$$

Then, the simple arithmetic mean $\hat{\mu}$ is calculated by

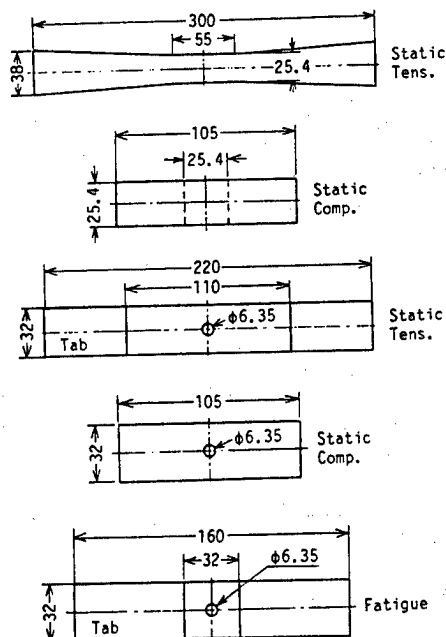


Fig. 1 Specimen configurations, unit=mm.

$$\hat{\mu} = (\sum n_j \hat{\mu}_j) / \sum n_j. \quad (2)$$

Figure 2 indicates the mean strength from all the data sets in each test case, though in some test cases the statistical test of the homogeneity of mean values was rejected. Therefore, this figure reveals a rough estimate of the mean strength. In case of the smooth specimens, the mean tensile strength drops slightly following the rise of temperature. The mean compressive strength decreases or does not change at low and room temperatures, but drops at 300°C. In case of the notched specimens, as the temperature rises, the mean tensile strength increases slightly or does not change and the mean compressive strength decreases. The high strength of T-800H fiber contributes the very high tensile strength in comparison with the compressive strength.

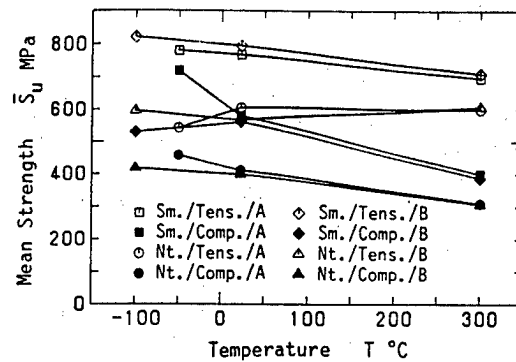


Fig. 2 Mean static strength.

Averaged Scatter of Static Strength

The measure of scatter is generally represented by the standard deviation or coefficient of variation in the normal distribution. This study assumes that the standard deviation or coefficient of variation is constant or common for the data sets in each test case defined above. The scatter estimates obtained from each data set in one test case are averaged and discussed. The averaged scatter estimate is expected to be better than individual estimate from each data set by an increase in the degree of freedom. Though, the mean strength is not assumed to be common in each test case.

Averaged standard deviation. The estimate of standard deviation in each data set, $\hat{\sigma}_j$, is given by

$$\hat{\sigma}_j = [\sum (x_{ji} - \hat{\mu}_j)^2 / (n_j - 1)]^{1/2}. \quad (3)$$

Therefore, the averaged estimate of standard deviation, i.e., the pooled estimate of standard deviation, with weights, $\hat{\sigma}$, can be calculated by

$$\hat{\sigma} = [\sum \{(n_j - 1) \hat{\sigma}_j^2\} / \sum (n_j - 1)]^{1/2}. \quad (4)$$

Figure 3 indicates obtained results. Besides $\hat{\sigma}$ for the test case of the smooth specimen, tensile test, and low temperature, $\hat{\sigma}$ for the tensile strength of the smooth specimens and the compressive strength of the notched specimens are not heavily influenced by temperature. As the temperature rises, $\hat{\sigma}$ for the tensile strength of the notched specimens is increased; however, that for the compressive strength of the smooth specimens is decreased. On comparison of $\hat{\sigma}$ for the tensile strength and that for the compressive strength in the smooth specimens, $\hat{\sigma}$ for the compressive strength is nearly

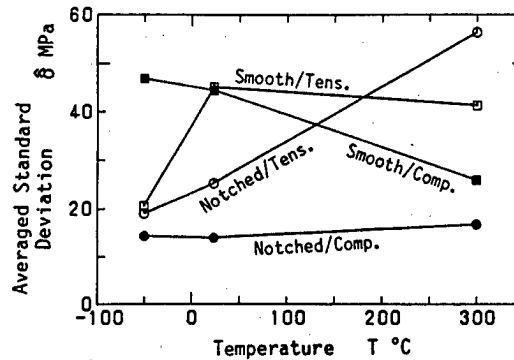


Fig. 3 Averaged standard deviation estimate with weights for static strength.

equal to or lower than that of the tensile strength, except for the test case of low temperature. On the other hand, for the notched specimens $\hat{\sigma}$ of tensile strength is higher than that of the compressive strength. Hence, if the measure of scatter is represented by the standard deviation, the scatter of compressive strength is not always higher than that of tensile strength.

Averaged coefficient of variation. The coefficient of variation, $\hat{\eta}_j$, in one data set is

$$\hat{\eta}_j = \hat{\sigma}_j / \hat{\mu}_j. \quad (5)$$

An appropriate method to average the coefficient of variation has not been found in ordinary text books, the authors proposed the following formula to get an averaged or pooled estimate, i.e., an unbiased estimator of the coefficient of variation with weights, $\hat{\hat{\eta}}$,

$$\hat{\hat{\eta}} = \frac{\sum [c_{2j} \hat{\eta}_j / \{1 + c_{2j}^2 (\eta^2 / n_j - 1)\}]}{\sum [c_{2j}^2 / \{1 + c_{2j}^2 (\eta^2 / n_j - 1)\}]} \quad (6)$$

where $1/c_{2j}$ is the constant to correct the bias of the standard deviation estimator and a function of sample size n . η is the common coefficient of variation. $\hat{\hat{\eta}}$ can be calculated by an iterative technique.

Figure 4 shows $\hat{\hat{\eta}}$, the averaged estimate of the coefficient of variation with weights. In case of the smooth specimens, besides $\hat{\hat{\eta}}$ for the tensile strength at the low temperature, $\hat{\hat{\eta}}$'s for both tensile and compressive strengths are approximately constant regardless of temperature. Of course, their values are apparently different. The value obtained for the compressive strength is larger than that for the tensile strength. In case of the notched specimens, $\hat{\hat{\eta}}$'s for both tensile and compressive strengths are almost the same at low temperature and increases as temperature rises. This value for the tensile strength becomes much higher than that for the compressive strength at +300°C.

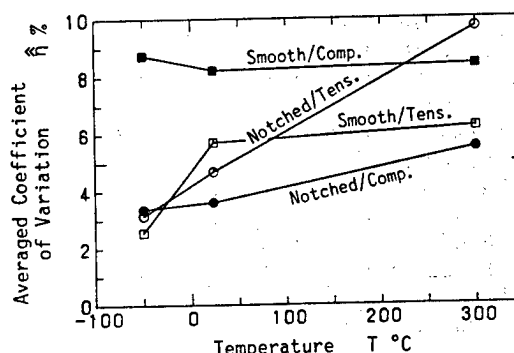


Fig. 4 Averaged estimate of the coefficient of variation with weights for static strength.

The averaged estimate of the coefficient of variation for the compressive strength is greater than that for the tensile strength in the smooth specimens; however, this relationship is reversed in the notched specimens. Since the coefficient of variation is expressed by Equation (5), the tendencies shown in Figure 4 are roughly explained by Figures 2 and 3.

Distributional Form of Tensile Strength in Smooth Specimens

Thirty observations of tensile strength of the smooth specimens at

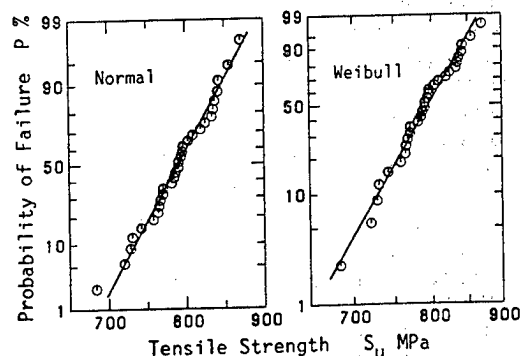


Fig. 5 Distribution of tensile strength of smooth specimens at room temperature on normal and Weibull probability paper.

room temperature are plotted in normal and Weibull probability paper and illustrated in Figure 5. Data fitness with a normal distribution is generally better than with a Weibull distribution, though the weakest is exceptional. The statistic of the modified Kolmogorov-Smirnov goodness-of-fit test[3] gives 0.077 for the normal distribution and 0.126 for the Weibull distribution. This means that the normal distribution fits quantitatively better with the obtained data than the Weibull distribution does.

FATIGUE TESTS

Static and fatigue tests for the fatigue test specimens illustrated in Figure 1 were conducted at NAL. At the same time, additional static tests were carried out at A company using the specimens made of the same lot of preregs. These results are mixed with those obtained at NAL. The static test results obtained here were not used in the analysis described above. Fatigue tests provided S-N relationships under three stress ratios, $R=0.1$, -1 , and $-\infty$, and were terminated at 10^5 load cycles, because the mission flight times of HOPE will be expected about ten. In order to investigate residual static strength, after 10^5 cycles the unbroken specimens were followed by static tests, i.e., tensile tests for the specimens tested under $R=0.1$ and compressive tests for those tested under $R=-1$ and $-\infty$.

Figure 6 presents obtained S-N relationships on semi-logarithmic graph paper. The net stress is represented by the maximum stress for $R=0.1$ and -1 , and the absolute value of the minimum stress for $R=-\infty$. Static test results are indicated at 0.25 cycles. When $R=0.1$, very high fatigue strength is shown due to the high strength of T-800H fibers. When $R=-1$, the lowest S-N relationship is obtained; however, the stress range is double the net stress expressed in this figure. When $R=-\infty$, fatigue strength is slightly higher than that under $R=-1$. This fact implies that under $R=-1$ compressive stress cycles mainly contribute to the fatigue damage and tensile stress cycles give small influence. Figure 6 indicates that fatigue life will be beyond 10^5 cycles at 65% of static strength at the worst case, $R=-1$. However, these results point out that consideration for fatigue damage is necessary when compressive stress cycles are anticipated.

Figure 7 illustrates the residual static strength (RSS) after 10^5 load cycles in a bar graph. Section lines in RSS bars indicate fatigue stress levels. When $R=0.1$, RSS is higher than the static tensile strength. This comes from the relaxation of stress concentration around the notch of the specimen. When $R=-1$ and $-\infty$, RSS is slightly

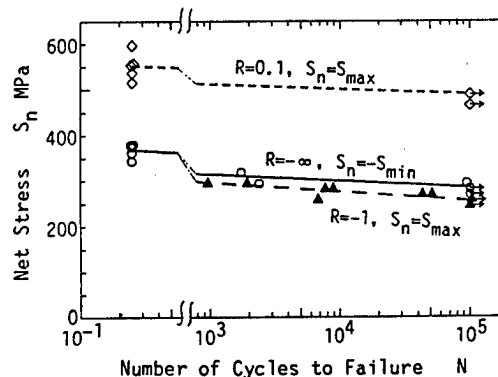


Fig. 6 S-N relationships of circular hole notched specimens at room temperature.

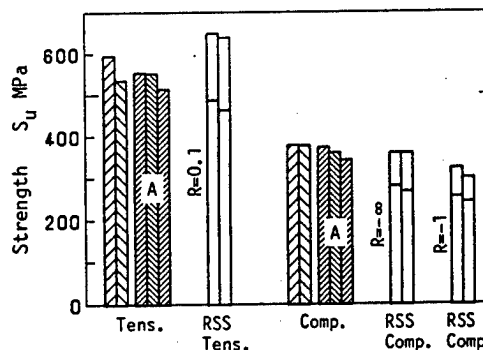


Fig. 7 Static strength and residual static strength (RSS) after 10^5 load cycles, fatigue stress indicated by a section line in RSS bars.

lower than the static compressive strength. This is explained by the reason that the delamination produced around the notch of the specimen by fatigue load cycles accelerates the delamination induced by static compressive stress. Therefore, it can be interpreted that fatigue damage gives positive influence on the tensile strength, but negative influence on the compressive strength.

CONCLUDING REMARKS

Static and fatigue tests were conducted on smooth and circular notched specimens of T-800H/PMR-15 laminates. Reliability of static strength under various temperatures and fatigue strength at room temperature is evaluated. Major results obtained are as follows:

1. The simple means of static tensile and compressive strengths were obtained and illustrated graphically.
2. The averaged estimates of standard deviation of static strength were calculated and given graphically.
3. The averaged estimates of the coefficient of variation of static strength were calculated and shown in a graph.
4. Distributional form of tensile strength of smooth specimens at room temperature fits better with a normal distribution than a Weibull distribution.
5. S-N relationships of notched specimens at room temperature were investigated for three stress ratios, $R=0.1$, -1 , and $-\infty$, and presented in a diagram.
6. Static tests of the unbroken specimens clarified that fatigue damage gives a positive effect on tensile residual strength and a negative effect on compressive residual strength.

ACKNOWLEDGMENT

The authors wish to express their hearty gratitude to the collaborators in obtaining the test results.

REFERENCES

- [1] McCleskey, S.F., Cushman, J.B., and Skoumal, D.E., "High Temperature Composites for Advanced Missile and Space Transportation Systems," Proc. AIAA/ASME/ASCE/AHS 23rd Structures, Structural Dynamics, and Materials Conf., 1982, pp. 212-222, AIAA Paper No. 82-0707.
- [2] Poveromo, L.M., "Polyimide Composites - Application Histories," High Temperature Polymer Matrix Composites, NASA CP-2385, 1985, pp. 339-358.
- [3] Mann, N.R., Schafer, R.E., and Singpurwalla, N.D., Methods for Statistical Analysis of Reliability and Life Data, John Wiley & Sons, 1974, p. 349.

Damage Mechanics for 3D composites

O. ALLIX, P. LADEVEZE

LABORATOIRE DE MECANIQUE ET TECHNOLOGIE
ENS CACHAN/CNRS/UNIVERSITE PARIS 6
61 avenue du Président Wilson
94235 CACHAN CEDEX - FRANCE

This paper deals with macro and meso-modelling of damage and fracture of tridirectional composites. Such models are used to predict the rupture of a structure or more generally to estimate its damage state compare to one or several ultimates states. Tridirectional composites, which are often used at high temperature, are made of fibres arranged in a regular pattern in the three directions of space. The voids between fibres are filled up by matrix. Contrary to laminates composites these materials offer a high strength in these three directions. Identification has been performed for a 3d carbon-carbon and a 3d evolutive composites of the AEROSPATIALE.

The first step was to develop a simple macro-modelling of this material which can be identified thanks to standard test. Traction and compression tests in different direction have been performed. Thus an homogeneous damage model has been developed. They have shown that damage phenomenon plays a prominent part in the material deterioration. An anisotropic model with one damage variable, associated with the shear behaviour, has been built up and tested for the 3D carbon-carbon composite.

To go further and get a better understanding of the damage process, the material has been studied at a more local scale. For 3D composites, between the macro scale of the structure and the micro scale of single fiber it exist an intermediate scale of its constituents : fibre-yarns matrix-blocks and their interfaces. The damage variables are assumed to be constant within the elementary cell. This means that we have chosen a preferential scale for the damage modelling which is called the meso scale. A meso-modelling of damage and anelastic phenomena, associated with the behaviour of each constituents has been construct. It allows (i) the optimization of the elementary cell of the composite in order to get a better global mechanical behaviour (ii) to analyze the damage behaviour of the structure near the edge or macro defect.

The homogeneous behaviour is rebuilt from the behaviour of the constituents. Thus the first difficulty is to determine the characteristics of fibre-yarns matrix-blocks and interfaces respectively. To obtain this information, which does not concern the homogeneous behaviour, non standard tests have been defined and realized. Some fibre-yarns have been taken out by machining and tested in tension, torsion and bending. In addition some compression test on samples without one fibre direction have been performed in order to get more information on the "in situ" behaviour of the matrix.

The reconstruction of the global behaviour, both in the linear and non-linear fields is realized thanks to simple model of scale changing. Actually it can been shown that the following approximations works quite well : under normal loading the axial strain is nearly constant in the cell, in addition, under shear loading, the shear stress distribution is nearly uniform in the cell. To take into account such properties a mixed model is used which allow us to get the anisotropic damage law and the anelastic global behaviour from a meso analysis of the elementary cell. Such an approach has allowed an improvement of the damage macro-modelling in the form of some coupling between shear effects. The non-linear behaviour is mainly due to the interfaces deterioration and the plasticity of the matrix block. The model we obtain has been checked for various solicitation and give good results.

Damage Mechanics For 3D Composites
O. Allix, P.Ladevèze

Laboratoire De Mécanique et technologie
ENS CACHAN/CNRS/UNIVERSITE PARIS 6
61 avenue du Président Wilson
94235 CACHAN CEDEX - FRANCE

ABSTRACT

This paper deals with modeling of damage and fracture of tridirectional composites, such as carbon-carbon, ceramic ceramic, or evolutive composites, and of its identification. A first approach consist in defining macro-damage modeling which are founded on an anisotropic damage theory. To go further, both in the understanding of the damage process and in the simulation of crack, mesomodeling, that is modeling of a composite at the scale of its main constituents are defined. In the case of three-directional composites the constituents are fiber-yarns, matrix-blocks and interfaces. The identification of the mesomodeling requires classical but also non-standard mechanical tests.

INTRODUCTION

The aim of this paper is to present some general tools and idea for the modeling and understanding of damage in the case of 3D composites such as carbon carbon ceramic ceramic or evolutive composites. For sake of brevity, the case of the three-directional carbon-carbon composites of the AEROSPATIALE, will be taken as an example. This material which is used at high temperature, are made of carbon-fibres arranged in a regular pattern in the three directions of space. The voids between fibres are filled up by carbon-matrix. Contrary to laminates composites these materials offer a high strength in these three directions. The first step in the investigation of this material was to develop and test an homogeneous damage model[1]. This study has shown that damage plays a prominent part in the material deterioration. To get a better understanding of the damage process, it was interesting to study it at a more local scale.

For 3D composites, between the macro scale of the structure and the micro scale of single fiber it exist an intermediate and preferential scale. It is the scale of the its constituents : fibre-yarns, matrix-blocks and their interfaces, which is called the meso scale. This scale allows a simple modeling of damage and anelastic phenomena, associated with the behaviour of each constituents. Such an approach allows us to optimize the elementary cell of the composite in order to get a better global mechanical behaviour.

The homogeneous behaviour is rebuilt from the the behaviour of the constituents. Thus the first difficulty is to determine the respective characteristics of fibre-yarns matrix-blocks and of interfaces. To obtain this information, which does not concern the homogeneous behaviour, non standard tests have been defined and realized. Some fibre-yarns have been taken out by machining and tested in tension, torsion and bending. In addition some compression test on samples without one fibre direction have been performed in order to get more information on the "in situ" behaviour of the matrix.

The reconstruction of the global behaviour, both in the linear and non-linear fields is realized thanks to simple models supported by the classical theory of asymptotic homogenization. Actually it can be shown that the following approximations works quite well : under normal loading the axial strain is nearly constant in the cell, in addition under shear loading the shear stress distribution is nearly uniform in the cell. To take into account such properties a mixed model is used which allow us to get the anisotropic damage law and the anelastic global behaviour from a meso analysis of the elementary cell. It is worth noting that the non-linear behaviour is mainly due to the interfaces deterioration, which is assumed to be uniform on each interface, and to anelasticity of the matrix

blocks[2]. The model we obtain, quite simple, has been checked for various sollicitation and give very satisfying results

SOME TOOLS FOR THE DAMAGE MODELLING

The idea we have followed is due to Kachanov[3] and Rabotnov[4]. First one adds a new internal variable in the thermodynamics sense to describe the damage state. The chosen damage indicator is the Young's modulus of the material. It is clear that the relative variation of the modulus $(E_0 - E)/E_0$ is characteristic of the damage level. For anisotropic materials, and then for composites, we developed this idea in [5]. The main features of the theory are presented hereafter. Let us consider a damaged material whose initial characteristics are denoted by '0' (no damage). The effective volume which is studied, is submitted to a stress perturbation σ^* , in the space direction \vec{n} .

The strain perturbations associated with σ^* and \vec{n} are :

- $\epsilon_L^*(\vec{n})$: longitudinal strain in the \vec{n} direction,
- $\epsilon_L^*(\vec{n}) + \epsilon_T^*(\vec{n}) + \epsilon_T^*(\vec{n})$: volumic strain in the \vec{n} direction.

T, T' denote two transversal and orthogonal directions with respect to \vec{n} , and orthogonal each to each. We define :

$$E(\vec{n}) = \frac{\sigma^*}{\epsilon_L^*(\vec{n})} \quad ; \quad \gamma(\vec{n}) = \frac{\sigma^*}{\epsilon_L^*(\vec{n}) + \epsilon_T^*(\vec{n}) + \epsilon_T^*(\vec{n})}$$

where $E(\vec{n})$ is the Young's modulus in the \vec{n} direction and $\gamma(\vec{n})$ is a less classical modulus, still in the \vec{n} direction. For an isotropic undamaged material, we have :

$$E(\vec{n}) = E_0 \quad \gamma(\vec{n}) = \frac{E_0}{1-2\nu_0}$$

The fundamental result is the following theorem ; the functions $E_0(\vec{n})$ and $\gamma(\vec{n})$ are independent and define entirely the Hooke's tensor of the material. It is to notice that they are not arbitrary functions : E depends on fifteen scalar coefficients, γ on six. The damage functions are defined by :

$$\delta(\vec{n}) = \frac{\gamma_0(\vec{n}) - \gamma(\vec{n})}{\gamma_0(\vec{n})} \quad d(\vec{n}) = \frac{E_0(\vec{n}) - E(\vec{n})}{E_0(\vec{n})}$$

The d and δ functions may be represented in the tridimensional space by two surfaces S_d, S_δ called

damage surfaces : $\vec{OM} = \vec{n} \cdot d(\vec{n}) \quad \vec{OM} = \vec{n} \cdot \delta(\vec{n})$

The central problem is, of course, to describe the damage state of the material with the minimum number of variables. If, for example, the damage surfaces may be approximated by means of two spheres, one obtains, for the damage, a two variable description which constitutes the real isotropic damage theory. More generally, the d and δ functions may be expanded in Fourier series. Thus, one obtains, depending on the choice of the truncation, relatively different damage kinematics. For composite media, the highest harmonics appear to be the most essential.

Modelling of the Damage Evolution. Coupling Damage-Anelasticity (or viscoanelasticity).

After choosing a damage kinematic, the construction of a theoretical model does not lead to special difficulties insofar as one uses the classical scheme of standard materials. It is a well-known procedure, the main difficulties consist in modeling :

- a different elastic "traction" and "compression" behaviour (microvoids and microcracks may open on shut depending on the case),

- the damage-anelasticity coupling.

For the first aspect of the problem, one will find in [5] various possible modelings from which some examples will be presented later on. The idea is to express this unilateral character in terms of energy. For the damage-plasticity coupling, a scheme which seems to work quite well, is to build the modelings upon quantities which are called "effective".

$$\text{- effective stress : } \tilde{\sigma} = K_0 \cdot K^{-1} \sigma \quad \text{- effective anelastic strain rate : } \dot{\tilde{\epsilon}}_p = K_0^{-1} \cdot K \dot{\epsilon}_p$$

where K denotes Hooke's tensor, σ , ϵ the stresses and strains. In other words, modelings are built upon the variables $\tilde{\sigma}$ and $\dot{\tilde{\epsilon}}_p$ which verify : $\text{Tr} [\tilde{\sigma} \cdot \dot{\tilde{\epsilon}}_p] = \text{Tr} [\sigma \cdot \dot{\epsilon}]$

With such a scheme, we noticed that the "traction" and "compression" behaviours did not have to be distinguished, even if they appear to be very different one from the other when hardening curves are considered. In order to measure the damages, it is strictly necessary to use loading and unloading.

MACRO DAMAGE MODELLING

For high strenght fiber composites one can suppose that only the shear moduli vary, the other elastic characteristics remaining constant. Moreover, one introduces only one scalar damage variable such that :

$$G_{12} = (1 - d) G_{12}^0 ; G_{23} = (1 - d) G_{23}^0 ; G_{31} = (1 - d) G_{31}^0$$

These expressions can be derived by homogenisation technics. For that model, the damage functions are : $\delta(\vec{n}) = 0$

And for \vec{n} not too near of an orthotropic direction where α, β, γ are the components of \vec{n} :

$$\frac{1}{1 - d(\vec{n})} \# \frac{\alpha^2 \beta^2 / G_{12}^0 + \beta^2 \gamma^2 / G_{23}^0 + \gamma^2 \alpha^2 / G_{31}^0}{\alpha^2 \beta^2 / G_{12}^0 + \beta^2 \gamma^2 / G_{23}^0 + \gamma^2 \alpha^2 / G_{31}^0} = \frac{1}{1 - d}$$

Damage evolution

$$\text{The conjugate quantity to } d \text{ is : } Y = \frac{\delta E_D}{\delta d} \Big|_{\sigma : \text{cst}} = \frac{1}{(1 - d)} E_\tau$$

where E_τ is the shear energy. The quantity Y is similar to the energy release rate it governs the damage evolution and then the rupture. For 3D Carbon-Carbon we propose the following model :

$$d = h [Y + g(Y, Z)] \text{ if } d < 1 \text{ otherwise } d = 1 ; Z = \langle \sigma_{11} + \sigma_{22} + \sigma_{33} \rangle_+ ; Y_t = \sup_{\tau \leq t} Y_\tau$$

h, g are functions depending on the material. For example let us consider the case of 3D carbon-carbon composites of the AEROSPATIALE

It is a tridirectional carbon-carbon composite. The carbon fibres are periodically arranged in the three directions of space. Along the first direction, the carbon fibres have a square cross-section made up with four strands of 3000 filaments each. The other fibres possess a rectangular cross-section made up with only two strands. The voids are filled up by carbon matrix. The density of this materials is about 2.

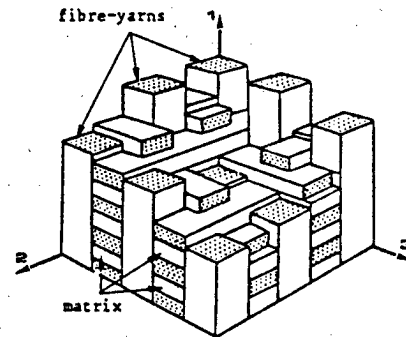


Fig 1 Description of the materials

These functions can be identified from compression and tension tests at 45° in an orthotropic plane.

The figure 2 presents experimental results for three tests :

- compression test at 45° (plane 1-2)
- tension test at 45° (plane 1-2)
- torsion test (axis 3)

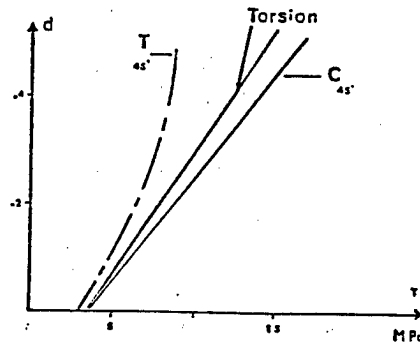


Fig 2 Damage evolution for several tests

Damage and anelasticity

The figure 3 shows the hardening function derived from tension and compression test at 45° (plane 1-2). Tension and compression behaviours are different.

The effective stress and strain are

$$\begin{aligned}\tilde{\sigma}_{ii} &= \sigma_{ii} & \tilde{\sigma}_{ij} &= \frac{\sigma_{ij}}{1-d} & \text{for } i \neq j \\ \dot{\tilde{\epsilon}}_{iip} &= \dot{\epsilon}_{iip} & \dot{\tilde{\epsilon}}_{ijp} &= \dot{\epsilon}_{ijp} (1-d) & \text{for } i \neq j\end{aligned}$$

The elasticity domain is defined by

$$\left[\left(\frac{\sigma_{12}^2}{G_{12}^0} + \frac{\sigma_{23}^2}{G_{23}^0} + \frac{\sigma_{31}^2}{G_{31}^0} + G_m^0 \right)^{1/2} - r \leq 0 \right]$$

where

$$\frac{1}{G_m^0} = \frac{1}{3} \left[\frac{1}{G_{12}^0} + \frac{1}{G_{23}^0} + \frac{1}{G_{31}^0} \right]$$

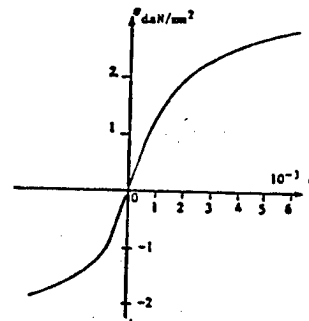


Fig 3 Tests at 30° (plane 1-2)

To describe the evolution of the effective plastic strain, one uses an associated model with isotropic hardening ie $r = l(p)$, l can be identified from a tension test at 45° (orthotropic plane)

Remarks and discussion:

To be complete, one has to add rupture criteria in the fibre-yarns directions : $-\epsilon_c \leq \epsilon_{ii} \leq \epsilon_T$

This model has been checked on numerous experimental and give satisfying results on tension and compression tests.

vertheless the global damage notion is not totally adequate to describe the deterioration of the material. Figure 3 shows the differences between the damage evolution in shear behaviour in tension at 45° (orthotropic plane) and in compression. A more refined analysis must therefore be set order to understand such phenomena.

SO DAMAGE MODELLING

if it is difficult to distinguish the different meso-constituents, a qualitative analysis of testimens after rupture shows that fibres-yarns were slipping during the test up to the point where interfaces were totally destroyed. So, the main assumption of the meso-modeling is that damage is to a progressive slipping of the fibre-yarns along their axis. Thus, besides matrix-blocks and -yarns we define interfaces between fibre-yarns and matrix-blocks as mechanical meso-tinent. Fibres-yarns Fibres-yarns interfaces are assumed to be very weak and brittle. Previous es have shown that fabrication processes greatly modify constituents characteristics. For ple the fibre-yarns modulus seems much higher than before fabrication. Thus, one of the main ulty is to measure the constituents characteristics after fabrication. Bending and torsion tests used on fibre-yarn specimens which were taken out of the material by machining, then scrapped

and calibrated to obtain a regular cross-section. Non standard compression tests were made on specimens for which one fibre-yarn was eliminated by machining.

Matrix block behaviour-modeling

The matrix possess isotropic properties. Their behaviour is elasto-plastic with damage; but the damage phenomenon of matrix blocks is not important as regard to the mean behaviour. So a simple Prandtl-Reuss model is chosen to describe its anelastic behaviour.

Interface behaviour-modeling

The fibers-yarn fibers-yarn interfaces are assumed to be very weak and brittle, the fibers-yarn matrix block interfaces seem to be elastic and damageable. Let us denote k_{Σ} the interface rigidity, $k_{\Sigma} = 0$ corresponds to perfect slipping and $k_{\Sigma} = +\infty$ corresponds to perfect bonding. The interface deterioration, which is assumed to be uniform on each interface, is describe thanks to a function f of Y and R , where:

$$Y = 1/2 \int_{\Sigma} \sigma^2 / k_{\Sigma} dS, z = \log k_{\Sigma}$$

R hardening variable, γ its dual variable, $f(Y, R) = g(Y) - R - R_0$

One has : $\dot{z} = \lambda_p \frac{\delta f}{\delta Y} - \dot{\gamma} = \lambda_p \frac{\delta f}{\delta R}$, where $\lambda_p > 0$ and $\neq 0$ only if $f = 0$ and $\dot{f} = 0$

Interface behaviour-modeling

The aim of identification is to determine a relation ship between the shear energy Y and the strength of the interface. An accurate analysis of the cell interface and the results of compression test with shear at 45° , allows these parameters to be found (Fig 4 -5).

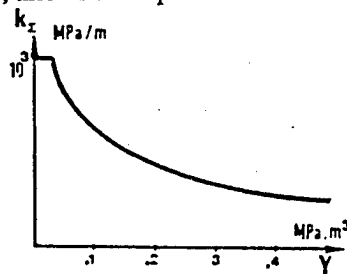


Fig.4: Interface strength versus shear energy

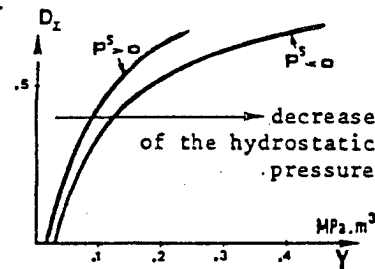


Fig.5: Interface damage evolution

RECONSTRUCTION OF THE MEAN BEHAVIOUR : HOMOGENISATION

By using the classical theory of asymptotic homogenisation [6] one can show that, in the orthotropic axis, the local shear stresses are nearly uniform, the local strain distributions in the fibre-yarns directions are uniform too. So we use, even in the non-linear field, a mixed formulation to rebuilt the mean behaviour knowing the meso one. The model we obtain is verified on different tests (fig.6-9).

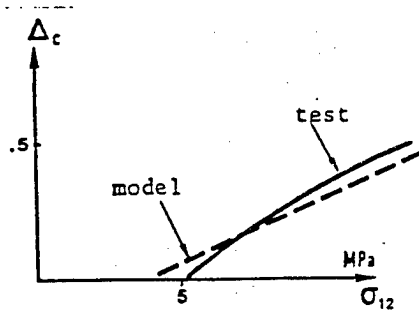


Fig.6: Damage evolution (normal direction)

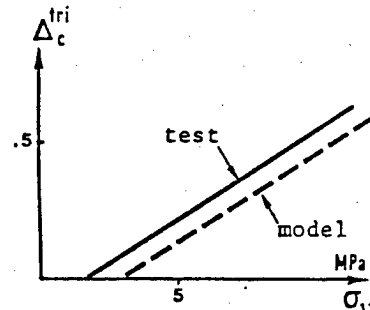


Fig.7: Damage evolution at 30°

SESSION II

ADVANCED MATERIALS

This page intentionally left blank

Processing and Properties of Ceramic-Matrix Composites for Applications in Severe Aerospace Environments

R. Naslain* and J.C. Cavalier**

* University of Bordeaux, Laboratory for Thermostructural Composites
(UMR 47, CNRS-SEP-UB1), Europarc, 1-3, Avenue Léonard de Vinci
33600 Pessac, France

** Société Européenne de Propulsion, BP 37
33165 Saint Médard-en-Jalles, France

ABSTRACT

Ceramic matrix composites (CMCs) made of ceramic fibers embedded in a ceramic matrix, offer the advantage (with respect to monolithic ceramics) of being tough and damage-tolerant materials. Such properties are observed when the fiber-matrix coupling is optimized, through the use of an interphase (e.g. pyrocarbon) during processing. Chemical vapor infiltration (CVI), based on the deposition of a solid from a gaseous precursor in the pores of a fiber preform heated at a moderate temperature and under a reduced pressure, is well suited to the processing of CMCs. 2D-SiC/C/SiC composites exhibit a non-linear stress-strain behavior in tension at room temperature and an outstanding crack propagation resistance. When protected against oxidation, 2D-SiC/C/SiC composites can be used in air up to at least 1200°C, the possible limiting parameters being the thermal stability of the fibers and the carbon interphase. A variety of parts have been already fabricated and tested for applications in the aerospace industry field.

INTRODUCTION

There is an increasing demand of high performance materials (in terms of fatigue resistance, stiffness and low density) in the aerospace industry field (e.g. in the design of structures for aircrafts, spacecrafts, satellites as well as in that of advanced jet and rocket motors). Polymeric matrix composites reinforced with e.g. carbon fibers (high tension or high modulus) or aramid fibers, are well suited to applications with service temperatures close to room temperature (i.e. up to about 200°C). The situation, in terms of available materials and technology is less satisfactory for those applications (e.g. heat shields, motor components) involving severe environmental service conditions (i.e. temperature ranging from 500 to 2000°C, vacuum, atmospheres containing oxygen). A few families of ceramic matrix composites (CMCs), including hot-pressed glass-matrix composites and CVI-processed SiC-matrix composites both reinforced with SiC-based fibers, are promising materials for such applications. However, our knowledge in this field is still limited.

ADVANCED CMCs

Any advanced CMC consists of at least three main components. The ceramic fibers, with a failure strain ϵ_m^R of the order of 1%, carry an important part of the load (if not all the applied load when the matrix undergoes microcracking). The fibers are often used as preforms (which are porous bodies fabricated e.g. according to weaving techniques). The ceramic matrix carries also part of the load (particularly at low strains) and protects the fibers against the effect of the environment. Since the matrix has a low failure strain (typically $\epsilon_m^R = 0.1\%$ or less), CMCs are referred to as inverse composites, i.e. when they are loaded, matrix fails first (at σ^D , it undergoes microcracking). The microcracks arising from matrix failure, which often propagate in mode I, generate notch effects upon the fibers. The resulting stress concentration at the crack tip is large enough to yield an early failure of the fibers when the fibers are too strongly bonded to the matrix. The fiber-matrix coupling is controlled during processing : (i) the coefficient of thermal expansion of the matrix should be lower (or of the same order) than that of the fiber and (ii) the chemical bonding should be limited. An interphase (the third component), is usually inserted between fibers and matrix. Often made of pyrocarbon or boron nitride, it acts as a mechanical fuse (deflecting the matrix microcracks from mode I to mode II in the vicinity of the fiber/matrix interface and thus protecting the fibers) and, additionally as a fiber binder and diffusion barrier. The interphase, a quite recent concept in CMCs, has a key role in the understanding of their tough mechanical behavior and effect of the environmental parameters.

CVI-PROCESSING OF CMCs

In the CVI-processing of CMCs, the starting materials are : (i) a porous fiber preform and (ii) gaseous precursors of the matrix and of the interphase (a first advantage of CVI lying in the fact that the same process can be used to form both materials).

The nature of the fiber preform depends on that of the related CMC part (and particularly on its loading scheme under service conditions). It can be a simple stack of fabrics maintained pressed together with a tooling (fig. 1) for thin wall structures or a more complex architecture (usually obtained by multidirectional weaving or knitting techniques) for thick wall structures or/and complex loading pattern. They would be referred to as 2D and nD (with $n \geq 3$) preforms. The ability of a fiber preform to be infiltrated by ceramic gaseous precursors depends on both its shape and dimensions as well as its pore spectrum.

In CVI, a solid (e.g. a ceramic material) is deposited within the pore network of a heated substrate (i.e. the fiber preform) as a result of heterogeneous chemical reactions taking place between the gaseous species of the precursor. The precursors commonly used are : CH_4 for carbon, CH_3SiCl_3 (MTS)- H_2 for SiC, $\text{NH}_3\text{-BX}_3$ (with $\text{X} = \text{F, Cl}$) for BN, $\text{BCl}_3\text{-CH}_4\text{-H}_2$ for B_4C or $\text{ZrCl}_4\text{-CO}_2\text{-H}_2$ for ZrO_2 [1]. In the CVI-processing of CMCs, the main objective is to fill as completely as possible the available open porosity with the ceramic material and thus to avoid an early sealing of the pores by the deposit

(bottle-neck phenomena). Two different phenomena control the rate of infiltration of the ceramic material in the pores : (i) the kinetics of the chemical reactions and (ii) the mass transfers of the reactants and products along the pores. In isothermal/isobaric CVI (ICVI), the mass transfers occur only by diffusion (both Knudsen and Fick diffusions, the former being predominant in pores of very small diameters). It has been established that under such conditions, the infiltration (in-depth deposition) is favored with respect to the deposition occurring on the external surface of the preform when (ii) is fast with respect to (i) which means that ICVI should be performed under low T, P conditions [1]. Moreover, the pore spectrum of the preform and the partial pressures of the various species in the gas precursor are also important parameters. In ICVI, the infiltration exhibits the following features : it is relatively slow, it yields some density gradient between the core of the material and its external surface (where the amount of deposit is always higher even under optimized conditions) and finally, it results in composites with a significant residual porosity (the infiltration process being stopped, for economical reason when Vp reaches a value of 10-15%).

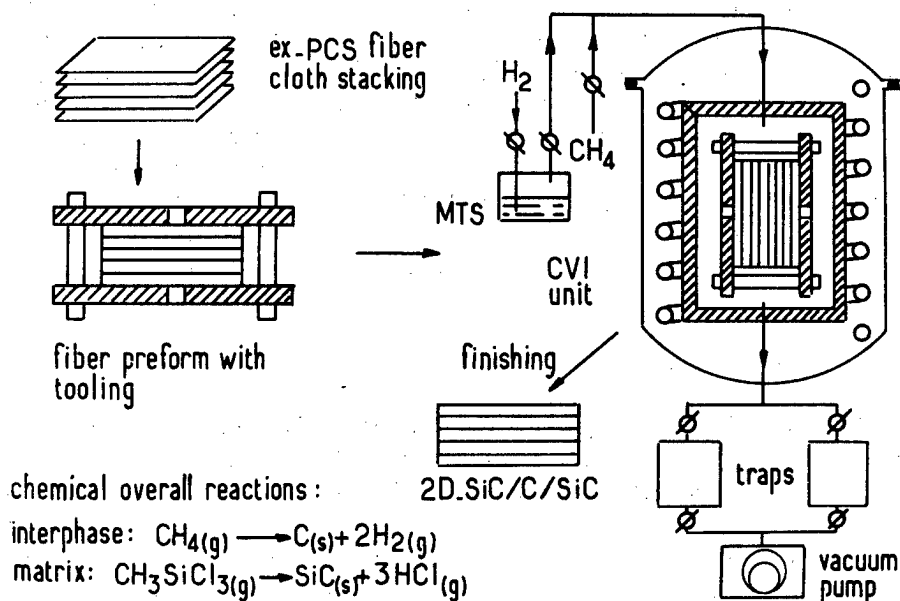


Fig. 1 : CVI-processing of ceramic matrix composites (schematic)

The feasibility of the ICVI-processing of CMCs has been established for a variety of ceramic materials including : C, SiC, B₄C, TiC, BN (and to a less extent Si₃N₄), Al₂O₃ and ZrO₂. However and as far as we know, it has been transferred to industry only for carbon and silicon carbide [2]. In order to increase the infiltration rate, it has been proposed to apply a pressure/temperature gradient to the preform, the mass transfers of reactants/products being by forced convection (FCVI) [3]. Under such conditions, the infiltration duration necessary to achieve a given residual porosity in a given preform has been reported to be reduced by one order of magnitude (with respect to ICVI). However, FCVI requires specific tooling and procedure. Moreover, it seems

doubtfull that the process could be applied to preforms of complex shapes. Conversely, a large number of preforms of complex shapes (which may be different from one another) are infiltrated simultaneously in the ICVI-process.

The various steps in the ICVI-processing of 2D-SiC/C/SiC composites are shown schematically in fig. 1. The starting material is a preform made of ex-polycarbosilane fibers (i.e. fabrics of Nicalon-type fibers). It is first infiltrated with a carbon interphase (a few 100 nm in thickness) and then with a SiC-matrix. It is noteworthy that such a processing approach has more common features with those of textile industry and chemical engineering than with the processing techniques used for the fabrication of classical ceramics.

MECHANICAL BEHAVIOR

Well-processed CMCs (i.e. composites in which the reinforcing potential of the fibers has not been degraded and the fiber/matrix coupling has been optimized, e.g. by use of a proper interphase) exhibit an outstanding mechanical behavior at room temperature, for ceramic materials [4].

When progressively loaded in tension, up to failure, a 2D-SiC/C/SiC composite exhibits a typical **non-linear** stress-strain behavior (load applied along one of the 1,2 axes corresponding to the warp and woof directions of the fiber cloths of the initial preform) (fig. 2) [5]. For $0 < \sigma < \sigma^D$, the matrix and the fibers behave elastically and the

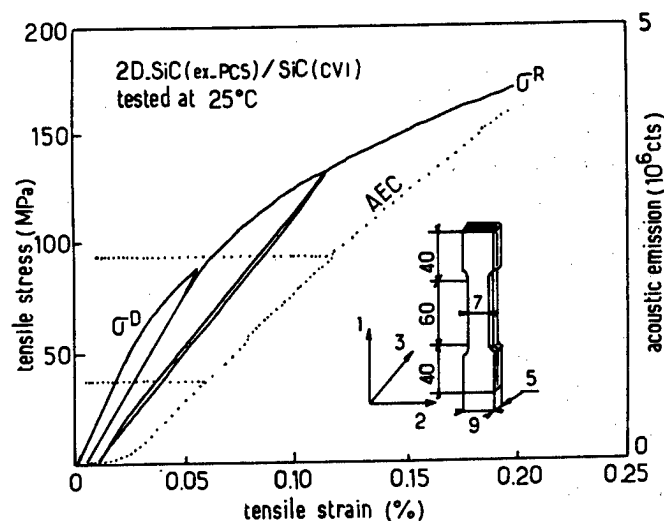


Fig. 2 : Mechanical behavior of a 2D- SiC/C/SiC composite loaded in tension (according to (5))

$\sigma = f(\epsilon)$ curve of the composite is linear elastic (the Young modulus being of the order of $E = 200$ GPa). For $\sigma^D < \sigma < \sigma^R$, the composite is progressively damaged (as evidenced by the high intensity of the acoustic emission signal). However, unloading and reloading cycles show that the material remains linear elastic, at least in a first approximation, with a decrease in stiffness (the residual strain at zero stress being negligible). It is worthy of note that the failure strain of 2D-SiC/C/SiC composites is very high, ranging from 0.2 to almost 1%, for a ceramic material (i.e. one order of magnitude higher than that

of the related monolithic ceramics). Such a behavior is directly related to the role played by the carbon interphase : when it is present, the brittle SiC-matrix can undergo a complete microcracking without any damage to the fibers. Under such conditions, the fibers become progressively debonded from the matrix (owing to the deflection in mode II of the matrix microcracks) and can be strained up to their intrinsic failure strain (1% for ex-PCS fibers).

All the damages that occur during loading, e.g. in a 3-point bending test performed on a notched specimen, absorb energy, therefore, the resistance to crack propagation of 2D-SiC/C/SiC is dramatically improved with respect to the related SiC monolithic ceramics [4, 5]. Thus, 2D-SiC/C/SiC composites are non-brittle and damage-tolerant materials, like metals (but for different reasons : in tough CMCs microcracking and other energy absorbing phenomena play a role similar to plasticity in metals).

EFFECT OF ENVIRONMENTAL PARAMETERS

The effect of environmental parameters (i.e. temperature, time and atmosphere) on the mechanical behavior of model unprotected 1D-SiC/C/SiC [6, 7] and coated 2D-SiC/C/SiC [8] composites has been studied recently. Two material parameters play an important role : (i) the nature of the fibers and (ii) the thickness of the carbon interphase.

High temperature tension tests performed under an **inert atmosphere** have shown that the room temperature failure stress of SiC (CVI) matrix 2D-composites is maintained up to about 1000°C. Beyond this limit, a decrease is observed for the composites made from ex-PCS fibers which is thought to be related to the thermal degradation of the fibers (Nicalon fibers are known to undergo microstructural change at $T > 1000 - 1200^\circ\text{C}$). However, at 1400°C, the failure stress is still 75% of that at ambient temperature. Conversely, an increase in failure stress is still observed for 2D-C/C/SiC composites with a peak value at 1200°C and a value still equal to $\sigma^R(25^\circ\text{C})$ at 1400°C. These results clearly show that the fiber properties govern the failure behavior of the composites at $1000 < T < 1400^\circ\text{C}$ under an inert atmosphere [2, 7].

SiC-based ceramics are known to exhibit a good resistance to oxidation at high temperatures which is related to the growth of a protective silica scale. It has been recently established that both ex-PCS fibers and SiC CVI-matrix have such a behavior, the oxidation rate of the former being higher than that of the latter, particularly below 1000°C [8]. Oxidation tests performed in air on unprotected 1D-SiC/C/SiC model composites have shown that two chemical phenomena occur : (i) the consumption of the carbon interphase yielding annular pores (whose size is that of the 0.1 - 1 μm interphase) and gaseous CO/CO₂ species and (ii) the oxidation of both the fibers and matrix resulting in the formation of silica. When the interphase is thin (i.e. 0.1 μm) and temperature high enough, this silica tends to seal the pores, mainly near the composite external surface, and the oxidation of the carbon interphase is stopped. Thus, the material is self-healing. Since this property is no longer observed at low temperatures (owing to the fact that the formation kinetics of SiO₂ becomes slow vs the oxidation of carbon), a coating (seal-coat) is usually applied to the composite at the end of the processing.

The effect of ageing treatments, performed at high temperatures in air, on the tensile mechanical behavior at ambient temperature of protected 2D-SiC/C/SiC

composites, has been discussed recently by Cavalier et al. [2]. The treatment has no significant effect on both σ^R (25°C) and ϵ^R (25°C) when it is performed below 800°C. At 1200°C, it results in no change in σ^R (25°C) but in a significant increase in ϵ^R (25°C). Finally, for $T > 1200^\circ\text{C}$, a decrease in σ^R (25°C) is observed (fig. 3). It thus appears that well-processed 2D-SiC/C/SiC composites can be used in air up to at least 1200°C. Recent applications of 2D-SiC/SiC ; 2D-C/SiC and 3D-C/SiC in the aerospace industry has been reviewed in (2).

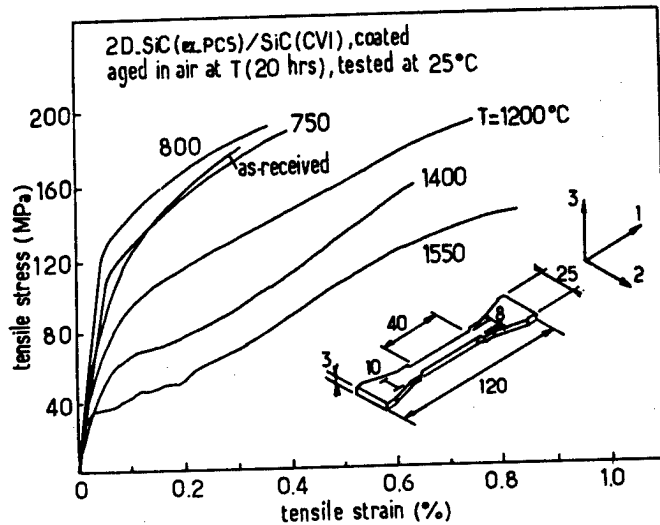


Fig. 3 : Effect of ageing treatments in air on mechanical behavior of 2D-SiC/SiC composites at ambient temperature (according to (2)).

REFERENCES

- (1)-Naslain, R. and Langlais, F. "CVD-processing of Ceramic-ceramic Composite Materials", Mater. Science. Research, 20 (1986) 145-164
 - (2)- Cavalier, J.C., Lacombe, A. and Rouges, J.M., "Ceramic Matrix Composites, New Materials with very high Performances", in "Developments in the Science and Technology of Composite Materials" (ECCM-3) (A.R. Bunsell P. Lamicq and A. Massiah, eds.), Elsevier Appl Science, 1989, pp. 99-110 (in french)
 - (3)- Stinton, D.P., Caputo, A.J. and Lowden, R.A.
- "Synthesis of Fiber-Reinforced SiC-composites by CVI", Amer. Ceram. Soc. Bull., 65/2 (1986) 347-350
- (4)- Lamicq, P.J., Bernhart, G.A., Dauchier, M.M. and Macé, J.G., "SiC/SiC Composite Ceramics", Amer. Ceram. Soc. Bull., 65/2 (1986) 336-338
 - (5)- Birbis, J.M., "Toughness Characterization of Ceramic Matrix Composite Materials", Thesis numero 395, Univ. Bordeaux, 6 dec. 1989 (in french)
 - (6)- Filipuzzi, L., Naslain, R. and Thebault, J., "Study of the Oxydation of 1D-SiC (Nicalon)/SiC (CVI) Composites with a Pyrocarbon Interphase", in Composite Materials for Applications at High Temperatures (Naslain, R., Lamalle, J. and Zulian, J.L., eds), AMAC-CODEMAC, 1990, pp. 289-301 (in french)
 - (7)- Filipuzzi, L., Camus, G., Thebault, J. and Naslain, R., "Effect of High Temperature Ageing Treatments on the Mechanical Behavior of Unidirectional SiC/SiC Fibrous Composites", Proc. 11th Risø Int. Symp. on Metallurgy and Mater. Sci., Structural Ceramics, Processing, Microstructure and Properties, 3-7, Sept. 90 (in press)
 - (8)- Filipuzzi, L. and Naslain, R., "Oxidation Kinetics of SiC-based Ceramic Fibers", Proc. 7th CIMTEC, Satellite Symp. 2, Montecatini Term, Italy, June 24-30, 1990, Elsevier (in press)

Fabrication and Properties of FGM

Ichiro Shiota *
Ryuzo Watanabe**

*Physical Properties Division,
National Research Institute for Metals

**Department of Materials Processing,
Faculty Eng. Tohoku University

ABSTRACT

Recent advancement of science requires high mechanical properties and high thermal resistivity in one material. Traditional coating or sticking of ceramics on metal often causes troubles at the interface by difference of thermal expansion coefficients between ceramics and metal. Functionally gradient materials(FGMs) are hopeful for relaxation of stress at the interface. Science and technology agency of Japan started a project to develop FGM. Four processes, gaseous, powder configuration, spraying and SHS processes, are adopted for fabrication. Each process has its own features in material system, size and properties, etc. A proper process and material system should be selected to fit its applying part.

INTRODUCTION

Recently, energy consumption has been enormously growing and limited energy resources are abruptly decreasing. One of the solution is developing a heat resistive structural material to improve the efficiency of energy utility. High strength, high modulus and high toughness are usually required for structural member and heat resistivity is important for energy efficiency. In the case of aero- or space use, high strength and high modulus to weight, i.e. high specific strength and high specific modulus are also important.

Generally speaking, metals have well balanced mechanical properties as a mechanical member. On the other hand, ceramics are superior to metals regarding heat resistance. Traditional alloys or dispersion strengthened metals has uniform composition, and the properties are also uniform as shown in Fig.1 a). These materials are difficult to have high mechanical properties and thermal resistance simultaneously. Then ceramics are often coated on a metal as shown in Fig.1 b). In this case, all properties have discontinuity at the interface. When the material is heated up, it is often broken at the interface by large thermal stress generated by difference of thermal expansion coefficients.

New idea was presented as shown in Fig.1 c), where the sharp interface was eliminated. This is the FGM(functionally gradient material). As the FGM is based on a new idea, no traditional methods can be applied to design, to fabricate and to evaluate. Therefore Science and Technology Agency of Japan has promoted a

project to develop FGM since 1987. There are various FGMs, e.g. various thickness and/or combination of materials, then a proper FGM should be used depending on applying parts. For example, a thin FGM layer is desirable, when a heat resistive material is coated on a cooled part. Because the cooling is effective up to the surface of the heat resistive layer. On the other hand, thick FGM is suitable for abrasive resistance. In this paper, fabrication and properties of FGMs are reported.

EXPERIMENTAL PROCEDURE

Fabrication processes of FGMs in the project are roughly classified into four; gaseous process, powder configuration process, plasma spraying process and SHS(self propagating high temperature synthesis) process. Less than 1mm of thickness is usually obtained by gaseous process, and more than 1mm by powder configuration and SHS processes. Spraying process is placed in the middle.

Gaseous Process

Compact and thin layers on a substrate can be obtained by gaseous process. The thickness of the layer is usually less than 1 mm, though it depends on fabricating time. Gaseous process is roughly divided into two methods; PVD(physical vapour deposition) and CVD(chemical vapour deposition).

PVD is the process to obtain a material from vaporized metal. If some reaction gas, e.g. oxygen, nitrogen or hydrocarbon is introduced in the metal vapour, oxide, nitride or carbide can be formed as a thin film on a substrate. If the flow rate of reaction gas is medium of 0 and sufficient amount to form ceramics, the deposited material consists of two or more phases(1). Resistance heating, electron beam heating or plasma heating by HCD (hollow cathode discharge) is usually used to evaporate the source metal. In this experiment, an HCD type instrument as shown in Fig.2, was used because the plasma can ionize the metal vapour to allow reaction with reaction gas to form ceramics. Specially degassed pure Ti or Cr was used for source metal. Pure nitrogen or pure propane was used for reaction gas. When the flow rate of the reaction gas was continuously increased from zero to sufficient flow rate to form a ceramics, the composition of the deposited film changes continuously from metal to ceramics.

In the CVD process, a metal or semi-metal halide gas is pyrolytically decomposed to form the metal or semi-metal film on a substrate. When a reaction gas is mixed in the halide, a carbide or a nitride can also be formed. Recently, plasma CVD or hybrid plasma CVD are popularly used, in which RF or RF+DC is applied during the reaction. In this project, an instrument as shown in Fig.3 was used(2). $\text{SiCl}_4 + \text{C}_x\text{H}_y + \text{H}_2$ mixture gas was used to form an FGM in which the composition was gradually changed from carbon to SiC.

Powder Configuration Process

This process is roughly divided into dry and wet processes. Dry process is an improved powder metallurgy(P/M) process. The P/M process involves the following sequent steps; the selection of combination of metals and ceramics, designing of the optimum compositional distribution, stepwise or continuous stacking of powder premixes according to the pre-designed compositional profile, the compaction and subsequent cold isostatic pressing of the stacked powder and sintering of the pressed compact. The spray deposition of the mixed powder was developed for the fine powder stacking as shown in Fig.4. Preliminary investigation have been carried out on several materials of heat resistive ceramics and ductile metals. Material combinations of zirconia/stainless steel and zirconia/molybdenum were investigated in detail to optimize the process variables.

Wet process is a method to use slurry(3). This FGM fabrication method is based on doctor blade process to prepare a thin sheet of ceramics. Metal and ceramic powders of various mixing ratios were blended with an appropriate binder materials, subjected to defoaming under low vacuum. Thin sheets of a given composition were prepared by doctor blade process. The thickness of a green sheet was in the range of several tens micron-meter and 2mm. The green sheets were layered in order of composition, and were pressed to form a stepwisely graded sheet material. The pressed sheet was debinded at an appropriate temperature and sintered. Overall process of this process is shown in Fig.5. The sintering balance problem which would cause various sintering faults was also specific to the method, as in the case of dry method. The variation of sintering rate with composition was minimized by controlling powder size distributions.

Spraying Process

Two types of spraying have been employed for the preparation of compositionally gradient coatings; single-gun method(4) and two-gun method(5).

In the case of single-gun method, metal and ceramic powders were fed into a spray gun through different ports and mixed in a flame. Fig.6 shows a schematic illustration for one-gun method. Low-pressure plasma spraying using single-gun was also investigated. The composition was controlled by changing the flow rates of powder carrying gas for two kinds of starting powders. The temperature distribution in the plasma flame, the passing time of powder particles in the flame and the velocity of liquid and semi-liquid droplets were controlled to obtain a defect-free and finely dispersed microstructure with well-defined compositional profile. These specific features of single-gun method were controlled by an appropriate design of plasma gun, electric current and voltage, plasma gas species and spraying distance between gun and substrate.

Two-gun method was also investigated in this project. Two plasma guns were obliquely settled above the substrate as shown in Fig.7. Metal and ceramic powders were introduced into different guns to form a coated layer of metal and ceramic mixture. The mixing ratio of two powders was controlled by changing the powder feeding rates of the both guns. Typical spraying condition for two-gun method in this project is shown in Fig.7.

SHS Process

SHS process was also applied to fabricate an FGM of the mixtures of metals and borides, carbides and nitrides(6,7). The constituent powders were stacked layer by layer according to the pre-designed profile in a mold, and were pressed isostatically at room temperature to form a green compact. The compact was placed in a pressure vessel, and was ignited at the one end. The synthesis reaction propagated towards the other end of the compact, while the compact densified under the isotropic pressure. Fig.8 shows SHS process using specially designed hydrostatic pressure vessel(6). Fig.9 shows an alternative SHS method to fabricate bulk FGM(7). The green compacts were mounted in a powdered ignition agent. The one end of the medium is ignited under isotropic gas pressure. The green FGM compact was heated with exothermic reaction of the medium up to ignition temperature and then eventually the SHS reaction occurred in the compact, along with the simultaneous densification. This method enabled to produce many FGM compacts at the same time.

RESULTS AND DISCUSSION

Gaseous Process

Ti to TiN, Ti to TiC, Cr to CrN FGM etc. were obtained by PVD. Crystal sizes of all the FGMs by PVD were of sub-micron order. A typical example of Ti

to TiN FGM is shown in Fig.10. No obvious boundary of metal and ceramics or grain boundary is observed in this figure. However, the size of knoop indentations decreases gradually from the bottom, to the top of the FGM, which indicates the gradual compositional change from Ti to TiN. Thermal stability of Ti to TiC FGM on a stainless steel substrate was investigated, and it was found that randomly oriented small crystal size of TiC was stable.

C/C composite is hopeful as an high specific strength and modulus material. However, preventing oxidation at a high temperature is essential for application. Traditional coatings of SiC on C often causes interfacial problems. Then C to SiC FGM on C by CVD was investigated in this project. Fig.11 shows the C content in NFGM(Non-FGM) from methane and propane, which were produced at 1173K under 1.3kPa(2). The C content depended on the source gas, even the deposition was achieved by the same SiC/C ratio in gas phase. From this result, it is obvious that control of the composition in FGM by using propane is easier than using methane. Higher pressure in the range of 1 to 40kPa is better to obtain a wide range of SiC/C ratio in FGM as shown in Fig.12(2). Morphology of the cross section of C to SiC FGM and corresponding Si distribution are shown in Fig.13(2).

Powder Configuration Process

In the case of dry process, main points are similar to the conventional powder metallurgy. However, powder compacts with different mixing ratios of metals and ceramics showed different sintering behaviours as shown in Fig.14. Fine adjustment of sintering behaviours was accomplished by the size control of the starting powders. Fig.15 shows an example of sintering adjustment in which sintering unbalance was almost eliminated, though with small difference in net shrinkage. The troubles caused by the sintering unbalance was avoided by pressure sintering, i.e., by hot pressing and hot isostatic pressing. At present disk-shaped samples were fabricated by hot pressing, while pressureless sintering was applied to short and long-sized cylindrical samples.

Sintered FGM shows a characteristic microstructural transition with compositional variation, as schematically shown in Fig.16. With increasing in the mixing ratio, the connectivity of the particles increases and a skeletal network is formed. The network changes to the alternative dispersive microstructure towards the other end of the material.

Minimum thickness of compositional control depended on the particle sizes of the starting powders and on the method of powder stacking. Conventional layer-by-layer process gave 0.2mm of minimum compositional control thickness, while thickness of 0.01mm was accomplished by the spray deposition technique which was shown in Fig.17.

Thermal expansion coefficient and thermal conductivity of the present metal-ceramic mixture were found to show a characteristic change with composition, as shown in Figs.18 and 19. Electrical conductivity showed similar tendency. The sinuos curves in these diagrams are explained qualitatively as a transition between two curves which are given by the maxwell relation for the two curves dispersive structures

In the case of wet process, thin sheets without defects have to be obtained in every compositional ratio of metal and ceramic powders. The defects are usually caused by shrinkage during drying process. Selection of proper specific surface area of powder was essential to avoid the defects(3). Sintering balance was also important as same as dry process(3). By thin sheet laminating process, disk-shaped FGMs of 30mm in diameter were obtained in the system of ZrO_2 -

$3Y_2O_3/Ni$.

Spraying Process

Low-pressure plasma spraying using single-gun under a pressure of 50-80 Torr. was successful to get uniform coatings. A finely controlled FGM of 4mm thickness was obtained for $ZrO_2-8Y_2O_3/Ni-20Cr$ by single-gun process.

Fig.20 shows an cross section of FGM of $ZrO_2-8Y_2O_3/Ni-Cr-Al-Y$ on a stain - less steel substrate by two-gun process. The spraying conditions are noted on the figure. Gradual compositional change is obviously observed in both figures. However, pores are observed at the top ceramics part. The pore content in right side is higher than the others. Therefore higher angle in Fig.7 is desirable for compact FGM.

SHS Process

The disk-rod shaped FGM in systems of TiC/Ni , TiB_2/TiC and TiC/Al_2O_3 were obtained by using powder mixture of Ti and C as the ignition agent. Though starting compositions were only for steps, the sintered product showed a continuous structural change as shown in Fig.21(6). The result of compositional analysis by EPMA revealed continuous compositional change(6,7).

CONCLUDING REMARKS

Four main processes were adopted to fabricate FGMs. Each process has its own features in material system, size and properties, etc. Though only a thin layer can be obtained by gaseous process, but the structural and compositional gradient can be controlled very finely. On the other hand, thick FGM can be obtained by processes using powders as starting materials, but minimum controlling range is larger than gaseous processes. A proper process and material system should be selected to fit its applying part.

ACKNOWLEDGEMENT

This investigation was granted as research sponsored by special coordination funds of STA for promoting science and technology. The research on fundamental techniques to develop functionally gradient material for relaxation of thermal stress.

REFERENCES

1. Shiota, I., Ozawa, E., Watanabe, O., "Prospects of Metal Nitride Intermediate Layer for FRM" Proc. ICCM-IV Tokyo, 1982, p1481
2. Sasaki, M., Wang, Y., Ohkubo, A., Hirai, T., Hashida, T., Takahashi, H., Hirano, T., "Fabrication of SiC-C FGM by CVD Process", Proc. 3rd FGM Symposium, 1989, p61 (in Japanese)
3. Yoshitake, A., Tamura, M., Shiota, I., Niino, M., "Fabrication of the Functionally Gradient Materials (FGM)-The State of the Art-", Proc. ESA Sympo on Space Applications of Advanced Structural Materials, 1990, in printing
4. Saitoh, T., Kitaguchi, S., Shimoda, N., Shiomi, Y., Koga, M., Takigawa, H., "FGM Coatings by Single-gun method", Proc. 3rd FGM Symposium, 1989, p5
5. Fukushima, T., "FGM Coatings by Single-gun method", Proc. 3rd FGM Symposium, 1989, 1
6. Miyamoto, Y., Nakanishi, H., Tanaka, I., Okamoto, T., Yamada, O., "Fabrication of TiC-Ni FGM by SHS under Gas Pressure", *ibid.*, p19
7. Sata, N., Yanagisawa, N., Nagata, K., Asano, O., Sanada, T., "Fabrication and Properties of TiB_2-Cu FGM by SHS Process", *ibid.*, p23
8. Mitoff, S. P., Properties Calculations for Heterogeneous Systems, *Advance in Material Research*, Vol. 3, John Wiley & Sons (1968), P305

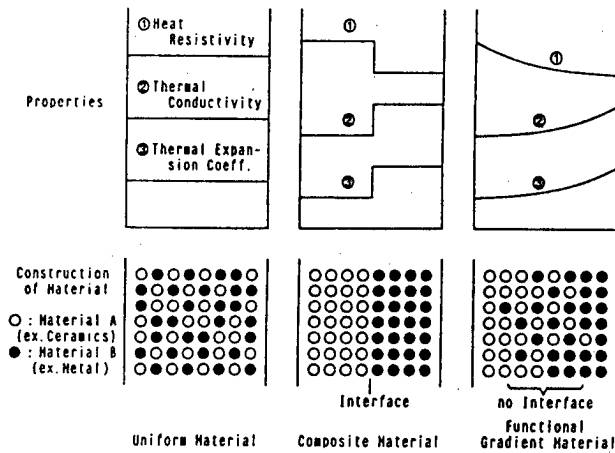
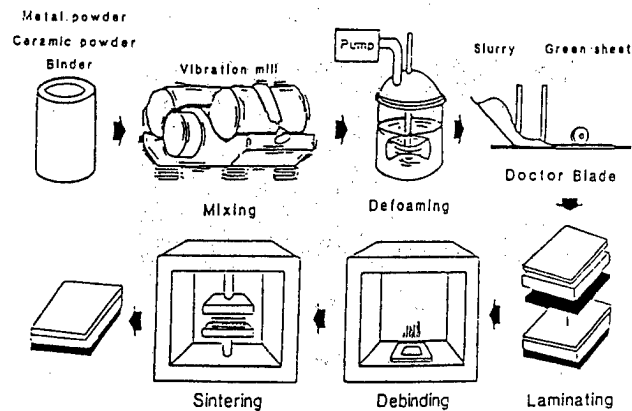
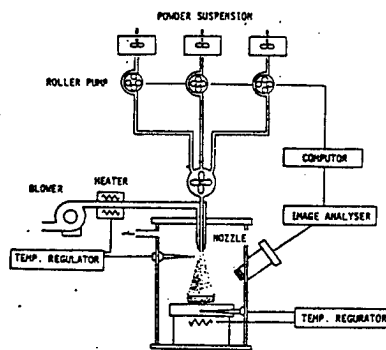
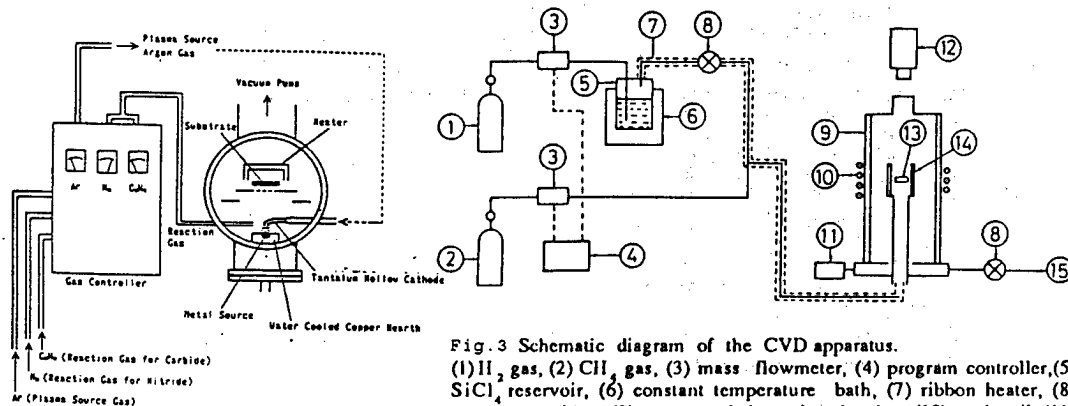


Fig. 1 Structure and properties of various materials



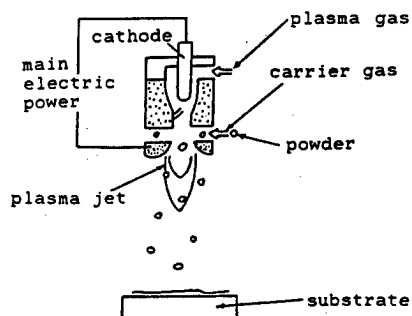


Fig.6 Single gun method

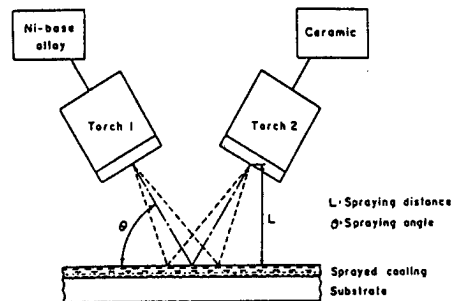


Fig.7 Two-gun method

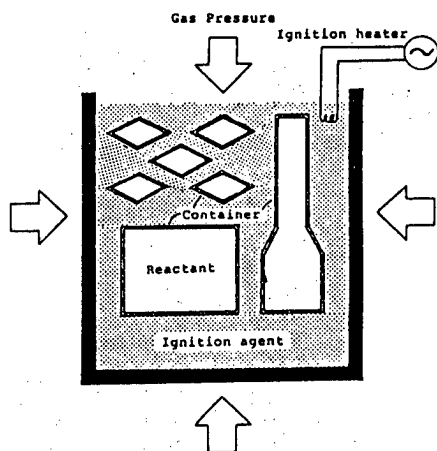


Fig.8 SHS process under gas pressure

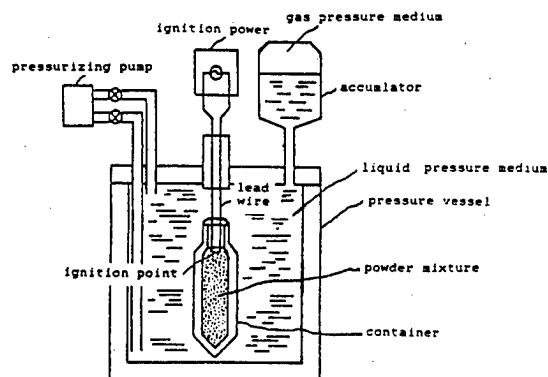


Fig.9 SHS process under hydraulic pressure

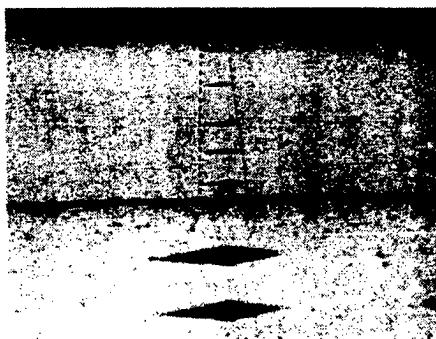


Fig.10 Ti to TiN FGM by PVD

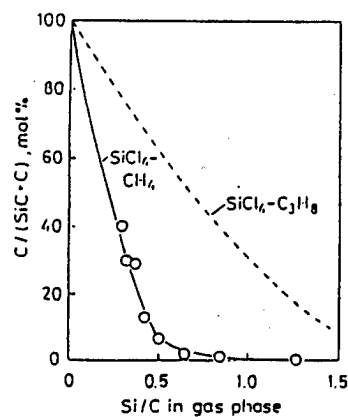


Fig.11 Si/C in gas phase vs. C/(SiC+C) in NFGM.
 $\text{SiCl}_4\text{-CH}_4$: 1773K, 1.3kPa
 $\text{SiCl}_4\text{-C}_3\text{H}_8$: 1773K, 40kPa

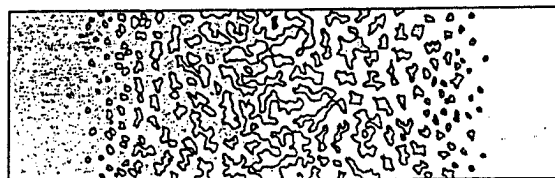
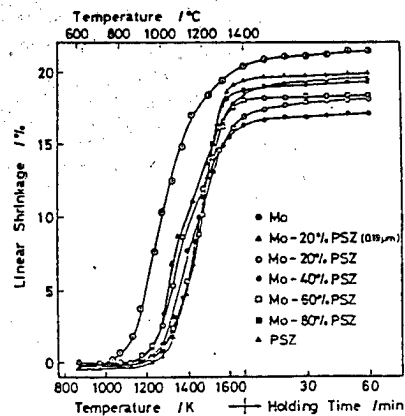
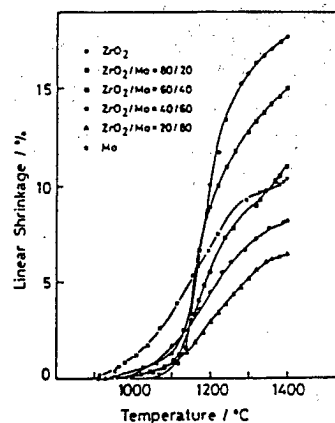
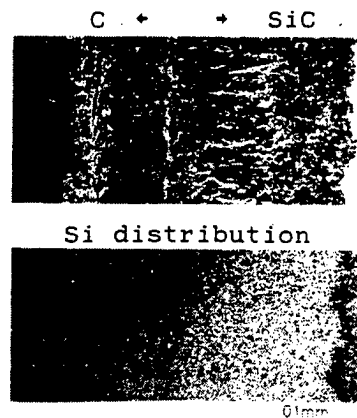
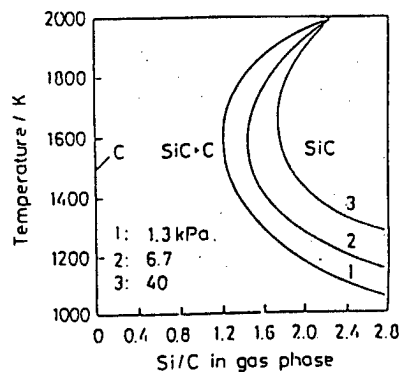
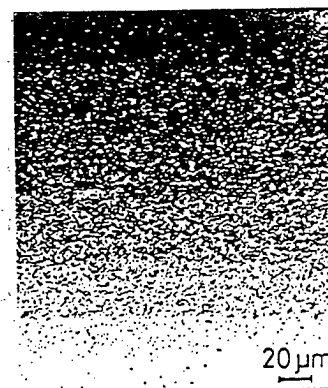


Fig.17 Powder-spray formed PSZ/SUS304 FGM



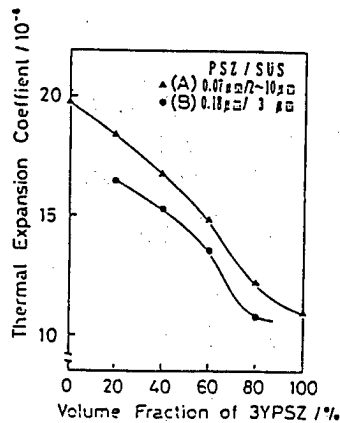


Fig. 18 Relation between thermal expansivity and composition.

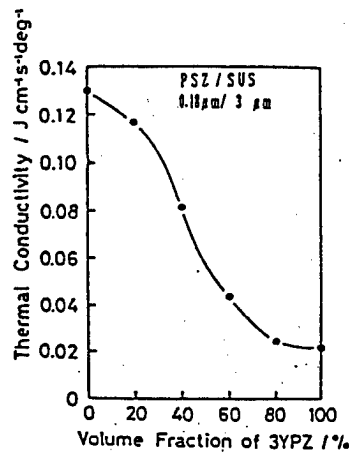
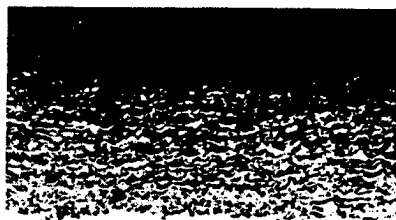
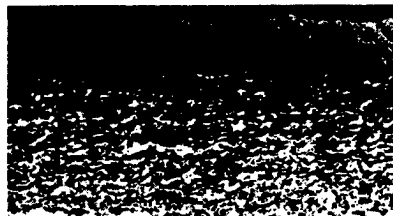


Fig. 19 Relation between thermal conductivity and composition.



71°



61°

Fig. 20 Micro-structures of graded coating
 operating current Ni-Cr-Al-Y:800A, Zr₂O₃/8Y₂O₃:1200A
 operating gas flow rate T₁, T₂: 45 l/min
 spraying distance 100mm
 spraying angle noted under each figure

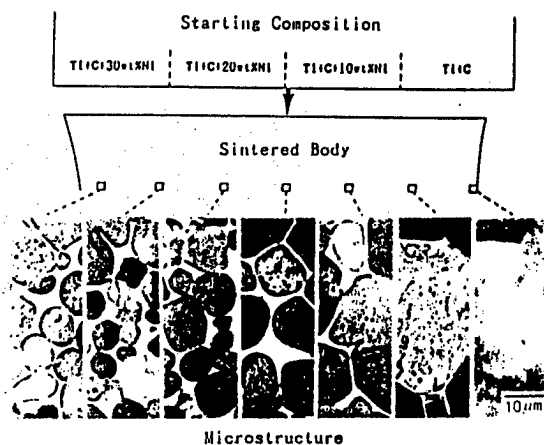


Fig. 21 Structure of TiC-Ni FGM

SILICON CARBIDE FIBRES REINFORCED SILICON CARBIDE AND GLASS CERAMIC COMPOSITES

M. Parlier, T. Grenier and J.-F. Stohr

**Direction des Matériaux,
Office National d'Etudes et de Recherches Aéronautiques (ONERA),
B.P. 72, F-92322 Châtillon Cedex, France**

ABSTRACT

Glass ceramic and covalent matrix ceramic composites are promising candidates for structural applications. Cost effective liquid processing routes either by injection moulding for the glass ceramic matrix or by infiltration of the fibre preform by a polymeric precursor and subsequent pyrolysis for the covalent matrix have been developed. This last processing route leads in the case of silicon carbide matrix to mechanical properties similar to that obtained by the conventional CVI technique. A micromechanics study has further confirmed the prime role of the fibre-matrix shear strength on the failure mode and mechanical properties of the composite, and the absolute necessity to control this parameter to insure a dissipative failure. An instrumented micro-indentation technique has been developed to achieve this end.

INTRODUCTION

The need for increased paying load in aeronautical civil aircraft as well as improved performance and efficiency in jet engines has resulted in a continuous decrease in the structure weight. This decrease in the structure weight leads to a large demand for the development of low density materials with an enhanced environmental resistance, able to operate at high temperatures under high stresses.

Moreover, among all the criteria involved in the choice of new structural materials, the cost/performance ratio is today of prime importance for aircraft and engine components and the development of new processing routes leading to shorter manufacturing cycles appears as one of the main ways to achieve sensible cost reductions.

Ceramic Matrix Composites (CMC's) appear as promising materials to meet the two former requirements, due to a unique set of combined properties:

- a high temperature capability up to 2000°C,
- high specific strength and stiffness,
- a low specific gravity,
- a good environmental resistance,
- a damage tolerant mechanical behaviour.

An illustration of the capability of ceramic matrix composites is given on Fig. 1, which compares the evolution of the specific strength of CMC's versus temperature with that of the main materials currently used in the aerospace industry. Among all the potential candidates, glass ceramic matrix and covalent matrix composites appear as the most prominent materials due to their ability of being processed by cost effective liquid routes.

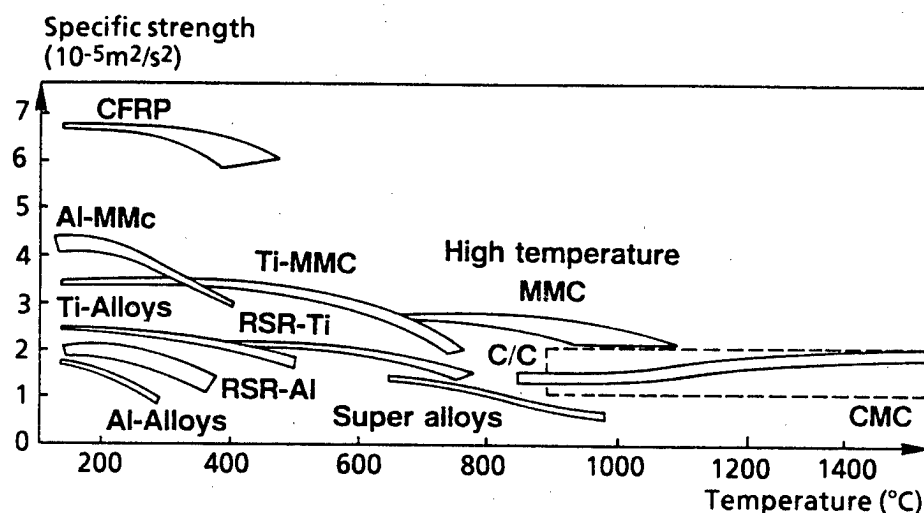


Fig. 1. Compared specific strength versus temperature for CMC and the materials most widely used in aeronautical industries

MECHANICAL BEHAVIOUR OF CERAMIC MATRIX COMPOSITES

Aveston, Cooper and Kelly (ACK) Model and SiC/Glass Ceramic Composite Behaviour

The non brittle rupture observed in some ceramic matrix composites - in fact it will be more accurate to say a dissipative failure - mainly originates from the weak bond between the fibre and the matrix allowing the matrix crack to be diverted or to outpass the fibres without breaking them, thus allowing multicracking of the matrix, without composite failure, to develop; on the opposite, if the fibre and the matrix are strongly bonded together, the crack grows straightforward, ignoring the fibres, thus leading to a brittle failure with a flat rupture surface. The understanding of this particular behaviour of CMC's constituted of two brittle phases was first proposed by Kelly et al. [1] who show that, in **unidirectional composites**, multifissuration of the matrix throughout the whole specimen cross-section occurs, leading to the specific shape of the stress-strain tensile curve illustrated on Fig. 2. This curve comprises the three following domains:

- a first elastic domain which ends with the first matrix crack;
- a plateau region corresponding to multicracking of the matrix occurring at the constant rupture stress of the matrix;
- finally, a linear stage corresponding to incremental loading of the fibres alone, leading to an apparent modulus of $E_f V_f$; this third stage ends at the failure stress of the fibres within the composite $\sigma_{fu} V_f$.

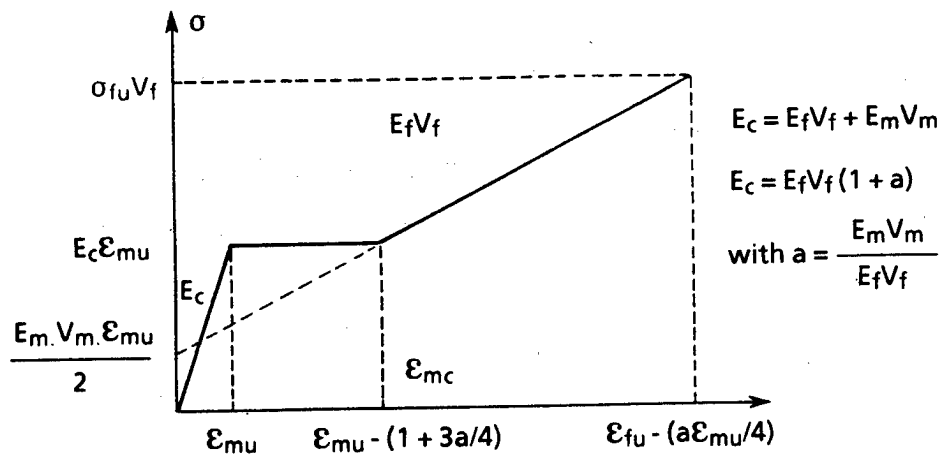


Fig. 2. Theoretical stress-strain curve according to the ACK linear mechanics approach

ACK further demonstrate by a keen micromechanics analysis based on a global energetic approach that the dissipative failure of the composite requires fibre-matrix debonding in front of the matrix crack, and that the rupture stress of the matrix within the composite - defined as the stress at which the first matrix crack has entirely crossed the specimen section - might be higher than that of the matrix alone.

In this former linear mechanics approach ACK made the assumption that the matrix rupture stress was unique, which is of course not the case since the rupture stress of ceramics is known to obey a Weibull distribution law. This distribution of the matrix rupture stress could of course account for the different shape of the tensile curve observed for most of unidirectional CMC's, which exhibits a somewhat smoother form with no plateau region as illustrated on Fig. 3 for a SiC/glass ceramic unidirectional composite. In fact, observation of SiC/glass ceramic composites specimens during the tensile test using an optical microscope reveals that the matrix cracks do not propagate instantaneously throughout the whole specimen cross-section as stated previously by ACK. Development of the matrix multicracking has thus been shown to happen in three stages:

- firstly, the nucleation of small microcracks, most of them appearing in the vicinity of the fibres at the end of the elastic domain (Fig. 3a);
- secondly, the growth of transverse macrocracks responsible for the composite stiffness loss (Fig. 3b);
- thirdly, the development of the macroscopic matrix multicracking throughout the whole specimen gauge length.

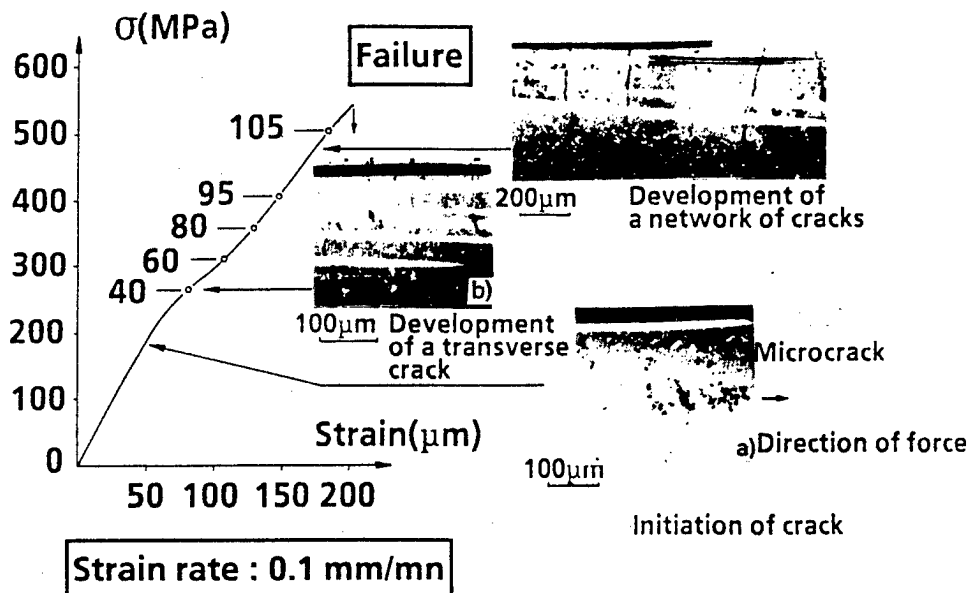


Fig. 3. Tensile stress-strain curve for a unidirectional SiC-Nicalon/LAS composite ($V_f = 37\%$) exhibiting the different damaging stages and the number of matrix macrocracks

A keen observation of the development of these macrocracks reveals that their growth rate is either stable or unstable depending upon their distance from the fibres: a fast growth rate was observed away from the fibres while a slow growth rate was always shown to exist in the immediate vicinity of the fibres. This influence of the matrix crack distance from the fibres on their growth rate clearly evidences the strong crack closing effect arising from the stiffener role played by the fibres. These observations lead to the following conclusions:

- the absence of a plateau region in the tensile curve of the SiC/glass ceramic composite is not due to pre-existing flaws within the matrix, but related to the matrix crack growth;
- a more accurate prediction of the CMC's behaviour in tension must rely on a local fracture mechanics approach, taking the crack growth stage into account.

Rupture Mechanics Approach of the Matrix Multifissuration

A local matrix crack growth modelization based on the same assumptions as those stated by ACK regarding the fibre-matrix load transfer by shear has been developed for a single fibre layer unidirectional composite by Pérès [2]. In this simulation, the crack growth rate is computed using an energy balance taking into account the energy released rate at the crack tip. The released energy ΔU during the crack growth, for a constant stress loading, is therefore half the value of the sum of the work done by the external forces and that resulting from the friction stresses during the glide of the fibres in their matrix sheaths. The variation of this work as a function of the crack length a , calculated for each step of the crack growth Δa , is plotted on Fig. 4a and 4b for a fully rigid fibre-matrix bond and a weak fibre-matrix bond respectively. The energy released at the crack tip is a pseudo-periodic function of the crack length with a series of minima, the lower each minimum, the higher the fibre-matrix cohesion.

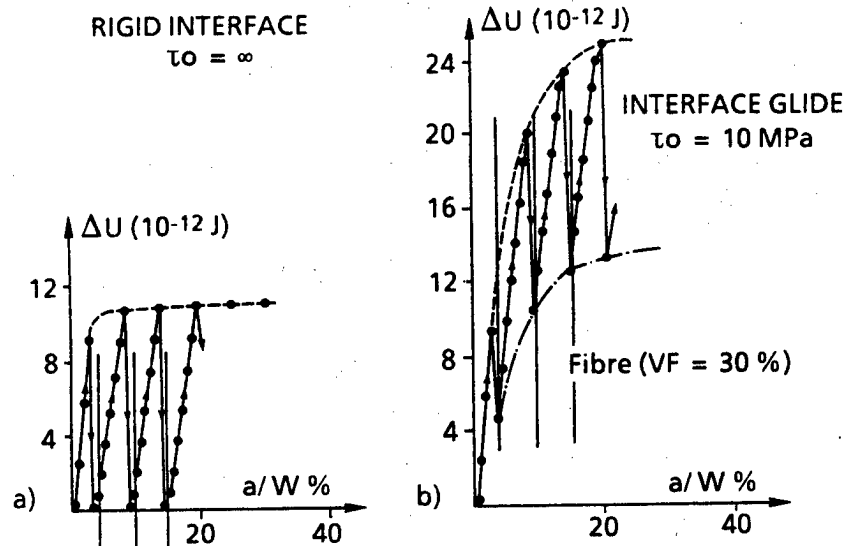


Fig. 4. Energy released at the crack tip during the crack growth for each propagation step
 a) With no fibre-matrix displacement at the interface
 b) With decohesion and glide at the fibre-matrix interface

The minimum value of the energy released at the crack tip increases during the crack growth so much the more as the interfacial shear strength decreases. The total energy released during the crack growth is well depicted by the area subtended by the pseudo-periodic curve. Therefore, a weak fibre-matrix shear strength will lead to a high value of the energy released during the crack growth, and then to a non-brittle dissipative failure.

This local crack growth computed simulation clearly evidences:

- firstly, the stiffener role played by the fibres in a way similar to what is observed in a stiffened metallic panel;
- secondly, the primary importance of the value of the fibre-matrix interfacial friction shear stress relative to the dissipative failure energy of the composite, the lower the friction stress, the higher the energy released at failure, provided that this friction stress remains higher than the threshold value τ_0 , insuring a sufficient fibre-matrix load transfer for the composite to work.

Therefore, processing of non-brittle CMC's requires an accurate control of this parameter, which can be achieved using the instrumented micro-indentation technique.

Instrumented Micro-indentation and Fibre-matrix Interface Control

The instrumented micro-indentation technique presents relative to the micro-indentation test first used by Marshall [3] the advantage of a precise determination of the fibre-matrix friction stress due to a simultaneous recording of the applied load and the fibre displacement.

A typical load-displacement curve exhibits the three following stages (Fig. 5):

- the first stage which corresponds to the indentation of the fibre ends with debonding of the fibre from the matrix;
- the second stage, which corresponds to the glide of the debonded length of the fibre in its matrix sheath, ends when the indenter reaches the matrix;
- the third one corresponds to the indentation of the matrix.

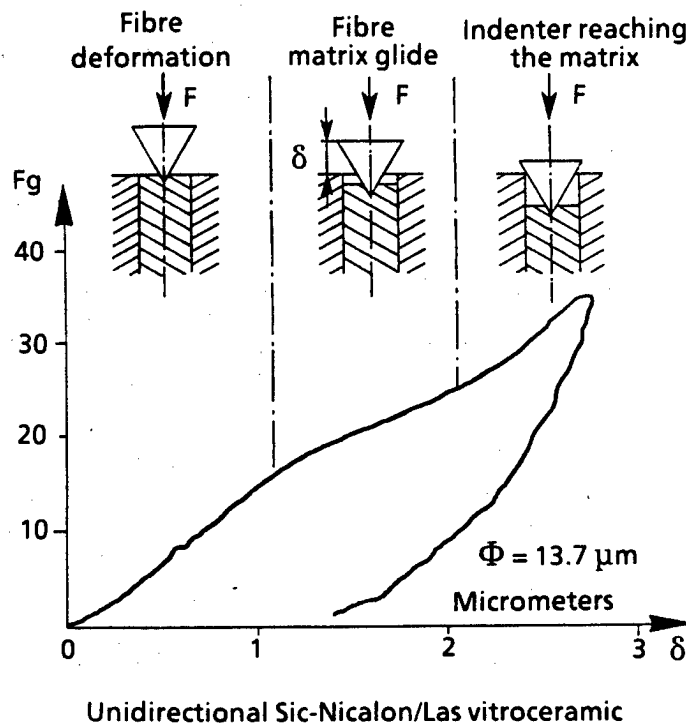


Fig. 5. Instrumented Vickers indentation test:
load versus displacement curve

Exploitation of the second stage of the load-displacement curve using a simple shear-lag analysis allows to derive a constant value of the interfacial friction shear stress.

As an illustration, Table 1 shows the results obtained with SiC/LAS composites manufactured at ONERA, using different fibre coatings, so as to achieve a precise control of the fibre-matrix interface characteristics.

TABLE 1. Mechanical properties of 1D SiC/LAS composites
in relation with the fibre-matrix
interfacial friction shear stress τ_i

Composites	τ_i (MPa)	Flexural strength	Feature of the rupture
SiC/LAS	11	1020	Dissipative (pull-out)
SiC+C/LAS	20	600	Rough rupture surface
SiC+Nb ₂ O ₅ /LAS	25	580	Rough rupture surface

It is then obvious that the flexural strength and the rupture mode are strongly related to the fibre-matrix interface friction stress. In that particular composite, a dissipative failure mode was only obtained with uncoated Nicalon fibres.

THE MAIN PROCESSING ROUTES IN USE FOR CERAMIC MATRIX COMPOSITES

Most of the ceramic composites in use today in the aerospace industry are designed starting from the fibre preform. Therefore, processing of these composite components cannot rely on the sintering technique in use for monolithic ceramics, for the two following reasons:

- the limited thermal stability of oxide or silicon-carbide fibres does not allow their hold at the temperature level of a sintering cycle;
- the constraining of shrinkage due to the presence of fibres will lead to wholly cracked components.

That are the reasons why CMC processing mainly relies on techniques based on the infiltration of the fibre preform. The matrix is then obtained by the decomposition of a gas phase, the infiltration of a liquid glassy phase or the pyrolysis of an infiltrated and cured polymeric precursor.

The Chemical Vapor Infiltration (CVI) Technique

CVI reactors for composite processing generally operate under isothermal conditions at low decomposition rates, thus allowing the manufacture of complex shape components with a good in-depth matrix homogeneity. However, this good homogeneity of the matrix can only be achieved through several infiltration cycles with intermediate machining of the components. This processing route leads to good quality components at the expense of long processing times (several months) which remain however acceptable for aerospace industry. CVI ceramic matrix composite processing has been developped in France by SEP [4] mainly for the production of SiC/SiC and C/SiC components today in use on rocket or turboprop engines.

Nevertheless, the long processing time necessary for the CVI manufacturing route has, for the time being, restricted the use of CMC components to the aerospace industry for cost effectiveness reasons. Improvements of the CVI technique in view of reducing the processing time have been proved to be successful. It is worth mentioning the low pressure reactor vessel designed by the ORNL in the United States [5], which allows a fifty-fold increase of the deposition rate; unfortunately, this processing technology is only fitted to the manufacture of thin components with not too intricate shapes.

The limitations of the CVI technique regarding the production cycle duration has resulted in search for more rapid and efficient processing routes.

Processing of Composites using Liquid Phase Infiltration of the Fibre Preform

Two different kinds of matrices are relevant of the liquid phase infiltration technique [6]:

- the glass-ceramic matrices, due to the fact that the glassy phase exhibits a viscosity allowing densification at a temperature compatible with the thermal stability of the fibres;
- covalent matrices such as SiC or Si_3N_4 for example, which can be obtained by the pyrolysis of polymeric precursors at a sufficiently low temperature to avoid any fibre degradation.

Glass-ceramic matrix composites. As an example the SiC Nicalon/LAS (lithium oxide, alumina, silica) composite can be processed using either hot pressing of prepreg tapes at a temperature insuring a viscosity below 5000 poises, or by injection moulding of the fibre preform at the same temperature level [2]. This last process is relevant of not too intricate shape components exhibiting a centre axis.

Covalent matrix composites processed from a polymeric precursor. The idea of using silicon based polymeric precursors to mould ceramic composites originates from the processing route used for carbon-carbon composites. However, the achievement of a SiC or a Si_3N_4 matrix is much more difficult than a carbon matrix due to the density difference between the polymeric resin and the ceramic leading to a high shrinkage, 75% as compared to only 35% in the case of carbon matrix composites.

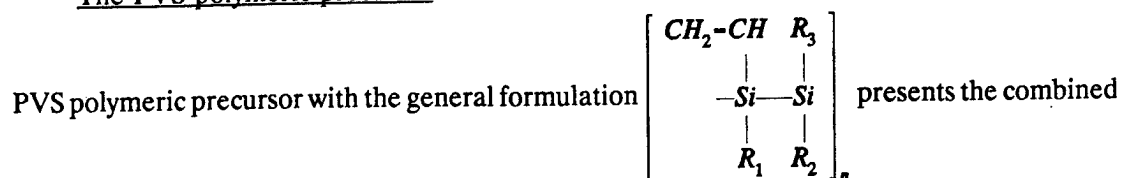
In order to overcome this difficulty, it is desirable to limit the role of the ceramic sprung from the resin to an efficient binder. To achieve this end a two-step infiltration process has been developed at ONERA [6]:

- the first step consists in an infiltration of the fibre preform by fine submicronic ceramic particles achieved using a colloidal filtration technique, which allows to fill 50% of the free volume within the fibre preform;
- the second step consists in an injection of the powder infiltrated preform with a suitable polymeric precursor followed, first by a curing cycle, then by pyrolysis.

This processing route allows the achievement of a sound composite with a residual porosity around 10% in the case of a 2D fibre preform.

However, these good results concerning the porosity can only be obtained provided that the polymeric precursor exhibits a combined set of properties allowing both a good matrix infiltration and a high ceramic yield. For this purpose, a specific polymer precursor of a silicon carbide matrix has been developed by ONERA and IRAP [7,8] while ATOCHEM has developed polymeric precursors of SiC/Si₃N₄ matrix [9,10]. As an illustration, the PolyVinyl Silane (PVS) developed at ONERA will be described in some more detail.

The PVS polymeric precursor.



set of properties required for ceramic matrix processing:

- a relatively low molecular weight ranging between 3500 and 4500 in order to achieve a sufficiently low viscosity at room temperature (20 poises) allowing the fibre infiltration at a temperature compatible with the gelification time;
- a thermoset behaviour - a pre-requisite in the case of a ceramic precursor - with a cross-linking temperature sufficiently below that of beginning of pyrolysis (Fig. 6), to avoid bubble forming during the curing cycle, which will lead to a high level of porosity.

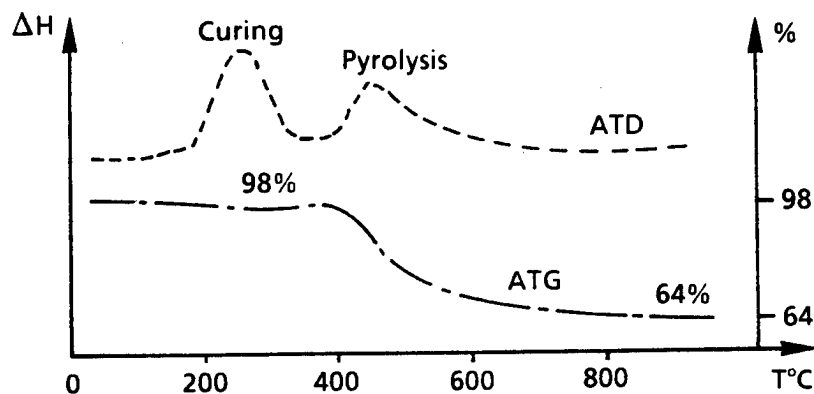


Fig. 6. Thermal characteristics of the PVS polymeric precursor

PVS exhibits a high matrix yield of 65% with a final composition of the ceramic product very near that of SiC-Nicalon fibres, as illustrated in Table 2.

Due to the overall good properties of the PVS precursor a flexible liquid processing route has been achieved for the manufacture of silicon carbide matrix composites. In order to check the reliability of the process, different silicon carbide fibres woven fabrics 1D, 2D, 3D have been used for composite processing based on the two-step infiltration previously described.

TABLE 2. Chemical analysis of the ceramic matrix and fibre obtained from polymeric precursors (weight %)

Ceramic	Species		
	SiC	SiO ₂	C
SiC (PVS)	68%	8%	24%
SiC (Nicalon)	66%	17%	17%

As shown in Table 3, the flexural rupture strength of the SiC/SiC composite processed by the liquid route compares favorably to that of composites processed by the CVI technology.

TABLE 3. Bending rupture strength (MPa) as a function of the processing route for SiC/SiC composites

Fibre architecture	Processing route		
	CVI (SEP)	CVI (Oak Ridge)	Liquid route (ONERA)
1D	700 (V _f = 0.45)	400 (V _f = 0.45)	500 (V _f = 0.45)
2D	350 (V _f = 0.45)	300 (V _f = 0.40)	200 (V _f = 0.30)
3D	-	-	250 (V _f = 0.45)

Potential Development of Ceramic-matrix Composites

Ceramic matrix composites have demonstrated their capacity as structural components in the aerospace industry, mainly for engine application due to their good specific strength at high temperatures (Fig. 7). Among the currently used composites, the SiC/LAS material appears very promising for a use up to 650°C with a further potential development up to 1000°C due to both its good properties (Table 4) and a cost effective processing route by injection moulding or hot pressing.

SiC/SiC and C/SiC materials present good properties up to 1200-1300°C for the first one, and 1500-1600°C for the second one. Moreover, it has been further demonstrated that these composites exhibit good fatigue resistance in that sense that no modification of the static mechanical properties (rupture strength, elongation to rupture) is observed after fatigue testing at room temperature [11] for loading conditions of either 35% of the static rupture stress, R = -1, 10⁶ cycles or 80% of the static rupture stress, R = 0.1, 10⁵ cycles; for the same loading conditions, a 20% drop in the Young's modulus is observed.

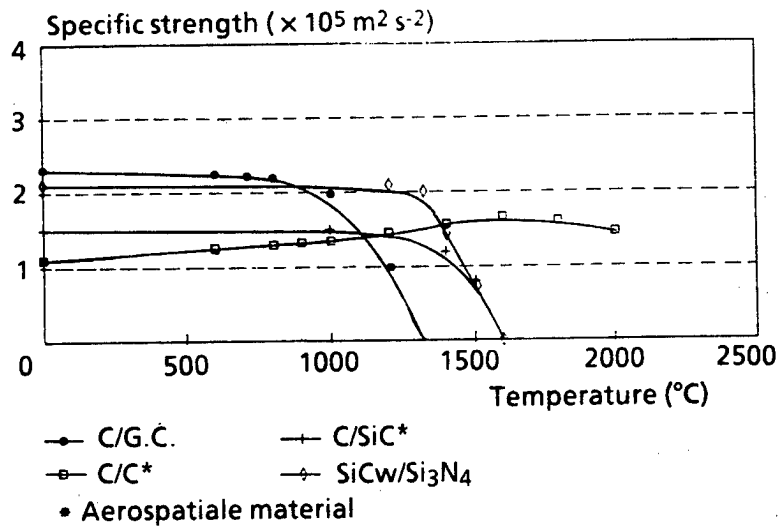


Fig. 7. Specific strength versus temperature for main ceramic matrix composites in use today

TABLE 4. Structural and mechanical resistance of the main CMC's in use today

Properties	Composites		
	SiC/LAS	SiC/SiC	C/SiC
Geometry of 2D woven fabrics	Satin weave	Plain weave	Plain weave
Total volume fraction of fibre	40%	40%	45%
Apparent specific gravity (g/cm^3)	2.5	2.5	2.1
Open porosity	2%	10%	10%
Ultimate bending strength (MPa)			
(typical values) 20°C	300	300	500
900°C	250	400	700

Moreover, the new processing route by liquid infiltration of the fibre preform offers the advantage of a short processing cycle and a reduced cost relative to the CVI technology used up to now, allowing to envisage applications of these materials out of the aerospace field.

CONCLUSION

1. The local analysis of the matrix crack growth has confirmed the former results obtained by ACK and further highlighted the prime importance of an accurate control of the fibre-matrix friction stress upon the mechanical properties (rupture strength, failure mode).

2. An instrumented micro-indentation test has then been developped, allowing a precise measurement of the fibre-matrix friction stress.
3. The feasibility of composite processing using the liquid route has been demonstrated for both glass ceramic and covalent matrices. For this latter matrix, a suitable polymeric thermoset SiC precursor has been developped and a two-step infiltration procedure defined.
4. The covalent matrix composites manufactured using the liquid route processing present mechanical properties equivalent to those processed by the conventional CVI technique.
5. The advantages of cost and processing time reduction together with the flexibility of this fabrication route regarding the matrix composition allow to consider applications of these materials out of the aerospace scope.

REFERENCES

- [1] Aveston J., Cooper G.A. and Kelly A., "Single and multiple fracture in properties of fibre composites", Conference Proceedings NPL, 15th IPC Science and Technology Press, Guildford (1971)
- [2] Pérès P., "Analyse théorique et expérimentale du rôle des paramètres de microstructure sur le comportement des composites à matrice fragile", INSA Thesis, September 5 (1988)
- [3] Marshall D.B., "An indentation method for measuring fibre friction stresses in ceramic composites", J. Amer. Ceram. Soc., vol. 67, n° 12 (1984)
- [4] French Patent 82.01025, "Structure composite de type réfractaire-réfractaire et son procédé de fabrication", January 22 (1982)
- [5] Stinton D.P., Caputo A.J., Lowden R.A., "Synthesis of fiber-reinforced SiC composites by Chemical Vapor Infiltration", Ceram. Bull., vol. 65, n° 2 (1986)
- [6] Jamet J.F., Anquez L., Parlier M., Ritti M.H., Pérès P., Grateau L., "Composite céramique : relations entre microstructure et rupture", L'Aéronautique & l'Astronautique, n° 123/124 (1987) p. 128-142
- [7] French Patent 89.00774, "Polysilanes et leur procédé de préparation", January 23 (1989)
- [8] Larché F., Elissalde D., Parlier M., Noireaux P., "Effect of the heat treatment temperature on the transformation of a SiC precursor", To be published in the proceeding of "International fine ceramics workshop", Nagoya (1990)
- [9] French Patent 87.18215, "Polysiloxalanes et leur procédé de préparation, leur utilisation comme précurseurs de céramique et lesdites céramiques", December 28 (1987)
- [10] Colombier C., "Studies of new polysilazanes precursor to Si-C-N-O ceramics", Proceeding of the 1st European Ceramic Society Conference, Maastricht, vol. I, June 18-23 (1989) p. 143-152
- [11] Jouin J.M., "Comportement sous chargement cyclique de composites céramique-céramique", Proceeding of the AMAC-CODEMAC congress, Bordeaux, editors: R. Naslain, J. Lamalle, J.L. Zulian, AMAC, April 29-30 (1990)

NEW MATERIALS DESIGN OF STRUCTURAL CERAMICS

-NANOCOMPOSITES-

K. NIIHARA and A. NAKAHIRA

Institute of Scientific and Industrial Research
Osaka University
8-1 Mihogaoka, Ibaraki-City 567, Osaka, Japan

ABSTRACT

Effects of SiC particulate dispersions on the mechanical properties have been investigated for Al_2O_3 and MgO ceramics. Both $\text{Al}_2\text{O}_3/\text{SiC}$ and MgO/SiC nanocomposites, in which SiC particles with nanometer size were dispersed within the matrix grains, were prepared by hot-pressing mixtures of fine powders less than $0.3\mu\text{m}$. In these nanocomposites, the mechanical properties such as hardness and fracture strength were significantly improved even at high temperatures above 1000 to 1200°C by SiC dispersions. The relationship between nanostructure and mechanical properties will be discussed for $\text{Al}_2\text{O}_3/\text{SiC}$ and MgO/SiC nanocomposites.

INTRODUCTION

Al_2O_3 and MgO ceramics have high potentials for structural applications, because of high hardness, good wear resistance and chemical inertness [1]. However, the availability of these oxide ceramics is greatly limited by low fracture toughness and strength, relatively poor thermal shock and creep resistances [2]. Thus, the improvement of mechanical properties for Al_2O_3 and MgO would expect the widespread applications as structural materials.

It is well known that the improvement of mechanical properties of ceramics has been achieved by the dispersion of particulate or whisker [3-5]. Although the whisker reinforcement leads to highly strong and tough ceramics, it makes difficult to obtain the dense ceramics and to achieve homogeneity [6]. For these three years, Niihara and his colleagues [7-13] have been investigating the ceramic nanocomposites in which the nano-size particles are dispersed within the matrix grains. In this paper, we describe the relationship between mechanical properties and microstructure for Al_2O_3 and MgO composites containing 5 to 33vol% SiC particles prepared by the hot-pressing technique. Special emphasis was placed on the understanding of the nano-scale microstructure design for improving the mechanical properties for these $\text{Al}_2\text{O}_3/\text{SiC}$ and MgO/SiC composites systems.

EXPERIMENTAL PROCEDURES

The $\alpha\text{-Al}_2\text{O}_3$ (average particle size of $0.4\mu\text{m}$ from Asahi Chemical Co.), and MgO (average grain size of $0.1\mu\text{m}$ from Ube Industries Ltd.), SiC (average particle size below $0.3\mu\text{m}$ from Ibiden Co.) were selected as starting powders.

The mixtures for $\text{Al}_2\text{O}_3/\text{SiC}$ and MgO/SiC composites systems containing various volume fraction of SiC particle were made by the conventional ball milling method in the highly pure acetone using the Al_2O_3 balls for 24h. The dried mixtures for $\text{Al}_2\text{O}_3/\text{SiC}$ and MgO/SiC systems were hot-pressed in N_2 atmosphere at 1600 to 1900 °C with applied pressure of 30MPa.

After the hot-pressed specimens were cut by diamond wheel and ground, the densities were measured by Archimedes methods using toluene for all composites. The components of both composites were determined by the X-ray diffraction analysis. The micro and nanostructure were examined by optical microscopy, scanning electron microscopy (SEM) and transmission electron microscopy (TEM). The hardness of these composites were measured by using a high-temperature Vickers hardness tester (Nikon, QM) up to 1300 °C. Tests were carried out in vacuum at the indenter load of 4.9N. The fracture toughness were determined by the indentation microfracture method with indenter load of 4.9 to 19.6N [14]. The fracture strength were estimated at room temperature to 1400 °C in air atmosphere by three-points bending with specimen dimension of 3x4x40mm. The tensile surfaces of specimen were polished to 1 μm diamond paste and the tensile edges were beveled.

RESULTS AND DISCUSSION

Micro and Nanostructure

As expected, the densities of composites prepared in this work were strongly dependent on the volume fraction of SiC dispersion and sintering temperature. For the $\text{Al}_2\text{O}_3/\text{SiC}$ system, the nearly full densities were observed at 1600 °C up to 5.1 vol%SiC, at 1700 °C for 10.5 vol%SiC and at 1800 °C for 17.2 to 32.7 vol%SiC. For the MgO/SiC composite system, the high densities of over 99% were obtained for the hot-pressed materials at 1700 to 1900 °C, depending on the volume fraction of SiC particles.

The X-ray diffraction analysis revealed that the $\text{Al}_2\text{O}_3/\text{SiC}$ and MgO/SiC composites prepared in this work were composed of $\alpha\text{-Al}_2\text{O}_3$ and $\beta\text{-SiC}$ and of MgO and $\beta\text{-SiC}$, respectively. The reaction phases were not detected. As shown in Fig.1, TEM observation revealed that the most of the fine SiC particles, typically less than 0.2 μm , were dispersed within Al_2O_3 grains for $\text{Al}_2\text{O}_3/\text{SiC}$



Fig.1 Micro and nanostructures for the $\text{Al}_2\text{O}_3/5\text{vol}\%\text{SiC}$ nanocomposites. Arrows indicate the SiC dispersions within the matrix.

composites and the same observation was also obtained for MgO/SiC composites. It was confirmed, therefore, that the nanocomposites, in which the second phase particles were dispersed within the matrix grains, could be successfully prepared by the conventional sintering method for both $\text{Al}_2\text{O}_3/\text{SiC}$ and MgO/SiC systems. The average grain sizes of Al_2O_3 and MgO were approximately 2 to $3\mu\text{m}$ for both composite systems prepared under the conditions above-mentioned.

Mechanical Properties

Fig. 2 shows the variation of fracture strength of $\text{Al}_2\text{O}_3/\text{SiC}$ composites with volume fraction of SiC. The strength of this composite increases significantly from 355 to 1017MPa and remains slightly-decreased strength 870MPa up to 33vol% SiC. The dependence of SiC dispersion on fracture toughness is quite similar to that of fracture strength, in which the fracture toughness increases from 3.25 to $4.70\text{MPam}^{1/2}$ at 5vol% SiC and remain the almost same toughness value up to 33vol% SiC. Furthermore, the maximum strength of $\text{Al}_2\text{O}_3/5\text{vol}\%$ SiC composites was improved to 1540MPa by annealing the polished specimens at 1300°C for 2h in air or Ar atmosphere.

This remarkable increase in strength of $\text{Al}_2\text{O}_3/\text{SiC}$ nanocomposites by SiC dispersions and annealing may be contributed to the grain size decrease of matrix, the healing of near-surface cracks generated by machining of specimens, the relaxation of local residual stress caused by the different thermal expansion coefficients between matrix and SiC and/or the subgrain boundaries formed within the Al_2O_3 matrix grains. The subgrain boundaries may be produced by the pinning and pile-up with hard SiC particles of dislocations due to highly localized stresses generated around SiC dispersions from the thermal expansion difference between Al_2O_3 and SiC dispersion during cooling down the specimens from sintering temperatures.

The fracture toughness and strength for MgO/SiC composites were shown in Fig.3. The strength of MgO/SiC composites is improved from 330 to 560 MPa by the addition of 20vol% SiC particles and the toughness increases from 1.1 to $3.3\text{MPam}^{1/2}$.

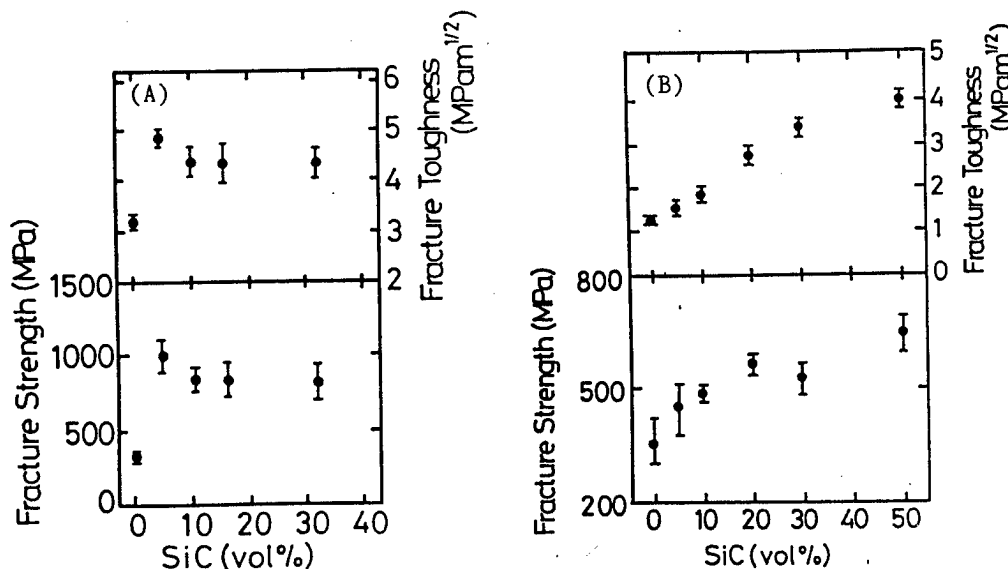


Fig.2 Variation of the fracture toughness and strength with the volume fraction of SiC dispersions for the $\text{Al}_2\text{O}_3/\text{SiC}$ (A) and MgO/SiC (B) nanocomposites.

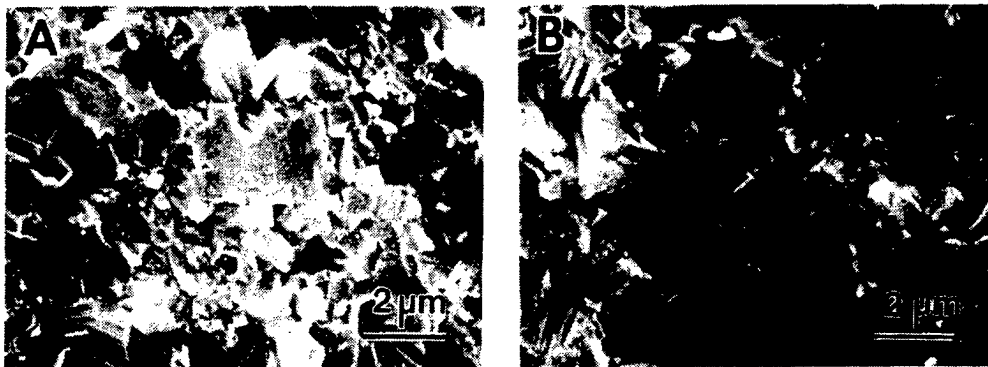


Fig.3 Fracture surfaces at room temperatures for the Al_2O_3 /5vol%SiC (A) and $\text{MgO}/10\text{vol}\%\text{SiC}$ (B) nanocomposites.

Although monolithic Al_2O_3 and MgO ceramics shows both trasgranular and intergranular fracture modes, the $\text{Al}_2\text{O}_3/\text{SiC}$ and MgO/SiC nanocomposites exhibit only the transgranular fracture mode, as shown in Fig.3. These results suggest that the SiC particles have the effect of encouraging the crack to pass through the grain rather than around the grain boundary. It might be thought that the transgranular fracture is produced by the tensile hoop stress of over 1000MPa around SiC particles within the Al_2O_3 and MgO matrix generated by thermal expansion mismatch between the matrix and SiC particles [15]. This high tensile stress will not produce the microcracking because the dispersed particle size is much smaller than the critical particle size in the $\text{Al}_2\text{O}_3/\text{SiC}$ nanocomposites, but the situation will not be always true for the MgO/SiC nanocomposites [16].

Based on these observations, it is reasonable to think that the main toughening mechanism for the $\text{Al}_2\text{O}_3/\text{SiC}$ nanocomposites is the crack deflection and the crack deflection and microcracking for the MgO/SiC nanocomposites. The radial compressive stress was also generated around the SiC dispersions by thermal expansion mismatch between the matrix and SiC particles. This compressive stresses can cancel out the shear stress generated at the grain boundary by the anisotropic thermal expansion of Al_2O_3 grain, which may result in grain boundary fracture [17]. Moreover, the TEM observation indicated that the above-mentioned subgrain boundaries are formed within the matrix grains by pile-up of dislocations. Therefore, it might be concluded that the high strength for $\text{Al}_2\text{O}_3/\text{SiC}$ and MgO/SiC nanocomposites is mainly attributed to the decrease in critical flaw size and the toughness increase associated with the dispersed SiC particles.

High-Temperature Hardness and Strength

Fig.4 shows the temperature dependence of Vickers hardness for the $\text{Al}_2\text{O}_3/\text{SiC}$ nanocomposites. These composites exhibit higher hardness at all test temperature range and smaller decreasing rates in hardness than those of monolithic materials. The degradations of high-temperature hardness for $\text{Al}_2\text{O}_3/\text{SiC}$ nanocomposites were significantly improved by the SiC dispersions. Similar improvement in hardness was also observed for the MgO/SiC nanocomposites. These results suggest that the SiC particulates dispersed within Al_2O_3 and MgO grains prohibit the high-temperature deformation and creep by the pinning of dislocations.

Fig.5 indicates the temperature dependences of fracture strength for the MgO/SiC nanocomposites. As is apparent in Fig.5, significant improvement in high-temperature strength was observed for the MgO/SiC composites. No reduc

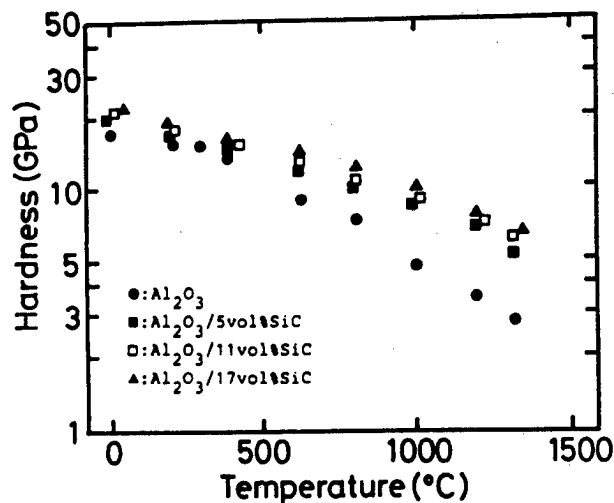


Fig.4 Temperature dependence of Vickers hardness for the Al₂O₃/nanocomposites.

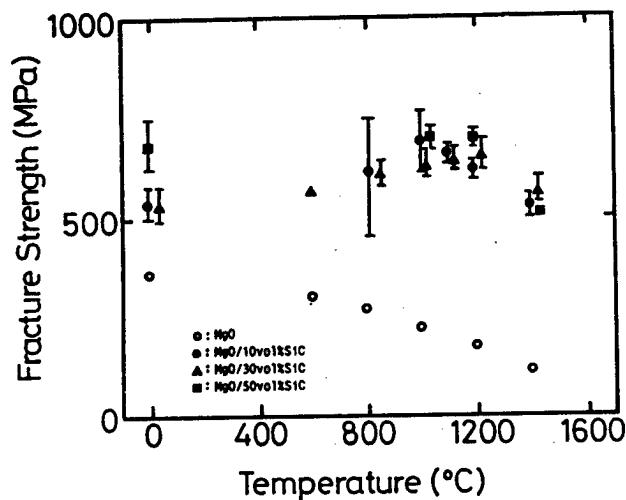


Fig.5 Temperature dependence of the fracture strength for the MgO/SiC nanocomposites.

tion in strength is observed up to 1400 °C for this nanocomposites. Especially at the temperature range from 1000 to 1400 °C, the MgO/30vol% SiC nanocomposite indicates the much higher strength than that at room temperature. The similar strength improvement was also observed for the Al₂O₃/SiC nanocomposites.

It is well known that the degradation in high-temperature strength is due to the grain boundary sliding and/or cavitation at the grain boundaries [18-21]. The radial compressive stresses around SiC particle is approximately some hundred MPa even at 1000 °C. Thus, it may be thought that this compressive stress could squeeze the grain boundary and inhibit the grain boundary sliding and/or the growth of cavities. Other possible mechanisms of improve-

ment in high-temperature strength are the creep prohibition by dislocation pinning with the SiC particle within matrix grains and the transgranular fracture enhanced by the tensile hoop stress around SiC particles.

CONCLUSIONS

The particulate nanocomposites were successfully prepared by conventional powder metallurgical technique. TEM observations revealed most of SiC particles were dispersed as nanometer-size inclusions within the Al_2O_3 and MgO matrix grains. These Al_2O_3/SiC and MgO/SiC nanocomposites showed the extremely high hardness and strength even at high-temperatures. This significant improvement in mechanical properties at room temperature may be attributed to the subgrain boundaries formed by the highly-localized residual stresses around the SiC dispersions generated by the thermal expansion mismatches between the matrices and SiC. The hardness and strength improvement at high temperatures may be associated with the dislocation pinning by hard SiC dispersions and the fracture mode change by localized stresses around the SiC dispersions within the matrix grains.

REFERENCES

1. R. Davidge and A.G. Evans, *Mater. Sci. Eng.*, 6(1970), 281.
2. J. Lankford, *J. Mater. Sci.*, 13(1978), 351.
3. R.P. Wahi and B. Ilschner, *J. Mater. Sci.*, 15(1980), 875.
4. F.F. Lange, *J. Mater. Sci.*, 17(1982), 225.
5. P.F. Becher and G.C. Wei, *J. Am. Ceram. Soc.*, 67(1984), C267.
6. M.G. Jenkins, A.S. Kobayashi, K.W. White and R.C. Bradt, *J. Am. Ceram. Soc.*, 70(1987), 393.
7. K. Niihara and A. Nakahira, *Proc. of MRS Meeting on Advanced Materials*, Vol.4, (1988), pp.129-133.
8. K. Niihara, A. Nakahira and T. Hirai, *J. of Japan Soc. of Powder Metall.* 36(1989), 165.
9. K. Niihara, *J. of Japan Soc. of Powder Metall.* 37(1990), 348.
10. K. Niihara, T. Hirano, A. Nakahira, K. Ojima and K. Izaki, *Proc. of MRS Meeting on Advanced Material*, Vol.4, (1988), pp.107.
11. K. Niihara, A. Nakahira, H. Ueda and H. Sasaki, *Proc. of 1st Japan Int. SAMPE Symp.*, (1989), 1120.
12. K. Izaki, H. Hakkei, K. Ando, T. Kawakami and K. Niihara, *Ultrastructure Processing of Advanced Ceramics*, Edited by J.M. Mackenzie and D.R. Ulrich, John Wiley & Sons, Inc., New York, (1988), pp.891.
13. K. Niihara, A. Nakahira, K. Suganuma, T. Hirano and K. Izaki, *J. of Japan Soc. of Powder and Powder Metall.*, 36(1989), 243.
14. K. Niihara, R. Morena and D.P.H. Hasselman, *J. Mater. Sci. Lett.*, 1, (1982), 13.
15. K. Niihara, A. Nakahira, T. Uchiyama and T. Hirai, "Fracture Mechanics of Ceramics, Vol. 7.", Edited by A.G. Evans, R.C. Bradt, F.F. Lange and D.P.H. Hasselman, Plenum Press, (1985), pp.103.
16. F.F. Lange, "Fracture Mechanics of Ceramics, Vol.2", Edited by R.C. Bradt, D.P.H. Hasselman and F.F. Lange, Plenum Press, (1974), pp.599.
17. R.W. Rice, *Proc. Brit. Ceram. Soc.*, 20(1972), 205.
18. A.G. Evans and A. Rana, *Acta Metall.*, 28(1980), 129.
19. A.G. Evans and T.G. Langdon, *Structure Ceramics*, *Progress in Materials Science*, 21(1976), 171.
20. R.M. Cannon and R.L. Coble, *Deformation Mechanisms in Ceramics*, Edited by R.C. Bradt and R.E. Tressler, Plenum Press, New York, (1975).
21. J.R. Porter, W. Blumenthal and A.G. Evans, *Acta Metall.*, 29(1981), 1899.

CERAMIC-METAL NANOCOMPOSITES

A. ROUSSET*, X. DEVAUX*, M. BRIEU*, A. MARCHAND**

*Laboratoire de Chimie des Matériaux Inorganiques U.R.A. CNRS 1311,
Université P. Sabatier, 31062 TOULOUSE-Cedex, FRANCE

**Laboratoire Louis Néel CNRS, 166X, 38042 GRENOBLE-Cedex, FRANCE

ABSTRACT

We prepared α alumina powders consisting of micronic grains in which iron or iron-chromium alloy clusters were homogeneously dispersed. Transmission Electron Microscopy studies showed that the metallic nanoparticles are monocrystalline and epitaxied in the alumina matrix. The crystallographic relationships between α alumina and the body centered cubic metallic phases are : $(111)[\bar{1}12]_{\text{M}} // (0001)[21\bar{3}]_{\alpha\text{-Al}_2\text{O}_3}$. Magnetic measurements displayed the superparamagnetic behaviour of the nanoparticles as well as their bimodal distribution. These nanocomposite powders were hot-pressed at about 1500°C. The resulting ceramics had a microstructure made of micronic alumina grains and metallic crystallites, with a size ranging from 10 to 100 nm. The larger part of metallic crystallites were intragranularly dispersed with a size lower than 50 nm. The study of cermet properties showed an improvement of alumina mechanical behaviour:

Bending strength ($\sigma_f = 850$ MPa), Fracture toughness ($K_{IC} = 8 \text{ MPa}\sqrt{\text{m}}$).

INTRODUCTION

Attempts at ceramics strengthening by metals, although already ancient, are still topical (1). Attractive results at the application level have been achieved in the case of non oxide ceramics. These were characterized by electronic structures and chemical bonding relatively close to those of metals. On the other hand, dispersing metals in oxides is much more difficult because of the poor wettability of oxides by metals. Therefore results were limited even if improvement has been noticed especially in Al_2O_3 -Mo and Al_2O_3 -Cr cermets (2,3). Toughening models show the interest of homogeneously dispersed small metallic particles, particularly submicron sized, in the ceramic matrix (4).

On a more fundamental level, preparing nanometric metallic particles in sintered or powdery oxides raises numerous problems which increasingly triggered the interest of research workers (5). Their investigations focus on elaboration methods, characterization as well as the study of specific properties: nature and influence of interfaces on mechanical, electric, magnetic, catalytic properties. So nanocomposites present an extremely wide activity field on which fundamental and applied research strongly converge.

Results in alumina powders containing nanoparticles of metal or alloy and also in cermets prepared by sintering the previous powders are presented.

RESULTS

Samples

Nanocomposite powders were generally obtained by reduction of solid solutions $\text{Al}_{2-2x}\text{M}_{2x}\text{O}_3$ ($x < 0.3$, $\text{M} = \text{Fe}, \text{Fe}_{0.8}\text{Cr}_{0.2}$). Cermets were produced by hot-pressing these powders at 1450-1500°C under vacuum. For each system $\text{Al}_2\text{O}_3/\text{Fe}$ and $\text{Al}_2\text{O}_3/\text{Fe}_{0.8}\text{Cr}_{0.2}$ proportions were 2, 5, 10, 15, 20 wt% of metallic phase. Tables 1 and 2 give the main characteristics of powders (Tab.1, Fig.1,2) and ceramics (Tab.2, fig.3,4) for 10% metallic phase. Various samples of Al_2O_3 -Fe nanocomposites were prepared : some with small intragranular particles surrounded by a FeAl_2O_4 spinel phase (sample 3, Fig.2), some with smaller particles but without aluminate layer (sample 2), other with bigger iron crystallites located outside the alumina grains (sample 1).

Sample	Phases	Alumina grain size	Average metallic particles size (nm)	specific area (m^2/g)
Al_2O_3 10Fe (1)	$\alpha\text{Al}_2\text{O}_3 + \gamma\text{Al}_2\text{O}_3 + \alpha\text{Fe}$	2-5 μm grains constituted with 0.1-0.3 μm sized crystallites	70	8.7
Al_2O_3 10Fe (2)	$\alpha\text{Al}_2\text{O}_3 + \alpha\text{Fe}$		5	2.3
Al_2O_3 10Fe (3)	$\alpha\text{Al}_2\text{O}_3 + \alpha\text{Fe} + \text{FeAl}_2\text{O}_4$		10	1.7
Al_2O_3 10 $\text{Fe}_{0.8}\text{Cr}_{0.2}$	$\alpha\text{Al}_2\text{O}_3 + \text{Fe}_{0.8}\text{Cr}_{0.2}$		8	2.3

TABLE 1 : Powdered nanocomposites characteristics.

Sample	Phases	Average alumina grain size (μm)	Average metallic particles size (nm)	Densification (%)
Al_2O_3 10Fe (2')	$\alpha\text{Al}_2\text{O}_3 + \alpha\text{Fe}$	#2	35	#99
Al_2O_3 10 $\text{Fe}_{0.8}\text{Cr}_{0.2}$	$\alpha\text{Al}_2\text{O}_3 + \text{Fe}_{0.8}\text{Cr}_{0.2}$	#2	35	#99

TABLE 2 : Massive nanocomposites characteristics.

Scanning electron microscopy on dense samples shows small alumina grains (about 2 μm) (Fig.3). During sintering, the average size of metal particles slightly increased. Most part of the metallic phase remained intragranular. The homogeneity of dispersion and the amount of intragranular particles increases as the growth of particles is limited. This phe-

nomenon particularly occurs in Al_2O_3 -Fe-Cr cermets.

Interfaces characterization

Bright field micrograph and electron microdiffraction pattern on Al_2O_3 -10Fe composite grain (sample 2) are presented in figures 5a and 5b. Dark field micrographs obtained with diffracted beams of $(2\bar{1}\bar{1}0)_{\alpha\text{Al}_2\text{O}_3}$ plans (Fig.5c) and $(10\bar{1})_{\alpha\text{Fe}}$ plans (Fig.5d) show that alumina grain and iron particles are monocrystalline. Comparison between bright field (Fig.5a) and dark field (Fig.5d) reveals that all metallic particles have the same crystallographic orientation. Crystallographic relationships between corundum lattice and iron lattice were deduced from the electron diffraction pattern (Fig.5b):

$$\begin{array}{ll} (10\bar{1})_{\alpha\text{Fe}} // (2\bar{1}\bar{1}0)_{\alpha\text{Al}_2\text{O}_3} & (101)_{\alpha\text{Fe}} // (0\bar{1}14)_{\alpha\text{Al}_2\text{O}_3} \\ (100)_{\alpha\text{Fe}} // (1\bar{1}02)_{\alpha\text{Al}_2\text{O}_3} & (001)_{\alpha\text{Fe}} // (1012)_{\alpha\text{Al}_2\text{O}_3} \end{array}$$

The investigation of additional microdiffraction patterns on the same grain studied along various crystallographic orientations leads to the general epitaxial relationship:

$$(111)[\bar{1}\bar{1}2]_{\alpha\text{Fe}} // (0001)[21\bar{3}]_{\alpha\text{Al}_2\text{O}_3}$$

The study of the Al_2O_3 -Fe-Cr system gave the same results. In the bulk cermets epitaxy is kept for intragranular metallic particles. Similar crystallographic relationships were noticed on thin films of body-centered cubic metals (Nb,Fe) epitaxied on sapphire (6,7).

Magnetic properties

Magnetic properties were only studied in powdered Al_2O_3 -10Fe composites (samples 1,2,3). Isothermal magnetization curves (Fig.6) and spontaneous magnetization graphs (Fig.7) show that sample 1 only contained ferromagnetic particles regardless of the temperature, whereas samples 2 and 3 show both ferromagnetic and superparamagnetic phases above 50 K. Assuming that only the Fe atom carries a magnetic moment, the magnetization values are displayed in Bohr magneton units (μ_B). Values of saturation magnetization at ambient temperature show that 47% of iron is ferromagnetic in sample 2 while 12% is in sample 3. Extrapolation of isothermal magnetization curves at 1.5 K to infinite provide a standard value for the magnetic moment per iron atom for sample 1 ($2.21\mu_B$) and for sample 3 ($2.09\mu_B$). The value for sample 2 is much higher ($2.50\mu_B$). This result can be explained either through a surface magnetism effect (8) or by the presence of paramagnetic Fe ions (9). Behaviour of sample 3 is completely specific. Analysis of hysteresis loops at low temperature shows a dissymmetrical loop such that $|H_c^+| - |H_c^-| < 0$. This shift changes with the temperature (Fig.8) and decreases towards 0 as the number of successive loops increases. This behaviour reveals the presence of an uncompensated antiferromagnetic phase as well as a ferromagnetic-antiferromagnetic exchange anisotropy. The antiferromagnetic compound is a $\text{Fe}_{1-x}\text{Al}_{2-x}\text{O}_4$ spinel phase ($x < 0.2$). The thickness of the phase surrounding iron particles is about 2.5 nm, thus this phase has a superantiferromagnetic behaviour beyond 50 K.

Mechanical properties

Mechanical properties were studied in 1450°C hot pressed nanocomposite powders. The transverse rupture strength was determined by the three-

point bending method and the K_{Ic} factor by the S.E.N.B. method.

Results in iron and Fe-Cr alloy are shown in figures 9, 10. Strengthening rises to a maximum for Al_2O_3 -5Fe composite. This behaviour is different for iron-chromium cermets. Strengthening increases beyond 5% and reaches bending strength value of 850 MPa and fracture toughness value of 8 $MPa\sqrt{m}$. These characteristics result from homogeneously dispersed and very small sized metallic particles. Figure 11 indicates that the higher the average size of particles is, the lower the mechanical properties are.

CONCLUSION

Results submitted in this paper show the interest of nanocomposites in fundamental as well as in applied research, even if extensive work is still need to achieve high-performance materials.

Controlling the size of metallic particles dispersed in alumina matrix makes it possible to obtain better mechanical properties than those mentioned in the literature for similar systems (2). Metallic particles size in the Al_2O_3 -Fe and in Al_2O_3 -Cr systems (3,10) already studied has not been reduced below 100 nm because particles were essentially intergranular. It seems similar studies had not been conducted in Al_2O_3 -Fe-Cr composites. Their mechanical properties are similar to these obtained for alumina based ceramic-ceramic composites (11). Controlling dimensions and size distribution of nanoparticles in ceramic matrices is a promising and interesting approach likely to raise original issues in the fields of elaboration and of mechanical and physicochemical properties.

REFERENCES

- 1- Aliprandi, G.; "Matériaux réfractaires et céramiques techniques"; Editions Septima; Paris; 1979.
- 2- McHugh, T.C.; Whalen, T.J.; Humenik Jr., M.; "Dispersion strengthened aluminium oxide"; J. Am. Ceram. Soc.; 49; 1966; 484-491.
- 3- Morgan, C.S.; Moorhead, A.J.; Lauf, R.J.; "Thermal-shock resistant alumina-cermet insulators"; Am. Ceram. Soc. Bull.; 61; 1982; 274-276.
- 4- Evans, A.G.; "High Toughness ceramics"; Mater. Sci. Eng. A; A105/106; 1988; 65-71.
- 5- Chakravorty, D.; "Organometallic route to nanocomposite synthesis"; Sadhana; 13; 1988; 13-18.
- 6- Qadri, S.B.; Claassen, J.H.; Broussard, P.R.; Wolf, S.A.; "Orientation relationship between thin films and sapphire substrates"; J. Less-Common Metals; 155; 1989; 327-330.
- 7- Anton, R.; Heinemann, K.; Poppa, H.; "The nucleation growth and oxidation of iron particles on α alumina"; Vide et Couches Minces; 201; 1980; 121-124.
- 8- Ohnishi, S.; Freeman, A.J.; Weinert, M.; "Surface magnetism of Fe (001)"; Phys. Rev. B; 28; 1983; 6741-6748.
- 9- Shull, R.D.; Ritter, J.T.; Bennett, H.L.; "Iron magnetic moments in iron/silica gel nanocomposites"; J. Appl. Phys.; 67; 1990; 4490-4492.
- 10- Klomp, J.T.; Lindenhovius, R.H.; "Microstructural and physical properties of Al_2O_3 -Fe cermets; Ceramurgia Int.; 4; 1978; 59-65
- 11- Bach, J.P.; "Elaboration et caractérisation de composites céramiques alumine-zircone préparées à partir de différents précurseurs; French Thesis; Saint-Etienne; 1989.

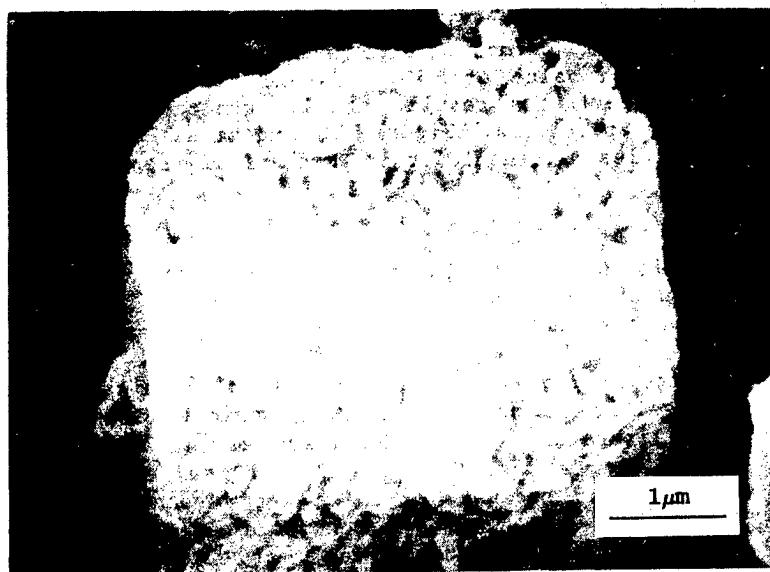


Fig.1. Scanning electron micrograph of Al₂O₃-10wt%Fe powder.

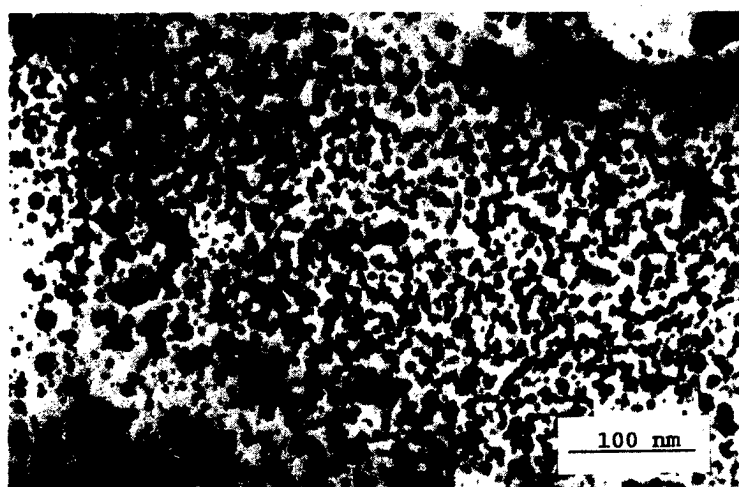


Fig.2. Transmission electron micrograph of Al₂O₃-10wt%Fe_{0.8}Cr_{0.2} powder.

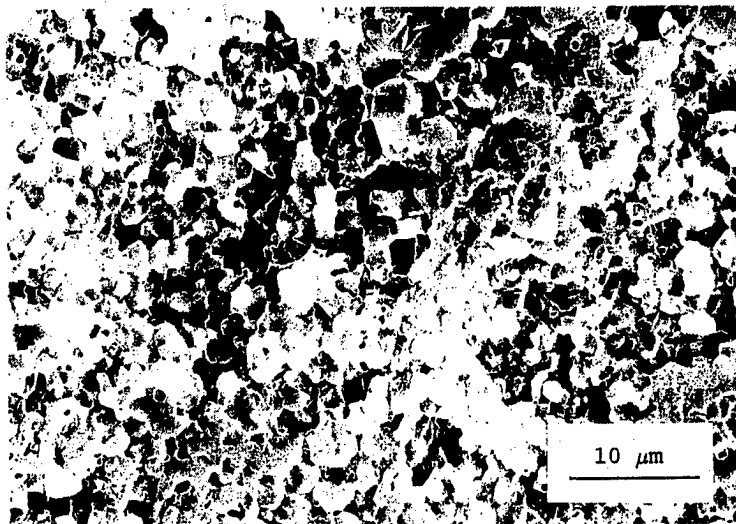


Fig.3. Scanning electron micrograph of Al_2O_3 -10wt% $\text{Fe}_{0.8}\text{Cr}_{0.2}$ cermet.



Fig.4. Transmission electron micrograph of Al_2O_3 -10wt% $\text{Fe}_{0.8}\text{Cr}_{0.2}$ cermet.

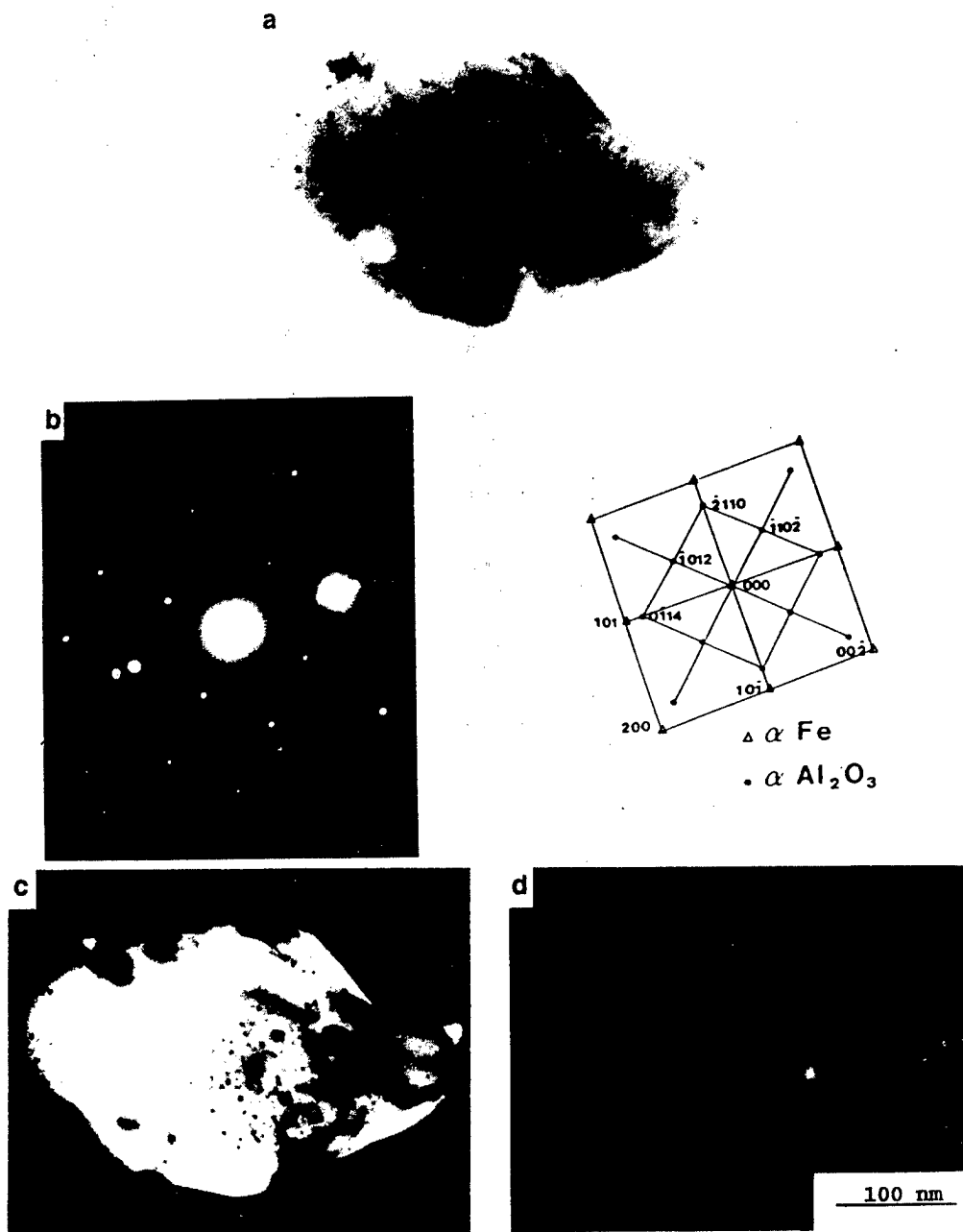


Fig.5. Transmission electron micrographs of Al₂O₃-10wt%Fe nanocomposite
 (a) Bright field of a composite grain. (b) Electron diffraction pattern of the same grain. (c) Dark field of Al₂O₃ grain. (d) Dark field of Fe particles.

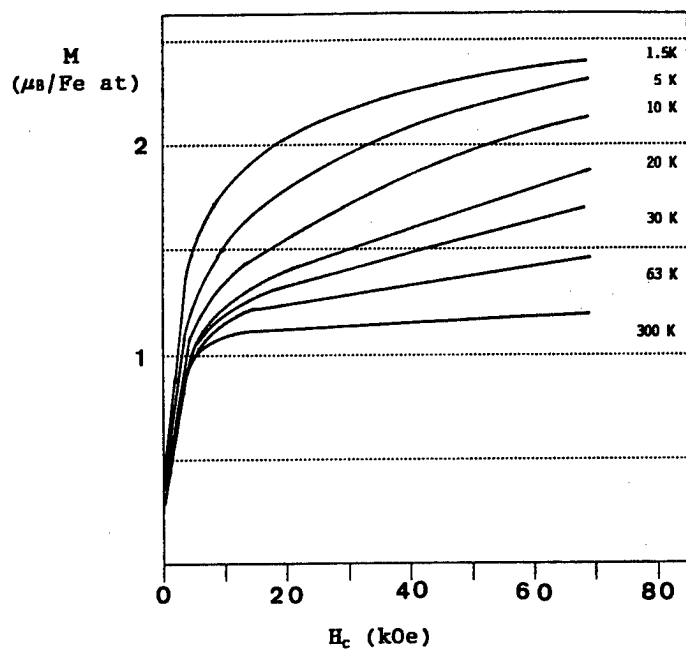


Fig.6. Isothermal magnetization of Al_2O_3 -10wt%Fe: sample(2).

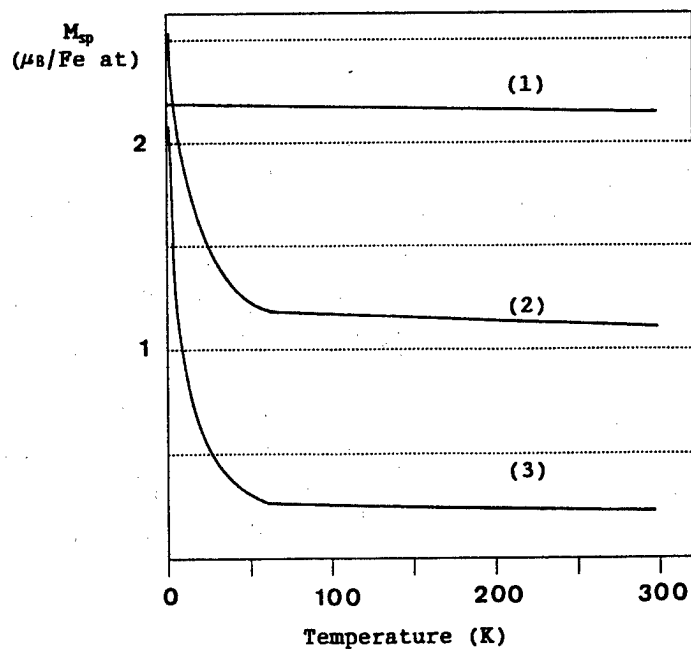


Fig.7. Spontaneous magnetization of Al_2O_3 -10wt%Fe: samples(1),(2),(3).

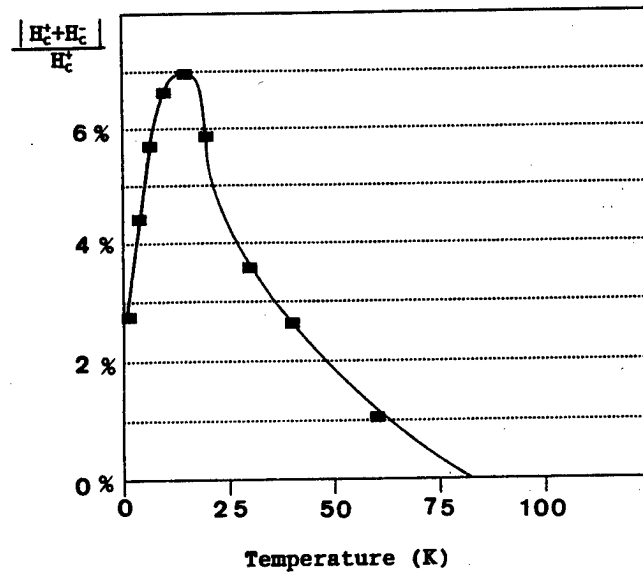


Fig.8. Graph $|H_c^+ + H_c^-| / H_c^+$ versus temperature, showing the hysteresis loop dissymmetry.

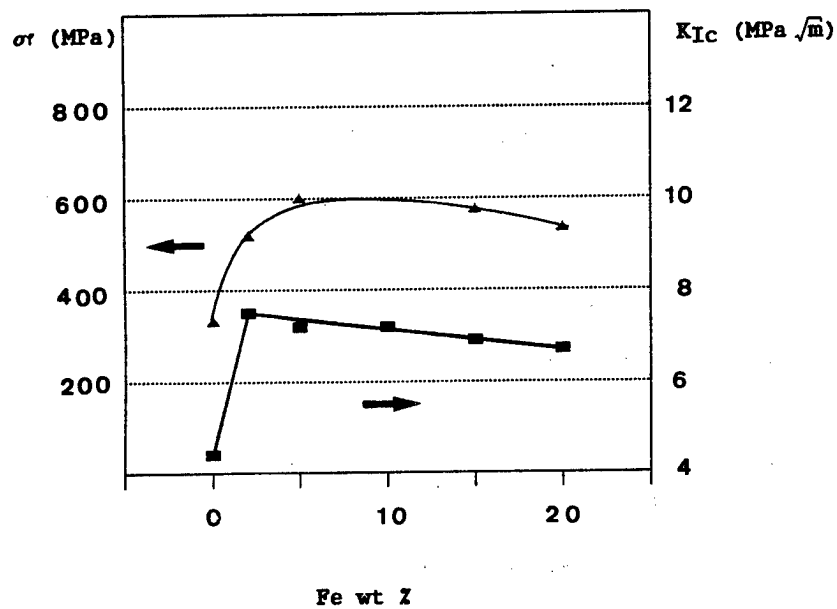


Fig.9. Fracture strength and fracture toughness of Al_2O_3 -Fe nanocomposites.

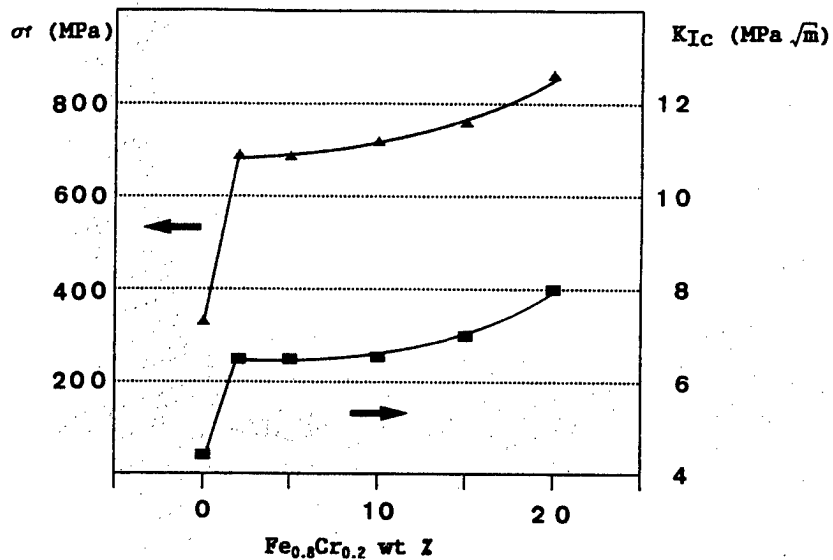


Fig.10. Fracture strength and fracture toughness of $\text{Al}_2\text{O}_3\text{-Fe}_{0.8}\text{Cr}_{0.2}$ nanocomposites.

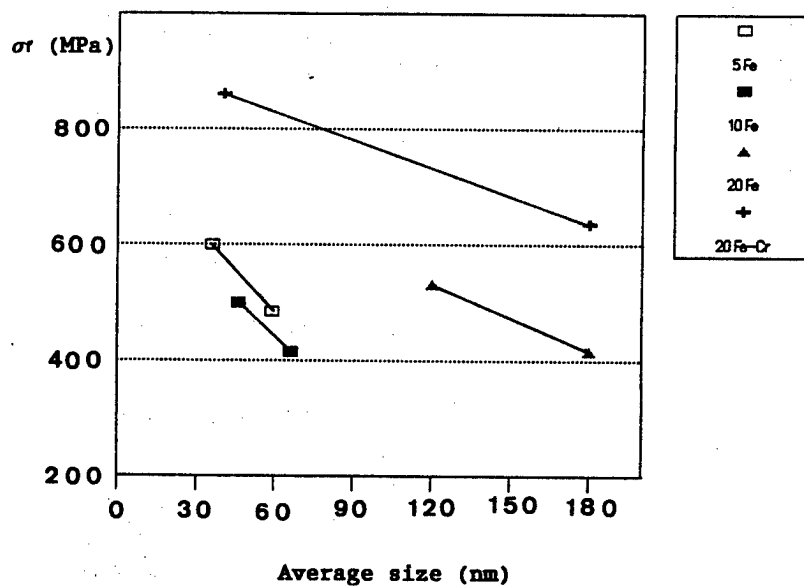


Fig.11. Fracture strength versus average size of metallic particles.

Fabrication of Three-Dimensional Fabric Composites and Their Mechanical Properties

Eiji Aoki, Takeshi Kitano , Yoshihiro Nagatsuka
Masahiro Funabashi and Kenji Fukuta*

Research Institute for Polymers and Textiles
1-1-4 Higashi, Tsukuba, Ibaraki Pref. 305 JAPAN

* Three-Dimensional Composites Research Corporation
2-1-6 Sengen, Tsukuba, Ibaraki Pref. 305 JAPAN

ABSTRACT

The influence of the structure of high density three dimensional(3D) fabrics woven by carbon fiber rovings and of number of filaments of a roving on the mechanical properties of their epoxy composites were investigated experimentally. Various mechanical properties of 3D fabric composites were also compared with those of laminated fabric composites. It was found that 3D fabric composites show very high shear strength, and that the mechanical properties of these materials tend to increase generally with decreasing the number of filaments and are influenced with structure composed of fiber rovings. Fracture toughness values are nearly similar for three directions and are nearly same as that of the laminated composite for fiber orientation. It is clearly shown at the stage of fracture that 3D fabric composites have higher resistance to delamination than laminated composites. It was found that carbon/Aramid hybrid 3D fabric composites have some excellent mechanical properties in comparison with those of single fiber woven 3D fabric composites.

Introduction

In recent years, fiber reinforced plastics(FRP) have become to be used in various industrial fields in accordance with the development of high performance fibers and matrix resins.

For typical examples of FRP, there exist laminated materials which are reinforced with uni-directionally oriented fibers and two-directionally oriented or woven fabrics such as plane-woven fabrics etc.. Multi-axial plane fabric like as a three axially woven fabric has begun to be taken attention as a good reinforcement of isotropic composite materials. However, all of these materials have laminated structures, and the mechanical properties between laminated structures are rather poor in comparison with those of fiber direction.

It is generally thought that three dimensionally fiber oriented fabric composites have many good properties in comparison with laminated composites, and are greatly expected as

advanced composite materials. However, we have many problems for development of fabrication of three dimensional(3D) fabric composites i.e, development of methods to get reliable fabrics and weave efficiently, and also development of processing methods to get composite materials.

Properties of 3D fabric composites may be influenced by the factors such as characteristics of fibers or bundle of filaments (fiber roving), number of filaments and structure of fabric composed of fiber rovings.

In this study, the influence of the factors mentioned above on the mechanical properties of 3D fabric composites impregnated with epoxy resins were investigated experimentally, and these properties were compared with those of laminated composites. Carbon fiber/Aramid fiber hybrid 3D fabric composites were also prepared to investigate their mechanical properties.

Preparation of 3D fabric composites

Two kinds of tri-axial three dimensional(3D) fabrics shown in Fig.1 including hybrid 3D fabrics, which are composed of warp, weft and vertical rovings were woven by the method developed in RIPT. One of them is orthogonally fiber oriented tri-axial 3D fabric called non-interlaced 3D fabric, and other also tri-axial 3D fabric in which fiber rovings run zig zag and interlace each other(interlaced 3D fabric).

Carbon fiber roving(CF) of which number of filaments are 3,000 (3Kf), 6,000(6Kf) and 12,000(12Kf) and Aramid fiber roving(AF) of 1 Kf were used for weaving of single fiber and hybrid fiber 3D fabrics. Diameters of these fibers are $7\mu\text{m}$ and $12\mu\text{m}$, respectively. Densities of fabrics were changed by weaving them with different pitches of rovings. Three kinds of epoxy resins were used as a matrix of 3D fabric composites. Bisphenol epoxy resin (Epoxy A) for samples of flexure, compression, shear and fracture toughness testing and heat resistant epoxy resin (Epoxy B) for impact testing were used. Another type of epoxy resin (Epoxy C) was also used for preparation of some impact testing samples. Solution of mixture of resin, curing agent and others was impregnated into 3D fabrics in a vacume chamber and then cured with the conditions recommended by manufacturers for each resin.

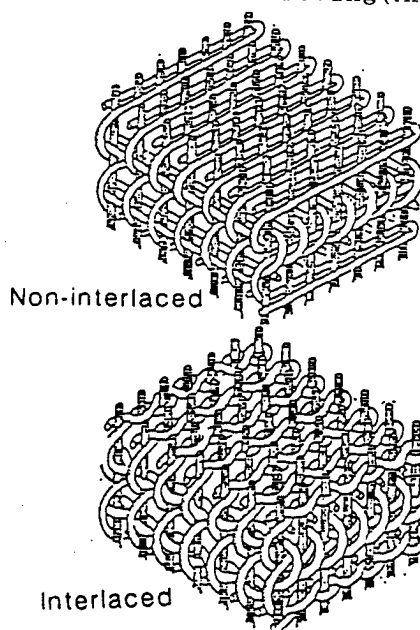


Fig.1 Perspective view of three-dimensional fabric

Mechanical testing

Tensile, flexure, compression and shear testings of 3D fabric composites were carried out by an Instron type machine. Shapes of test samples and conditions of testing are summarized in Table 1. Each sample was cut from the block or plate of 3D fabric composite materials by a diamond cutter.

Fracture toughness testing conditions, methods to obtain data and their analyses were followed by ASTM-E399 of Compact Testing. Electro-Hydraulic Servo Machine was used for testing. Fracture toughness of laminated composites were also measured and compared with those of 3D fabric composites.

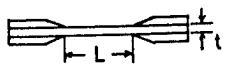
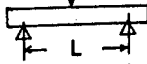
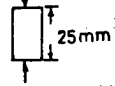
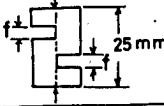
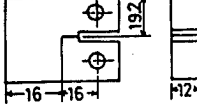
Two kinds of impact testings, Izod impact and Falling body impact testing were carried out for plate type 3D fabric composites.

Influence of number of filaments of fiber roving on mechanical properties

Non-interlaced 3D fabrics were woven by using CF bundles having different numbers of filaments and impregnated with Epoxy A. Laminated plane fabric composites composed of same fiber and matrix resin were also prepared for mechanical testing. Tensile, flexural and compressive strength and modulus, and also shear strength of these materials were measured and are summarized in Table 2.

Flexural and compressive strengths and their moduli of 3D fabric composites increase generally with decreasing the number of filaments, and are similar to those of laminated (2D) composites. For measurement of shear properties of 3D fabric composites, short beam method was applied at first stage.

Table 1 Dimensions of test specimens and test conditions for various mechanical properties

Item	Test specimen	Testing condition
Tension		L = 180mm (20°C) t = 5mm
Flexure		12x12x215mm Span(L) = 190mm Cross head speed 5mm/min
Compression		13x13x25mm Cross head speed 1mm/min
Shear		13x13x25mm t = 1mm Cross head speed 1 mm/min
Fracture toughness		40x38.4x12mm

		3D-1	3D-2	L.C(2D)
No. of filaments		3Kf	6Kf	3Kf
Content Vf%		52.6	50.4	57.1
Specific gravity		1.51	1.49	1.53
Tensile	Strength MPa	—	746	—
	Modulus GPa	61.8	56.1	62.9
	Specific modulus GPa	40.9	37.7	41.1
Flexure	Strength MPa	760	673	736
	Specific strength MPa	503	452	481
	Modulus GPa	55.3	51.1	55.7
Compression	Specific modulus GPa	36.6	34.3	36.4
	Strength MPa	477	415	459
	Specific strength MPa	316	272	300
Shear	Modulus GPa	61.4	48.5	62.7
	Specific modulus GPa	40.7	32.6	41.6
	Shearing strength MPa	> 163	> 161	42.1
Poissons ratio		—	0.13	—

3D : Three dimensional fabric composite
L.C : Laminated fabric composite

however, it was found that the method is not suitable because the deformation in the sample are similar to those by compression testing. New shear testing method by using samples shown in Table 1 instead of short beam method was applied in this study. Even for the sample of this shape, complete shear fracture could not be obtained because the space of notch (1mmx6.5mmx6.5mm) cut in the specimen are closed by deformation accompanied by compression. In Table 2, shear stresses when the space of notch part is closed are shown, however, real strength may be larger than these. It is assumed from the result that the values of 3D fabric composites obtained by this method are larger than four times of shear strength of laminated composites, which are easily fractured by short beam method.

From the measurement of strain distribution and also relations between stress and strain at various positions under flexure testing of 3D fabric composites, it was found that these materials show deformation like as that of isotropic material.

Fracture toughness of 3D fabric composites

Fracture toughness of 3D and laminated (2D) fabric composites were measured by compact testing method following ASTM-E399 Standard. Recording the curves of load-deformation along the direction of load, fracture toughness value, KQ was calculated from the maximum load. Some typical curves of load-deformation for two kinds of composites (3D and 2D) are shown in Fig.2. Values of maximum load obtained from the curves and fracture toughness values KQ or G_{IC} calculated from maximum loads are shown in Table 3. Maximum load and fracture toughness, KQ in direction perpendicular to laminated fabrics of 2D fabric composites are approximately 1/27 th of those in direction parallel to oriented fibers, however, these values of 3D fabric composites show the corresponding maximum loads and fracture toughness to the content of fiber in three directions, X, Y and Z.

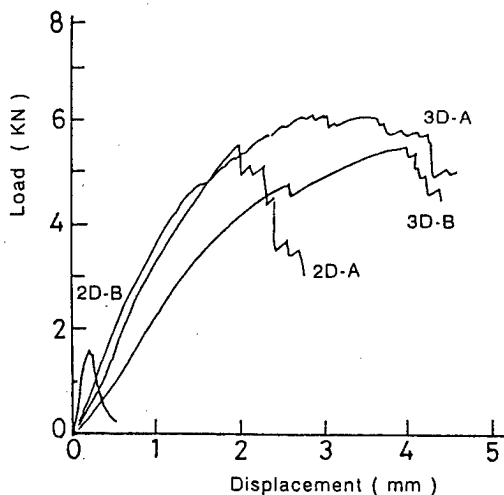
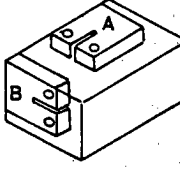
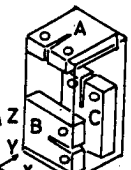


Fig.2 Fracture toughness test of laminated (2D) and 3D fabric composites

Table 3 Fracture toughness of 3D fabric and laminated (2D) fabric composites

Structure of composite	2 D		3 D		
Crack plane orientation	A	B	A	B	C
Max. load P (N)	5462	201	5266	5688	4805
Fracture toughness KQ (N/mm ^{3/2})	777	28	752	812	694
G_{IC} (N/mm)	51	1	107	127	—
Remark Crack plane orientation					

From these results, it becomes clear that 3D fabric composites may be good isotropic materials.

Impact properties

The results of impact testing for 3D and 2D fabric composites are shown in Table 4. Izod impact value of non-interlaced 3D fabric composite(NI) is generally larger than that of laminated fabric composite(L). However, impact value of interlaced 3D fabric composite(I) is similar to that of laminated fabric composite. These results may be because the weaving density of I sample perpendicular to thickness of test specimen (plate type) is not so high and the disorder of fiber orientation occurs during processing. From the results of Izod impact testing for other three samples(I, NI and L) impregnated with Epoxy C, it can be said that impact value of NI sample is largest in three samples and also value of L sample is smaller than those of NI and I samples. The impact values of 3D fabric composites seem to increase with decreasing the number of filaments of rovings.

Fig.3 shows some typical curves of impact load as a function of time for three kinds of samples (NI, I and L), which were measured by using a falling body impact tester. From the figure, it can be found that the change of load as a function of time shows very different appearance between 3D fabric composites(NI and I) and laminated fabric composite(L). From the observation of the appearance of fracture of these samples, it is found that the delamination of L sample appears clearly in comparison with 3D fabric composite samples(NI and I).

CF/AF hybrid 3D fabric composites

In order to get more functional and more "tailored designed" composite materials,

Table 4 Izod impact values of 3D fabric and laminated(2D) fabric composites

Structure	Fiber volume fraction (%)	Izod impact value (J/cm ²)
Non-interlaced 3D fabric	48.4	11.0
Interlaced 3D fabric	49.3	8.7
Laminated fabric	51.1	8.6

Notchless test
Size of test specimen W:10mm,t:5mm,L:60mm
Matrix : Epoxy resin B

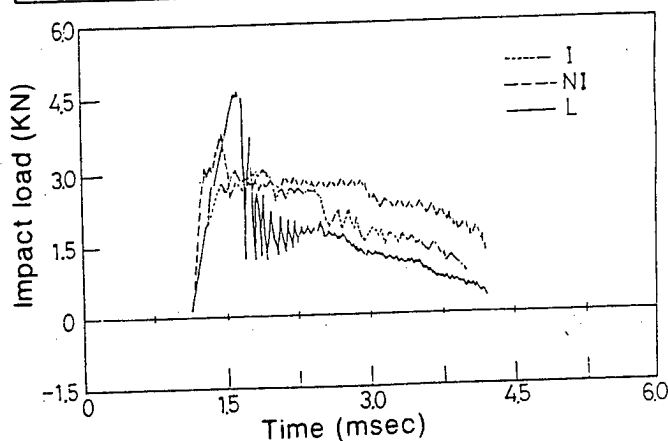


Fig.3 Time dependent impact load (Falling body impact testing)
NI : Non-interlaced 3D fabric
I : Interlaced 3D fabric
L : Laminated fabric

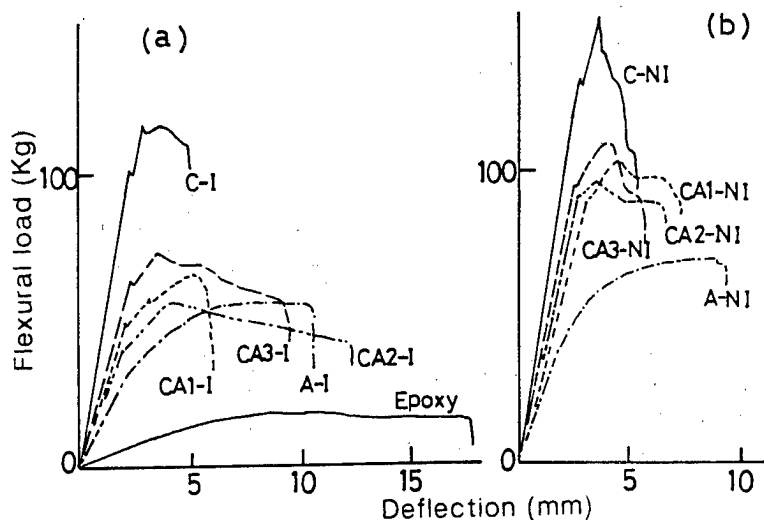


Fig.4 Flexural load vs. deflection curves of Carbon fiber/Aramid fiber hybrid 3D fabric composites
(a) Interlaced 3D fabric (b) Non-interlaced 3D fabric

CF/AF hybrid 3D fabric composites were fabricated and their mechanical properties were investigated experimentally. Typical load-deflection curves under flexure testing are shown in Fig.4 for hybrid 3D fabric composites composed of carbon fiber(CF) and Aramid fiber(AF) with various combinations. Fig.4(a) and (b) show the results of interlaced(I) and non-interlaced(NI) hybrid 3D fabric composites, respectively. It was found from the figure that AF 3D fabric composites(A-I and A-NI) show very different behavior from those of CF 3D fabric composites(C-I and C-NI) and that hybrid 3D fabric composites show intermediate behavior between CF and AF 3D fabric composites for both interlaced and non-interlaced type composites. For impact and shear properties of hybrid 3D fabric composites, we could find some characteristic behavior.

Summary

In this study, the influence of structure and number of filaments of tri-axial three dimensional fabric composites woven by carbon fiber rovings on various mechanical properties were investigated experimentally, and these properties were compared with those of laminated fabric composites. Carbon fiber/aramid fiber hybrid 3D fabric composites for more functional and "tailored designed" composite materials were also investigated. It was found that CF 3D fabric composites show very good shear, fracture toughness and impact properties in comparison with those of laminated fabric composites and are rather good isotropic materials, however, these mechanical properties are influenced by weaving structure and also number of filaments of rovings. For hybrid 3D fabric composites, some interesting results were obtained for getting high performance and functional composite materials.

Growth, structure and properties of Fe/Ru hexagonal superlattices

M.F.Ravet*, M.Maurer**, J.C.Ousset* and M.Piecuch*

*Laboratoire Commun CNRS Saint-Gobain, CRPAM, BP 109,
54704 Pont-à-Mousson (France)

**Compagnie Saint-Gobain, Les Miroirs, Cedex 27
92096 Paris-la-Defense (France)

ABSTRACT

Metallic multilayers and superlattices are thin films composite nanomaterials in which the composition is modulated by alternating deposition of different metals.

During the last few years, multilayers and superlattices have given rise to a great interest from both fundamental and technological point of view, due to the sophisticated deposition techniques which allow to tailor new structures with interesting physical properties.

For the first time, we have synthesized hexagonal Fe(x)/Ru(y) superlattices in a single crystal phase by Molecular Beam Epitaxy. The bidimensional epitaxial structure was checked by Reflexion High Energy Electron Diffraction. The sharpness of the interfaces was observed by Transmission Electron Microscopy in cross section and by simulations of small angle X-Ray scattering patterns. The epitaxial growth of Fe layers (up to 14Å) sandwiched by Ru layers (as thin as 4Å) stabilizes a perfectly hexagonal expanded structure.

According to magnetic measurements, the Fe atoms carry a magnetic moment with an in-plane anisotropy and with an evidence of coupling through Ru layers.

1. INTRODUCTION

For about twenty years, elaboration of synthetic composite materials at a nanometric scale has become possible because of the development of sophisticated deposition means such as sputtering and Molecular Beam Epitaxy (MBE) which offers the ability to grow artificial structures by depositing in alternance different elements layer by layer. In the field of semiconductors, the epitaxial growth by MBE of single crystal systems with quasi-ideal interfaces has allowed to get superlattices and new structures which initiated a new generation of electronic devices.

More recently, it was taken advantage of the sputtering techniques to synthesize artificial structures consisting of alternating thin layers of a metallic high electronic density element with high reflective power, such as tungsten, and a low electronic density element such as carbon or silicon, in the aim to get synthetic periodic systems for UV-X-ray optics[1]. The components may be amorphous or microcrystalline. In this field of optical applications, the quality of the interfaces and their evolution with respect to thermal treatments is of a crucial importance[2].

Moreover, epitaxy offers the possibility to synthesize transition metal films possessing modified structures as compared with stable phases[3]. Regarding the magnetism of metals, it is interesting to study the effect of a controlled variation of interatomic distances and anisotropic effects and on the magnetic properties. The potential technological applications of magnetic multilayers and superlattices are in the field of magnetic recording or magnetoresistive sensors[4].

In this context, the case of metallic Fe deserves attention. Indeed, Fe may present different allotropic phases, the bcc and fcc structures and a hcp structure under high pressure (above 130kbars)[5]. The bcc form is magnetic when it is in bulk form, whereas fcc and hcp are not.

According to theoretical predictions, both fcc and hcp bulk phases should undergo a transition to a magnetic state at volume expansion of order of 5% [6].

The purpose of our work was to stabilize Fe layers with an hexagonal structure by epitaxial growth with a transition metal, Ruthenium, possessing a stable hcp structure and to elucidate the effect of the Fe layers stretching on the magnetic properties.

2. DESCRIPTION OF SUPERLATTICES.

When two metallic pure elements are alternatively deposited on a substrate, the multilayer stacking is constituted by a periodic gradient of electronic density with a modulation wavelength Λ . The layers may grow in the amorphous, polycrystalline or textured crystalline state. The Fe/Al system is an example of this type of multilayer[7]. When the deposition rates are low enough (less than 1Å/sec) and when the structural and thermodynamical considerations are adequate, both lattices may fit each another and the growth of layers may be single crystalline, included at the interfaces. If the difference between the two materials is small enough, then the layers can be constrained to match perfectly by introducing a coherency strain into each layer. The as-obtained stackings are usually called metallic superlattices. Metals because of their elastic properties are good candidates for such artificial structures, although their high evaporation temperatures and chemical properties need specific conditions of elaboration.

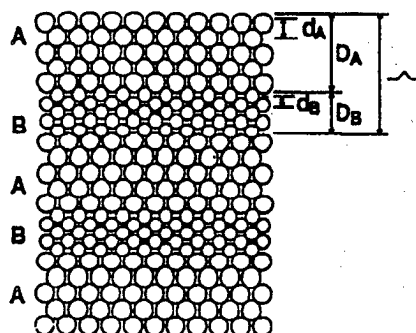


Fig.1. Structure of a superlattice.

Three kinds of modulations are combined. The single crystal stacking is constituted by elements A and B layers of D_A and D_B thicknesses consisting in n_A and n_B layers with lattice parameters d_A and d_B respectively. The modulation wavelength is given by $\Lambda = D_A + D_B$.

In the following, the respective thickness of layers will be called x and y .

3. GROWTH OF IRON ON RUTHENIUM AND OF Fe_x/Ru_y SUPERLATTICES.

Though there is a huge mismatch between lattice parameters of hcp Ru ($a=2.71\text{\AA}$, $c=4.28\text{\AA}$) and of an hypothetical hcp Fe phase at ambient pressure ($a=2.53\text{\AA}$, $c=4.06\text{\AA}$), the thermodynamical considerations, evaluated by the empirical approach[8] are suitable to stable Fe/Ru interfaces. So we have prepared epitaxial films by deposition of Ru and Fe layers in a RIBER EVA32 MBE. The Fe and Ru molecular beams were produced by electron beam gun evaporation in an Ultra High Vacuum chamber (10^{-10} torr during evaporation). The layer thickness was monitored by quartz microbalances.

The first stage consisted in getting a single crystal Ru surface. Buffer layers of (0001) ruthenium with a thickness from 200Å to 400Å have been grown on (1 $\bar{1}$ 20) oriented sapphire and (0001) mica. The temperature of the substrate was chosen as a compromise to obtain a good epitaxy without interdiffusion. The crystalline quality, the atomic scale flatness of the growth front and orientation of the Ru surfaces were checked in-situ by RHEED (Reflexion High Energy Electron Diffraction). Then we have deposited Fe on this (0001) Ru surface. RHEED patterns gave the proof of an epitaxial growth of an in-plane hexagonal structure of Fe on Ru.

We could determine that the critical number of atomic layers, i.e. the maximum layer number for keeping the single crystal bidimensional structure, was about 14 Å, i.e. 7 atomic layers. Over this number, the RHEED patterns became broad. A phase transition probably occurred because the coherency strains were relieved.

In order to elucidate the occurrence of the hexagonal structure of Fe in the tridimensional state, we have deposited by the same way Ru on Fe then Fe on Ru, and so obtained or the first time[9] a periodic stacking of single crystal artificial structures. Fig.2 gives the scheme of the Fe_x/Ru_y superlattices we gained. The smallest thickness we have realized in a superlattice was 4Å, i.e. 2 monolayers, for each component.

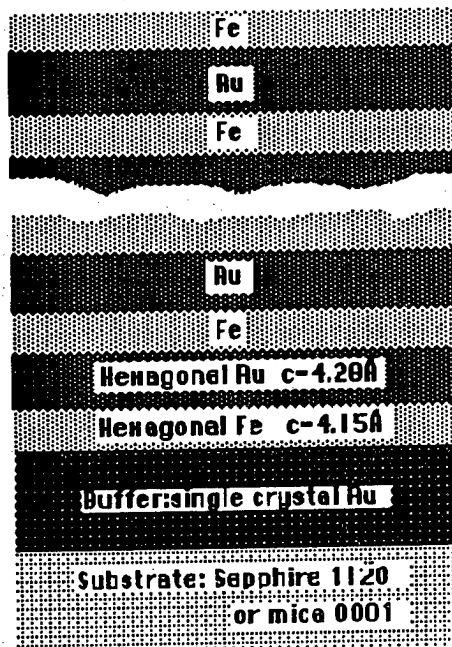


Fig.2. Fe_x/Ru_y Superlattice

4. STRUCTURAL PROPERTIES OF Fe/Ru SUPERLATTICES.

4.1. Structure of Fe_x/Ru_y superlattices.

Towards an electromagnetic radiation, the superlattice must be considered as a modulated electronic density where three periods are in competition: interplanar distances d_A and d_B of components A and B, and the period of the modulation Λ . The scattering amplitude by such a one dimensional system is given by:

$$I(q) \propto S(q)^2 \cdot F(q)^2$$

where q is the modulus of diffusion vector, $F(q)$ the structure factor and $S(q)$ the modulation function. These functions have been calculated for Fe/Ru superlattices[10].

The experimental consequence is the presence of modulation peaks at low angles (small q) and diffraction peaks at higher angles surrounded by satellites, the intensity of which depends on the respective position of maxima in functions $S(q)$ and $F(q)$.

X-ray diffraction experiments have been performed on a High Resolution PHILIPS Diffractometer using a 4 crystals monochromator which delivers a pure $\text{Co K}\alpha_1$ radiation ($\Delta\lambda/\lambda=2.3 \cdot 10^{-5}$) and a parallel beam (13°).

In all cases, even in the thinnest superlattice $\text{Fe}(4\text{\AA})/\text{Ru}(4\text{\AA})$ on Fig. 3, diffraction pattern presents small angle scattering peaks and high angle satellites around the principal peaks of the superlattice, as a proof of well periodic structures with sharp interfaces. The real period Λ is deduced from their position, and, when compared to the nominal values, allows a precise calibration of deposition rates of Fe and Ru.

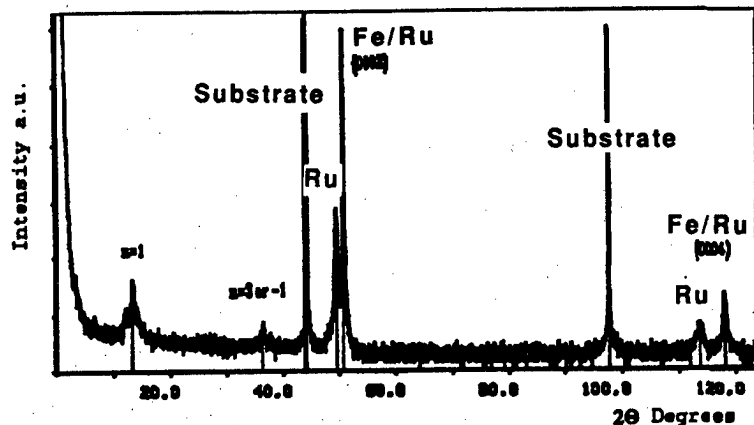


Fig.3 X-Ray diffraction pattern on Fe(4Å)/Ru(4Å)

High angle diffraction patterns with the diffusion vector q perpendicular to the surface show clearly that the (0001) axis is parallel to the growth direction, i.e. the (000 2 *l) planes are oriented in the sample plane. However, the tridimensional hcp structure is not demonstrated by such data. The hcp ABAB...versus cfc ABCABC... stackings sequences have to be elucidated. At present, the most convincing arguments in favor of the hcp ABAB...stacking structure merges from powder diffraction patterns on ground superlattices showing only characteristic peaks of hexagonal symmetry, and from the observation of (1123) diffraction peaks corresponding to out-of-plane hexagonal crystallographic axes.

From the precise determination of the (000 2 *l) and out-of-plane peaks positions, we have deduced the values of a and c mean lattice parameters, we have plotted them versus $x/(x+y)$ and extrapolated to pure Fe ($y=0$). This leads to values of $a_{Fe}=2.64\text{\AA}$ and $c_{Fe}=4.15\text{\AA}$ which are surprisingly large compared with the expected values in an hypothetical hcp Fe structure $a_{Fe}=2.53\text{\AA}$ and $c_{Fe}=4.08\text{\AA}$.

Indeed, that is to be related to the stretched Fe basal planes due to the pseudomorphic epitaxy with Ru. The atomic volume calculated from those distances 12.8\AA^3 is expanded by 10% at least in comparison with the bcc, fcc or the hypothetical hcp Fe phase (11.5\AA^3). That is the most interesting structural result with respect to the physical properties we aimed.

4.2. Interfaces

The sharpness of the Fe/Ru interfaces is a critical point in the understanding of the stabilization of hcp Fe epitaxial layers and on its effect on the magnetic properties. A qualitative insight into the interfaces sharpness relies in the observation of diffraction peaks at low angles and satellites around the (000 2 *l) superlattice peaks. Moreover, quantitative data are achieved by simulation of X-Ray diffraction patterns. The recursive model we used[10] describes the superlattice as an atomic stacking where on the one hand a disorder coefficient similar to a Debye-Waller factor represents the interface roughness, and on the other hand a random thickness error by Monte Carlo calculations is introduced. The best fits were obtained with a roughness of 1Å and a thickness error of 2Å. This last value is quasi equal to $c/2$, i.e. a monolayer. That is understandable if we consider that the main imperfections in the superlattices are monoatomic steps. A confirmation of that merges from the observation of modulation peaks for the thinnest superlattice Fe(4Å)/Ru(4Å), i.e. Fe(2 monolayers)/Ru(2 monolayers).

Observations by cross-sectional Transmission Electronic Microscopy give a direct view of the stacking. On Fig.4-a in High Resolution[11] conditions, there is an evidence of coherence between Fe and Ru atomic layers, and of well defined interfaces. However, dislocations clearly come up from the interface with the sapphire substrate and increase through the Ru buffer and the stacking. That means that the substrate surface quality is a crucial condition for a regular single crystal superlattice. Fig.4-b shows how in a superlattice Fe(21Å)/Ru(43Å), a long range roughness occurs from the bottom to the surface of the stacking. The lattice strains have relieved because the Fe thickness is higher than the critical one.

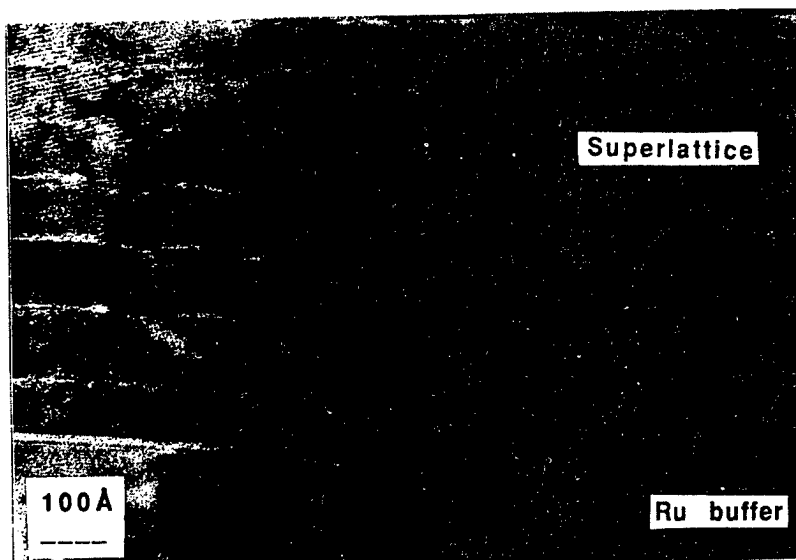


Fig.4-a

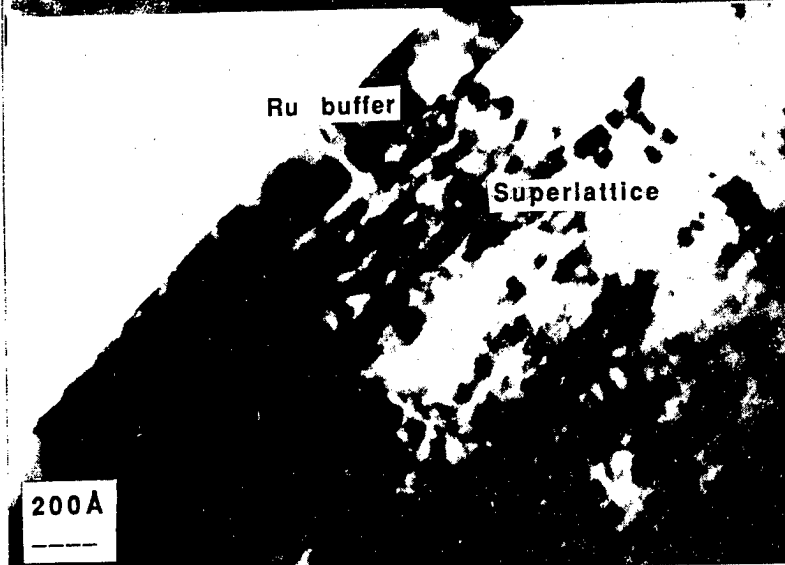


Fig.4-b

Fig.4. Cross-sectional TEM

4-a. HRTEM on a $\text{Fe}(x=12\text{\AA})/\text{Ru}(78\text{\AA})$ superlattice grown on a 200\AA Ru buffer and a sapphire substrate.

4-b. TEM on a $\text{Fe}(x=21\text{\AA})/\text{Ru}(43\text{\AA})$ superlattice grown on a 200\AA Ru buffer and a mica substrate.

5. MAGNETIC PROPERTIES OF Fe/Ru SUPERLATTICES.

Mössbauer spectroscopy experiments have been achieved with the aim of gaining a microscopic view on the Fe magnetism and also to characterize the local structure around the Fe atoms[12]. All the samples exhibit a doublet at room temperature resulting from a quadrupole splitting due to a 6-fold local axial symmetry. These results agree with the hexagonal structure of Fe/Ru superlattices.

Two different families of samples have been investigated for their bulk magnetic properties by SQUID magnetometry. In the first family, the Ru thickness was kept constant (24\AA) and the Fe thickness was changed. The absence of spontaneous magnetization in Fe layers thinner than 4 monolayers and a subsequent increase of $1.7 \mu\text{B}$ per atom in the additional layer suggests that the 2 Fe layers at the interface with Ru are non-magnetic, whereas the next ones are fully polarized, with a moment of $1.7 \mu\text{B}/\text{Fe}$. This is not too far from theoretical predictions[6] and must be

related to the volume expansion 10% for the Fe layers due to the pseudomorphous growth with Ru. The absence of Fe magnetism at the interfaces is certainly due to a strong hybridization of the Fe electronic bands with the broader bands of Ru and gives another insight of the sharpness of interfaces.

In the second family of samples, the Fe thickness has been kept constant (12Å) to check the interactions through the Ru layers. From the typical hysteresis curves, there is an evidence of an orientation of magnetic moments in the plane, and of saturation magnetization and coercitive field larger for the sample with thinner layers of Ru. That means that a magnetic coupling between Fe layers through Ru layers clearly occurs. More detailed investigations concluded to an antiferromagnetic interlayer coupling which becomes very weak for a Ru thickness of about 12 monolayers.

Concerning transport properties, very weak residual resistivities (less than $1\mu\Omega\text{cm}$) is a further evidence of a high degree of order in the superlattices, particularly at the interfaces. Recent magnetoresistance measurements have shown very small negative components at low magnetic fields, but for the moment there is no evidence of giant magnetoresistance unlike that has been observed in other systems[4].

6. CONCLUSION.

Throughout the example of Fe/Ru superlattices, we have shown that it is possible to tailor new artificial modulated metallic materials with sharp interfaces (one atomic layer), and to display interesting structural and physical properties.

Fe epitaxially grown by MBE on Ru is stabilized in an expanded (10% in volume) hcp metastable structure. Consistently with theoretical predictions this new phase corresponds to a magnetic state.

We have elaborated Fe/Ru superlattices with sharp interfaces. Correlatively, the magnetic interfaces are also sharp. Except for two atomic layers near the interface, the Fe sites carry a large moment. Magnetization and magnetoresistance suggest that a coupling occurs between the Fe layers and through the Ru layers. This coupling could be antiferromagnetic but there is no giant magnetoresistance.

The successive stages of the study we have described may be applied to other systems where Fe could be associated with other metals.

ACKNOWLEDGEMENTS.

The authors are indebted to J.J. DEMAÏ from the Service de Microscopie Electronique de l'Université NANCY I for his cross-sectional TEM observations (Fig.4-b) on ultramicrotome cut samples.

REFERENCES

1. E.SPILLER, Proceedings of the Mat. Res. Soc. Symp. **56** 419 (1986)
2. V. DUPUIS, M.F. RAVET, M. PIECUCH and C. TETE, Proceedings of the SPIE **1140** (1989) 57
3. HONG M., WOLF S. and GUBSER D.C. (Editors), Metallic Multilayers and Epitaxy, (Metallurgical Society, Warrendale, PA) 1988
4. P. ETIENNE, G. CREUZET, A. FRIEDRICH, F. NGUYEN-VAN-DAU, A. FERT, and J. MASSIES, Appl. Phys. Lett., **53**, 162 (1988)
5. D.I.C. PEARSON and J.M. WILLIAMS, J.Phys. F **9** (1979) 1797
6. J.KUBLER, Solid State Com. **72** (1989) 631
7. J.F. BOBO, P. DELCROIX, J.C. OUSSET, M.F. RAVET, and M. PIECUCH, MRS Proceedings, Symp. C, STRASBOURG Spring Meeting 1990, (to appear)
8. A.R. MIEDEMA and J.W.F. DORLEIJN, Surf. Sci **95** (1979) 447
9. M. MAURER, J.C. OUSSET, M.F. RAVET, and M. PIECUCH, Europhysics Lett. **9** (1989) 803
10. M. PIECUCH and L. NEVOT, Metallic Multilayers, A.CHAMBEROD and J.HILLAIRET editors. Materials Science Forum **59** (1990) 93
11. A. BOURRET and J.L. ROUVIERE, MRS Proceedings of the Spring Meeting San Francisco (1990) (to appear)
12. M. MAURER, J.C. OUSSET, M. PIECUCH, M.F. RAVET, and J.P. SANCHEZ MRS Symp. Proc. **151** (1989) 99

This page intentionally left blank

POSTER SESSION

APPLICATION

AND

CAD/CAM

This page intentionally left blank

THE USE OF INFRARED THERMOGRAPHY TO THE QUALITY ASSESSMENT OF COMPOSITE MATERIALS USED IN MILITARY SHIP BUILDING.

Francis LESBRE

Délégation Générale pour l'Armement,
Service Technique des Constructions et Armes Navales
8 Bd Victor, 75732 PARIS CEDEX 15

ABSTRACT

The French Navy has been using composite materials, either monolithic or sandwiches for several years, in ship building. These materials are used on surface vessel hulls such as mine hunters and on several submarine structures.

In order to guarantee a sufficient level of reliability and durability, the DCN had to developped specific methods for the non-destructive testing of these materials such as infrared thermography.

This technique consists of monitoring the structure surface temperature with a infrared camera, after a given excitation. This method can be used with either a mechanical (vibrothermography) or photothermal excitation (photothermography). An experimental set-up using this technique was developed for testing composite structures at the dockyard.

1. INTRODUCTION

The French Navy has been using composite materials, either monolithic or sandwiches, for several years in ship building. A presentation of some of the industrial composite production of the French DCN (Direction des Constructions Navales) was reported at the first French-Japanese seminar of composite materials held in March 1990 at Paris [1]. It has been shown that the use of composite materials are various : ship construction (hull of minehunter), elements of submarines, torpedos, radomes...

In order to guarantee a sufficient level of reliability and durability, the DCN had developped specific methods for non-destructive testing of these materials. One of the most interesting methods is the infrared thermal inspection, which is specially convenient to inspect quickly large surface of structures. This method can be used either with a mechanical excitation : "vibrothermography", or with photothermal excitation : "photothermography".

2. HEAT TRANSFER IN COMPOSITE MATERIALS

The governing three-dimensional differential equation in the case of anisotropic materials is given by :

$$(1) \partial/\partial x_i (k_{ij} \partial T/\partial x_j) + \bar{Q} = \rho c \partial T/\partial \tau$$

for $i, j = 1, 2, 3$ where k_{ij} is the thermal conductivity tensor, T is temperature, \bar{Q} is internal heat generation rate per unit volume, c is the specific heat, ρ is the density, and τ is time.

Because an IR camera allows measurements of the temperature field only at the surface of the specimen, it is then necessary to use a bidimensional approximation of Equation 1. If the thickness t of the specimen is small compared with some other dimensions, one can consider that the temperature $T(x,y,z)$ and the heat generation rate \bar{Q} are constant over the thickness, to obtain :

$$(2) \quad t \frac{\partial}{\partial x_i} (k_{ij} \frac{\partial \theta}{\partial x_j}) - \alpha \theta + Q = \rho c \frac{\partial \theta}{\partial \tau}$$

for $i, j = 1, 2$, where θ is surface temperature rise above ambient, α is a radiative and convective heat loss coefficient, ranging about $10/\text{m}^2/\text{K}$ for CFRP, and Q is the heat generation rate per unit area. During vibrothermographic tests, a steady state field of temperature is obtained (at least for the time scale of the camera) and is given by :

$$(3) \quad t \frac{\partial}{\partial x_i} (k_{ij} \frac{\partial \theta}{\partial x_j}) - \alpha \theta = -Q$$

for $i, j = 1, 2$. This equation describes the different heat transfer mechanisms involved during a vibrothermographic test. The interaction of internal flaw surfaces during vibration is represented by the term Q . Therefore, because of the diffusion of heat, the observed thermal picture θ is a fuzzy and mistaken representation of the real damage state in the material. Equation (3) can be solved to obtain a map of Q by using the temperature field digitized and stored into a memory computer.

3. VIBROTHERMOGRAPHY.

Vibrothermography uses high-frequency, low-amplitude mechanical vibrations to induce localized heating in a material. The frequency of excitation is varied in such a way that local flawed regions are set into local resonance. A very strong source of energy dissipation frequently develops as a result of the interaction of internal flaw surfaces during local vibration motions.

Vibrothermography has been proved very useful in the detection of impact damage in many plastics materials such as sandwich composite panels or glass-epoxy panels [2]. Composite laminate specimens of CFRP and GFRP were impacted by dropping steel cylinders from different heights to have different impacts energies, ranging from 5 to 20 Joules. The specimens were attached to a piezoelectric shaker and then vibrated. The frequency of excitation was chosen by sweeping it between 10 and 20 kHz until the best thermal contrast around the damaged regions was obtained. The specimens were then vibrated at a fixed frequency. When a steady-state field of temperature was obtained, the resulting thermal patterns were recorded.

A standard IR camera, an Agema AGA 780, was used in this study. The video signal is digitized by an 8-bit analog-to-digital convertor at 500 kHz sample rate and sent at the same rate into a screen buffer; The data are then transferred into a personal computer by direct memory access (DMA) channel.

Some examples of the results are given in pictures 1 to 6. Fig. 1 is a vibrothermogram of a CFRP specimen impacted with an energy of 20 J. The frequency of excitation was 19 kHz. This vibrothermogram was made by averaging 100 thermograms taken from a steady-state temperature field and by subtracting the reference picture recorded before the test. Also a spatial filtering has been done. These processing allows to increase the ratio signal maximum over noise. Therefore, the impact area is clearly indicated by the hot spot in the center of the picture. The two curves on the top and the left are cross section of the temperature field for an abscissa and ordinate indicated by the black window in the center of the picture. Figure 2 is a 3-D representation of the same picture. Figure 3 and 4 are a heat source map computed by the use of the temperature field of fig 1 and 2. The effects of the conduction are eliminated, and the heat source boundary is clearly delineated.

Fig 5 is a vibrothermogram of a GFRP specimen impacted at two different locations. Figure 6 is a 3D representation of the same picture. The impact energy was J. The

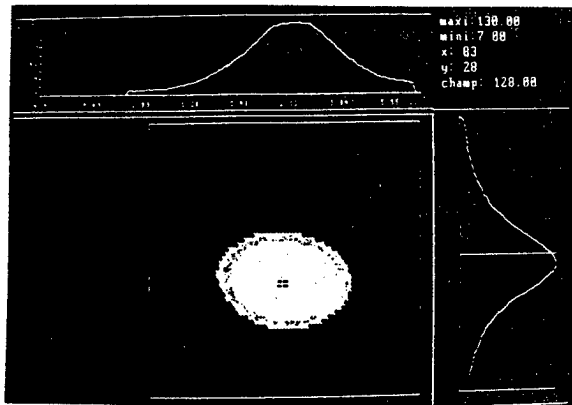


Fig1 : vibrothermogram of impacted CFRP specimen, with averaging 100 thermogramms and spatial filtering.

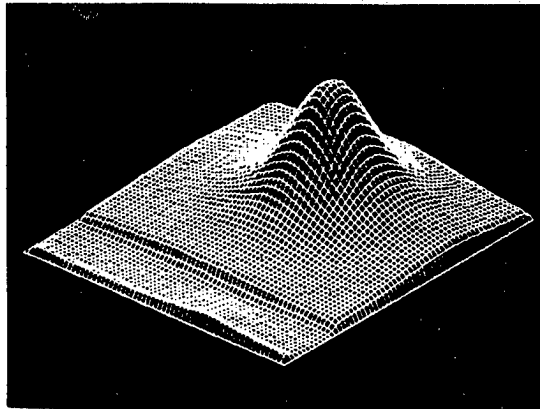


Fig2 : 3-D representation

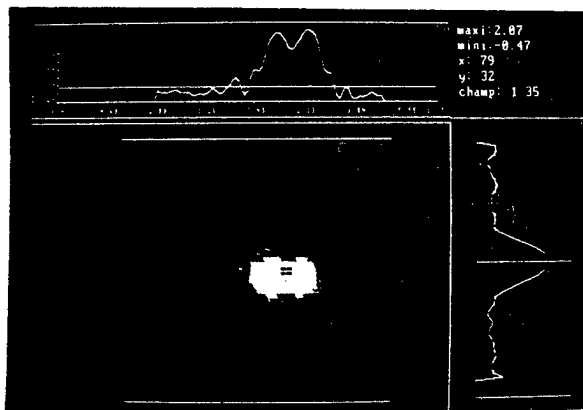


Fig 3 : Heat source map computed by the use of temperature field of fig.1.

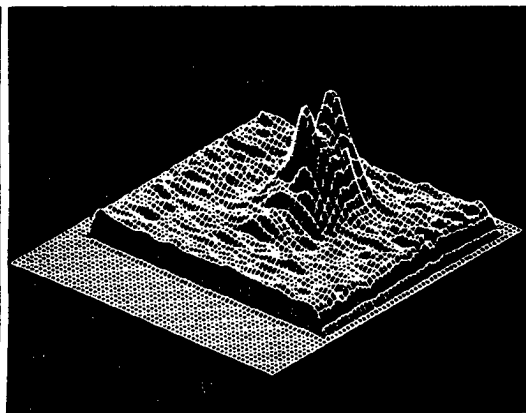


Fig 4 : 3D-representation

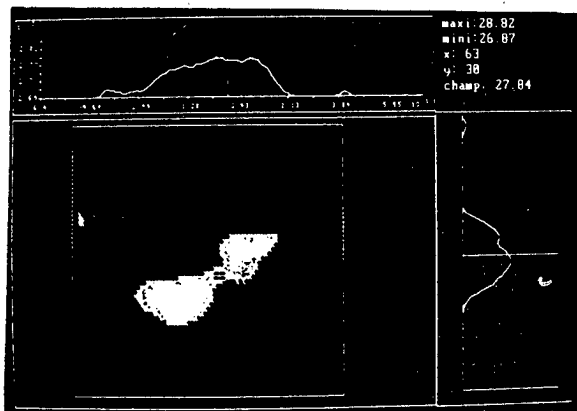


Fig.5 : Vibrothermogram of GFRP specimen impacted at two different locations.

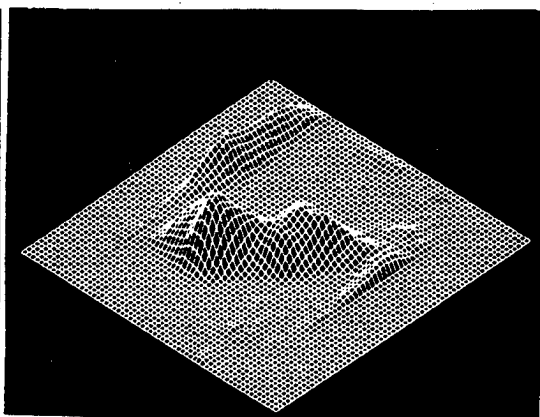


Fig 6 : 3D-representation

specimen was vibrated at a frequency of 18 kHz. In this case, the damage area is easily located because the thermal conductivity of the GFRP (in the fiber direction) is about 20 times lower than the thermal conductivity of a CFRP. The effects of heat conduction are reduced, thereby increasing the sharpness of the temperature gradients by the same amount.

As a conclusion, vibrothermography allows a good detection and characterization of impacts damages on samples, if digital image processing techniques are used, specially when dealing with poor to noise ratio images.

4. PHOTOTHERMOGRAPHY

4.1 Description of the technique

Photothermography is based upon the observation of the temperature surface of a material after deposition of a transient heat flux at its surface. If defects or inclusions are present in the material depth, they will give rise to thermal discontinuities and hot spots, which are to be detected by the infrared camera.

This technique was at the research and development stage for the last five years and gave rise to a semi-industrial equipment [3], which is shown figure 7 and 8. This system is enough compact to allow on site testing. It is made of the following elements :

- A linearly focused heat source
- An infrared camera (AGEMA 780) , with a real time frame grabber
- A two axes frame
- A PC compatible computer
- Several specifically designed softwares

The digitization can be obtained with two modes :

Line scanner mode : In this mode, the vertical mirror is fixed and the camera delivers only infrared lines. An image is formed by the vertical motion of the two axis frame. The scanning rate is controlled by the computer.

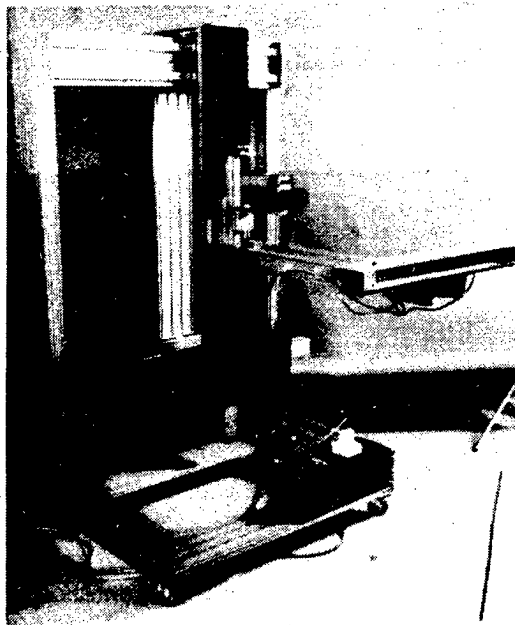


Fig. 7 and 8 : Picture of the photothermography equipment

Image mode : In this mode the infrared camera delivers infrared picture at a frame rate of 25 images/seconds. The heat deposition is made by the infrared tube moved by the two axis frame at the surface of the specimen.

4.2 Experimental results as samples

Several tests were performed as samples of GFRP materials with simulated defects. These defects were made of polyamide pieces inserted into the material. Results are obtained with three modes:

Surface heat deposition and image mode digitization: In this case, samples are illuminated by a surface heat deposition device. The infrared camera is used in its natural image scanning mode. Figure 9 present a thermal picture obtained on a defect after a digital processing. The filter used removed the gradient of temperature at the surface.

Line heat deposition and image mode digitization : This mode allows an easy set-up of all parameters, but the heat deposition is not optimised. Figure 10 presents an infrared image obtained on the defect as figure 9. The vertical thermal profil shows a temperature gradient.

Line heat deposition and line scanner digitization : Figure 11 shows a reconstructed picture of the defect previously discussed. In this case, on can see a good density of heat repartition.

4.3 On site testing

On site testing of real structures have been carried out in a ship yard. Tests were performed on submarines structures. In this case, heat deposition were performed by an infrared focused line heater. Tested structures were made of GFRP sandwich-panels with a syntactic foam. Total panel sizes were 7 x 5 meters. Several natural defects were detected at the foam/GFRP interface. Figure 12 give an example of the thermogram obtained.

CONCLUSIONS

The ever increasing use of composite materials in the military ship building has lead the DCN to develop several methods of Non Destructive Testing, in order to assess a good level of quality and reliability of these structures. Infrared techniques are particularly convenient for these testing.

Vibrothermography does not require external heat deposition and allows to obtain a good detection and characterization of impact damages on GFRP and CFRP samples. This method is specially convenient on relatively little structures.

Photothermography is based upon the monitoring of surface temperature after heat deposition, and is of more general use. An automated device was developed. It allows a good detection and characterization of artificial, such delaminations, on sandwiches and monolithic composites.

On site tests were performed on large structures. Natural defects were detected which proves the efficiency of this methods to testing the composite materials used in the military ship building.

REFERENCES

- [1] F.LESBRE, F.TERRAIL, "Advanced Composite Materials applied to military shipbuilding", French-Japanese Seminar on composite materials, Paris Le Bourget (13-14 mars 1990)
- [2] P.POTET ET F.LESBRE, "Contribution de la vibrothermographie à la caractérisation de l'endommagement des matériaux composites", Sixièmes Journées Nationales sur les composites, JNC6, Paris (1988), p.261-272.
- [3] C.ABJEAN, F.LESBRE, P.POTET, "Développement d'un banc de contrôle automatique par thermographie infrarouge de matériaux intéressant la construction navale militaire", Colloque international: Les Avancées Européennes en Essais Non Destructifs, Toulouse France (17-19 octobre 1989), p.219-232.

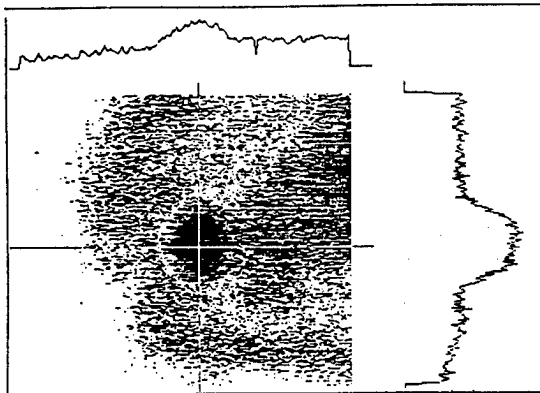


Fig 9

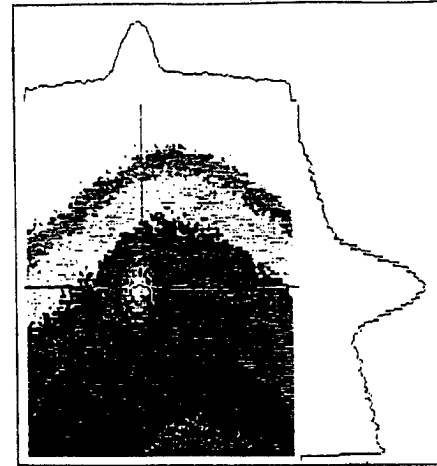


Fig 10

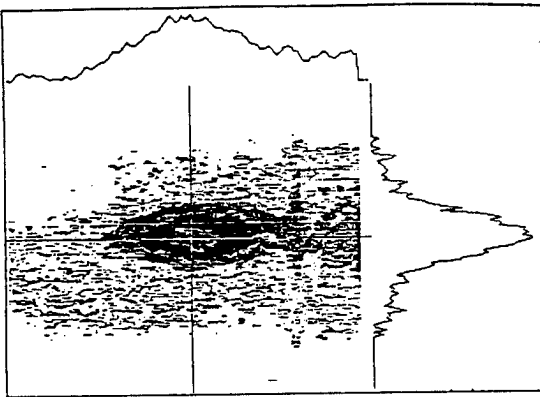


Fig 11

Fig 9 : Surface heat deposition
and image mode digitization.
Fig 10 : Line heat deposition
and image mode digitization.
Fig 11 : Line heat deposition
and line scanner digitization.

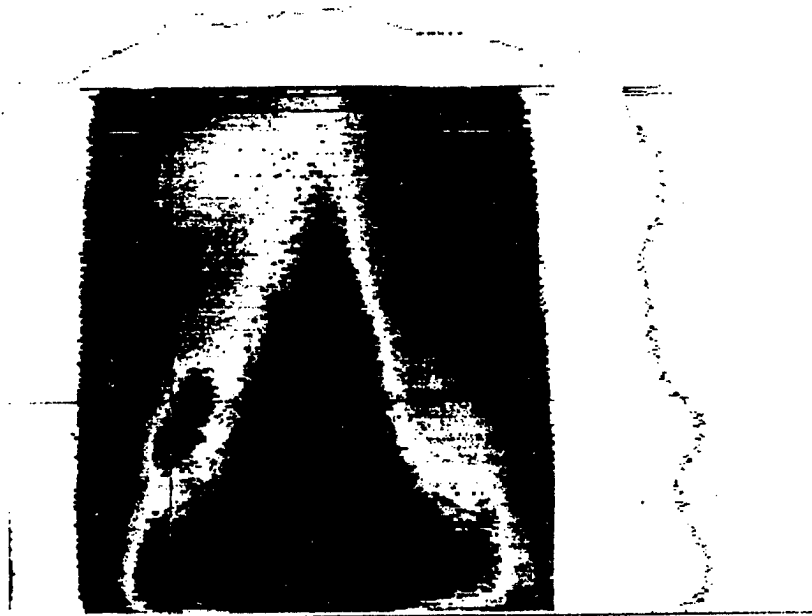


Fig 12 : Photothermogram on a on-site structure of GFRP/syntactic foam panel.

MATERIALS FOR CRYOGENIC BEHAVIOR

M. SABRIE, ALSTHOM

This page intentionally left blank

C o m p u t e r A i d e d D e s i g n

D. E. R o u v r a y * a n d P. D e s t u y n d e r **

* E n g i n e e r i n g S y s t e m s I n t e r n a t i o n a l s

** C o n s e r v a t o i r e N a t i o n a l d e s A r t s e t M e t i e r s

This page intentionally left blank

Development of High Performance
Carbon-Carbon Composites for Space Applications

Tadashi MATSUSHITA*, Hidehiko MITSUMA*, Tomoyuki KOBAYASHI* ,
Hirotoshi NAKAYAMA**, Akihito SAKAI**, Nobuo TSUCHIYA***, and Tsuneo KINJO***

- * Tsukuba Space Center, National Space Development Agency of Japan, 2-1-1, Sengen, Tsukuba, Ibaragi 305, Japan
- ** Gifu Technical Institute, Kawasaki Heavy Industries, LTD. 1, Kawasaki-cho Kakamigahara Gifu 504, Japan
- *** High-Technology Research Laboratories, Kawasaki Steel Corporation, 1, Kawasaki-cho, Chiba 260, Japan

Abstract

Carbon-Carbon (C/C) is a light weight refractory composite, and a prime candidate material for hot sections of space vehicles which are exposed to severe aerodynamic heating during re-entry. A resin char process was chosen for making C/C, and 2D carbon cloth and phenolic resin were selected for the preforming materials, to get high strength and to enable relatively complex shape forming. To prevent oxidation at high temperature, we have established multilayer coating method whose main coating is Chemical Vapor Deposited (CVD) SiC. Preliminary data acquisition tests are conducted, and some trial products such as an integral skin-stringer panel and other shaped components were fabricated to develop forming process and to demonstrate the feasibility of the material system.

Introduction

Carbon-Carbon (C/C) is a light weight refractory composite, and a prime candidate material for hot structures and Thermal Protection Systems (TPS) of space vehicles which are exposed to severe aerodynamic heating during re-entry. Excellent mechanical properties at elevated temperatures up to 1700 °C make this composite suited for the hot section of reusable space vehicles.

Reinforced Carbon-Carbon (RCC), the first generation of C/C for space applications, was used as the nose cone and the wing leading edge material of the Space Shuttle Orbiter (Ref.1). Now, development of the advanced C/C is in progress and our study is focused on advanced space transportation systems such as H-II Orbiting Plane (HOPE) (Ref.2) and other spaceplane concepts. Advanced material development, oxidation-protection coating, material characteristics testing, and fabrication of components are described in this paper.

Material Development

Preforming materials, reinforcement structure, and fabrication process were evaluated to generate high strength C/C composites. Because the developing target is structural members for spaceplanes, formability of large, complex shaped parts were considered in the evaluation. So, methods which would not give structural components in these several years were rejected.

Table 1 Classification of Carbon-Carbon Composites by Reinforcement Structure

Reinforcement Structure	Advantages	Limitations	Total Evaluation
UD (Uni-directional)	<ul style="list-style-type: none"> High fiber volume fraction Highest in-plane strength Fiber orientation flexibility (easy to get anisotropic laminate) 	<ul style="list-style-type: none"> Conformability for Complex shaping 	Fair
2D (Two-directional)	<ul style="list-style-type: none"> Formability and conformability for complex shaping High in-plane strength as UD in case of quasi-isotropic stacking 	<ul style="list-style-type: none"> Fiber orientation possibility 	Excellent
3D (Three-directional)	<ul style="list-style-type: none"> High interlaminar shear strength High fracture toughness 	<ul style="list-style-type: none"> In-plane strength Preformability & conformability for shaping 	Good

Reinforcement structure for C/C composites is classified as UD, 2D, or 3D reinforcement, like the Polymer Matrix Composites (PMC). Advantages and limitations of each reinforcement structure are listed in Table 1. As a result, 2D carbon cloth and phenolic resin were selected for the preforming materials.

Candidate fabrication process of C/C composites are

- Hot Press,
- Hot Isostatic Pressing (HIP),
- Chemical Vapor Infiltration (CVI),
- Resin Impregnation (Resin Char).

From the view points of formability and fabricating cost, resin impregnation process was selected. The process is common for C/C composites fabrication, and was applied to Reinforced Carbon/Carbon(RCC) of the Space Shuttle Orbiter (Ref.3). The process is charted in Fig.1 A net shape cured preform is carbonized, then impregnation and carbonization/graphitization are repeated several times to fill pores in matrix by carbon.

Oxidation-Protection Coating

C/C composites keep their strength at over 2000°C in non-oxidation environments. But they oxidize rapidly over 500 ~ 600 °C in the air. So, a critical technical issue for C/C is coating technology to prevent oxidation. The target temperature of oxidation-protection coating has been set to 1700°C, based on aerodynamic heating calculations of the HOPE(Ref.4).

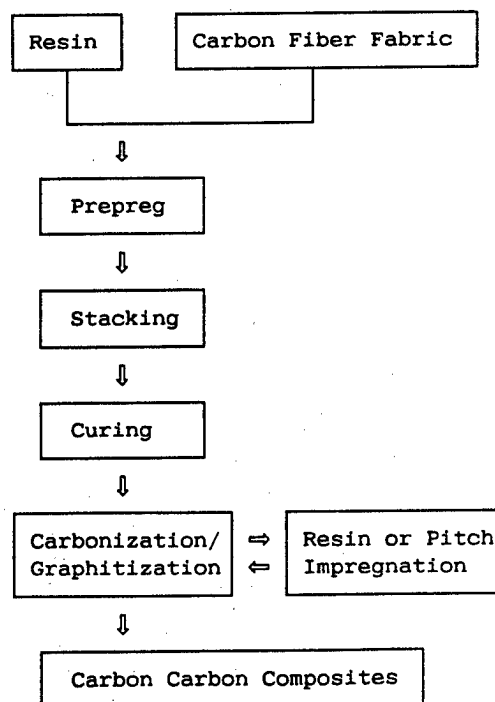


Fig.1 Production Scheme of Resin Impregnation Process

Coating materials are requested not only their own characteristics such as heat resistance and low volatility, but also chemical and mechanical compatibilities with C/C substrate. And weight reduction by thinning coating layer is required especially for space applications. Among ceramic materials which meet the requirements, Silicon Carbide (SiC) has been selected as most feasible material.

Table 2 Techniques for Coating

Glass-type Ceramic Coating
Diffusion/Conversion Coating
Solution Ceramic Coating
Plasma Spray
Chemical Vapor Deposition
Physical Vapor Deposition

Typical techniques for ceramic coating are listed in Table 2. Among them, Chemical Vapor Deposition (CVD) technique can generate tight and pure coating layers which endure 1700°C. But if the CVD-SiC layer is directly deposited on C/C substrate, delamination will occur by difference of thermal expansion. To resolve this problem, we inserted a thermal stress relaxation layer between C/C substrate and CVD-SiC layer. And more, SiO₂ overcoating was added to seal micro cracks of CVD-SiC layer.

Coated samples were evaluated by plasma flame exposure tests. High speed air flow from plasma gun dynamically heated the sample to 1300, 1500, and 1700°C. Six minutes exposure was repeated ten times for each temperature. As the results shown in Fig. 2, total weight losses were less than 30mg which was 0.6% of original sample weight. And more, bullet shaped specimens, whose nose radius were 17.5mm, survived arc heated wind tunnel tests.

Weight loss [mg]

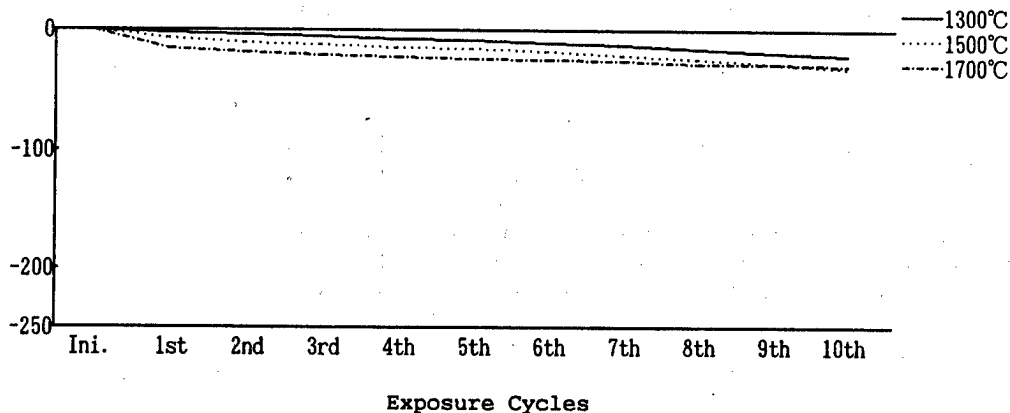


Fig. 2 Weight Loss after Plasma Flame Tests

Material Characteristics Testing

Typical data from preliminary data acquisition test results of developed C/C are shown in Fig. 3. As compared with NASA RCC design allowables (Ref. 1), which are also shown in Fig. 3, much higher values have been obtained. The effects of temperature, coating, and testing methods are also evaluated. The example of the results are listed in Table 4. No strength reduction due to high temperature or coating have been recognized.

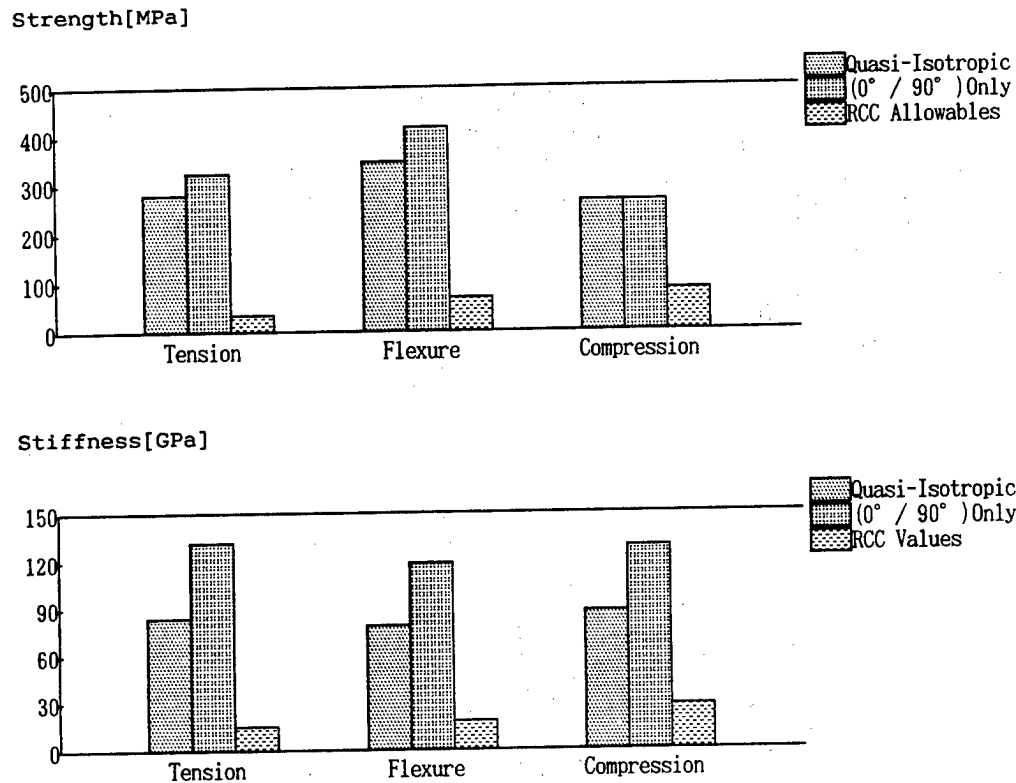


Fig.3 Preliminary Data Acquisition Test Results

Table 4 Effect of Temperature, Coating, Testing Method on Flexural Properties

Test Temperature	Coating	Testing Method	Strength [MPa]	Stiffness [GPa]
-50°C	No	4 points	371	74
Room Temp.	No	4 points	347	79
Room Temp.	Coated	4 points	360	75
Room Temp.	Coated	3 points	439	68
1700°C	No	3 points	448	64
1700°C	Coated	3 points	551	90

Fabrication of Components

Structural members of spaceplanes and those of other space applications have relatively complex shapes. So, some trial products were fabricated to develop forming process and to demonstrate feasibility of the material system.

An integral skin-stringer panel simulating a prime structural member of a spaceplane hot structure was successfully fabricated (see Fig.4). The panel is 500mm width by 1000mm length, and stiffened by three blade-type stringers.

A nosecone-like component (Fig.5) is 380mm in diameter and 200mm in height, and have small radius of curvature. A leading edge-like component was also fabricated to demonstrate complex shape formability (Fig.6).

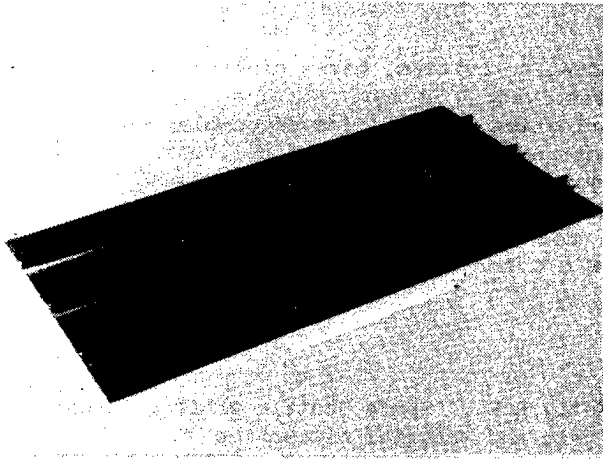


Fig.4
Integral Skin-Stringer
Panel



Fig.5
Nosecone-like
Component

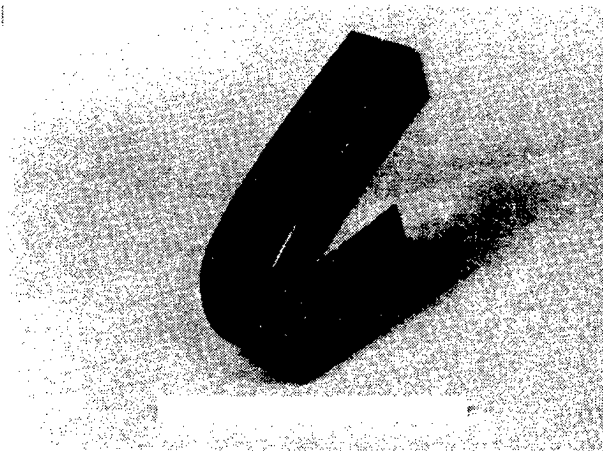


Fig.6
Leading Edge-like
Component

Conclusion

As a result of the development activities, basic problems on fabricating structural members have been resolved. We have obtained high strength and high modulus C/C materials, fabrication technologies of complex shaped components, and oxidation-protection coating system up to 1700°C. Next targets are design data acquisition, joining technology such as thermal-stress-free fasteners, and low-cost coating technology for relatively low temperature areas. Work in these areas is now ready to start. We hope advanced space transportation vehicles made of C/C and other advanced materials go to space in late 1990's.

References

1. Johnson, D.W., Curry, D.M., Kelly, R.E., "Space Shuttle Orbiter : Leading Edge Structural Design/Analysis and Material Allowables," AIAA paper 86-0949, 1984
2. T.Ito, S.Matsubara, H.Katsuta, T.Akimoto, Y.Takizawa, "Development Scenario of H-II Orbiting Plane, HOPE," 38th IAF Oct.10-17, 1987
3. Curry, D.M., Scott, H.C., Webster, C.N., "Material Characteristics of Space Shuttle Reinforced Carbon-Carbon," 24th International SAMPE, 1979
4. T.Kobayashi, T.Matsushita, H.Mitsuma, H.Tamura, H.Atumi, "Research and Development of the Primary Structural Members and Thermal Protection System for HOPE," Proc. of 27th Aircraft Symposium, 1989

ADVANCED JOINT OF 3-D COMPOSITE MATERIALS FOR SPACE STRUCTURE

T. Yamamoto, Mitsubishi Heavy
Ind., LTD. Nagoya, Japan
T. Hirokawa, Shikishima Canvas
CO., LTD. Omihachiman, Japan

ABSTRACT

Advanced joint of graphite/epoxy composite materials reinforced by three dimensional(3-D) fabrics has been designed, fabricated for prototype and evaluated.

Graphite fiber reinforced plastic materials have advantages of its lightweight and high strength for use in space structure. Specially, light joint of composite truss structure for the satellite component is one of most important technical subjects.

Compressive strength and tensile strength of advanced joint were measured and fabrication cost was evaluated. Materials and fabrication costs were cut down 28% and the weight of 16% was reduced comparing with uni-directional tape laminated composites.

1. INTRODUCTION

Composite materials reinforced by such fibrous structure are not only lightweight but are superior in specific strength, specific rigidity and low thermal expansion, so that they have great value not only in the above-mentioned applications but also in many other industrial field. The strength characteristics of such composite materials are largely dependent on the fiber content, weave and construction, matrix and the like of the fibrous structure used as a reinforcement.

However, the known technology can be applied only when fibrous structure is comparatively simple in profile or configuration and only when various portions of each fibrous structure are comparatively uniform in fiber density. Moreover, in the manufacture of a fibrous structure having an intricate profile, a cutting operation must be performed which may cause breakage of fibers leading to reduction of strength. Also, the known technology does not provide a usable means for manufacturing a bottomed hollow element, i. e., a hollow member having a bottom wall, and when it is

desired to assure a great reinforcing effect in a selected direction, it is necessary to increase the strength of the entire fibrous structure, so that the resulting fibrous structure has not the disadvantage of increased weight. Moreover, in forming an article having corners using laminated fabric material, the resin forms pools which causes a decrease in strength or a sacrifice of strength at the joint.

It is an object of this advanced joint, therefore, to provide a fibrous structure for reinforcing a composite material having a complicated profile, particularly a bottomed hollow pillar-shaped element having lateral projections such as fins, and which is capable of displaying high strength in a selected direction and is free of any remarkable fiber breakage or resin pools.

2. CONCEPT OF 3-D STRUCTURE

Fig. 1 shows the basic fiber arrangement that was used on Advanced joint. Fig. 2 shows an integrally woven 3-D advanced joint. This orthogonary woven 3-D fibrous structure consists of yarns arranged in three directions X, Y and Z and is integrally woven as to form the final configuration of the structure without using such methods as stitching and chemical bonding. Bottom layers of the hollow square-pillar portion of the body is made thicker than top layers of it. Two fins are outwardly extending from points at two corners on the bottom wall at the angle of 45 degrees.

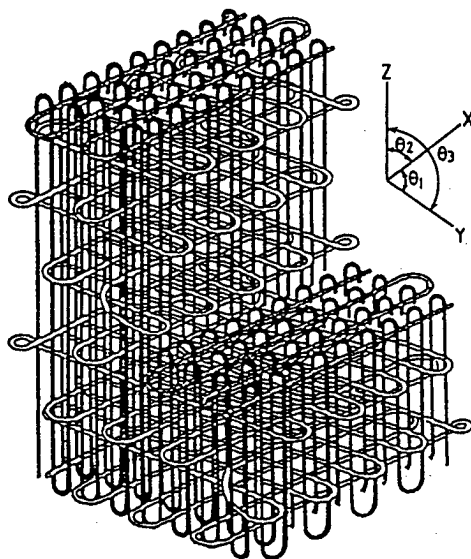


Fig. 1 BASIC FIBER ARRANDEMENT

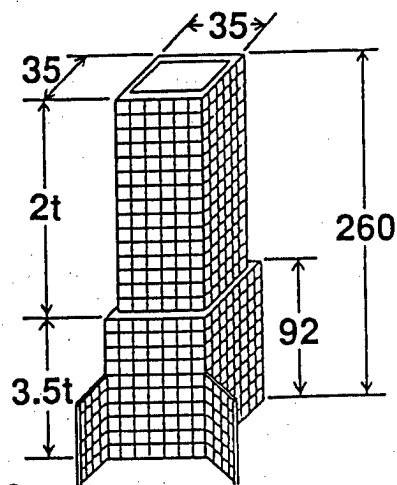


Fig. 2

**THE SCHEMA OF ADVANCED
JOINT OF 3-D COMPOSITE
MATERIALS**

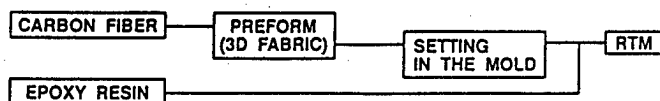
2.1 MOLDING PROCESS

Molding processes for 3-D fabric are shown in Fig.3. This figure also shows the comparison of fabrication processes between 3-D and prepreg. 3-D molding processes is less complicated than prepreg. The properties of epoxy resin just used are shown Table-1. This epoxy resin is very popular, but we have had some modifications of resin matrix to minimize cracks in the resin.

Table-2 shows the processes of resin transfer molding used in 3-D Advanced Joint.

Fig. 3 COMPARISON OF MOLDING PROCESS

3D FABRIC



PRE-PREG

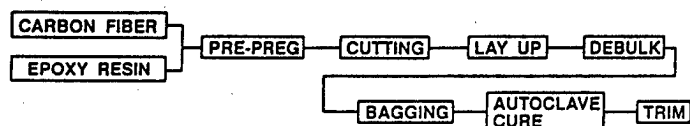


Table-1 TYPICAL PROPERTIES OF EPOXY RESIN

PROPERTY		VALUE	
Base resin		$\text{TGDDM} \left(\begin{array}{c} \text{N,N,N',N'-tetraglycidyl amino diphenyl Methane} \\ \text{G} \quad \text{G} \\ \text{G} \quad \text{N} \text{---} \text{CH}_2 \text{---} \text{C}_6\text{H}_4 \text{---} \text{N} \text{---} \text{C}_6\text{H}_4 \text{---} \text{N} \text{---} \text{G} \\ \text{G} \quad \text{G} \end{array} \right) \text{G} \text{---} \text{CH}_2 \text{---} \text{CH} \text{---} \text{CH}_2 \text{---} \text{G}$	
Density	kg/dm ³ (Lb/in ³)	1.27	(0.046)
Tg	°C (°F)	210	(410)
Viscosity (Pa.S)	at 80 °C	4	
	at 100 °C	0.6	
Flexural strength MPa		230	(33.5)
Flexural modulus MPa		4100	(596)

Table-2 RTM PROCESSES

ITEM		PROCESSES
Temperature for resin transfer	°C (°F)	120 (248)
Injection Rate	cm ³ /min	2.8
Curing temperature	°C (°F)	180 (356)
Curing pressure	kg/cm ² (psi)	50 (714)
Curing Time	Hr	2

3. MECHANICAL PROPERTIES TEST

Advanced joint was fastened to the test jig by 3/8 inch diameter bolt.

The schema of mechanical property test is shown in Fig. 4.

Maximum 6400kg of compression load was applied to advanced joint, and then tensile load was applied until advanced joint was failed. Test results of mechanical property test are shown in Table-3.

In case of compression test, no evidence of failure was observed. Advanced joint was failed at 6100kg in tensile load. Failure was occurred at outersurface of the bottom board around bolt hole.

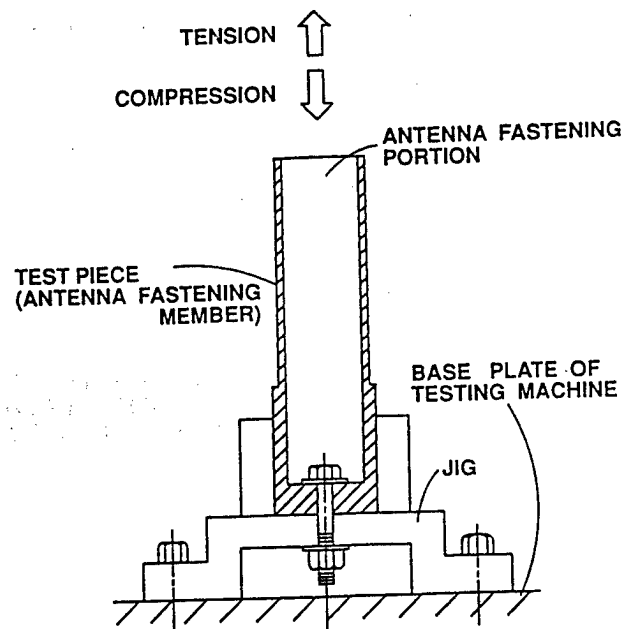


Fig. 4
THE SCHEMA OF MECHANICAL PROPERTIES TEST

4. COMPARISON OF WEIGHT AND COST

A fibrous structure according to the present advanced joint and a comparative one manufactured in a conventional manner, i.e., comprising laminated two-dimensional parts, were impregnated with the same epoxy resin and, after curing, antenna fastener members were formed, respectively. The fastener members were then subjected to tensile and

compression tests on a testing installation as illustrated Fig. 4. The data thus obtained are shown in Table-4.

It should be appreciated also that manufacturing cost for the joint formed from the fibrous structure of the present advanced joint decreased by 72% with respect to the comparative one.

This is due to the fact that the present advanced joint does not require conventional operations, laminating, cutting, fabricating, and adhesive bonding. Weight per one joint decreased by 84%.

Table-3 RESULTS OF MECHANICAL PROPERTY TESTS ON ADVANCED JOINT OF 3-D COMPOSITE MATERIALS


TEST METHOD	FAILURE LOAD	FAILURE MODE
COMPRESSION	(> 6400 kg)	NO EVIDENCE OF FAILURE OBSERVED AT 6400 kg
TENSION	6100 kg	TENSILE FAILURE OCCURED AT BOTTOM 

Table-4 COMPARISON OF WEIGHT AND COST BETWEEN 3-D ADVANCE JOINT AND 2-D COMPARATIVE (UD LAMINATED JOINT) THAT HAS SIMILAR FAILURE LOAD WITH ADVANCED JOINT

ITEM	3-D ADVANCED JOINT	2-D COMPARATIVE
WEIGHT (g)	183	218
MANUFACTURING COST	72	100

5. CONCLUSION

In accordance with these tests it is now possible to manufacture a fibrous structure for reinforcing a composite material having a bottomed cylindrical or pillar shape and fins extending outwardly from the periphery of the body. Despite of its complicated shape, this fibrous structure comprises uninterrupted lengths of yarn arranged linearly and integrally so that the strength or tenacity of the yarn is assured to be used to the maximum extent. Furthermore, the pattern and the lay-up density of yarns can be freely selected in accordance with the designed distribution of strength. Therefore, the weight of the fibrous structure can be reduced while the necessary strength characteristics are maintained. As the result, it is now possible to meet the stringent requirements of space and aircraft applications.

Furthermore, since these advanced joint do not call for a cutting operation, there is no incidence of yarn breakage. Moreover, as these structure does not involve a gluing, bonding, seaming or other joining operation for intricately shaped portion which have heretofore been required, the peeling or detachment of the yarn at such positions can be effectively precluded.

6. BIOGRAPHIES

Tetsuya Yamamoto is presently a Senior Engineer of materials and processes on advanced composite in Nagoya Aerospace Systems, Mitsubishi Heavy Ind., LTD. He has over 20 years experience in adhesive bonding and composite technology.

Tetsuro Hirokawa is presently a Leader of Advanced composite Materials Group in Shikishima Canvas Co., LTD. He has over 10 years experience in weaving technology including 3-D fabrics, 2-D thick fabrics and special shaped fabrics.

SUPERPLASTIC FORGING OF SiCw REINFORCED ALUMINUM ALLOY

T. Tsuzuku, A. Takahashi, C. Fujiwara, A. Sakamoto
Mitsubishi Heavy Industries Ltd. Nagoya Aerospace Systems Works
10, Oye-cho, Minato-ku, Nagoya 455 Japan

ABSTRACT

Plastic deformation behavior at elevated temperature and room temperature mechanical properties after deformation of SiCw reinforced aluminum alloy (referred to as SiCw/Al) were investigated in order to optimize the condition of isothermal forging. The flow stress of SiCw/Al decreases radically with increasing temperature, and superplastic flow ($m \geq 0.3$) can be obtained at the temperature higher than (solidus-30)°C and at the strain rate higher than $5.0 \times 10^{-2} \text{ s}^{-1}$. Tensile strength of deformed SiCw/Al strongly depends on the deformation temperature, and the highest strength was obtained when SiCw/Al was deformed superplastically at the temperature just below the solidus line of the matrix. Based on these results the deformation condition of SiCw/Al was optimized, and a model missile wing was successfully fabricated by isothermal forging, which revealed significant weight advantage of SiCw/Al wing over the conventional wing.

INTRODUCTION

SiCw/Al is characterized by high strength and high stiffness with little anisotropy, and relatively good workability compared with continuous fiber reinforced aluminum alloy. SiCw/Al is manufactured either by powder metallurgy or by squeeze casting, and these manufacturing technologies have been established basically. Authors, however, further investigated the manufacturing process of squeeze casting to obtain the better mechanical properties in SiCw/Al, and they developed ultra high strength material, 27%SiCw/7075Al. The tensile strength of this material is more than 1,000 MPa, which is comparable with that of continuous fiber reinforced aluminum alloys.

Applicability of SiCw/Al for structural members of advanced aerospace components became broader by the development of high strength materials, and now the development of fabrication technologies has become the key for actual application of SiCw/Al. However,

tensile ductility of SiCw/Al is relatively low, so that studies of forging and rolling of SiCw/Al have not been completely successful.

In this study, plastic deformation behavior at elevated temperature and room temperature mechanical properties after deformation of SiCw/Al, which are essential for development of plastic forming technologies, were studied in connection with chemical compositions of matrix alloys, volume fraction of SiCw, and manufacturing process.

MATERIAL AND EXPERIMENTAL PROCEDURE

Development of High Strength SiCw/Al

In the manufacturing process of SiCw/Al by squeeze casting, the technical key points to improve the strength of SiCw/Al are to refine SiCw as much as possible before fabricating SiCw preform and to adopt high strength aluminum alloy as matrix. Based on this philosophy, high strength material, 27%SiCw/7075Al, was developed, and tensile strength more than 1,000MPa was achieved in the extruding direction. Refining of SiCw has effects to reduce the internal defects such as cluster of SiCw and/or imperfect infiltration of matrix alloy, and to make dispersion of SiCw uniform. SiCw in extruded bar is preferentially aligned along the extruding direction, which results in anisotropic mechanical properties. Tensile strength in transverse direction, however, is about 800MPa, which is only 25% lower than that in longitudinal direction.

Experimental Materials and Procedure

Materials used in this study are listed in Table 1. Materials were manufactured by squeeze casting and they were extruded by the ratio of more than 10 to get an alignment of SiCw along the extruding direction. Refining of SiCw before fabricating preform was applied for manufacturing SiCw/7075Al, but not applied for SiCw/6061Al.

The plastic deformation behavior of the materials was examined by constant strain rate compression test. The compressive specimen were prepared from the extruded bar as shown in Fig.1 so as to compress the material perpendicular to the alignment of SiCw. Tensile strength were examined under -T6 condition of the matrix, in the direction of SiCw alignment.

RESULTS AND DISCUSSION

Deformation Behavior

Fig.2 and Fig.3 show the flow stress as a function of temperature for SiCw/6061Al and SiCw/7075Al respectively. In both materials, flow stress decreases with increasing temperature and it drops sharply above the temperature which is lower than the solidus line of the matrix by about 80 °C. Above that temperature, the flow stress of SiCw/Al

is lower than that of the matrix alloy which is squeeze casted and extruded as the same as SiCw/Al. The lower flow stress of SiCw/Al at the high temperature is attributable to the fine grain structure, and main mechanism of the deformation is supposed to be grain boundary sliding. And it is also suggested that sliding at the SiCw/matrix interface may be contributing to the deformation, because the higher the volume fraction of SiCw is, the lower the flow stress is. Fig.4 and 5 show the flow stress of SiCw/Al as a function applied strain rate at various temperature. The strain rate sensitivity index "n" becomes larger than 0.3, in another words, superplastic flow is observed at high temperature and high strain rate condition. Threshold temperature for superplastic flow is lower than solidus line by about 30°C in both SiCw/6061Al and SiCw/7075Al.

Cracking Susceptibility

Closed symbols in fig. 4 and 5 exhibit the deformation conditions under which cracks occurred by the 50% reduction. SiCw/6061Al often cracked when it was deformed under superplastic conditions (fig.4). Fig.6 shows the representative cracking morphologies observed in SiCw/6061Al. Specimen were deformed nonuniformly which results in nonuniform crackings. These local deformation is supposed to be due to the nonuniformity in dispersion of SiCw. In these specimen, flow stress of SiCw rich portion is lower than that of SiCw poor portion at high temperature as shown in Fig.2, and SiCw rich portion deforms preferentially to lead the nonuniform deformation and cracking. Therefore SiCw/Al should be uniform in dispersion of SiCw without cluster of SiCw and/or imperfect infiltration of matrix metal, to be deformed superplastically. SiCw/7075Al, which were manufactured by using refined SiCw, never showed these kinds of nonuniform deformation and cracking, so that it is clear that refining of SiCw before fabrication of SiCw preform is effective not only for improving mechanical properties at room temperatures, but also for improving formability under superplastic conditions.

Mechanical Properties of Deformed SiCw/Al

Fig.7 shows tensile strength of extruded SiCw/7075Al and of upset forged SiCw/7075Al as a function of forging temperature. Tensile strength of deformed SiCw/Al strongly depends on deformation temperature. Especially, marked degradation of strength is observed in the specimen deformed above the solidus line of the matrix. This kind of degradation is also observed in just heated (not deformed) materials as shown in Fig.8. The degradation, however, was not observed in the specimen heated with hydrostatic pressure, so that the degradation is thought to be caused by crackings which occurred at the interfaces of partial liquid phase and solid phase. Below the solidus temperature, the higher the deformation temperature is, the higher the strength of deformed SiCw/Al is and as the results, the maximum strength is obtained from the specimen deformed superplastically at the temperature just below the solidus line. The results for

SiCw/6061Al is shown in Fig.9. Dependence of tensile strength at room temperature upon deformation temperature is the same as that for SiCw/7075Al. However, tensile strength is improved by forging, since SiCw/6061Al billet includes a lot of internal defects such as cluster of SiCw and/or imperfect infiltration of matrix metal. Effect of the strain rate on strength of deformed SiCw/Al is not found in this study clearly.

Isothermal Forging of Missile Wing Model

Based on the fundamental studies, fabrication trial of the missile wing model was conducted. High strength 27%SiCw/7075Al was selected as the material and an extruded bar was used in order to get the alignment of SiCw from the bottom to the top of the fin. The optimum deformation condition is as follows, from the view points of plastic deformation characteristics and of mechanical properties after deformation.

Temperature; $T = 450^{\circ}\text{C} \sim 480^{\circ}\text{C}$

Strain rate; $\dot{\epsilon} \geq 5.0 \times 10^{-2} \text{sec}^{-1}$

Isothermal forging of missile wing model was carried out in two steps. At first extruded bar was flattened, and then the plate was forged in matched die to get net shape in thickness. Fig.10 shows the forged missile wing model after finish machining, in which no defect was detected by X-ray, ultrasonic and penetrant inspections. Tensile strength of missile wing model was 930~1030MPa in direction from the bottom to the top of the fin, and 730 ~830MPa in the intersecting direction. Comparing to conventional wing made of PH stainless steel, more than 50% of weight reduction can be achieved by replacing with SiCw/Al.

CONCLUSION

- (1) SiCw/Al shows superplastic flow at the following condition.

Temperature ; $T \geq (\text{solidus}-30)^{\circ}\text{C}$

Strain rate ; $\dot{\epsilon} \geq 5.0 \times 10^{-2} \text{sec}^{-1}$

At this condition, the higher the volume fraction of SiCw is, the lower the flow stress is, which suggest that slidings between the SiCw and the matrix may occur as well as grain boundary sliding.

- (2) Refining of SiCw before fabricating SiCw preform is effective not only for improving mechanical properties at room temperature, but also for improving formability under superplastic conditions.
- (3) Tensile strength after plastic deformation is strongly affected by deformation temperature, and the maximum strength is obtained when SiCw/Al is deformed superplastically at the temperature just below the solidus line.
- (4) Missile wing model is fabricated successfully by isothermal forging and significant weight advantage over the conventional wing is confirmed.

Table 1 Materials used in this study

MATRIX	Vf of SiCw	SOLIDUS LINE
6061Al	18%, 27 %	583°C
7075Al*	13%, 20%, 27%	480°C **

*Chemical composition were modified to Al-7.5Zn-2.5Mg-1.6Cu-0.2Cr (wt.%) in order to achieve high strength.

**Solidus line was determined from the flow stress v.s. temperature curve shown as fig.3.

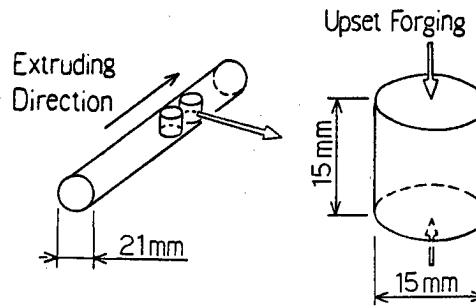


Fig.1 A schematic of preparation of specimen and upset forging

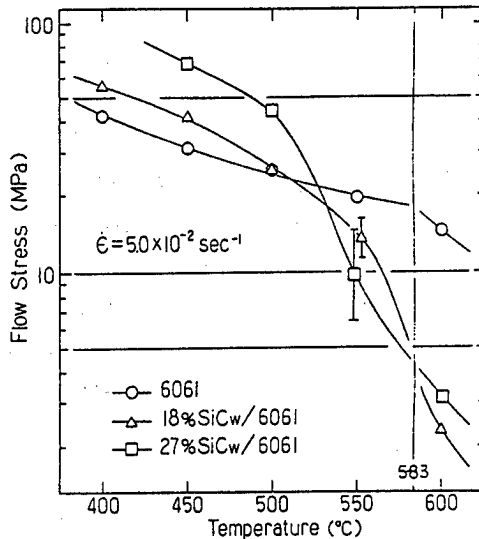


Fig.2 Flow stress as a function of temperature for SiCw/6061Al

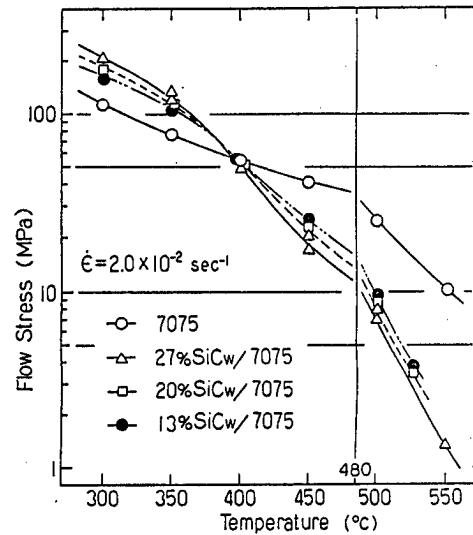


Fig.3 Flow stress as a function of temperature for SiCw/7075Al

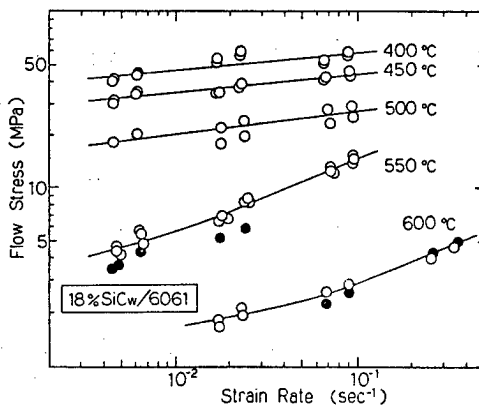


Fig.4 True stress as a function of strain rate for SiCw/6061Al

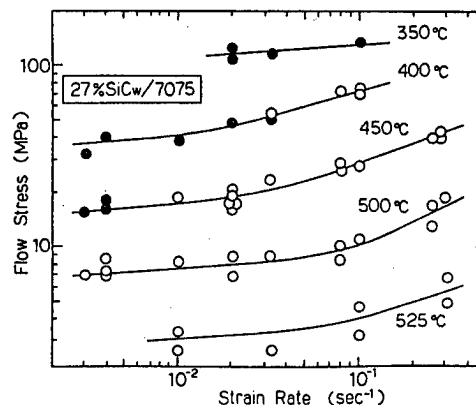


Fig.5 True stress as a function of strain rate for SiCw/7075Al

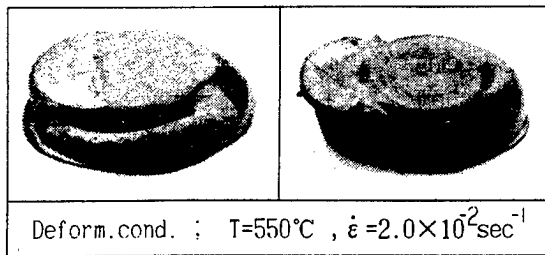


Fig.6 Nonuniform deformation and cracking observed in 27%SiCw/6061Al

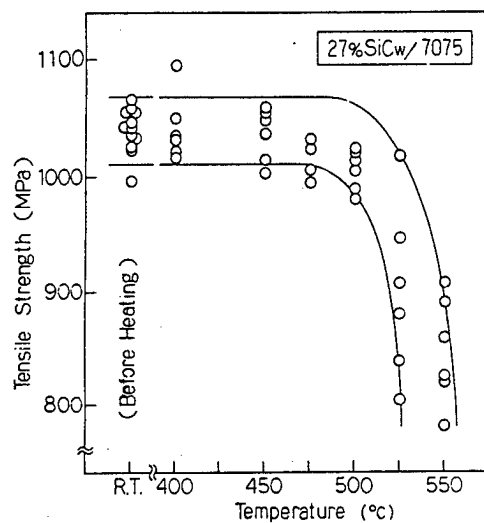


Fig.8 Tensile strength of SiCw/7075Al held at various temperature for 2 hours

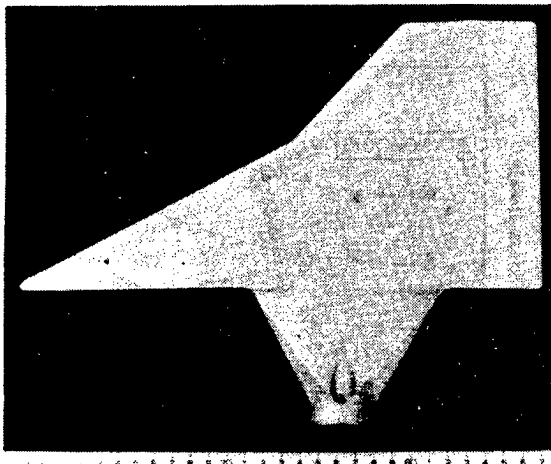


Fig.10 Missile wing model fabricated by isothermal forging

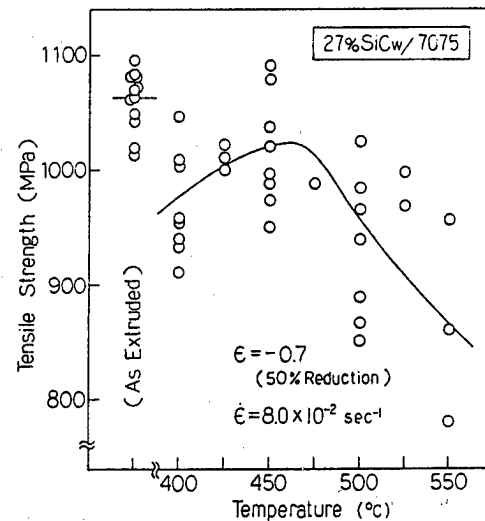


Fig.7 Tensile strength before and after upset forging as a function of deformation temperature for SiCw/7075Al

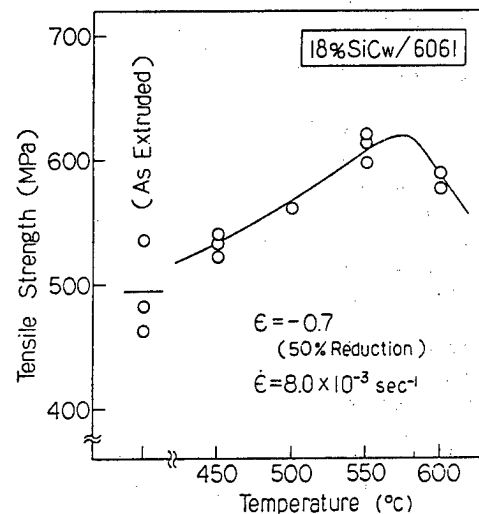


Fig.9 Tensile strength before and after upset forging as a function of deformation temperature for SiCw/6061Al

APPROACH TO CONTROL OF FIBRE ORIENTATION ON FRTP IN INJECTION MOULDING

Tsuneo.Hirai*, Tsutao Katayama* and Mitomo Hirai**

* Doshisha University, Kyoto 602 Japan

** Osaka Prefectural College of Technology,
Neyagawa-city Osaka 572 Japan

ABSTRACT

The fibre orientation in an injection moulded Fibre Reinforced Thermo-Plastics (FRTP) product depends on the flow pattern during moulding. It is difficult, but desirable to predict the orientation and control it by any means available. The method described in this paper imposes a restriction to flow at the flow front throughout the operation. The restriction is found to create not just a stable flow front but stable flow throughout the body.

INTRODUCTION

The injection moulding of fibre reinforced plastics is replacing other materials and methods in the manufacture of components because of the productivity of the process and the quality of the products, particularly strength and specific stiffness. However, the process still has many problems such as brittle weakness along the weld lines and warpage during thermal diffusion, influenced by the fibre orientation.

Fibre orientation, which depends on the flow pattern during the mould filling process, cannot be easily controlled during the injection moulding process. This is especially so for complex die configurations, although changing the position of the gate may give some control. In order to prevent warpage i.e. out-of-plane displacements, and improve rigidity at the required positions, it is necessary to predict and control the fibre orientation.

In this paper the flow pattern and hence the fibre orientation are controlled by restriction the flow front throughout the moulding process. Two investigations are described, one using a simple cylindrical mould fed from one end by a disc-shaped gate with a centered sprue and the other using a flat mould with a glass window for viewing and photographing the flow under free and restricted flow conditions.

FIBRE ORIENTATION OF CYLINDRICAL PRODUCTS

Experiments were carried out on the moulding of cup-shaped components using the transfer moulding process shown in Fig.1. This

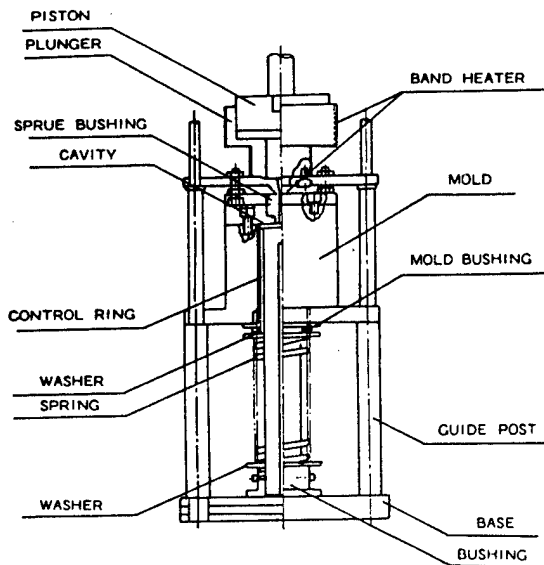


Fig.1 Shape and dimension of the specimen.

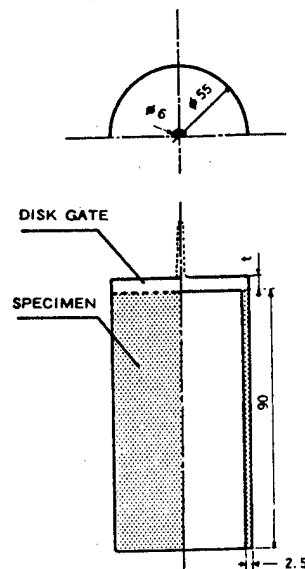


Fig.2 Schematic diagram of the model instrument.

process was used in place of injection moulding from cost considerations, in view of the small number of experiments. A sliding control ring is positioned in the cylindrical cavity of the apparatus, to control the movement of the flow front. It was shown that fibre orientation could be controlled satisfactorily using a spring to apply a counter pressure to the control ring, as shown in Fig.1. Fibre orientation is observed using soft X ray photography. Carbon fibres electroplated in copper, which are visible under X ray radiation were used as tracer fibres.

Experience has shown that similar characteristics are observed when moulding using glass fibre reinforcement with up to 20 weight% glass content. To evaluate the effects of fibre orientation in a component and achieve a reduction in the influence of the skin layer, experiments were made using polyethylene with tracer fibres to model the behaviour of high polymers, with the fibre orientation influenced by the factors described above.

The distribution of the fibre orientation in the disk gate is observed on concentric circles as shown in Fig.3. The lines shown in the diagram are drawn so that the direction gives the mean fibre orientation and the length shows the orientation factor. It can be readily appreciated that rigid rotation of a fibre during flow depends on the configuration ratio of the channel, that is the extrusion ratio of the inlet area of A_0 to the extruded area A , or $R=A_0/A$.

Fibres tend to align

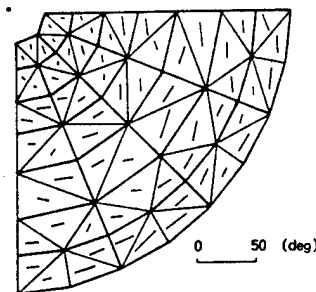
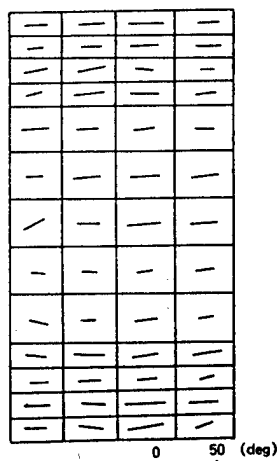


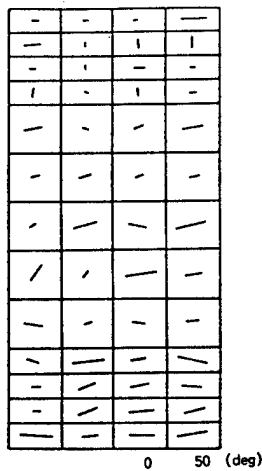
Fig.3 Diagram of the orientation in the disk gate.
(thickness of gate: $t=2.5\text{mm}$,
cross-head speed: $cs=50\text{mm/min}$,
controlling flow front(C.F.))

along a stream line for $R > 1$ and become perpendicular to the line for $R < 1$, for example during radial flow in the disc gate.

The distributions of fibre orientation in the cylindrical part of the mould are shown in Fig.4(a) and Fig.4(b) as having different patterns for the same thickness of gate disc and cylindrical wall and the same free flow front condition. Variations around the circumference are shown along the rows and progressive changes in orientation are indicated down the columns.



(a)



(b)

Fig.4 Diagram of the orientation in the case of free flow front. ($t=2.5\text{mm}$, $cs=50\text{mm/min}$)

Fig.5 Diagram of the orientation in the case of controlling flow front. ($t=2.5\text{mm}$, $cs=50\text{mm/min}$, C.F.)

The first and second rows might indicate an unstable flow condition which could be due to variations in viscosity.

The tangential orientation of fibres at the periphery of the disc gate might be transferred to the end of the cylinder, since R for the transition is unity for the case shown in Fig.4(a). If the configuration of the transition is considered to be from radial spread to cylindrical flow the fibre orientation after the transition might be arranged along the stream line, since the flow out of the junction can be considered as a convergent phase. One of the results supporting this flow model is shown in Fig.4(b).

Cup shaped components are generally required to resist hoop stress, calling for a circumferential fibre orientation. The method of controlling the flow front by means of the slide ring has been developed to achieve this objective. The

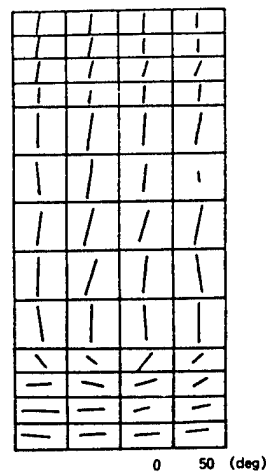


Fig.6 Diagram of the orientation. ($t=9.0\text{mm}$, $cs=50\text{mm/min}$, C.F.)

results shown in Fig.5 confirm that the method is successful.

Experiments were then carried out using thicknesses of disc gate greater than the cylinder wall thickness. The fibre orientation diagram for a 9mm disc gate thickness is shown in Fig.6. The fibre direction is parallel to the flow direction, since the value of R is considered to be greater than unity in the transition region.

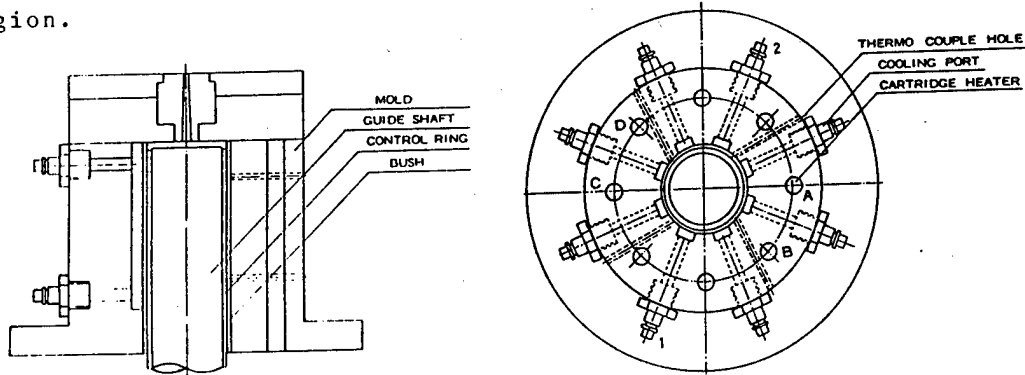
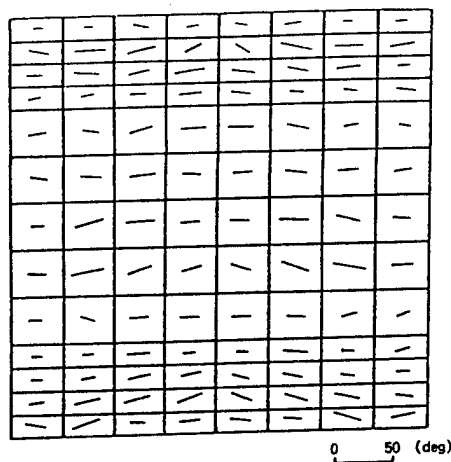
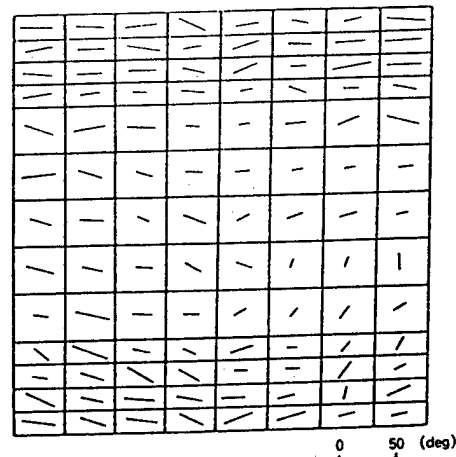


Fig.7 Schematic diagram of the mold.
(Cooling parts:1,2, Heating parts:A,B,C,D)



(a) In the case of controlling flow front



(b) In the case of free flow front

Fig.8 Diagram of the orientation with temperature gradient.
($t=1.0\text{mm}$, $cs=50\text{mm/min}$)

Finally an attempt is made to develop a method of controlling the fibre orientation by incorporating a temperature gradient control system using longitudinal cooling pipes and heaters spaced around the circumference and resulting fibre orientation diagrams are shown in Fig.7 and Fig.8 respectively. The effect of the slide ring restricting the flow front is given in Fig.8(a) and for the free flow front in Fig.8(b).

The temperature is highest over the centre columns of the diagrams and lowest at the edge columns. The extrusion ratio over the transition region between disc gate and cylindrical cavity is

less than unity, therefore the fibre orientation to be come aligned circumferentially for the steady flow condition shown in Fig.8(b). After careful examination of the configuration of the fibres in the diagram it is concluded that the complex formation of the flow front and the rigid rotation of the fibres to the flow

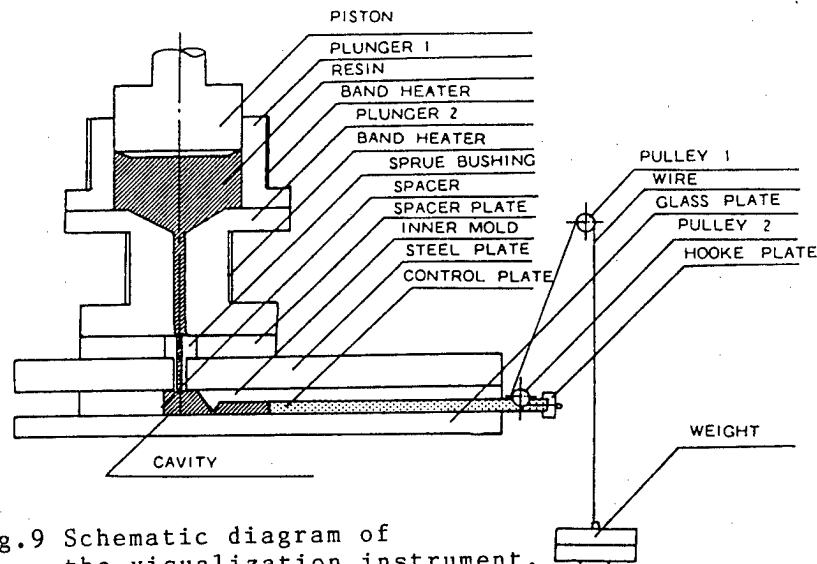
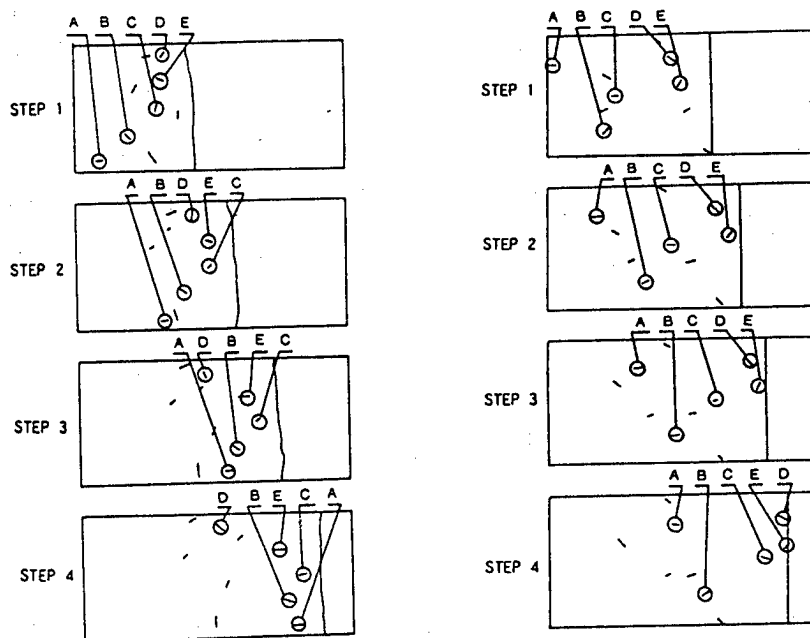


Fig.9 Schematic diagram of the visualization instrument.



(a) In the case of free flow front (b) In the case of controlling flow front

Fig.10 Diagram of the tracer fiber orientation.
($v=10\text{mm/sec}$)

direction is due to the effect of the higher temperature region. In spite of these complex effects, the fibre orientation could be controlled fairly well by using the slide ring to control the flow front, as shown in Fig.8(a).

VISUALISATION OF FIBRE ORIENTATION

Motions of the fibres during moulding cannot be observed using the equipment shown in Fig.1. Fibre movement and flow of resin were revealed in experiments using the visualisation mould with a glass window shown in Fig.9. The mould has a film gate and a control plate. Counter pressure was applied by means of a dead weight and pulley system. A sequence of photographs was taken through the window, giving the diagrams shown in Fig.10. In the case of the free flow front each tracer fibre rotated as flow proceeded and the shape of the flow front changed gradually, as shown in Fig.10(a). For the controlled flow front the tracer fibres undergo almost no rotation (Fig.10(b)).

DISCUSSION

In the disc gate a velocity gradient occurs along a fibre so that it tends to rotate and become perpendicular to the flow direction.

When the gate thickness is greater than the cylinder wall thickness, flow into the wall is convergent and it is observed that fibres rotate to become parallel to the flow direction. It seems that the disordered fibre orientation occurring with a free flow front is caused by disturbances to flow due to surface contamination, and surface defects in the mould. In the case of the free flow front it is found that orientation is also affected by temperature gradients over the surface of the cavity.

It is found that fibre orientation is stabilised by controlling the flow front by means of the slide ring or control plate, in spite of the disturbances due to surface defects, contamination and temperature gradients.

It might be possible to adapt the design of the mould and product to utilise this method of controlling the flow front for some commercial products.

CONCLUSION

The following results are obtained,

- (1) By controlling the flow front, it is found that the steady cavity filling process can achieve the desired fibre orientations.
- (2) The fibre orientation in the cylindrical wall is controlled by the thickness of the disc gate.

REFERENCES

1. T.Hirai, T.Katayama and M.Hirai, Proceedings Int. Sympo. on Composite Materials and Structures, 1098-1103(1986).
2. M.Hirai, T.Fukuda, T.Hirai and T.Katayama, Proceedings of the 7th Int. Conference on Composite Materials, Vol.1, 147-152(1989)
3. T.Hirai, T.Katayama, M.Hirai and M.Yoneda, J. of The Society of Materials Science Japan, Vol.34, No.378, 256-261(1985). (in Japan)

Structural Analysis of Laminated Cylinder

Akiko Nakazono, Yoshifumi Nakano

Tsukuba Research Laboratory,
Sumitomo Chemical Co., LTD.

6-Kitahara, Tsukuba, Ibaraki 305, Japan

ABSTRACT

The structural analysis system of laminated cylinders by closed form solution has been developed. The capabilities of this system are as follows.

- For given laminated cylinder geometry and loads, the ply stresses and strains are calculated by the point stress analysis method.
- Any combination of axial tension/compression load, internal/external pressure, torsional load, bending moment, and nonmechanical load can be applied.
- The ply stresses and strains (all components ; $r, \theta, z, r\theta, \theta z, zr$) of thick cylinder can be calculated.
- Both first ply failure and progressive failure analysis are available.
- Either Tsai-Wu or Maximum stress failure criterion can be selected.
- Critical buckling loads are determined under the combined loading condition. The contribution of each load is considered by interaction equation.
- The natural frequencies of free vibration are calculated for a given cylinder geometry and given boundary conditions (free, simply supported, and fixed ends).

We can quickly design and analyse almost all cases of laminated cylinders by using our own software system.

INTRODUCTION

Recently composite structures are widely used both in commercial and aerospace applications. The cylindrical structure which is one of the basic structural elements is widely used, because it is easy to be manufactured. For example filament winding or rolling table methods are usually used.

In designing composite structures, it is very important to make the best of orthotropy. In analysing thin walled laminated cylinders under various loads, not only first ply failure analysis but also progressive failure analysis is necessary. That would be of great help to consider the failure mechanism, whether material failure(matrix crack, fiber break, etc.) or buckling failure.

Composites in Japan are mainly used in sport and leisure application, especially fishing rods and golf shafts, which are subjected to bending moments. When the thin walled cylinder is under bending, it is necessary to consider the ovalization of cross section(called Brazier effect)[1].

In many cases of cylinder applications, thick cylinders with radius-to-thickness ratio of 5 or even lower are being used. We often need through-the-thickness normal and shear components of stress and strain which we cannot analyse by the shell theory. Then we need to calculate all components (6 components) of stress and strain without the limit of radius-to-thickness ratio by solving the basic differential equations of cylinder with equilibrium condition of the stress and continuity condition of the displacement at each interface and boundary conditions.

These are why we have developed our own softwares to design and analyse the laminated cylinder, although the program by Whitney, et al. is already well-known[2].

ANALYSIS METHOD

The design and analysis system for laminated cylinder consists of two modules. One is for thick walled cylinders and the other is for thin walled cylinders. Cylinder geometry and coordinate system are shown in Fig.2. The basic assumptions of the softwares are as follows.

Basic Assumptions

1. Cylinder constructed of homogeneous orthotropic sheets bonded together
2. Each ply obeys Hook's law
3. Small displacements : $|u|, |v|, |w| \ll t$
 Small strains : $|\epsilon_r|, |\epsilon_\theta|, |\epsilon_z|, |\gamma_{rz}|, |\gamma_{r\theta}| \ll 1$

Only for thin walled cylinder

4. Cylinder has constant midplane radius, R and thickness, t
5. Cylinder is thin : $R, L \gg t$
6. Through-the-thickness shear strains $\gamma_{rz}, \gamma_{r\theta}$ are negligible
7. Through-the-thickness normal strain ϵ_r is constant along r -axis[3]

The capabilities of these modules are shown in TABLE 1. and Fig.1

EXAMPLES

The examples of analysis using our system are shown below.

Example. 1 : Residual stresses that come from temperature change and thermal expansion coefficient mismatch are calculated both with finite element method (3-dimensional solid element) and with this system. Fig.3 shows a good agreement with both solutions.

Example. 2 : The result of progressive failure analysis of the angle-ply laminated cylinder under torsional load is shown in Fig.4 compared with the result of the test. In the analysis the temperature change after curing is considered and Tsai-Wu failure criterion is used. The torque-shear strain curve calculated by thick walled module is much the same as the one by thin walled module. Fig.4 implies that the cylinder will fail when fiber compressive failure is occurred in a -90° layer.

Example. 3 : The stress distributions of thick/thin cylinders which are subjected to internal pressure are compared in Fig.5. The stress gradient along the thickness is larger as the thickness increases.

TABLE 1 Module Capabilities

	Thin-Walled Cylinder	Thick-Walled Cylinder
Radius/Thickness	> 5	All
Stress and Strain components	$\theta, z, \theta_z, (\epsilon_r = \text{const})$	$r, \theta, z, \theta_z, z_r, r\theta$
Output points	Outer and inner surface of each ply	
Strength	First Ply Failure Analysis Progressive Failure Analysis With buckling	
Failure Criteria	Tsai-Wu Criterion, Maximum Stress Criterion	
Load	<p>All loads can be combined</p> <ul style="list-style-type: none"> • Nonmechanical Load (Temperature Change, Moisture Concentration) • Mechanical Load (Axial Tension/Compression, Torsion, Internal/External Pressure) (Bending, Transverse Crash) <p>For these two loads, Consider ovalization of cross section (Brazier effect) Output stresses and strains at Tension/Compression side of each ply</p>	
Buckling	<p>Appliable Load</p> <ul style="list-style-type: none"> • Axial Compression • Pressure • Torsion • Bending <p>Interaction Equation $R_c + R_p + R_t^2 + R_b \geq 1$ (buckled) < 1 (unbuckled) $R = \frac{\text{(applied stress)}}{\text{(critical buckling stress)}}$</p>	can not calculate
Natural Frequency	<ul style="list-style-type: none"> • Arbitrary set of boundary conditions is applicable (free, simply supported, fixed) • Initial forces are applicable (axial force, pressure, torsion) 	can not calculate

CYLINDER ANALYSIS

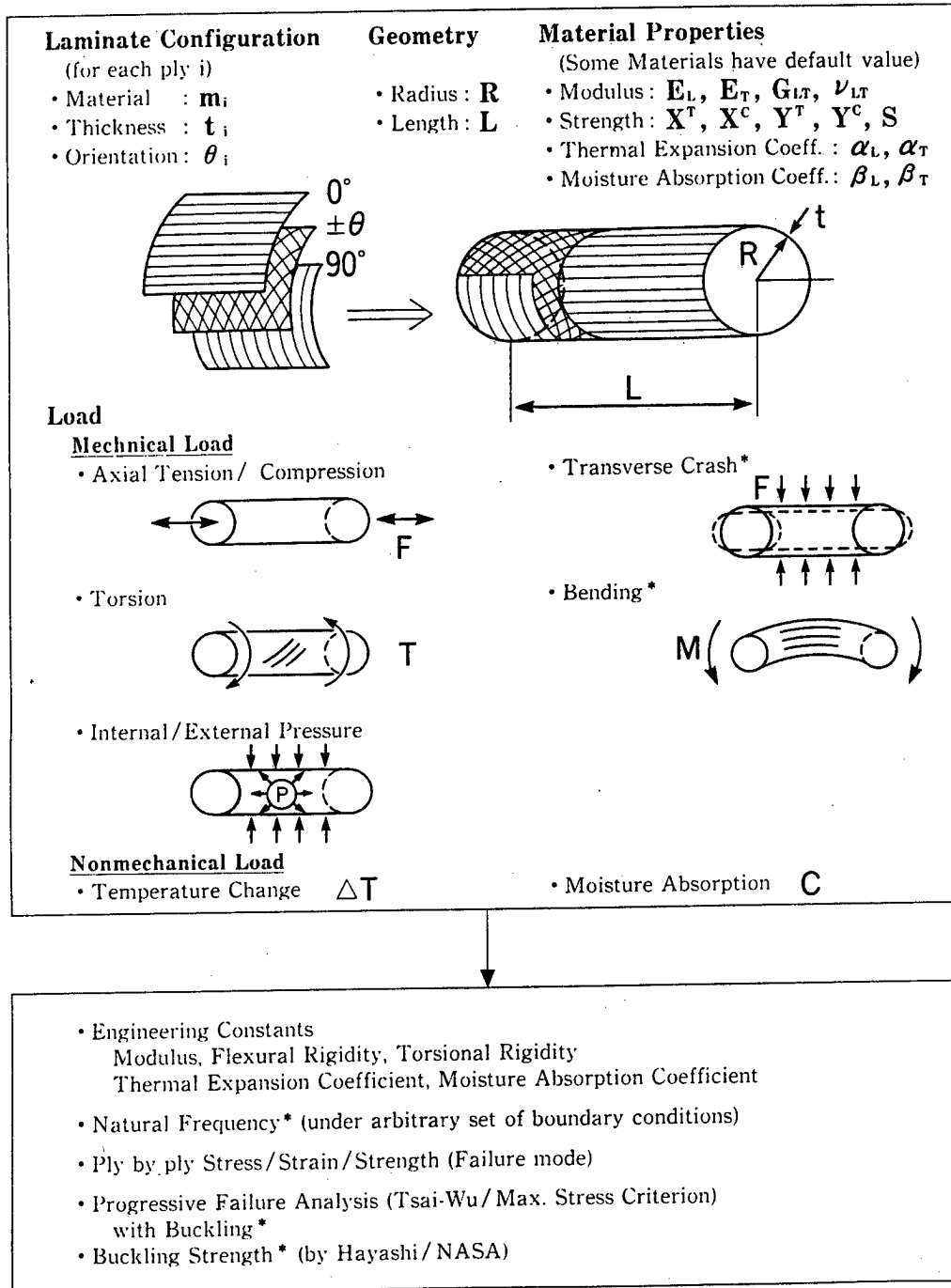


Fig. 1 Capabilities of Cylinder Analysis System

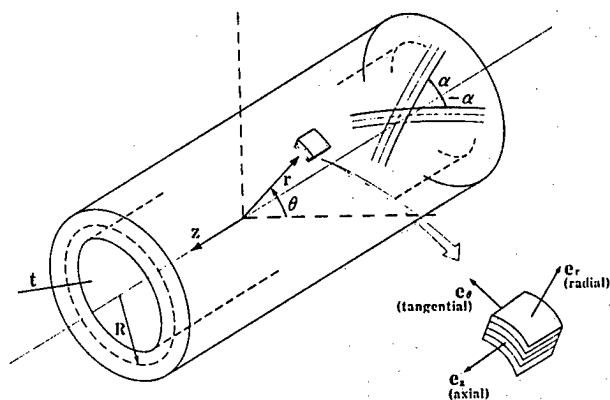


Fig. 2 Cylinder Geometry and Coordinate System

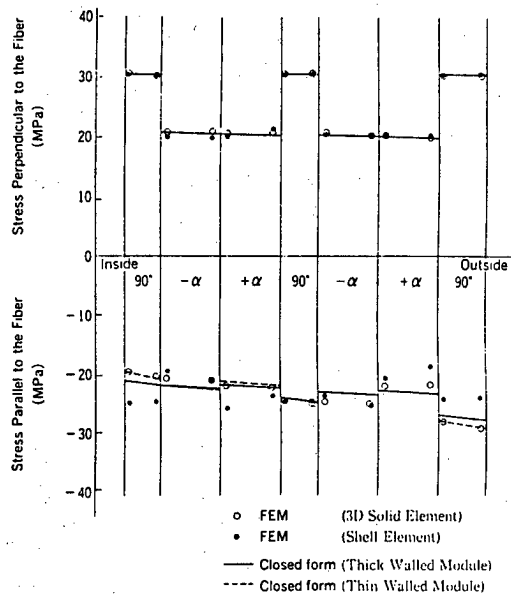


Fig. 3 Distribution of Stress Caused by Temperature Change ($\Delta T = -100^\circ\text{C}$)

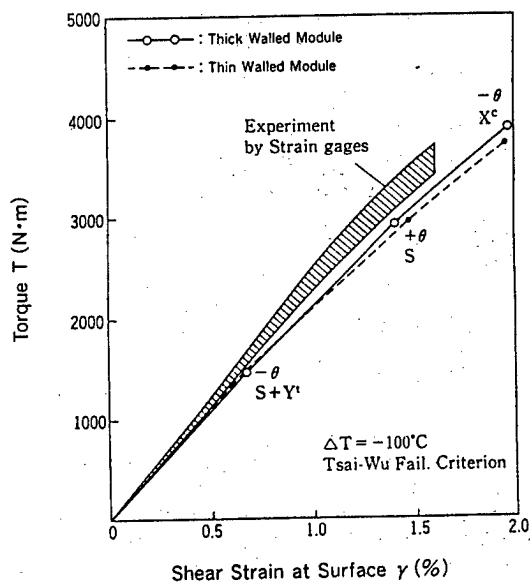


Fig. 4 Torque-Shear Strain Curve of Torsion Tube Test Laminated Cylinder [$\pm\theta$] $\phi 50/40 \times 15\text{mm}$, at R.T.

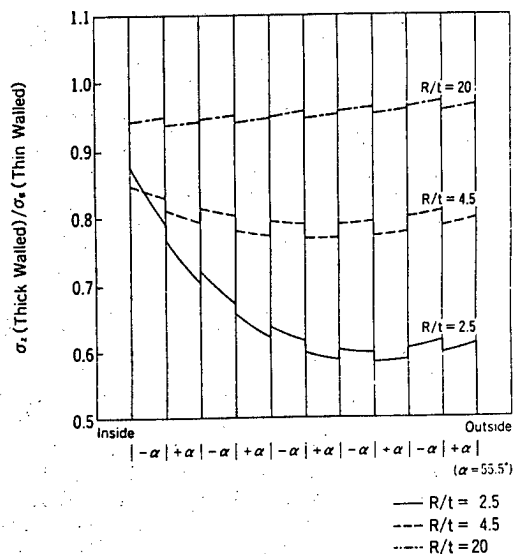


Fig. 5 Distribution of Stress Subjected to Internal Pressure

CONCLUSION

The structural analysis system of laminated cylinders by closed form solution has been developed. Anybody can quickly design and analyse almost all cases of laminated cylinders by choosing items in the menus.

REFERENCES

1. Ed. by Hayashi, T.; Composite Material Technology (Fukugou Zairyou Kougaku); Japan Science Technology Pub. (Nikkagiren); Sept. 1971
2. Whitney, J. M. and Gillespie, J. W. Jr.; CYLAN, Cylinder Analysis, Users Manual; Center for Composite Materials, Univ. of Delaware; Aug. 1984
3. Whitney, J. M.; "On the Use of Shell Theory for Determining Stresses in Composite Cylinders"; J. of Composite Materials; Vol. 5, July, 1971, pp. 340-353.
4. Dong, S. B., Pister, K. S., and Taylor, R. L.; "On the Theory of Laminated Anisotropic Shells and Plates"; J. of the Aerospace Sciences; Vol. 29; Aug., 1962, pp. 969-975.
5. Whitney, J. M. and Halpin, J. C.; "Analysis of Laminated anisotropic Tubes under Combined Loading"; J. of Composite Materials; Vol. 2, No. 3, July, 1968, pp. 360-367.
6. Pagano, N. J. and Whitney, J. M.; "Geometric Design of Composite Cylindrical Characterization Specimens"; J. of Composite Materials; Vol. 4, July, 1970, pp. 360-378.
7. Vicario, A. A. and Rizzo, R. R.; "Effect of Length on Laminated Thin Tubes under Combined Loading"; J. of Composite Materials; Vol. 4, April, 1970, pp. 273-277.
8. Pagano, N. J.; "Stress Gradients in Laminated Composite Cylinders"; J. Composite Materials; Vol. 5, April, 1971, pp. 260-265.
9. Cohen, D. and Hyer, M. W.; "Residual Stress in Cross-Ply Composite Tubes"; CCMS-84-04, VPI-E-84-16; Virginia Polytechnic Institute & State University
10. Buckling of Thin-Walled Circular Cylinders; NASA-SP-8007; NASA Space Vehicle Design Criteria (Structure); Aug. 1968
11. Becker, H., and Gerard, G.; "Elastic Stability of Orthotropic Shells"; J. of Aerospace Science; Vol. 29, No. 5, May, 1962, pp. 505-520.
12. Ed. by C. R. C. Japan; Handbook of Structural Stability; CORONA Pub.; March, 1971
13. Cheng, S., and Ho, B. P. C.; "Stability of Heterogeneous Anisotropic Cylindrical Shells under Combined Loading"; AIAA Journal; Vol. 1, No. 4, April, 1963, pp. 892-898.
14. Jones, R. M.; "Buckling of Circular Cylindrical Shells with Multiple Orthotropic Layers and Eccentric Stiffeners"; AIAA Journal; Vol. 6, No. 12, Dec., 1968, pp. 2301-2305.. Errata, Oct., 1969, p. 2048.
15. Dong, S. B.; "Free Vibration of Laminated Orthotropic Cylindrical Shells"; The J. of Acoustical Soc. of America; Vol. 44, No. 6, 1968, pp. 1628-1635.

NEW THERMOPLASTIC POLYIMIDE COMPOSITE FOR AIRCRAFT STRUCTURE

T. Nagumo
Aerospace Engineering Division.
Fuji Heavy Industries, Ltd.
Utsunomiya, Tochigi, Japan

and

H. Sakai
Central Research Institute.
Mitsui Toatsu Chemicals, Inc.
Sakae, Yokohama, Japan

ABSTRACT

Fiber reinforced composite materials on thermoplastic resins have been aggressively developing, which have excellent fracture toughness and processability, compared to thermoset resin based composite materials are expected to be used as the primary structural materials of aerospace, especially for their heat resistance, in addition to the advantages mentioned above. As a result of our continuous efforts, the new thermoplastic polyimide resin based composite material has been developed, which has twice Hot-Wet compression strength of Epoxy resin based composite material and Compression After Impact (CAI) of 36 kgf/mm². And new structure-fabrication techniques using their thermoplastic property can be confirmed effective to provide a sufficient structural property. In this paper, the mechanical properties, processability, and fabrication techniques will be reported.

1. INTRODUCTION

Recently, advanced composite based on epoxy is widespread used throughout the aerospace. However conventional epoxy system composite are limited to continuous use in high temperature environment more than about 120~130 °C. So it is necessary to develop high temperature resistance materials and to improve existing materials in order to apply these advanced composite to a future supersonic aircraft structure. Meanwhile, the matrix resin characteristics affects basic composite performance, also has a tendency that high temperature resistance property and toughness property are not compatible each other. Therefore, a considerable amount of efforts has been directed toward the development of high performance composite by the combination of new innovative resins and high performance carbon fiber. Especially, the toughness property increment is one of the important subjects to balance with high temperature resistance property. In these conditions, improved resin matrix composites and high temperature thermoplastics have been emerging as shown in Figure 1. Most importantly, high temperature thermoplastic resin matrix composite offers the sufficient potential for high damage tolerant property as well as low cost fabrication compared to conventional resin matrix composite. The objective of this study is to challenge the development of new thermoplastic polyimide composite and low cost design and manufacturing techniques for a future supersonic transport aircraft structures. This paper will review the present state of developed technology with reference to mechanical property and processing of new thermoplastic polyimide composite.

2. TARGET OF MATERIAL DEVELOPMENT

High temperature resistance requirement of aircraft construction material is decided by aircraft cruising performance and service environment. In this study, a hypothesis was made for a primary structure applications in Mach 2.5 transport aircrafts to develop new advanced composite, which is near the limitation of resin matrix composites. So, the target of material development was established as shown in Table 1, to overcome the problems associated with mechanical property and processings of present resin matrix composites. High temperature resistance which is hard to define mechanically, was the degree of about 177 °C cruising in service. And glass transition temperature (T_g) required more than 220 °C because practical experiences suggest the long-time service is about 50 °C below the T_g of matrix resins. Mechanical property, particularly compressive characteristics is the most critical in structural design, required equivalent to or more than state-of-the-art toughened epoxy system composite in ambient and 177 °C, wet conditions. Processing temperature required below 400°C which is much higher than curing temperature of epoxy matrix composite, but seemed almost the limitation of customers processing capability about same as for APC-2. In addition fusion bonding quality required equivalent to the conventional film adhesive bonding quality.

3. RESULT AND DISCUSSION

3.1 Matrix resin and prepreg development

In general high temperature thermoplastic resin more than $T_g=200$ °C tends to require high temperature processing conditions, their number is not so large until recently. However new thermoplastic polyimide resin (PIX) could be developed to satisfy with forementioned target of material development using modification techniques from LAR C-TPI [1] as shown in Figure 2, being worked under licensing agreement between Mitsui Toatsu Chemicals and NASA-Langley Research Center. PIX resin exhibits crystalline, solvent resistance and high thermal stability, beside its melt viscosity is appropriately low to impregnate into the carbon fiber rovings. PIX resin properties were shown in comparison with PEEK, conventional epoxy in Table 2. Development of PIX prepreg was conducted to produce continuously using resin melt impregnation method into intermediate modulus high strength carbon rovings as shown in Figure 3. Prepreg width is 200mm, volume fraction is 60%. Subsequently, it was confirmed that adequate plied panels could be produced without noticeable composite inner defects.

3.2 Basic mechanical property

The mechanical evaluation result of developed PIX composite is shown in Figure 4, Figure 5. These results suggested PIX composite is superior to other materials in hot wet resistance and toughness property. Particularly, 0° compression strength is hot wet condition such as 121 °C, wet and 177 °C, wet was extremely improved compared to the strength of typical conventional composite as T300/epoxy. Compression strength after 1500LB IN/IN impact was more than twice of conventional epoxy matrix composite and exceeded the strength of directing PEEK matrix composite toward the practical structural applications. And forementioned target such as 100 kgf/mm² compression strength in 177 °C, wet condition could be satisfied. However, in other basic property data except for 0° compression and compression after impact, it was recognized there exists a dispersed properties seemed to be affected by composite panel quality deviation. So the quality review will still be necessary to investigate what parameter affects composite property.

3.3 Processability

In practical application of thermoplastic resin matrix composite, there is a possibility that both prepreg and composite panel will be a material respectively dependent on the fabrication structure in producing various aircraft structures. Processability evaluation was carried out for PIX prepregs and consolidated composite sheets. As a result, appropriate prepreg consolidate condition and composite panel forming condition was shown in Figure 6 and Figure 7. Prepreg consolidate condition was required 400°C , $20\sim 30\text{ kgf/cm}^2$ beyond the conventional thermoset composite curing condition but also one fourth of conventional epoxy matrix composite curing time. On the other hand, although composite panel forming seemed to be a peculiar method different from the processing of thermoset resin matrix composite, these condition was required 400°C , 35 kgf/cm^2 . This reason would be supposed PIX melt-flow helps a smooth interlayer slip followed by fusion bond in higher temperature to produce good quality composite structure during forming process. Therefore, it was confirmed PIX resin composite has obvious advantage of being easy to increase producibility of structure fabrication, but severe condition should be inevitably applied for a short time to produce the structure.

3.4 Bonding property

Bonding method has been considered to be important in application of composite to a aircraft structure. This study reviewed the applicability of several unique bonding methodology beside conventional adhesive bonding [2] and evaluated the possibility whether PIX resin matrix composite could be applied because PIX resin is a true thermoplastic. In adhesion bonding, good bond quality could be obtained with a special chemical etching treatment regardless PIX resin repels thermoset adhesive resin characteristically. On the other side, several fusion bonding was conducted to assess which methodology will become a candidate for future bonding technology. Figure 8 showed the several results of bonding shear strength tests. Besides, it was understood these methods except for ultrasonic are approximately equivalent to the adhesive bonding, and their time required to conduct was outstanding shorter than a conventional method. However, in detail outside heat fusion bonding such as hot iron consumed longer time than other fusion bonding. So, totally induction fusion bonding was considered to be a future candidate by means of selecting suitable inductive materials.

3.5 Fabrication of structure

In this study, stringer, flame and skin structure as a fuselage element were practically produced and fabricated by induction and outside heat fusion bonding on the assumption of fabricating the Fastenerless fuselage structure as shown in Figure 9. Stringer size is $510\text{ mm}(\text{L}) \times 90\text{ mm}(\text{W}) \times 25\text{ mm}(\text{H})$ as shown in Figure 10. Flame size is $450\text{ mm}(\text{L}) \times 51\text{ mm}(\text{W}) \times 80\text{ mm}(\text{H})$ as shown in Figure 11. Small tube model as a fuselage skin is $160\text{ mm}(\phi) \times 300\text{ mm}(\text{L})$. These fabrications were basically according to the forementioned condition of prepreg consolidation, press forming and fusion bonding method. Especially bonded stringer and bonded flame figure are complicate, there had been a anxiety that PIX resin deterioration, interlaminar void and wave of fiber rovings are occurred in high temperature and longer processing conditions. However, it was confirmed both bonded stringer and bonded flame quality are almost good, beside small tube model manufactured by tape winding is also considered good as a first trial. Finally subcomponent fuselage structure was produced as shown in Figure 12. Size is $580\text{ mm}(\text{L}) \times 450\text{ mm}(\text{W}) \times 80\text{ mm}(\text{H})$. This structure could be fabricated by fusion bonding method with some considerations of facility and fusion bonding film. Fusion bonding method including fusion bonding film property was considered to be important, because complicate preformed structure will be distorted more easily affected by the temperature of fusion bonding when composite matrix resin is same as fusion bonding film. Therefore, polyimide relative new fusion bonding film, which melt flow

begins at lower temperature than PIX resin melting temperature was developed and applied to this subcomponent structure. And it was confirmed bonding quality was almost good as same as the element bonded structures.

4. CONCLUSION

In summary, developed PIX is one of the promising materials as would be expected that could offer significant mechanical and processing property advantages, particularly in high temperature resistance, damage tolerance and being able to apply fusion bonding. However, on the contrary of high performance a mount of study still remain to be done to develop a low lost manufacturing of actual aircraft structures. Therefore, next subject will be not only the improvement of PIX composite toward the easy and low cost manufacturing characteristic material, but also the establishment of further detail technique in order to be able to apply to a future supersonic transport aircraft.

5. ACKNOWLEDGMENTS

This work was conducted in cooperation of Fuji Heavy Industries and Mitsui Toatsu Chemicals, and the part of The Research and Development of Innovative Aircraft Structures with High Performance Thermoplastic Composite sponcered by The Society of Japanese Aerospace Companies.

This paper reported here is admitted by the Society of Japanese Aerospace Companies.

6. REFERENCES

- [1] A.K.St. clair and T.L.St. clair,
A Multi-Purpose
Thermoplastic Polyimide,
SAMPE Quartely, October 1981,
PP20-25.
- [2] T.Nagumo, H.Nakamura et al,
Evaluation of PEEK Matrix
Composite, International SAMPE
Symposium, Preprints, vol.32, 1987,
PP396-407

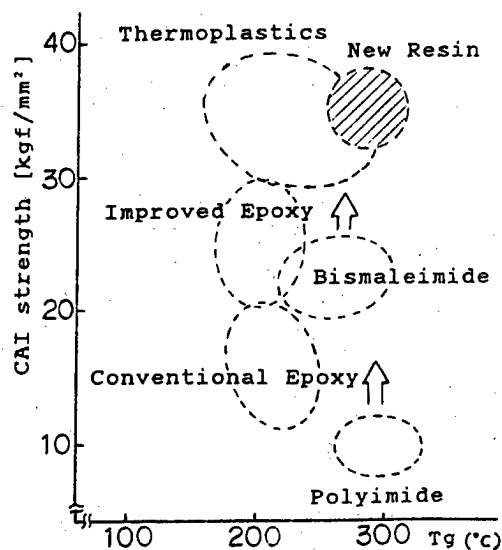


Figure 1. Relationship of CAI and Resin Tg

Table 1. Target of Material Development

TEST ITEMS	TARGET
Heat resistance	$T_g \geq 220^\circ\text{C}$
0° Compression strength	RT: $\geq 140\text{kgf/mm}^2$ HTW: $\geq 100\text{kgf/mm}^2$
C.A.I. 1500 lb·in/in	RT: $\geq 32\text{kgf/mm}^2$ HTW: $\geq 22\text{kgf/mm}^2$
Processing temperature	Less than 400°C
Fusion bonding	Equivalent to adhesion bonding

RT: ambient temperature, humidity.
HTW: 177°C , wet.

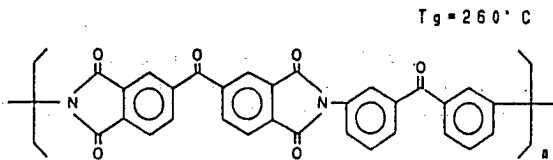


Figure 2. Structure of LARC-TPI

Table 2. Properties of PIX, PEEK EPOXY Resin

PROPERTY	UNIT	PIX	PEEK	EPOXY
T_g	$^\circ\text{C}$	252	143	200
T_m	$^\circ\text{C}$	388	334	-
FLEX. STRENGTH	Kgf/mm^2	14	15	18
FLEX. MODULUS	Kgf/mm^2	400	380	400

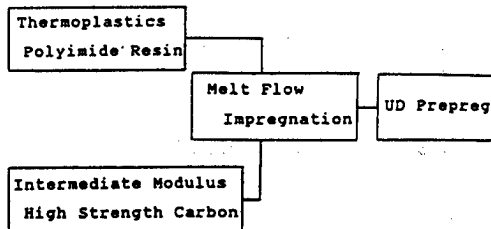


Figure 3. Production Flow of Prepreg

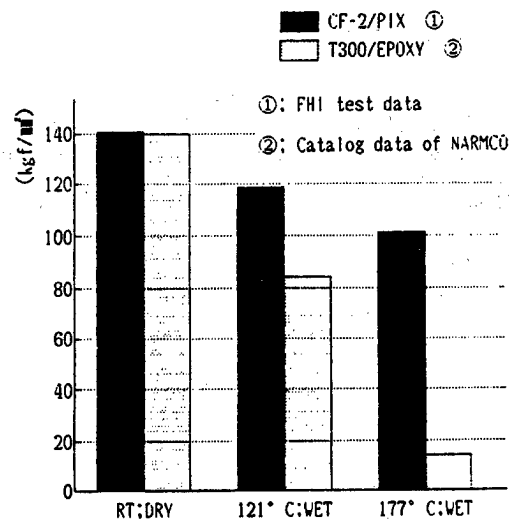


Figure 4. 0° Compression Strength

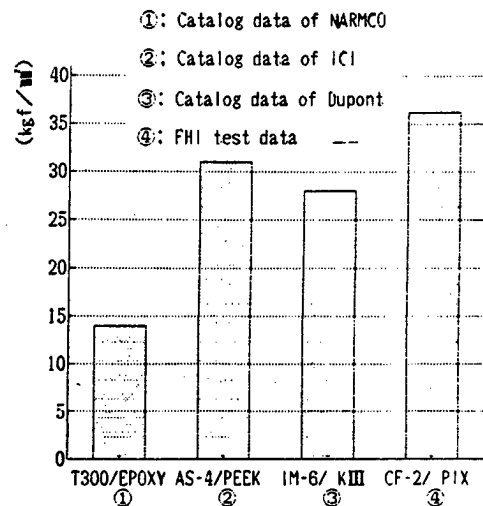


Figure 5. Compression Strength After Impact

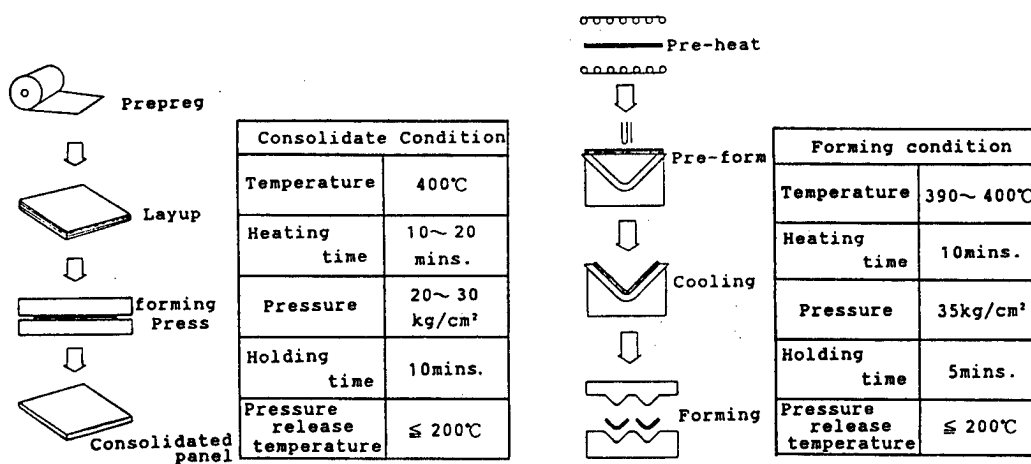


Figure 6. Prepreg Consolidation

Figure 7. Panel Forming

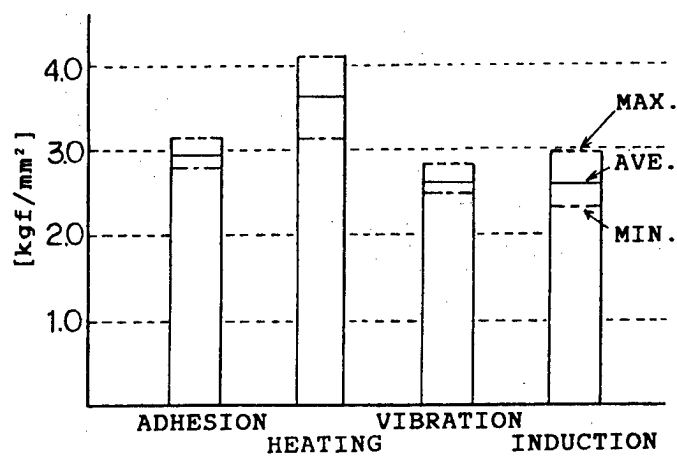


Figure 8. Shear Strength of Different Bonding Methods.

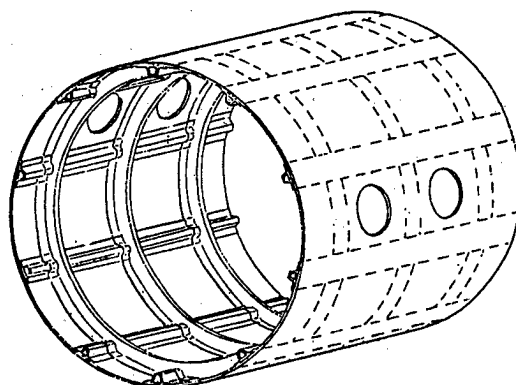


Figure 9. Fastenerless Fuselage Structure



Figure 10. Fusion Bonded Stringer Structure

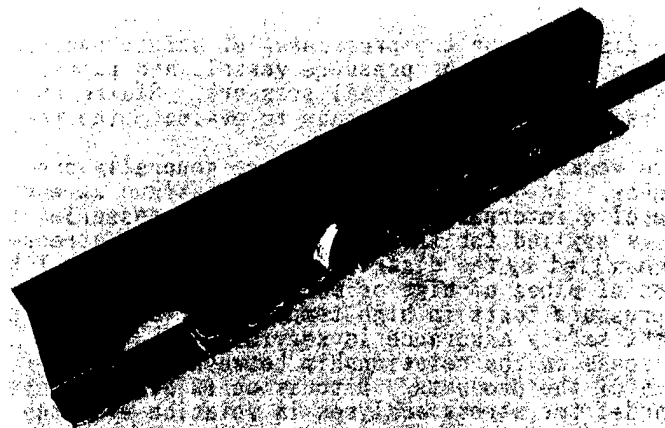


Figure 11. Fusion Bonded Flame Structure

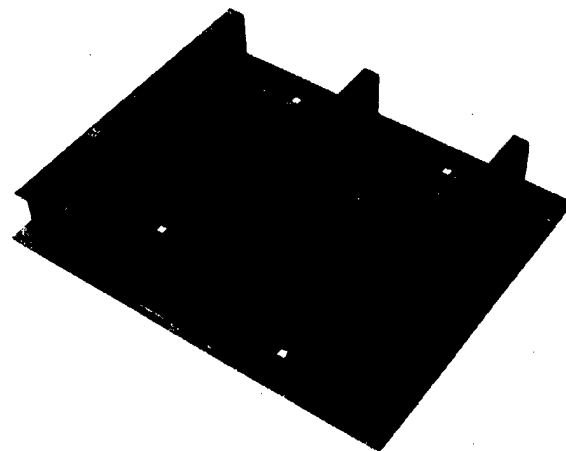


Figure 12. Fastenerless Subcomponent Fuselage Structure

Safety Evaluation and Design of Filament Wound Structures
— Cases of Pressure Vessels and Pipes —

Masanori Kawahara*, Takao Mori*, Yoshihiro Hirase*,
Akihiko Kato** and Toshio Ishihara*

- * Advanced Technology Research Center, NKK Corporation
1-1 Minamiwatarida-cho, Kawasaki-ku, Kawasaki 210, Japan
- ** Polymer Products Department, NKK Corporation
1-2, 1-chome Marunouchi, Chiyoda-ku, Tokyo 100, Japan

ABSTRACT

This paper discusses on the procedures of safety evaluation of filament wound products in the cases of pressure vessels and pipes. In these products, the prevailing loads are the internal pressure. Static and cyclic pressure tests are generally used as basic means to evaluate the performance and safety in service.

In pressure vessels, metallic liners are generally used to assure the gas-tightness. In order to increase the fatigue strength of metallic liners under cyclic internal pressures, an over-pressuring treatment, autofrettage, is applied for the control of residual stresses. Fracture modes can be also controlled by the distribution of reinforcing fibers.

In the case of pipes of high or medium pressures, cyclic pressure tests or long term pressure tests in high temperature water provides critical criteria for the safety assurance in service.

Authors discuss on the relationship between features of damages and design criteria of the products. Discussion is also directed to the selection of numerical model for stress analyses in relation with the features of damages.

INTRODUCTION

Filament winding technologies are extensively used to manufacture various composite products[1,2]. Each product has its own criteria to be taken into account for design and safety evaluation. Some criteria are based on basic rules of fracture in composite materials, and others are rather to evaluate the performance under some specific service conditions.

This paper discusses on the procedures of safety evaluation of filament wound products in the cases of pressure vessels and pipes. In these products, the prevailing loads are the internal pressure. Static and cyclic pressure tests are generally used as basic means to evaluate the performance and safety in service. Design has been performed on the basis of stress analysis by using appropriate numerical models, such as netting theory, laminate theory, or finite element methods[3-8].

Safety criteria depend much upon the laminate structures. In the first place, existence of fluid-tight layer is the most influencing item for design and safety evaluation. Pressure vessels are often fabricated by winding of reinforcing filaments on a metallic liner, which acts as airtight layer. Pipes are often fabricated by winding of fibers on a mandrel, which is to be removed after the curing of resin to fix the wound fibers. Authors took the case of a pressure vessel as an example with airtight layer, and the case of a pipe as an example without specialized layer for airtightness. Table 1 briefly shows the comparison of these two cases.

Table 1 Comparison of Two Cases: Pressure Vessel and Pipe

	Pressure vessel	Pipe
fluid-tightness	metallic liner	comosite itself
final failure	"burst" No care for micro fissures in resin or at resin-fiber boundaries	"weep" or "leak" Leak occurs through micro fissures in resin or at resin-fiber boundaries
criteria for final failure	maximum tensile stresses (or strains) of fibers	maximum tensile or shear stresses (or strains) in resin or at the resin-fiber boundaries
comments on safety in service	Fatigue life of metallic liner is to be improved. → Autofrettage (compressive residual stresses in liner)	Properties of resin-fiber boundaries is to be controlled. → Surface treatment of fibers
models for stress analysis	Netting theory is better	Laminate theory is better
tests for safety evaluation	① Raw material tests ② Tests for vessels Burst tests Pressure cycle tests at ambient temp. at high & low temp. Thermal cycle tests Bonfire tests Gunfire tests	① Raw material tests ② Tests for pipes Internal pressure tests in short term in long term (in hot water) cyclic Axial tests Bending tests

CASE OF PRESSURE VESSELS

Pressure vessels were fabricated by winding of resin-impregnated filament on a metallic liner. Liner material was Al 6061 alloy T6 tempered. Filament was high strength glass fiber, T-glass. Resin system was epoxy type.

Figure 1 schematically shows the laminate structure of the vessel. The vessel has three layers: metallic liner layer, helical winding FRP layer, and hoop winding FRP layer.

Figure 2 shows exterior view of a burst vessel. Location of burst can be controlled by an excess winding of reinforcing fibers.

Figure 3 shows fissures formed on the surface of a burst vessel. A few number of fissures initiate, already at the stage of autofrettage, along fiber direction. As the pressure increases and approaches to the burst level, tiny fissures initiate in transversal direction of fibers. Such a feature of damages justifies the approach of netting theory.

Figure 4 schematically shows the effect of autofrettage, to introduce compressive residual stresses in metallic liner.

Table 2 shows the specification of vessels.

Table 3 shows an example of results in a series of safety assurance tests.

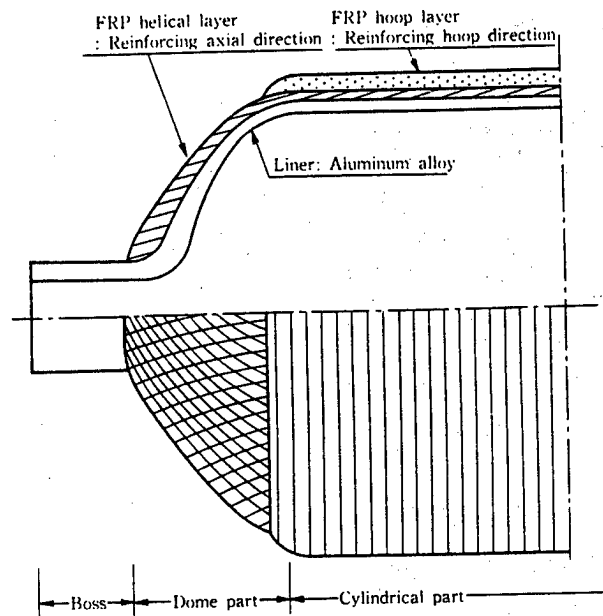


Fig. 1 Laminate structure of fabricated FRP pressure vessel



Fig. 2 Exterior view of a bursted pressure vessel



Fig. 3 Fissures formed on surface of a bursted pressure vessel

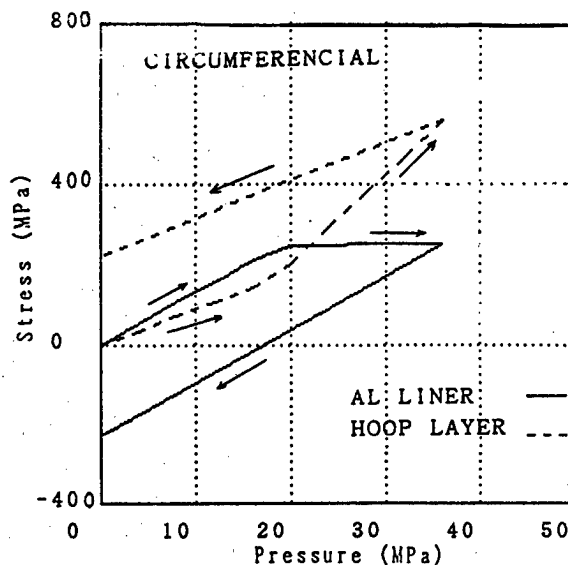


Fig. 4 Effect of autofrettage to introduce compressive residual stresses in metallic liner

Table 2 Specification of the Pressure Vessel

Capacity	: 5.1 litres	Service temperature	: -51 to 91°C
Weight	: 4.9 kg	Service life	: 15 years
Outer diameter	: 156 mm	Re-inspection period	: 3 years
Maximum filling pressure : 300 kgf/cm ² (29.4 MPa)			
Test pressure : 500 kgf/cm ² (49.0 MPa)			
Minimum burst pressure : 900 kgf/cm ² (88.2 MPa)			

Table 3 Prototype Tests for a Filament Wound Pressure Vessel

Test	[Cycling conditions]		Cycles	Burst Pressure (after cycling) kgf/cm ² (MPa)
	Temperature °C	Pressure kgf/cm ² (MPa)		
Virgin burst	ambient	0~500(49.0)	1	1,140(111.8)
Pressure cycling at ambient temp.	① ambient	0~500(49.0)	1	
	② ambient	0~300(29.4)	10,000	
	③ ambient	0~500(49.0)	30	990(97.0)
Pressure cycling at hi. & lo. temp.	① ambient	0~500(49.0)	1	
	② 93	0~300(29.4)	5,000	
	③ -51	0~300(29.4)	5,000	
	④ ambient	0~500(49.0)	30	995(97.5)
Thermal cycling	① ambient	0~500(49.0)	1	
	② ambient	0~300(29.4)	10,000	
	③ ambient	0~500(49.0)	30	
	④ 93~-51	300 29.4	20	1,050(102.9)
Bonfire	fire by kerosine and wood	300(29.4) <<filling>>	Vessel must be sound until completely vented from safety valve.	

CASE OF FRP PIPES

FRP pipes were fabricated by winding of E glass impregnated epoxy type resin. Long term internal pressure tests in hot water are considered indispensable for FRP pipes destined to high pressure use.

Figure 5 shows an exterior view of a FRP pipe

Figure 6 shows photograph of micro-structure in a failure pipe. Fissures initiate in resin or at resin-fiber boundaries. Leak took place along these fissures.



Figure 5 Exterior view of a FRP pipe

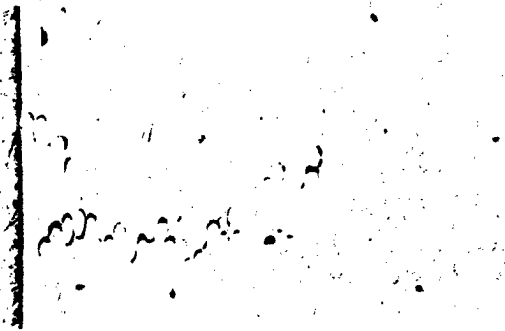
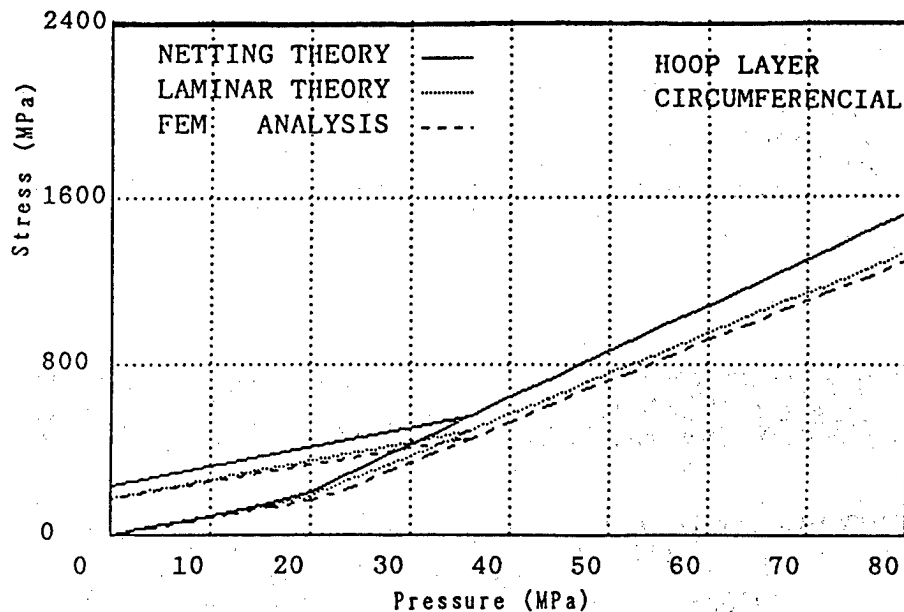


Figure 6 Micro-structure in a failure pipe

STRESS ANALYSIS MODEL FOR DESIGN

Stress analyses of filament wound structure are often conducted by netting theory, based on fiber strength. Loads are considered to be supported only by the reinforcing fibers. Strength of resin is neglected. On the contrary, laminate theory, based on mechanical properties of uni-directional laminates, takes into account the strength of resin between fibers and/or the joint strength between resin and fibers. Finite element methods have capability to apply to more complexed problems; such as elasto-plasticity, contact boundaries, cracked bodies, etc by using appropriate special elements.

Figures 7 shows an example of results in stress analyses conducted by using netting theory, laminate theory, and conventional finite element methods.



Figures 7 An example of results in stress analyses: comparison among netting theory, laminate theory and conventional FEM

DISCUSSION AND CONCLUDING REMARKS

Fracture of composite materials includes multiple phenomena of degrading in each composing material. Some damage may be vital to the function of the product, but the other may not. Each product has its own criteria to be taken into account for design and safety evaluation.

Laminate structure is one of the most important factor to influence upon the items of safety evaluation. In the case of pressure vessels with metallic liner layer, fissuring in resin is of little importance, but fatigue of liner materials is the biggest item to consider in design and safety evaluation.

In order to set a good safety criterion, it is necessary to understand well the features of damages in the structure as well as the role and the function of the product.

REFERENCES

- [1] Ford, r.a., 1st Intern. Conf. on Automated Composites, (1986-9), 4/1, Nottingham, England.
- [2] Wilson, b.a., 34th Intern. SAMPE Symposium and Exhibition, (1989-5), 2429, Reno, U.S.A.
- [3] NASA Computer Code CR72124, 1966.
- [4] DOT FRP-1 Standard, 1981.
- [5] Fukunaga, H. and Uemura, M., J. of JSASS, Jpn., 29-331(1981), 432.
- [6] Uemura, M., J of JSCM, Jpn., 13-1(1987), 10.
- [7] Takehana, T., Presented at Annual Meeting of HPGSI of Japan, Jpn., (1988).
- [8] Nakagiri, T., "Presence and Future of Pressure Technology", Jpn., HPI(1989).

PRODACOM : Property Database for Advanced Composite Materials for Future Industries

Mitsunori Miki* and Yoshio Minoda**

* Aeronautical Engineering, University of Osaka Prefecture
4-804 Mozu-umemachi, Sakai 591, Japan

** Research and Development Institute
of Metals and Composites for Future Industries
3-17-7 Tranomon, Minato-ku, Tokyo 105, Japan

ABSTRACT

A property database of advanced composite materials is developed and referred to as the PRODACOM. The data model is relational, but it also has hierarchical and network structures taking the special nature of composite property data into consideration. The data sheet for the collection of the data is made after investigating each item of materials properties and making trial entries by many researchers. The computer programs for input, search, and output are made and tested. The hardware of the system is a desktop computer with an optical disk storage equipment and a laser printer. Graphical data such as specimen geometries, curing profiles, and stress-strain curves, are also stored and managed by using an optical image scanner and an image data management program. The statistical analysis of the stored data is also conducted.

INTRODUCTION

Advanced composite materials such as graphite/epoxy, graphite/polyimide, SiC/polyimide, and aramid/epoxy are going to be used in primary structures of airplanes and aerospace structures. The development of such materials will also contribute to the improvements of the performances of automobiles, robots, and other precision machines.

In 1981, Ministry of International Trade and Industry, Japan started the System for the Research and Development of Basic Technologies for Future Industries where basic researches on new materials, biotechnology, and new functional devices were conducted. One of those researches is the research and development of composite materials. The target of this research is to increase the strength under high temperature. Table 1 shows the typical goal strengths of composites being developed. It should be noted that the goal strengths are set to 90% reliability with 95% confidence level, which are equivalent to B-value in MIL specifications.

Table 1 *Typical goal strengths of composite materials being developed for future industries.*

	Room-temp. strength	High-temp. strength
Polymer composites	2350 MPa	2115 MPa at 250 °C
Metal composites	1470 MPa	1320 MPa at 450 °C

Note: Strength is in 90% reliability with 95% confidence level.

Many companies, national institutes and research laboratories, and universities have been carrying out the development, investigation of the evaluation methods, and testing of the materials in cooperation. The authors have been engaged in the development of the database of the material properties of the composites. This database (PRODACOM: PROperty Database of Advanced COMposites) is the first full-scale database of composite materials in Japan and the present number of property data is more than ten thousand. The database also includes data on modulus, fracture strain, Poisson's ratio, compressive strength, energy release rate, impact energy, fatigue strength, physical and chemical properties. The number of data is presently increasing.

This paper presents the outline of the development of the database and the statistical analysis of the tensile, flexural and shear strengths of polymer matrix composites and metal matrix composites using the PRODACOM. The results obtained from the frontier composites will yield useful design guidelines in airplane and aerospace applications.

PROBLEMS IN MATERIALS DATABASE

The development of the database of the materials properties of advanced composites is not easy since the following problems exist:

- (1) Necessary properties are different for different composites.
- (2) Values of the properties are changed with testing conditions such as specimen geometry and loading method.
- (3) Detailed data have not been published yet since they are related to high technology.
- (4) The procedures of searching data are not uniform, that is, the way to utilize a database is not clearly defined.
- (5) Standard testing methods have not been established for some material properties of advanced composites.
- (6) The database management system should include statistical analysis of data since the design allowable of materials should be defined from their reliability.
- (7) The quality of the data should be identified by a certain means.
- (8) The database should include graphical data such as specimen geometries, curing profiles, and stress-strain diagrams.
- (9) The database does not come of itself. Producers, users, and researches of materials have to cooperate to develop it.

FUNDAMENTAL DESIGN OF DATABASE

The database consists of two sub-databases: PMC (polymer matrix composites) and MMC (metal matrix composites) databases. Each database consists of 17 files as shown in Fig. 1 where the field names of each file are presented. The datamodel adopted for a file is basically relational, but the files have a hierarchical structure as shown in Fig. 2.

HARDWARE AND SOFTWARE

The computer system for the database consists of mainframe RIPS (Research Information Processing System) of Agency of Industrial Science and Technology, MITI (Ministry of International Trade and Industry, Japan) at Tsukuba near Tokyo and workstation FACOM 9450. The workstation has been equipped with a hard disk drive, a flexible disk drive, an optical disk drive, a laser printer, a dot matrix printer, an image scanner, and a plotter as shown in Fig. 3. The literal data is up-loaded to the mainframe or down-loaded to the workstation while the graphical data is stored only in the optical disk which has the memory capacity of 1.2 GB (giga bites) for a 5" optical disk.

The software consists of three categories of computer programs: one is for literal data, one is for graphical data, and one is for statistical analysis. The literal data management programs are written in EPOACE of Fujitsu which is one of the popular relational database language while the graphical data are handled by using EPOIMAGE of Fujitsu which reads graphical data by the image scanner, stores them in the optical disk, and search required data. The statistical analysis consists of the calculation of general statistics, the inference of the Weibull parameters, and the determination of A- and B-allowables of the material strength. Their programs are written in BASIC.

STATISTICAL ANALYSIS USING THE DATABASE

Table 2 shows the number of data of the database at the end of 1989. Data have been accumulated from that time on. Statistical analysis of tensile, flexural, and shear strengths is performed using the database. The results obtained from a lot of data of advanced composites reveal many important facts.

Figure 4 shows the strength distributions of the longitudinal tensile strength of graphite woven fabric/ polyester (Torayca cloth 6343/Polymal X-440, [0/90]x12plies) and graphite(T400)/polyimide, UD, $V_f=67\%$) at room temperature on Weibull paper. A good fit to two-parameter Weibull distribution is found. The mean values are 480 and 2400 MPa, respectively, and the coefficients of variation (CV) are 5.6 and 3.5%, respectively. These values show that the materials have excellent performance for primary structural elements.

Figure 5 shows the distribution of the shape parameters of the Weibull distribution for unidirectional graphite composites. It is found that the distribution fits well to Normal distribution and the mean value and the CV of the shape parameter are 19.7 and 29.7%, respectively. These values are very important for reliability designs with advanced graphite composites.

For important materials, the cross-checks of test data between the company where the materials are developed and the government research institutes are carried out to ensure the reliability of the test data. Figure 6 shows the comparison between the company data and the cross-checked data. The difference between the mean values is 2 to 4% and it can be considered that the data are very reliable although the tests of high strength unidirectional composites are very difficult.

Figure 7 shows the relation between the mean value and the CV of the tensile and bending strengths of polymer composites. The CV is less than 10% when the mean value is more than 500 MPa, but the CV is exceeding over 30% when the mean value is less than 500 MPa. This means that the strength becomes high and its variation becomes small when the fibers are well aligned. Thus, the guideline for the design of composite structures are: 1) For high strength applications, high reliability design can be performed by designing the geometry of the structure such that the load is applied accurately along the fiber direction, and 2) For intermediate strength applications, a sufficient value of the safety factor is needed. It should be noted that the CV remains around 5% though the strength of advanced composites increases remarkably. The similar relations for the shear strength of PMC and the tensile strength of MMC are shown in Figs. 8 and 9.

CONCLUDING REMARKS

The first largest database of the material properties of advanced composites has been successfully developed in Japan. However, a problem arises on the interchange of the data with other nations because the literal data except numerical data are written in Japanese and two-byte Japanese character code is used. Additional work for the translation from Japanese to English version will be needed for international data exchange.

This work was performed under management of Research and Development Institute of Metals and Composites for Future Industries, sponsored by Agency of Industrial Science and Technology, MITI.

Table 2 No. of the strength data in the database at the end of 1989.

Material	Tension	Compression	Bending	Shear	Impact	Others	Total
FRP	1545	150	680	1477	103	216	4171
FRM	2868	60	34	15	6	103	3086

1. Material file (Format P1)			8. Compressive property file (Format P8)		
A	Number	S05	A	Number	S05
B	Affiliation	S30	B	Specimen number	S10
C	Name	S30	C	Test environment	S15
D	Date	S12	D	Test direction	S05
E	Document No.	S12	E	Compressive strength	V08
F	Composite system	S30	G	Compressive fracture strain	V08
G	Constitution	S64	G	Compressive modulus	V08
H	Stacking sequence	S64	H	Comment	S10
I	Fiber content	V05	I	Test link	S05
J	Void content	V05	9. Shear property file (Format P9)		
K	Ply thickness	V05	A	Number	S05
L	No. of plies	V05	B	Specimen number	S10
M	Plate thickness	V05	C	Test environment	S15
N	Curing condition	S30	D	Test direction	S05
O	Curing condition link	S01	E	Shear strength	V08
P	Drawing link	S01	G	Shear fracture strain	V08
Q	Stacking sequence link	S01	G	Shear modulus	V08
R	Material comment link	S01	H	Comment	S10
2. Laminate construction file (Format P2)			I	Test link	S05
A	Number	S05	10. Poisson's ratio file (Format P10)		
B	Construction detail	S64	A	Number	S05
C	Material link	S05	B	Specimen number	S10
3. Curing condition file (Format P3)			C	Test environment	S15
A	Number	S05	D	Test direction	S05
B	Curing condition detail	S64	E	Poisson's ratio	V08
C	Material link	S05	F	Comment	S10
4. Material comment file (Format P4)			G	Test link	S05
A	Number	S05	11. Energy release rate file (Format P11)		
B	Material comment	S64	A	Number	S05
C	Material link	S01	B	Specimen number	S10
5. Test condition file (Format P5)			C	Test environment	S15
A	Number	S05	D	Type	S05
B	Test item	S32	E	Crack length	V08
C	Test method	S32	F	Energy release rate	V08
D	Test specimen	S32	G	Comment	S10
E	Test environment	S32	H	Test link	S05
F	Test direction	S32	12. Bending property file (Format P12)		
G	Property link	S05	A	Number	S05
H	Material link	S05	B	Specimen number	S10
I	Test comment link	S05	C	Test environment	S15
6. Test comment file (Format P6)			D	Test direction	S05
A	Number	S05	E	Bending strength	V08
B	Test condition detail	S64	G	Bending fracture strain	V08
C	Material link	S05	G	Bending modulus	V08
7. Tensile property file (Format P7)			H	Comment	S10
A	Number	S05	I	Test link	S05
B	Specimen number	S10	13. Physical & chemical property file (Format P13)		
C	Test environment	S15	A	Number	S05
D	Test direction	S05	B	Density	V08
E	Tensile strength	V08	C	Thermal expansion coeff.	V08
G	Tensile fracture strain	V08	D	Thermal distortion temp.	V08
G	Tensile modulus	V08	E	Td(Air)	V08
H	Comment	S10	F	Specific heat	V08
I	Test link	S05	G	Coeff. of thermal transfer	V08
			H	Tg	V08
			I	Td(N ₂)	V08
			J	Diffusional activation energy	V08
			K	Factor D ₀	V08
			L	Constant a	V08
			M	Constant b	V08
			N	Test link	S05

Fig. 1-1 Data items in each file. One alphabetical character denotes a data field designation followed by a field name and format. Data format is represented by letter S for string data and by letter V for numerical data, followed by the number representing the size of the field. (continued on the following page)

14. Impact property file (Format P14)

A	Number	S05
B	Specimen number	S10
C	Test environment	S15
D	Test direction	S05
E	Impact strength	V08
F	Comment	S10
G	Test link	S05

15. Foreign object impact property file (Format P15)

A	Number	S05
B	Specimen number	S10
C	Test environment	S15
D	Test direction	S05
E	Impact value	V08
F	Comment	S10
G	Test link	S05

16. Fatigue property file (Format P16)

A	Number	S05
B	Specimen number	S10
C	Test environment	S15
D	Test direction	S05
E	Stress ratio	V04
F	Maximum stress	V08
G	No. of cycles (mantissa)	V04
H	No. of cycles (exponent)	V04
I	Fracture parameter	V04
J	Comment	S10
K	Test link	S05

17. Environmental property file (Format P17)

A	Number	S05
B	Specimen number	S10
C	Test environment	S15
D	Test direction	S05
E	Tg	V04
F	Tensile modulus	V06
G	Damping	V06
H	TMR	V04
I	WVR	V04
J	Comment	S10
K	Test link	S05

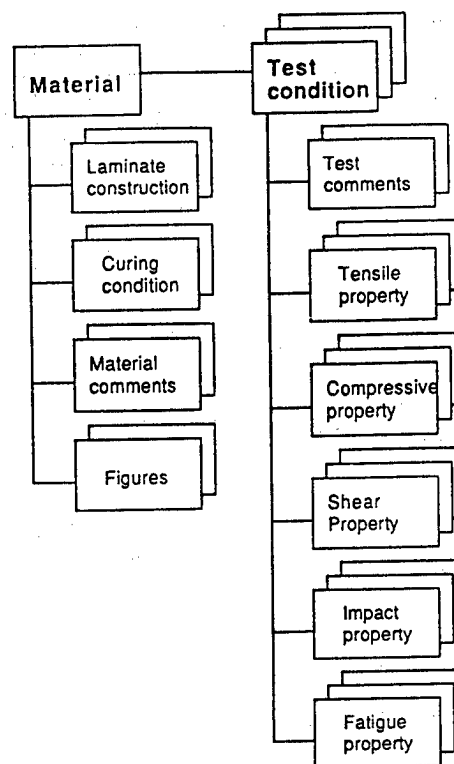


Fig. 2 Hierarchical structure of the data files.

Fig. 1-2 (continued from the previous page)

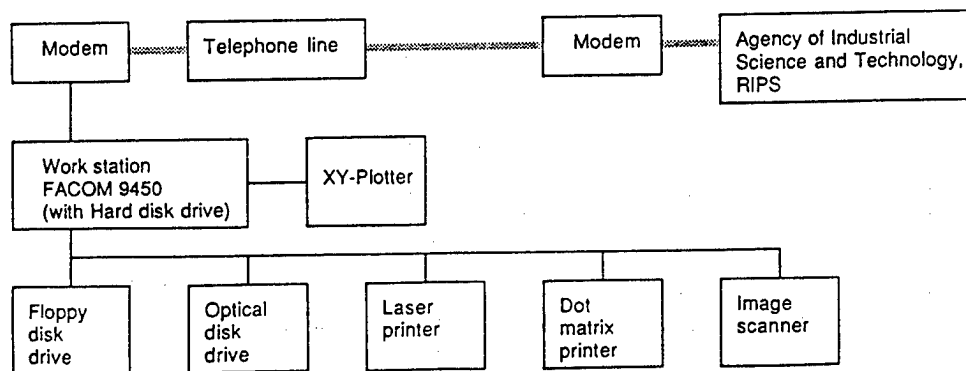


Fig. 3 Block diagram of the database hardware system.

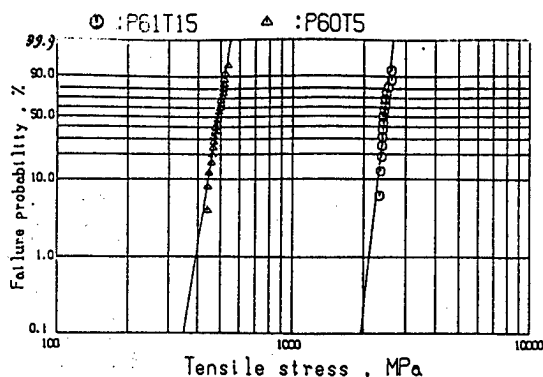


Fig. 4 Typical tensile strength distributions of graphite composites. P61T15:Torayca-cloth/polyester. P60T5:T400B/polyimide

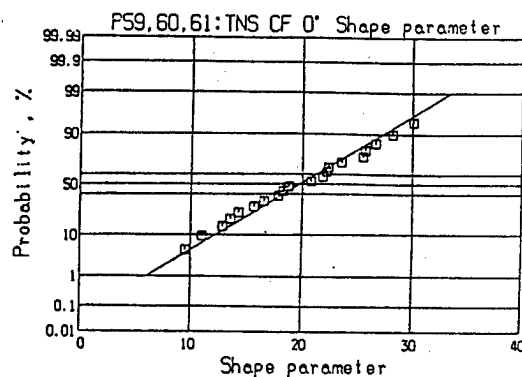


Fig. 5 The distribution of the shape parameters of unidirectional graphite composites on Normal paper.

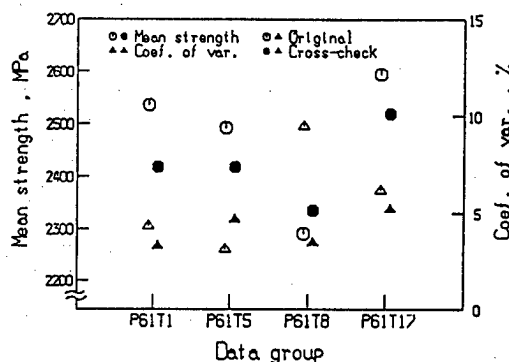


Fig. 6 The difference between the original test data and the cross-checked data obtained by the government research institutes.

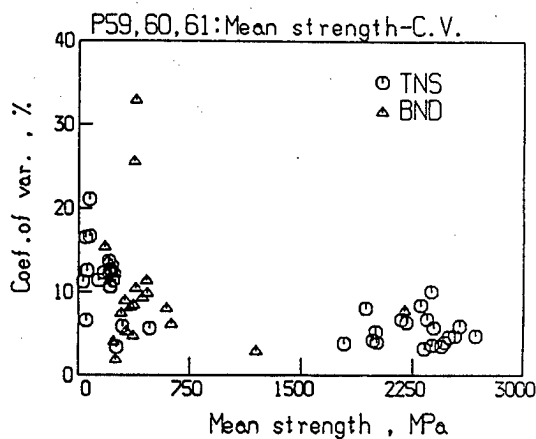


Fig. 7 The relation between the mean strength and the coefficient of variations of the tensile and bending strengths of PMC.

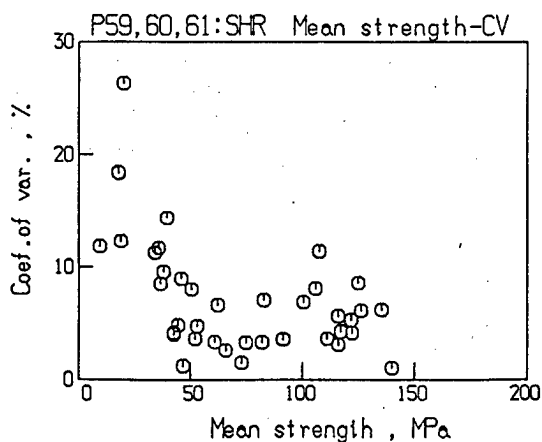


Fig. 8 The relation between the mean strength and the coefficient of variations of the shear strength of PMC.

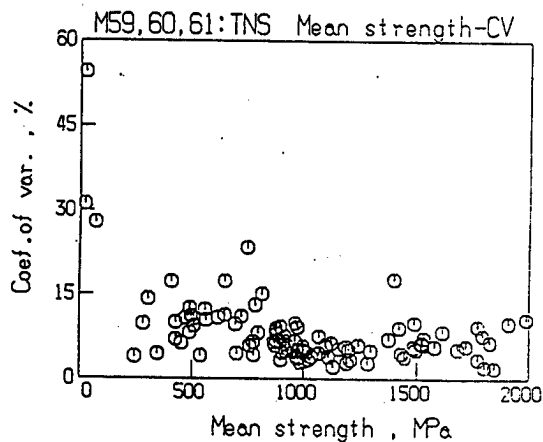


Fig. 9 The relation between the mean strength and the coefficient of variations of the tensile strength of MMC.

Japan-France Friendship Communication Monument
Colossal Structure Composed of Innovative Materials

Hiroshi Saito
Secretariat of the Japanese Committee
for the Japan-France Friendship Monument
Chuo-ku , Kobe 650, Japan

ABSTRACT

The countries of Japan and France are currently working together on a project to construct a monument on Awaji Island in Hyogo Prefecture to commemorate the 200th anniversary of the French Revolution, in the same spirit as the construction of the Statue of Liberty about 100 years ago in the United States in commemoration of the 100th anniversary. Intended to express the theme of "communication" and featuring a simple gate-like design, this monument will serve as both the starting point and the ending point of a "Tropic of Poetry" linking France and Japan. As befits a monument of the 21st century, innovative materials will be used extensively in the structure. Although this project poses a number of technical questions, the joint effort to overcome all difficulties through advancing technological development will in itself promote deeper communication between the two nations. I should like to give you a brief explanation of this project in the hope that such knowledge will help win your support for the construction of a colossal structure using innovative materials.

BACKGROUND TO THE CONCEPT OF THE MONUMENT

The countries of Japan and France are currently working together on a project to construct a monument to commemorate the 200th anniversary of the French Revolution in Japan (Awaji Island, Hyogo Prefecture), aiming at widening "communication that supports new friendly exchange between the two nations and the global society in the 21st century.

This project was first proposed in September of 1986 by the Japan-France Symbol Association, the promoting organization on the French side. Two design competitions were held in France and at the final judging held in June of 1989, the work by architect Patrick Berger entitled "Awaji: Garden of Tropics" (collaborator: J.P. Nouhaud, writer) was chosen as the winning design.

Eight representatives from Japan, including architects Arata Isozaki and Tadao Ando, and writer Sakyo Komatsu, were invited to attend the final judging.

Following the donation of the concept design on January 10, 1990, the Japanese side began taking action aimed at promoting the realization of the

project by joining efforts around the Japanese Committee for the Japan-Friendship Monument (established in December 1989; president: Eishiro Saito, president of the Federation of Economic Organizations) which was set up to organize nationwide support.

CONCEPT OF "AWAJI: GARDEN OF TROPICS"

The prize-winning work by architect Patrick Berger, entitled "Awaji: Garden of Tropics", features a simple form reminiscent of the arches often seen among the relics of ancient Greece or Rome, besides having something in common with the "torii" (gateway to Shinto shrines in Japan).

The design, as shown in Fig. 1, consists of a bronze table (305 m long x 30 m wide x 6 m thick) supported by 4 glass pillars (12 m wide x 18 m deep x 80 m tall).

This structure, with an apparently simple design, will serve as a structure symbolizing "friendship, exchange, and communication".

A proposal was made to the effect that granite dating back almost 2 billion years from Batz Island in the Bretagne region France would be carried to Awaji Island to serve as the flagstone for the monument; and, the Japanese side would donate a Japanese garden to the quarry site.

The imaginary line linking Batz Island and Awaji Island would be called the "Tropic of Poetry". Scenes of various places found along this line would be filmed using a French observation satellite and projected on a screen at the monument site in order to turn it into a base for communication.

The concept design further proposes a total of 8 gardens to express various facets of communication, including a "Garden of History" and a "Garden of Memories".

Besides innovative materials, this monument features new technical proposals befitting the 21st century, both structurally and technologically, and its realization will only be accomplished by uniting the technical expertise of both sides.

Structural Outline of the Monument

The bronze table, as shown in Fig. 2, comprises 16 modules of wooden beams (composite wood), which represent the number of language groups in the world; each wooden beam is tensed by two prestressing cables (diameter: 13.2 cm). A steel plate (thickness: 6 cm), which resists compressive force, will rest on top of these beams, and the table itself will be covered with a bronze plate (mean thickness: 10 mm) all around.

Each supporting glass pillar, as shown in Fig. 3, comprises elementary glass cubes (each 2-meter cube) and carbon fiber rods (each 8 cm x 8 cm); and, the carbon fiber rods constitute the supporting cubic grid structure.

According to the initial computations, it is estimated that a prestressing load of about 65,000 tons and a shearing force of about 5,200 tons will be applied to the table. The table, which is a compound structure of wood, steel, and prestressing cable, and the support, which is a compound structure of glass and carbon rod, are expected to present sufficient resistance to these loads.

THE OSAKA BAY AREA AND A NEW SYMBOL ON AWAJI ISLAND

A series of major national projects, including the Akashi Kaikyo Bridge, the Kansai International Airport, and the Osaka Bay Route Highway, are now being integrally promoted in the Osaka Bay Area, and this area is expected to serve as a major base of international exchange in Japan in the future.

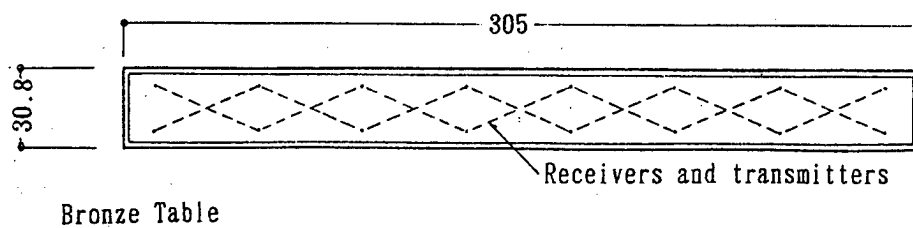
Awaji Island, the future site of the monument, is now in the midst of being transformed into a large-scale high-quality "Awaji Resort" making the best of the beautiful coastline and the abundance of nature there to offer a new dimension in our lifestyle in the future.

The Akashi Kaikyo Bridge, upon completion, will provide a direct link between the Keihanshin area and Shikoku Island. Taking into account the fact that the new Kansai International Airport will be also be very close, the proposed monument site should be judged to have all the ideal conditions.

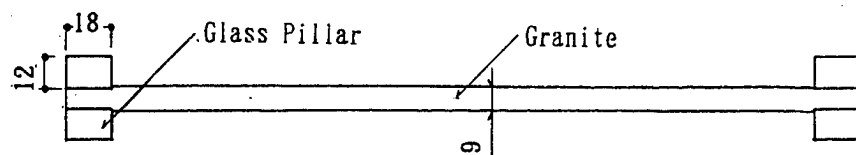
Furthermore, from the monument site, one could see the Akashi Kaikyo Bridge right below and the panoramic view of Osaka Bay should be superb.

This monument is certain to become a symbol of the Osaka Bay Area and the Seto Inland Sea in the 21st century.

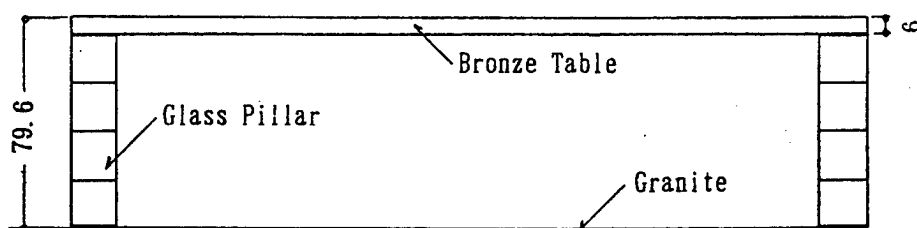
For this purpose, we should like to join the technological know-how of our two nations in order to overcome a series of problems so as to complete this monument befitting the 21st century.



Bronze Table



Glass Pillar and Granite



Elevation

Unit:m

Fig.1. General drawings of Monument

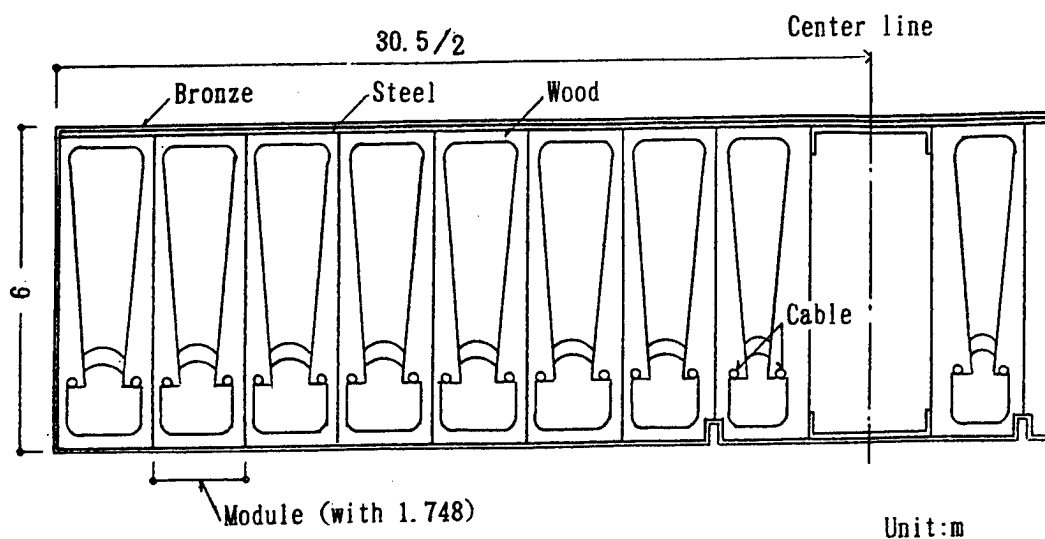


Fig. 2. Cross section of Bronze Table

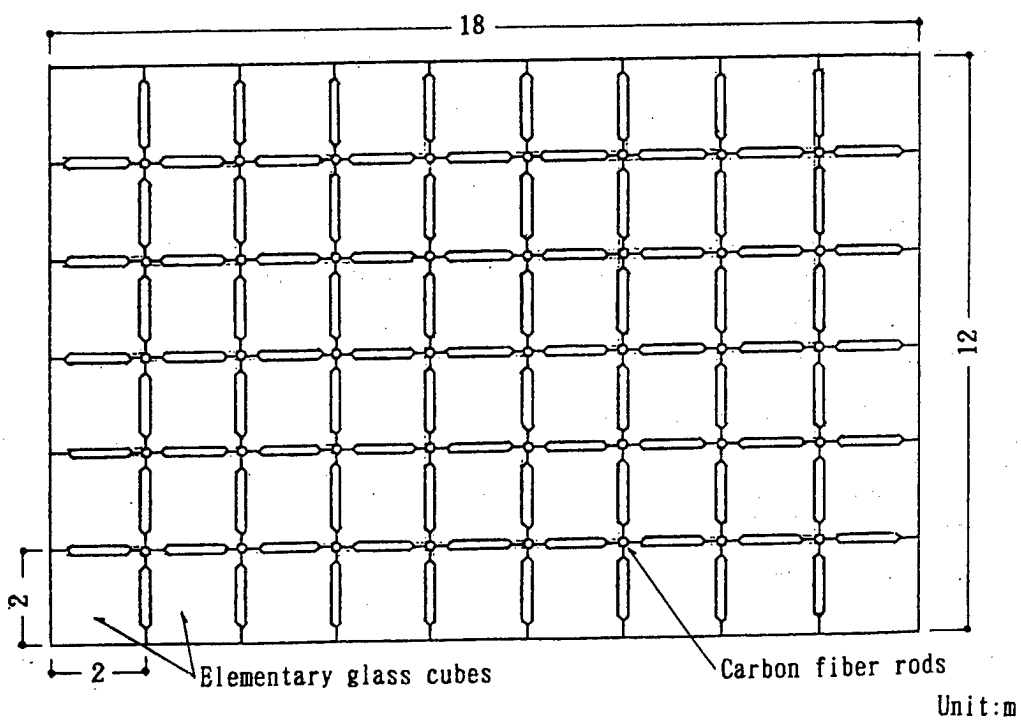


Fig. 3. Cross section of Glass Pillar

COMPUTER AIDED MICRO-DAMAGING AND FRACTURING CHARACTERIZATION OF COMPOSITE MATERIALS FOR NON LINEAR STRUCTURAL ANALYSES AND CRASH SIMULATIONS

Dr. L. T. KISIELEWICZ
ESI Japan
3-7-16 Uehara, Shibuya-ku, Tokyo 151, Japan

and

Dr. ANDOH K.
Penta Ocean Construction Co., Ltd.
2-2-8 Koraku, Bunkyo-ku, Tokyo 112, Japan

ABSTRACT

A general use of composite materials in industrial structures design requires that appropriate design criteria and corresponding analysis procedure be available in order to take advantage of the qualities of these materials. Considering the fact that damage in these materials start to develop at rather low load levels, an accurate modeling of the microscopic behavior is needed. Such analysis procedure, including a specific material model for composite, has been developed and industrially validated in the past years. It has been developed in such a way that it allows to use, in many cases, the available finite element packages.

INTRODUCTION

The merits of using fiber matrix material in many structural applications are gaining increasing recognition. However, to benefit fully from these materials, a meaningful design procedure must permit some degree of internal damage within the composite, such as matrix micro-cracking or delamination between layers, insofar that the safety of the structure is not impaired. Typically matrix micro-cracking may initiate at 20% of ultimate load with the first fiber failure occurring at 40% of ultimate load. Using these load levels as design criteria would negate the benefits of composite materials and lead to overly conservative structural designs.

To assess a material ultimate strength for structural member design, one must predict the initiation and propagation of material fracture, meaning macroscopic material separation. Fracture is linked to the nucleation, growth and coalescence of micro-flaws, whether natural (initial Imperfections) or load induced, into macro-flaws. Applying this phenomenology to composite materials requires that micro-damaging of both constituents be taken into account.

Most finite element packages lack a material model capable of representing the different constituents of composites. However, they still can prove very valuable structural design tools insomuch that response curves be provided for the critical structural members. An adequate analysis procedure must be developed where these response curves are generated at the modelling stage.

GENERAL ANALYSIS PROCEDURE

Figure 1 shows the flow chart of the general design procedure. In this procedure, the critical member of the composite structure are first analyzed with PAM FISS in order to generate the structural response curves for their loading conditions. This is done by developing a detailed finite element model of these members and deriving the structural response curve by incrementing the load applied to the member. This first step is only carried out when the finite element package to be used for the global structural analyses lacks the Bi-Phase model or any equivalent model to represent the multi-constituent structure of the composite material.

Following that initial step, for these cases, an equivalent model of the critical members can be derived by using the structural response curves. The non critical members, typically those members which will remain in the linear range, can be modeled using the homogeneous material properties available in all finite element packages

Analytical iteration are carried out in the classical way by interpreting the results of the analyses. In the case that one or more critical members do not fulfill the design criteria and need to be redesign, the design loop must be restarted.

In the cases where the structural analysis package does have the Bi-Phase model, or an equivalent model, the first step of the procedure can be skipped as the critical members can be modeled with appropriate material properties.

COMPOSITES STRUCTURAL CHARACTERIZATION

Composite Structural Behavior

When loading a composite members at levels less than 20% of the ultimate load, the composite material is fully bonded and traditional continuum mechanics theory apply. However, with increasing loading, fiber and matrix damage tend to progress independently within the two constituents which then obey independent mechanical and failure criteria [2]. In that case, a homogeneous material model can hardly reproduce the behaviors for all possible layouts of structural members. A special material model is thus needed to account for the different damaging processes of the matrix and the fibers.

Bi-Phase Model

The Bi-Phase model is an ESI proprietary material model adapted to unidirectional long fiber reinforced composites or composite fabrics [1]. This model is illustrated on the figure 2 hereunder. The stiffness and the strength of its elements are calculated by superimposing the effects of an orthotropic material constituent (the matrix of the composite), and of a unidirectional constituent (the fibers), with or without deformation compatibility. Each material constituent has its own rheological properties, e.g. elastic plastic, or elastic brittle orthotropic, or a micro-fracturing brittle damage law for the matrix and a unidirectional elastic brittle damage law for the fibers. Upon incremental loading, the stresses are calculated separately for each constituent and damage (matrix cracking, fiber rupture) can propagate independently, based on the criteria chosen for each constituent.

A multi directional laminate is modeled by stacking through the thickness several unidirectional elements with the fibers oriented along different directions with respect to a global reference frame.

PAM FISS™ package

ESI's PAM FISS™ is a special purpose finite element package for damage and fracture mechanics. It contains the Bi-Phase model and allows for arbitrary three dimensional geometries, static and dynamic loading, including impact, contact and interface sliding, and thermal loading. Figure 3 hereunder illustrates the major features of PAM FISS™.

The specialized damage and fracture mechanics option of PAM FISS™ allow to zoom on areas of stress concentrations via mesh size reduction, to propagate crack or delamination fronts along directions independent from the finite element mesh orientation, and to automatically evaluate several damaging and toughness criteria.

Industrial Validation

Developing new material models and analysis procedures is not an end by itself. It requires an industrial validation, comparing analytical results with tests, in order to be applicable in industrial applications. This general rule has been applied to the Bi-Phase model and to the PAM FISS™ package.

Industrial validation of the Bi-Phase material model and of the PAM FISS™ package has been carried out during for several years, mainly in the fields of aerospace and defense [1][4][5]. More recently these tools have been used and validated for other industrial fields. The reports of these projects will be reported publicly in the coming months.

It is beyond the scope of this presentation to detail the results of these industrial validations. The interested reader can refer to ESI Japan to get more details on it.

TYPICAL APPLICATION : CRASH SIMULATION

While not the most typical, the above procedure is illustrated here for the case of the numerical simulation of the crash of composite structure. It is not typical because the simulation tool used, PAM CRASH™, does have the Bi-Phase model implemented in it. It was thus not necessary to proceed with the two-step analysis. However, this case has been selected because it shows that advanced numerical techniques, such as the one used for structural crash simulations, can be used for structures made of advanced materials, such as the LFRP composites.

PAM CRASH™ is a widely used package for the numerical simulation of metallic structures crashes. In that field, especially in the cases of transportation artifacts, such as automobiles and rolling stocks, PAM CRASH™ is recognized worldwide.

In the case of structures made of composite material, few results have ever been shown and no industrial solution is available for the numerical simulation of crashes. Following several years of preliminary investigation and initial validation, the Bi-Phase model has been implemented in the PAM CRASH™ package and a major industrial investigation has been undertaken. The detailed results of this project will be reported publicly later. In this communication, preliminary qualitative results are shown.

Figure 4 shows the collapse modes of a box beams submitted to low velocity axial crash, one being made of ductile metal, and the second of LFRP composite, with a wall made of a sandwich structure. In that project, PAM FISS™ was used to calibrate the Bi-Phase model for the particular composite used. Simple coupon tests were simulated and the results were compared with actual tests results. The crash of the box beam then simulated using PAM CRASH™ and the results were compared with test results.

CONCLUSIONS

An analysis procedure has been presented to replace the traditional approach of analyzing an equivalent homogeneous anisotropic continuum by a two-step analysis. The traditional allowable stress criterion is replaced by a realistic numerical simulation of the initiation and propagation of damage for the critical members of the structure.

This procedure allows to take advantage with reliability of the merits of composite materials (low weight for high strength) and still using in most application cases the existing analysis tool, i.e. the non linear finite element packages.

REFERENCES

- [1] A. de Rouvray, P. Dowlatyari, E. Haug - Validation of the PAM FISS / Bi-Phase Numerical Model for the Damage and Strength Prediction of LFRP Composite Laminates - MECAMAT 89 International Seminar on Mechanics and Mechanisms of Damage in Composites and Multi-materials - St. Etienne, France - November 1989

- [2] L. Holloway - Composite Materials in Structures - University of Surrey Press - 1976
- [3] D. Ulrich, A.K. Pickett, E. Haug, J.C. Bianchini - Crash Simulation for Metallic, Sandwich and Laminate Structures - AGARD 66th Structures and Materials Panel Meeting - Luxembourg - May 1988
- [4] A. de Rouvray, E. Haug, P. Dowlatyari, P.W. Beaumont, M. Spearing - Advanced Model Development and Validation for Composite Damage Mechanics - ESA Workshop "Advanced Structural Materials : Design for Space Applications" - March 1988
- [5] E. Haug, P. Dowlatyari, A. de Rouvray - Industrial Calculation of Damage Tolerance and Admissible Stress in Components made of Composite Materials using the PAM FISS / Bi-Phase Material Model - International Colloquium on Spacecraft Structures - Toulouse, France - December 1985
- [6] A. de Rouvray, E. Haug - Failure of Brittle and Composite Materials by Numerical Methods - Chapter 4 in Structural Failure - Proceedings of the International Symposium on Structural Failure, MIT - Boston, USA - June 1988

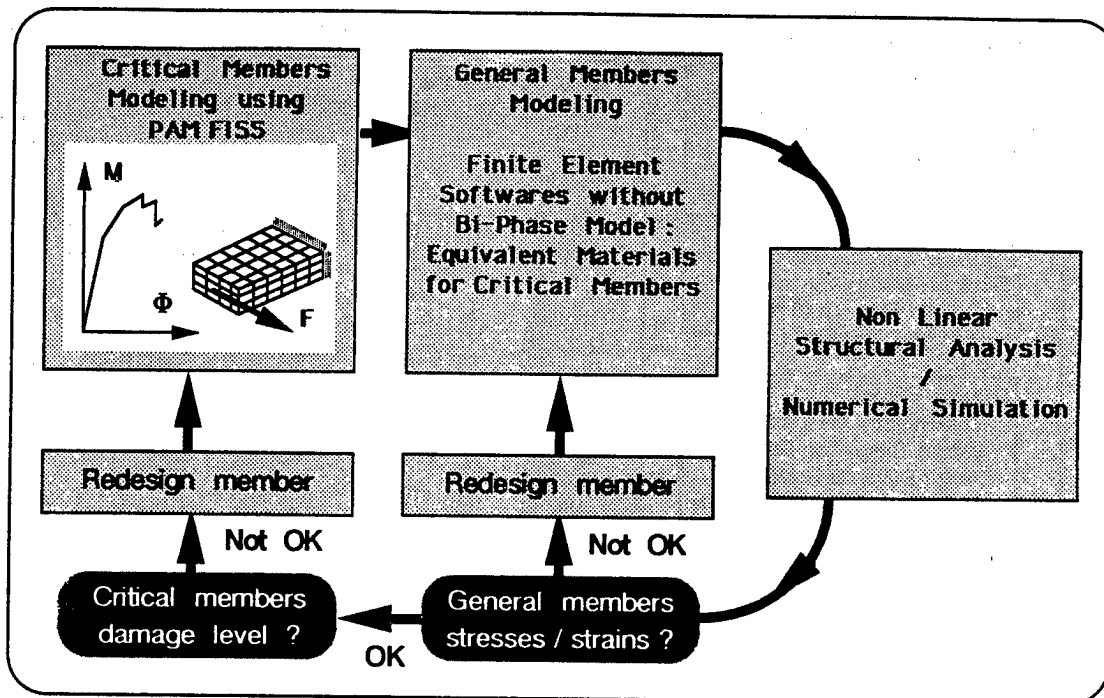


Figure 1 - General Flowchart of Procedure for Structural Analysis of Composites

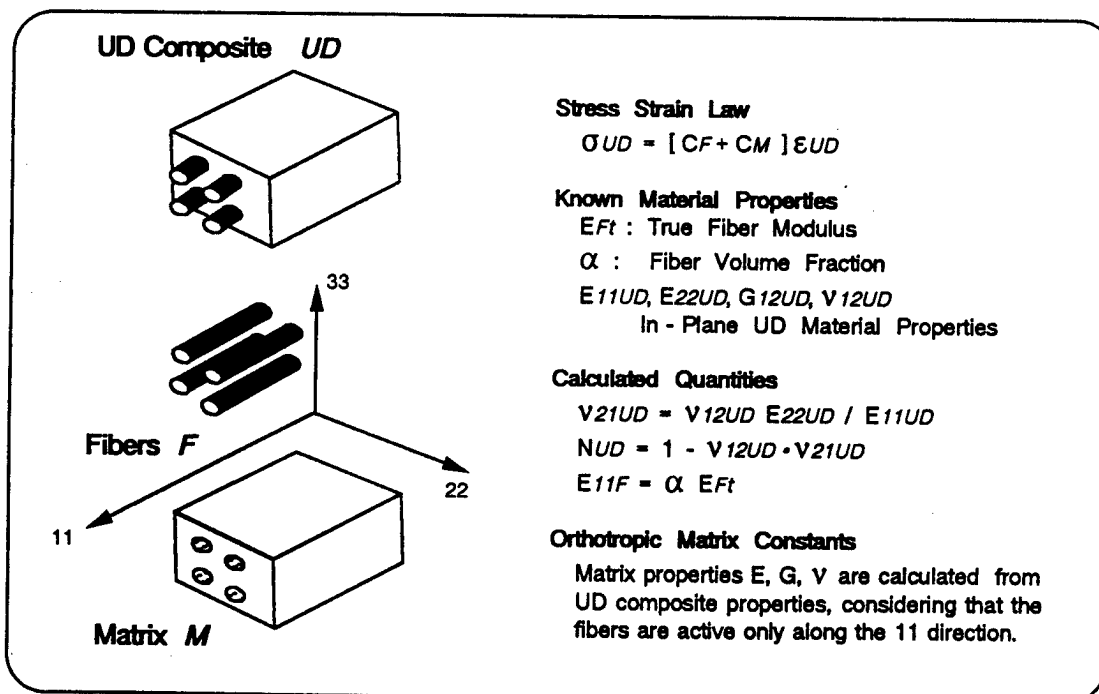


Figure 2 - Bi-Phase Material Model for LFRP Composites

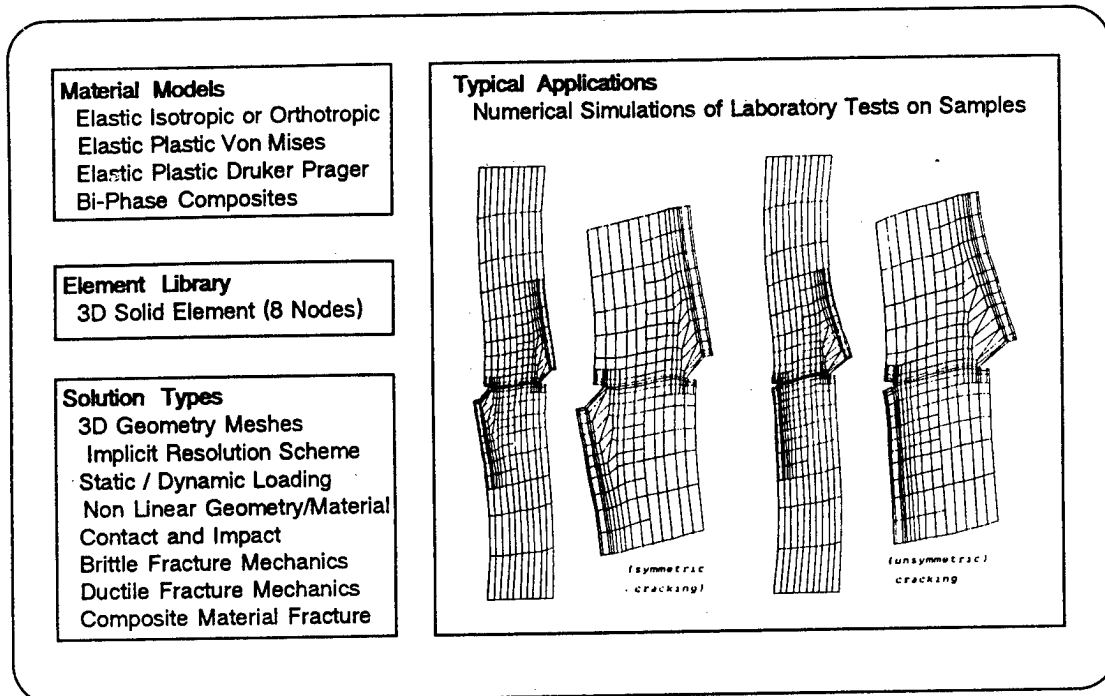


Figure 3 - PAM FISS™ Features and Typical Applications

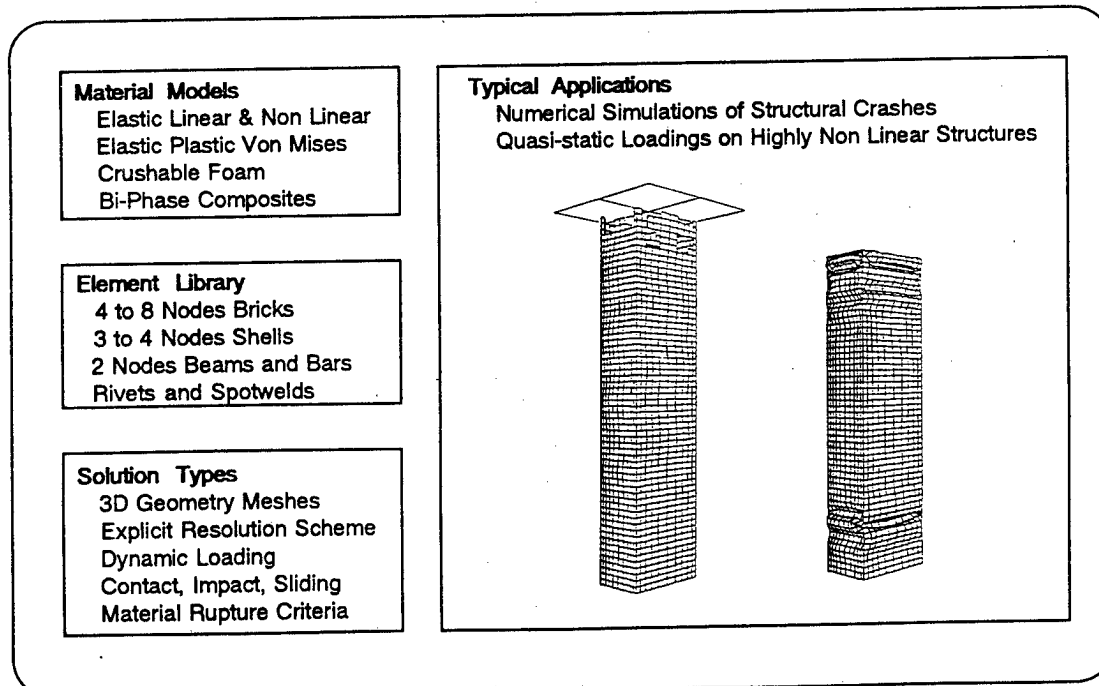


Figure 4 - PAM CRASH™ Features and Application to Crash of Composites

Grafting of Glass Surface

P. Chartier

Saint-Gobain Recherche
39, Quai Lucien Lefranc, 93303 Aubervilliers, France

ABSTRACT

Surface grafting is a treatment which consists in covalently binding molecules or polymer segments to a substrate. This paper reports how to provide new glass surface properties by chemical grafting.

First, polymer grafted glass fibers are presented, which exhibit high activated area and therefore good potentiality to adhesion and adsorption.

Then, molecular glass grafting is described: the deposition of self-assembled monolayers of organosilicon compounds on glass can induce important modification of wetting, adhesion and chemical properties of glass surfaces. Data concerning microstructure characterization and macroscopic properties of these grafted monolayers are given. Polymer grafting is also reported.

Applications of grafting for design multimaterials in the glass industry are evoked.

INTRODUCTION

Surface treatments have been a subject of interest and importance for many years, and are now used in all industries in order to create new physical and chemical properties at the surface of traditional materials. A large number of surface treatments has been developed, depending on the nature of the substrate and application. Both the wide range of Saint-Gobain materials, which includes glass, cast iron, ceramics and paper, and the will to develop new multimaterials, explains why the surface treatments area is of great interest for Saint-Gobain.

The present paper focuses on an emerging chemical surface treatment: grafting, which consists in covalently binding small molecules or polymer segments to a substrate. Grafting is commonly used for producing surface modified polymer and silica supports for separation techniques (1), and is starting to be extended to other fields (2).

In glass industry, two types of application of grafting can be considered:

- 1) controlled interfaces
- 2) activated surfaces

The first one involves adhesion and friction properties to be modified (composites, adhesive bonding...) whereas the second one includes adsorption capacities aspects (catalysis, sensors...).

This paper especially reports how to modify, by grafting, physico-chemical properties of glass and polymer surface; consequences on wettability, surface activity and adhesion behavior of these materials are described.

MATERIALS

Glasses and polymer of industrial interest were used for experiments : float glass plates, E and C glass fibers from Saint-Gobain and one polyurethane (PU). Chemicals employed in the preparation of grafted layers were from Petrarch (silanes) and Aldrich (other compounds), and were used as received.

POLYMER GRAFTED GLASS FIBERS

Polymer grafted glass fibers were obtained from conventional glass fibers used for insulation or reinforcement of plastics. Firstly pretreated with a thermal activator, fibers were then chemically grafted in aqueous solution by unsaturated monomers, such as acrylics, which polymerized on the active surface sites, forming covalent bonds at the interface. Experimental conditions have been chosen in such a way that fibers were highly grafted by strongly bound, weakly crosslinked polymer chains, in order to significantly increase the number of surface sites compared to naked fibers. Grafting ratios in the range of 50-100 % of the initial fibers weight have been obtained in this way, that leads to a specific area of about 100 m²/g.

The microstructure of these grafted fibers was characterized by microscopy : complete coverage of the fibers by the coating was observed in the case of polyacrylic acid graftings. Moreover, swelling experiments were carried out in several media. It was observed (figure 1) that this kind of coating exhibited a high affinity for polar species, such as water, alcohols and amines, and ions. This surface treatment constitutes a valuable tool for controlling interfaces and obtaining activated surfaces.

SELF-ASSEMBLED MONOLAYERS ON GLASS

Self-assembled monolayers of silanes onto float glass were obtained according to procedure reported elsewhere (3); it consists in dipping clean glass substrates into a solution containing a small amount of silane diluted in a mixture of chlorinated and aliphatic solvents. Then treated glass samples were rinsed with pure solvents and dried at ambient temperature.

The adsorption of long-chain silanes on flat glass was investigated using wettability measurement, X-ray reflectivity, Fourier Transform Infra Red (FTIR) spectroscopy and desorption tentative experiments. Glass plates treated with octadecyltrichlorosilane (OTS) exhibited very low surface energy : for example, water forms droplets which move freely at the surface, providing contact angle equal to 105° , that corresponds, according to Fowkes's theory (4), to a surface energy of about 30 mJ/m^2 . Water adhesion to glass surface is thus five times decreased following OTS treatment.

X-ray reflectivity experiments showed that the adsorbed layer was highly dense and approached thickness of about 2.1 nm, within 0.1 nm to the OTS length. Polarized specular reflectance FTIR spectroscopy confirmed these results: adsorption of OTS to float glass surface can lead to formation of closely packed monomolecular films, essentially perpendicular to the surface. Models for grafting mechanism of long-chain silanes and structure of self-assembled monolayers are proposed in figure 2.

Ageing experiments made on OTS treated glass samples showed that self-assembled monolayers do exhibit high resistance to hot water and moisture. Thus, because of their non polar moieties exposition, their closely packing and very strong binding to the surface, grafted OTS molecules cannot be easily removed.

Potential applications of self-assembled monolayers are very numerous. By using silanes with various terminal groups, one may expect to obtain both passivation and activation coatings in order to, for example, repel water, protect glass surface against chemical attacks or promote adhesion with polymers.

GRAFTING OF POLYMER SURFACE: AN ALTERNATIVE TO PROMOTE GLASS/POLYMER ADHESION

Chemical surface modification of polyurethane (PU) films was studied by grafting acrylic monomers under electron radiation, with the aim of increasing the hydrophilic behavior of PU. The experimental process consisted in spreading over the PU surface an aqueous solution containing the monomer, then submitted it to electron beam of several hundreds keV energy and several Mrads dose. Then treated PU was rinsed with water in order to remove ungrafted species.

Measurement of surface energy by the contact angle method showed that hydrophilicity of PU films was considerably increased by the grafting: initially of about 5 mJ/m^2 , polar component of the surface energy reached approximately 30 mJ/m^2 after grafting.

Impact of this surface grafting on adhesion properties of PU films with glass was also demonstrated using a conventional peel test. We can see on figure 3 that adhesive strength reached more than one hundred N/cm at the glass/grafted PU interface.

Applications of this grafting process may be found in several areas: laminated flat glass, coatings for glass fibers, and so on...

CONCLUSION

It was shown that grafting techniques can induce important modification of the physico-chemical properties of glass and polymer materials. The wide variety of these techniques, combined with the innovative character of this area, makes grafting very attractive for sectors where controlling interfaces becomes predominant, such as advanced composites materials.

REFERENCES

- (1) Foucault, A., Rosset, R., *Analisis*, **17**(9), (1989), 485-507
- (2) "Chemical Modified Surfaces in Science and Industry", Ed. Leyden, D.E., Collins, W.T., Gordon and Breach Science Publishers, New-York, 1988
- (3) Sagiv, J., *J. Amer. Chem. Soc.*, **102**(1), (1980), 92-98
- (4) Fowkes, F.M., *Ind. Eng. Chem.*, **56**(12), (1964), 40-46



10 μ m

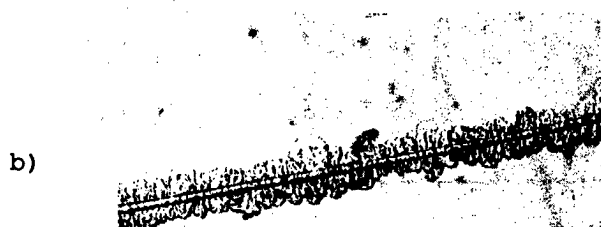


Fig.1: Microscopic views of an acrylic polymer grafted glass fiber
 a) in dry environment
 b) swollen into water

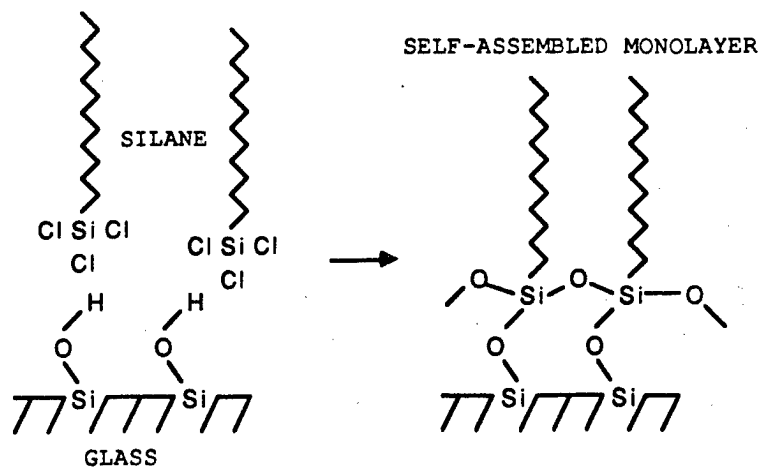


Fig.2: Hypothesis of adsorption mechanism of self-assembled monolayer of silane on glass

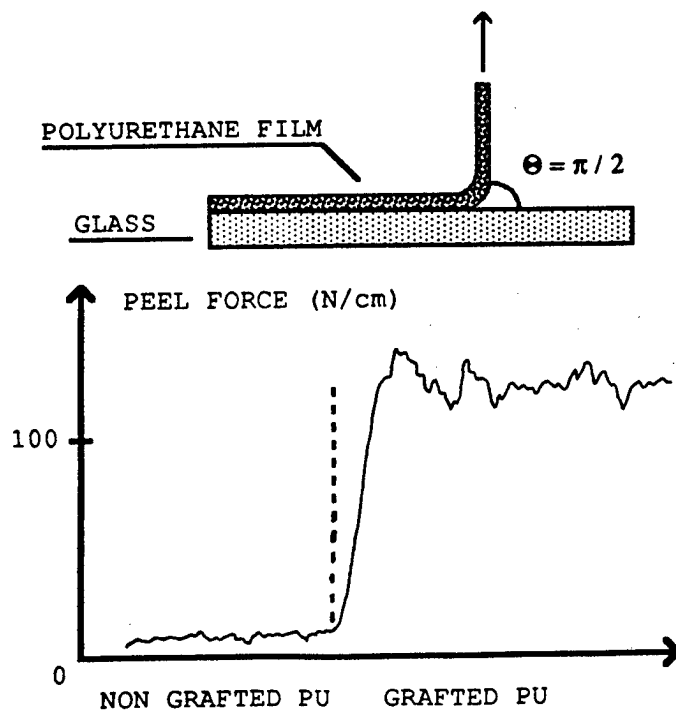


Fig.3: Peel curve of glass/polyurethane assembly
Influence of grafting polyurethane

INFLUENCE OF THE REACTION ZONE ON THE INTERFACIAL SHEAR STRESS IN SiC / TITANIUM ALLOY COMPOSITE.

G.LAMANTHE, Y.KAGAWA# and A.OKURA****

***Inst. of Industrial Science , The University of Tokyo,
7-22-1, Roppongi, Minato-ku, Tokyo 106, Japan.**

***on leave from SNECMA , 91003 - Evry , France.**

****Inst. of Space and Astronautical Science,
3-1-1, Yoshinodai, Sagamihara, Kanagawa 229, Japan.**

ABSTRACT

The influence of the reaction zone thickness on the shear properties of SiC fiber-reinforced titanium based composites (SCS6/commercially pure titanium or Ti-6Al-4V alloy) has been investigated. The Shear-lag model analysis is applied for the determination of interfacial shear debonding stress and frictional sliding shear stress of the composite during indentation test (fiber push-out).

To study the behaviour of the complex interface between fiber and matrix the composite is modelled following three concentric cylinders models. The influence of the heat treatment will be taken into account with the variation of the thickness of the reaction zone. Some numerical applications are discussed here.

INTRODUCTION

SiC fiber-reinforced titanium alloy composites are being considered for applications in advanced gas turbine engines. During exposure to processing and service temperatures, the composites develop reactions at the fiber-matrix interface, which can damage the mechanical behaviour of the composite material.

In this work, the effect of the reaction zone, and the degradation of the fiber on the strength of the composite material is studied by determining the interfacial shear strength with analytical models (Shear Lag theory and concentric cylinders models [2,3]) and experimental tests (push out indentation).

EXPERIMENTAL PROCEDURE

Material :

Ti-based composite material was obtained by hot pressing at 900°C under 100 MPa during 1h, of titanium sheets with SCS6 fibers. The Ti-6Al-4V alloy matrix composite was fabricated by hot-isostatic pressing.

Push-out indentation test :

Using a fiber push-out technique (Figure 1) the interfacial debonding load and the maximum sliding load were measured for varying lengths of embedded fibers. The interfacial properties can then be evaluated (shear debond stress τ_d and sliding friction stress τ_f).

ANALYSIS OF THE INTERFACIAL MECHANICAL PROPERTIES

Debonding and sliding analysis :

The application of the Shear-lag model gives an estimation of the debonding stress. The analysis of sliding friction [1] allow the evaluation of a coefficient of sliding friction ($\mu = 0.15$) and of residual compressive stress on the interface σ_0 .

Residual stress calculation :

To study more precisely the behaviour of the complex interface between SiC fibers and titanium or Ti-Al6-4V alloy the composite was modelled as an assembly of SiC bar, thin-walled reaction zone t and thick-walled titanium alloy matrix as shown on figure 2 [2,3].

If we assume that the reaction zone consists of TiC [4], because of the difference between the elastic moduli and between the coefficients of thermal expansion of the materials, the value of σ_o is particularly high ($\sigma_o = 500\text{MPa}$). Figure 3 compares normalized stresses between fibers and interface, and interface and matrix, respectively σ_{im} and σ_{fi} , calculated following the two models. As a function of reaction zone thickness both give the same kind of result; the absolute value is higher in the case of [2] which seems less accurate. In this case we could predict that the fracture will occur between the reaction zone and the matrix ($\sigma_{im} < \sigma_{fi}$). But this result is not consistent with the experimental observations.

Before heat treatment if we consider amorphous carbon in the "reaction zone" σ_{im} and σ_{fi} have closer values.

PERSPECTIVES

The experimental results have yet to be completed and compared with previous studies [4,5]. Then the effect of the heat treatment will be considered with the variation of the reaction zone thickness t and of the reaction products. Hardness measurements and microstructural characterizations of the matrix, fiber and reaction zone are also being carried out to discuss the experimental results.

REFERENCES

- [1] D.K.SHETTY.- J. Am. Ceram. Soc., 71 [2] C107-C109 (1988)
- [2] H.NAYEB-HASHEMI and J.SEYYEDI -. Met.Trans A, 20A, 1989, 727-739.
- [3] C.H..HSUEH, P.F.BECHER and P.ANGELINI -
J .Am. Ceram. Soc. ,71 [11] 929-933, Nov.88
- [4] C.JONES, C.J.KIELY and S.S.WANG -
J. Mater. Res.,4 ,[2], 327-335, Mar/Ap.89
- [5] Y.LEPETITCORPS, R.PAILLER and R.NASLAIN -
Comp. Sc. Technology, 35, 207-214, (1989).
- [6] C.J.YANG, S.M.JENG and J.M.YANG - Scripta Met. 24, 469-474, 1990.

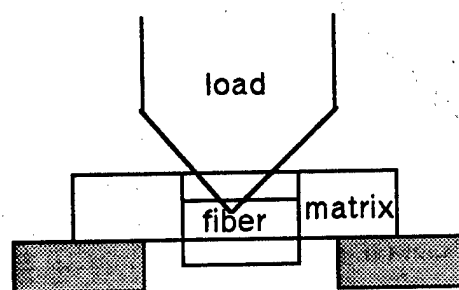


Figure 1 : Geometry of the indentation test

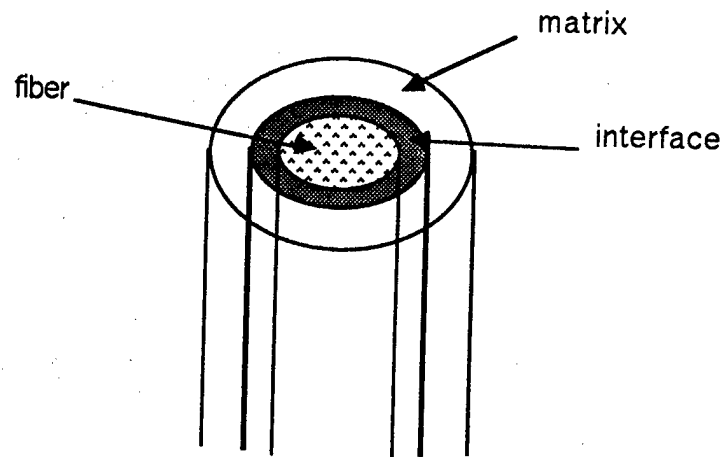


Figure 2 : Three concentric cylinders model

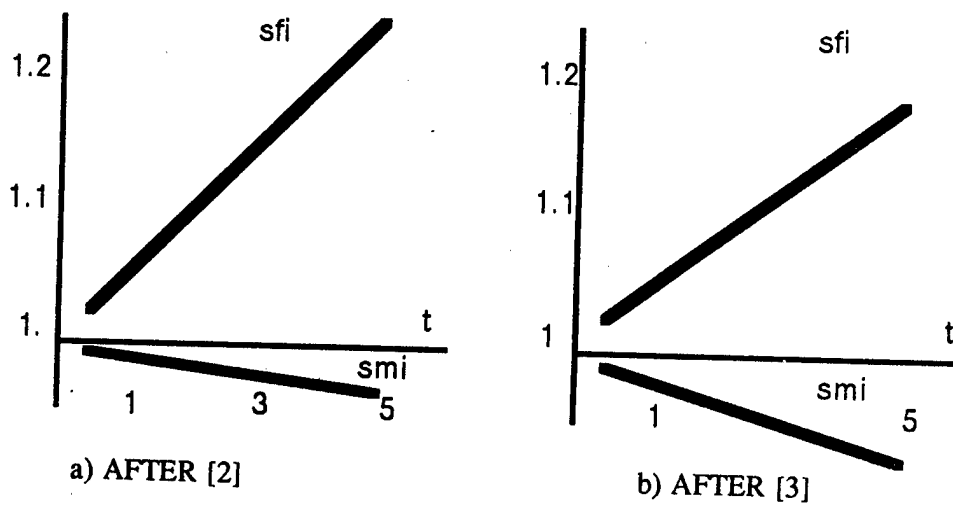


Figure 3 : Normalized stress between the three layers versus reaction zone thickness t (μm)

This page intentionally left blank

SESSION III

INTERFACE
AND
COATINGS

This page intentionally left blank

PLASMA SPRAYED CERAMIC COATINGS
P. Fauchais, A. Vardelle, M. Vardelle, J.F. Coudert, A. Grimaud
URA 320 CNRS, University of Limoges France

ABSTRACT

In this paper is presented what is the state of the art in the plasma spraying of ceramics coatings. The importance of the design of the plasma torch is first emphasized. Then the heat and momentum transfers problems between the plasma jet and the injected particulates are discussed with the heat propagation phenomenon enhanced for ceramic particulates especially the agglomerated ones. The way the particulates flatten is then discussed with the strands and passes formation and the importance of the coating temperature monitoring during spraying to limit the cracks formation and improve the thermomechanical properties of the coatings.

1. INTRODUCTION

When temperature and/or load increase, materials are subjected to corrosion, and/or wear and if material chemistry provides the mechanical properties it often does little to provide sufficient corrosion or wear resistance. These problems were solved by use of a thin layer of a second material (coating) applied to the component surface (often by thermal spraying) which provide corrosion, wear, thermal resistance without degrading the mechanical properties of the substrate. Plasma spraying has extended drastically the capabilities of the thermal spray coatings by accomodating coating materials with very high melting points such as ceramics, cermets, refractory alloys and superalloys. The advent of the space age in the late 1950' has brought about a need for higher performance materials, which helps the development of plasma sprayed coatings. The success of these coatings in aircraft engineering (still the largest market) has led the applications in other fields such as paper, steel, textile, chemical, mechanical, oil and gas industries. Now plasma spraying is a permanent part of the mechanical engineering discipline and the sales increase of about 12%/year since four years /1 to 7/.

In plasma spraying the heat source is a d.c. arc where the gas blown between a stick type thoriated tungsten cathode and a nozzle shaped anode is partly heated in a plasma column before exiting as a jet at high velocity but with a low density in either air (APS), or in inert controlled atmosphere (IPS), or soft vacuum (VPS or LPPS). The design of this heat source will be the subject of the first section, however limited to APS.

The particulates (size distributions between a few μm and 100 μm), injected radially in the plasma jet either inside the nozzle (but downstream the arc root) or outside it, are accelerated, heated and, if possible, melted during their flight in the jet. This means of course that only materials which melting temperature is at least lower by 300K from their evaporation or

decomposition temperature can be sprayed. The heat and momentum transfers to the particulates are the key points to obtain a molten state upon impact. The second section will be devoted to the study of these phenomena under thermal plasma spraying conditions.

The particulates splat onto the substrate and the previously deposited layers and are cooled down very fast (up to 10^6 K/s at the beginning which is equivalent to splat cooling). The way they splat depends on their molten state and velocity upon impact. The resulting lamellae pilling up together with the cracks generated by the stresses relaxation (stresses due to quenching of the splats, temperature gradients within the coatings and differences in expansion coefficients between the substrate and the coating). The last section will deal with the coating built up and the thermal problems involved.

2. PLASMA JET GENERATION

It involves very complex physical phenomena at the electrodes and 3 D flows which are laminar within the plasma jet core and the plasma column inside the torch (due to the high temperatures, low density and high viscosity of the plasma) while they are turbulent in the plasma fringes as well as in the closely entrained surrounding gas /11 to 13/. Thus it explains why the plasma torches development has been mainly empirical since decades / 14 to 16 /.

The electrons necessary to create the plasma column are emitted at the conical tip of a stick type thoriated tungsten cathode by thermoionic emission (see fig. 1). According to the exponential term in the Richardson-Dushman's law, a very small diameter of a molten pool (a few tenths of mm^2) is sufficient to provide the requested electron density /17/. A complete modelling is complex and only empirical formulae to determine cathode shapes and dimensions have been established /18/.

From this small emitting spot the plasma expands (see fig. 1) pumping part of the plasma gas injected close to the cathode tip. This expansion / 8, 17/ depend on:

- the way the gas is injected in the arc chamber (radially, longitudinally, along the surface of the cathode cone, as a vortex).
- the arc current which increases the electrical radius corresponding roughly to the 8000 K isotherm.

Thus the design of the arc chamber is very critical especially for the plasma gas injection. The length of the plasma jet (characterized for example by the 8000 K isotherm) varies easily in a ratio of 1.5 for the same plasma gas flowrate and nature and almost the same power level when changing the gas injector /19/ as shown in fig. 2.

The length of the nozzle depends on the plasma column diameter relative to that of the nozzle. The arc strikes at the anode nozzle wall (see fig. 1) by one or a few tiny plasma columns (when the cold boundary layer close to the wall is hot enough) which are continuously fluctuating under the action of the drag force resulting from the "cold" plasma gas fraction flowing in the fringes of the arc and the $j \times B$ forces /8/ (see fig. 1). These fluctuations result in arcing modifying continuously the length of the electrically conducting plasma column. This continuous movement of the arc root helps in preserving the integrity of the anode, the thermal flux at the anode reaching $10^{10} - 10^{11} \text{ W/m}^2$. These fluctuations of the plasma column length (linked to the gas aerodynamic in the nozzle) coupled with the negative resistance of the arc, react on the power supply which brings in its own fluctuations and all these phenomena induce pulsating plasma jets which length varies at frequencies between 1 kHz (pure argon) and a few tens of kHz (Ar - H₂ plasmas).

As the plasma jet exits the nozzle it encounters a steep laminar shear at the outer edge of the jet /21/ (see fig. 1). This large velocity difference causes the flow around the nozzle exit to roll up into a ring vortex which is pulled downstream with the flow, allowing the process to repeat itself

again at the nozzle exit. Adjacent vortex rings have the tendency to coalesce to form larger vortices. The perturbed vortices start to entangle themselves with adjacent rings resulting in large scale eddies and the onset of turbulent flow. That results in the first large scale entrainment of surrounding atmosphere. The mixing and diffusion processes eventually reaches the center line of the jet foretelling the end of the plasma core. When the surrounding atmosphere is air, the oxygen dissociation at 3500 K cools down very fast the plasma jet and shortens its length as shown by the measurements of Roumilhac /19/.

This turbulent mixing depends strongly on the plasma jet velocity which is however a parameter very difficult to measure /8/. Of course the plasma jet velocity, for given arc chamber and nozzle, increases with the total arc current I , the total gas flowrate m°_{pl} and the hydrogen percentage. As shown by the measurements of Brossa and Pfender /22/ with probes in a Ar plasma flowing in air, the rate of air pumping increases with arc current and gas flowrate. Such measurements are confirmed by those of Roumilhac /19/ :

As a conclusion it is important to emphasize the complexity of the phenomena involved in the creation of a spraying plasma jet. The temperature and probably the velocity distributions depend strongly on the nozzle and arc chamber designs, nozzle diameter and shape, arc current, total plasma gas flowrate and nature and they are difficult, if not impossible, to predict. It must be kept in mind that two plasma torches, even if their design characteristics seems to be identical, working with the same arc current and total gas flowrate and nature may produce quite different plasma jets resulting in very different melting conditions for the particulates.

The plasma viscosity plays also a great role in the mixing with the surrounding atmosphere as shown by the measurements of Roumilhac /19/ for Ar-He (40-60% vol) plasma jets which length is the same as that of Ar-H₂ (80-20% vol) jets with a power level 1.5 time higher.

3. HEAT AND MOMENTUM TRANSFERS TO THE PARTICULATES

As already emphasized (see introduction) heat and momentum transfers to particulates under thermal plasma conditions are very complex and many papers have been devoted since the seventies / 9, 10, 23 to 26 for example /. Many possible phenomena playing a role in transfers have been accounted for but for the same phenomenon many expressions are proposed. To make a choice between them a comparison with experimental data has to be made. Unfortunately the experimental data / 27 to 29 for example / on particulates result from statistical measurements on N particulates passing in the measurement volumes during a given time and thus such measurements do not allow really to choose /30/. However such models, related to momentum and heat transfers to a unique particulate, are very useful to predict, at least qualitatively, what are the tendencies.

3.1 Transfer to a Unique Particulate

The motion of the injected particulate is established by a force balance /10/ often resumed to the Newton's force equal to the drag force in which the drag coefficient is usually derived from a corrected Stokes formula. In this formula the Drag coefficient has to be corrected for the steep temperature gradients between the particulate and its surrounding, the vaporization of the particulate, the non continuum effect (already important at atmospheric pressure for particulate diameters below 10 μm).

For a given injection velocity of the studied particulate, provided the plasma jet temperature and velocity distributions are known (see section 2) , the integration of the equations of motion allows to calculate the velocity components of the particulate, from which the trajectory may be obtained by further integration for the position vector.

Such calculations show the great importance of the particulate initial velocity on its trajectory

depending on the plasma jet temperature and velocity distributions /29, 31, 38/.

Particulate heating

The temperature history of the particulate is determined by an energy balance at the particulate surface which include the energy transfer from the plasma to the particulate, the energy required for heating the vapor from the particulate surface temperature to that of the plasma and the latent heat of change. Of course in case of melting and/or vaporizing (which occurs generally with ceramics in Ar-H₂ plasmas) a moving boundary problem has to be solved /10, 31/.

Usually the heat transfer coefficient h is obtained from the familiar Nusselt number, of course using, as for C_D , correction factors to account for the steep temperature gradients. In general convection represents little compared to conduction /23/ and h can be expressed as:

$$h = 2 \bar{\kappa} / d_p$$

where $\bar{\kappa}$ is the mean integrated thermal conductivity of the plasma gas and d_p the particulate diameter.

With ceramic particulates sprayed with Ar-H₂ plasmas (for which the heat transfer is drastically enhanced by the hydrogen with its high mean thermal conductivity $\bar{\kappa}$ /23/) heat propagation phenomenon occurs according to the low thermal conductivity κ_p of the material (it occurs as soon as $\bar{\kappa} / \kappa_p > 0.03$). This is illustrated in fig 3 for dense zirconia particulates (fused and crushed, stabilized with 8% wt yttria) with two sizes(30 and 60 μm) flying in an Ar-H₂ plasma jet at a 30 kW power level. It can be seen that the 30 μm particulate reaches a maximum surface temperature of 3700 K, while the center temperature is higher than the melting temperature after 80 mm trajectory. On the contrary for 60 μm particulate if the surface temperature is higher than the melting temperature the center temperature reaches hardly the melting temperature 80 mm downstream of the nozzle exit where the spraying substrate is usually disposed. This phenomenon is enhanced when agglomerated particulates, with lower thermal conductivity, are used. This is illustrated in fig. 4 showing the temperature evolution (surface and center) versus time of these 60 μm particulates respectively fused and agglomerated immersed in an infinite Ar-H₂ plasma (23% H₂ in vol.) at 10000K. As the melting state controls the particulates flattening upon impact it is not surprising to see the differences exhibited by the Vickers Hardnesses of coatings sprayed at 40 kW with an Ar-H₂ plasma jet (50 slm - 15 slm) with different sizes and morphologies of the particulates (see table 1). It is to be noticed that H measurements with a 5N load represent well the coating cohesion depending strongly on the particulates flattening upon impact. It is worth to be noticed that the best results are obtained with the fused and crushed particulates between 45 and 10 μm , the worst corresponding to agglomerated particulates in the size range - 90 + 45 μm . The -106 + 10 μm size range containing small particulates gives better results than the - 90 + 45 μm one, the small particulates, in general well melted, contribute to the coating consolidation. The sintered agglomerated particulates with a lower heat propagation phenomenon exhibits values intermediate between fused and agglomerated particulates.

3.2 Particulates Distribution

The real situation correspond to the injection of particulates having a size distribution, eventually a shape distribution (in most cases neglected) and an injection velocity distribution. For establishing a mathematical model it requires the repetition of the calculation for a single particulate with different initial states. Moreover the results must be corrected by considering the coupling effect between the particulates and the plasma jet which is usually called the load effect. Load effect calculations have been performed by Lee and Pfender /32/ for an argon plasma jet and by Proulx et

al /33/ for an Ar-H₂ plasma jet which characteristics were measured at the lab for a power level of 29 kW. In both cases the calculations show that this load effect modifies the plasma velocity distribution when the ratio m_p/m_g is higher than 0.25 and the plasma temperature distribution when it is higher than 0.5.

The trajectory distribution results from the product of the size and injection velocity distributions /31/. With small particulates the injection velocity distribution is very broad (between 0 or 70 m/s for alumina particles - $21 + 15 \mu\text{m}$ in diameter /29/) and thus the resulting trajectory distribution is also rather broad.

On the contrary for bigger particulates (- $90 + 45 \mu\text{m}$) with a larger size distribution, the injection velocity distribution is narrower (between 1 and 15 m/s) resulting in almost the same trajectory distribution as that obtained with the - $21 + 15 \mu\text{m}$ size distribution. Fig. 5a and b illustrates the corresponding velocity and mean surface temperature distribution in a plane 75 mm downstream of the nozzle exit for the fused zirconia particulates considered for the hardness measurements depicted in section 3.1. As expected from the heat transfer calculations, in spite of their highest velocity the - $45 + 10 \mu\text{m}$ particulates reaches the highest surface temperature. Statistically the mean surface temperature of the - $106 + 10 \mu\text{m}$ particulates is between that of the - $45 + 10$ and - $90 + 45 \mu\text{m}$ particulates (according to the presence of the small particulates).

To conclude it is to be noticed that the corresponding particulates radial flow distribution forms the deposition strand when moving the torch relatively to the substrate. The strand thickness will be controlled by the particulates mass flowrate, the deposition efficiency (usually between 40 and 60%, part of the particulates being not molten enough to stick to the surface) and the relative torch-substrate velocity.

4. COATING GENERATION

All the processes involved in coating generation will not be described here (for more details see /2,4,7/ for example) but only the points which are linked to thermal effects will be emphasized. Although the crucial importance of thermal effects and mechanical exchanges between the impinging molten particulates and the substrate or the previously deposited layers has been stressed in a number of theoretical analyses /2,34,35/ very few experimental data are available.

Two thermal histories play an important role:

- that of individual particulates as they impact the substrate.
- that of the strands and passes, these evolutions being of course linked to the particulates temperatures and velocities upon impact.

When studying the resulting splats upon a flat steel substrate, Houben /35/ has shown the strong influence of the heat content compared to that of the velocity. The well molten particulates form pancake type with a good central contact with the substrate (and many microcracks relaxing quenching stresses), while poorly molten ones form flower type splats with a much reduced contact area.

Such shapes result in very different thermomechanical properties of the coatings, these ones depending strongly on the contact between the splats as illustrated for example by the measurements of Pawlowski et al /36/. Recent temperature measurements of the splats during their impact and cooling /37/ have shown their very rapid cooling (1500 K within 6 to 30 μs according to the substrate nature) resulting in quenching stresses in the contact area, stresses relaxed by microcracks, plastic flow or creep /38/.

When spraying, the strands (corresponding to the pilling up of already solidified lamellae) are generated in times corresponding about to a few tens of mm/sec depending on the relative velocity torch-substrate. They cool down rather slowly (depending on their thickness) from

temperatures close to that of the individual solidified splats (1500-2000°K) to a temperature controlled by the substrate and coating during spraying (cooling generally achieved by air jets blown at the coating cooling surface).

Moreover, as in general, plasma sprayed parts have a cylindrical symmetry the substrates are rotated while the torch is moved parallel to the axis of symmetry. If very high rotation velocities can be achieved, translation velocity can hardly be more than 1 m/sec. Thus, depending on the substrate size, the strands will overlap more or less and this overlapping, resulting in pass thicknesses, play a very important role in their cooling /39/, role which has not been yet systematically studied. Finally the resulting temperature of the successive passes depends on their thickness and cooling also function of the spraying distance.

More precisely the coating temperature during spraying should be monitored to limit the gradients within the coating and the cooling of the substrate and coating also monitored after spraying. This will reduce the cooling stresses arising from the differential thermal contraction between the successive passes as well as between the substrate and deposit. Such stresses often relaxed by cracks propagation reduce drastically the adhesion, cohesion and mechanical properties of the coatings /40/.

It is not clear at the moment, depending on substrate and coating nature, which are the best conditions for substrate and coating temperature evolution during spraying because of the lack of systematic data but it plays a critical role in the coating resistance to thermal cycling /39/. Moreover the problem is very complex when spraying ceramic coatings on metal substrates in air because at the beginning the substrate heating (to limit as much as possible its oxidation) has to be limited while the adhesion between the successive ceramic passes is enhanced when their surface temperature increases.

CONCLUSION

Plasma spraying is one of the most versatile method to apply a wide variety of coatings on almost any substrate. However its development over the last two decades has been largely empirical and it is only for a few years that, with the development of new measurement techniques and improvement of modelling, plasma spray technology is emerging from art to science.

The coating is formed particulate by particulate, a new one impacting on an already solidified one, resulting in a lamellar structure. By measuring the velocity and surface temperature as well as the diameter of the particulates just before impact and by following their cooling versus their morphology, the substrate nature and surface roughness and the cooling by gas jets, a better understanding of coating formation will result. The measurement techniques are now available but this task will be long and difficult to account for the trajectory and size distribution of the particulates and the heat propagation phenomena taking place.

Beside the splats, the way the successive passes temperature has to be controlled for a given substrate and coating nature is not yet at all understood, even if the resulting residual stresses, often relaxed by cracks, condition the coating service resistance especially on thermal cycling.

The influence of the particulates size and injection velocity distributions has started to be understood with the new measurements techniques for particulates in flight (giving distributions of velocity, surface temperature, diameter, evaporation) however the effort has to be pursued in connection with the strands and passes formation as well as the way the splats are formed.

At last a very important problem is still pending : that of the plasma torches. The way they are designed (essentially empirical up to now) conditions very strongly the plasma jets velocity and temperature distributions and at the moment the used plasma torches are still from the "middle age". The way the particulates are injected can also be drastically improved for example by injecting them through the cathode thus improving their residence time.

All this is a big challenge for the searchers for the next decade.

REFERENCES

1. Rykalin N.N., Kudinov V.V., Pure and Appl. Chem., Vol. 48, p. 299, 1976.
2. Zaat J.H., Ann. Rev. Mater. Sci. Vol. 13, p. 9, 1983.
3. Apelian D., Mat. Res. Soc. Symp. Proc. Vol. 30, p. 91, 1984.
4. Thermal Spraying, Practice, Theory and Application, 1985.
5. Technology forecast, Advanced Materials and Processes, Vol. 133, N°1, p. 8, 1988.
6. D'Angelo C., El Joundi H. Advanced Materials and Processes, Metal Progress, Vol. 12, p. 41, 1988.
7. Fauchais P., Grimaud A., Vardelle A., Vardelle M., Ann. Phys. Fr. Vol. 14, p. 261, 1989.
8. Fauchais P., Coudert J.F., Vardelle A., Vardelle M., Grimaud A., Roumilhac P., Nat. Proc. NTSC 87, Orlando Fl., (Pub.) AIME p.11, 1988.
9. Pfender E., Pure and Applied Chemistry, Vol. 57, n°9, p. 1179, 1985.
10. Pfender E., Plasma Chemistry, Plasma Processing, Vol. 9, n°1, p. 1675, 1989.
11. Delawari A.H., Szekely J., Plasma Chem., Plasma Processing, Vol. 7, n°3, p. 317, 1987.
12. Lee Y.C., Pfender E., Plasma Chemistry, Plasma Processing, Vol. 7, n°1, p.1, 1987.
13. Chyou Y.P., Pfender E., Plasma Chemistry, Plasma Processing, Vol. 9, n°1, p. 291, 1989.
14. Fauchais P., Rev. Int. Hautes Temper. et Refract., Vol. 5, p. 71, 1968.
15. Andrews C.W., Surfacing Journal July, p. 1, 1974.
16. Jurewitz J. et al., ISPC 7, Vol. 3, p. 1, 1974.
17. Pfender E. Electric Arc and Arc Gas Heaters, in gaseous Electronics, (Ed.) Hirsh M.K., Oskam J.J., Academic Press N.Y., Vol. 1, 1978.
18. Jukov M.F., Experimental investigations of plasmotrons (in Russian) (Pub.) Nauka, Novossibirsk, URSS, 1977.
19. Roumilhac P., Thèse de l'Université de Limoges, University of Limoges, France, March 12th. 1990.
20. Spores R., Pfender E., Thermal Spray Technology, Conf. Proc. (Pub.) ASM International p. 85, 1989.
21. Brossa M., Pfender E., Plasma Chemistry, Plasma Processing, Vol. 8, n°1, p. 75 (1988).
22. Bourdin E., Fauchais P., Boulos M.I., Int. J. Heat Mass Transfer, Vol. 26, p. 567, 1983.
23. Joshi S.V., Park J.Y., Taylor P.R., Richardson L.S., Int. J. Heat Mass Transfer, Vol. 29, n°10, p. 1565, 1986.
24. Chen Xi, Pure and Applied Chemistry Plasma Processing, Vol. 60, n°5, p. 1565, 1986.
25. Chyou Y.P., Pfender E., Plasma Chemistry Plasma Processing, Vol. 9, n°1, p. 45, 1989.
26. Vardelle M., Vardelle A., Fauchais P., Boulos M., A.I.Ch.E. Vol. 29, p. 236, 1983.
27. Vardelle M., Vardelle A., Fauchais P., Boulos M., A.I.Ch.E. Vol. 34, p. 567, 1988.
28. Fauchais P., Vardelle M., Vardelle A., Coudert J.F., Metallurgical Transactions Vol. 20 B, p. 263, 1989.
29. Vardelle M., Vardelle A., Fauchais P., Experimental determination of drag and heat transfer coefficients under thermal plasma conditions, submitted to Plasma Chemistry Plasma Processing.
30. Vardelle A., Thèse de doctorat d'Etat, University of Limoges, July 1987, France.
31. Lee Y.C., Pfender E., Plasma Chemistry Plasma Processing, Vol. 7, n°1, p.1, 1987.
32. Proulx P., Mostaghimi J., Boulos M., ISPC 8(ed.) Prof. Akashi, Univ. of Tokyo, Vol. 1, p. 13, 1987.
33. Mc Pherson R., Thin Solid Films, Vol. 83, p. 297, 1981.
34. Houben J.M., Doctoral Thesis, Univ. of Eindhoven, N.L., (1988).
35. Pawlowski L., Lombard D., Fauchais P., J. Vac. Sci. Technol., Vol. A3, n°6, p. 2494, 1985.

37. Moreau C., Cielo P., Lamontage M., Dallaire S., Vardelle M., Impacting particle temperature monitoring during plasma spray deposition, submitted to J. of Phys. E. Sci. Instrum.
38. Howard S.J., Clyne T.W., Interfacial fracture toughness of vacuum plasma sprayed coatings, Sym.D., EMRS Strasbourg May 1990.
39. Gitzhofer F., Bernard D., Fauchais P., Martin C., Boulos M., in Thermal Spray Technology, Conf. Proc. ASM International p. 27, 1989.
40. Hobbs R.H., Reiter H., In Thermal Spray, Advances in Coatings Technology, Conf. Proc. (Pub.) ASM (Int.) p. 285, 1988.

TABLE 1

Size Range	Fused and Crushed	Agglomerated Sintered	Agglomerated
- 45 + 10 μm	550		
- 106 + 10 μm	505	434	388
- 90 + 45 μm	375	298	248

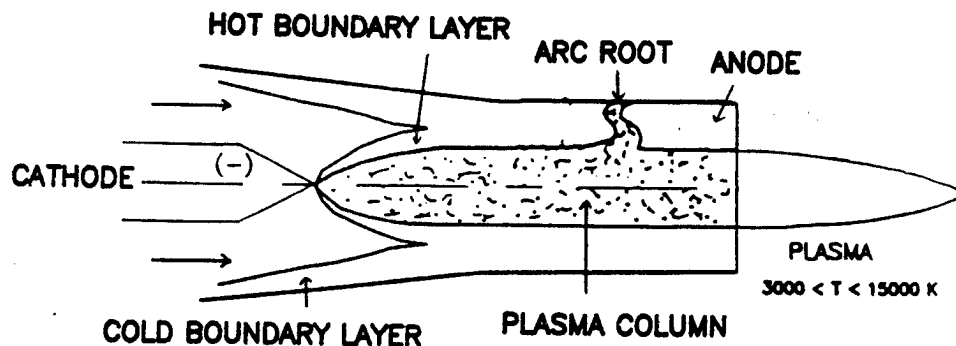


Fig.1 : Principle of a spraying D.C. plasma torch

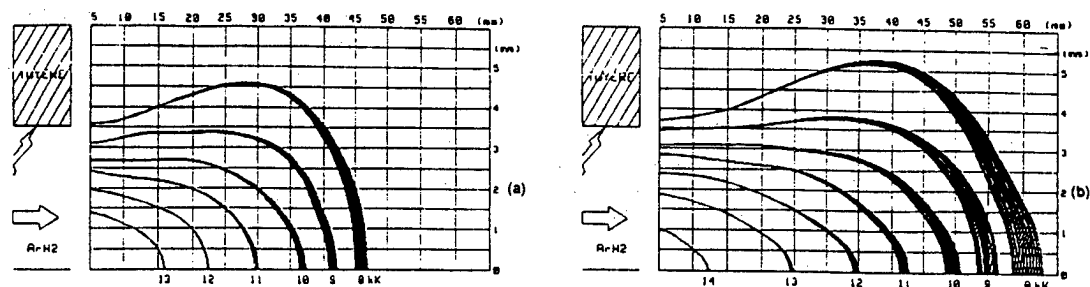


Fig. 2 : Isotherms of an Ar-H₂ (30 slm - 12 slm) plasma jet, 35 kW, nozzle diameter 7 mm, (a) radial plasma gas injection (b) axial plasma injection.

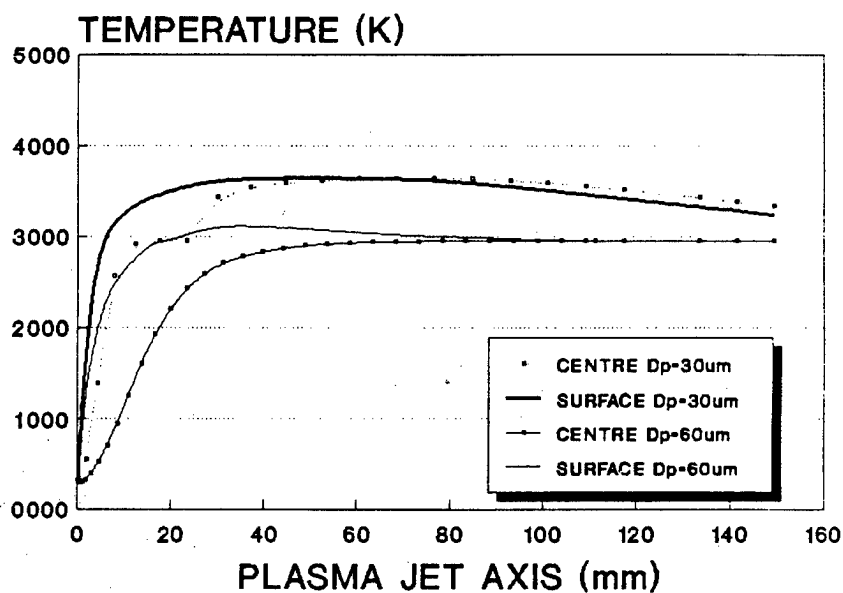


Fig 3 : Surface and center temperature of 30 and 60 μm in diameter particulates (ZrO₂ + 8% Y₂O₃ wt) injected in an Ar-H₂ plasma jet : 30 kW, Ar 50slm, H₂ 15slm, nozzle diameter 8 mm.

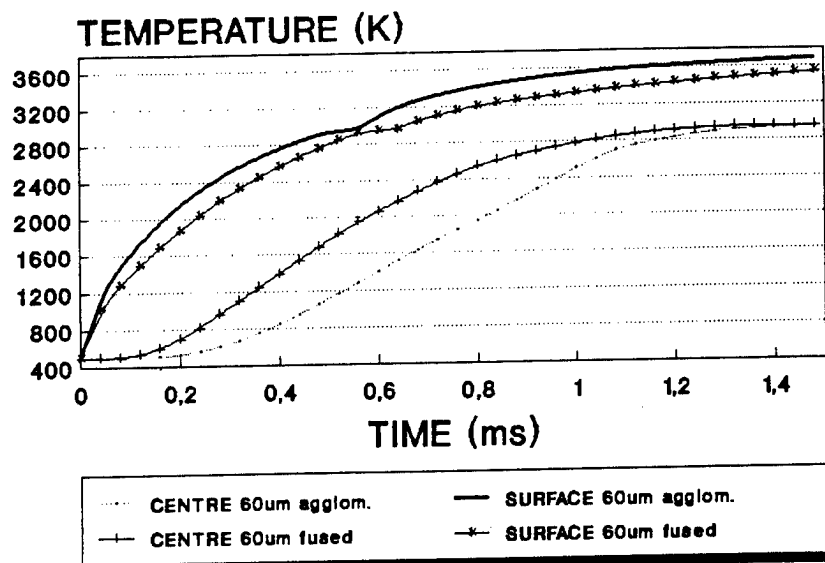


Fig. 4 : Surface and center temperature of zirconia particulates (stabilized with 8% Y_2O_3) fused and agglomerated immersed in an infinite plasma at 10000K (Ar-H₂ 20% vol.).

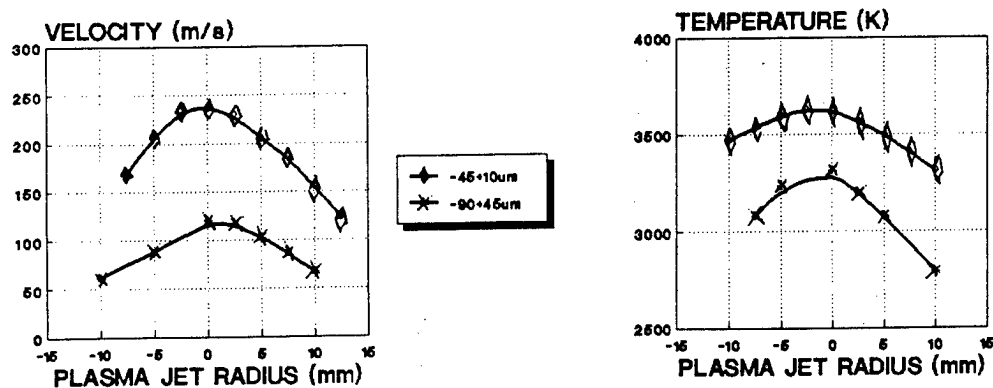


Fig. 5: Velocity (a) and Surface temperature (b) distributions 75 mm downstream of the nozzle exit) fused zirconia particulates respectively - 45 + 10, - 90 + 45 μm in flight in an Ar-H₂ plasma jet (40 kW, 50 slm Ar, 15 slm H₂).

Recent Advancement in Thermal Barrier Coatings

H. Takeda, T. Suzuki, M. Ito and M. Nakahashi

***Toshiba Research and Development Center
1 Komukai-Toshiba, Saiwai, Kawasaki, 210, JAPAN***

ABSTRACT

The authors' successful results on thermal barrier coating (TBC) development programs including a Japanese national project for gas turbine high temperature dynamic parts such as turbine blades, have encouraged the actual use of TBCs. The application of TBC has yielded the high efficiency, high durability, and long life of the base metals of gas turbines.

This paper reports some remarked properties of TBCs obtained in the program and recent research results on advanced technologies which have improved TBC reliability. The advanced technologies include non-destructive thickness evaluation methods and laser treatment for obtaining a smooth and anti-erosion surface.

The thickness measurement method using an eddy current is basically available to evaluate a plasma sprayed ZrO_2 coating non-destructively when calibration data can be obtained for a standard specimen. Fluorescent material doping to a ceramic layer is effective for evaluating or indicating effective thickness of the TBC without destructive investigation.

Controlled laser irradiation to a plasma sprayed ceramic layer of a TBC densifies the surface portion resulting in a high anti-erosion property.

INTRODUCTION

TBC is the most simple method to obtain a high efficiency gas turbine without any system design change. Only by coating a thin ceramic layer to usual gas turbine hot parts, it can decrease the heat loss which reduces gas turbine efficiency. However, TBCs for hot parts are laid under very severe conditions, and their properties depend on the applied techniques and materials. Therefore, it is important to solve these problems to apply TBC for actual use.

Usually, a TBC consists of a metal alloy bond coat and a ceramic overcoat, both formed by plasma spraying. The plasma spraying technique is a very effective method to apply a thick film onto a substrate in a very short time. However, this rapidness makes it difficult to control the uniformity of the coating layer, especially case of applying to a complex surface configuration, such as gas turbine airfoils.

The authors have developed computer controlled plasma spraying system for the gas turbine airfoil to establish a uniform coating technique, and have evaluated the coated airfoils in a 1400°C class gas turbine test facility.

Besides coating uniformity, TBC reliability depends on the material system. It is necessary to find optimum ceramic and bond layers by adopting some evaluation method such as a heat cycle test, hot corrosion test, oxidation test and so on.

Non-destructive evaluation of a TBC is also important to control and keep its quality during plasma spraying or actual use. The authors have developed new methods because there have been no techniques for such purposes.

An erosion problem will occur when TBC is used in a particle rich combustion gas environment, because of the high porosity of a ceramic layer. The laser irradiation technique has been developed to increase the anti-erosion property by densifying the surface portion of the ceramic layer.

TBC SUMMARY

Principle of TBC

Generally, the gas turbine operating temperature which is closely related to system efficiency, is dominated by the hot parts' metal wall temperature. Therefore, lowering the metal wall temperature without energy loss is very important to raise system efficiency. TBC has been developed for such a purpose.

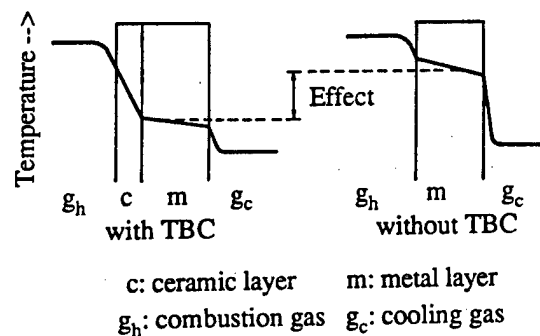


Fig. 1 TBC effect principle

Figure 1 explains the TBC effect. The effect of TBC becomes clear by comparing airfoils with and without TBC. In Fig. 1, two airfoil models which have air cooling systems are under the same condition. The left hand model is for an airfoil with a TBC. In this case, the heat from the hot gas to the cooling air through the airfoil metal wall is reduced by a low thermal conductivity ceramic layer (that is, a TBC). This causes to lower the metal wall temperature without changing other thermal conditions.

The effect of TBC depends on the heat transfer condition at the airfoil surface, the thermal

conductivity of the materials, and so on. Figures 2 and 3 show the calculated TBC effect. In these figures, the most important point is that a large temperature reduction is obtained by only a two or three hundred micron thick ceramic layer.

It is important to notice that the TBC effect is obtained only in the parts where a cooling system is adopted.

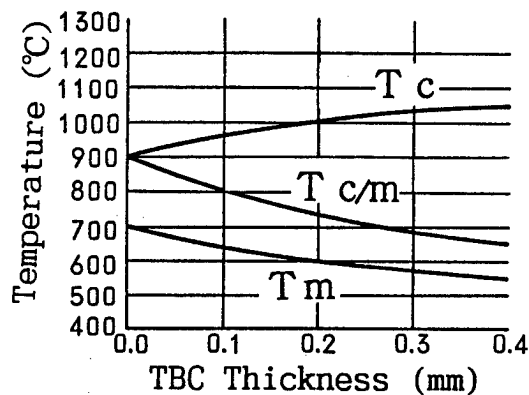


Fig. 2 Calculated TBC effect: Influence of thermal transfer coefficient

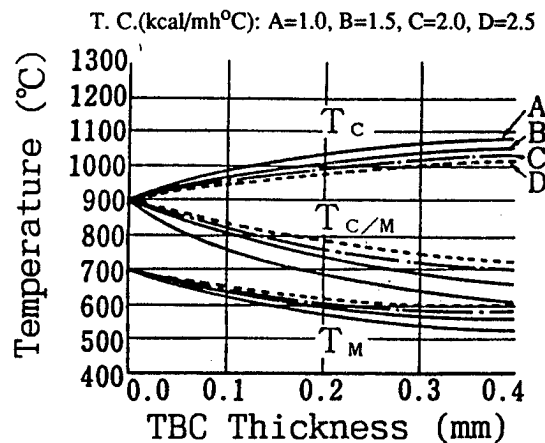


Fig. 3 Calculated TBC effect: Influence of thermal conductivity(T.C.) of ceramics

In both figures, thermal conditions noted below are common.

heat transfer at the surface: $10,000 \text{ kcal/m}^2\text{h}^\circ\text{C}$, hot gas temperature: $1,200^\circ\text{C}$, cooling gas temperature: 400°C , metal wall thickness: 2 mm , bond metal layer thickness: 0.1 mm , T.C. of metal layer: $30 \text{ kcal/mh}^\circ\text{C}$

TBC Materials and Formation

A TBC usually consists of two layers, a metal bond layer and a ceramic top layer. The role of the metal bond layer is to combine the substrate(hot parts metal wall) and the ceramic top layer sufficiently and to protect the metal wall from oxidation and corrosion at high temperature. Therefore, the metal layer materials are basically the same as heat resistant material compositions. In the early days of TBC development, simple composition alloys, such as Ni-Al or Ni-Cr, were used. After recognizing the importance of a metal layer, MCrAlY(M=Ni, Co and their alloys) type alloys have been developed and have shown remarked properties.

The properties demanded of a ceramic layer are as follows:

- low thermal conductivity---basic property for a thermal barrier;
- high temperature stability---no material change should be accepted, because TBC is used at a high temperature for a long time;
- high thermal expansion coefficient close to that of a metal---thermal expansion coefficient mismatch between the ceramic layer and the metal wall causes thermal fatigue damage.

From these reasons, stabilized ZrO_2 has been selected as the most applicable ceramic for TBC.

These metal and ceramic layers are usually formed by the plasma spraying method. The

plasma spraying method is a very useful technique to form a comparatively thick coating in a short time, which is a very important factor for industrial applications. Figure 4 shows a typical TBC microstructure formed by plasma spraying. Some quantity of pores in the ceramic layer are observed. These pores play an important role in TBC. The thermal expansion coefficient of the ceramic layer is intended to be close to that of metals, as mentioned above, but it is impossible to adjust it perfectly. This causes large a thermal stress for a large temperature gap even when the thermal expansion mismatch is small. Under this condition, the existence of pores decreases the stress by its high compliance. However, the existence of pores causes the degradation of mechanical properties. It is very important to maintain optimized porosity by controlling the plasma spraying conditions.

EXPERIMENTAL AND RESULTS

Selection of Materials for TBC

Partially stabilized ZrO_2 satisfies the thermal properties demanded of TBC. Problems in the actual use of TBC are dominated by durability that depends on the high temperature properties of the metal bond layer. From this point of view, the authors investigated the effect of the metal bond layer composition on the thermal fatigue property of the TBC. Figure 5 shows the thermal fatigue test result for several TBC specimens with different composition bond metal layers. The thermal fatigue test was carried out by inserting the specimen in two different temperature furnace alternately. The higher temperature furnace was kept at $1100^\circ C$ and the lower one was kept at $280^\circ C$. The holding time in each furnace was 30 minutes. In Fig. 5, the superiority of the MCrAlY type bond metal, especially NiCoCrAlY, is shown.

Automated Plasma Spraying Technology Development

The authors developed a microcomputer controlled plasma spray gun actuator to apply TBC uniformly to turbine blades and vanes that have a very intricate

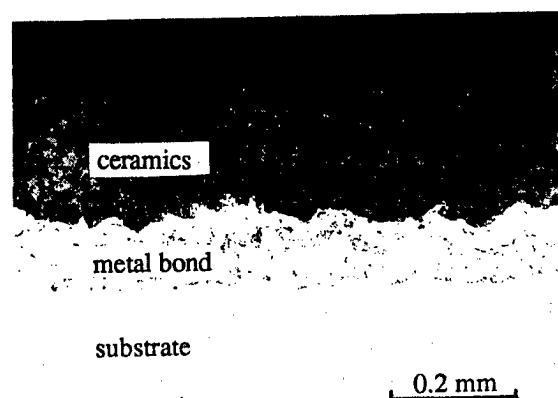


Fig. 4 TBC microstructure

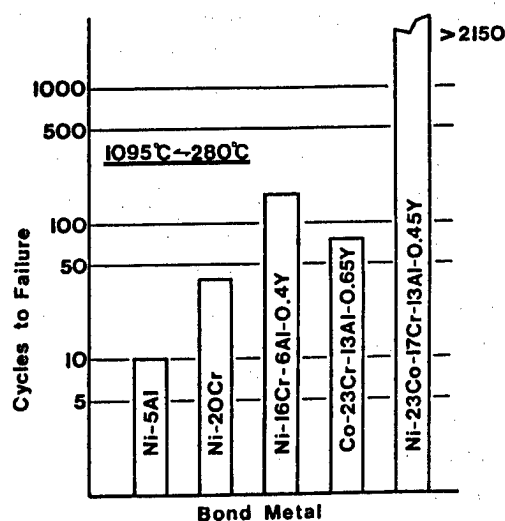


Fig. 5 Effect of bond metal layer composition on TBC thermal fatigue test

configuration. There are three major factors in plasma spraying technology to gain high performance coating. They are a constant and high speed scanning rate, constant distance from the gun to the substrate, and the rectangularity of the plasma flame and substrate. A high response actuator can act desirable motion by teaching these factors to a computer. A uniform thick coated layer is observed in Fig. 6.

Non-destructive Coating Layer Thickness Evaluation

The TBC thickness distribution survey during spraying and the remaining thickness investigation during actual usage without damaging the coating are very important factors to maintain high quality. The authors tried two different types of non-destructive evaluation methods and obtained interesting results. In one method, eddy current was used and showed a good relation between the data obtained by this method and the data obtained by destructive means, that is, cross-sectional microscopic observation. Figure 7 shows one experimental result for this method. In the other method, fluorescence technology was used. Doping a small quantity of fluorescence material to a TBC ceramic layer, it irradiates fluorescence light when the layer is irradiated by ultra violet ray. When the ceramic layer is designed to consist of several layers that contain a different dopant in each layer, its thickness is easily confirmed using ultra violet ray without destruction.

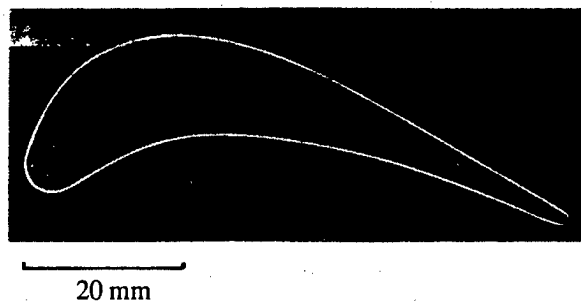


Fig. 6 Cross-section of a uniform coated vane

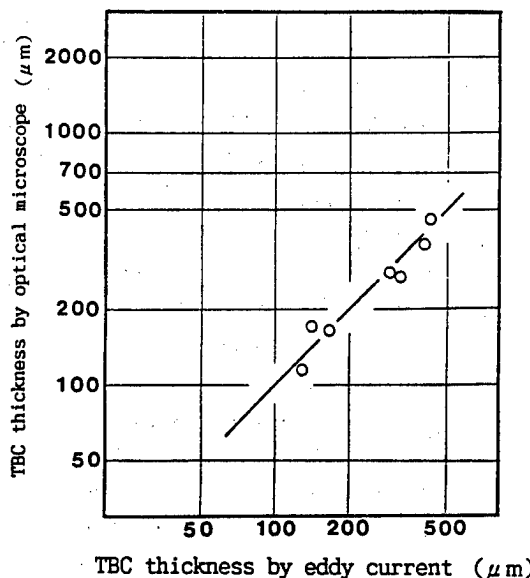


Fig. 7 Comparison of data for two TBC thickness measurement method

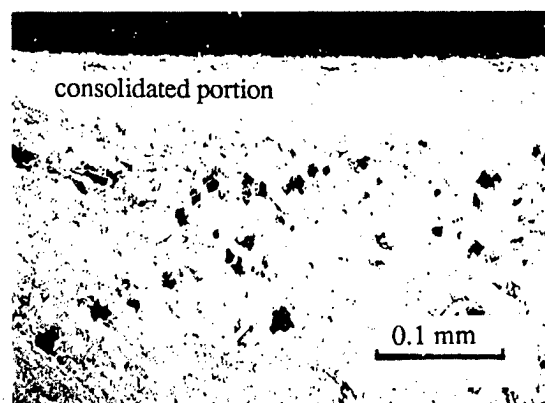


Fig. 8 Microstructure of laser surface treated TBC

High Temperature Gas Turbine Test for TBC Coated Blades and Vanes

100 TBC applied vanes and 64 TBC applied blades were installed in a 1400°C class test gas turbine and their TBC effect and durability were investigated. An approximately 40 hour test proved the feasibility and durability of TBC for industrial use.

Laser Surface Consolidation

Plasma sprayed ZrO_2 was irradiated by a laser beam to consolidate its surface to increase its anti-erosion property. A limited thick portion of the layer was melted and consolidated at an optimum condition. It should not be consolidated completely, to retain the effectiveness of porosity forward thermal stress. Figure 8 shows the controlled consolidation of a ceramic layer obtained by such an optimum irradiation condition. The consolidated layer showed a good anti-erosion property the same as sintered ZrO_2 (see Fig. 9).

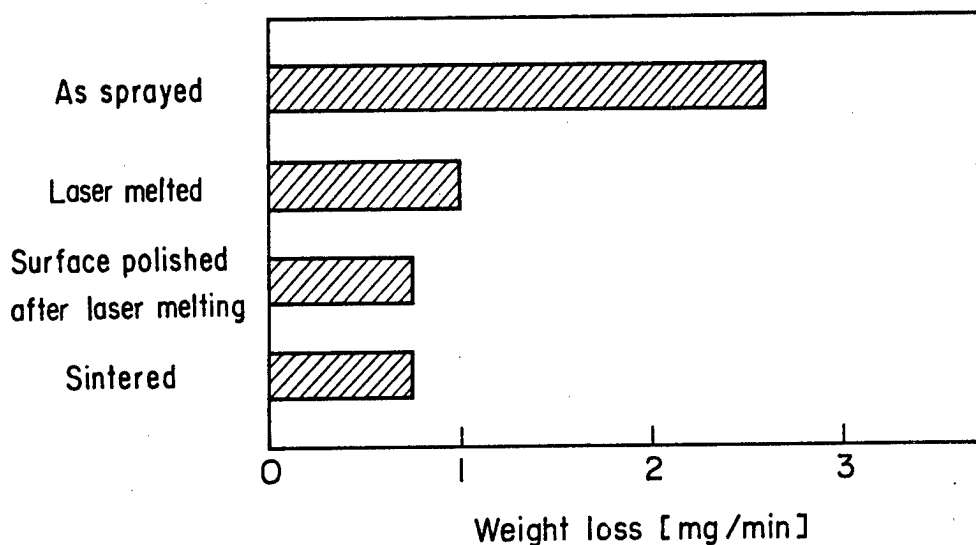


Fig. 9 Erosion property of surface treated TBC

SUMMARY

The recent advancement of TBC technology has been introduced. The authors have recommended the application of this technology to actual systems from experimental results. A highly quality controlled TBC promises a high efficiency of the system, long life of hot parts, and so on.

CARBON FIBRE COATING AND ITS INFLUENCE ON THE MECHANICAL BEHAVIOUR
OF THE COMPOSITES

J. BOUIX, R. FAVRE, C. VINCENT, H. VINCENT

Université de LYON-I, Laboratoire de Physicochimie Minérale
(URA 116 du CNRS) , 43 boulevard du 11 novembre 1918 , Bât. 731
69622 Villeurbanne (France)

S. CARDINAL, P. FLEISCHMANN, P.F. GOBIN, P. MERLE

INSA de LYON, GEMPPM (URA 341 du CNRS), 20 avenue A. Einstein
Bât. 502, 69621 Villeurbanne (France)

Summary. This paper concerns on one hand the elaboration and the properties of carbon fibres coated with carbides by a particular C.V.D. and on the other hand the elaboration by squeeze-casting and the mechanical behaviour of Al-matrix composites reinforced by these fibres.

I. COATING OF CARBON FIBRES WITH CARBIDES BY R.C.V.D.

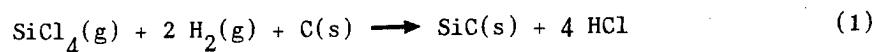
I.1. Aim, principle and advantages of R.C.V.D.

In the domain of ceramic and metallic matrix composites, the most important drawbacks of the carbon fibres are the chemical reactivity of carbon at middle and high temperature with air and metals such as aluminium and, on the other hand, their poor wettability by molten metals.

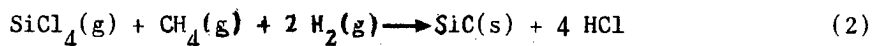
Therefore, it could be interesting to coat each single strand of a carbon fibre with a thin, but adherent and uniform layer of materials able to withstand the chemical action of air or metals, to improve their wettability and to keep their high mechanical properties.

We will describe in the first part of this paper the process for coating the T300 fibres (ex-PAN, 6K) which have been embedded by squeeze-casting in an alloyed aluminium matrix, this coating consisting of SiC, B₄C or TiC.

This coating is obtained thanks to a particular chemical vapor deposition (CVD) called reactive CVD (RCVD) in which only one element of which the carbide consists (SiC for example) is carried on by the gas phase whereas the carbon is taken off from the fibre itself. At a convenient temperature occurs the reaction:



The reaction (1) needs the contact between the carbon substrate and the gas phase, which provides the most important advantage of RCVD in comparison with classical CVD consisting of the reaction:



As a matter of fact, this classical reaction (2) does not make it possible to avoid a preferential deposition on the peripheral strands with a welding of these strands to each other, because the gaseous reactants react in the peripheral zone of the fibre and do not have time to diffuse into the core.

At the contrary, the reaction (1) is self-controlled : the gas phase comes into contact with the peripheral strands, which induces the formation on these strands of a carbide layer which isolates the substrate from the gaseous reactants. Then, the speed of the reaction (1) decreases strongly on these strands, because its continuation involves the diffusion of C or SiCl_4 through this layer. Therefore, the remaining gaseous reactants can diffuse into the fibre to coat each strand as far as the core. This thickness of the carbide layer is at last much more uniform than by classical CVD and it is not necessary to work at low pressure to enhance the gas diffusion.

I.2 Elaboration of the coated fibres

The coating is achieved in a pilot plant shown on figure 1 and giving 300 m coated for each run. The initial fibre unrolls in the axis of a cylindrical horizontal quartz reactor, between two stainless pulleys set in stainless chambers. The whole system is tight and dried in vacuo. The heating is achieved by H.F. induction as well as by Joule effect on the fibre itself with two contacts on the pulleys. A gas distribution system allows every possible composition of the H_2 -Ar- MCl_n mixture and the gas stream flows in the opposite direction with regard to that of the fibre.

The thermodynamic computation and the experimental study allowed us to determine the set of parameters (temperature of the fibre, composition of the gas phase, total gas flow, time of contact between the fibre and the gas mixture) giving an uniform coating of 0.01 to 0.1 micron thickness for different carbides and different fibres (ex-PAN, ex-PITCH, high tensile strength or high modulus).

For example, with a T300 (6K) fibre, a B_4C coating of average thickness equal to 0.05 micron (determined by chemical analysis) is obtained in the following conditions:

- temperature of the fibre : 1350°C
- total gas flow : 75 cm³ per min
- H_2/BCl_3 molar ratio : 1.5
- Speed of the fibre : 24 m per hour (time of contact: 2 min)

1.3. Characteristics of the coated fibres

The uniformity of the coating is illustrated by the figure 2, showing the Si K α X image of SiC coated elementary strands and by the figure 3, showing partially oxidized SiC coatings after burning the carbon fibre at 1000°C in air.

The presence of oxygen (0.1%) and nitrogen (7%) in the initial T300 fibre induces the formation of oxyde and nitride in the carbide layer: the figure 4 shows the XPS spectrum of aSiC coating containing SiO and SiO₂ and the figure 5 shows the XPS spectrum of a B_4C coating containing BN. This nitride is quite absent in coated ex-PITCH fibres.

The mechanical properties of the coated fibres have been determined on elementary strands ($l = 20$ mm, $s = 0.1$ mm.min⁻¹). The Young modulus remains nearly constant and the tensile strength decreases as the thickness of the coating increases. The figure 6 shows that this decay remains very slow up to a thickness of 0.08 micron for B_4C and 0.05 micron for SiC.

The resistance to oxidation has been tested by determining the weight loss in air a 600°C as a function of time. The T300 initial fibre has loss 100% of its weight after 75 min. After 2 hours, this loss is equal to 7% for a 0.05 micron SiC coated fibre and remains near 0% with B_4C coating of the same thickness (figure 7).

II. INFLUENCE OF THE COATING ON THE MECHANICAL BEHAVIOUR OF THE COMPOSITE

In order to test the efficiency of the coating for the chemical

protection of the fibre during the processing of the composite and its influence on the strength of the interface between the fibre and the matrix, acoustic emission (A.E.) during tensile tests correlated with Scanning Electron Microscopy of the fractured composite were used.

II.1. Principle of the method

We have used results of a previous study on the characterization of the fibre-matrix bond in a single SiC filament-aluminium matrix composite [1].

By simulating theoretically a tensile test by finite element method and by using the Weibull's distribution of the fibre fracture stresses and a model for load transfer between the fibre and the matrix (Kelly model)[2], it is possible to obtain the theoretical curve of the cumulated breaks number N versus the tensile strain of the composite. That corresponds to a reference curve for analysing experimental results. On the other hand, measurements performed during a tensile test of the single filament composite leads to counting and to the localization of the fibre breaks. Therefore the experimental curve for the cumulated breaks number as a function the measured tensile strain can be determined. Experimental results(fig.8) show that the same final level (i.e. the same critical length L_c which is the usual parameter which is used to define the fibre matrix bond) can be reached by different ways. Two other parameters may thus characterize the fibre-matrix bond :

- the gap between the first experimental break and the beginning of the calculated curve. This parameter can be connected with a damage induced by the processing of the composite.

- the ratio of the experimental slope $dN/d\epsilon$ to the calculated one. A ratio having a value very lower than unity can be considered as relevant from a very bad bonding with a very small load transfer while a value near unity indicates a good load transfer.

II.2. Application to 6K coated or non coated fibre composite

We studied the influence of the coating on the fibre matrix interface, using a 6 K fibre composite embedded in a 6061 matrix in T6 condition.

These composites were elaborated by the squeeze casting technique. The fibres used were either non coated T300 fibres or fibres coated with SiC, B_4C or TiC. In this case, no theoretical approach of the fibre rupture can be done. It is however possible to use the results of the theoretical study on the monofilament composite in order to define some experimental parameters for A.E. measurements allowing the comparison of the influence on the behaviour of the composite, of the various coated or non coated fibres. These parameters are :

- the initial strain ϵ_0 at which fibre break begins, which should allow a comparison between the strength of the various fibres

- the slope of the A.E. curve $N = f(\epsilon)$ which can be used to compare the strength of the interface between the fibre and the matrix. This slope was defined in our experiments by the parameter $\epsilon - \epsilon_0$, where ϵ is the strain which corresponds to $N/N_0 = 0,7$, where N_0 is the maximum number of A.E. events.

Figure 9 gives the ϵ_0 and $\epsilon - \epsilon_0$ values obtained for the various samples. Each point of the diagram of this figure corresponds to the ϵ_0 and $\epsilon - \epsilon_0$ values obtained with the same sample.

Three different domains corresponding to different fibres can be delimited :

- the domain corresponding to non-coated carbon fibres with $0 < \epsilon_0 < 0,8\%$ and $1\% < \epsilon - \epsilon_0 < 2,5\%$

- the domain corresponding to SiC or B_4C coated fibres with $0 < \epsilon_0 < 1,5\%$ and $1\% < \epsilon - \epsilon_0 < 2,5\%$

- the domain corresponding to TiC fibres with $0 < \epsilon_0 < 0,8\%$ and $1,5\% < \epsilon - \epsilon_0 < 3,5\%$.

This diagram shows an evident spread of ϵ_0 values corresponding to SiC or B₄C coated fibres toward large ϵ_0 values. These coatings seem thus to protect the fibre from the degradation during the processing of the composite, as the mean ϵ_0 values for non-coated fibres is lower. (It must also be underlined that the three lowest ϵ_0 values for SiC or B₄C coated fibres correspond to the same elaboration operation which could thus not have been done in good conditions).

On the contrary TiC coated fibres exhibit ϵ_0 values in the same range as non-coated fibres. Moreover the $\epsilon - \epsilon_0$ values for these fibres are significantly higher than for all the other fibres. This would signify that TiC coatings lead to a bad load transfer between the fibre and the matrix.

The study of the total acoustic emission level (figure 10) reveals also two kinds of behaviour. The total amount N_0 of acoustic emission events during a tensile test is much more higher in the case of SiC or B₄C coated fibres than in the other cases (more than one order of magnitude).

Scanning electron microscope observation of the fibre rupture (fig 11) show two different kinds of rupture : a brittle rupture in the case of non-coated or TiC coated fibres, while the existence of pull-out is observed in the case of SiC or B₄C coated fibres.

Thus comparing the behaviour of non-coated and of B₄C or SiC coated fibres, the existence of pull out may be explained by the effective protection of the fibres by the carbide layer during the processing of the composite, the identical range of $\epsilon - \epsilon_0$ values, leading to conclude that the load transfer between the fibre and the matrix is not significantly modified by the presence of these coatings.

On the contrary in the case of TiC coatings, the large $\epsilon - \epsilon_0$ values indicates a bad load transfer between the matrix and fibres probably due to the high reactivity of TiC with the Al matrix. The fact that the rupture of the fibres remain brittle as in the case of non-coated fibres could be explained by the lower value of rupture strength of the TiC coated fibres as shown by table I.

coating	σ_R (MPa)
non-coated	3150
B ₄ C	3000
SiC	3120
TiC	1500

Table I : Rupture strength of coated or non coated fibres.

It must be underlined that the differences in total A.E. level can be explained by the type of rupture observed. One E.A. event corresponds, in the case of the brittle fracture observed for TiC coating or non-coated fibres, to the collective and simultaneous rupture of many fibres. On the contrary it corresponds to the rupture of one single filament or a few filaments, in the case of B₄C or SiC coatings.

II.3. Mechanical properties of unidirectionnal composite

Unidirectionnal composites were realized by the technique of squeeze-casting. The volume fraction of the fibres was 55%. The matrix was a 6061 alloy in T6 condition. Four points flexure tests were performed on these specimens.

Table II gives the mean value of the rupture strength obtained for the various composites :

coating	None	B ₄ C	SiC	TiC
σ_r (MPa)	410	990	1050	425

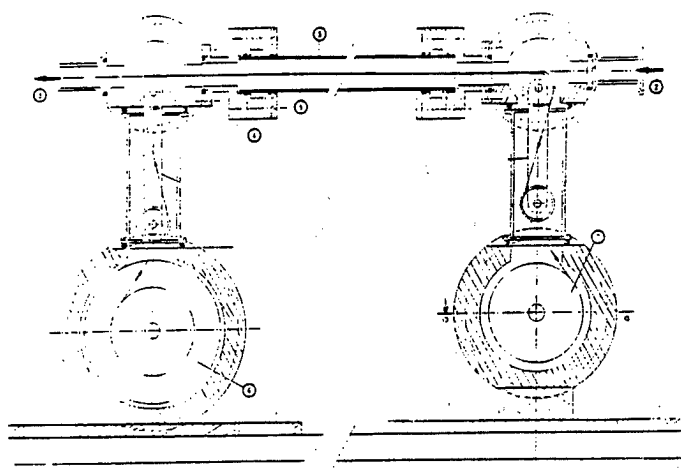
It can be seen that an effective improvement of the mechanical properties of the material is obtained with B₄C or SiC coated fibres, as the rupture strength is in that case approximately twice that obtained with other fibres.

CONCLUSION

A complete interpretation of the mechanical behaviour of the composite can only be done by a theoretical analysis including the Weibull's characteristics of the fibres embedded in the matrix. It is however possible to draw from the present experiments some qualitative conclusion on the influence of the coating. Our results show that B_4C and SiC coatings provide an effective chemical protection of the fibre as well against oxydation as during the processing of the composite leading to better mechanical properties. This seems not to be the case for TiC coatings.

References

- 1- R. HAMMAN, R. FOUGERES, D. ROUBY, P. FLEISCHMANN, P.F. GOBIN, F. LONCA-HUGO, M. BOIVIN, Mem. Sci. Rev. Met., décembre 1989, 789-797
- 2- A. KELLY, W.R. TYSON. "Fibre Strengthening Materials" in High Strength Materials, Zackay V.F., John Wiley and Sons, New York (1965), 578-602



- 1- carbon fibre
- 2- gas inlet
- 3- gas outlet
- 4- cooler
- 5-Quartz tube
- 6-7- stainless pulleys

Figure 1 : Pilot plan

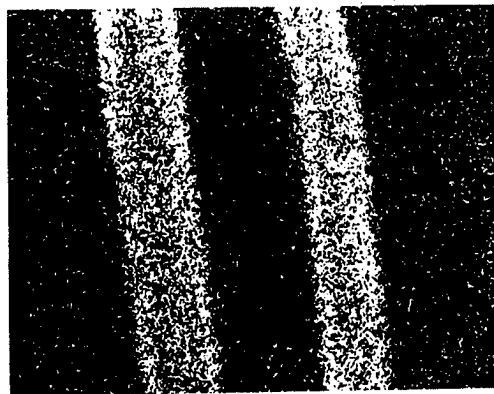


Figure 2 : Si K α X image on a SiC coated fibre

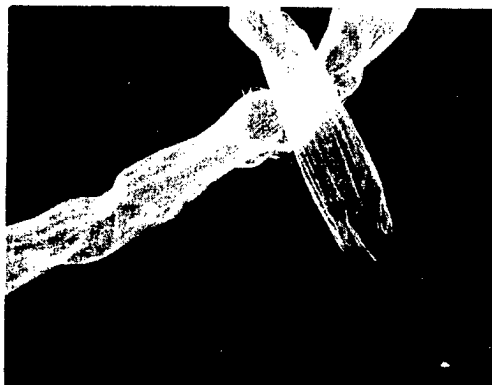


Figure 3 : SiC coated fibre after burning at 1000°C in air

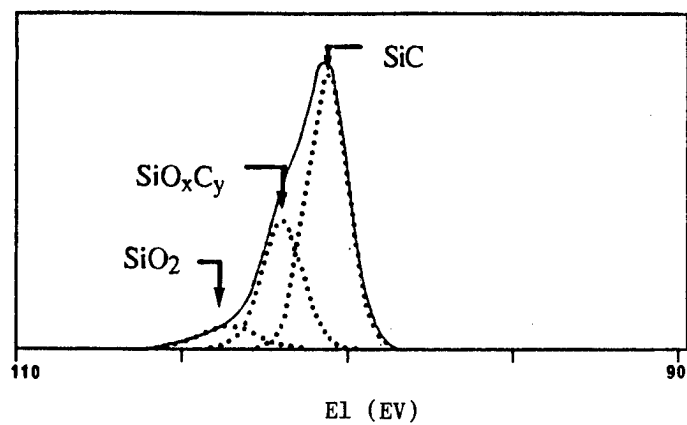


Figure 4 : XPS spectrum of SiC coated fibre

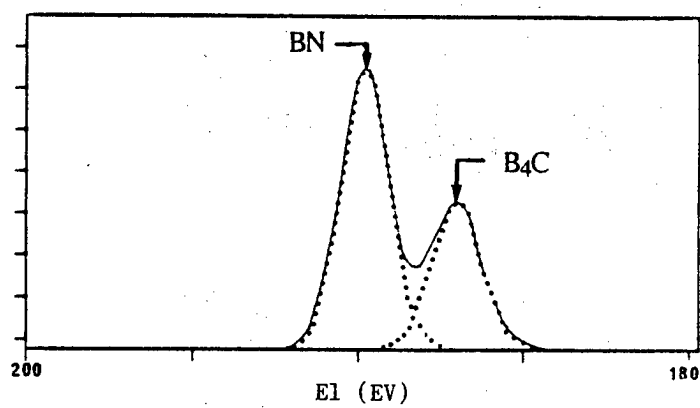


Figure 5 : XPS spectrum of B_4C coated fibre

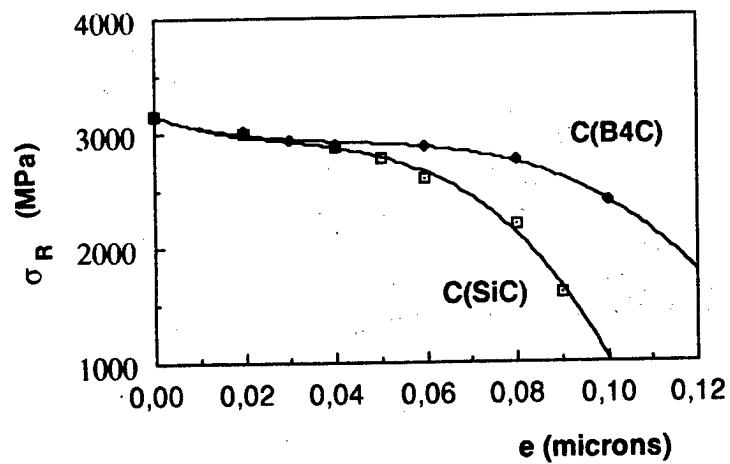


Figure 6 : Tensile strength of coated fibres as a function of the thickness of the coating (SiC, TiC, B_4C)

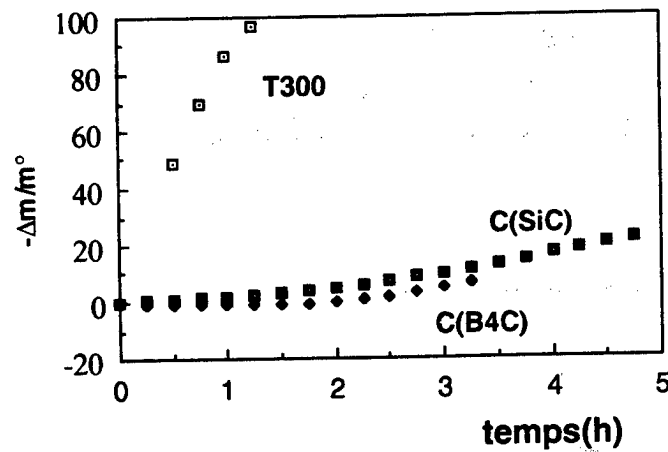


Figure 7 : Weight loss of the initial T300 fibre and of SiC, B_4C and TiC coated fibres in air at 600°C as a function of the time

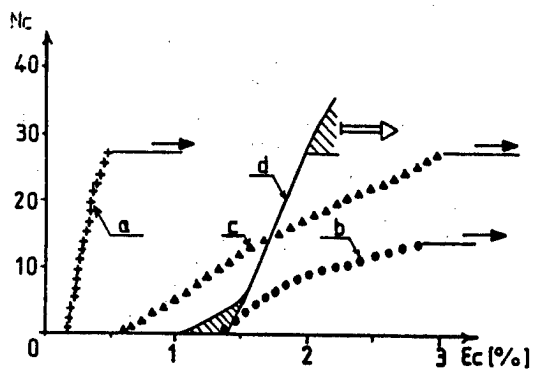


Figure 8 :

Comparison between theoretical curve of multiple crack phenomenon (d) and experimental curves (a, b, c)

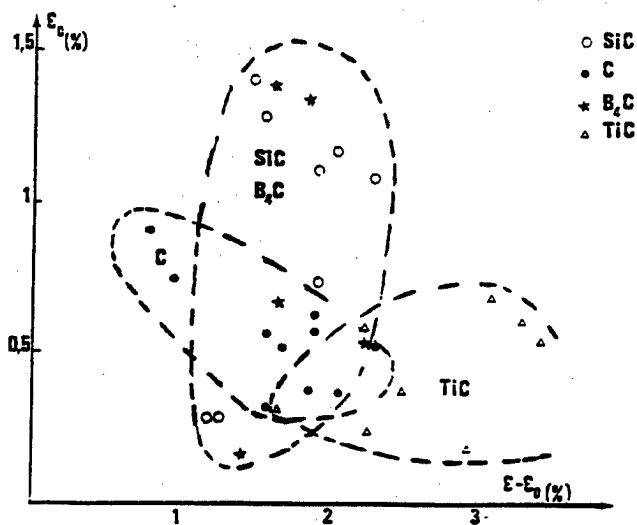


Figure 9 :

Variation domain of A.E. parameters ϵ_0 and $\epsilon - \epsilon_0$ as a function of the nature of the coating.

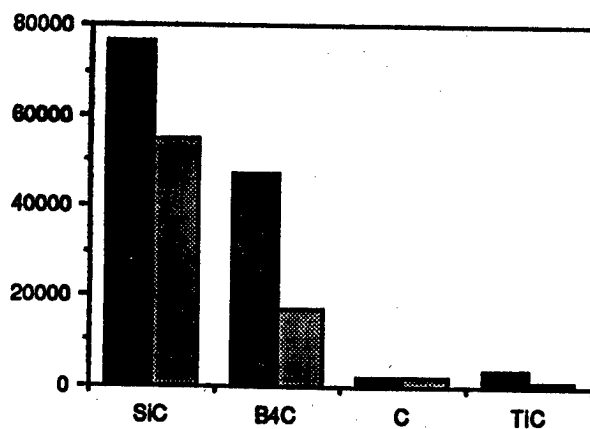
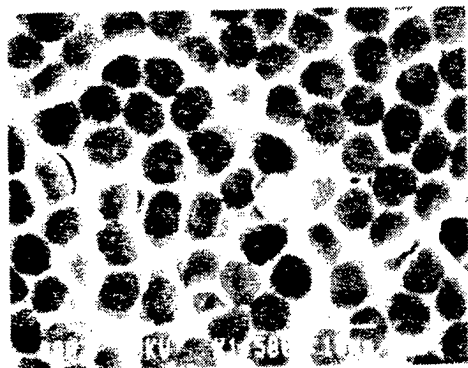
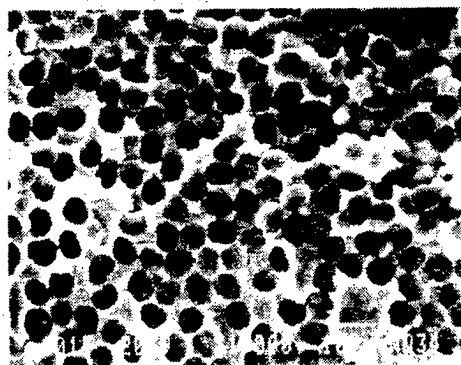


Figure 10 :

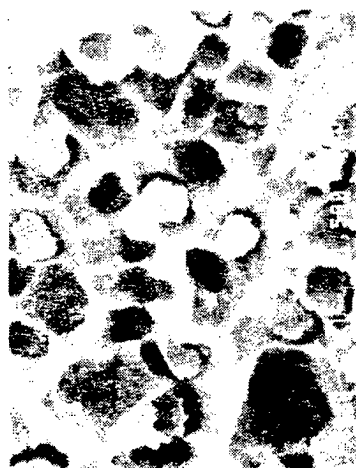
Total acoustic emission level (two different experiments) as a function of the nature of the coating.



a



b



10μm

c



10μm

d

Figure 11 :

S.E.M. observation of the rupture of the fibres.

- brittle rupture in the case of non coated (a) or TiC coated fibres(b)
- pull out in the case of SiC (c) or B₄C (d) coated fibres

Laser and Plasma Hybrid Spray Coatings on Carbon Fiber Reinforced Composite Materials

H. Shimura*, S. Sasaki*, K. Hasegawa** and K. Hirano***

* Mechanical Engineering Laboratory, Tsukuba, Ibaraki 305, Japan.

** Chemical Research Center, Kawasaki Steel Co.,
Kawasaki-cho, Chiba 260, Japan.

*** Chemical Research Laboratory, Nippon Steel Co.,
Nakahara-ku, Kanagawa 211, Japan.

ABSTRACT

To improve the oxidation resistance of C/C composites, the concept of environment resistant multi-layer coating was proposed. The laser and plasma hybrid spray system was developed for the purpose of applying the coating which permits C/C composites to be used in an oxidative gaseous condition at higher temperatures. This system is coupled the high power CO₂ laser with the low pressure plasma spraying equipment. Using this hybrid method, the multi-layer coatings of WC/MoSi₂/ZrO₂ were synthesized on monolithic carbons in a preliminary experiment. The formed thick coating films were high dense and stable at 2000 °C in inert atmosphere.

1. Introduction

C/C composites are materials with excellent physical properties such as low density, high rigidity, low thermal expansion, and high resistance to high temperature and wear. Because of these properties, C/C composites are increasingly used in super precision machine elements which require small deformation under force and heat. The excellent wear resistance of C/C composites makes the material ideal for the production of brakes. This material is also used in the production of turbine blades which are subject to high temperatures in service. To use this material in the production of super precision machine elements, coatings must be added to give a flat surface. The desired processing is then done on the coating. Furthermore, the material may not be used at temperatures of 500 °C or above if the atmosphere causes oxidizing effects. For this reason, it is necessary to provide an oxidation resistant coating on the surface. If the material is to be used in the production of turbine blades which are to be operated in a high temperature environment, the material must be provided with an erosion and corrosion resistant coating, in addition to an oxidation resistant and a thermally resistant coating.

In this paper, we present a laser and plasma hybrid spray system. The actual coating formed on a carbon material using this system is also shown in this paper. The system has been developed for the purpose of applying a coating which permits C/C composites to be used in an oxidation gas atmosphere at high temperatures.

2. Concept of Environment Resistant Coating

To improve the oxidation resistance of C/C composites, we propose a 5-layer coating as described below.

(1) Coating Which Emphasizes Adhesion (1st Layer)

The carbide generation temperature is high. This coating is a material whose carbide generation speed is slow in the temperature range of 1500 to 2000°C. This material must have low thermal expansion because C/C composites have low thermal expansion (Mo, W, WC, etc.).

(2) Self-Sacrificing Oxidation Resistant Coating (2nd Layer)

This material reacts with oxygen that has permeated through the coating on the upper level, so that oxygen will not be passed to the coating on the lower level (MoSi₂, WSi₂, etc.).

(3) Oxygen Inhibiting Coating (3rd Layer)

Oxides generally allow oxygen to permeate through them at high temperatures. Oxygen will reach this layer since the fourth and fifth layers on the higher level are made of oxides. A self-sacrificing oxygen barrier is provided in the second layer. The third layer is considered necessary to extend the life of the second layer (Pt, Ir, Rh, etc.).

(4) Heat Resistant Coating (4th Layer)

This coating will protect the inner coatings from sudden external temperature changes. The material used is a heat resistant oxide ceramic of a low thermal conductivity (ZrO₂, etc.).

(5) Erosion and Corrosion Resistant Coating

This coating resists wear due to collisions with particles in the operating environment, as well as corrosion due to reactive gas (ThO₂, etc.).

A conceptual drawing is shown in Figure 1. This multi-layer structure is required since no single material available today is suitable for protecting C/C composites at a temperature near 2000 °C. The coatings discussed in this paper may be applied to the production of gas turbine blades currently used in applications such as aircraft jet engines. In these applications, NiCoCrAlY and other materials constitute the first layer on the blade base material (Ni-base super alloy) and provide adhesion and oxidation resistance. The second layer consists of MoSi₂ and other self-sacrificing oxidizing coatings. The third layer is ZrO₂ and other heat, erosion and corrosion resistant coatings, respectively.

Using this production method, the selection of a material for the first coating is considered the most difficult because its reaction with carbon, its thermal expansion and other factors must be studied carefully.

3. Spraying System

Methods to coat C/C composites and other carbon material include the CVD method and the spraying method. The CVD method will form a good adhesive coating on carbon material, but it is difficult to increase the film thickness. For the ordinary low pressure plasma spraying method, it is difficult to improve adhesion and porosity. To improve these properties, the material surface temperature must be increased. For some spray materials to be used, the base metal must be heated to at least 2000 °C, and this is a difficult task.

In the prototype laser and plasma hybrid spraying method presented here, heating to a temperature above 3000 °C is possible using a high output laser (CO₂ gas laser) of 10kW power class. Adhesion is also improved by the reaction of the base metal with the spray material, resulting in the formation of carbide at the interface. The porosity is also expected to improve because the sprayed material is also heated and dissolved. Figure 2 is a conceptual draw-

ing and photograph of the spraying system.

4. Experimental Method

4.1 Spraying Method

Some basic experiments on multi-layer coatings for improved environment resistance of C/C composites were done. A laser and plasma hybrid spray was used to and a coating was formed on monolithic carbon as follows:

(1) Mo-Base Coating

Mo (coat 1), Mo-MoSi₂ (coat 2), Mo-MoSi₂-PSZ (ZrO₂ including 6% Y₂O₃)(coat 3).

(2) W-Base Coating

A W or WC coat was used instead of a Mo coat.

Figure 3 shows the dimensions of the spraying test piece used.

4.1.1 Low Pressure Plasma Spray

According to a study¹⁾ on the coating of carbon material with a low pressure plasma spray (LPPS), the base material must be heated to 1000 °C or above to facilitate the formation of carbide in order to improve Mo adhesion. In our experiments, however, the plasma heating did not result in a temperature rise as expected, and it was difficult to form a sprayed coating even when the atmospheric pressure and other spraying conditions were changed (for example, the pressure was adjusted between 50 and 300 mm Hg in Ar atmosphere, and the He mixing ratio was increased in the plasma to increase the plasma temperature).

4.1.2 Laser Heated Spraying

Low pressure plasma is not suitable for producing a coating with good adhesion because the reaction of the base metal with the spray material is limited due to insufficient preheating of the base metal. In addition, heating using heaters or high frequency entails great difficulties. By irradiating a carbon material with a high output carbon dioxide gas laser (maximum output 10kW), the irradiated face can be heated to above 2000 °C in a few seconds (using 3 kW of power and a focus diameter of approximately 5 mm). Coating experiments were conducted by using laser heating and plasma spraying simultaneously. In this spraying method, the material is heated by a laser before plasma spray has started, and heating is stopped as soon as plasma spraying has started.

The material to be sprayed was irradiated and heated by a laser while fed at a 2 mm pitch at a scanning speed of 2000 mm/min. The heating duration was 3 minutes.

4.1.3 Laser and Plasma Hybrid Spraying

In this spraying method, laser irradiation is continued during plasma spraying. An improved porosity of coating is expected because the material is sufficiently heated even when plasma spraying is being done, and hence the sprayed coating is melted again.

The spraying was done while the plasma and the laser were irradiated and the material to be sprayed was fed at a 2 mm pitch at a scanning speed of 2000 mm/min. The preheating with the laser was done in the same manner as the laser heating and spraying. On the multi-layer coating, the second and third coatings were formed using only low pressure plasma spraying.

4.2 Heating Test

Heating tests were done because a coating to be used on gas turbine blades must be stable even at temperatures above 1500 °C. Since the carbon material

used in the tests was not fully coated, heating experiments at temperatures up to 2000 °C were conducted in an inert atmosphere (vacuum or Ar gas).

5. Experimental Results

5.1 Film Porosity

The photograph in Figure 4 shows a cross-sectional view of a laser heated and plasma irradiated Mo coating. The spray conditions are given in Table 1. Figure 5 is a photograph of a cross-section of a Mo coating which was formed with the laser and plasma hybrid spray method. The spray conditions are the same as for the laser heated spray (Table 1). A comparison of Figures 4 and 5 shows that the hybrid sprayed coating (Figure 5) has better porosity. Figure 6 shows a cross-sectional view of a monolithic carbon which was coated with three layers of Mo-MoSi₂-PSZ. The photograph in Figure 7 shows the cross section of a coating consisting of two layers (W-MoSi₂) formed on C/C composites.

5.2 Results of Heating Tests

The results of heating tests up to 2000 °C in Ar atmosphere or in vacuum are summarized in Table 2. Table 2 indicates that the coating with WC used in the first layer is stable even at high temperatures. Table 3 shows the change in coating components after tests (the coating was analyzed from above the surface using X-ray diffraction). The WC coating is coexistent with W₂C at high temperatures. An inter-layer diffusion of elements is also observed in the case of multi-layer coating.

6. Summary

1. The formation of a thick coating on carbon material, which has been considered a difficult problem, is now possible using laser and plasma hybrid spray method.
2. Further study is needed on the selection of the coating material which contacts the carbon directly and on the stability of the oxygen barrier material at high temperatures.
3. The stability of the coating at high temperatures must be improved by realizing an inclined inter-layer structure for multi-layer coating.

REFERENCES

- (1) Костиков В.И, Шестерин Ю.А, ПЛАЗМЕННЫЕ ПОКРЫТИЯ, Москва Металлургия(1978).

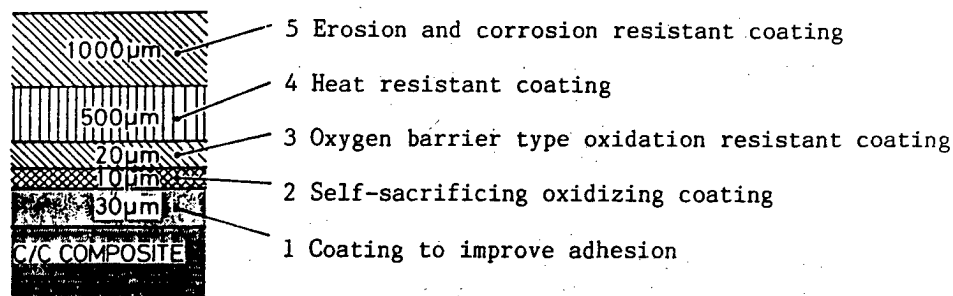
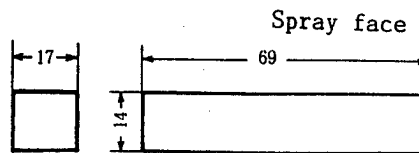
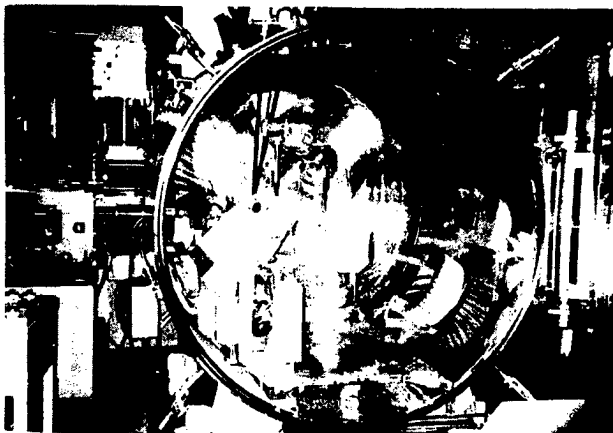


Fig.1. Conceptual Diagram of Super Environment-Resistant Multi-Layer Coating



Unit:mm

Fig.3. Dimensions of Test Piece

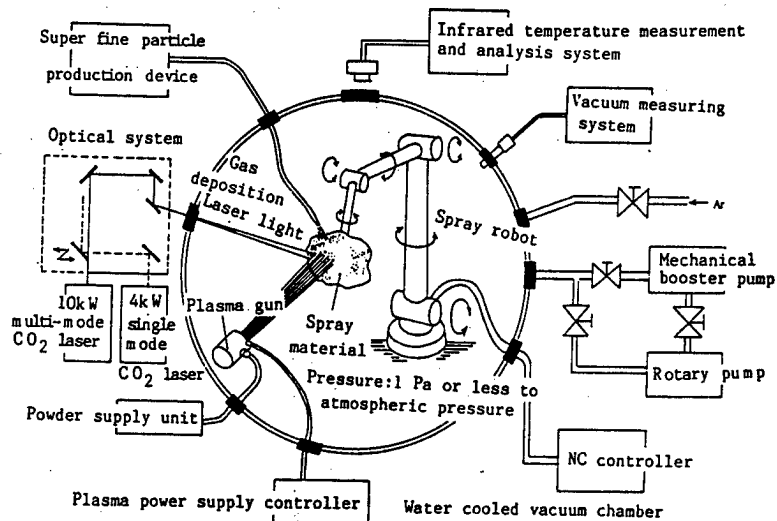
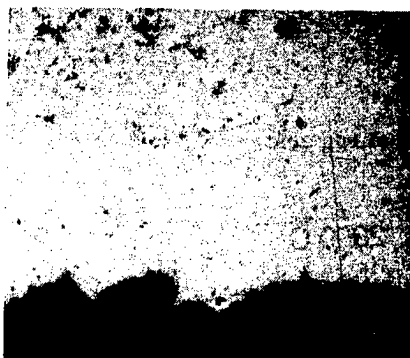
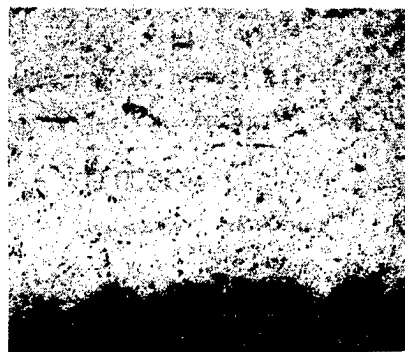


Fig.2. Conceptual Diagram of Spray System and photograph of the spraying system



125 μ m

Fig.4. Laser Heated, Plasma Sprayed Mo Coating



125 μ m

Fig.5. Hybrid Sprayed Mo Coating

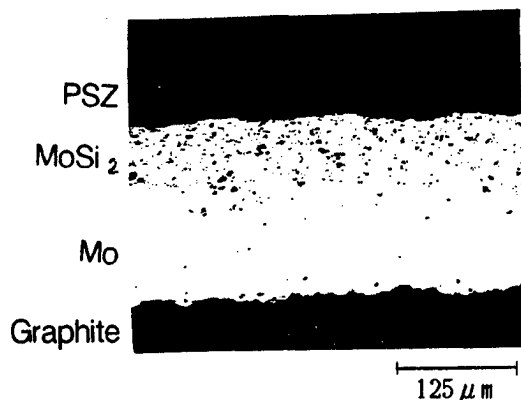


Fig.6. An Example of Multi-Layer Coating

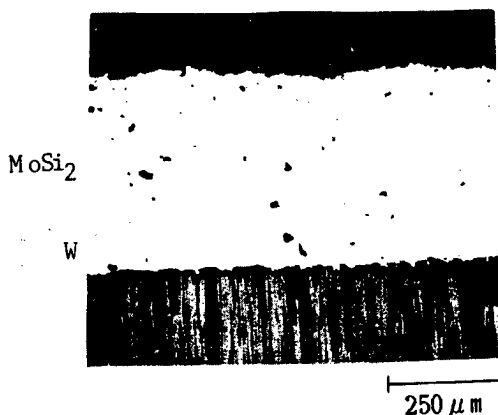


Fig.7. Cross-Sectional View of W-MoSi₂ Coated UD-C/C

TABLE 1. Spray Conditions	
Chamber pressure:	100 Torr (Ar)
Spray gun:	Plasmadyne SG-100
Arc gas (Ar):	50 psi (50l/min)
Auxiliary gas (He):	0 psi
Powder gas (Ar):	15 psi (3.93l/min)
Powder feedrate:	55g/min
Current:	800A
Voltage:	33V
Laser irradiation	
powder:	3kW

TABLE 2. Results of High Temperature Tests			
	1000°C	1500°C	2000°C
WC	○	○	○
W	○	○	X
Mo	○	○	
MoSi ₂ /W	X	X	
MoSi ₂ /WC	X	X	
○ No delamination			
X Delamination or crack			

TABLE 3. Products Formed by Reaction between Coating and Base Material at High Temperatures

		1000°C	1500°C	2000°C
WC	W ₂ C+WC	W+W ₂ C+WC	W+W ₂ C	W ₂ C+WC
W	W	W	W	W+W ₂ C+?(?)
Mo	Mo	Mo	Mo	
MoSi ₂ /W	?	MoSi ₂ (W+W ₂ C)	MoSi ₂ (WC)	
MoSi ₂ /WC	?	MoSi ₂	MoSi ₂ +?(WC)	

INTERFACE INFLUENCE ON MECHANICAL PROPERTIES OF COMPOSITES

Jean-Pierre FAIVRE
VETROTEX INTERNATIONAL
SAINT-GOBAIN GROUP
B.P. 929
73000 CHAMBERY - FRANCE

ABSTRACT

Cohesion of a composite is obtained by a good fitting between fibers and resin but many properties of such a material do not depend primarily on the quality of this interface. For instance, stiffness depends first of all on the glass content.

On the contrary, other properties are strongly influenced by the performances of the interface or the interphase. This paper presents several cases where this kind of correlation exists.

- Ageing : protection of the fibers by a coating strongly hinders degradation of standard mechanical properties (shear or bending).
- Impact : with constant processing conditions, impact properties can be much improved even if static stiffness or strength are not modified. Examples with reinforced thermoplastics and injected BMC will be presented.
- Toughness : toughness measured by crack propagation experiments on both reinforced thermoplastics and unidirectional thermosets is again very dependent on the nature of the interphase.
- Transverse stress : this property is of primary importance on the global behaviour of a structure and it is very sensitive to the interface.

These examples show that an improvement or an optimum can be reached in many specific properties even if the basic properties of the material are not affected.

INTRODUCTION

A minimal level of interface properties is required to get a material formed with two or more individual constituents. When this level is reached, the basic composite properties depend on the glass content : for instance, stiffness of a unidirectionnal glass reinforced epoxy increases linearly with the volume ratio of glass ; this property is more or less independent of the quality of the interface.

On the contrary, many other properties depend heavily on the nature of the interface. In this paper, some of these will be reviewed : ageing properties in the presence of water and in severe conditions ; impact properties for both thermoplastic and thermoset reinforced polymers ; toughness and transverse strength. In each case, examples are presented of an improvement of performance by a suitable choice of interface.

AGEING

A good control of the ageing properties of a composite depends on the performances of the fibre, of the resin, and of the interface. These behaviours have to be studied in ambient and severe conditions. To simulate ageing in ambient conditions, accelerated ageing in hot water is favoured as water seems to be of primary importance in this process. E Fiberglasses and resin perform less favourably while ageing (Fig. 1) and the choice of a suitable resin is a key point : epoxy resin are especially recommended if excellent ageing properties are required. But for a given system (fibre + resin), the interface can greatly modify the resistance to ageing. In table 2, interlaminar shear strength of a series of experimental unidirectionnal epoxy laminates is presented. Fibre (nature, diametre, yield) is constant, resin (constituents and cure cycle) is also constant. The only changes are minor modifications in interface : great modifications result in ageing performances.

Ageing in severe conditions is another requirement. Parts of reinforced thermoplastics in cars are for instance in contact with antifreeze liquid based on glycol. This product is generally at a high temperature. A study of impact performance of a range of RTP has shown that a clear improvement in flexural and impact properties is obtained with a change in the interface constituents. A new product is under development in our laboratories. Fig 3 shows the evolution of flexural strength for a standard product and for a new development product between 0 and 100 hours in the presence of a mixture of glycol and water at high temperature.

IMPACT BEHAVIOUR

The presence of glass fibres in a resin modifies its impact behaviour : Fig 4 shows the Charpy impact properties of standard polypropylene and polyamide against the glass content in volume, but for a given formulation the nature of the interface can change the impact resistance.

In an injected thermoset like ZMC300[®], besides improvements in mixing and injection, a modification of interface has increased filamentarisation and subsequently, impact properties : at constant processing conditions, the increase in impact resistance is over 50 %. Fig 5 is a view of these products which shows the visual differences with this new product.

The large use of glass reinforced thermoplastics in the automotive industry also requires good impact properties for this product. A continuous research effort allows the improvement of impact performances like Charpy or Izod energies. Evolution of Charpy impact energy is summed up in Fig 6 for a polyamide 6-6 30 % glass fibre for 20 years.

TOUGHNESS

Toughness is a basic property of any material. It allows the understanding of some of its macromechanical performances. This property is widely studied for composites (1,2,3). In using the test studied by the VAMAS group, different products have been tested in mode I delamination growth. Test samples are double cantilever beams of unidirectional reinforced epoxy with a thin film of teflon introduced as initiation crack. In an experiment, different samples have been tested : epoxy resin system, manufacturing, and cure cycle were kept constant. Only the fibre was different. Results are expressed in R curve and the initiation and propagation energies can be observed.

Each curve is the result of 14 samples tested at different initiation lengths. On Fig 7, results of 3 products have been plotted. Product A is a composite with a very weak interface, with no interactions between fibres and resin. Product B is a standard industrial strand for which mechanical performances are generally considered as good. Product C is a new product developed for specific use in epoxy resin : the interface is then very strong ; it has been controlled in different tests. These major differences in performances between products are only connected to interface. This result has consequences for the general behaviour of final products when a part is under stress. Results of the same kind but with smaller differences have been observed on reinforced thermoplastics tested in compact tension or notched bending.

TRANVERSE TENSION

Performances of glass reinforced resin in this test are weak. Strain limit is less than .5 % : first cracks appear generally in this direction. It is of primary importance to increase this limit. Transverse tests are developed in many laboratories and there is much literature available on this subject. PETERS (4,5) has developed interesting techniques to measure the intrinsic transverse strength by the use of a Weibull statistics. More simple methods have been used to detect the transverse strength in our laboratory : a unidirectional laminate is shaped and tested on a universal dynamometer. Significant results are obtained on different products. Table 8 gives strain for the first cracks detected by acoustic emission and the failure strain for different strands. Again clear differences are noticed between products with weak or medium interfaces and a product with strong adhesion.

CONCLUSION

Interface can be characterized by the adhesion between glass and resin and by the modifications it introduce in the physical nature of the "interphase". Any macroscopical behaviour of a composite has to be explained by the properties of its constituents, and by the main aspects of the interface.

Improvements in performance can be obtained by a judicious choice of key influencial factors : depending on the performance required, there is generally an optimum to reach in each of these properties ; this optimum has to be the result of a compromise.

REFERENCES

- 1) Fracture Mechanics Of Anisotropic Plates.
E.WU, Composites Materials, Vol. 2, 1988.
- 2) Application Of Fracture Mechanics To Graphite Fiber-reinforced Composites.
C. BATHIAS, R. ESNAULTS and J. PELLAS, Composites, July 1981, p.195-200.
- 3) Composite Interlaminar Fracture : Effect Of Matrice Fracture Energy.
D.L. HUNSTON, Composites Technology Review, p.176, 1986.
- 4) On Cross-Ply Cracking In Glass- and Carbon-Fiber Reinforced Epoxy Laminates.
P.W.M. PETERS, T.W. CHOU, Vol. 18, N°1, January 1987, Composites.
- 5) A New Method To Determine The Fibre-Matrix Bond Strength.
P.W.M. PETERS, Interfacial Phenomena In Composite Materials '89,
Editor F.R. JONES, Published by Butterworths, p.59-62.

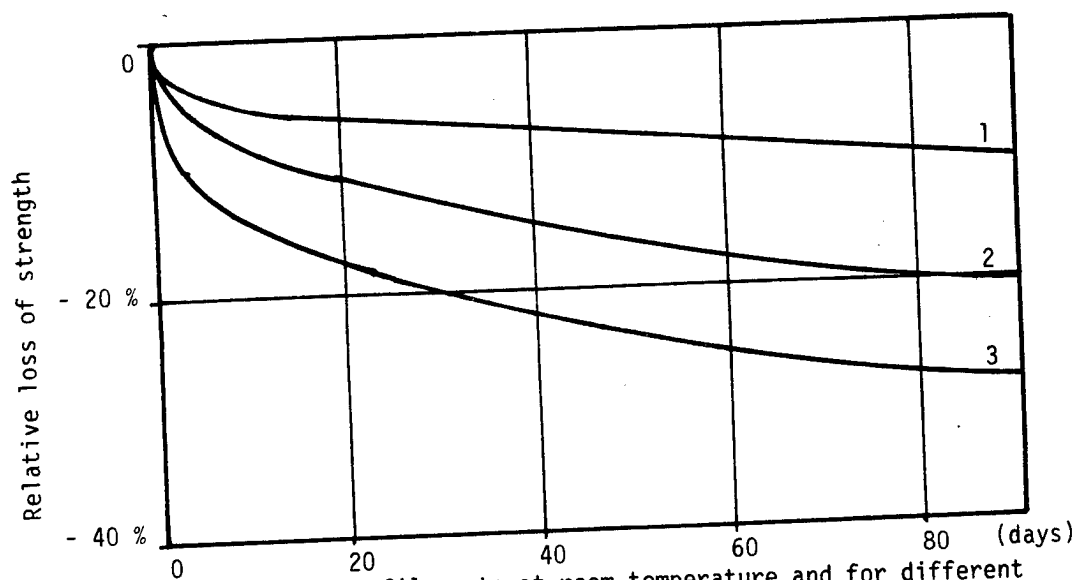


Fig. 1 : Ageing of E glass filaments at room temperature and for different ratios of humidity. (1 : 0%RH, 2 : 65%RH, 3 : 100%RH)

	Initial strength	Strength after treatment	Loss
A	78.8 Mpa	56.6 Mpa	- 28 %
B	79.9	59.5	- 25 %
C	78.9	47.4	- 40 %
D	78.5	54.6	- 30 %
E	76.9	40.7	- 47 %
F	78.1	43.1	- 45 %

Table 2 : Interlaminar shear strength before and after ageing (72 hours in boiling water) for a series of development strands.

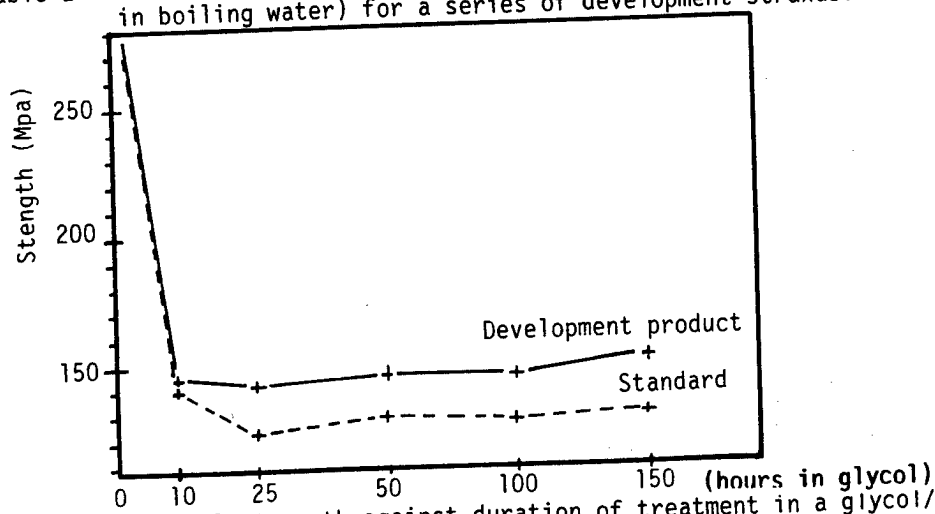


Fig. 3 : Flexural strength against duration of treatment in a glycol/water mixture at high temperature.

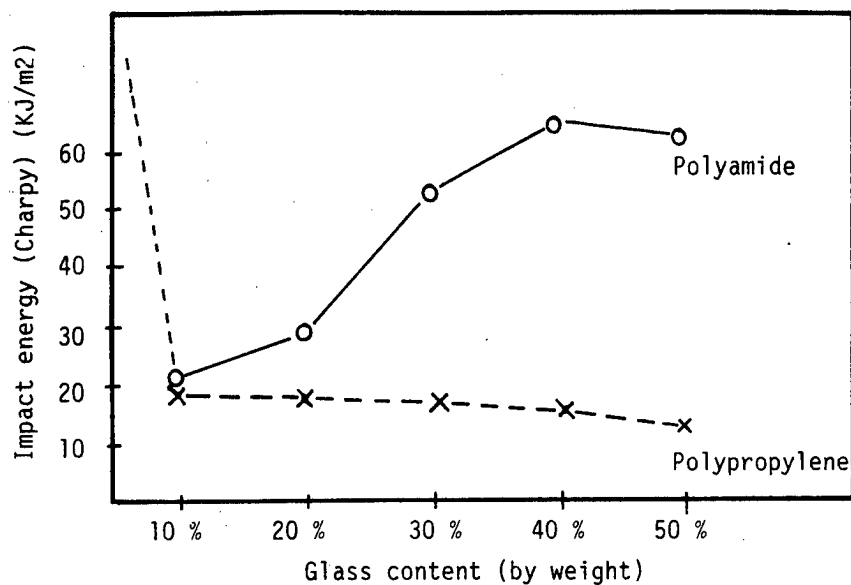


Fig. 4 : Influence of glass content on Charpy Impact resistance.

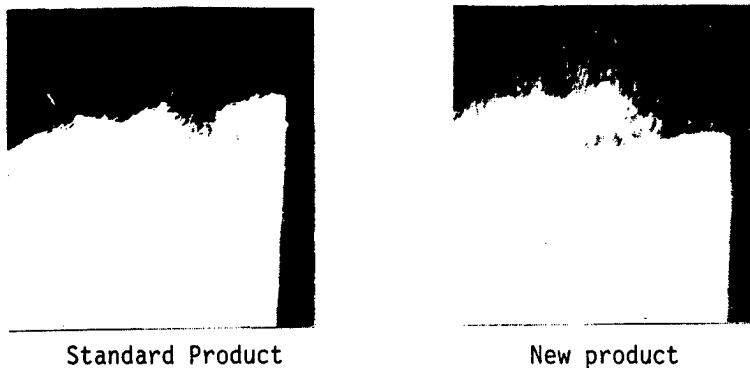


Fig. 5 : SEM pictures of damaged zones for a standard and a recently developed injected thermoset.

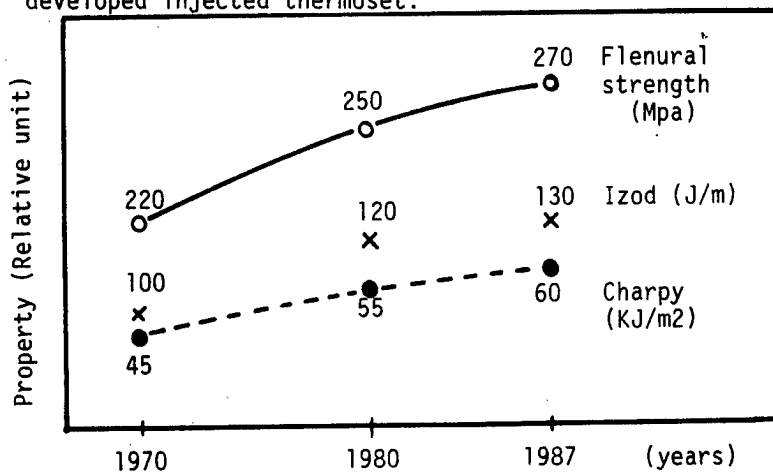


Fig. 6 : Improvement of mechanical performances on VETROTEX industrial products over 20 years. (standard polyamide).

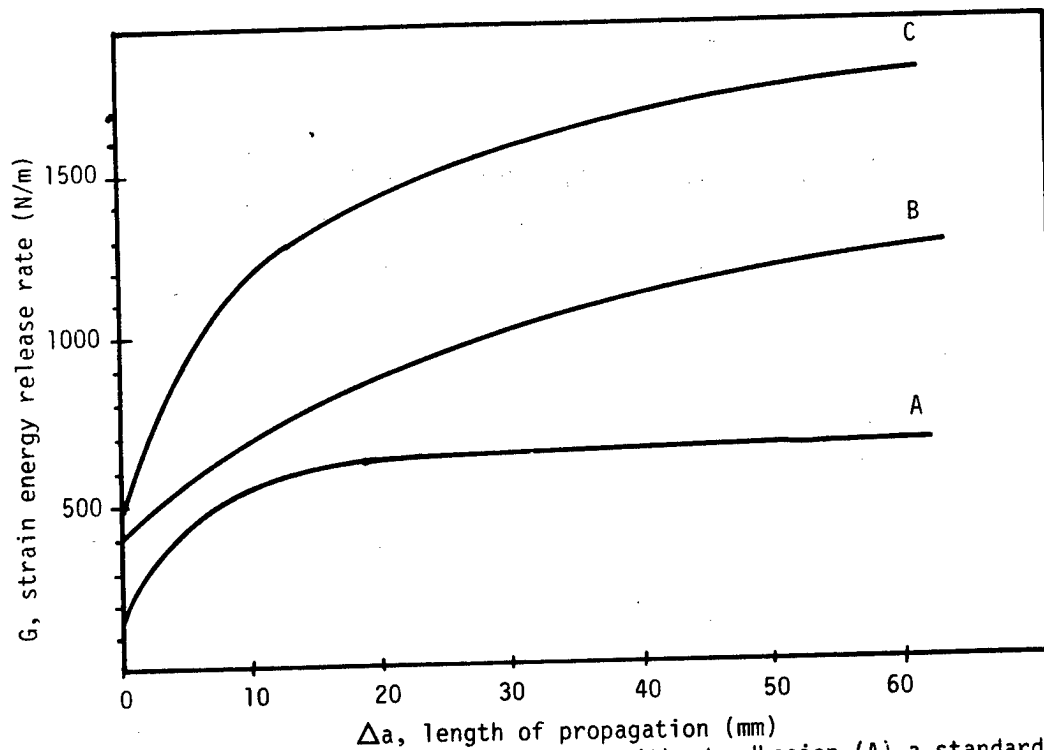


Fig. 7 : Toughness (R curve) of a product without adhesion (A), a standard product (B), and a specific product (C). Epoxy resin.

Product	Strain at first damage %	Failure strain %
A	0.18	0.25
B	0.36	0.67
C	0.43	0.97

Table 8 : Strain at first damage and failure strain in tranverse tension. See references on figure 7.

DATABASE AND COMPUTER ASSISTED
MANUFACTURING

H. VIELLARD, CODATA-FRANCE

This page intentionally left blank

SESSION IV

DATABASE

This page intentionally left blank

IDAM: A DESIGN ASSIST SYSTEM FOR COMPOSITE MATERIALS

M. YOSHIOKA*, M. HOJO*, K. KEMMOCHI*,
K. Ban** and S. IIYAMA***

- * Industrial Products Research Institute,
Higashi, Tsukuba, Ibaraki 305, Japan
- ** Rehabilitation Engineering Center for Employment
Injuries, Minato-ku, Nagoya, Aichi 455, Japan
- *** Toyo Engineering Corp. Research Center,
Togo Fujimi, Mobarra, Chiba 297, Japan

ABSTRACT:

Composite materials have advanced characteristics which make it possible to design their properties. However, it is difficult for product designers who are familiar with conventional isotropic materials to utilize composite materials. A design assist system that will make it easier for product designers to use composite materials is necessary.

In this report, the concept for a system which assists the access to the composite materials database (IDAM: Intellectual Database Access Manager) is proposed. A pilot system based on this concept and the results of its execution are introduced. The IDAM offers mechanical properties of composites through the retrieval of the database or simulations.

1. INTRODUCTION

In the material engineering field many factual databases have been developed. The usage of factual databases in this field has shifted from "knowing the properties of materials to "utilizing the properties for products design"¹⁾²⁾. In composite material engineering in Japan, however, very few factual databases have been developed³⁾, and the purpose of these databases remain "knowing the properties of materials".

Composite materials have many special characteristics which isotropic materials do not have. In particular, the characteristics which make it possible to design properties are very useful for designing products. This characteristic, however, complicates the properties of the materials, and also makes it difficult for products designers who are familiar with conventional isotropic materials to use it.

The importance of composite materials for database lies in the "designing properties of materials" rather than "knowing the properties of materials". So the database should contain not only mechanical properties data as materials but also information for "designing properties", for example, properties of the material components (fiber and resin), single lamina properties, ply orientations, etc. Consequently, a composite materials database is more complicated than databases of other material, and this makes it difficult to use for those

who have little or no knowledge of composite materials. Thus, a system for assisting users in accessing the database is necessary.

Therefore, the authors have developed an application system called IDAM (Intellectual Database Access Manager) which offers information concerning "designing properties of materials" based on the user requirements. The IDAM's functions are to retrieve experimental data of mechanical properties from the factual database, and based on user's demands, to simulate the properties of materials whose constituent components are available in the factual database.

In this report, the concept of the IDAM and examples of execution by the prototype system based on the concept are presented. The prototype system can be applied to simple laminated composites.

2. THE CONCEPT OF THE IDAM⁴⁾

The IDAM is a retrieval support tool for accessing a composite materials database. The IDAM is a system which presents the properties data of various composite materials by retrieving them from the factual database or by simulating mechanical behavior. Figure 1 shows the configuration of the IDAM. The system has four subsystems.

(1) CONTROL SUBSYSTEM controls the main process flow in the IDAM. It has the following functions: input of user's demands, issuing the retrieval command to the database and selecting the applicable fracture criteria for the simulation.

(2) KNOWLEDGE BASE is the aggregate knowledge required for running the control subsystem. In the pilot system, it contains the knowledge concerning the selection of fibers and matrices, the lay up angles, the retrieval commands, etc.

(3) COMPOSITE MATERIALS DATABASE is the factual database containing the properties of laminates, single ply, fibers and matrices. With the database management system, it is possible to retrieve the data by SQL (Structured Query Language), the standardized language⁵⁾ for database access. By using SQL for retrieval of database, it make possible to keep independence of the IDAM from the database management system.

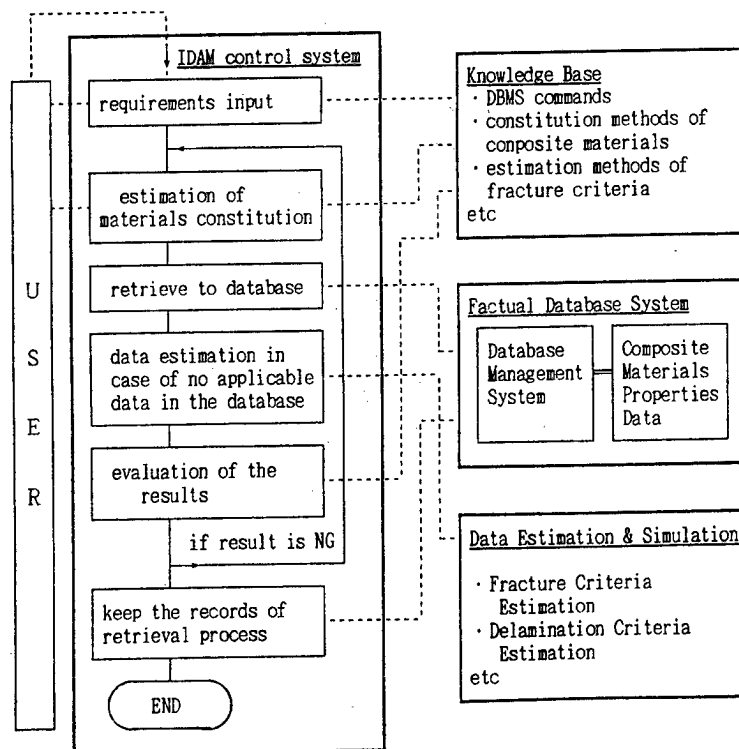


Fig. 1 concept of the IDAM

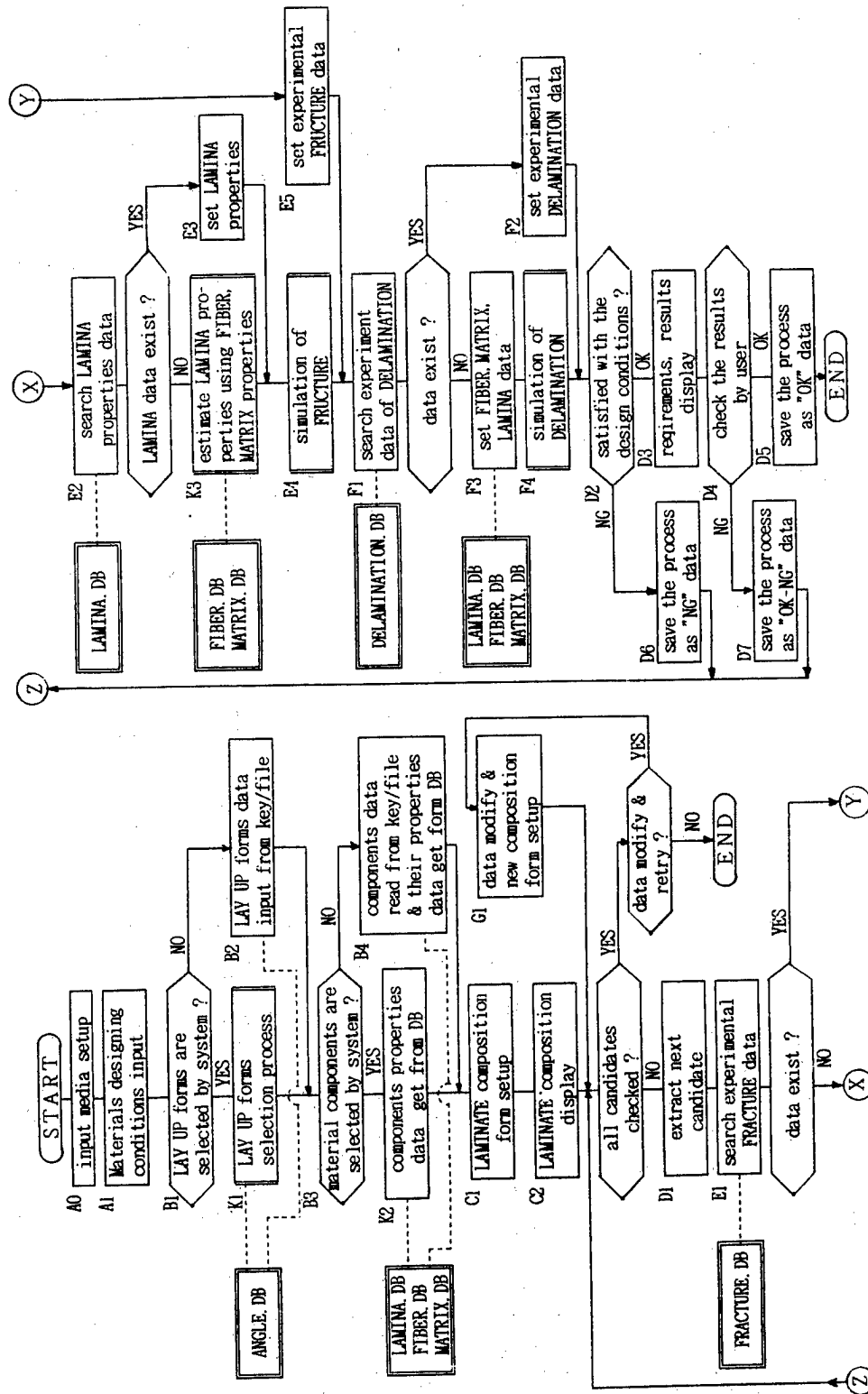


Fig. 2 Program flow of the IDAM

(4) SIMULATING FRACTURE STRENGTH SUBSYSTEM estimates the mechanical properties of laminates. In this subsystem, fracture load and delamination load are calculated for the requested conditions using one of the four fracture criteria selected by the users.

3. PILOT SYSTEM REALIZED

3.1 The functions of the pilot system

In the pilot system, the following functions are realized:

(1) Experimental or estimated value of load for fracture and delamination onset are presented by retrieval from the factual database or by simulation using the data retrieved.

(2) For the estimation of strength, four fracture criteria⁶⁾⁷⁾ are available: Wu tensor theory, Tsai-Hill theory, Maximum stress theory and Maximum strain theory.

(3) The user can select one of the three criteria (stress, strain and delamination) to evaluate retrieved or simulated values. The results of the criteria are saved in a file along with the data relieved or simulated above.

(4) The user can change the requirements of laminates input in first. Then, the above operations can be executed continuously.

(5) The system contains some intellectual algorithms to select constitution of laminates, for example, fiber, matrices and ply orientations.

(6) User requirements can be entered by key input or by file input. For the case of key input, users can enter their requirements by responding inquiry of the system. The system selects a series of candidates of lay up angles, fibers, and matrices based on use requirements using knowledge database. For the case of file input, all candidates should be selected by users and written in the input file. This process will be explained in chapter 4.

3.2 The program flow

The program flow of the pilot system is shown in figure 2. The program is written in C language on the UNIX operating system. Informix-ESQL/C is used as the database management system. The data or the commands transfer between the program and the management system is done through the SQL language.

3.3 The database files

The data base is composed of nine data files. The detail contents of each data files are shown in figure 3. Here, FRACTURE.DB and DELAMINATION.DB have link pointers to LAMIDSTRUCT.DB, ANGLESTRUCT.DB, and LTHICKSTRUCT.DB in order to make a relations between the experimental data and information of their specimen.

4. THE PROGRAM EXECUTION ENVIRONMENT and TEST RUN

4.1 The environment for running the program

The pilot system runs on the EWS(Sun 3/80 made of Sun Micro Systems Inc.) which has 16MB main memory and 110MB disk storage system. As the operating system, the UNIX 4.3 BSD (Sun OS V.4.0.3) is used and the informix-ESQL/C is used as the database management system.

angle.db

field name	contents
anglebase_id	ID of lay up angle unit
anglebase	lay up angle unit
anglestru_id	ID of lay up angle
anglestructure	lay up angle from
tlayer	Number of plies

lamina.db

field name	contents
l_id	Lamina ID
lname	Lamina name
f_id	Fiber ID
m_id	Matrix ID
vf	Volume fraction of fiber
pop	Popularity grade
l_xt	0° Tensile strength
l_xc	0° Compressive strength
l_yt	90° Tensile strength
l_yc	90° Compressive strength
l_s	Shear strength
gc	Fracture toughness

fiber.db

field name	contents
f_id	Fiber ID
fname	Fiber name
fkind ^{*1)}	Fiber material
f_xt	Tensile strength
f_el	Longitudinal modulus
f_e3	Transverse modulus
f_g23	Shear modulus
f_pl2	Poisson's ratio
f_pl3	Poisson's ratio

*1) "H_STRENGTH" or "H_ELASTIC"

matrix.db

field name	contents
m_id	Matrix ID
mname	Matrix name
mkind ^{*2)}	Matrix material
m_xt	Tensile strength
m_e	Yang's modulus
m_p	Poisson's ratio

*2) "POLY" or "EPOXY" or "PEEK"
(Polyester)

fracture.db

field name	contents
lstr_id	ID for reference to lamidstruct.db
astr_id	ID for reference to anglestruct.db
tstr_id	ID for reference to lthickstruct.db
tlay	Number of plies
fl_st	1st. ply failure stress
fl_ex	1st. ply failure strain [X-dir]
fl_ey	1st. ply failure strain [Y-dir]
fl_pl	1st. ply failure place
fm_st	Max. load stress
fm_ex	Max. load strain [X-dir]
fm_ey	Max. load strain [Y-dir]

lamidstruct.db

field name	contents
lamidstru_id	ID of lamina constitution
l1	Lamina ID of 1st ply
:	:
l16	Lamina ID of 16th ply

anglestruct.db

fields name	contents
anglestru_id	ID of angle constitution
a1	Angle of 1st ply
:	:
a16	Angle of 16th ply

delamination.db

field name	contents
lstr_id	ID for reference to lamidstruct.db
astr_id	ID for reference to anglestruct.db
tstr_id	ID for reference to lthickstruct.db
tlay	Number of plies
dl_st	Delamination stress
dl_pl	Delamination place

lthickstruct.db

field name	contents
lthickstru_id	ID of thickness combination
t1	Thickness of 1st ply
:	:
t16	Thickness of 16th ply

Fig. 3 Detail contents of data files

4.2 Example of execution

Figures 5 and 6 show the results of a test run for the required conditions data by file input shown in figure 4. In this case, two types of composite candidates based on the requested conditions are evaluated.

Figure 5 shows the result for the evaluation of the first selected candidate (T300/#3601,(0/45/-45/90)2s). "*" mark in the column "REQUEST" row "MAX LOAD" means that the evaluation is carried out based on MAX LOAD in this example. The result shows that the experimental data of fracture strength was in the database (the "Exp" mark in the column "CAL_RESULT" indicates the real tested value), and its value satisfied the requested condition. The delamination load was not in the database, thus it is estimated by simulation (the "Sim" marks in the column "CAL_RESULT" show simulated values).

Figure 6 shows the result for the evaluation of the second candidate laminates (T300/#3620,(0/45/-45/90)2s). In the case of this result, the real tested data of fracture strength for selected laminates was not in the database, therefore the fracture load value was estimated by simulation. The delamination load .RM 2.6" data is obtained from the database, but the location of the delamination is obtained by simulation because this data is not in the database.

5. CONCLUDING REMARKS

A concept for a system which assists users in accessing the database for composite materials was proposed. The system assists users to take suitable mechanical properties of composites through the retrieval of the database or the simulations based on the retrieved data. A pilot system developed based on the concept and example of its execution were presented.

At present, the pilot system can only be applied to simple shaped composites, and the simulated fracture strength value have also not enough accuracy for designing products. The system, however, shows a form of database for composite materials in the future.

Acknowledgment.

The IDAM was developed as the joint research by Industrial Products Research Institute and Research Center of Toyo Engineering Corporation.

The authors would like to

```
## test.dat
## ***** Request condition *****
# Target laminate thickness (mm) :2.5
# Laminate thickness allowance (mm) :1.5
# Width (mm) :10.0
# Applied load (kgf) :10000.0
# Max allowable strain [X-dir] (%) :1.0
# Max allowable strain [Y-dir] (%) :0.35
# Stiffness ratio [Ey/Ex] :1.0
# Stiffness ratio [Ex/Gxy] :2.0
# Design criteria :1
# Fracture criteria :1
##
## ***** Hybrid information *****
# Hybrid[h] or non-hybrid[n] :n
##
## ***** Lamina thickness *****
# Lamina thickness (mm) :0.125
##
## ***** Constitution of laminate *****
# Total candidate number :1
##
## -----< Candidate 1 -----
# Constitution :0/45/-45/90/0/45/-45/90/0/-45/45/0/90/-45/45/0
##
## ***** Material *****
# Total candidate number :2
##
## -----< Candidate 1 -----
# Lamina id :1
# Fiber id :1
# Matrix id :2
# Lamina name :T300/#3601
# Fiber name :T300
# Matrix name :#3601
# Volume fraction :0.6
##
## -----< Candidate 2 -----
# Lamina id :2
# Fiber id :1
# Matrix id :3
# Lamina name :T300/#3620
# Fiber name :T300
# Matrix name :#3620
# Volume fraction :0.6
##
```

Fig. 4 Input conditions of test run by file

*** REQUEST DATA & CALCULATED RESULTS [1] ***

EVALUATION ITEMS	REQUESTS	CAL. RESULTS	JUDGE
LAMINATE THICKNESS(mm)	1.000 - 4.000	2.000	
WIDTH (mm)	10.00		
APPLIED LOAD (N)	10000.00		
STRAIN UNDER (α -dir) (%)	1.00	0.93	
APPLIED LOAD (γ -dir) (%)	0.35	0.32	
DESIGN CRITERIA	1.Max load		
FRACTURE CRITERIA	1.Tsai_Wu		
MAX LOAD (N) (MPa)	* 10000.0 (250.0 ~ 1000.0)	12437.0 :Stim (621.9)	
80% MAX LOAD (N) (MPa)		9949.6 :Stim (497.5)	
1st PF LOAD (N) (MPa)		6520.1 :Stim (326.0)	
1st PF PLACE (Layer)		4 :Stim	
DELAMINATION LOAD (N) (MPa)		7600.0 :Exp (380.0)	
DELAMINATION PLACE(Layer)		2 - 3 :Stim	
LAMINATE (deg)	0/ 45/-45/ 90/ 0/ 45/-45/ 90/ 90/-45/ 45/ 0/ 90/-45/ 45/ 0		
LAMINA ID	: 2/ 2/ 2/ 2/ 2/ 2/ 2/ 2/ 2/ 2/ 2/ 2/ 2/ 2/ 2		
FIBER ID	: 1/ 1/ 1/ 1/ 1/ 1/ 1/ 1/ 1/ 1/ 1/ 1/ 1/ 1/ 1		
MATRIX ID	: 3/ 3/ 3/ 3/ 3/ 3/ 3/ 3/ 3/ 3/ 3/ 3/ 3/ 3/ 3		
VOLUME FRACTION :	0.600/0.600/0.600/0.600/0.600/0.600/0.600/0.600/0.600/0.600/0.600/0.600/0.600/0.600/0.600/0.600		
LAYER THICKNESS :	0.125/0.125/0.125/0.125/0.125/0.125/0.125/0.125/0.125/0.125/0.125/0.125/0.125/0.125/0.125		
LAMINA NAME	: 2-1300/#3620		
FIBER NAME	: 1-T300		
MATRIX NAME	: 3-#3620		
LAMINATE Ex(MPa):	54790.988007		
Gc (N/mm):	(NO DATA)		

COMMENT : THIS RESULT WAS [OK-DATA]

Fig. 6 Result of test run for No.2 candidate

thank T.Fukai, Y.Shirasaka and T.Shinogaya of Toyo Engineering Corporation for their considerable help in the system development. We also would like to acknowledge the great assistance of Prof. K.Takahashi of Nagoya Institute of Technology and Director R.Hayashi of Industrial Products Research Institute.

REFERENCES

- 1)Iwata, S., "Expert Systems Interfaces for Materials Data Bases", ASTM STP 1017, 1989,175-184.
- 2)Parsaye, K. et al., "Intelligent Databases", John Wiley & Sons, Inc., 1989, 201-216.
- 3)Miki, M. et al., "Database Management System For Composite Materials", French-Japanese Seminar on Composite Materials: Preceding, Use and Database, 1990.
- 4)Yoshioka, M. et al., "Development of a New Access Methods for Factual Database of Composite Materials (in Japanese)", Sen-i Gakkai Preprints, 1989, S-99.
- 5)Date, C. J., "A guide to the SQL standard", Addison-Wesley Publishing Company Inc., 1987, 1-6
- 6)Takahashi, K. et al., "Composite Structures", 2 (1984), 91-104.
- 7)Soni, S. R., "A Comparative Study of Failure Envelopes in Composite Laminas", Journal of Reinforced Plastics and Composites, 2(1983), 34-42.
- 8)O'Brien, T. K., "Characterization of Delamination Onset and Growth in a Composite Laminate", ASTM STP 775, 1982, 140-167.

Data Format, Structure and Transfer for Material Databases

by Eric JULLIARD
Association Française de Normalisation
(AFNOR)

1 - Introduction

The growing use of computer techniques need a growing amount of computerized information.

The basic elements to be taken into consideration to ensure a proper use of this information are :

the software tools needed to generate the basic information under a computer-readable form, transforming information into 'data',

the software applications to process these data.

1.1 - generation of data

Two major problems occur here :

a huge amount of information available only under paper form,
which has to be reconsidered for being properly computerized :

- .too much paper
- .not so well adapted to computerization

a number of software tools already existing, used independently to generate data with specific data models and data formats, which are not compatible to each other :

- .many 'computerization islands'
- .no compatibility

The paradox is that, on one hand, there is a great lack of computerized information and, on the other hand, there is no consistency in the generation of data, leading to duplication of work, redundancies and, finally, depreciation of the quality of final data within the information system.

1.2 – processing of data

The increasing number of data processing systems and software applications running independently and using specific data formats prevent from using and exchanging data from one application to an other.

The result is that it is necessary to create many times the same data elements.

1.3 – what is the issue ?

To enable the description, storage and exchange of data so that they can be used on many systems within many applications, it is necessary to define :

- .a neutral data model,
- .neutral data formats,
- .a neutral data structure,
- .a neutral exchange format.

from basic concepts defining :

- .the objects to describe in the database,
- .the use and processing of relating data.

A set of specifications has been established in 1988/1989 within the French standardization as a contribution to European standardization to deal with that problem.

This presentation is intended to present these specifications (Z99 standards).

2 – A neutral data model

2.1 – basic requirements

The Z99 specifications have been initially established to define the working methods and programming principles to describe, enter, store and distribute data relating to industrial components on magnetic media, under a neutral digital form.

These data are then to be integrated in all data processing applications for which they are required.

The very first software applications for which the Z99 specifications have been established are Computer Aided Design applications (CAD systems).

However, experience showed that they could be used not only for CAD, but also for other applications involving similar description of industrial components, such as Purchase or Maintenance.

Moreover, it has been stated that, a component being described through a set of characteristics, the Z99 description could be used to describe, in the same manner, data relating to materials.

Thus, a material is considered as a component and the same kind of description applies to it.

2.2 - basic concepts

The library defined within the Z99 specifications is :

multisectorial

the objects described in the library can belong to the Mecanical Industry (such as nuts, bearings, steel bars, etc.), the Electronics Industry (such as condensators, electronic cards, electrical motors, etc.) or the Civil Engineering and Building Construction Industry (such as windows, sand, concrete, etc.).

multisource

the description of the objects in one given library can come from National or International standards, industrial catalogues or even company standards

multisupplier

the information relating to the objects described in a given library can come from various sources, such as different vendors, standardization institutions, or even such or such internal department of a given company

multiapplication

the library should be able to run on different applications, either CAD or other applications

2.3 - basic principles

The 4 basic principles applying to data in a Z99 library are :

unicity

one given data relating to one given object shall be entered in the library only once by the data supplier owning this data.

No specific rule is given in Z99 about the way to do it, but the storage data structure allow such a rule to be implemented.

traceability

each data in the library shall be referred to the data supplier who has entered this data in the library.

This is achieved by giving each data supplier an identification number which is a prefix to all data.

This identification number is delivered at a Company level (one company = one identification number).

quality

each data supplier has to define a suitable quality control system to ensure that the data entered in the library are in conformance with the original data.

The choice of the system belongs to the data supplier himself.

integrity

for each library of a given supplier, a 'signature' is generated from the corresponding data.

The user can check this signature when he gets the library from this supplier to ensure that there has been no alteration of the data

2.4 – the data model

2.4.1 – the data structure description

The main point about the Z99 model is that the data structure is described independently of the data themselves.

The data structure description only explains how the data are organized.

Thus, the data and the structure are independent.

2.4.1.1 – object -> reference document

The object (component or material) it is intended to describe in the library is defined through the declaration of the characteristics (parameters) relating to it as they appear in a reference document.

This document may be a standard, an industrial catalogue, or even a company standard.

It may be available under a paper form, but could be under a digital form.

The main point is that the document in question is the REFERENCE document, which means that the only true information is in that specific document (or file) and that this document (or file) will be used as the only reference in case of problem.

2.4.1.2 – reference document -> data sets

A reference document is composed of data sets.

A data set is defined as a logical element, having some coherent properties, in which the characteristics (parameters) attached to the described object are organized of a specific manner.

The kind of information relating to the described object depends on the data set type :

data set type : table

the parameters are organized in lines and columns, the head of the columns being the names of the parameters, each line being a set of values (numerical or other).

data set type : view

a 'view' type data set is an extract or junction of other data sets of 'table' type.

This is useful to create a virtual table, which does not exist physically, by joining tables by a reference constraint using one or more of their common attributes.

data set type : image

the parameters are presented for information in an image (for example in a pixel file) as an illustration to provide the user with a visual help.

data set type : algorithm

the value of one parameter is calculated from values of other parameters (stored in the library or keyed-in when required) through an algorithm.

data set type : text

the parameters are located in a text.

This text may include a simple naming of the parameters or even definitions, etc.

2.4.2 – the data

Each data set comprises a number of parameters.

The way the parameters are organized depends upon the data set type.

However, for each data set entered in the library, a file or table is created containing the corresponding data.

This file or table may be inside or outside the library.

The name of this file or table is the name of the data set as declared in the data structure description.

3 – Neutral data format and structure

The neutral format defined by the Z99 specifications is based on a relational data model.

It is in strict conformance with the ISO 9075 standard defining the SQL query language.

Many Database Management Systems (DBMS) available on the market are conforming to this standard.

It is to be noticed that the format defined within Z99 is a storage format, and may not necessarily be the final operation format, even if this format may be suitable for some applications.

3.1 – overall architecture

All the data within the Z99 library itself are stored in relational tables described according to ISO 9075.

There are 3 kinds of tables :

3.1.1 – general tables

These tables are used for :

- .the data suppliers identification (SI),
- .the data suppliers locations (SA).

As Z99 defines a multisupplier library, data from several data suppliers may be included in one given library.

The general tables are used to register the data suppliers whose data are in the library.

3.1.2 – structure tables

These tables are used by each data supplier to :

- .define a general classification (domains, or 'fields'),
- .define, for each field, the reference documents which are registered,
- .describe, for each document, the data sets,
- .describe, for each data set, the parameters concerned,
- .define, for each field, the objects described in the documents,
- .describe, for each object, the relevant parameters,
- .describe, for each object, the identifier of this object,
- .describe, for each object, inheritance mechanism if relevant.

3.1.3 – data

3.1.3.1 – data tables

All the data belonging to 'table' type data sets are stored, within the library itself, in relational tables.

For each data set of 'table' type, a data table is created.

The name of this data table is the name of the data set it refers.

3.1.3.2 – view-definition tables

The data defined in a 'view' type data set are described through a relational view, which specifies a combination or a junction of existing data tables.

Such a relational view has to be expressed within the library, using the SQL syntax.

This is done through a view-definition table, in which the SQL statement 'create VIEW as select...' is stored as an ASCII text.

The name of the relational view defined in this view-definition table is the name of the data set it refers.

The name of the view-definition table itself is the same as the data set, except the first character, replaced by 'V'.

3.1.3.3 – data files

The data relating to other data sets than tables or views are stored in external files, using given formats.

So can be stored :

- .images, in **pixel files** using various formats,
- .text, in **text files** like ASCII files,
- .algorithms.

4 – Neutral exchange format

It is not sufficient to have a neutral data model enabling the description of various models of objects without having rules to enable the exchange of data relating to such models.

The Z99 specifications define a neutral exchange format, so that the data structures and data can be exported from the Z99 library to be integrated in various applications.

All the data are exported in ASCII or EBCDIC files.

As the Z99 specifications define a meta-library, three types of exchange files can be defined :

4.1 1 – library definition file

This file contains the definition of the library.

This definition consists of the list of the tables, fields and formats defined within the Z99 specifications.

The corresponding data are tabulated in the file using the following :

TABLE_NAME	FIELD_NAME	FIELD_FORMAT
------------	------------	--------------

4.2 – data structure files

For each structure table defined within the Z99 specifications, a file is created, containing the tabulated data describing the structure of the data themselves.

As an example, the file for RD (reference document table) is the following :

SCY	SCO	DC	RDDC	LC	RDTI	RDTD	RDTs	RDRL
-----	-----	----	------	----	------	------	------	------

4.3 – data files

Depending upon the data set types, the data files are even exported with their own formats (in the case of external files), or as tabulated files ('table' and 'view' types data sets).

When they are exported as tabulated files, the same as before applies :

Data set number : S1234567

17	0,6	2	0,8	0,05
37	0,6	2	0,8	0,05
..

4.4 - Import

Importing these files, it is necessary to :

- .generate the tables by interpreting the 'library definition file',
- .fill the data structure tables with the corresponding export files,
- .create the data and view-definition tables from the data structure,
- .fill the data tables with the corresponding export files.

5 - Conclusion

A material being considered as a component, the description would be the following :

- .the material is referred in a reference document
- .this material is identified through a designation,
- .this material has characteristics (parameters), like dimensions, physical or chemical properties, etc.,
- .some characteristics may refer a test method defined in some other reference document,
- .these characteristics have values,
- .etc.

Thus, the Z99 specifications enable a neutral description, storage and exchange of the relevant data.

Z 99-001

SUPPLIER
Field

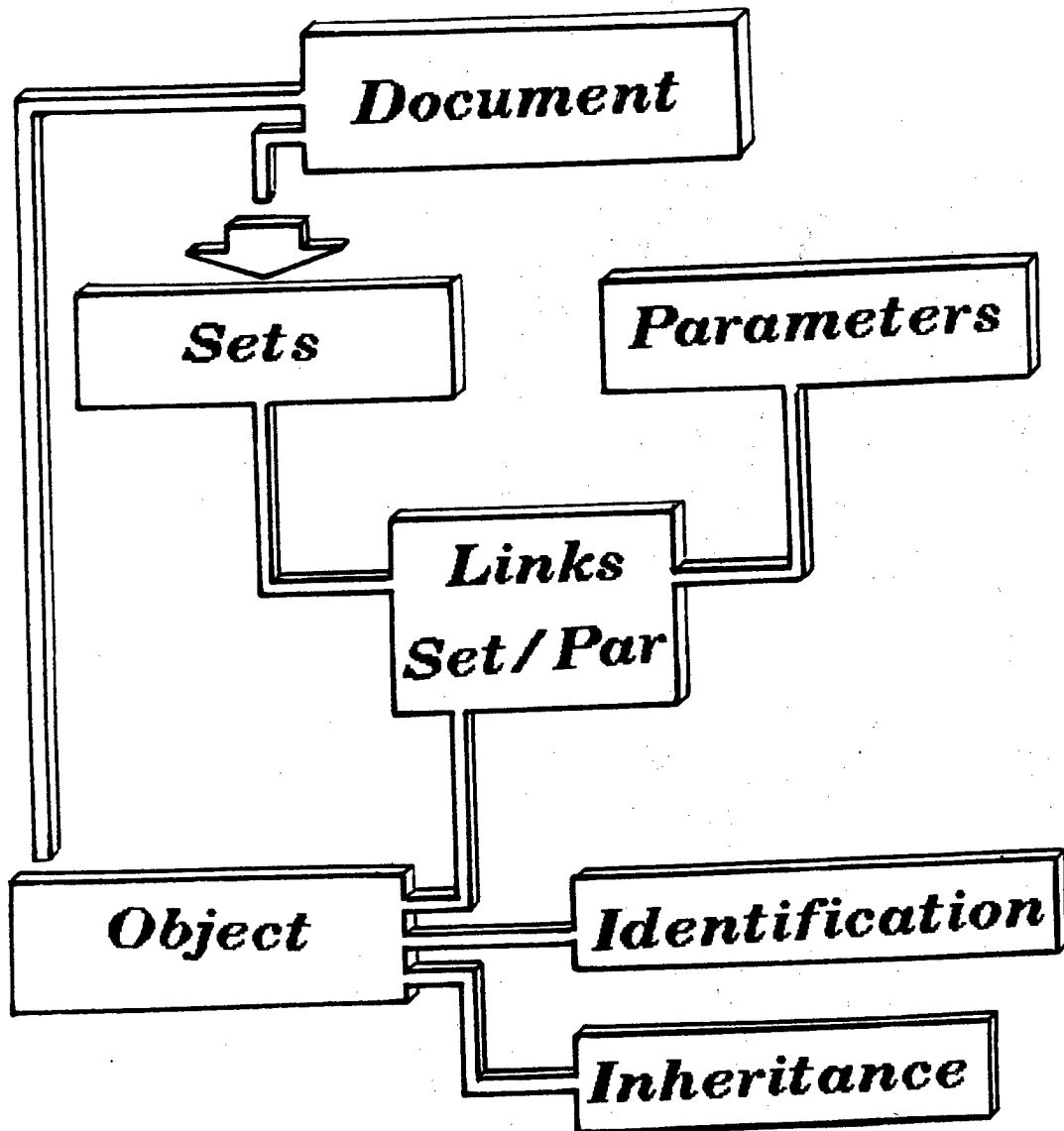
DOCUMENT

DATA SETS

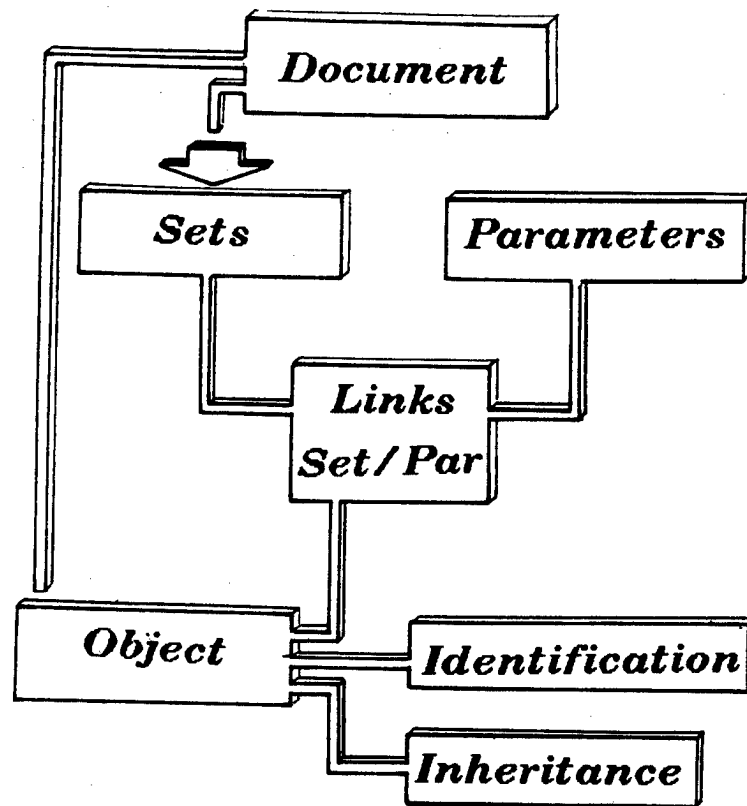
PARAMETERS

TECHNOLOGICAL NODES
Inheritance
Identification

***Country
Supplier
Field***



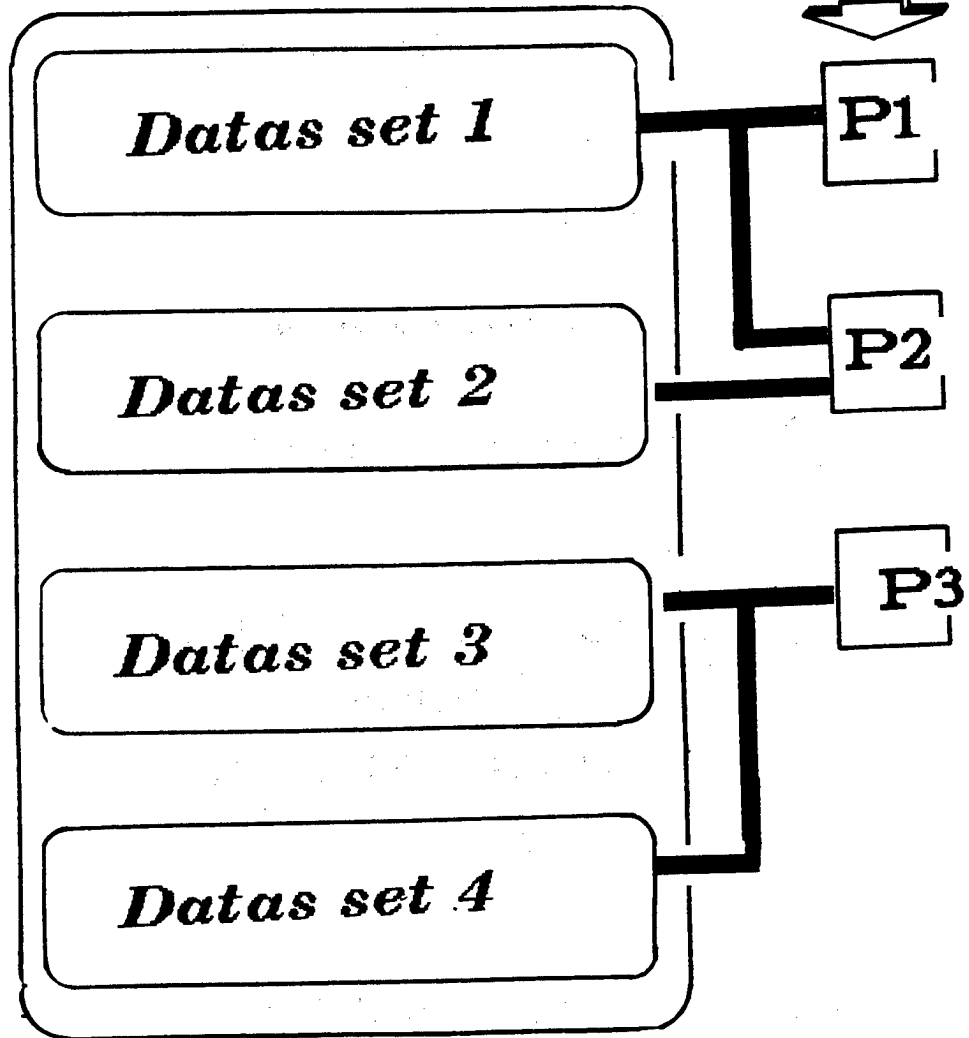
*Country
Supplier
Field*



DOCUMENT



Parameters



- DATA -

Tables (3 types)

⇒ **Suppliers tables**

⇒ **Structures tables**
Fields
Document view
Object view

⇒ **Data tables**

- DATA - Typology

5 types



Text (X)



Parameters table (T)



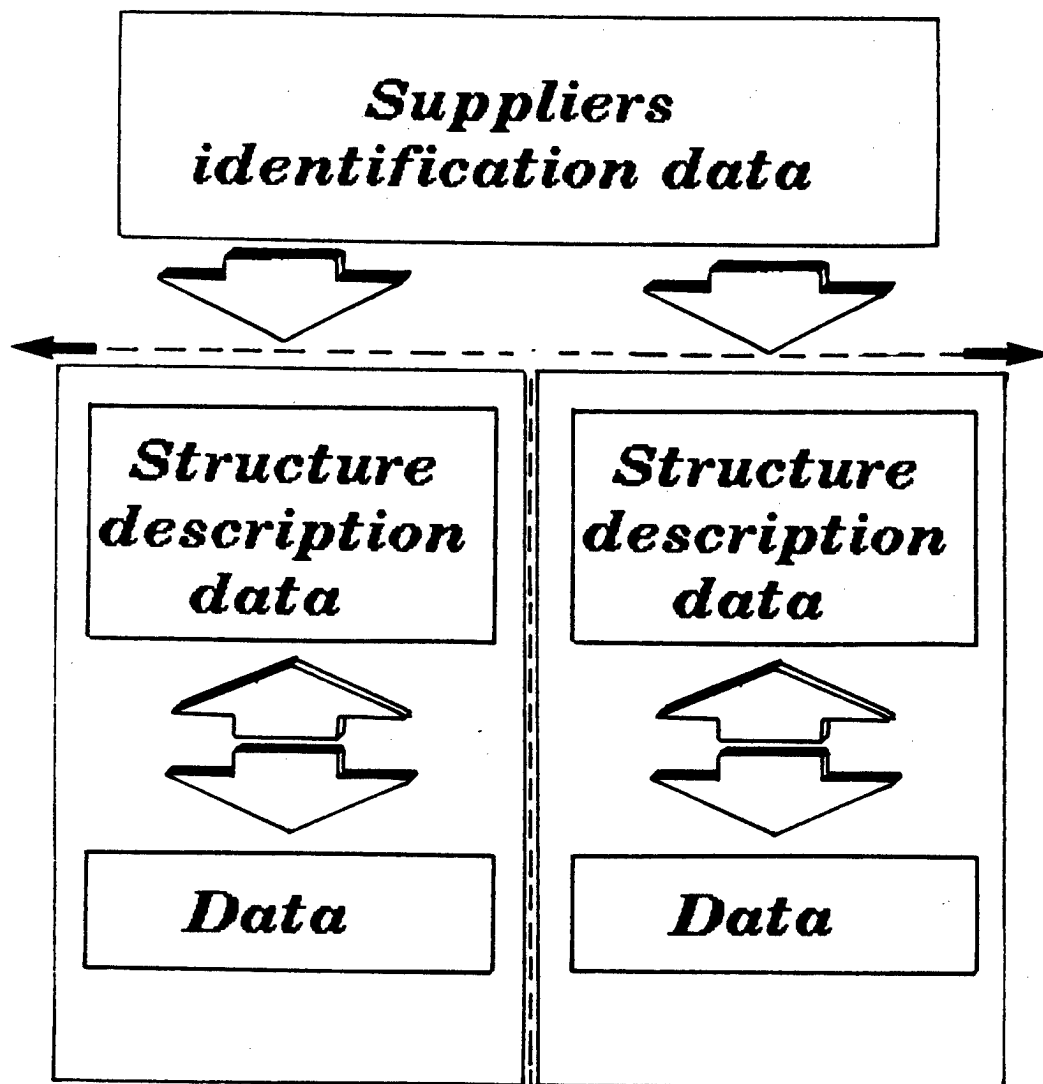
Image (I)



View (V)



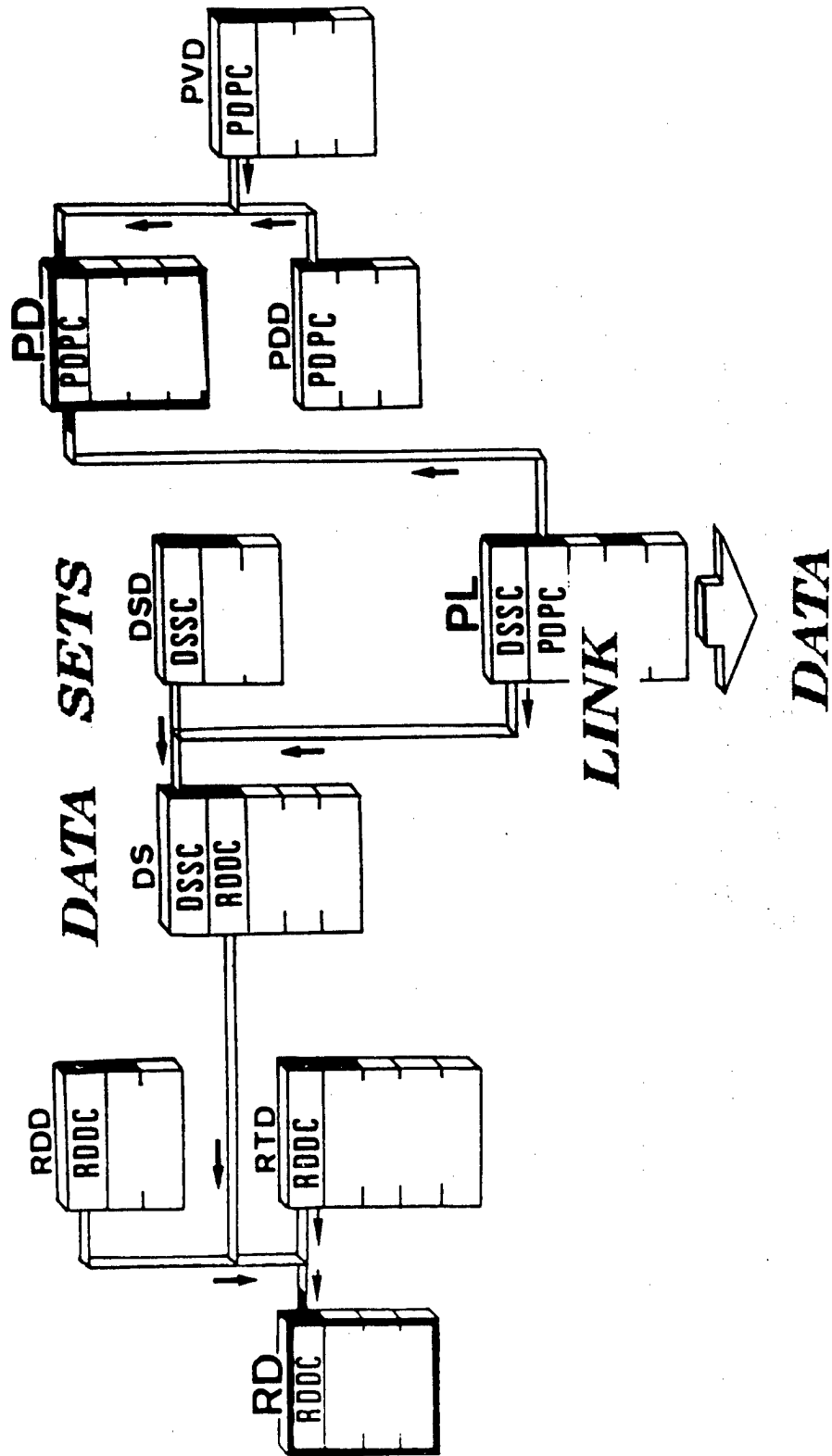
Algorithm (A)



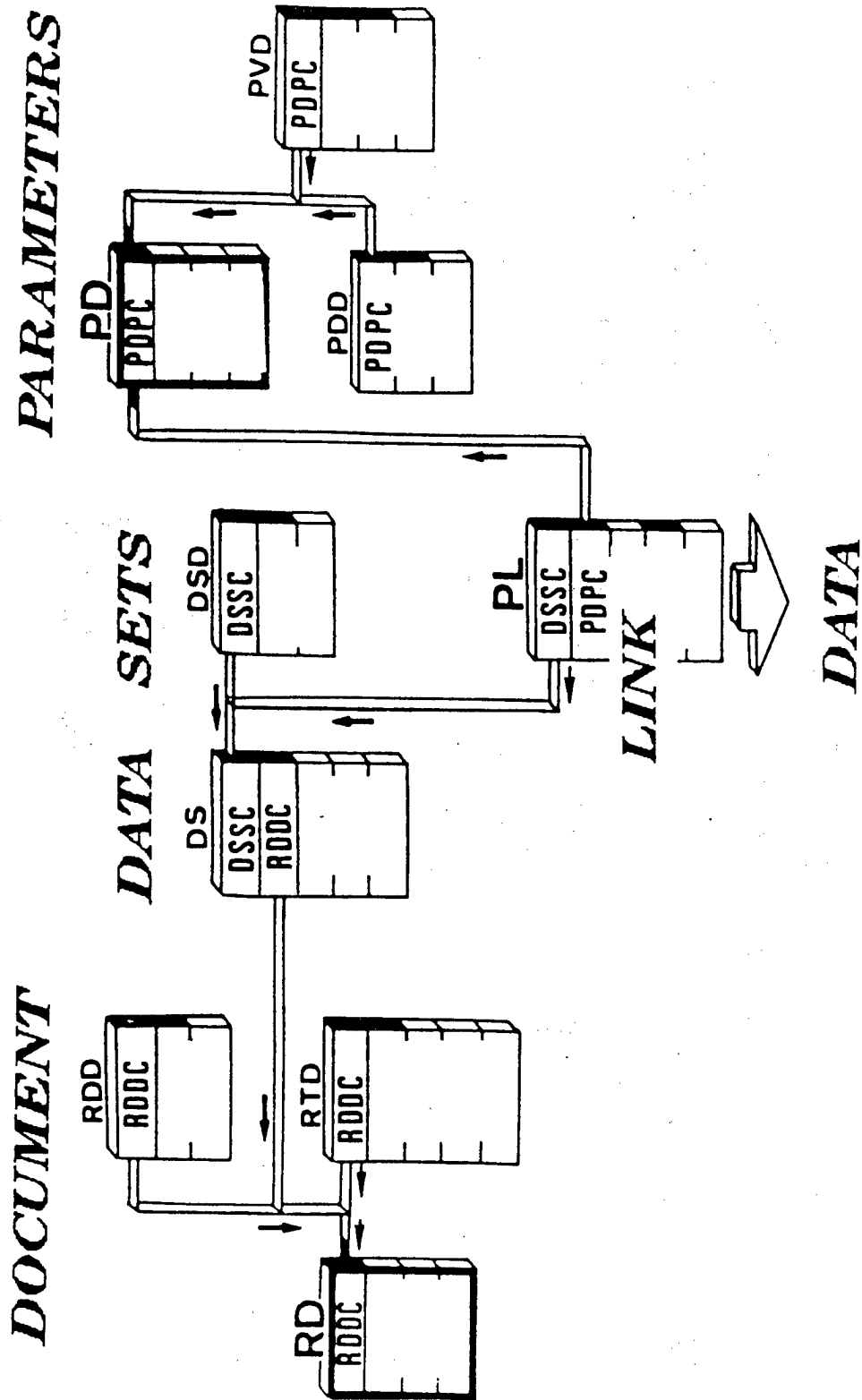
DOCUMENT VIEW

PARAMETERS

DOCUMENT



DOCUMENT VIEW



DATA TRANSFER

***''Character'' file form
(ASCII or EBCDIC)***

-» T1

***Data base
tables definition datas***

-» T2

Structure definition

-» T3

Data

Tables definition

	<u>RD . EXP</u>	
RD	DC	CHAR(3)
RD	RDDC	CHAR(9)
RD	RDDD	CHAR(8)
RD	RDDI	CHAR(80)
RD	RDDS	CHAR(6)
RD	RDRL	NUMBER(1)
RD	SCO	CHAR(4)
RD	SCY	CHAR(2)

	<u>DS . EXP</u>	
DS	DC	CHAR(3)
DS	DSDR	CHAR(80)
DS	DSSC	CHAR(9)
DS	DSSD	CHAR(1)
DS	DSST	CHAR(1)
DS	RDDC	CHAR(9)
DS	SCO	CHAR(4)
DS	SCY	CHAR(2)

Neutral format

Structure tables data

RD.DAT

FR A001 E22 DFA012338 E22315
19780601 ENR 1

FR A001 01A DFA018315 E25107
19830601 ENR 1

FR A001 01A DFA030024 E25401
19830901 ENR 1

DS.DAT

S00000143 DFA030024 0100/001
X FR A001 01A

S00000079 DFA012338 0300/001
X FR A001 E22

S00000080 DFA012338 0400/001
X FR A001 E22


S00000081 DFA012338 0500/002/1
X FR A001 E22

S00000082 DFA012338 0600/002/2
I FR A001 E22

➡ S00000083 DFA012338 0700/003/3.1
T FR A001 E22

Structure tables data

Links table

 S00000083 P00330000 d	IX	FR A001 E22 mm NUMBER(5,2)	2
S00000083 P00410000 D		FR A001 E22 mm NUMBER(5,2)	3
S00000083 P00850000 B		FR A001 E22 mm NUMBER(3,1)	4
S00000083 P00360002 rsmin		FR A001 E22 mm NUMBER(5,2)	5
S00000083 P00380000 Série	IX	FR A001 E22 CHAR(5)	1

Neutral format

Data

<u>S0000083.DAT</u>				
17	0,6	2	0,8	0,05
37	0,6	2	0,8	0,05
17	1	2,5	1	0,05
37	1	2,5	1	0,05
17	1,5	3	1	0,05
37	1,5	3	1,8	0,05
17	2	4	1,2	0,05
37	2	4	2	0,05
17	2,5	5	1,5	0,08
37	2,5	5	2,3	0,08
17	3	6	2	0,08
37	3	6	3	0,08
17	4	7	2	0,08
37	4	7	3	0,08
17	5	8	2	0,08
37	5	8	3	0,08
17	6	10	2,5	0,1
37	6	10	3,5	0,1
17	7	11	2,5	0,1
37	7	11	3,5	0,1
17	8	12	2,5	0,1
37	8	12	3,5	0,1
17	9	14	3	0,1
37	9	14	4,5	0,1
17	10	15	3	0,1
37	10	15	4,5	0,1

**Development
of
Fatigue Strength Design Support System**

Toshio Shuto, Takamasa Ochiai
Engineering Systems Section, Knowledge Systems Department
Mitsubishi Research Institute, Inc.
3-6, Otemachi 2-chome, Chiyoda-ku, Tokyo 100, Japan

ABSTRACT

Fatigue strength design not only requires advanced technology but also necessitates broad scope of expertise in the relationship of fatigue data and analysis area with products, etc. The objective of this system is to use computer and support the process of fatigue strength design of structure. The area of design to be supported by this system includes: high cycle fatigue design, low cycle fatigue design, crack growth analysis and fatigue design for welded joint. This paper describes the design concept and capabilities of this system.

1. INTRODUCTION

Functions computer system should have for supporting mechanical engineer in his design work would be summarized as follows:

- 1) CAD/CAM system
- 2) Simulation of mechanical behavior
- 3) Database system for mechanical design

Among these three, a number of systems have been developed for 1) and 2), and we can find excellent ones on the market. But concerning 3), there has been so far developed few systems which fit for use.

To see the application fields of mechanical design support system, on the other hand, they are structural static characteristics and structural dynamic characteristics. The applications have proven to be successful, but systems which can support fatigue strength design of mechanical structure is still very few.

Fatigue strength design not only requires advanced technology but also necessitates expertise in broad range. Consequently, most mechanical engineers have carried out a rough design about fatigue strength and supplemented it with the enough allowance for safety rate or left the strength design to the so-called 'strength specialist'.

Under these circumstances, a system has been developed for helping design work by combining fatigue strength database and the expertise in strength design. The overview and design concept of the system are described as follows.

2. OVERVIEW OF THE SYSTEM

The system has the following capabilities to support design work of which process requires consideration of fatigue characteristics.

2.1 Database Retrieval Function

This is the function to figure out fatigue limit, fatigue strength at N cycles, etc. through S-N curve based on the database of the experimental data of materials. The database is further broken down into three databases, ie., database on fatigue strength of metallic material and database on fatigue crack growth rates of metallic material, both developed by the Society of Materials Science, Japan (JSMS), and database on low cycle fatigue strength of metallic material, which was developed at our institute. The last one was developed with particular reference to the "JSME Data Book: Fatigue of Metals IV, Low Cycle Fatigue Strength" of the Japan Society of Mechanical Engineers (JSME), and designed to the maximum possible extent to be equivalent to the basic data format of the databases of JSMS.

The following updates are made on the version 2 of the system:

- Information in the data sheet of National Research Institute for Metals (NRIM) is added to make fact data more substantial.
- Number of retrievals and numerical range is tabulated by retrieval item to make re-retrieval more efficient.
- The function to register the coefficient of S-N curve is added for materials frequently used.

Figures 1 and 2 represent database retrieval menu and display of retrieval results.

Mathematical model for S-N curve. The following 2 methods are adopted as mathematical model for S-N curve, following the proposition by Nishijima, et al.

(1) By-linear curve (applied to materials of which fatigue limit is existent). To decide the straight line of ramp by principal component analysis method first, and then, using the estimated standard deviation of fatigue strength obtained as a result, to decide the height of the horizontal straight line by probit analysis. The formula of S-N curve is thus given as follows:

$$Y = (A/2) \{ |X-D| - (X-D) \} + E \quad (1)$$

In short, S-N data is summarized as the three parameters, ie., slope of ramp, crimp point D, and the height of horizontal line E.

(2) Application to the materials of which fatigue limit is not existent. The probit analysis using weighing coefficients is adopted with the assumption that dispersion is not dependent on number of cycles, but it appears as normal distribution. Average S-N characteristic and dispersion level are statistically estimated, and skew hyperbola with sloped straight line and horizontal line as asymptote is adopted as a mathematical model for S-N curve in this case.

$$(Y-E)(Y+AX-D)=C \quad (2)$$

2.2 Fatigue Strength Design/Analysis/Evaluation Function

Basic function for fatigue strength design/analysis and materials to be designed/analyzed by this system are shown in Figure 3. Materials to be designed and analyzed are observed in three aspects, ie., structure, material, and external force. In other words, in terms of structure, a material is observed if it has a simple shape with well-defined stress distribution pattern or not, in terms of material, if it has well-defined fatigue limit like steel or not, and in terms of external force, if its external force is constant load or variable load. Materials are observed in the combination of these aspects in design and analysis.

2.3 Expert System

Fatigue strength design is a field not theoretically well organized yet. In such field, know-how and expertise are regarded as more important. For example, there are certainly a number of methods to describe the process of crack growth, but the most important thing is how we use these methods properly according to the characteristics and shape of material. This system has succeeded in representing these know-hows and expertise as production rule so that the optimal design/analysis will be easily done. Nine knowledge bases are available for inference now.

2.4 User Interface and Structure of the System

As aforementioned, this system has three different functions. However, in the process of actual fatigue design, we not only use fatigue experimental data, but also requires various analytical algorithms and expertise in all. In order to effectively use the capabilities of the system under this circumstance, and to assist user with the information appropriate for his level and purpose, the system operates on UNIX-based engineering workstation, using multi-window.

To realize the easy use of users, the display of the system is divided into two phases and five types and each division is allocated to a certain function. The emphasis is also put on the modularization to enhance productivity. The outline of the structure of the system is shown in Figure 3.

3. ENDING REMARKS

The objective of this system is to assist mechanical engineer in fatigue strength design of mechanical structure so that he can select optimal material. The system offers various capabilities, but there still remain problems. Some of the problems are as follows:

- 1) Strengthening database. To increase fact data by adding public data of welded joint, creep, etc.
- 2) Improvement of user interface. To make user interface more interactive and responsive, figures and icon should be used as a control. The database registration process should be interactive.

We are working on these problems to make the system better.

REFERENCES

- (1) Shuto, T., "Development of Expert System for Selecting Mechanical Material", The 11th Seminar of Soc. Mat. Sci., Japan, 1988.
- (2) Nishijima, S., "Statistical Analysis of the Small Sample of Fatigue Data", Vol. 46, No. 412, pp.1303-
- (3) Nishijima, S., "Statistical Analysis of Fatigue Test Data", J. Soc. Mat. Sci., Japan, Vol. 29, No. 316.
- (4) Ochiai, T., "Database for Fatigue Strength Design", The 175th Seminar of JSMS, 1990, pp.63-72.

設定項目	単位	設定値
1. 提供コード		JIS SNCM439
2. 材料名		
3. 厚さ		
4. 長さ		
5. 引張力	Kg/mm ²	
6. 引張力強さ	Kg/mm ²	
7. 伸び	%	
8. 絞り	%	
9. 衝撃試験		
10. 衝撃試験片形状		
11. 衝撃吸収エネルギー	Kg ^{1/2} m	
12. 応力集中係数		1.00
13. 試験片形状		
14. 試験片寸法 (幅/厚さ)	mm	
15. 試験片寸法 (長さ/直径)	mm	
16. 測定形式		RB (回転曲げ (均一))
17. 実験開始—実験終了		
18. 試験データ数		
19. 応力条件	MPa	M (平均応力一定)
20. 応力比または応力		0.50
21. 試験温度	deg	20.00
22. 試験雰囲気		

(キャンセル) (実行)

Stress vs. Time

Evaluate

Equivalent Stress vs. Time

詳細な検索情報を表示しますか?

Figure 1. Sample Database Retrieval Menu

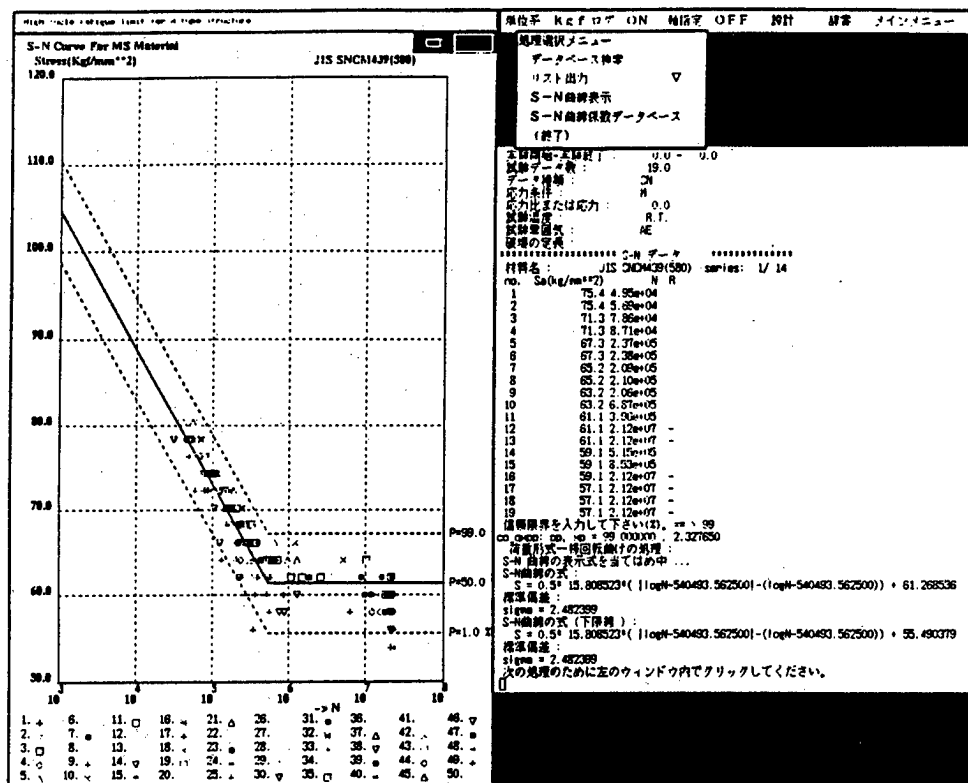


Figure 2. Sample Display of Database Retrieval Results

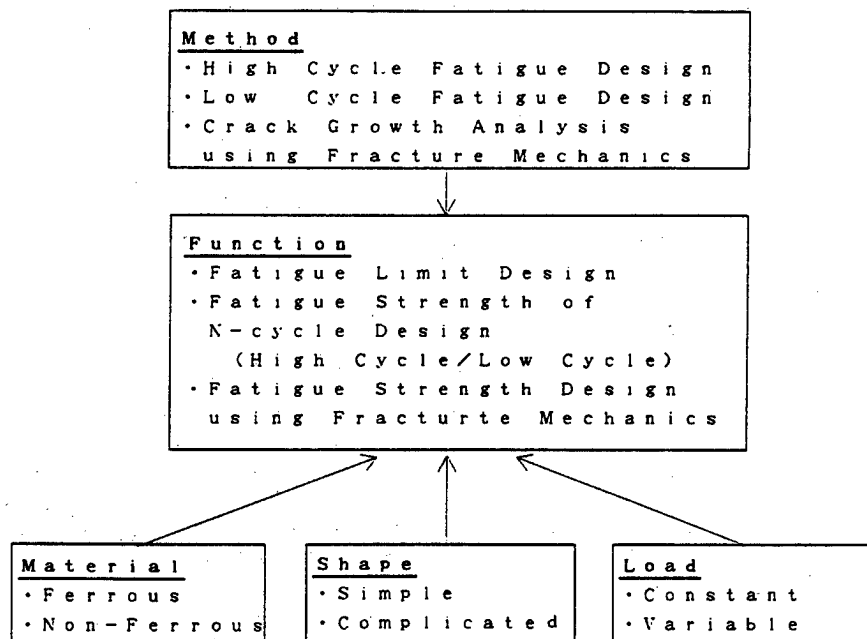


Figure 3. Basic Capabilities of This System

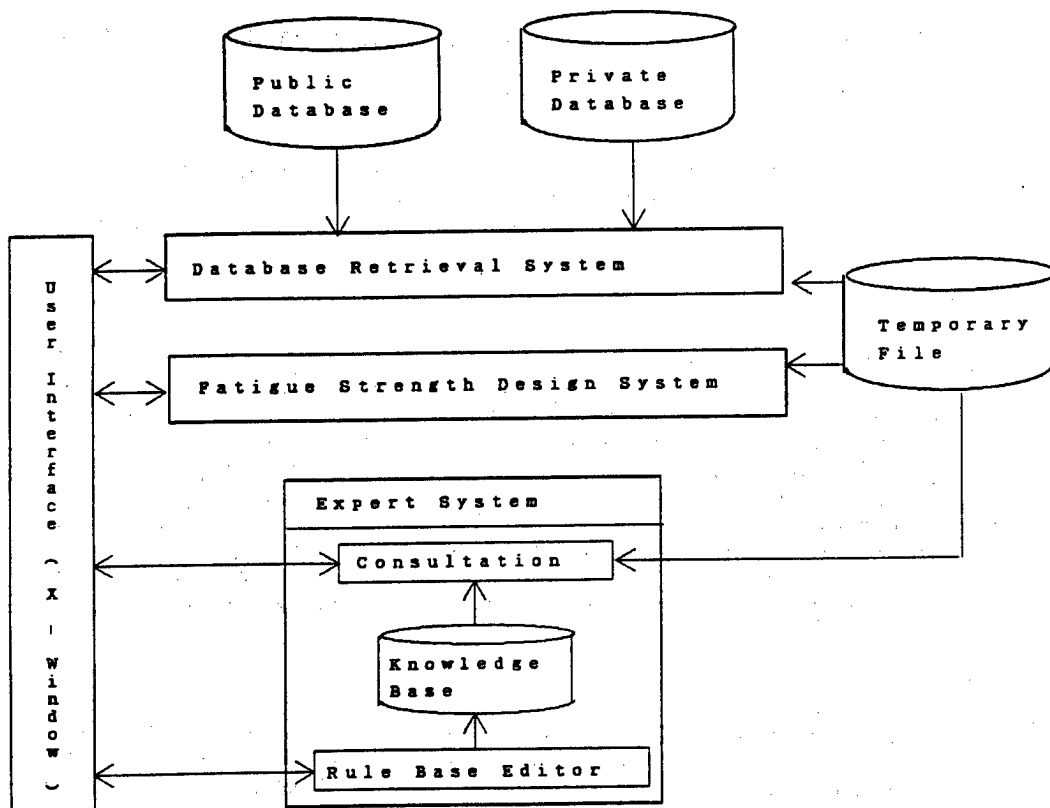


Figure 4. Structure of the System

JICST/NRIM Materials Database for Engineering Steels and Alloys

Y.Monma*, K.Kanazawa*, M.Sakamoto*, S.Nishijima*,
K.Suzuki**, and K.Simura**

*National Research Institute for Metals (NRIM)
Meguro-ku, Tokyo 153, Japan

**Japan Information Center of Science and Technology (JICST)
Chiyoda-ku, Tokyo 100, Japan

ABSTRACT

A comprehensive database for materials strength of engineering steels and alloys has been developed under a joint research between NRIM and JICST. The nucleus data was taken from NRIM's Creep and Fatigue Data Sheet Program. The user via public telephone network can issue query commands to search tensile, creep and fatigue data of 60+ steel and alloys. The retrieved data can be statistically analyzed, and the regression curves together with the raw data plots are output on the user's graphic display. Six types of graphs corresponding tensile, creep-rupture, high-cycle fatigue, low-cycle fatigue, fatigue crack growth and cyclic stress-strain diagrams are available. The database has been put into the public on-line service of JICST's JOIS-F since March 1990.

INTRODUCTION

With the development of computer technology, a number of materials databases have been built in many countries. Particularly databases for metallic materials are flourishing[1-3]. The materials database is regarded as one of key technologies for the advanced CAD/CAM/CAE applications. It also has become of major interest for the search of new materials. The NRIM has conducted comprehensive testing programs of creep and fatigue; NRIM Creep Data Sheet (CDS) and Fatigue Data Sheet (FDS). The JICST has been responsible for the public on-line service of factual database for science and technology. In view of this situation, NRIM and JICST signed for the collaboration to develop a materials database for engineering steel and alloys. This paper describes the metadata, query commands, report formats, and the data analysis of database. The database operates on a mainframe computer in JICST, and has accessibility through the public telephone network in Japan. The database management system used is ADABAS.

DATA SOURCE

The nucleus data collected for the database is NRIM Creep and Fatigue Data Sheets, which has been obtained by the long-term testing program at NRIM and published so far as the NRIM Creep and Fatigue Data Sheet series. The NRIM data contains 3,000 test points for elevated-temperature tensile, 9,000 test points for creep-rupture (accumulated rupture times is 1.2×10^8 h), and 35,000 test points for high-cycle fatigue (accumulated cycles to failure is 5×10^{11}) for more than 60 steels and alloys. It also includes about 100 data points ruptured beyond 100,000h.

METADATA

Prior to the system design of the database, we conducted a survey for the potential users. With regards to the purpose of materials strength database, the following four areas were identified:

- 1) Design analysis of structural components
- 2) New materials development
- 3) Residual life prediction
- 4) Strength analysis to comply with the rule

It was considered that a comprehensive metadata is needed in order to cover the user needs. As listed in Table 1, more than 200 record items were chosen for the metadata. The quantity of test data is summarized in Table 2.

Table 1. Summary of Metadata

Category	No. of Items	Example of Record Items
Material Source	72	Standard Code, Material Name, melting Process, Deoxidation Product Form, Nonmetallic Inclusion, Chemical Composition, Room Temp. Strength, Data Source, Year,...,etc.
Welding	23	Welding Method, Welding Position, Reinforcement, Joint Shape, Groove Design, PWHT, ...,etc.
Tensile	20	Machine Type, Specimen Sampling, Specimen Shape, Environment, Test Temp., Strain Rate, Yield Strength, Tensile Strength, Elongation, Reduction of Area,...,etc.
Creep	24	Machine Type, Specimen Sampling, Environment, Test Temp., Stress, Time to Rupture, Rupture Elongation,...,etc.
Fatigue	65	Test Type, Machine Type, Specimen Sampling, Specimen Shape, Stress Concentration Factor, Test Environment, Test Temp., Stress Ratio, Stress Amplitude, No. of Cycles to Failure, Strain Wave Form, Strain Amplitude, Crack Length, Crack Growth Rate, Stress Intensity Factor,...,etc.

Table 2. Summary of Data Size

Test Mode	No. of Heats	No. of Data Sets	No. of Data Points
Tensile	274	274	2,712
Creep-Rupture	273	273	5,722
High-Cycle Fatigue	524	964	16,223
Low-Cycle Fatigue	37	81	466
Fatigue Crack Growth	37	48	4,399
Cyclic Stress-Strain	34	102	1,247
Total	1,179	1,742	30,769

QUERY COMMANDS[4]

A wide variety of query commands is available. The query allows flexible commands such as the right-truncated as well as full-spell search, range search. The logical operations adds further flexibility to the query commands. For the user friendliness the history and help are provided. Tagged keywords are provided for the search of processing and testing conditions.

DATA ANALYSIS

On-line data analysis is available for the following 6 materials property data.

1) Elevated-temperature tensile strength:

Polynomial regression of temperature for logarithmic strength

$$\log(St) = A_0 + A_1T + A_2T^2 + \dots + A_kT^k \quad (k \leq 5)$$

where St = yield strength or ultimate tensile strength (MPa),
 T = temperature (deg C)

2) Creep-rupture times:

Manson-Haferd parameter method with optimized parameter constants.

$$\log(tR) = (T_k - B_1)(A_0 + A_1X + A_2X^2 + \dots + A_kX^k) + B_2 \quad (k \leq 5)$$

where tR = time to rupture (h), T_k = temperature (K), $X = \log(S)$,
 S = stress (MPa), others ($B_1, B_2, A_0, A_1, A_2, \dots, A_k$) are determined to produce smallest sum of residuals.

3) High-cycle fatigue life:

Bilinear (simultaneous) regression analysis.

$$\log(Sa) = (A/2)\{|\log(Nf) - D| - (\log(Nf) - D)\} + E$$

where Sa = stress amplitude (MPa), Nf = number of cycles to failure,
 $E = \log(Sw)$, $A = -M_0$ (slope), $D = \log(Nw)$, Sw = endurance limit (MPa),
 Nw = minimum Nf at Sw .

4) Low-cycle fatigue life:

$$\log(Ee) = K_e \log(Nf) + \log(Ce), \log(Ep) = K_p \log(Nf) + \log(Cp), E = Ee + Ep$$

where Ee = elastic strain (%), Nf = number of cycles to failure,
 Ep = plastic strain (%), and Ee and Ep are constants.

5) Fatigue crack growth rate:

Log-log linear and asymptotic to delta-K threshold by weighting.

$$(dA/dN) = C_0 \cdot (DK^{M_0} - DK_{th}^{M_0})$$

where da/dN = fatigue crack growth rate (m/cycle), DK = range of stress intensity factor, DK_{th} = threshold of DK , and C_0 and M_0 are constants.

6) Cyclic stress-strain curve:

$$\log(St) = Mp \cdot \log(Ep) + \log(Cp), \log(St) = Mt \cdot \log(Et) + \log(Ct)$$

where St = stress (MPa), Ep = plastic strain range (%),
and Et = total strain range (%).

It should be noted here that only one model for each property was implemented for first phase of system design. The evaluation models were chosen on the basis of the experience in NIRM[5].

GRAPHICS

The system can send graphical image data to the user terminal. A terminal with Tektronix 401X graphics emulator is required to draw diagrams on the display. The retrieved data can be plotted with or without the regression curves. A special command ($\%FIT$) is used to invoke the data evaluation module. Figures 1-4 are typical examples of data analysis.

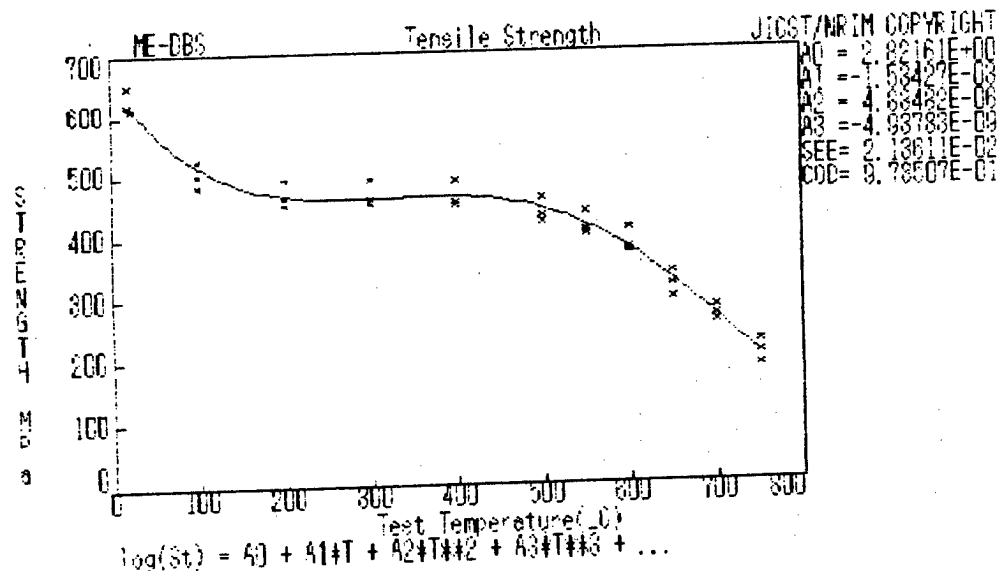


Fig.1. Example of data evaluation of tensile strength for SUS304H steel.

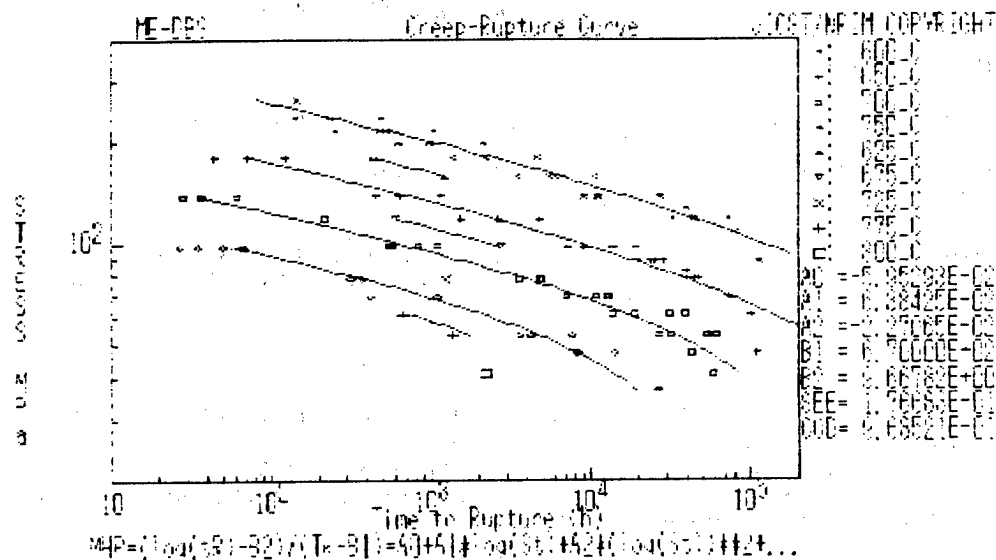


Fig.2. Example of data evaluation of creep-rupture for SUS304H steel.

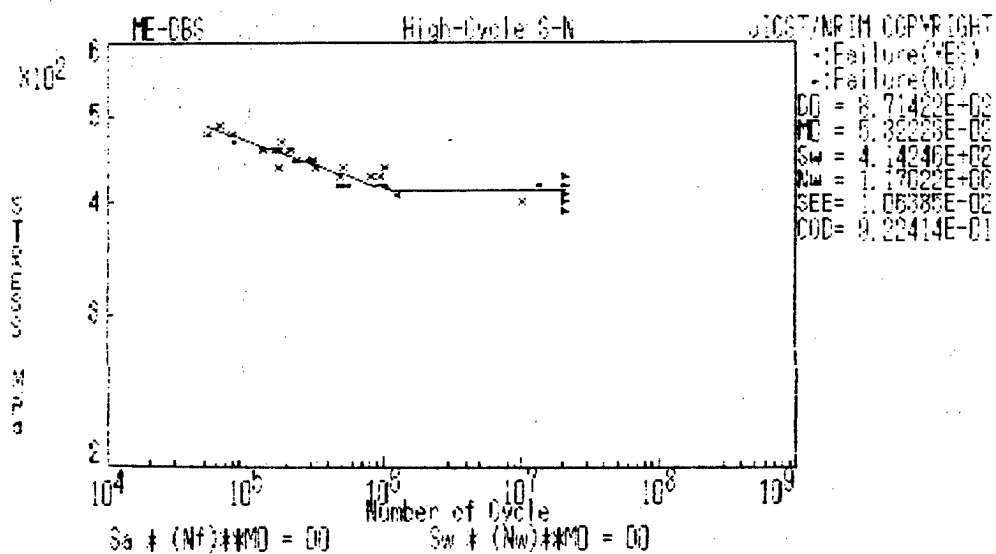


Fig.3. Example of data evaluation of fatigue for a carbon steel (S45C).

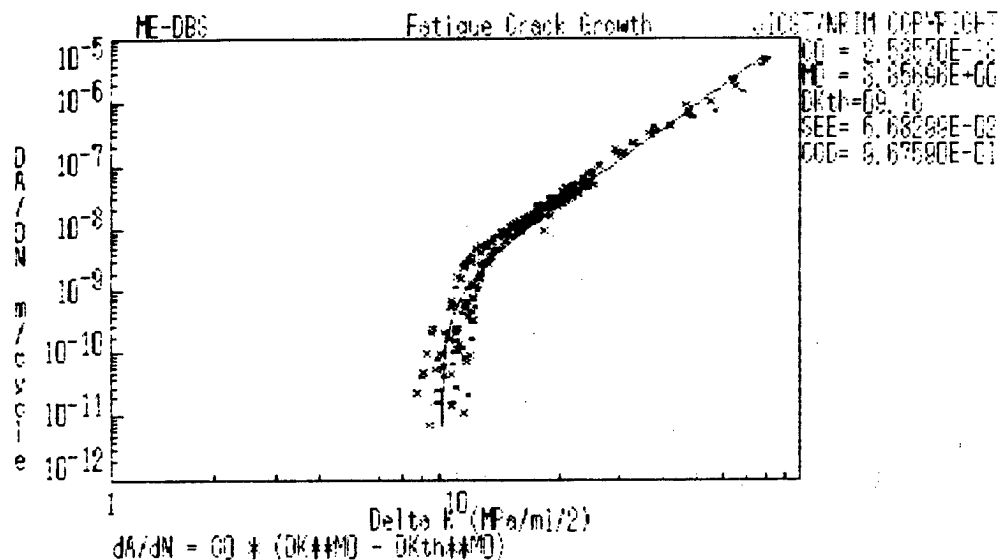


Fig.4. Example of data evaluation of fatigue crack growth of a low alloy steel.

FUTURE DEVELOPMENT

Improvements must be made on many points. The update of raw data will be made at least annually. In addition to the NRIM data, the existing data from SMSJ (Society of Materials Science, Japan) and ISIJ (Iron and Steel Institute of Japan) are planned to include. Additional data evaluation methods are needed to meet more advanced demands. The user interface should be improved for better user friendliness. The command language is not so easy to learn. Currently very limited menu is available in the current version. The policy of down-load up-load has not been fixed.

CONCLUSION

This paper has outlined major functions that NRIM/JICST Database for Engineering Steels and Alloys (ENSTAL), which is the first materials database available to Japanese public. Finally, suggestions have been made for the future improvement.

References

- [1] CODATA Task Group on Materials Database Management: International Register of Materials Database Managers (1989).
- [2] H.Kroeckel, K.W.Reynard and J.Rumble: Factual Materials Databanks, VAMAS TWA10 Report (1987).
- [3] S.Nishijima, Y.Monma and M.Kanao: Computerization and Networking of Materials Data Bases, ASTM STP 1017 (1989).
- [4] K.Suzuki, K.Shimura, Y.Monma, M.Sakamoto, H.Morishita and K.Kanazawa: Joho-Kanri, 33(1990), p.332.
- [5] S.Nishijima, Y.Monma and K.Kanazawa: Significance of Data Evaluation Models in Materials databases, VAMAS Technical Report No.6 (in press).

CERTIFIED REFERENCE MATERIALS (CRMs)

AN INTERNATIONAL DATA BANK

COMAR

JP. CALISTE - LABORATOIRE NATIONAL D'ESSAIS, PARIS, FRANCE

ABSTRACT

The analytical quality management, the establishment of validated methods according to the traceability and performance testing, and on another hand the existence of more than 100 producers of CRMs in the world offering 10.000 CRMs, are the bases of the necessity of the setting up of an international Data bank.

Starting from the analytical activity needs LNE (FRANCE) has defined a general code for indexation, developed the associated programs and established an international cooperation between JAPAN-IIII, USA-NIST, UK-LGC, FRG-BAM, USSR-VNIIMSO, CHINA-SRMC.

Analytical chemistry is one of the foundations of modern society. It underpins the work of government, commerce and industry and is vital for the enforcement of law, the maintenance of public health, the protection of the environment and the manufacture of quality products.

IT HAS BEEN ESTIMATED THAT ABOUT 5 % OF THE GROSS NATIONAL PRODUCT OF DEVELOPED COUNTRIES IS DEVOTED TO CHEMICAL MEASUREMENTS.

For measurements to be effective they must be reliable and widely accepted. The demands being placed on laboratories are increasing both in terms of the technical difficulty and concern for factors such as cost and quality.

The absence of reference materials use often leads to calibration difficulties and large measurement uncertainties. The resultant inaccuracy has financial and time penalties together with inadequate support for important regulation, policy and investment decisions.

On these bases it is very important to :

- awareness of analytical quality problems,
- and measurement traceability underpinned by reference materials

In this context the importance of the use of CRMs can be easily demonstrated, but before to develop more in detail the functions and the structure of the data bank COMAR it can be useful to remind the ISO definitions :

Reference material is :

"A material or substance one or more properties of which are sufficiently well established to be used for the calibration of an apparatus, the assessment of a measurement method, or for assigning values to materials".

Certified reference material CRM is :

"A reference material one or more of whose property values are certified by a technically valid procedure, accompanied by or traceable to a certificate or other documentation which is issued by a certifying body".

EXEMPLES OF INTERROGATION

In order to understand the purpose of the data bank according to the analytical chemistry needs it will be presented two kinds of exemples :

- one concerning the selection of pure iron (purity greater than 99.99 %)
- the second about the selection of sulfer in fuel (sulfer less than 0,5 %)

From these exemples (presented in details by slides) it is possible to see that the user has the possibility to select :

- the field of application (petroleum products for exemple)
- the elementary composition according to a range (lower and upper values)
- but also the name of the CRM
 - the form
 - the producer
 - and the country of origine

For each step of the interrogation the number of CRMs selected is displayed and by function keys it is possible to display or to print information about each CRM selected ; including commercial reference and contact name associated to the information about the producer.

THE STRUCTURE OF THE DATA BANK

Five parts of information are the bases of the data bank :

- general information
 - name
 - trade reference
 - field of application
 - year of certification
- Elementary composition : in order to describe the elementary composition this part allows to give the concentration (% , ppm,ppb) for each element associated to the relative precision and information about the quality of the value (certified, indicative, estimated).
- Molecular composition : the same structure is used in order to describe the molecular composition each molecule is identified by its Registry Number of the Chemical Abstract Service.
- Physical property : each physical property is identified by the ISO code and the SI units are used, a range specifies the certified value and parameters can be indicated.
- conventionnal property : in this case (hardness for exemple) the identification of this property is done by the reference to the standards that describe this property.

HISTORY OF THIS PROJECT

1980	ISO-REMCO recommendation about the indexation code, bases of a future data bank
1982	Demonstration of this data bank including 500 CRMs issued from french producers
1983	Collaboration with NBS (USA) about the portability between coding center
1984 - 1985	Creation of the first international part of the data bank with the collaboration of BAM (RFA) and NPL (UK)
1988 - 1989	Establishment of cooperation with USSR, JAPAN and CHINA
16 mai 1990	Signature of a Memorandum of Cooperation with all the participants to the setting up of the data bank COMAR. LNE is in charge of the Central Secretary

ACCESS TO THE INFORMATION

FOR JAPAN THE CODING CENTER FOR COMAR IS THE

- INTERNATIONAL TRADE AND INDUSTRY INSPECTION INSTITUTE (IIII) OF MITI 2.49.10 NISHIHARA SHIBUYA-KU TOKYO
- CHEMISTRY DEPARTMENT M. Y. MIYAKOZAWA
- PHONE TOKYO (481) 1921
- FAX TOKYO (481) 1920

According to the MEMORANDUM this Institute code CRM for Japan and recieve from the Central Secretary the International Data Bank COMAR, and in Japan, is the sole distributor with in that country.

The Materials Design Support Systems with Case-Based Reasoning

Yuzuru Fujiwara

(University of Tsukuba, Institute of Electronics
and Information Science Tsukuba, 305 JAPAN)

Abstracts

One of the most important functions in experts' brain is induction or learning, and this paper show that an example of Case-Based Reasoning. Most of databases and knowledge bases produced in the field of materials are hardly satisfactory to specialists of corresponding fields due to lack of sufficient contents in databases and knowledge bases as well as necessary functions of system.

There are many available information , while the present state of the arts to construct DB and KB is far from managing and using to the maximal extent most of the information.

This paper describes a new information model called MIB : SORITES (Materials Information Base : Self Organizing Receptor Interconnection Systems), which can handle semantics through dynamic structures of information.

The model is based on flexible representation of concepts and relationship among concepts, and directed links in the structures may be of types as many as necessary e.g. super classes - subclasses, causes - results, structures - properties, functions - mechanism and so on. The model is consisted of a set of hypergraphs in which nodes can be simple nodes, sets of nodes, sets of links or any combination of nodes and links. That is a node is a set of objects with abstract data type attributes, and a link is dynamic and carries meaning as specified relationship among nodes.

The model has been applied to the research information bases of polymer, Organic Synthesis and non - linear optical materials. The last are shown as examples here.

1. Introduction

Computer and softwares have been used to support research and development of science and technology, Large accumulation of programs numerical calculation, bibliographic and factual databases, and expert systems being implemented in various fields are available and are used extensively.

One of the major problems in producing databases is identification of the entities unless small databases are of concern. Another is access to data according to contents. Although both problems seem to be simple, it is not the case, because they are related with meaning of data, which is one of the furthest goals of computers. Various data models have been proposed to increase capabilities of database management systems. For example, the relational model is very popular because it is easy to use and is theoretically well-founded. Many attempts are reported to extend the model e.g. RM/T (the extended relational model by Codd), ADT (abstracts data type by Stonbraker), abstractions by Smith and so on, and to overcome restrictions of a basic form of the relational model which requires that values are atomic and may not be structured. This means that data should be simple and that you may not input complicated data necessary for materials design. The network model is flexible and the hierarchical model has been used widely, while they have same problems as those mentioned above.

It is to be noted that the registry numbers and standard nomenclature may not be the solution of the issues.

2. Information contained in materials

Polymer is taken as an example in a database called OPM-IBS (Optical Materials Information Base System) which contains bibliographic, spectral, graphic and text data of C-13 NMR of polymers, and has been compiled for seven years. It has comprehensive data in this particular field and the contents are of high quality in

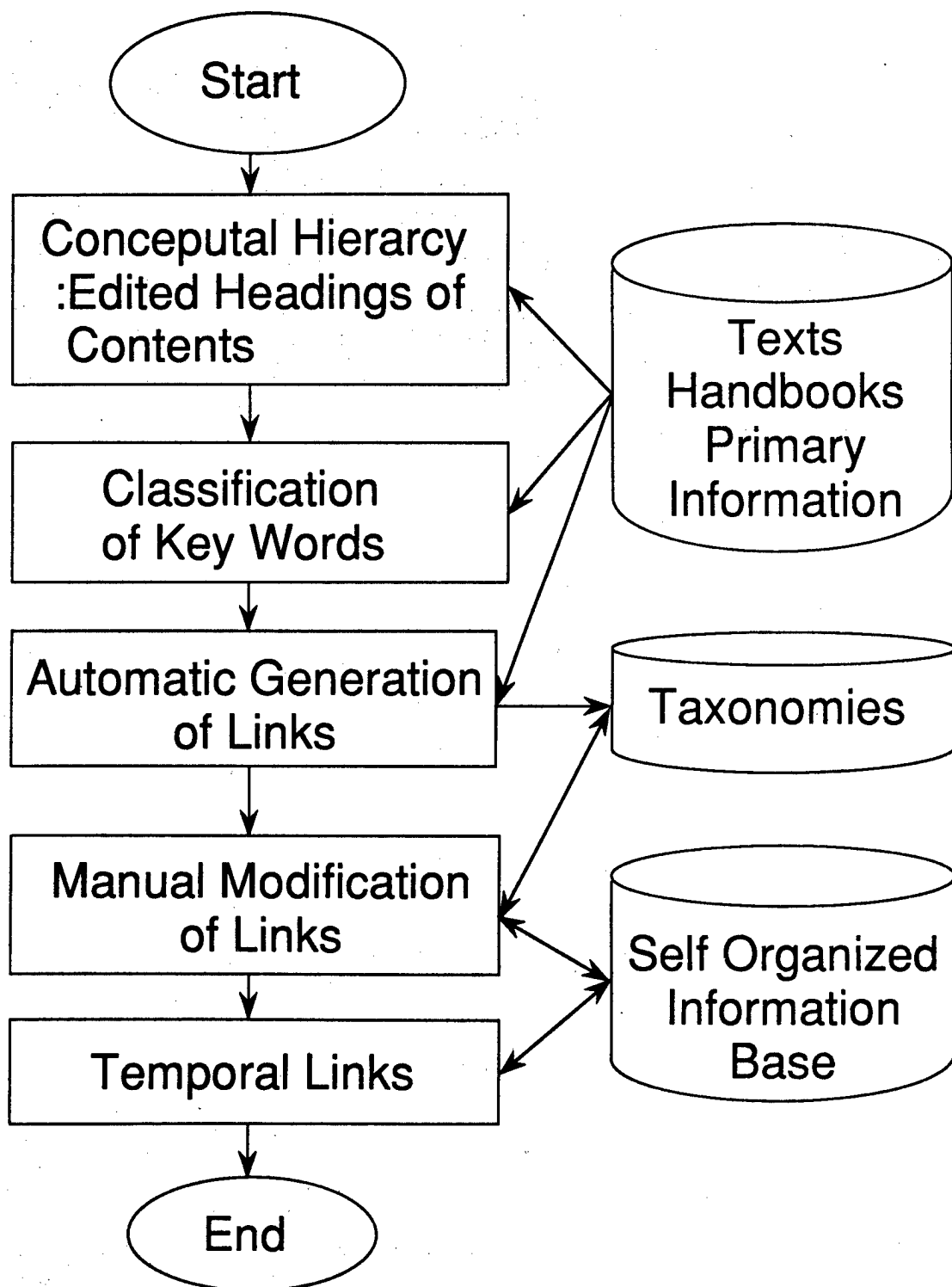
the sense of critical evaluation as well as contents of information necessary for research and development.[1].

In order to describe polymeric materials, it is necessary to include not only structures of repeating units but also other structural and nonstructural information, as shown in Figure 1; where explicit structural information contains that of repeating units, stereoregularity, irregular structures (e.g., branches, chain ends, head-to head addition of vinyl monomer, 1/2 or 3/4 addition in 1/4 addition of polyisoprene), degree of polymerization, and dispersion; implicit structural information contains that of production processes (e.g., hydrogenated PIP/EPR), reactions (e.g., chlorinated PE), starting monomer (e.g., polyvinylalcohol from polyvinyl acetate); related structural information contains that of additives, catalysts and so on; and nonstructural information of the types of properties (e.g., high density PE), processes (e.g., high pressure polymerization), use (e.g., engineering plastics) [1-3].

Although polymeric materials have many attributes to be described, all of them are not usually obtained. The lack of data is significant and the material cannot be fully specified. Moreover, it is not always required to know the value of every attribute, but the generic classes of materials are of concern. Sometimes, all of these attributes are not sufficient to describe compounds and yet further information is required such as isotope substitution, higher order structures and so on.

On the contrary, minor differences between distinct values may be neglected from a practical point of view. In a word, polymeric materials are mixtures of many kinds of isomers and homologues, and the required specification depends on the view of the user, where the corresponding sets of attributes are combinations of all attributes irrespective of the levels. Therefore, the constitution of key attributes must be dynamic and may not be unique.

Fig. 1 Self Organization of Information by Taxonomies



Systems for material design have components of the analysis of requirements, the structure design, the design of process and composition, and the estimation and evaluation of candidate structures, which are the major part of material design.

A particular example of material design is briefly sketched in Figure 1 to give a clear image of the design engine.

Requirement analysis may be performed automatically to some extent by preparing a thesaurus and a taxonomy of technical terms. Therefore, the design engine must be capable of giving an appropriate interpretation of requirements provided with a taxonomy ranging from a use level to a basic property level of materials. Moreover, the prepared structures of terms may not always give a complete analysis for requirements, and a supplementary interpretation should be given from the outside.

In this case, the design engine should be able to recognize the part it cannot interpret, then to show the part and request instructions to accept new concepts, resulting in reconstruction of the thesaurus. In other words, it is desirable for the design engine to have a learning mechanism.

1) Structure design. After those requirements are analyzed a set of basic property descriptions is obtained. The first step of structure design is to give model structures of the target material which is adapted to these property descriptions. This is accomplished basically by searching correspondence between structures and properties (a kind of knowledge base) stored in the taxonomy.

However, it is clear that many logical conflicts could occur during reasoning steps if a simple deductive inference method were applied. In the actual process, material designers have to content themselves with adapting a starting model material to a

subset of descriptions, and to fitting the remainder of the descriptions, in an effort to identify new descriptors where there are conflicts.

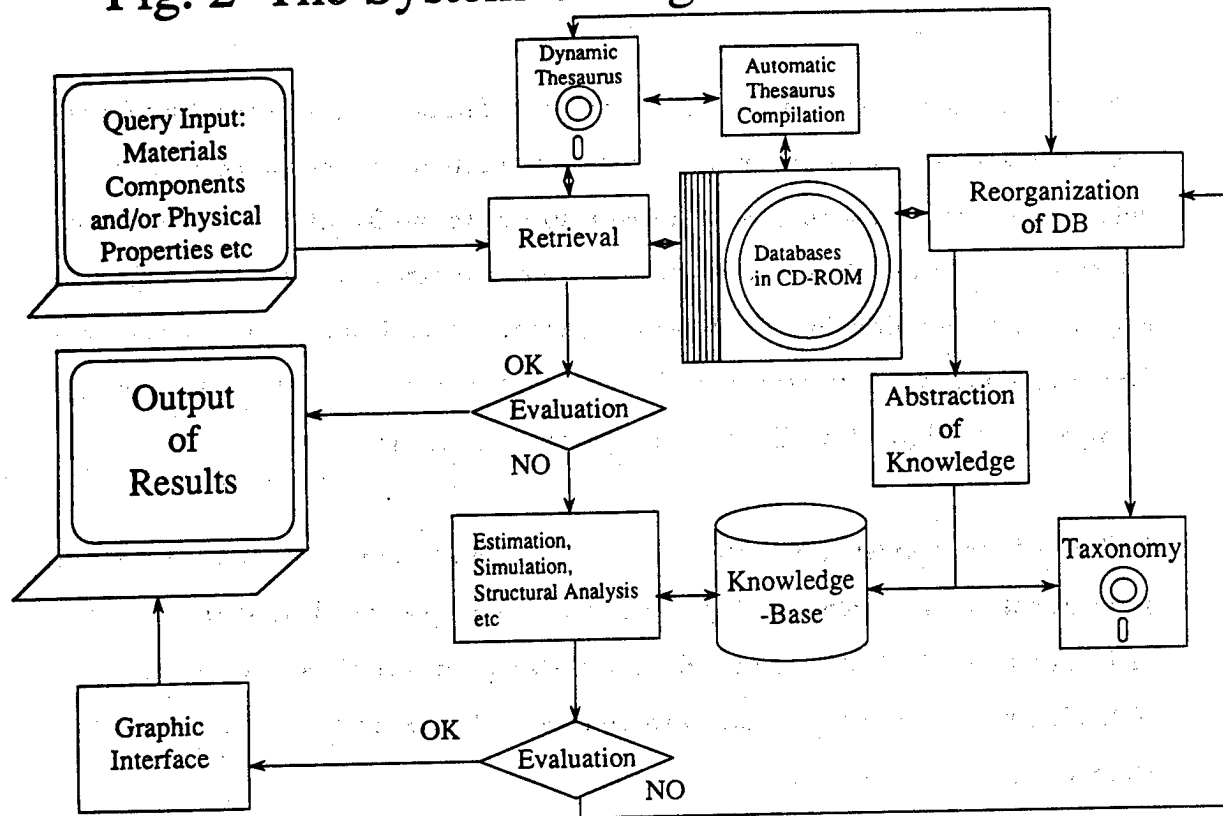
The second step of structure design is the optimization of the model structure through structural modification. As mentioned above, the model structure only fulfills constraints, so it is necessary to change the substructures to accommodate other requirements. The governing principle for this optimization is after the "additive property". It is the assumption that the property of a whole structure can be considered as the sum of properties of the constituent substructures, giving a guideline for structural modification.

While this estimation should be considered a preliminary hypothesis to be tested by experiments, it should be noted that knowledge enables a designer to estimate it. Therefore, it is necessary for the design engine to provide a set of correspondences between properties and substructures so that it can give any combination of repeating units. This set of correspondences can be regarded as a kind of representation form of semantics about properties in terms of (sub)structures. Further, it is possible to combine the set with the thesaurus and the taxonomy of technical terms, so it may be considered as part of a representation scheme of semantics of expertise.

2) Process and composition design. There are various steps in process design and composition design, including combining materials, additional reagents, etc., and controlling their concentrations. It is necessary for the design engine to appropriately apply the knowledge as such to the given requirements, although this function requires semantic analysis and dynamic structurization of knowledge.

3. OP-IBS System Features

Fig. 2 The System Configuration of OPM-IBS



Since a huge quantity of data and knowledge is needed for a material design system, it is vital, in order to manage such a system, to introduce database techniques. It seems promising to use a relational database for this purpose due to its logical clarity. However, to adopt a relational database as an integrated system for data and knowledge of material design, the following functions should be added:

1) Support for inference. In logical programming such as PROLOG, the relationship between the logic view of the relational database and inference is clear. Logical schemas are very useful for deterministic inference of the "if A then B" variety, whereas it is less good at handling heuristic reasoning. Both types of inference are needed in material design systems, and some hybrid knowledge representation scheme is required to accommodate both of them.

2) Support for taxonomy and related inheritance/defaults. It is known that frame-based knowledge representation is effective in the domain where the ratio of data to data descriptors is close to 1 (3). This corresponds to the fact that frame taxonomy seems to closely match our intuition about how to structure the world. It also suggests enticing directions for processing inheritance, defaults, etc. While data for material design range from that of the ratio 1:1 to that of the ratio 1:thousands, it is important for data of small ratio to support the taxonomy.

3) Support for complex data types. Most of the conventional database systems support only very simple data types such as integer, real number, string, etc., and lack functions which define new data types and support them. Therefore, it is difficult for them to process data with diverse modalities and complexities such as chemical graphs, time, etc.

In this respect, ADT-INGRES developed by Stonebraker et al. shows a direction which uses an abstract data type in a relational database context (4). In ADT-INGRES, each individual column of a relation is regarded as ADTs (Abstract Data Types), and the implementation details are hidden from the level of application software. Operations are defined in terms of procedures written by programming language C which supports both database access and ADTs. In particular, it suggests that many of the problems concerning non-first normal form relation would be solved by using query command QUEL.ADTs.

4) Support for metadata access. Metadata (data on data) are usually stored in a dictionary and cannot be accessed by the user. Such an implementation could not be qualified as a development type system which would handle data dynamically, and this means that metadata handling should be possible as far as the data manipulation language is concerned, as well as that of application data.

Reference

- 1) Y. Fujiwara, T. Nakayama and N. Ohbo; "Computer Aided Design System for Polymeric Materials" The Role of Data in Scientific Progress : CODATA-Elsevier 237-276 (1985)
- 2) Y. Fujiwara and N. Ohbo; "Databases and Knowledge Bases as Scientific Tools" CODATA Bull, 64 23-27
- 3) A. Nishioka, K. Hatada and Y. Fujiwara; "Polymer C13-NMR Database System with Bibliographic, Numerical, and Graphic data" Anal. Chem. Japan 36 (1) 64-66 (1987)
- 4) Y. Fujiwara; "CAPDAS: Polymer Database on CD-ROM" Information Management of Japan 30 (10) 967-978 (1988)
- 5) Y. Fujiwara, W. G. Lee, Y. Ishikawa, A. Nishioka, K. Hatada and N. Ohbo; "A Dynamic Thesaurus for Intelligent Access to Research Databases" Proc. the 44th FID Congress: Information-Knowledge-Evolution 44 (3) 61-69 (1988)
- 6) Y. Fujiwara, H. Murakami, T. Yamagishi, N. Ohbo and T. Nakayama; "A C-13 NMR Databases System with Spectral Analysis and Estimation Functions for Polymer Research" Japan and Germany Spectral Databases Workshop (1988)

Products Data Banks Requirements from Industrial Users

Daniel R. Vinard

Saint-Gobain Recherche
39 quai Lucien Lefranc, F.93303 AUBERVILLIERS

ABSTRACT

Industrial needs for Computerized Scientific and Technical Information, cannot be restricted to the "so-called" scientific data only. From base materials to components, products and applications, nobody can draw a precise line.

"Validated" data is certainly a prime concern for industrial R&D labs but the data banks providing such data are not likely to cover, in the next future, the bulk of the needs of Industry.

A more "pragmatic" approach has to be considered, including the available technico-commercial data, naturally explicated by the proper labelling for their expected "quality".

The development of such "pragmatic" databanks, will induce, later on, the consultation of the more scientific ones.

Industrial needs expressed by the industrial users themselves should be integrated at the real start of the conception of the systems, and not afterward ! ...

MARKET "PULL" : FROM "MATERIALS" TO "PRODUCTS" DATA BANKS

The recent publication of the GUIDE DES BANQUES DE DONNEES FACTUELLES FRANCAISES SUR LES MATERIAUX 1989 : Catalog of French Factual Data Banks on Materials) available at CODATA France, is clearly showing the need for "Products" Information.

Indeed, 40 Data Banks (refer to the enclosed detailed chart), covering most of the industrial activity (adhesive, aluminum, aeronautic, car industry, building and civil engineering, metals, mechanics and ceramic and glass) are presented with the full description of their access (public or under private contract), including pictures of the key screens (most of them being "videotex" assisted).

Many of these data banks include "components", commercial products and catalogs. When possible, the "friendly access use" is preferred to the scientific "sophistication". Some Materials DataBank "purists" may regret these features ! However they should take this opportunity to meditate on the requirements expressed by the users (industrial in particular) and may consider this "photography" of the "real" activity on databanks in our country as a warning against purely scientific constructions, fascinating at the first glance, but disappointing afterward when seeking for users ! ...

INDUSTRY REQUIREMENTS

The proliferation of commercial systems, testifying their vitality, is not, however, truly satisfactory, since the scattering of information under many systems and configurations will obviate, on the long term, the development of coherent information systems.

Therefore, the priority seems to be, at the moment, to reach an agreement on a **common standard for data storage (or, at least, for data exchange)**.

The Research labs, the manufacturing plants and the marketing services, are generating a continuous flow of valuable numerical data (material properties and behavior, quality control regulations, statistics, ...) which are un-uniformly stored in too many systems, generally adapted to the precise local function, but improper to be communicated to other locations, or used for other functions.

This need for a coherence in the formats is even more important in the case of the "products" data banks, since the potential users are widely diversified and would not access to commercial transactions without the possibility of a common language with the industrial suppliers of their materials and products.

CAD/CAM and modelling purposes are good illustrations of the need to access in a comprehensive way to valuable data : A Pilot Demonstration Program, gathering about 20 European is studying the feasibility of the concept of data storage for CAD/CAM.

The "Products" data banks seem to be ahead of the "Materials" in this area. As an example, the AFNOR Z-99 standard, homologated by EEC, for the "components" used in CAD/CAM has been developed by a large group (110 in France) of industrial users : We are presently studying the adaptation of this standard to "straight" materials.

An other priority is the **"graphic" presentation** of industrial data (drawings, curves, charts, ..).

"Videotex" has brought a readily available solution for all terminals, including the less sophisticated ones (such as the "Minitel" which is a the free disposition of any telephone contractant in France, and explain the success of the videotex databanks). However the screen definition and the speed of transfer is far from the levels required for transfer of pictures and detailed drawings.

Videodiscs, locally associated with the connected terminals can illustrate the databanks output with the features which cannot be conveniently expressed otherwise by textual or numerical data.

RNIS (Réseau Numérique à Intégration de Service) will be widely developed in most of the french cities at the end of 1990 : it will transfer data at 64.000 bits/s and therefore will be suitable for image and drawings data.

Last, but not least, is the "friendly access" requirement which is the key of the effective use of computerized data by industrial users. The increasingly large volumes of information cannot be restricted to the lonely access of the information "specialists". Training of researchers and technical users may overcome many of the present hints which inhibit the present consultation of Databanks. However a major effort has to be made by Databank producers to adapt themselves to the "friendly access" concepts of their potential users.

EXAMPLES OF INDUSTRIAL PRODUCTS DATA BANKS

The following examples are presented to illustrate the diversified needs for factual information.

SG-PROMAT (Saint-Gobain Products and Materials)

SAINT-GOBAIN is a multinational Group covering large sectors of the industry of materials (glass, ceramic, metal, cement, wood, ..).

Aside from the scientific and validated computerized data data banks which are vital for researching in an area such as glass (including the links with the expert systems), a complete system is available to all companies of the Group SAINT-GOBAIN (113 through the world) for storage and access to data pertaining to their materials and products.

It can describe and retrieve, in numerical as well as textual terms, any material produced or used by the Group (from paper products to reinforced concrete component, including, cast iron, glass and ceramics). As an exemple of other potential use, scientific equipments, with their proper characteristics (NMR, ESCA, SIMS, Infra-red ..) of each Research Laboratory within the Group can be located through the world, for proper use.

The system is operated on Télésystèmes Questel, as a private base with several levels of confidentiality, assisted by videotex and videodisc interfaces.

Building and Civil Engineering areas.

The following list, illustrates once more, the development of a large number of videotex, easy to access, systems which are favored by the users.

Name	Producer	Nature of informations	Videotex access
NORIANE	AFNOR	Standards	Questel
ARIANE	FNB	Products and related data	
ACERMI	CSTB	Certification of insulating products	3615
ADETEL	BTP	Manufacturers and products	3614
ARIABAT	FNB	Manufacturers and products	3615
BAT2000	Atel.2000	Enterprises, Standards, Contracts	3615
BODACC	Official	Enterprises	3613
COROTEL	Corona	Paints	3614
CYCLOPE	CSTB	Products and companies	3615
EAUDOC	Johanet	Water : Equipments and supplies	3615
GIMM	GIMM	Wood products	3614
HABITAT88	CSTB	Constructions	3615
IMCC	AIMCC	Products	3614
INFOBAT	SOCOTEC	Products and insurance standards	3629
INSEE	INSEE	Economic data	3615
MAZDA	MAZDA	Lighting products	3615
MEMOBAT	Entrepreneur	Enterprises and products	3615
MONITEL	Moniteur	Enterprises, Products, Contracts	3615
RUBSON	Rubson	Waterproofing products	3614
RUTILE	CSTB	Technical agreements on products	3615
SAGERET B	SAGERET	Enterprises	3614
URBA	BTP Ministry	Products reglementations	3617
USNOUV	Usine Nouv.	Economic data on products	3615

N.B. 3613-14-15-17-29 are the codes for minitel (and prices levels)

ANNEX

GENERAL TABLE OF MATERIALS AND PRODUCT DATABANKS INCLUDED IN THE "GUIDE DES BANQUES DE DONNEES FACTUELLES FRANCAISES SUR LES MATERIAUX 1989" (Catalog of French Factual Data Banks on Materials available at CODATA France).

Name	Content	Producer	Field
ACERMI	Aide au choix des matériaux isolants certifiés du bâtiment	CSTB Champs sur Marne	Bâtiment
ADEP	Propriétés thermodynamiques et de transport de corps	Centre de Recherche et d'Etudes Céramiques Université de Limoges	Thermodynamique
ADHEMIX	Caractéristiques des colles structurales du marché français	CEA/DAM, Monts	Adhésifs

Name	Content	Producer	Field
ALUSELECT (1)*	Aide à la sélection des principaux alliages d'aluminium de	European Aluminium Ass., Voreppe	Aluminium
ARIAGEC (2)	Informations sur les opérations de recherche en génie civil	PROGEC/MRT, Paris	Génie civil
ARIANE (3)	Techniques, réglementations, produits et fabricants du bâtiment	IFB-CATIEP, Paris	Bâtiment
ARTEMISE (4,5)	Chimie des roches et minéraux, géologie, pétrographie. Domaines ignés, métamorphiques et sédimentaires	CRPG, Vandoeuvre	Géochimie
BADGE-DAN	Exploitation et valorisation de données du sous-sol national en vue de l'aménagement	ENSG/INPL, Vandoeuvre	Géochimie
BASALTE	Ensemble de résultats d'essais d'usage interne effectués au CSTB	CSTB, Champs sur Marne	Bâtiment
CETIM ADHESIFS	Aide à la conception et à la mise en oeuvre d'assemblages collés	CETIM, Saint Etienne	Adhésifs
CETIM DIAMANT	Aide à la conception de pièces et d'ensembles mécaniques	CETIM, Senlis	Mécanique
CETIM FATIG	Calcul de tenue en fatigue de pièces mécaniques principalement en acier	CETIM, Senlis	Mécanique
CETIM FIMAC (7)	Caractéristiques mécaniques et physiques des polymères et composites	CETIM, Nantes	Plastiques composites
CETIM SICLOP (8)	Guide de choix d'aciers de construction pour traitements thermiques	CETIM, Senlis	Mécanique
CIMBETON (9)	Aide au choix des ciments et bétons données techniques et commerciales	CNC, Paris	Bâtiment
COMPOSITE DATA	Mise en oeuvre, caractérisation, application des matériaux composites	Inst. Mat. Composites Pessac	Composites
CYCLOPE	Matériaux, produits, procédés et systèmes nouveaux du bâtiment	CSTB, Paris	Bâtiment
DATAROC	Roches exploitées en carrière: essais mécaniques, physiques, chimiques et minéralogiques	LCPC, Paris	Géologie
FATIGUE (10)	Résultats d'essais de fatigue de matériaux métalliques, utilisés dans l'aéronautique	Aérospatiale, Suresnes	Aéronautique
FEU	Résultats d'essais de résistance au feu d'éléments de construction du bâtiment	CSTB, Champs sur Marne	Bâtiment

Name	Content	Producer	Field
GEOBANQUE (11,12)	Données géologiques, hydrogéologiques, géologiques et géotechniques du sous-sol français	BRGM, Orléans	Géologie
GEPROC	Essais mécaniques de caractérisation d'éprouvettes en matériaux composites	Avions Marcel Dassault, Saint Cloud	Aéronautique
GUIDE DE CHOIX ENGIN-PLAST (13)	Guide de choix des matières plastiques pour le moulage des pièces industrielles	Engin-Plast Chatenay-Malabry	Plastiques
G3F	Guide de choix de matériaux composites et adhésifs	G3F, Villeurbanne	Composites, adhésifs
HYDROGENE-DATA (14,15)	Aide à la recherche d'information sur les interactions hydrogène-matériaux	ENSCP, Paris	Thermodynamics
INFOBAT (16)	Produits et procédés qualités du bâtiment: informations et actualités	Socotec, Paris	Bâtiment
INFOVISION (17)	Aide à la recherche de produits et de fabricants dans le domaine des roulements	Sonovision Vélizy Villacoublay	Mécanique
MECAROC (18)	Propriétés mécaniques et physiques de pierres de construction du Génie Civil	I.U.T. de la Rochelle Université de Poitiers	Bâtiment
PMC (19)	Aide au choix des matériaux de construction et d'entretien des chaussées	LCPC, Paris	Génie civil
PROCOP-M (20)	Calcul d'écoulement de polymères injectés, résistance de polymères et composites	Cisigraph, Rungis	Plastiques composites
QUARTZ	Résultats d'essais acoustiques sur des éléments de construction de bâtiment	CSTB Champs sur Marne	Bâtiment
REFDATA (21,22)	Aide à la recherche de matériaux de référence pour l'étalonnage	LNE, Paris	Matériaux de référence
RP3L (23)	Aide au choix des matériaux plastiques Rhone-Poulenc: calcul de dimensionnement	Rhone-Poulenc, Lyon	Plastiques
RUTILE	Informations signalétiques sur les avis techniques du bâtiment	CSTB, Paris	Bâtiment
SG-PROMAT (24,25)	Matériaux, produits et compétences du Groupe Saint Gobain	Saint Gobain Paris la Défense	Bâtiment mécanique
SOPREMA-ETANCHEITE	Produits d'étanchéité destinés au bâtiment	Soprema Gennevilliers	Bâtiment
SPAO (26)	Guide de sélection technique des polymères du marché européen	LNE, Paris	Plastiques
THERMODATA (27-29)	Propriétés thermodynamiques des éléments, composés minéraux et alliages métalliques	Thermodata, Saint Martin d'Hères	Thermodynamique
THERMOSALT (30)	Propriétés thermodynamiques des mélanges de sels fondus	SETT, Univ. de Provence, Marseille	Thermodynamique
VULCAIN-BDM (31-33)	Matériaux et traitements pour la mécanique, la micromécanique et le décolletage	CT DEC, Cluses AFNOR, Paris La Défense	Mécanique

**DEVELOPMENT AND APPLICATION OF RELIABILITY ASSESSMENT
DATABASE FOR HEAVY APPARATUS EQUIPMENTS AND STRUCTURES**

Takao Inukai, Nagatoshi Okabe

Applied Mechanics Group, Metals and Applied Mechanics Department
Heavy Apparatus Engineering Laboratory, TOSHIBA Corporation
Suehiro-cho, Tsurumi-ku, Yokohama 230, Japan

1. ABSTRACT

Reliability database is essential to the improvement and reliability prediction of various products, as well as its model changes, structural modifications of new developed products, and optimum reliability design. Such database can be utilized in two various fields including reliability tests and maintenance. Failure database underlying reliability information can be divided roughly into experimental database and field database. This paper will introduce next two example of database and reliability analysis.

- 1) Field database for vacuum circuit breaker (VCB) as a sample of representative heavy electric switch gear.
- 2) Material strength database for in-service degradation of steam turbine components.

2. FIELD DATABASE FOR VACUUM CIRCUIT BREAKER

2.1 Formatting for Actual Delivery and Failure Data

Field data is based on operating conditions and failure information of VCBs delivered to various customers and being used in various applications. Standard items should be recommended so that the following typical information may be obtained.

- i) Types of products
- ii) Histories of the products (including periods of operation, the number of switching, and maintenance conditions)
- iii) Environmental and application conditions
- iv) Failure conditions (including portions out of order, parts in trouble, failure modes, and symptoms)
- v) Effects and actions against failure (including the degree of difficulty in recovery)

Such works aim at utilizing the past highly reliable empirical field data of VCBs.

As shown in Table 1, data is divided into [A] actual delivery record data and [B] failure data.

A database covering actual delivery records is a parameter for reliability analysis. This requires correct actual delivery records. The needed information items include VCB types, customers, delivery dates, serial product numbers, and the number of delivered VCBs. The types must be so coded to make it possible to

identify the structures of vacuum valves used, rated applied current, rated interrupting current, and the presence or absence of TNRs. In addition, this coding must be such that it contributes to understanding customers' classifications, customers' names, and frequencies of using VCBs.

The failure database must cover errors, including part failure found during maintenance and inspection, which force products to be put out of operation. The information items should include dates on which failure occurs, its phenomena, actions against it, test numbers, and the number of VCBs out of order. The failure phenomena codes must be subdivided into category, portion, element, and degree of importance. The category codes should serve for knowing either of (i) machinery, (ii) electricity, (iii) chemistry, and (iv) environment which the failure is related to. The portion codes should serve for understanding what portion the failure occurred at. The element codes should serve for identifying the improper part. The degree of importance codes should serve for identifying effects of the failure. In addition, the cause of failure codes should serve for understanding what the failure originates in. The action against failure codes should serve as information data permitting the identification of permanent or tentative actions.

2.2 Configuration of Multi-Item Retrieval System

Data must be retrieved selectively from the reliability database, depending on the application and the object subjected to reliability analysis. For the retrieval system, the following items in [A] actual delivery data and [B] failure data serve as retrieval keys.

[A] Delivery records : Types of VCBs, customers, and delivery dates.

[B] Failure records : Date on which failure occurs, failure phenomena, and causes of failure.

The combination of (i) single-item retrieval and (ii) multi-item retrieval as well as a masking function by symbol # makes very diverse retrieval possible.

Example(1): The specification of type = ##10## retrieves all VCBs rated at 10kV and incorporating motors.

Example(2): The specification of customer = P##, delivery date = 8##, and improper portion = F## retrieves all the VCBs delivered to electric power companies in 1980s and whose mechanical parts were out of order.

Example(3): The VCBs which meet conditions of example (1) and (2) are retrieved (multi-item retrieval).

2.3 Reliability Analysis of VCBs Based on Delivery Records and Failure Data

Reliability data is characterized by the fact that the number of non-failure data (incomplete data) pieces proving VCBs' reliability is much more than the number of failure data (complete data) pieces. The representative reliability analysis means for both complete and incomplete data is Nelson method which is also called hazard method⁽¹⁾⁽²⁾⁽³⁾. Hazard method provides a reliability analysis method comprising two steps. The first step is to determine a hazard $h(t)$ from actual data, and a cumulative hazard $H(t)$ from the accumulation of a series of $h(t)$. The second step is to identify the distribution of failure data and probabilistic parameters on basis of the failure probability $F(t)$ which is obtained from $H(t)$.

Hazard means probability of failure in the subsequent unit period and hazard $h(t)$ is defined as following equation.

$$h(t) = \frac{f(t)}{R(t)} = \frac{f(t)}{1-F(t)} = -\frac{dR(t)/dt}{R(t)} \quad (1)$$

Where $R(t)$ is reliability, $F(t)$ is probability of failure and $f(t)$ is failure probability density function.

Cumulative hazard is defined as follows.

$$H(t) = \int_0^t h(t) dt \quad (2)$$

Using $H(t)$ the reliability $R(t)$ is expressed as follows.

$$R(t) = \exp[-H(t)] \quad (3)$$

Thus, cumulative failure probability $F(t)$ can be obtained as following expression. As shown in equation(4), $F(t)$ is determined from VCB's operation and failure data, which is independent of the distribution.

$$F(t) = 1 - \exp[-H(t)] \quad (4)$$

VCB's reliability depends on the reliability of many structural components being so called system reliability. Thus, the life of a VCB depends nearly on the minimum life of its components. Theoretically, Weibull distribution depending on the minimum life of components seems to be most adapted to the VCB's life distribution. For reliability analysis of VCB's operation and failure data, $F(t)$ is expressed as two parameter Weibull distribution. As an example, Fig.1 shows the life data on Weibull plot sheets. The life data has been acquired by retrieving field data under three conditions. Fig.1 shows that the life data follows the two parameter Weibull distribution at any conditions.

On the other hand, it is possible that reliability analysis of VCB's life distributions is covering the number of operations. Fig.2 shows the example of VCB's life distribution covering the number of operations and their regression line.

3. MATERIAL STRENGTH DATABASE FOR STEAM TURBINE COMPONENTS

3.1 Introduction

Steam turbines in fossil power plants are used in high temperature steam and are operated as long as 20 years or more. Because of such operating condition, the material strength of steam turbine components known to degrade due to coarsening of carbide or precipitating of impurity in the grain boundary.⁽⁴⁾

Therefore, in order to maintain reliability of fossil power plants, the establishment of material strength database taken from the retired components and the development of reliability analysis system are sought after.

In this section, the material strength database system which is taken into account of material degradation information and reliability analysis example will be introduced.

3.2 System Configuration

As shown in Fig.3, the material strength database system is composed of a database and three subsystem such as retrieval, property analysis and reliability analysis. The material strength database, which is the raw data obtainable from the material strength tests, is prepared in the form of the Japan Society of Materials Science data sheets for fatigue strength of metallic materials by revision depending on various properties of strength, in order to note also the in-service degradation material properties. It is made possible to enter the data such as the material history after the mill sheet formation (service temperature, operation time, load, number of operation, etc.), basic strength property data (tensile, impact, hardness, etc.), plant name, component name and sampled portion.

The retrieval subsystem is used to output the desired data in the form of numeric values or graphics by the way of inputting retrieval items. Retrieval is executed for each items successively to perform narrowing into the required data. For this purpose, the material strength database is divided into various files including only the necessary data for each retrieval item, and the useless

reading of unwanted data is eliminated through the combination of the supplier code and test number, thereby shortening the retrieving time.

The property analysis subsystem expresses in the formula of material data obtained through the retrieval by making a parameter analysis on the basis of the other basic material strength properties and/or metallurgical properties.

The reliability analysis subsystem estimates the probabilistic material strength from the scatter between the experimental values and estimated values obtained by the property analysis. It is applicable to make a probabilistic estimation for the life or strength of steam turbine component materials.

3.3 Reliability Analysis for Creep Rupture Strength

Using a result of performing a retrieval under retrieval conditions shown in Table 2, an example of reliability analysis for creep rupture strength will be explained. Fig. 4 shows the creep rupture property of the retrieved data, and the creep rupture property inclines to lower with the lowering in hardness. The creep rupture property can be expressed as a function of hardness.

$$P = C(\sigma) H_v + D(\sigma) \quad (5)$$

$$C(\sigma) = C_1 + C_2 \log_{10} \sigma + C_3 (\log_{10} \sigma)^2 \quad (6)$$

$$D(\sigma) = D_1 + D_2 \log_{10} \sigma + D_3 (\log_{10} \sigma)^2 \quad (7)$$

Where, P is Larson Miller parameter, σ is stress, and C_1 - C_3 , D_1 - D_3 are material constants.

Using this expression, Fig. 5 shows the comparison between experimental value and estimation value from hardness.

Then, the ratio (μ) of experimental value against estimation value of creep rupture strength was plotted in form of Weibull plot sheet as shown in Fig. 6. In this case, three parameter Weibull distribution is better agreement with actual data, especially lower probability data compared to two parameter Weibull distribution.

Using the three parameter Weibull distribution obtained above, statistical interval estimation of the creep rupture strength was conducted. Fig. 7 shows the example of creep rupture strength distribution on condition of temperature of 566C, hardness H_v of 240, and creep rupture life of 100,000 hours. The upper and lower range means 99% confidence level and center line means 50% confidence level.

4. CONCLUSION

(1) Focusing on a vacuum circuit breaker as typical heavy electric apparatus, this study has constructed the reliability database and developed the retrieval system. And the Nelson method was applied to Weibull analysis on field database to estimate parameters required for reliability analysis.

(2) With an example of creep rupture data on in-service degradation materials of steam turbine components, the material database system was described. The statistical distribution of creep rupture strength was revealed to fit the three parameter Weibull distribution.

5. REFERENCE

- (1) W. B. Nelson, J. Quality Technology, 1-1, 27 (1967).
- (2) W. B. Nelson, G. E. Research & Development Center, TIS Report 68-C-007 (1968).
- (3) W. B. Nelson, J. Quality Technology, 1 (1969).
- (4) K. Kimura et. al., Current Japanese Materials Research, 3 (1988).

Table 1 Data Sheet for VCB Delivery and Failure Record

[A] Delivery Record						[B] Failure Record					
Flag	Type	Customer	Delivery Date	Job No.	Number of Delivery	Failure Date	Phenomena	Cause	Action	Test No.	Number of Failure
	A120X100T	P12F	73X	1820900	999	80X	N2N3	D2	K	1193	0001
Type VGA2 + A2 VGA5 + A5 VK + K VY + Y						Year Month Electric Mechanic Chemistry Environment					
Power : P Export : E Rail : R						D: Design A: Assembly T: Test P: Production G: Technology L: Setting C: Customer					
						Permanent K: OK L: Need(Not yet) N: Not yet Not yet					
						Tentative - OK OK Not yet					

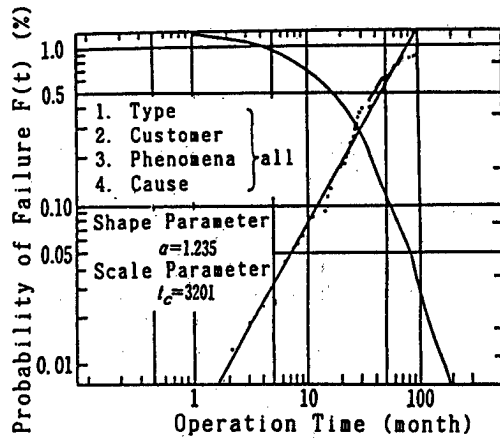


Fig. 1-1 Retrieval Example for VCB Reliability Data

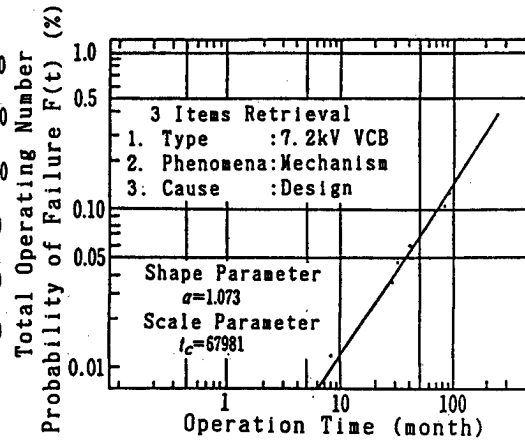


Fig. 1-2 Retrieval Example for VCB Reliability Data

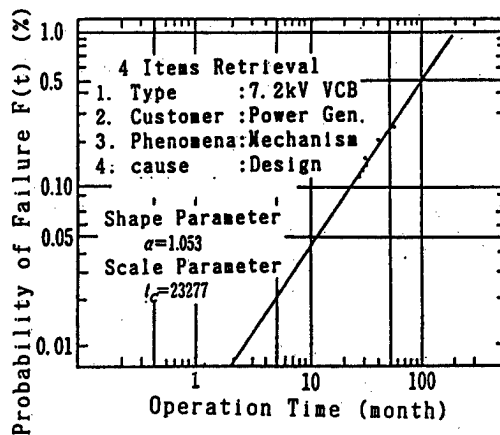


Fig. 1-3 Retrieval Example for VCB Reliability Example

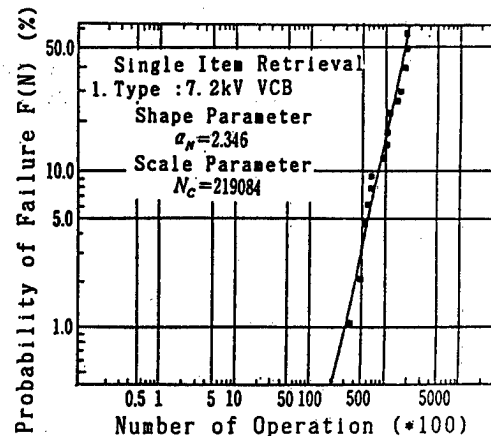


Fig. 2 Reliability Analysis Example for VCB against Number of Operation

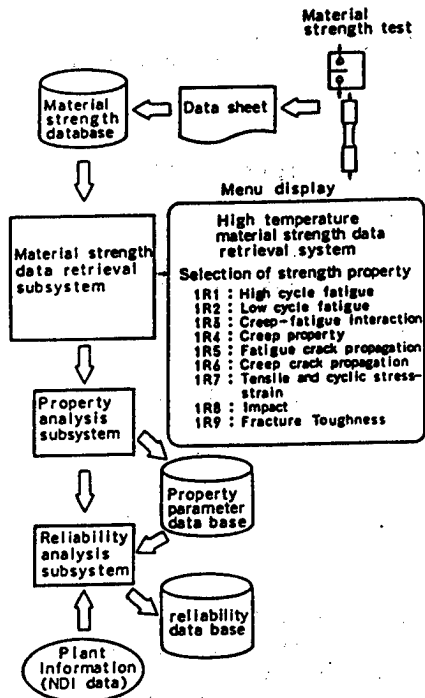


Fig. 3 System Configuration

Table 2 Input Item for Retrieval Example

Retrieval Condition	Input Item
Retrieval Method	Retrieval Key System
Material	CrMoV Forging Steel
Test Piece	Smooth
Test Environment	Air
Surface Treatment	None
Heat Treatment	Quench and Tempered
History	Used
Heat Treatment	None
Hardeness(Hv)	1 Upper254.9 Lower245.0 2 Upper214.9 Lower205.0 3 Upper174.9 Lower165.0

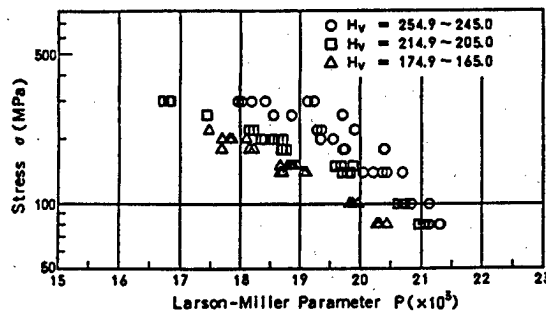


Fig. 4 Retrieval Result (Creep Rupture Property)

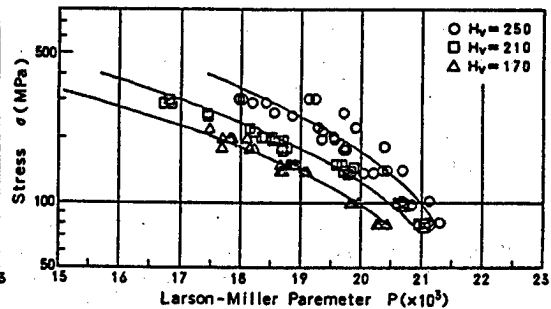


Fig. 5 Comparison of Standardized Creep Strength and Estimate Creep Strength from Hardness

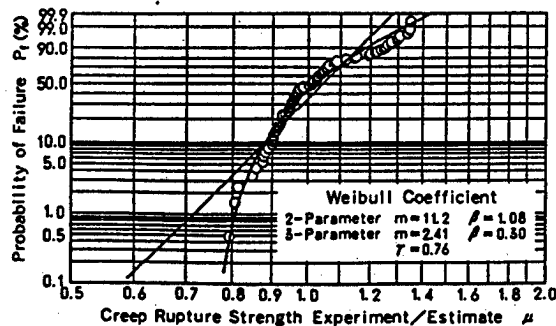


Fig. 6 Weibull Distribution Showing Dispersion of Experimental Values of Creep Rupture Strength from Estimated Values

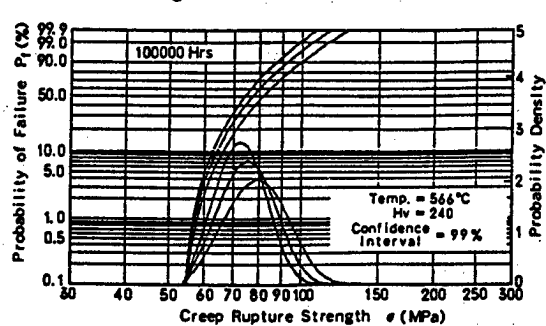


Fig. 7 An Example of Statistical Estimation of Creep Rupture Strength

The "Cetim-Matériaux" Database

H.P. Lieurade, C. Lebreton

Centre Technique des Industries Mécaniques (CETIM)

52, Avenue Félix Louat-60304 SENLIS- Cédex- France

Tel : (33) 44.58.32.66 ; Telex :140006 F ; Fax: (33) 44.58.34.00

Abstract

CETIM-MATERIAUX is a Material Database especially aimed at selecting materials having the correct set of required properties, i.e. multi-criteria searching is the main aim. It covers information on the properties of metals, plastics, organic matrix composites, adhesives and lubricants. The data concern physical and mechanical properties of engineering materials, special attention being given to wear, fatigue and corrosion.

There is also a set of associated software which can be used on PC independently of the main data base : CETIM-SICLOP (Optimisation of steel selection), CETIM-FATIG (Fatigue design), CETIM-TELEMAC (Selection of reinforced polymers and composite materials), CETIM-ANASTRA (Calculation of mechanical, thermal and hygrometric characteristics of polymer matrix composites, taking into account fibre orientation and layering).

After outlining the differences between databases, simulation software and expert systems, the authors describe the principle of interrogation of CETIM-MATERIAUX and give a brief presentation of CETIM-SICLOP.

Introduction

For many years, CETIM has been providing materials information to the mechanical industries, published guides (e.g. : [1 to 3]) and developed methodologies to help with selecting the right material/treatment combination which, for the lowest cost, will enable a mechanical component to withstand the operating stresses. It has now also been developing for several years a Material Data Bank and a set of Associated Software.

Before describing the main features of the CETIM-MATERIAUX Data Bank and of CETIM-SICLOP, we will try to define what is meant by the terms "data base" and "associated software" and to what extent these different computer tools can contribute to selecting materials. We would also like to insist on the limits of these products.

Database and Associated Software

A data base, is primarily a collection of data. The different material databases may be classified according to the following characteristics :

- THE TYPES OF DATA they contain,

- Test results : either specific results of individual tests (raw test data) or data sets which as a group are descriptive of some measured characteristics,

- Calculated values : certain characteristics cannot be measured directly but are determined by means of a mathematical analysis of raw test data (e.g. the Larson-Miller parameter for creep). Some banks might even contain interpolated or extrapolated values,

- Synthesis of test data : either average or typical values -the result of the analysis of one or more data sets to indicate the 'normal' or average behaviour of a material- or certified values such as those often found in standards, -mainly minimum or maximum values-

- THE MATERIALS covered (steels, cast-irons, aluminum and other metallic alloys, plastics, organic matrix composites, adhesives and lubricants in the case of the CETIM Database),

- THE NATURE OF DATA

- either TECHNICAL

- . Application characteristics (physical properties, mechanical characteristics, fatigue, wear, corrosion...),

- . Processing (Processability and processing parameters),

- or ECONOMICAL (cost, availability,...) NATURE OF DATA.

The CETIM-MATERIAUX Database deals mainly with syntheses of test data although it may also contain individual test results. Besides application characteristics, the CETIM-MATERIAUX data base tackles the processability aspects but does not include any economical data.

But a Database is also a structure : the input formats including the compulsory metadata (e.g. test temperature) and the useful secondary information (optional input, e.g. ghost line direction and surface roughness of specimens used for establishing fatigue design curves) and the possible links between the different data entities and with the thesaurus. Figure 1 outlines the main features of the CETIM-MATERIAUX Database structure. It can be noted that this structure takes into account the fact that a material does not intrinsically possess the characteristics required by the designer. - A material name only defines a potential for obtaining these characteristics corresponding to various structural states which can be obtained through a transformation (sequence of mechanical, surface, heat, ... - treatments)- This structure also allows you to deal with the inheritance of property values between products obtained through transformations of the same material.

The primary function of a Database is to allow the extraction of the data it contains. The structure of factual databases is generally much more complex than that of bibliographic databases. Except for a few specialists of a bank, it is not conceivable to content oneself with the query language (SQL in the case of Cetim) associated with our Database Management System (Oracle).

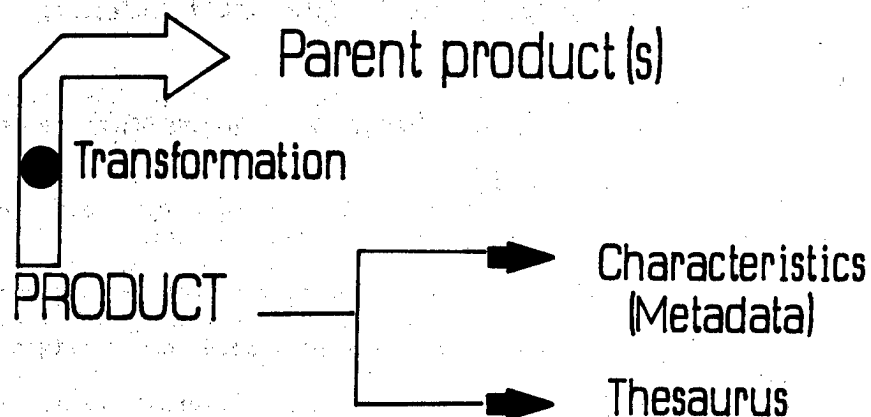


Fig 1. Main features of The CETIM-MATERIAUX database structure

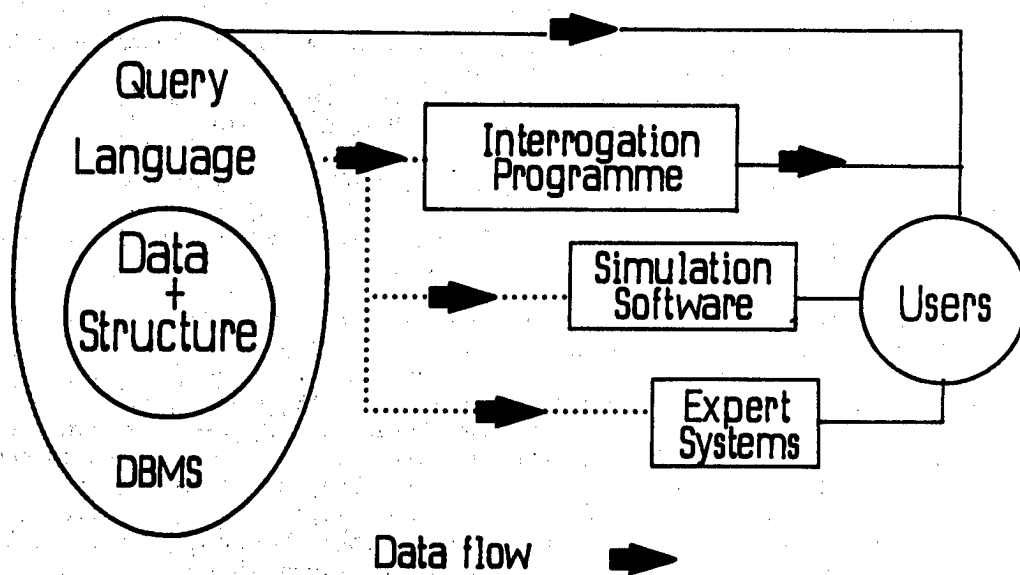


Fig. 2 Different ways of accessing data

Cetim-Matériaux is consulted via a user-friendly menu driven interface. Nevertheless, it is to be understood that an consultation programme is only aimed at helping the user in formulating his question and presenting the results of his query. As shown in Figure 2, the user can only get the data which are in the database. For material selection purposes, this is generally not sufficient. The associated software include some analytical knowledge (e.g. to calculate the response of a steel to heat treatment in CETIM-SICLOP). The last step would be to develop a complete Intelligent Knowledge System including expert knowledge with an inference engine containing logic and analytical capabilities to solve material problems.

Consultation of Cetim-Matériaux

1.- Search by name	
Integration into the search context	
Thesaurus key words	Characteristic values
2 Family	8 Physical properties
3 Material	9 Elastic moduli
4 Form	10 Static Mechanical propert.
5 Role	12 Fatigue
6 User industries	12 Friction / Wear
7 Characteristic	13 Corrosion
	14 Processability
16 Suppliers	15 Specific to adhesives
17 Specific Selection Programmes*	
ENTER YOUR CHOICE _____	

Fig. 3. Extract of the main menu of CETIM-MATERIAUX.

Two main ways of consulting are available. The first option of the menu allows the selection of product(s) the name(s) of which is (are) known or partially known. The other options allow a multicriteria selection by specifying key words of the thesaurus and/or required characteristic values. For both ways of interrogation, the list of selected products is then displayed and the user can select one product in order to visualize the information (description, characteristics, source of reference ...) concerning it. We may note that to assess the quality and reliability of the data, every piece of information is indexed to its source document which can be consulted during the session.

Search context. After introducing a search criterion, either a thesaurus key word (an assisted mode allows you to go down the hierarchy of the different thesauruses and choose a key word among those displayed.) or a characteristic value (as seen in figure 4, we may also have to specify certain metadata) the criterion is integrated into the search context if there exist products that comply. This context then can be activated to search the Database for appropriate materials. It can be modified at any stage to expand or reduce the number of products selected.

* : Option 17 is intended for later developments and will allow, for example, access to specific modules to help select adhesives.

Find products where PROOF STRESS		
Measured under the following conditions		
Orientation	1- Longitudinal 2- Long Transvers 3- Short transverse	
	4- Radial 5- Axial 6- Tangential	
Temperature : Either T (= 20 deg. C, room temperature by default)		
or T>= _____ and/or T<= _____ deg. C		
IS	>= _____ MPa	and/or <= _____ MPa

Fig. 4. Example of an input screen (extract).

Presentation of CETIM-SICLOP

CETIM-SICLOP, a software package designed to provide help in selecting steel grades, rapidly determines the following :

STEEL GRADES* which meet
the mechanical and structural REQUIREMENTS
according to the SHAPE and DIMENSIONS of the part and
standard HEAT TREATMENT conditions or those specified by the user.

CETIM-SICLOP also forecasts the profile of the characteristics inside a part, determines and optimizes heat treatment conditions and dimensions. It comes with a Database consisting of nearly 200 steel grades and its own management system. CETIM-SICLOP also includes a certain number of special functions especially designed for the heat treaters : determination of the severity of quench, utilization of a previously stored steel record (part geometry + severity of quench). CETIM-SICLOP is a menu-oriented conversational software package with an on-line help system.

The operator can use one of the fourteen simple shapes to describe its part and specify one of the following characteristics : Hardness (Rockwell C, Brinell, Vickers), percentage of martensite, ultimate tensile strength, 0.2% offset proof stress, elongation at rupture, reduction in area, fatigue limit in rotary bending. Figure 5 gives output examples

* : Heat treatable structural steels only.

Conclusions

Public access to Cetim-Matériaux will be available in 1991 via the X25 networks at a speed of 2400 bauds with a VT100 terminal emulation - This corresponds to the recommendations of the Code of Practise developed by the "Materials Data Base Demonstrator Programme" task group. Cetim-Matériaux was among the eleven European data banks selected by the CEC for this programme- We may also note that Cetim-Matériaux can be interrogated either in English or French and that the associated software are available.

SteelSet

Grade	Treat.		Quenched		TEMPERED						7	
	Q	Tem. °C	Hardness HRC	Ma %	Hardness HRC	UTS MPa	Ys0.2 MPa	El. %	RA %	Fat MPa		
32CRM012	0	600	45.5	83	28.3	924	756	20	63	481	STEELS	
42CRM04	0	600	45.5	82	28.4	927	757	20	63	481		
30CRNIMO8	0	600	50.0	98	28.4	928	797	21	66	498		OUT OF
35CRNIMO6	0	600	49.6	96	28.6	932	794	21	66	497		
34NICRM01	0	600	49.7	96	28.7	934	795	21	65	497	16	
50CRV4	0	600	50.5	86	30.6	980	810	19	62	503		

Martensite percentages less than 50 % are given for information only as well as Ys0.2%, fatigue and particularly Elongation, RA for Ma < 50%.

Cetim-Siclop El.0789 Cq Dma/418

←: Profile

↑ ↓ Pgup, Pgdn, home, end

Esc: Quit

F5: Print

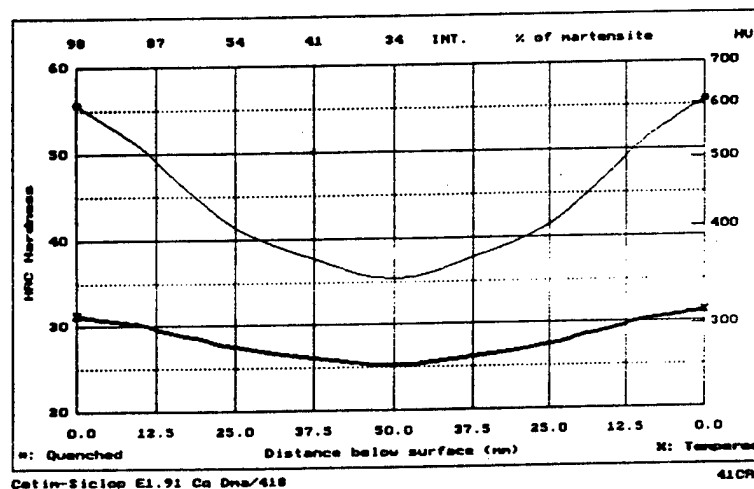


Fig. 5. Screen displaying a search results (top) and graphic representation of an hardness profile within a shaft (bottom). The upper curve corresponds to as-quenched hardness and the lower curve to a quenched and tempered state.

Bibliography : 1- F. Convert, F. Lacroisey & A. Pailleux, Guide de aciers outils pour travail à froid sur presse, Ed. Cetim (1978). 2- TOURNIER C. and PEYRE J.P., Choix des traitements superficiels, Ed. RPM-CETIM, Collection Matériaux en mécanique (1986). 3- Manuel des traitements de surface à l'usage des bureaux d'études, ed. Cetim-Club des traitements de surface (1987).

ACKNOWLEDGMENTS. The support of MRT (help decision N° 87.k.0455) and the collaboration of the DGA are acknowledged.

This is a U.S. Government publication. Its contents in no way represent the policies, views, or attitudes of the U.S. Government. Users of this publication may cite FBIS or JPRS provided they do so in a manner clearly identifying them as the secondary source.

Foreign Broadcast Information Service (FBIS) and Joint Publications Research Service (JPRS) publications contain political, military, economic, environmental, and sociological news, commentary, and other information, as well as scientific and technical data and reports. All information has been obtained from foreign radio and television broadcasts, news agency transmissions, newspapers, books, and periodicals. Items generally are processed from the first or best available sources. It should not be inferred that they have been disseminated only in the medium, in the language, or to the area indicated. Items from foreign language sources are translated; those from English-language sources are transcribed. Except for excluding certain diacritics, FBIS renders personal and place-names in accordance with the romanization systems approved for U.S. Government publications by the U.S. Board of Geographic Names.

Headlines, editorial reports, and material enclosed in brackets [] are supplied by FBIS/JPRS. Processing indicators such as [Text] or [Excerpts] in the first line of each item indicate how the information was processed from the original. Unfamiliar names rendered phonetically are enclosed in parentheses. Words or names preceded by a question mark and enclosed in parentheses were not clear from the original source but have been supplied as appropriate to the context. Other unattributed parenthetical notes within the body of an item originate with the source. Times within items are as given by the source. Passages in boldface or italics are as published.

SUBSCRIPTION/PROCUREMENT INFORMATION

The FBIS DAILY REPORT contains current news and information and is published Monday through Friday in eight volumes: China, East Europe, Soviet Union, East Asia, Near East & South Asia, Sub-Saharan Africa, Latin America, and West Europe. Supplements to the DAILY REPORTs may also be available periodically and will be distributed to regular DAILY REPORT subscribers. JPRS publications, which include approximately 50 regional, worldwide, and topical reports, generally contain less time-sensitive information and are published periodically.

Current DAILY REPORTs and JPRS publications are listed in *Government Reports Announcements* issued semimonthly by the National Technical Information Service (NTIS), 5285 Port Royal Road, Springfield, Virginia 22161 and the *Monthly Catalog of U.S. Government Publications* issued by the Superintendent of Documents, U.S. Government Printing Office, Washington, D.C. 20402.

The public may subscribe to either hardcover or microfiche versions of the DAILY REPORTs and JPRS publications through NTIS at the above address or by calling (703) 487-4630. Subscription rates will be

provided by NTIS upon request. Subscriptions are available outside the United States from NTIS or appointed foreign dealers. New subscribers should expect a 30-day delay in receipt of the first issue.

U.S. Government offices may obtain subscriptions to the DAILY REPORTs or JPRS publications (hardcover or microfiche) at no charge through their sponsoring organizations. For additional information or assistance, call FBIS, (202) 338-6735, or write to P.O. Box 2604, Washington, D.C. 20013. Department of Defense consumers are required to submit requests through appropriate command validation channels to DIA, RTS-2C, Washington, D.C. 20301. (Telephone: (202) 373-3771, Autovon: 243-3771.)

Back issues or single copies of the DAILY REPORTs and JPRS publications are not available. Both the DAILY REPORTs and the JPRS publications are on file for public reference at the Library of Congress and at many Federal Depository Libraries. Reference copies may also be seen at many public and university libraries throughout the United States.